1977

TURBULENT CHARACTERISTICS OF FLOW OVER RIPPLES.

MAHMOUD KAMEL. GIRATALLA
University of Windsor

TURBULENT CHARACTERISTICS OF FLOW OVER RIPPLES

A DISSERTATION

SUBMITTED TO THE FACULTY OF GRADUATE STUDIES THROUGH THE DEPARTMENT OF CIVIL ENGINEERING IN PARTIAL FULFILLMENT OF THE REQUIREMENTS FOR THE DEGREE OF DOCTOR OF PHILOSOPHY AT THE UNIVERSITY OF WINDSOR

by

MAHMOUD K. GIRATALLA

WINDSOR, ONTARIO, CANADA

1977

ABSTRACT

This thesis presents a mathematical simulation of flow over ripples along with experimental confirmation.

Experiments were conducted to establish the conditions of initiation and development of ripples in a mobile bed channel. Turbulence characteristics, including intensities, scales and Reynolds stresses, were measured by the hot-film anemometry technique over a sand mortar casting of a natural ripple bed, a smooth and sand-roughened artificial ripple bed and a smooth and sand-roughened flat bed.

A flow visualization method using the doubly refracting technique was used to investigate the shear pattern for the flow of milling yellow solution over the above mentioned beds.

A mathematical model to simulate the flow pattern over a ripple bed was developed. The finite element technique was adopted to solve the governing equations of the problem.

A comparison was made of the turbulence characteristics measured by the hot-film anemometer for the different smooth and sand-roughened beds.

Velocity and shear stress distributions obtained experimentally from the hot-film anemometry, the Pitot tube and the flow visualization methods for the different beds were analyzed.

Velocity and shear stress distributions, and also the separation pattern of flow in the lee of the ripple obtained theoretically were compared with the experimental results obtained from different methods.

A comparison between the experimental results of this study and those reported by other researchers was made. An explanation for the observed discrepancies in bed shear along the ripple is suggested.

ACKNOWLEDGEMENTS

In the memory of my parents

The author wishes to express his sincere gratitude to his supervisor, Dr. J.A. McCorquodale, for his valuable suggestions, guidance and encouragement during the course of this study. The comments of the members of this thesis committee are also appreciated.

The writer is grateful to the Department of Civil Engineering in the University of Windsor for the opportunity of carrying out this research.

Thanks are also due to my wife, Ann, for her encouragement and in typing the manuscripts of this thesis.

The financial assistance offered by the National Research Council of Canada is greatly acknowledged.

TABLE OF CONTENTS

***

LIST OF FIGURES

Figure | Page

Figure		Page
50-54.	Vertical Velocity and Shear Stress Distributions 44" D/S from the Screen for Different Beds - Obtained from Flow Visualization Analysis	200-204
55-59.	Isoshear and Isovelocity Patterns 44" D/S from the Screen for Different Beds - Obtained from Flow Visualization Analysis	205-209
60.	Shear Stress Variation at 0.125" Above Different Beds - Obtained from Flow Visualization Technique	210
61.	The Typical Arrangement of the Six Nodes Triangular Elements of the Finite Element Method	211
62.	The Typical Arrangement of the Three Nodes Triangular Elements of the Finite Element Method	212
63.	Finite Element Solution of the Stream Function for Laminar Flow Model	213
64.	Finite Element Solution of the Stream Function for Turbulent Flow Model	214
65.	Theoretical Vertical Velocity Distribution Along the Middle Ripple for Laminar Flow Model	215
66.	Theoretical Vertical Velocity Distribution Along the Middle Ripple for Turbulent Flow Model	216
67.	Velocity and Shear Stress Distributions Along the Ripple Obtained from the Mathematical Models	217
68.	Correlation of Hot-Film Anemometry Measurements Over the Cast Natural and Rough Artificial Ripple Beds	218
69.	Correlation of Pitot-tube Measurements Over the Cast Natural and Rough Artificial Ripple Beds	219
70.	Reynolds Shear Stress Obtained from Hot-Film Anemometry Measurements Versus Bed Shear Stress Measured by the Pitot-tube	220
71.	Comparison Between the Hot-Film Anemometry and Pitot-tube Measurements Over Rough Artificial Ripple Bed	221
72.	Comparison Between the Hot-Film Anemometry and Pitot-tube Measurements Over Cast of a Natural Ripple Bed	222

Figure		Page

Figure | Page

LIST OF PHOTOGRAPHS

LIST OF TABLES

CHAPTER ONE

INTRODUCTION

1.1 General Remarks

In the case of channel flow with granular bed material, the moving sediment along the bed can distort the bed into a variety of different shapes as shown in Fig. 1.

At low velocities the bed does not move at all. As the velocity is steadily increased, the threshold of movement is reached and the bed begins to move. On further increase of the velocity, the bed develops ripples. At higher velocities larger periodic irregularities, known as dunes, appear on the bed. With increasing velocity, the dunes are erased leaving a flat bed. Further increase in the velocity leads to the formation of sand waves. As the Froude number increases, the surface waves become so steep that they break; and at the same time there is a gradual movement upstream of the whole wave system. These sand waves are then called antidunes.

No completely satisfactory theories have yet been put forward to explain the mechanism of ripple bed forms. Most of the previous work, which has been done on bed forms, overlooked the early ripple stage of bed formations. Previous studies by Raudkivi[79], Khanna[50], and Rifai and Smith[83], indicated that the turbulent characteristics of the flow play an important role in ripple formation.

Previously, mathematical studies of flow over ripples were attempted using one of two approaches. The first group of studies was based on stochastic analysis. Yalin[116] used this approach to study the conditions of detachment of an individual grain, initiation of sediment transport and the non-fluctuating and fluctuating lift forces acting on the granular bed material. The second group of studies was based on a mathematical solution of potential flow over a linearlized boundary composed of periodic series to simulate the bed forms. Kennedy[46] and Marcer and Hague[66] are the most recent researchers who used this approach.

1.2 Objectives and Scope

The main objective of this research was the measurement and simulation of turbulent flow over a ripple bed.

Hot-film anemometry, being one of the most reliable and refined techniques known to-date to measure turbulence characteristics, was chosen as the basic instrumentation in the experimental study. Rigid bed models were used as the bed boundary to permit more exhaustive studies with the hot-film probes which are subject to damage in an active mobile bed channel.

A mathematical model to simulate the flow pattern over ripple beds was developed using the finite element technique to solve the governing Poisson and Helmholtz vorticity equations of the flow field.

Another objective of this research was the development of a new experimental flow visualization technique using "milling-yellow" solution to study the shear patterns of flow over rigid beds. The doubly refractive characteristics of the milling-yellow solution allowed the visual study of these shear patterns.

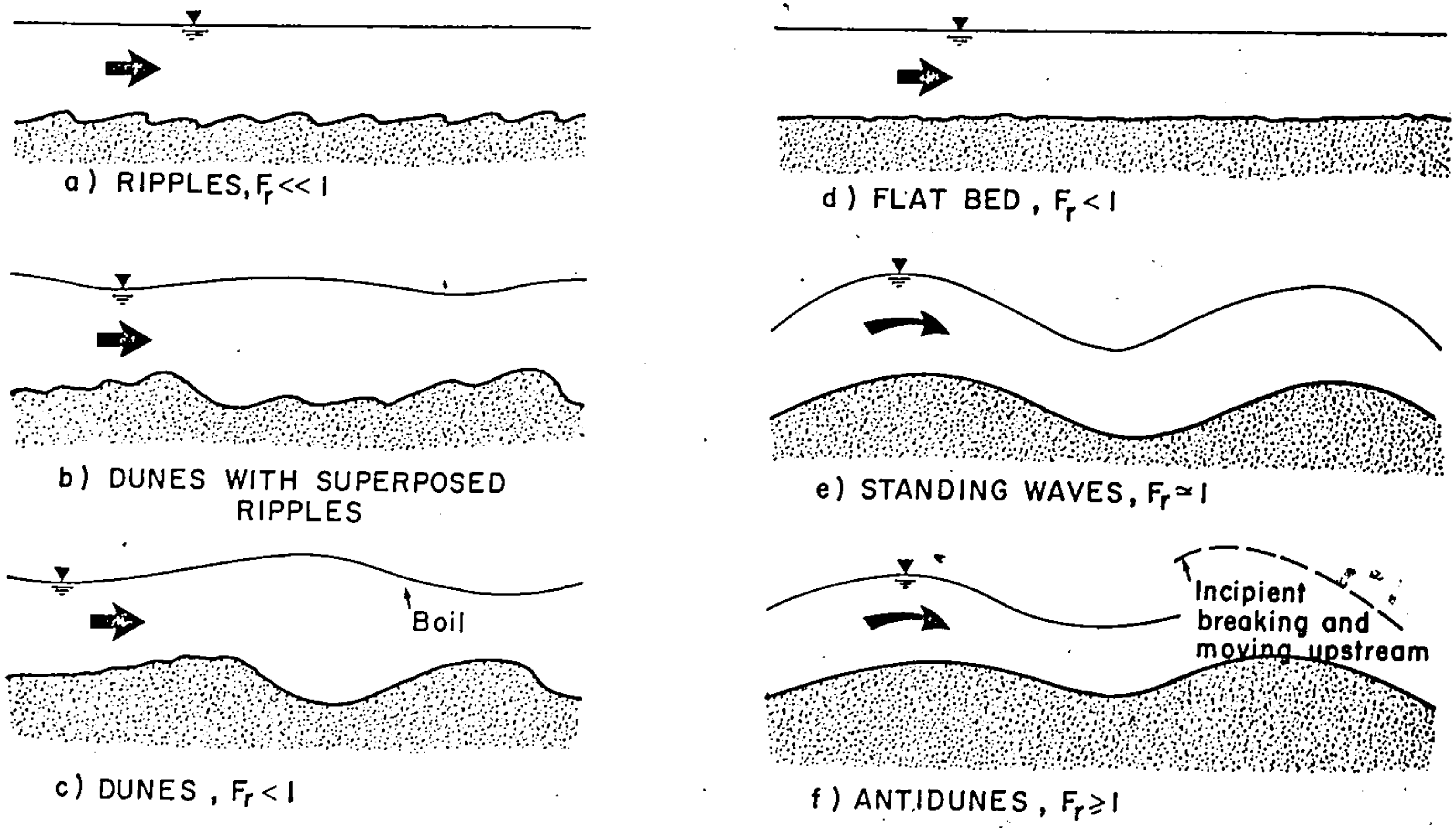

Fig. 1 - Forms of bed roughness in alluvial channels, after Simons and Richardson reference (96)

CHAPTER TWO

LITERATURE SURVEY

2.1 Bed Formations

2.1.1 General Comments on Ripple Formations

As early as 1883 in England, Darwin[19] published the results of experiments on sand ripple formations due to oscillatory motion. He concluded that a vortex sheet exists between two parallel currents due to a high velocity gradient. This vortex sheet is unstable in nature and eventually will break up into a series of vortices. Darwin did not explain the significance of such a vortex sheet, nor did he investigate the velocity gradient causing ripples.

Also in England, Bagnold[4] conducted extensive research on the formation of sand dunes caused by wind. He explained that desert dunes are due to the instability of the bed caused by the bombardment of sand grains.

Exner[24] established a differential erosion equation for two-dimensional flow in the form

$$\frac{\partial \eta}{\partial t} + K \frac{\partial v}{\partial x} = 0$$

where η is the elevation of the bed relative to time t, K is a factor relating sediment discharge to flow velocity,

v is the flow velocity near the bed, and

x is the distance in the downstream direction.

Using his equation, which indicates that the change in bed elevation is due to longitudinal variation of bottom velocity, Exner showed that if a symmetrical sand wave is taken as an initial bottom surface, it will be transformed in course of time into an asymmetrical wave with a gentle upper slope and a steep lower slope. However, he did not give the reason how a longitudinal variation of velocity can exist if the bottom is originally plane.

Anderson[3] reasoned that in case of shallow flow, surface waves may affect the alluvial bottom and cause sand waves. Considering the interaction between surface waves and sand waves, and using Exner's equation of erosion, he obtained a relationship between the Froude number and the depth-wave length ratio. He did not explain the case of deep flow having sand ripples along the bed or desert dunes formations without a free surface.

Gilbert[29] and Inglis[41] postulate that the origin of ripple lies in an uneven movement of the sediment caused by the uneven flow of water. Liu[60] explained that ripples are caused by the instability of the interface between the fluid and the bed.

Descriptions of the development of different bed patterns have been given by many investigators, for example: Simons and Richardson[95, 96]. They divided the forms of bed roughness, on the basis of their shape, resistance to flow, and sediment transport, into two regimes, the lower and upper flow regimes, with a transition zone in between. The bed forms are ripples and dunes in the lower flow regime, and plane bed, standing waves and antidunes in the upper flow regime. The bed form in the transition zone is variable, ranging from that which is typical of the lower flow regime to that for the upper regime.

Different sets of criteriá, based on experimental evidence and physical reasoning were chosen by Shields(93), Langbein(54), Liu(60), Bagnold(5), Bogardi(8) and others(27,22,38) in order to predict the range of occurrence of each bed configuration, respectively. They all provide different sets of curves which could be used for practical application, keeping in mind the limitation imposed by each, according to its experimental limits.

Yalin in 1964(116), and Znamenskaya in 1969(31), and others(26,94) have concentrated on the study of the variation of the average ratio between the length and height of ripples and dunes. Typical values of this ratio are in the range of 6 to 25.

Inglis(41) and Falkner(25) reported that no ripples were found on the sand bed with sand sizes larger than approximately 0.6 mm.

In 1963 Raudkivi(77) studied flow conditions for the particular case of flow of water over a cohesionless sand bed when ripples form. He described the mechanism of ripple formation as a disturbance in the plane surface by a chance piling-up, when the threshold conditions of sediment transport are exceeded. This surface disturbance establishes an interface or surface of discontinuity in the flow similar to that with flow past a negative step. In his excellent explanation he stated that where the core of this interface meets the sand boundary, it excavates more material because of increased turbulent agitation in the interface between the wake and main stream. This extra material entrained cannot be supported by flow over a plane boundary. The turbulent agitation is a maximum where the core of the interface meets the boundary and decrases with distance downstream. The additional entrained material settles out as it passes downstream, away from the stronger agitation of the core region, leading to a new ripple face. This settling out is a function of the decay of agitation. The interface turbulence decreases moving downstream the new ripple face, but the surface drag increases because of the convergence of flow.

Hill[37] reported a general investigation of the occurrence of bed forms. From the Bagnold number, the number with which the ratio of shear stress to dispersive pressure varied, he reasoned that when this ratio becomes greater than the coefficient of friction of sand at rest, the system becomes unstable. A relationship was determined to find the point at which ripples would replace the flat bed. The data available generally supported his assumption, however, there was little data for ripple conditions because the flat bed was usually displaced by dunes. A curve based on an empirical relationship was suggested to determine the point at which the flat bed ceased to exist because of dune formation.

Hill and Srinivasan[38] have considered the occurrence of different bed forms as an instability in the flat bed flow. A general functional relationship has been developed for the instability of a flat bed when it tends to be replaced by either dunes or ripples.

Their experiments indicated that two distinct relationships exist for the two instabilities with a region of transition in between where either instability may occur. From the stability function, the occurrence of different bed forms could be predicted.

In 1971 William and Kemp[114] carried out a research to investigate the mechanism of the initiation of ripples in natural sands under turbulent water flow. Ripples were found to form on a flat bed from small deformations caused by the random action of high turbulent velocities close to the bed. A derivation of the criteria for ripple formations was given in terms of a line on Shield's graph. Additional experiments were made in which the grain Reynolds number was varied by varying the temperature and thus the viscosity of the water. Their results suggested that the described mechanism of ripple formation does not operate for grains larger than 600 micron at normal temperatures.

In 1972 William and Kemp[115] continued their experiments on the initiation of ripples by artificial disturbances. They found that ripples may be produced on flat channel beds by artificial disturbances, at lower flows than those at which ripples form naturally. The artificial disturbance used, consisted of vertical thin plates set normal to the flow. These plates produced separation eddies, and the motion of grains at the flow reattachment point was observed. They related the development of a ripple train downstream of the disturbance to the bed shear stress measured upstream of the disturbance. The initiation of ripples in these circumstances was also related to the height of the disturbance, the water depth, and grain diameter, in addition to the normal parameters of Reynolds number and Shields mobility number.

Yang[118] revealed, after reviewing the existing literature, some disadvantages of using Shield's diagram as the criterion for incipient motion of sediment particles in an alluvial bed. He introduced a new criterion based on avarage flow velocity, fall velocity, and shear velocity Reynolds number, which led to a dimensionless unit stream power equation for sediment transport. More than 1,000 sets of data from both laboratory flumes and natural streams published by different authors were used to support his argument.

Pratt[75] examined his results of a laboratory investigation of the flow over a graded 0.49 mm sand within the framework of Bagnold's theory for the flow of cohesionless grains in fluid and general agreement was found between the experimental and predicted behaviour. Bagnold's primary and secondary bed features were shown to correspond to ripple type and dune type bed-forms respectively. The subdivision of the secondary features between intermediate, flattened dunes, and developing dunes was seen to occur at a particular ratio of the bed load to the associated intergranular fluid stress at each of the four depths of flow investigated.

The premise that ripple formation is due to turbulence was favoured by some hydraulic engineers such as Velikanov[108], Tison[104] and Von Karman[109]. Velikanov was able to prove mathematically that turbulence could cause erosion and deposition along the bottom. Tison found that ripples were present in turbulent flow only.

Yalin[116] gave his interpretation of why and how sand waves occur. Waves on the free surface resulting from the discontinuity at the beginning of the mobile bed produce antidunes. Disturbance in the structure of turbulence resulting from discontinuity of the plane initial bed produces dunes. Deformation of the unstable bed surface resulting from any local discontinuity in the plane bed produces ripples. Yalin distinguished between ripples and dunes with respect to their origin of occurrence. While dunes are assumed to be produced by the largest eddies of turbulent flow, ripples are inhibited by the turbulence in the vicinity of the bed. He claimed that ripples are essentially dependent on the nature of the fluid and the size of the grains, and possibly on the bed shear stress.

2.1.2 Flow Characteristics Over Ripples

The problem of resistance to flow over alluvial beds has been tackled by many investigators to estimate the friction factors of different bed forms.

Einstein and Barbarossa(21) divided the bed resistance into two parts. The first part of the resistance is associated with the rough sand grain surface. The second part is transmitted to the boundary in the form of normal pressures at the different sides of each sand dune or ripple. They found from river measurements that the second part, which is the form resistance of the bed irregularities, is a function of the sediment transport alone.

Engelund(22) in his theoretical approach followed the Einstein-Barbarossa subdivision of the total drag. Basically he calculated the surface drag in terms of the sand grain roughness and the form drag as the Carnot expansion loss.

Shen[91] analyzed the experimental data collected at many research laboratories. He came to the conclusion that with uniform size materials the variation of resistance due to the sediment bed irregularities is a function of both the sediment transport rate and the Reynolds number based on the fall velocity of the sediment particle.

Garde and Raju[28] proposed new parameters to describe the resistance of an alluvial stream. They claimed, after reviewing the reliability of the resistance relationship given by Einstein-Barbarossa, Liu and Shen, that their own relation is far more satisfactory in predicting the resistance of an alluvial stream.

Vanoni and Hwang[107] expressed the friction factor for flow over a ripple bed in terms of height, hydraulic radius and a newly introduced "exposure parameter" to account for the areal concentration of ripples. Their experimental results clearly show the advantage of using the exposure parameter to find the friction factor.

In 1967 Raudkivi[78] examined the variation of friction factor in fluvial channels in terms of the governing principles. His laboratory measurements showed that local surface drag on a bed covered by bed forms varies from zero at the reattachment region of the surface of discontinuity formed at a crest, to a maximum at the next crest downstream. On exceeding a critical temporal mean value of the shear velocity, the friction factor increases rapidly as ripples form and reaches a peak value where the steepness of the bed forms is a maximum. As the velocity increases, more dunes of decreasing steepness were formed which lead to a transitional flat bed, for which the friction factor has approximately the initial flat bed value. With the formation of antidunes, Raudkivi found that the friction factor increases again. Raudkivi[77] also presented and examined velocity, pressure and shear stress measurements along different bed profiles.

Chang[12] found that, for flow over ripples in alluvial channels, the grain-roughness friction factor can be satisfactorily determined from Nikuradse's formula. The form roughness friction factor was found to be proportional to the exposure parameter and inversely proportional to mean relative height of the ripples, and, also proportional to the coefficient of expansion loss. The latter was found to be a function of the mean relative height of the ripples.

Crickmore[16] studied the effect of flume width on bed form characteristics. His experimental results obtained from three different flume widths showed that the form height, form length and spectral width increase with increasing width of flume. He also suggested that the transport can be obtained from the product of the avarage height of the dunes and their speed.

Grass[34] used the hydrogen bubble wire technique to measure the distributions of critical instantaneous bed shear stress associated with the observed movement of individual surface grains. Critical flow conditions were then predicted by equating the lower extremes in these characteristic critical shear stress distributions to the upper extremes in the distribution of instantaneous bed shear stress produced by the particular type of background flow under consideration. His method yielded sufficiently consistent results to suggest an extension to Shield's curve for small grain Reynolds numbers.

Squarer[99] investigated the bed form geometry in a curved channel and a straight flume which were subjected to the same nominal flow conditions, by using statistical analysis of records of stream bed profiles. A quantitative comparison was made in terms of the autocorrelation, spectral density and probability density function of a process, defined by the bed elevation. The same statistical functions were used to evaluate the bed friction factor and ripple celerities. He found that the total rate of sediment transport in the curved channel is approximately fifteen times as much as that of straight flume for the same nominal flow conditions.

Laursen et al(56) carried out experiments of air flow in a closed conduit with smooth and rough schematic triangular shaped bed forms placed symmetrically at the top and bottom of the conduit. Pressure distributions and boundary shear stress were measured using the Preston-tube.

Jonys(43,44) studied experimentally the mechanics of bed forms. Velocities, pressure distributions, boundary shear stress and geometry of bed forms were measured within actively translating light weight sediment beds. Statistical analysis was carried out to select only the stable bed forms for his study. He related the pressure gradient on bed forms to their surface slope. Jonys found that maximum pressure gradient occured at locations of maximum bed-form surface slope, i.e., at locations of maximum particle entrainment, and the minimum pressure gradient corresponded with location of zero particle entrainment.

Sheen(90) carried out turbulence measurements in the flow over a sand-coated artificial ripple bed. He presented velocity and turbulence components at various stations along the ripple.

Rifai and Smith[83] used a series of rigid triangular elements, placed on the bed of a laboratory flume to simulate alluvial channel bed features. Their study showed that the energy spectra expressed by the frequency of the turbulence throughout the flow is higher than that for comparable flow over a rigid plane bed, due to the higher frequency turbulence arising from the eddies in the lee of the elements. They found experimentally that the macro scale of turbulence is approximately equal to the height of the triangular element.

Khanna[50], using hot wire anemometry in an air medium, measured the mean velocity distribution, angle of flow, static pressure distribution and longitudinal turbulence intensity, along a typical smooth wooden wave with flow characteristics of the domain of ripples and dunes. From his observations, skin friction coefficient, form drag, shear stress and boundary layer thickness have been evaluated.

Thomas[102] carried out experiments on particles transport in a round pipe in an attempt to establish a correlation of the sand waves forming in closed pipes and open channels. He observed that equally spaced clumps or islands formed at velocities only slightly greater than those required to initiate particle movement. Thomas presented a good correlation between his results and those reported by Simons et al[97] on sand dune formation in an open flume. He concluded that sand waves in closed pipes, open flumes, rivers and channels are closely related phenomena and hence any theories must account for the data from all these systems. The equation that he proposed was based, in part, on Helmholtz instability.

In spite of the previous extensive experimental work in investigating the early stages of bed formation, it was felt that one of the significant areas overlooked by previous investigators is the measurement of turbulent characteristics of flow of the domain of natural ripples.

The experimental measurements over mobile beds were always limited to either Pitot-tube or hydrogen bubble techniques where no information of the turbulent characteristics of flow over ripples can be revealed. Other investigators[50,90] have carried out turbulence measurements using the hot-sensor anemometry technique over simplified two-dimensional ripple models that were not completely representative of the actual three-dimensional ripple formation. Khanna[50] measured turbulence characteristics of air flow over smooth sand waves that do not represent an actual ripple formation. Sheen's[90] experiments were carried out on water flow over a two-dimentional sand-roughened ripple bed model.

The difficulties encountered in turbulence measurements over sandy mobile bed are recognized. The moving particles will damage the delicate sensors if such approach is attempted. However, in the present research an exhaustive study with the hot-film probes was initiated to investigate the turbulent characteristics of water flow over a rigid cast of a three-dimensional natural ripple formation and a representative two-dimensional sand-roughened model of a ripple bed. Flow characteristics over a smooth ripple model, and smooth and sand-roughened flat beds were also studied, Pitot-tube measurements were also undertaken over the natural mobile ripple bed and the rough and smooth rigid beds. In this manner a complete satisfactory comparison of the flow characteristics over the natural mobile bed, cast of the natural ripple, the artificial ripple and the flat beds can be achieved.

2.1.2 Mathematical Models of Flow Over Ripples

Analytical treatment of turbulent flow past boundaries of regular periodic form has been of interest to many investigators. The first of these, presented by Lamb[53] and Milne-Thomson[67] has considered irrotational flow over a sinusoidal boundary as a simple example of a time-dependent motion rendered steady by a simple Galilean transformation. This formulation has later been used by Kennedy[46] and Reynolds[81], to examine the stability of flows over erodible beds in alluvial channels. Treating the fluid motion as irrotational achieves considerable mathematical simplification and yields at least a description of the behavioural features of the flow outside the boundary layer region. Many other important properties, however, are not revealed unless shear forces and rotational aspects of the flow are introduced into the mathematical model. The second approach to the problem utilizes the one dimensional method of analysis which was introduced by Boussinesq[9] and further developed by Masse[61] and Iwasa[42]. It has been applied to flow over a rigid, wavy bed by Engelund and Hansen[23], and to flow over erodible beds originally by Exner[24] and more recently by Reynolds[81]. Using the one dimensional method of analysis, Kennedy[47] developed an energy equation for shearing flow over a bed of regular sinusoidal form, retaining the curvilinear and convective terms. The formulation has been linearized and examined, and found to yield a practically complete description of the array of surface wave configurations accompanying various flow conditions and bed geometries.

Recently, Mercer and Haque[66] presented a ripple flow profile model based on potential flow over a linearized boundary composed of a periodic series of modified wedges and eddy shear lines as an advancement on sinusoidal profile models. Velocity and pressure data taken from a styrofoam replica of the profile model were compared to those obtained theoretically assuming irrotational flow and also to those obtained theoretically assuming inviscid rotational flow. The latter showed fair agreement with their experimental results. This model gave a solution for a simplified boundary condition with frictionless ideal flow.

It was felt that applying the finite element technique[120] as a sophisticated mathematical model simulating the real flow under prescribed intricate boundary conditions would provide a new approach in modelling ripple behaviour.

2.2 Hot-Film Anemometry

The analysis and measurements of King in 1915[51] relating the convective heat transfer from small heated wires to the measurement of fluid motions is generally accepted as the beginning of hot wire anemometry. The use of hot-films, however, is much more recent. One of the earliest developments was that by Ling and Hubbard in 1955[58,59]. While differences between films and wires do exist, the operating principle is the same. Thus, when discussing the techniques of hot-wire anemometry, the comments apply as well to hot-films.

Since King's early experiments, literally thousands of articles have been published in which hot-wire techniques were used. The majority of these were concerned with the study of turbulence in air streams, particularly in wind tunnels. A representative list of thirty-six such works which report some of the most important turbulence measurements has been compiled by Cooper and Tulin[15]. Of these, the work by Laufer[55] as a thorough investigation of mean and fluctuating quantities in a two dimensional air channel flow is the most significant.

Techniques of construction of the sensing element and methods of operation in air streams for flows ranging from a few feet per second to measurements in hypersonic wind tunnels have been well developed. A reproducibility of ±2% in the measured turbulence characteristics is generally expected. With liquids, however, the situation is different, where many problems which are not encountered in air may arise.

In early turbulent studies, the results were not much better than qualitative reproducibility of about ±50%. These include reports in 1950 and 1956 on the study of the effect of turbulent intensity on skin friction in ship model towing tests[10,101]. Others include the ocean turbulence studies at the Pacific Naval Laboratories between 1951 and 1956[70] with later reports in 1959[33,71] and 1962[32].

In more recent studies quantitative results have been obtained. These include the momentum transfer study in two phase liquid-liquid flow by Darby[18], velocity profiles in the transition region in an open channel by Carruthers[11], and the analysis of the turbulent free shear layer in channel flow by Sabin[86].

A fundamental study of turbulence by Bankoff and Rosler[6] in 1962 once again vividly demonstrated the problems associated with liquid turbulence measurements. They used a hot-film anemometer to measure velocity distributions, intensities and scales of turbulence, and spectral energy distributions in a free jet. Rust accumulation from the connections in galvanized piping, entrained air bubbles and electrolytic deposition of metallic ions from the water on the hot-film caused considerable difficulties. Drift in mean velocity readings (probe voltage) was as great as 75% per hour.

Roberts[84] was able to obtain satisfactory results by using well-filtered, degassed and de-ionized hydraulic oils. Raicheln[76] was also successful in measuring turbulence characteristics in carefully cleaned water.

Dell'osso[20] employed single and crossed hot-film to investigate the turbulence characteristics in open channel flow.

McQuivey alone[63] and with Richardson[64,65] made extensive measurements of turbulence characteristics of water flow in open channels. The effect of fluid-borne contaminants on the voltage/velocity relation was studied by comparing turbulence measurements made in clean and very dirty water for hydraulically rough and smooth open-channel flow. They conclude that dirt and air bubbles accumulating on the sensor decrease the mean voltage for a given velocity but in the domain of frequencies encountered in water, do not affect the frequency response of the sensor to velocity fluctuations. Thus, for a given sensor, there is a unique family of voltage/velocity relations which can be defined by calibration with different overheat ratios. Their verification was limited to a degree of contamination of the probe which changed the voltage/velocity relation the same as would occur when the overheat ratio decreased from 1.10 to 1.07.

Resch[80] has also obtained experimental results of turbulence in water flow using unidirectional, conical and wedge shaped probes.

2.3 Flow Visualization

Even though Maxwell[62] first observed the phenomena of double refraction in liquids in 1866 little work has been done with its direct application in the field of fluid mechanics.

It was not until 1924 that Humphery[40] first used vanadium pentoxide solutions to show qualitatively the difference between laminar and turbulent flow. The earliest attempts at quantitative measurements from flow double refraction were reported by Alcock and Sadron[2], using sesame oil, they claimed to be able to determine velocity gradients within approximately 0.1 mm of a solid boundary.

Hauser and Dewey[35] used bentonite solutions for qualitative and quantitative studies of velocity profiles in two dimensional laminar flow.

Peebles, Garber and Jury[73] were apparently the first to use an aqueous solution of milling-yellow dye to obtain stress patterns through and around various configurations. Peebles, Prados and Honeycutt[72] reported on the optical and physical properties of milling-yellow in 1954. This report was followed in 1955 and 1957 by reports of Peebles and Prados[74], using milling-yellow to study fully developed laminar flow through straight converging and diverging channels.

Wayland and Sutera[110,111,112,113] have conducted experiments on the laminar and turbulent flow in the annular space between eccentric rotating cylinders to clarify the optical calibration data obtained from concentric cylinders to the analysis of general two dimensional laminar flow.

Thurston and Schrog[103] investigated the dynamic birefringence of aqueous solutions of milling-yellow. They conducted an experiment with a confined fluid layer between two rigid parallel planes, one plane being fixed and the other plane executing a sinusoidal motion.

Scheuner[88] obtained the velocity profiles, in the boundary layer for various flow rates of milling-yellow solution in a four by four inch tunnel, from the interference pattern created by parallel flow along a flat plate. His experimental results compared favourably with theoretical Blasius boundary layer velocity distributions. He also analyzed qualitatively the flow past a cylinder.

Ousterhout[68] presented his results of milling-yellow solution flowing over immersed bodies in a uniform velocity field. It was possible to determine the shape of velocity profiles within a boundary layer by interpreting the interference fringes as lines of constant strain rate. Regions of instability, vortex shedding and turbulence were also determined.

Ahimaz[1] suggested an experimental approach using the milling-yellow solution and the scattered light technique to study the three-dimensional state of flow and the stress at a point in the fluid.

CHAPTER THREE

THEORY AND DEVELOPMENT OF THE MATHEMATICAL MODEL

3.1 Introduction

In this chapter a mathematical model simulating the flow pattern over a ripple bed is presented. The flow is represented by a Poisson Equation, relating stream function to vorticity and a modified Helmholtz Vorticity Equation in the forms:

$$\frac{\partial^2 \psi}{\partial x^2} + \frac{\partial^2 \psi}{\partial y^2} + \omega = 0 \qquad 3.1$$

and

$$\frac{\partial \omega}{\partial t} + \frac{\partial}{\partial x} \left\{ U\omega - (\nu + \varepsilon) \frac{\partial \omega}{\partial x} \right\} + \frac{\partial}{\partial y} \left\{ V\omega - (\nu + \varepsilon) \frac{\partial \omega}{\partial y} \right\} = 0 \qquad 3.2$$

Theoretical derivation of Eqs. 3.1 and 3.2 is given by Zaghloul[119].

It should be noted that an eddy viscosity term has been added to the kinematic viscosity in the Helmholtz Equation to account for the actual turbulent flow conditions.

The finite element technique is adopted to solve the governing equations. This method is primarily based on limiting the real system with an infinite degrees of freedom to a finite number of degrees of freedom so that the computer solutions can be obtained.

The finite element technique which was developed originally as a concept of structural analysis [14], has been applied by Zienkiewicz[120] to problems dealing with fluid flow.

3.2 The Finite Element Formulations

3.2.1 Poisson Equation

Eq. 3.1 is the two dimensional form of Poisson Equation for an incompressible fluid.

By the calculus of variations, the equivalent formulation of Eq. 3.1 is the requirement that the double integral given in Eq. 3.3 and taken over the whole region should be minimized.

$$\chi = \iint \left[\tfrac{1}{2} \left\{ \left(\frac{\partial\psi}{\partial x}\right)^2 + \left(\frac{\partial\psi}{\partial y}\right)^2 \right\} - \omega\psi \right] dxdy \qquad 3.3$$

The procedure used to derive the necessary matrix formulation of Eq. 3.3 was achieved by dividing the region into a number of finite triangular elements. These triangular elements are assumed to be interconnected at six discrete nodal points, the three vertices and the three midpoints of the sides of every triangle.

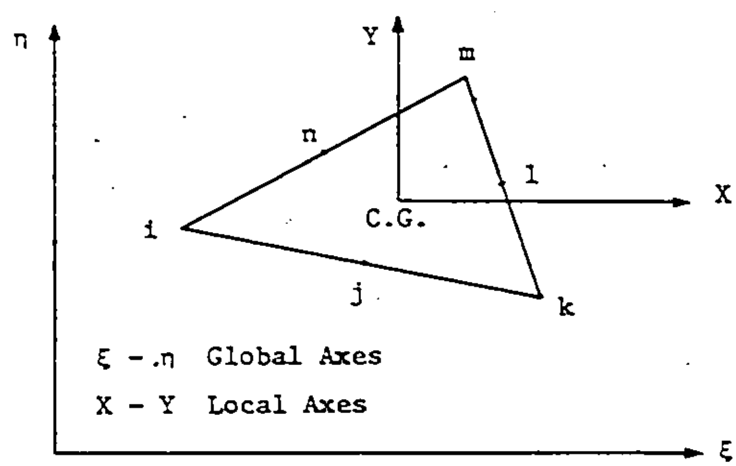

Fig. 2. The Characteristics of a 6-nodes Triangular Element

Fig. 2 shows a typical triangular element with the nodes i, j, k, l, m and n numbered in an anticlockwise order. If the six nodal values of ψ define the function within each element, then ψ can be expressed as a matrix of single column written as

$$\{\psi\}^e = (\psi_i, \psi_j, \psi_k, \psi_l, \psi_m, \psi_n) \qquad 3.4$$

The choice of six nodal points to define the stream function ψ is necessary to yield non-zero second derivatives of ψ with respect to x and y in order to calculate ω from the Poisson Equation.

Assuming the ψ values can be represented by the local X and Y co-ordinates, that is, co-ordinates referred to local axes situated at the centroid of the element, in the form

$$\psi = \alpha_1 + \alpha_2 x + \alpha_3 y + \alpha_4 x^2 + \alpha_5 xy + \alpha_6 y^2 \qquad 3.5$$

which is the compatible form of the second degree polynomial type equation.

Now, define the matrix $[C]$ such that,

$$[C] = \begin{bmatrix} 1 & x_1 & y_1 & x_1^2 & x_1 y_1 & y_1^2 \\ 1 & x_2 & y_2 & x_2^2 & x_2 y_2 & y_2^2 \\ 1 & x_3 & y_3 & x_3^2 & x_3 y_3 & y_3^2 \\ 1 & x_4 & y_4 & x_4^2 & x_4 y_4 & y_4^2 \\ 1 & x_5 & y_5 & x_5^2 & x_5 y_5 & y_5^2 \\ 1 & x_6 & y_6 & x_6^2 & x_6 y_6 & y_6^2 \end{bmatrix} \qquad 3.6$$

where subscripts 1, 2, 3, 4, 5 and 6 indicate the nodes i, j, k, l, m and n respectively.

And the inversion $[C]^{-1}$ as

$$[C]^{-1} = \begin{bmatrix} C_{11} & C_{12} & C_{13} & C_{14} & C_{15} & C_{16} \\ C_{21} & C_{22} & C_{23} & C_{24} & C_{25} & C_{26} \\ C_{31} & C_{32} & C_{33} & C_{34} & C_{35} & C_{36} \\ C_{41} & C_{42} & C_{43} & C_{44} & C_{45} & C_{46} \\ C_{51} & C_{52} & C_{53} & C_{54} & C_{55} & C_{56} \\ C_{61} & C_{62} & C_{63} & C_{64} & C_{65} & C_{66} \end{bmatrix} \qquad 3.7$$

Also, define the vector $[E]$ as

$$[E] = [\, 1,\ x,\ y,\ x^2,\ xy,\ y^2 \,] \qquad 3.8$$

Using Eqs. 3.4 to 3.8, one obtains

$$\{\psi\}^e = [C] \; \{\alpha\}^e$$

or

$$\{\alpha\}^e = [C]^{-1} \; \{\psi\}^e \qquad 3.9$$

and

$$\psi = [E] \; \{\alpha\}^e$$

or

$$\psi = [E] \; [C]^{-1} \; \{\psi\}^e \qquad 3.10$$

$$= [W_i,\ W_j,\ W_k,\ W_l,\ W_m,\ W_n] \; \{\psi\}^e$$

where

$$W_i = C_{1i} + xC_{2i} + yC_{3i} + x^2C_{4i} + xyC_{5i} + y^2C_{6i} \qquad 3.11$$

Differentiate ψ with respect to x yields

$$\frac{\partial\psi}{\partial x} = \psi_x = \left[\frac{\partial E}{\partial x}\right] [C]^{-1} \{\psi\}^e \qquad 3.12$$

and

$$\left[\frac{\partial E}{\partial x}\right] = [E_x] = [0,\ 1,\ 0,\ 2x,\ y,\ 0] \qquad 3.13$$

Therefore,

$$\psi_x = [N_i,\ N_j,\ N_k,\ N_l,\ N_m,\ N_n] \{\psi\}^e \qquad 3.14$$

where

$$N_i = C_{2i} + 2xC_{4i} + yC_{5i}$$

Also, the differentation $\frac{\partial}{\partial\psi_i}(\frac{\partial\psi}{\partial x})$ can be written as

$$\frac{\partial}{\partial\psi_i}\left(\frac{\partial\psi}{\partial x}\right) = \frac{\partial\psi_x}{\partial\psi_i} = N_i \qquad 3.15$$

Similarly,

$$\frac{\partial\psi}{\partial y} = \psi_y = \left[\frac{\partial E}{\partial y}\right] [C]^{-1} \{\psi\}^e \qquad 3.16$$

and

$$\left[\frac{\partial E}{\partial y}\right] = [E_y] = [0,\ 0,\ 1,\ 0,\ x,\ 2y] \qquad 3.17$$

Therefore,

$$\psi_y = [M_i, M_j, M_k, M_l, M_m, M_n] \quad \{\psi\}^e \qquad 3.18$$

where

$$M_i \doteq C_{3i} + xC_{5i} + 2yC_{6i}$$

and

$$\frac{\partial}{\partial\psi_i}\left(\frac{\partial\psi}{\partial y}\right) = \frac{\partial\psi_y}{\partial\psi_i} = M_i \qquad 3.19$$

With the nodal values of ψ defining uniquely and continuously the function throughout the region, the 'functional' χ can be minimized with respect to these values. To achieve this, one should first evaluate the contributions to each differential, such as $\frac{\partial\chi}{\partial\psi_i}$, from a typical element, then adding all such contributions and equating these to zero. It is noted that only the elements adjacent to the node i will contribute to $\frac{\partial\chi}{\partial\psi_i}$. The differentiation of Eq. 3.3 with respect to ψ yields

$$\frac{\partial\chi^e}{\partial\psi_i} = \iint \left[\left(\frac{\partial\psi}{\partial x}\right) \frac{\partial}{\partial\psi_i}\left(\frac{\partial\psi}{\partial x}\right) + \left(\frac{\partial\psi}{\partial y}\right) \frac{\partial}{\partial\psi_i}\left(\frac{\partial\psi}{\partial y}\right) - \omega \frac{\partial\psi}{\partial\psi_i}\right] dxdy \qquad 3.20$$

Substituting Eqs. 3.14, 3.15, 3.18 and 3.19 in Eq. 3.20 and arranging one obtains

$$\frac{\partial\chi^e}{\partial\psi_i} = \iint \Big([N_i, N_j, N_k, N_l, N_m, N_n] N_i \quad \{\psi\}^e$$
$$+ [M_i, M_j, M_k, M_l, M_m, M_n] M_i \{\psi\}^e \Big) + F_i \qquad 3.21$$

where

$$F_i = - \int\int \omega \frac{\partial\psi}{\partial\psi_i} \, dxdy = - \int\int \omega \, W_i dxdy \qquad 3.22$$

where W_i is defined by Eq. 3.11.

If ω can be assumed as constant within an element, then the integral of Eq. 3.22 reads

$$F_i = - \omega \int\int (C_{1i} + xC_{2i} + yC_{3i} + x^2C_{4i} + xyC_{5i} + y^2C_{6i}) \, dxdy \qquad 3.23$$

which requires to be evaluated over the area of the triangle, this becomes

$$F_i = - \omega\Delta \, (C_{1i} + \overline{x}C_{2i} + \overline{y}C_{3i} + \overline{x^2}C_{4i} + \overline{xy}C_{5i} + \overline{y^2}C_{6i}) \qquad 3.24$$

where $\overline{x}$ and $\overline{y}$ are the co-ordinates of the centroid, that is,

$$\overline{x} = (x_i + x_k + x_m)/3 \; ; \quad \overline{y} = (y_i + y_k + y_m)/3 \qquad 3.25$$

and

$$\Delta = \int\int dxdy = \text{area of the triangle}$$

Adopting the local co-ordinate system, implies

$$\overline{x} = \overline{y} = 0$$

Therefore, $$F_i = - \omega\Delta C_{1i} \qquad 3.26$$

Eq. 3.20 is written for one of the six nodes forming an element. For this element, a matrix of a single column of the six differentials $\frac{\partial \chi^e}{\partial \psi_i}$, $\frac{\partial \chi^e}{\partial \psi_j}$, $\frac{\partial \chi^e}{\partial \psi_k}$, $\frac{\partial \chi^e}{\partial \psi_l}$, $\frac{\partial \chi^e}{\partial \psi_m}$, and $\frac{\partial \chi^e}{\partial \psi_n}$ gives the final equation as

$$\left\{\frac{\partial \chi}{\partial \psi}\right\}^e = \left\{\begin{array}{c} \frac{\partial \chi^e}{\partial \psi_i} \\ \frac{\partial \chi^e}{\partial \psi_j} \\ \frac{\partial \chi^e}{\partial \psi_k} \\ \frac{\partial \chi^e}{\partial \psi_l} \\ \frac{\partial \chi^e}{\partial \psi_m} \\ \frac{\partial \chi^e}{\partial \psi_n} \end{array}\right\} \tag{3.27}$$

Eq. 3.27 can be written in a condensed matrix form as

$$\left\{\frac{\partial \chi}{\partial \psi}\right\}^e = [h] \ \{\psi\}^e + \{F\}^e \tag{3.28}$$

where $[h]$ is the stiffness matrix given by

$$[h] = \begin{bmatrix} N_iN_i & N_iN_j & N_iN_k & N_iN_l & N_iN_m & N_iN_n \\ N_jN_i & N_jN_j & N_jN_k & N_jN_l & N_jN_m & N_jN_n \\ N_kN_i & N_kN_j & N_kN_k & N_kN_l & N_kN_m & N_kN_n \\ N_lN_i & N_lN_j & N_lN_k & N_lN_l & N_lN_m & N_lN_n \\ N_mN_i & N_mN_j & N_mN_k & N_mN_l & N_mN_m & N_mN_n \\ N_nN_i & N_nN_j & N_nN_k & N_nN_l & N_nN_m & N_nN_n \end{bmatrix}$$

$$+ \begin{bmatrix} M_iM_i & M_iM_j & M_iM_k & M_iM_l & M_iM_m & M_iM_n \\ M_jM_i & M_jM_j & M_jM_k & M_jM_l & M_jM_m & M_jM_n \\ M_kM_i & M_kM_j & M_kM_k & M_kM_l & M_kM_m & M_kM_n \\ M_lM_i & M_lM_j & M_lM_k & M_lM_l & M_lM_m & M_lM_n \\ M_mM_i & M_mM_j & M_mM_k & M_mM_l & M_mM_m & M_mM_n \\ M_nM_i & M_nM_j & M_nM_k & M_nM_l & M_nM_m & M_nM_n \end{bmatrix} \qquad 3.29$$

and

$$\{F\}^e = -\omega\Delta \begin{Bmatrix} C_{1i} \\ C_{1j} \\ C_{1k} \\ C_{1l} \\ C_{1m} \\ C_{1n} \end{Bmatrix} \qquad 3.30$$

Eq. 3.28 is derived for one element, to obtain the equation of the minimization of the whole region, one has to assemble all the differentials of χ and equate each to zero, that is,

$$\frac{\partial \chi}{\partial \psi_i} = \Sigma \frac{\partial \chi^e}{\partial \psi_i} = 0 \qquad 3.31$$

the summation being taken over all the elements. Using Eq. 3.28 in Eq. 3.31 yields

$$\frac{\partial \chi}{\partial \psi_i} = \Sigma\, \Sigma\, h_{in} \psi_n + \Sigma F_i = 0 \qquad 3.32$$

the summation being taken over all the elements and nodes.

3.2.2. Helmholtz Equation

Eq. 3.2 is the two dimensional form of Helmholtz Equation for an incompressible fluid, in which

$$\left(\frac{\partial}{\partial x} (U\omega) + \frac{\partial}{\partial y} (V\omega) \right) \text{ is the convective term}$$

and

$$\left(\frac{\partial \omega}{\partial t} - \nabla (\nu + \varepsilon) \nabla \omega \right) \text{ is the diffusion term}$$

The convective term in Helmholtz Equation is assumed to be constant over the element during one time step, that is an average value

$$\overline{\left(\frac{\partial}{\partial x}(U\omega) + \frac{\partial}{\partial y}(V\omega)\right)}^{e} = \text{constant} = \overline{C}^{e}$$

$$t = t \text{ to } (t + \Delta t)$$

or

$$\overline{\left(U\frac{\partial \omega}{\partial x} + \omega\frac{\partial U}{\partial x} + V\frac{\partial \omega}{\partial y} + \omega\frac{\partial V}{\partial y}\right)}^{e} = \overline{C}^{e}$$

or

$$\overline{\left(U\frac{\partial \omega}{\partial x} + V\frac{\partial \omega}{\partial y} + \omega\left(\frac{\partial U}{\partial x} + \frac{\partial V}{\partial y}\right)\right)}^{e} = \overline{C}^{e}$$

but the continuity equation states

$$\frac{\partial U}{\partial x} + \frac{\partial V}{\partial y} = 0$$

therefore, the convective term can be written as

$$\overline{\left(U\frac{\partial \omega}{\partial x} + V\frac{\partial \omega}{\partial y}\right)}^{e} = \overline{C}^{e} \qquad 3.33$$

Furthermore, within an element, the expression $(\nu + \varepsilon)$ in the diffusion term is assumed to be represented by an average value, that is

$$\nabla(\nu + \varepsilon)\nabla(-) \equiv \overline{(\nu + \varepsilon)}^{e}\nabla^2(-) \qquad 3.34$$

then, Helmholtz Equation can be rewritten as

$$\left(\frac{\partial^2\omega}{\partial x^2} + \frac{\partial^2\omega}{\partial y^2}\right) - \frac{1}{(\nu + \varepsilon)_e}\left(\overline{C}^e + \frac{\partial\omega}{\partial t}\right) = 0 \qquad 3.35$$

Using the above averaging process tends to damp temporal instabilities caused by vortex shedding in the solution as pointed out by Zaghloul.[119]

In a similar manner to that used for the Poisson Equation, the equivalent variational formulation to Eq. 3.35, is the requirement that the integral given in Eq. 3.36 below and taken over the whole region, should be minimized, or

$$\chi = \iint_{\text{all elements}} \left[\tfrac{1}{2}\left\{\left(\frac{\partial\omega}{\partial x}\right)^2 + \left(\frac{\partial\omega}{\partial y}\right)^2\right\} + \frac{1}{(\nu + \varepsilon)_e}\left(\overline{C}^e + \frac{\partial\omega}{\partial t}\right)\omega\right] dxdy \qquad 3.36$$

in which, however, $\frac{\partial\omega}{\partial t}$ may be treated as implied by Zienkiewicz[120], as an invariant. The differentiation of Eq. 3.36 with respect to the unknown ω_i gives

$$\frac{\partial\chi^e}{\partial\omega_i} = \iint \left[\left(\frac{\partial\omega}{\partial x}\right)\frac{\partial}{\partial\omega_i}\left(\frac{\partial\omega}{\partial x}\right) + \left(\frac{\partial\omega}{\partial y}\right)\frac{\partial}{\omega_i}\left(\frac{\partial\omega}{\partial y}\right) + \frac{1}{(\nu + \varepsilon)_e}\left(\overline{C}^e + \frac{\partial\omega}{\partial t}\right)\frac{\partial\omega}{\partial\omega_i}\right] dxdy \qquad 3.37$$

The same pattern of the triangular elements employed in section 3.2.1 was used to derive the matrix formulation of Eq. 3.37. The vorticity within each element was defined only on the three vertices of the triangle i, k and m, numbered in an anticlockwise direction, then ω can be expressed as

$$\{\omega\}^e = \begin{Bmatrix} \omega_i \\ \omega_k \\ \omega_m \end{Bmatrix} \qquad 3.38$$

Adopting the three node element to define the vorticity ω is sufficient. This is true since the first derivatives of the vorticity with respect to the co-ordinates x and y only, are required in the variational formulation of the Helmholtz Equation.

Assuming that the ω values can be represented by the local X and Y co-ordinates in the form

$$\omega = \alpha + \beta x + \gamma y \qquad 3.39$$

which is the compatible form of the first degree.

Then for each node, one can write

$$\omega_i = \alpha + \beta x_i + \gamma y_i \qquad 3.40a$$

$$\omega_k = \alpha + \beta x_k + \gamma y_k \qquad 3.40b$$

$$\omega_m = \alpha + \beta x_m + \gamma y_m \qquad 3.40c$$

or in a matrix form

$$\{\omega\}^e = \begin{bmatrix} 1 & x_i & y_i \\ 1 & x_k & y_k \\ 1 & x_m & y_m \end{bmatrix} \begin{Bmatrix} \alpha \\ \beta \\ \gamma \end{Bmatrix} = [CM] \begin{Bmatrix} \alpha \\ \beta \\ \gamma \end{Bmatrix} \qquad 3.41$$

Solving for α, β and γ in terms of the nodal values ω_i, ω_k and ω_m by the method of determinants assuming

$$2\Delta = \det \begin{vmatrix} 1 & x_i & y_i \\ 1 & x_k & y_k \\ 1 & x_m & y_m \end{vmatrix} = 2 \text{ (area of triangle i, k, m)}$$

$$\Delta_1 = \det \begin{vmatrix} \omega_i & x_i & y_i \\ \omega_k & x_k & y_k \\ \omega_m & x_m & y_m \end{vmatrix}$$

$$\Delta_2 = \det \begin{vmatrix} 1 & \omega_i & y_i \\ 1 & \omega_k & y_k \\ 1 & \omega_m & y_m \end{vmatrix}$$

$$\Delta_3 = \det \begin{vmatrix} 1 & x_i & \omega_i \\ 1 & x_k & \omega_k \\ 1 & x_m & \omega_m \end{vmatrix}$$

Then

$$\alpha = \frac{\Delta_1}{2\Delta} \qquad 3.42a$$

$$\beta = \frac{\Delta_2}{2\Delta} \qquad 3.42b$$

$$\gamma = \frac{\Delta_3}{2\Delta} \qquad 3.42c$$

Substituting the values of Eqs. 3.42a, 3.42b, and 3.42c in Eq. 3.39, and arranging, yields

$$\omega = \frac{1}{2\Delta}\Big[(a_i + b_i x + c_i y)\,\omega_i + (a_k + b_k x + c_k y)\,\omega_k + (a_m + b_m x + c_m y)\,\omega_m\Big] \qquad 3.43$$

in which,

$$a_i = x_k y_m - x_m y_k \qquad 3.44a$$

$$b_i = y_k - y_m \qquad 3.44b$$

$$c_i = x_m - x_k \qquad 3.44c$$

Then, ω can be expressed in a matrix form as

$$\omega = [L_i,\ L_k,\ L_m] \begin{Bmatrix} \omega_i \\ \omega_k \\ \omega_m \end{Bmatrix} = [L]\ \{\omega\}^e \qquad 3.45$$

where

$$L_i = \frac{a_i + b_i x + c_i y}{2\Delta}$$

Differentiate ω with respect to x and y respectively, one obtains

$$\frac{\partial\omega}{\partial x} = \frac{1}{2\Delta}\left[b_i,\ b_k,\ b_m\right]\ \{\omega\}^e \qquad 3.46a$$

$$\frac{\partial\omega}{\partial y} = \frac{1}{2\Delta}\left[c_i,\ c_k,\ c_m\right]\ \{\omega\}^e \qquad 3.46b$$

Also,

$$\frac{\partial}{\partial\omega_i}\left(\frac{\partial\omega}{\partial x}\right) = \frac{1}{2\Delta}\cdot b_i \qquad 3.47a$$

and

$$\frac{\partial}{\partial\omega_i}\left(\frac{\partial\omega}{\partial y}\right) = \frac{1}{2\Delta}\cdot c_i \qquad 3.47b$$

Substitute Eqs. 3.46a, 3.46b, 3.47a and 3.47b in Eq. 3.37 one obtains

$$\frac{\partial\chi^e}{\partial\omega_i} = \frac{1}{(2\Delta)^2}\int\int\left(\left[b_i,\ b_k,\ b_m\right]\ \{\omega\}^e\, b_i + \left[c_i,\ c_k,\ c_m\right]\ \{\omega\}^e c_i\right)dxdy$$

$$+ \int\int\left\{\frac{\overline{C}^e}{\overline{(\nu+\varepsilon)}^e}\,\frac{\partial\omega}{\partial\omega_i}\right\}dxdy + \int\int\left\{\frac{1}{\overline{(\nu+\varepsilon)}^e}\cdot\frac{\partial\omega}{\partial t}\cdot\frac{\partial\omega}{\partial\omega_i}\right\}dxdy \qquad 3.48$$

or

$$\frac{\partial\chi^e}{\partial\omega_i} = h_i\ \{\omega\}^e + Q_i + R_i$$

The final equation for one element can be written in a matrix form as

$$\left\{\frac{\partial\chi}{\partial\omega}\right\}^e = [h]\ \{\omega\}^e + \{Q\}^e + \{R\}^e \qquad 3.49$$

where $[h]$ is the stiffness matrix written as

$$[h] = \frac{1}{4\Delta}\begin{bmatrix} b_ib_i & b_ib_k & b_ib_m \\ b_kb_i & b_kb_k & b_kb_m \\ b_mb_i & b_mb_k & b_mb_m \end{bmatrix} + \frac{1}{4\Delta}\begin{bmatrix} c_ic_i & c_ic_k & c_ic_m \\ c_kc_i & c_kc_k & c_kc_m \\ c_mc_i & c_mc_k & c_mc_m \end{bmatrix} \qquad 3.50$$

Following the assumption that both $\overline{C}^e$ and $\overline{(\nu + \varepsilon)}^e$ are constants within an element, then, the second term on the right hand side of Eq. 3.49, that is, $\{Q\}^e$ can be written as

$$Q_i = \frac{\overline{C}^e}{\overline{(\nu + \varepsilon)}^e} \iint \left(\frac{\partial\omega}{\partial\omega_i}\right) dxdy = \frac{\overline{C}^e}{\overline{(\nu + \varepsilon)}^e} \iint L_i \, dxdy$$

$$= \frac{\overline{C}^e}{\overline{(\nu + \varepsilon)}^e} \frac{1}{2\Delta} \iint (a_i + b_ix + c_iy)\, dxdy$$

$$= \frac{\overline{C}^e}{\overline{(\nu + \varepsilon)}^e} (a_i + b_i\overline{x} + c_i\overline{y}) \;/2$$

Since the local co-ordinates of the centroid of the element are zero, that is, $\overline{x} = \overline{y} = 0$.

Therefore,

$$Q_i = \frac{1}{\overline{(\nu + \varepsilon)}^e} \cdot \frac{\overline{C}^e \cdot a_i}{2}$$

Thus, finally the simple result obtained is,

$$\{Q\}^e = \frac{\overline{C}^e}{2\overline{(\nu + \varepsilon)}^e} \begin{Bmatrix} a_i \\ a_k \\ a_m \end{Bmatrix} \qquad 3.51$$

To calculate $\overline{C}^e$, recall Eq. 3.33 as

$$\overline{C}^e = \overline{(U \frac{\partial \omega}{\partial x} + V \frac{\partial \omega}{\partial y})}^e$$

The first derivatives of the vorticity ω with respect to the co-ordinates x and y can be deduced from Eq. 3.39 as

$$\frac{\partial \omega}{\partial x} = \beta$$

and

$$\frac{\partial \omega}{\partial y} = \gamma$$

Then Eq. 3.33 can be written as

$$\overline{C}^e = \overline{(U\beta + V\gamma)}^e \qquad 3.52$$

The right hand side of Eq. 3.52 is evaluated for every element using

$$U = \frac{\partial\psi}{\partial y} = \alpha_3 + \alpha_5\bar{x} + 2\alpha_6\bar{y} = \alpha_3 \qquad 3.53a$$

and

$$V = -\frac{\partial\psi}{\partial x} = -\alpha_2 - 2\alpha_4\bar{x} - \alpha_5\bar{y} = -\alpha_2 \qquad 3.53b$$

Note that $\bar{x}$ and $\bar{y}$ are the local co-ordinates of the centroid of the element, that is, $\bar{x} = \bar{y} = 0$. The values of β and γ can directly be calculated from the relation

$$\begin{Bmatrix} \alpha \\ \beta \\ \gamma \end{Bmatrix} = \begin{bmatrix} 1 & x_i & y_i \\ 1 & x_k & y_k \\ 1 & x_m & y_m \end{bmatrix}^{-1} \begin{Bmatrix} \omega_i \\ \omega_k \\ \omega_m \end{Bmatrix} = [CM]^{-1} \{\omega\}^e \qquad 3.54$$

To evaluate the third term on the right hand side of Eq. 3.49, that is, $\{R\}^e$, recall Eq. 3.45 as

$$\omega = [L] \{\omega\}^e$$

Therefore,

$$\frac{\partial\omega}{\partial t} = [L] \left\{\frac{\partial\omega}{\partial t}\right\}^e \qquad 3.55$$

but,

$$R_i = \frac{1}{(\nu + \varepsilon)^e} \iint \left(\frac{\partial\omega}{\partial t} \cdot \frac{\partial\omega}{\partial\omega_i}\right) dxdy \qquad 3.56$$

or

$$R_i = \frac{1}{(\nu + \varepsilon)^e} \iint [L] \left\{\frac{\partial\omega}{\partial t}\right\}^e \cdot L_i \cdot dxdy \qquad 3.57$$

The final form for all nodes reads

$$\{R\}^e = \frac{1}{(\nu + \varepsilon)}^e \int\int [L] \left\{\frac{\partial\omega}{\partial t}\right\}^e [L]^T \cdot dxdy \qquad 3.58$$

Noting that the first product is a scalar, one obtains

$$\{R\}^e = \frac{1}{(\nu + \varepsilon)}^e \left(\int\int [L]^T [L] \; dxdy\right) \left\{\frac{\partial\omega}{\partial t}\right\}^e \qquad 3.59$$

or

$$\{R\}^e = [p] \left\{\frac{\partial\omega}{\partial t}\right\}^e \qquad 3.60$$

with

$$[p] = \frac{1}{(\nu + \varepsilon)}^e \int\int [L]^T [L] \cdot dxdy \qquad 3.61$$

or

$$[p] = \frac{\Delta}{(\nu + \varepsilon)}^e \begin{bmatrix} L_i L_i & L_i L_k & L_i L_m \\ L_k L_i & L_k L_k & L_k L_m \\ L_m L_i & L_m L_k & L_m L_m \end{bmatrix} \qquad 3.62$$

Evaluation of the term $\overline{(\nu + \varepsilon)}^e$ will be dealt with in detail in Chapter 8 "Results of the Computer Simulation".

The final form of Eq. 3.49 is now

$$\frac{\partial\chi}{\partial\omega_i} = \Sigma\,\Sigma \; h_{im}\omega_m + \Sigma\,\Sigma \; p_{im} \frac{\partial\omega_m}{\partial t} + \Sigma \; Q_i = 0 \qquad 3.63$$

or

$$[H]\{\omega\} + [P]\left\{\frac{\partial \omega}{\partial t}\right\} + \{Q\} = 0 \qquad 3.64$$

in which $[H]$ is the stiffness matrix of the whole assembly, and $[P]$ is a matrix assembled by precisely the same rules as the stiffness matrix from the components of $[p]$.

Solution of Eq. 3.64 has been achieved by assuming that in the interval of time Δt the value of $\left\{\frac{\partial \omega}{\partial t}\right\}$ vary linearly with time. Thus, on integrating

$$\{\omega\}_t = \{\omega\}_{t-\Delta t} + \left(\left\{\frac{\partial \omega}{\partial t}\right\}_{t-\Delta t} + \left\{\frac{\partial \omega}{\partial t}\right\}_t \right) \cdot \frac{\Delta t}{2} \qquad 3.65$$

or

$$\left\{\frac{\partial \omega}{\partial t}\right\}_t = - \left\{\frac{\partial \omega}{\partial t}\right\}_{t-\Delta t} + (\{\omega\}_t - \{\omega\}_{t-\Delta t}) \cdot \frac{2}{\Delta t} \qquad 3.66$$

Substituting in Eq. 3.64 at time t gives the following recursion formula

$$([H] + \frac{2}{\Delta t} [P]) \{\omega\}_t = [P] \left(\frac{2}{\Delta t} \{\omega\}_{t-\Delta t} + \left\{\frac{\partial \omega}{\partial t}\right\}_{t-\Delta t} \right) - \{Q\}_t \qquad 3.67$$

or

$$[S] \{\omega\}_t = [V]_{t-\Delta t} - \{Q\}_t \qquad 3.68$$

Thus $\{\omega\}_t$ can be evaluated by solving the system of simultaneous equations provided the values of $\{\omega\}$ and $\left\{\frac{\partial \omega}{\partial t}\right\}$ are known at time $t-\Delta t$.

At the first step, only the values of $\{\omega\}_{t=0}$ are known. However, from Eq. 3.64, the values of $\left\{\frac{\partial\omega}{\partial t}\right\}_{t=0}$ can be determined. Thus the solution of

$$-[P]\ \left\{\frac{\partial\omega}{\partial t}\right\}_{t=0} = \left([H]\ \{\omega\}_{t=0} + \{Q\}\right) \qquad 3.69$$

will result in the initial values. With the initial values of $\{\omega\}_{t=0}$ and $\left\{\frac{\partial\omega}{\partial t}\right\}_{t=0}$ are now known, solutions of Eqs. 3.67 and 3.66 will result in the subsequent values of $\{\omega\}_t$ and $\left\{\frac{\partial\omega}{\partial t}\right\}_t$ respectively.

The equations to be used in the solution and the order in which they are solved are summarized in Chapter 8.

CHAPTER FOUR

PRINCIPLES OF THE HOT-FILM ANEMOMETRY AND THE FLOW VISUALIZATION TECHNIQUES

The basic principles of the hot-film anemometry and the flow visualization techniques that were used to measure the flow characteristics are outlined in this chapter.

4.1 Hot-Film Anemometry

4.1.1 Introduction

The detecting element of a hot anemometer is either wire or film, which is heated by an electric current. The sensor is cooled by the flowing fluid, causing the temperature to drop and, consequently, the electric resistance of the sensor to diminish.

The total amount of heat transferred depends on:

a) the flow velocity,

b) the difference in temperature between the sensor and the fluid,

c) the physical properties of the fluid, and

d) the dimensions and physical properties of the sensor.

Generally (b) and (d) are known. If (c) is known or kept constant, the flow velocity can be measured; or if (a) is known or constant, a variation in the fluid physical properties can be detected.

The sensor is cooled by heat conduction, free and forced convention and radiation. However radiation and free convection effects are negligibly small under usual operating conditions.

For carrying out measurements of turbulent velocity fluctuations, one of two different methods could be applied, the constant current or the constant temperature technique.

In the first method the electric current "I" is kept constant while the temperature and hence the electric resistance change with the fluctuating velocity. In the second method, the temperature and so the electric resistance are kept constant while the electric current fluctuates with the velocity.

In the constant current anemometer, the finite thermal capacitance of the sensor affects the sensitivity and the phase relations so that turbulence can only be measured up to a frequency around 1000 HZ. The constant temperature anemometer, however, employs a feedback technique that minimizes the effect of thermal lag, thereby increasing the upper frequency limit by a factor of several hundred up to 400 KHZ.

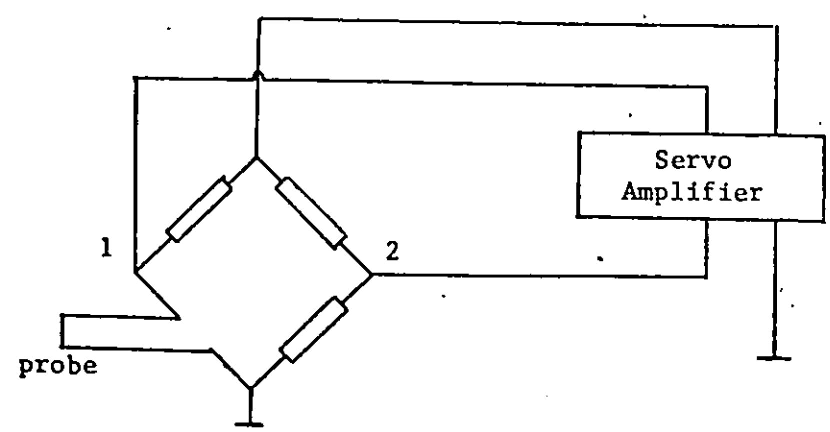

Fig. 3 Constant Temperature Anemometer Circuit

Throughout the hot anemometry measurements in this research the constant temperature technique was adopted. This system consists of a Wheatstone bridge of which the probe, consisting of the probe body, probe prongs and probe sensor, forms a part and a servo amplifier as shown in Fig. 3.

Electric current from the servo amplifier flows through the bridge, thus heating the sensor. The output current of the amplifier is controlled by the bridge unbalance, that is, the error signal between points (1) and (2) in Fig. 3. The amplifier is polarized so that a change in probe resistance due to cooling will result in an increase in amplifier output current.

4.1.2 Basic Equations

4.1.2.1 General

The heat transfer from the sensor to a flowing incompressible fluid may be described in terms of the dimensionless groups of Nusselt (N_u), Prandtl (P_r) and Reynolds (R_e) as suggested by Kramers[52] in the form

$$N_u = 0.42\, P_r^{0.2} + 0.57\, P_r^{0.33} \cdot R_e^{0.5} \qquad 4.1$$

where

$$N_u = \frac{ad}{K}$$

$$P_r = \frac{c_p \cdot \mu}{K}$$

$$R_e = \frac{\rho U d}{\mu}$$

in which

- a – heat transfer coefficient
- K – heat conductivity of fluid
- μ – absolute viscosity of fluid
- c_p – specific heat of fluid at constant pressure
- ρ – density of fluid
- g – gravitational acceleration
- U – velocity of fluid
- d – equivalent diameter of the sensor

The values of the fluid properties appearing in the dimensionless groups refer to the average temperature T_{av}.

$$T_{av} = \frac{T_s + T_f}{2}$$

where

- T_s – sensor temperature, and
- T_f – fluid temperature.

Eq. 4.1 has proved to be valid in the range

$$.01 < R_e < 10000$$

which is sufficiently wide for all practical applications of hot-film anemometry.

The heat per unit time transferred to the fluid from a sensor with equivalent length ℓ is

$$a\pi d\ell \quad (T_s - T_f)$$

or, with the value of "a" according to Eq. 4.1

$$\pi K\ell \quad (T_s - T_f) \left[0.42 \quad (P_r)^{0.2} + \quad 0.57 \quad (P_r)^{0.33} \quad (R_e)^{0.5}\right]$$

For thermal-equilibrium conditions, this heat loss per unit time must be equal to the heat generated per unit time by the electric current through the sensor, that is, it must be equal to I^2R_s where

I - the electric heating current, and

R_s - the total electric resistance of the sensor.

Thus for the thermal equilibrium one obtains

$$I^2R_s = \kappa \quad \pi K\ell \quad (T_s - T_f) \quad \left[0.42 \, P_r^{0.2} + 0.57 \, P_r^{0.33} \, R_e^{0.5}\right] \qquad 4.2$$

where κ is a conversion factor equal to 4.2, if the left hand side is obtained in joules per second, and the right hand side is obtained in calories per second.

The temperature dependence of the electric resistance of the sensor gives an effect of first order; it is on this effect that the use of a hot wire or film as an anemometer is based. This temperature dependence may be expressed as follows

$$R_s = R_o \left[1 + \sigma \, (T_s - T_o) + \sigma_1 \, (T_s - T_o)^2 + \ldots\right] \qquad 4.3$$

where

R_o - resistance at a reference temperature T_o

σ, σ_1 - temperature coefficients of the electric resistivity of the sensor.

Usually, under the normal operating conditions, the quadratic term may be disregarded, since σ_1 is much smaller than σ.

Disregarding the quadratic term in Eq. 4.3, the temperature difference $(T_s - T_f)$ in Eq. 4.1 can easily be expressed in terms of $(R_s - R_f)$, where R_f denotes the electric resistance of the sensor at the fluid temperature T_f, one obtains

$$T_s - T_f = \frac{R_s - R_f}{\sigma R_o} \qquad 4.4$$

The relation 4.1 can then be written

$$I^2 R_s = \frac{\kappa \ \pi K \ell}{\sigma} \cdot \frac{R_s - R_f}{R_o} \left[0.42 \ P_r^{0.2} + 0.57 \ P_r^{0.33} \ R_e^{0.5}\right] \qquad 4.5$$

Eq. 4.5 can be written in the form

$$\frac{I^2 R_s^2}{R_s (R_s - R_f)} = A + BU^n \qquad 4.6$$

where

$$A = 0.42 \frac{\kappa \ \pi K \ell}{\sigma R_o} (P_r)^{0.2} \qquad 4.7$$

$$B = 0.57 \frac{\kappa \ \pi K \ell}{\sigma R_o} (P_r)^{0.33} \left(\frac{\rho d}{\mu}\right)^{0.5} \qquad 4.8$$

and $n = 0.5$

Eq. 4.6 is the basic equation in hot-sensor anemometry.

For the constant temperature (constant resistance) technique in turbulence measurements, Eq. 4.6 can be written as

$$E^2 = R_f^2 \cdot a\,(a - 1)\quad(A + BU^n)$$

or

$$E^2 = A' + B'U^n \qquad 4.9$$

in which a = the overheating ratio = R_s/R_f and E = the mean voltage. In water, the overheating ratio (a) is usually set between 1.03 and 1.10. Values of (a) higher than 1.10 are not used in water because the temperature of the probe would cause boiling.

In practice, the factors A' and B are not calculated according to the relations 4.7 and 4.8, but, are determined experimentally by performing a calibration test to obtain a relation in the fotm E = f(U). To convert the voltage fluctuations sensed by the hot-film anemometer to velocity fluctuations, the following assumptions are made:

1) In a two dimensional flow, the velocity vector $\vec{U}$ can be expressed by a mean value U and fluctuation components u and v.
2) The sensor held perpendicular to the flow is sensitive only to the mean and fluctuating component of the velocity perpendicular to the hot-film; that is, the film is sensitive to the first order of u and is only affected by the second order of v.
3) The relation between mean voltage and mean velocity can be used to convert voltage fluctuations to velocity fluctuations.

4) The change in the slope dE/dU of the calibration curve is small over the range of the velocity fluctuations encountered during a measurement; thus, the tangent to the voltage/velocity curve at the mean velocity can be used to convert voltage fluctuations to velocity fluctuations.

5) The fluid properties, overheating ratio, film dimensions and angle of attack are constant; that is, the heat transfer is a function of only the velocity of flow.

The above assumptions are used to derive the formulae to calculate the turbulence characteristics as described in the following subsections.

4.1.2.2 Turbulence Intensity

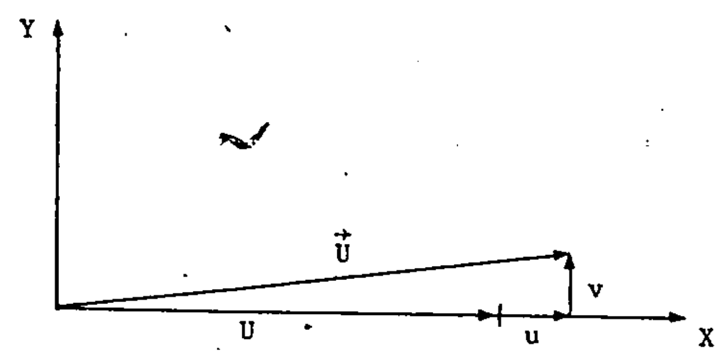

Fig. 4 Definition Sketch of Velocity Vector

The velocity vector for a hot-film (Wedge-probe) placed perpendicular to the mean flow as shown in Fig. 4 reads

$$\vec{U}^2 = (U + u)^2 + v^2 \qquad 4.10$$

The derivative of the velocity vector becomes

$$d\vec{U} = \frac{1}{\sqrt{(U + u)^2 + v^2}} \left[(U + u)\ du + vdv\right] \qquad 4.11$$

Similarly, the derivative of the voltage output from the anemometer reads

$$dE = \frac{\partial E}{\partial U}\ dU \qquad 4.12$$

It is also assumed that $|U| >> |u|$ or $|v|$. Therefore Eqs. 4.11 and 4.12 reduce to

$$dU = du \qquad 4.11a$$

$$\text{and} \quad dE = \frac{dE}{dU}\ du \qquad 4.12a$$

According to Sandborn [87] and Hinze [39], the general assumption is that dE = e, and du = u (i.e. the derivatives are equal to the fluctuations).

Using this assumption, Eq. 4.12a becomes

$$e = \frac{dE}{dU}\ u \qquad 4.13$$

The root-mean-square of the voltage fluctuation is normally the measured output of the hot-film anemometer. Therefore Eq. 4.13 can be written as

$$e' = \frac{dE}{dU}\ u' \qquad 4.14$$

in which

u' = rms of the velocity fluctuations, or, the turbulence intensity.

e' = rms of the voltage fluctuation and is usually measured by RMS voltmeter inserted in the anemometer circuit. Such a voltmeter is designed to measure the root-mean-square value of AC voltage from the definition

$$e' = \sqrt{\overline{e^2}} = \sqrt{\frac{1}{T}\int_0^T e^2 dt} \qquad 4.15$$

and

$\frac{dE}{dU}$ = the slope of the calibration curve and is known as the sensitivity of the probe "S".

Therefore Eq. 4.14 can be written as

$$u' = \sqrt{\overline{u^2}} = \frac{e'}{S} \qquad 4.16$$

4.1.2.3 Reynolds Stresses

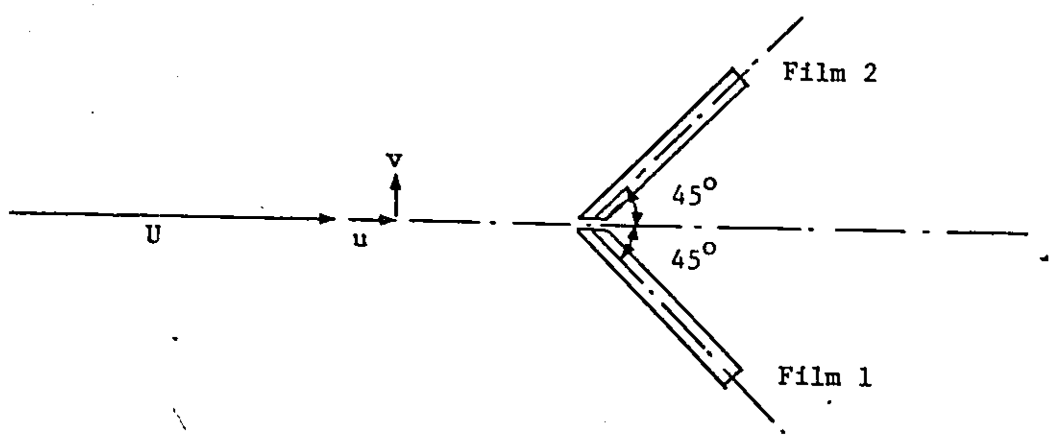

Fig. 5 Sketch of the Velocity Components in Relation With the V-Probe

Consider a V-probe consisting of two mutually perpendicular films that is placed on an angle of 45° to the direction of the mean flow velocity as shown in Fig. 5. In practice each film is equally sensitive to the longitudinal component of flow velocity fluctuation "u" and the vertical component "v". Thus the output of the two films denoted by subscripts (1) and (2) are respectively

$$e_1 = S_1 (u + v)$$

$$e_2 = S_2 (u - v)$$

where S_1 and S_2 are sensitivity factors. The sum and difference signals are then

$$e_s = e_1 + e_2 = u (S_1 + S_2) + v (S_1 - S_2)$$

$$e_d = e_1 - e_2 = u (S_1 - S_2) + v (S_1 + S_2)$$

If the RMS of e_s and e_d, that is, $\sqrt{\overline{e_s^2}}$ and $\sqrt{\overline{e_d^2}}$, and also the correlation, $\overline{e_s e_d}$ can be measured, the turbulence intensities u' and v' and Reynolds stress $-\rho\overline{uv}$ can then be calculated by solving the following three simultaneous equations

$$\overline{u^2} \cdot (S_1 + S_2)^2 + 2\overline{uv} \ (S_1^2 - S_2^2) + \overline{v^2} (S_1 - S_2)^2 = \overline{e_s^2} \qquad 4.17$$

$$\overline{u^2} \cdot (S_1 - S_2)^2 + 2\overline{uv} \ (S_1^2 - S_2^2) + \overline{v^2} (S_1 + S_2)^2 = \overline{e_d^2} \qquad 4.18$$

$$\overline{u^2} \cdot (S_1^2 - S_2^2) + \overline{uv} \left[(S_1 + S_2)^2 + (S_1 - S_2)^2\right] + \overline{v^2} (S_1^2 - S_2^2) = \overline{e_s e_d}$$

4.19

where

$$u' = \sqrt{\overline{u^2}}$$

and

$$v' = \sqrt{\overline{v^2}}$$

In the practice of hot-film anemometry, a summing unit to compute e_s and e_d, and an analog correlator to measure $\overline{e_s e_d}$ are inserted in the V-probe circuit.

4.1.2.4 Eulerian Macro and Micro Scales of Turbulence

The correlation of the fluctuating velocity component in the direction of flow "u" at a fixed point in the flow field at two different instants t' and t'-t can be written as

$$\overline{u(t') \cdot u(t'-t)}$$

or its correlation coefficient as

$$\rho(t) = \frac{\overline{u(t') \cdot u(t'-t)}}{u'^2} \qquad 4.20$$

where the average is taken with respect to "t'". The Eulerian Macro scale of turbulence "Λ" is defined as

$$\Lambda = \int_0^\infty \rho(t)dt \qquad 4.21$$

The macro scale "Λ" may be considered to be a rough measure of the longest connection in the turbulent behaviour of u(t).

The equation for the osculating parabola in the vertex of the ρ curve reads

$$\rho(t) = 1 - \frac{t^2}{\lambda^2} \qquad 4.22$$

where $\rho(t)$ is the normalized autocorrelation function for a small value of time delay "t". λ is known as Eulerian Micro scale of turbulence, which is a measure of the most rapid changes that occur in the fluctuations of u(t). The micro scale can be also considered as a measure of the dissipation of kinetic energy of the flow field into heat by the effect of molecular viscosity.

4.2 Flow Visualization

4.2.1 Definitions

i) Polarized Light

In ordinary light, the light vector is not restricted in any sense and may be considered to comprise a number of arbitrary transverse vibrations. When the vibration pattern of the Electromagnetic wave exhibits a preference as to the transverse direction of vibration, the light is considered to be polarized. There are three kinds of polarized light:

1. plane polarized light,
2. circularly polarized light,
3. elliptically polarized light.

ii) Plane Polarizers

Plane polarizers are optical elements which absorb the components of the light vector not vibrating in the direction of the axis of the polarizer. When a light vector passes through a plane polarizer, this optical element absorbs that component of the light vector which is perpendicular to the axis of polarization and transmits the parallel component, as illustrated in Fig. 6.

The amplitude of the light vector is given by

$$A = a \sin \omega t \qquad 4.23$$

where $\omega = 2\pi f$, the circular frequency of light. The absorbed and transmitted components of the light vector are

$$A_a = a \sin \omega t \sin \delta$$

$$A_t = a \sin \omega t \cos \delta$$

where δ is the angle between the axis of polarization and the light vector.

iii) Wave Plates

Certain materials have the ability to resolve the light vector into two orthogonal components and, moreover to transmit each of these components at a different velocity. A material exhibiting this property is called doubly refracting. The doubly refracting plate illustrated in Fig. 7 has two principal axes labelled 1 and 2.

The transmission of light along axis 1 proceeds at velocity c_1 and along axis 2 at velocity c_2. If $c_1 > c_2$, axis 1 is called the fast axis and axis 2 the slow axis.

If this doubly refracting plate is placed in a field of plane-polarized light such that the light vector A_t makes an angle β with axis 1, then upon entering the plate, the light vector is first resolved into two components, which are given by

$$A_{t_1} = A_t \cos\beta = a\cos\delta\sin\omega t\cos\beta = K\sin\omega t\cos\beta$$

$$A_{t_2} = A_t \sin\beta = a\cos\delta\sin\omega t\sin\beta = K\sin\omega t\sin\beta$$

where $K = a\cos\delta$.

The light components A_{t_1} and A_{t_2} travel through the plate with different velocities c_1 and c_2 respectively. They will emerge from the plate with a relative phase shift as shown in Fig. 8.

The angular retardation for each component is given by

$$\Delta_1 = \frac{2\pi h}{\lambda}(n_1 - n)$$

$$\Delta_2 = \frac{2\pi h}{\lambda}(n_2 - n)$$

where

n - the index of refraction of air

n_1, n_2 - the indices of refraction in the direction of the fast and slow axes of the wave plate

λ - wave length of light

h - thickness of the wave plate

Therefore, the angular phase shift Δ will be given by

$$\Delta = \Delta_1 - \Delta_2 = \frac{2\pi h}{\lambda} (n_1 - n_2) \qquad 4.24$$

Upon emergence from a general wave plate exhibiting a retardation Δ, the two components of light are described by the equations

$$A'_{t_1} = K \cos\beta \sin(\omega t + \Delta)$$

$$4.25$$

$$A'_{t_2} = K \sin\beta \sin\omega t$$

When the doubly refracting plate is designed to give an angular retardation of $\frac{\pi}{2}$, it is called a quarter wave plate.

4.2.2 The Stress Optic Law in Two Dimensions

If a liquid, at rest, with the property of double refraction is viewed in polarized light, it exhibits an index of refraction, n_o, which is the same at all points and at all planes. However, with flowing fluid, a two-dimensional state of stress is induced. Optically, the liquid becomes doubly refracting and exhibits properties very similar to those of the wave plates. The principal axes of stress at any point in the medium becomes the fast and slow axes.

The theory which related the changes in the index of refraction to the state of stress is due to Maxwell, who reported this phenomenon in 1853. Maxwell noted that the changes in the indices of refraction are linearly proportional to the stresses induced in the model and follow the relationships

$$n_1 - n_o = c_1\sigma_1 + c_2\sigma_2 \qquad 4.26a$$

$$n_2 - n_o = c_1\sigma_2 + c_2\sigma_1 \qquad 4.26b$$

where

n_o - the index of refraction of the model in the unstressed state

σ_1, σ_2 - the principal normal stresses

n_1, n_2 - the indices of refraction along the two principal axes associated with σ_1 and σ_2 respectively

c_1, c_2 - the stress optic coefficients

Subtracting Eq. 4.26b from Eq. 4.26a, one obtains

$$n_1 - n_2 = (c_1 - c_2)\ (\sigma_1 - \sigma_2) = c\ (\sigma_1 - \sigma_2) \qquad 4.27$$

Combining Eqs. 4.24 and 4.27, yields

$$\Delta = \frac{2\pi h}{\lambda} c\ (\sigma_1 - \sigma_2)$$

$$\tau_{max} = \frac{\sigma_1 - \sigma_2}{2} = N \cdot f \qquad 4.28$$

where

τ_{max} - the maximum shear stress acting along the bed

N - $\frac{\Delta}{2\pi}$, relative retardation in terms of a complete cycle of retardation, 2π

f - $\frac{\lambda}{2hc}$ = sensitivity constant

The function of the polariscope is to yield the value of N at all points in the model.

4.2.3 Effect of a Stressed Model in a Circular Polariscope (Dark Field Arrangement)

If the light is followed as it passes through the different parts of the polariscope shown in Fig. 9, an expression for the transmitted horizontal component of the light vector A through the analyzer can be obtained.

First by employing Eq. 4.24, the light emerging from the first quarter wave plate can be expressed as

$$A_1' = \frac{\sqrt{2}}{2} K \sin\left(\omega t + \frac{\pi}{2}\right) = \frac{\sqrt{2}}{2} K \cos \omega t \text{ (along the fast axis)}$$

$$A_2' = \frac{\sqrt{2}}{2} K \sin \omega t \text{ (along the slow axis)} \qquad 4.29$$

The components of light A_1' and A_2' propagate from the first quarter-wave plate and enter the model as illustrated in Fig. 10. These components are resolved when they impinge upon the model into two new components A_1'' and A_2'' along the σ_1 and σ_2 axes, and expressed as

$$A_1'' = A_1' \cos\left(\frac{\pi}{4} - \alpha\right) + A_2' \sin\left(\frac{\pi}{4} - \alpha\right)$$

$$A_2'' = A_2' \cos\left(\frac{\pi}{4} - \alpha\right) - A_1' \sin\left(\frac{\pi}{4} - \alpha\right) \qquad 4.30$$

Combining Eqs. 4.29 and 4.30 gives

$$A_1'' = \frac{\sqrt{2}}{2} K \left[\cos \omega t \cos \left(\frac{\pi}{4} - \alpha\right) + \sin \omega t \sin \left(\frac{\pi}{4} - \alpha\right)\right]$$

$$A_2'' = \frac{\sqrt{2}}{2} K \left[\sin \omega t \cos \left(\frac{\pi}{4} - \alpha\right) - \cos \omega t \sin \left(\frac{\pi}{4} - \alpha\right)\right] \qquad 4.31$$

The two components A_1'' and A_2'' propagate through the model with different velocities and emerge out of phase by a relative amount Δ. If this relative phase difference Δ is divided between the two components, with $+\Delta/2$ applied to A_1'' and $-\Delta/2$ applied to A_2'', then the amplitudes of these components upon emergence from the model become

$$A_1''' = \frac{\sqrt{2}}{2} K \left[\cos \left(\omega t + \frac{\Delta}{2}\right) \cos \left(\frac{\pi}{4} - \alpha\right) + \sin \left(\omega t + \frac{\Delta}{2}\right) \sin \left(\frac{\pi}{4} - \alpha\right)\right]$$

$$A_2''' = \frac{\sqrt{2}}{2} K \left[\sin \left(\omega t - \frac{\Delta}{2}\right) \cos \left(\frac{\pi}{4} - \alpha\right) - \cos \left(\omega t - \frac{\Delta}{2}\right) \sin \left(\frac{\pi}{4} - \alpha\right)\right] \qquad 4.32$$

The light emerging from the model, propagates to the second quarter wave plate and enters it according to the diagram shown in Fig. 11. The components A_1''' and A_2''' are resolved onto the fast and slow axes of the second quarter wave plate and are then denoted as A_1^{iv} and A_2^{iv} where

$$A_1^{iv} = A_2''' \cos \left(\frac{\pi}{4} - \alpha\right) + A_1''' \sin \left(\frac{\pi}{4} - \alpha\right)$$

$$A_2^{iv} = A_1''' \cos \left(\frac{\pi}{4} - \alpha\right) - A_2''' \sin \left(\frac{\pi}{4} - \alpha\right) \qquad 4.33$$

By substituting Eqs. 4.32 into Eqs. 4.33, one obtains

$$
\begin{aligned}
A_1^{iv} = \frac{\sqrt{2}}{2} K \Big[& \sin\left(\omega t - \frac{\Delta}{2}\right) \cos^2\left(\frac{\pi}{4} - \alpha\right) \\
& - \cos\left(\omega t - \frac{\Delta}{2}\right) \cos\left(\frac{\pi}{4} - \alpha\right) \sin\left(\frac{\pi}{4} - \alpha\right) \\
& + \cos\left(\omega t + \frac{\Delta}{2}\right) \cos\left(\frac{\pi}{4} - \alpha\right) \sin\left(\frac{\pi}{4} - \alpha\right) \\
& + \sin\left(\omega t + \frac{\Delta}{2}\right) \sin^2\left(\frac{\pi}{4} - \alpha\right) \Big] \\
A_2^{iv} = \frac{\sqrt{2}}{2} K \Big[& \cos\left(\omega t + \frac{\Delta}{2}\right) \cos^2\left(\frac{\pi}{4} - \alpha\right) \\
& + \sin\left(\omega t + \frac{\Delta}{2}\right) \sin\left(\frac{\pi}{4} - \alpha\right) \cos\left(\frac{\pi}{4} - \alpha\right) \\
& - \sin\left(\omega t - \frac{\Delta}{2}\right) \cos\left(\frac{\pi}{4} - \alpha\right) \sin\left(\frac{\pi}{4} - \alpha\right) \\
& + \cos\left(\omega t - \frac{\Delta}{2}\right) \sin^2\left(\frac{\pi}{4} - \alpha\right) \Big]
\end{aligned}
\qquad 4.34
$$

If it is assumed that the $\frac{\pi}{2}$ relative phase shift which occurs as the light passes through this quarter wave plate is applied in a positive sense to the A_1^{iv} component, then the emerging light components A_1^{v} and A_2^{v} may be expressed as

$$
\begin{aligned}
A_1^{v} = \frac{\sqrt{2}}{2} K \Big[& \cos\left(\omega t - \frac{\Delta}{2}\right) \cos^2\left(\frac{\pi}{4} - \alpha\right) \\
& + \sin\left(\omega t - \frac{\Delta}{2}\right) \sin\left(\frac{\pi}{4} - \alpha\right) \cos\left(\frac{\pi}{4} - \alpha\right) \\
& - \sin\left(\omega t + \frac{\Delta}{2}\right) \sin\left(\frac{\pi}{4} - \alpha\right) \cos\left(\frac{\pi}{4} - \alpha\right) \\
& + \cos\left(\omega t + \frac{\Delta}{2}\right) \sin^2\left(\frac{\pi}{4} - \alpha\right) \Big] \\
A_2^{v} = {} & A_2^{iv}
\end{aligned}
\qquad 4.35
$$

Finally, the light enters the analyzer as shown in Fig. 12. The light components A_1^v and A_2^v are further resolved into vertical and horizontal components. The vertical components are absorbed in the analyzer and the horizontal components are transmitted to give the light vector A

$$A = \frac{\sqrt{2}}{2} (A_2^v - A_1^v) \qquad 4.36$$

Substituting Eq. 4.35 into Eq. 4.36 and expanding and simplifying gives

$$A = \frac{1}{2} K \sin \frac{\Delta}{2} \left[\cos (\alpha + \omega t) - \sin (\alpha - \omega t)\right] \qquad 4.37$$

The intensity I of the light is proportional to the square of the amplitude, hence

$$I = K' \sin^2 \frac{\Delta}{2} \left[\cos (\alpha + \omega t) - \sin (\alpha - \omega t)\right]^2 \qquad 4.38$$

The extinction (that is, I = 0) is possible only when either

$$\sin^2 \frac{\Delta}{2} = 0$$

or

$$\left[\cos (\alpha + \omega t) - \sin (\alpha - \omega t)\right]^2 = 0$$

Practically, the second term does not produce extinction which can be recorded, since the angular frequency ω of the light is beyond the range of any recording equipment.

Hence, $I = 0$ only when $\sin^2 \frac{\Delta}{2} = 0$ or $\frac{\Delta}{2} = N\pi$ where $N = 0, 1, 2, 3, \ldots$ etc.

The loci of these points of extinction produce the isochromatic fringes, which are defined as lines along which the principal stress difference $(\sigma_1 - \sigma_2)$, equals a constant depending upon the order N of the fringe.

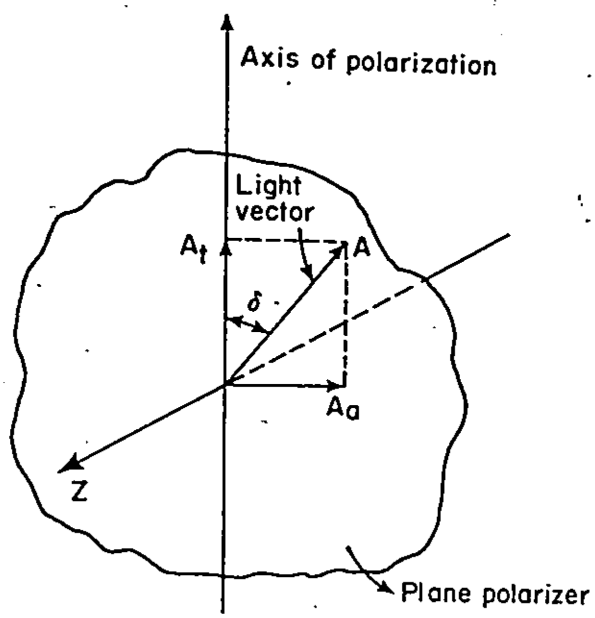

Fig. 6 - Absorbing and transmitting characteristic of a plane polarizer.

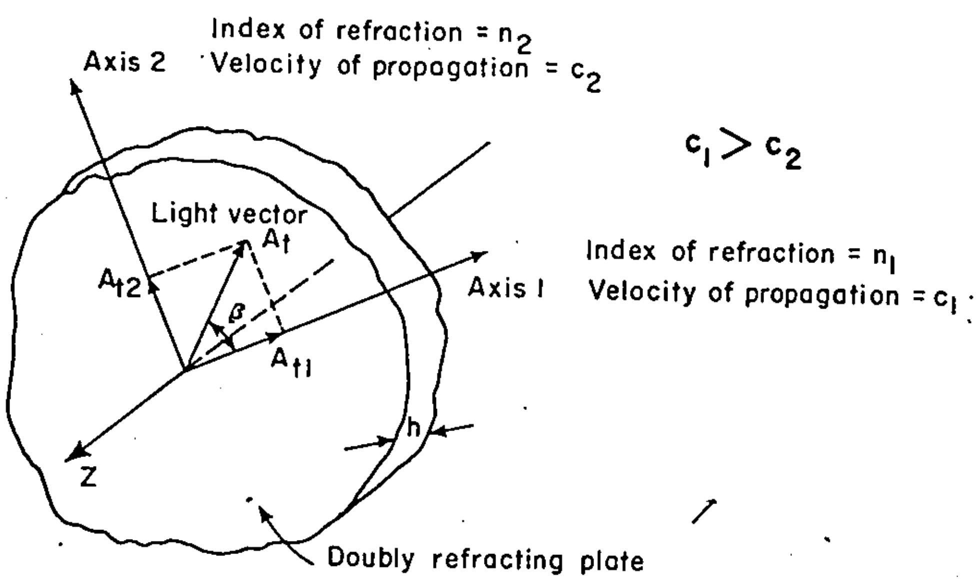

Fig. 7 - A plane - polarized light vector entering a doubly refracting plate.

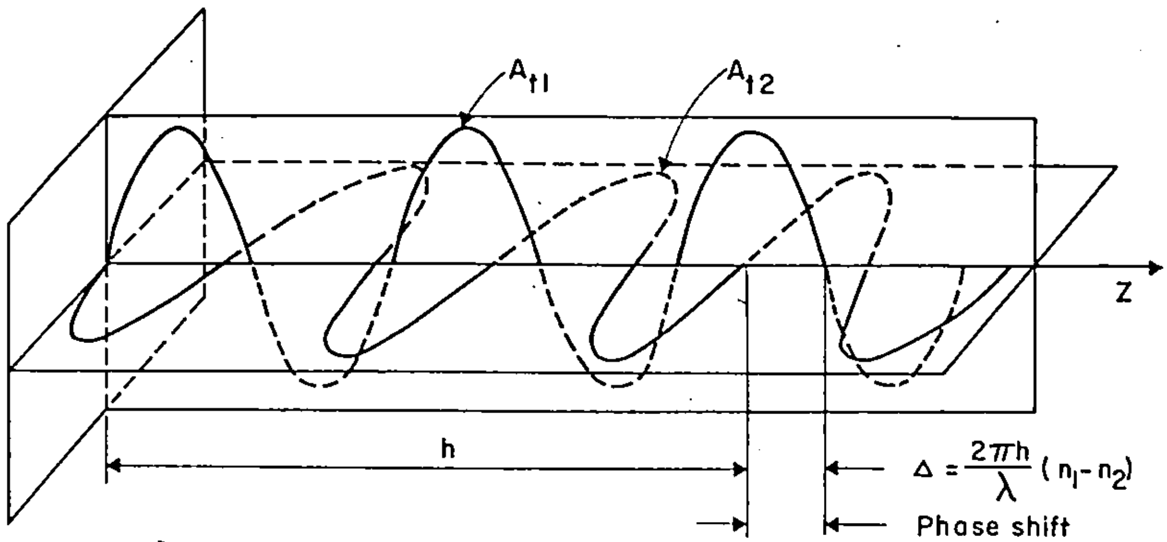

Fig. 8 - Retardation produced by wave plate.

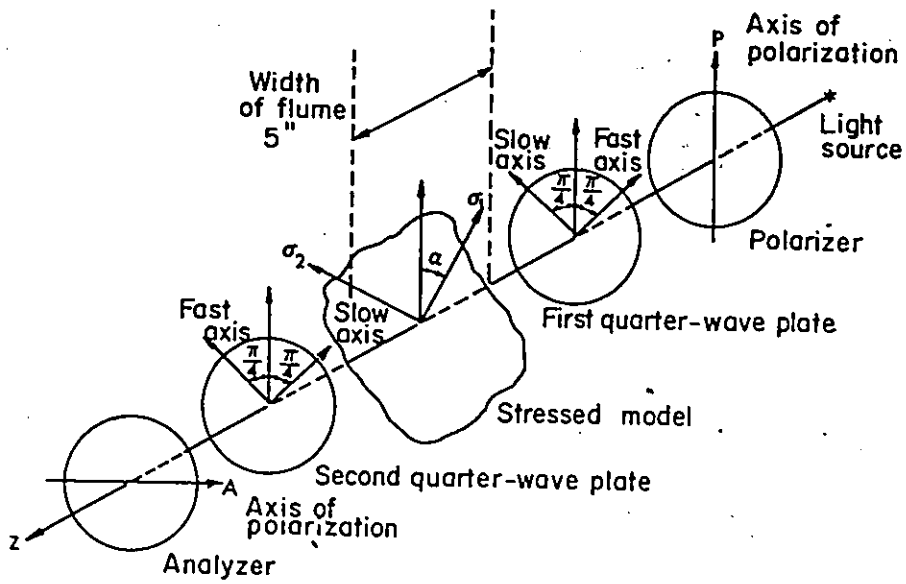

Fig. 9 - A stressed photoelastic model in a circular polariscope (arrangement A - crossed polarizer and analyzer - crossed quarter - wave plates. After Dally & Riley reference (17)

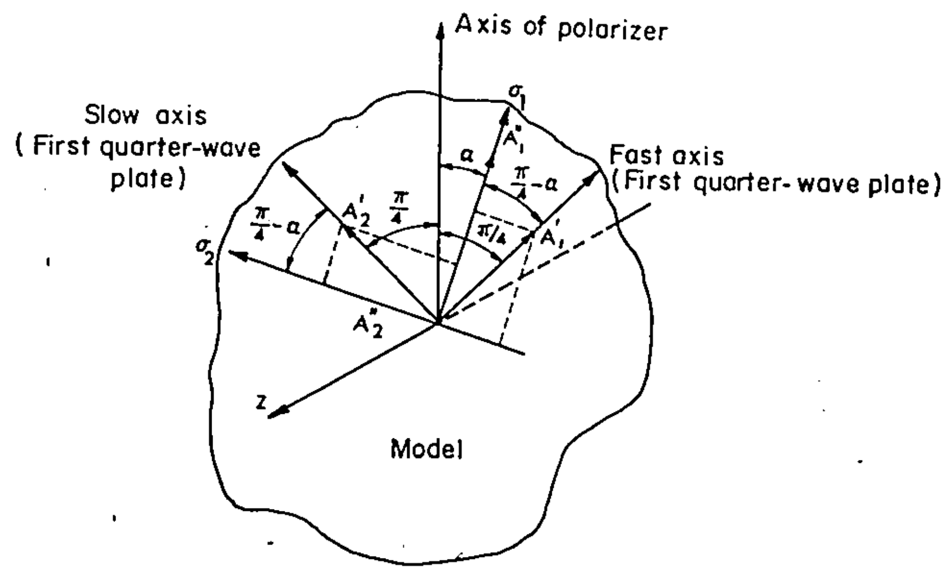

Fig. 10 - Resolution of the light components as they enter the stressed model.
After Dally & Riley reference (17)

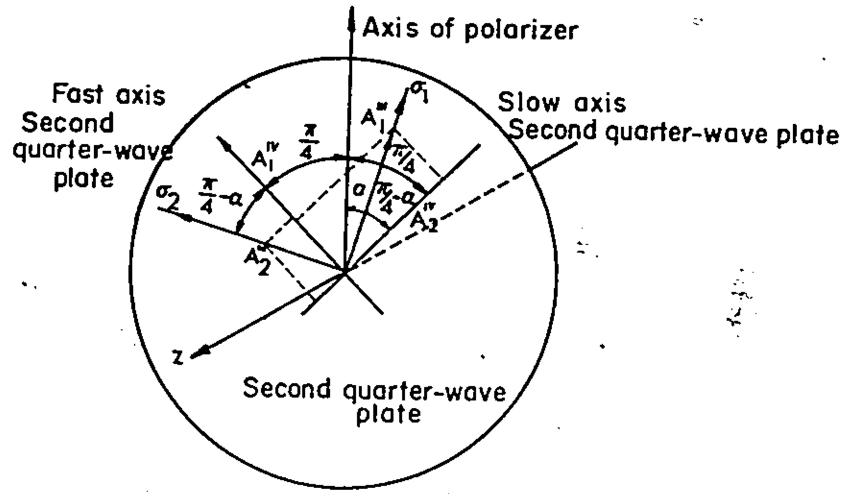

Fig. 11 — Resolution of the light components as they entre the second quarter wave plate. After Dally & Riley reference (17)

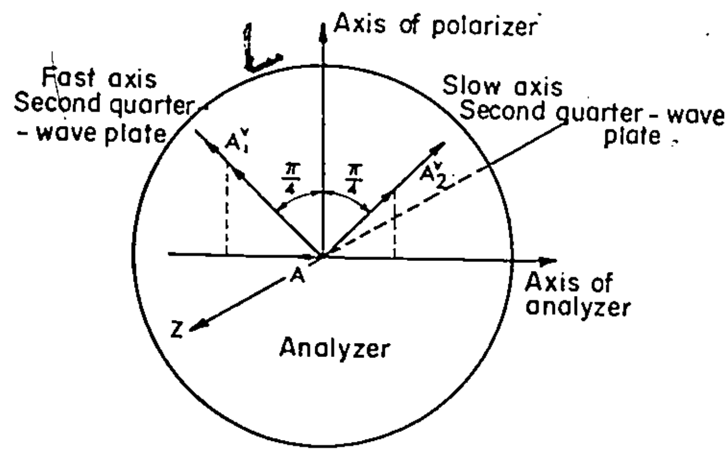

Fig. 12 — Components of the light vectors which are transmited through the analyzer (dark field) After Dally & Riley reference (17)

CHAPTER FIVE

LABORATORY EQUIPMENT AND INSTRUMENTATION

Complete descriptions of laboratory equipment and instrumentation are presented and discussed in this chapter. The basic equipment consisted of:

1) A specially designed flume
2) Pitot static tube and manometer
3) Hot-film anemometer and associated correlator probes
4) Flow visualization instruments consisting of viscometer, polariscope and photographic equipment

5.1 The Flume

A bronze centrifugal pump of one quarter horsepower was used to circulate the fluid in the flume. The flow entered the 6 feet (180 cm) long by 2 feet (60 cm) high and (5.0 ± 0.1) inch, (12.7 ± 0.3) cm, wide plexiglass flume from the end, where a fiber filter and a honeycomb flow straightener were installed. These were installed to filter the flow from any suspended impurities and to minimize the turbulence in the flume. At the downstream end of the flume the fluid was collected in a 2.5 feet (75 cm) wide by 2.5 feet (75 cm) long by 2 feet (60 cm) high plexiglass sump to be recirculated to the flume through a 2.5 inch (6.4 cm) diameter copper pipe.

The flow conditions were controlled by two brass valves positioned at each end of the flume. An orifice meter of (1.50 ± 0.03) inch, (3.8 ± 0.1) cm, throat diameter was installed in the 2.5 inch (6.4 cm) pipe entering the flume. The orifice meter was connected to a flow meter which was calibrated to measure the rate of flow. The specific gravity of the liquid used in the manometer was 2.95.

The flow characteristics over mobile and rigid beds were investigated. Uniform size Ottawa sand of D_{50} = 0.2 mm was selected for the mobile bed analysis. Five different rigid beds were installed in the flume at different times, as required, to perform the rigid bed analysis. The rigid beds are a cast of the natural ripple bed, smooth and sand-roughened artificial ripple bed and smooth and sand-roughened flat bed.

A schematic layout and the dimensions of the flume are shown in Fig. 13. Photo. 1 shows a view of the apparatus. Photo. 2 shows a view of the flow meter. Photos. 3 and 4 show a view of the cast of the natural ripple bed and the sand-roughened artificial ripple bed respectively.

The following considerations were taken into account in the design of the flume.

1) The flowing fluid should not come into contact with any material which reacts with the milling-yellow solution.

2) Two rubber pipes, each one foot (30 cm) long, were used to isolate any vibration from the pump to reach the flume.

3) The five inch (12.7 cm) flume width was selected, not to introduce difficulties in the flow visualization part of the study.

4) The equipment was portable which allowed its operation in laboratories with temperature control.

5.2 Pitot-Static Tube

A Pitot-tube was used to measure the total and static heads at different points in the flow field. The Pitot-tube has an external diameter of 0.125 inch (0.32 cm) and internal diameter of 0.046 inch (0.12 cm). The difference between the total and static pressures, at the point of measurement, was read on an inclined manometer adjusted at a slope of 10:1. The liquid used in the sloping manometer has a specific gravity of 1.75. Photo. 10 shows a view of the Pitot-tube and the sloping manometer.

5.3 Hot-film Anemometry Equipment

5.3.1. Hot-film Probes

Two different probes were used throughout the hot-film anemometry measurements of this study, namely:

i) The 55A83 DISA Wedge-probe:

This probe has a nickel film that is placed on the sharp edge of a wedge consisting of the quartz substrate. A 2 μm quartz layer protects the nickel film against mechanical and chemical influences and insulates it electrically. Photo. 5 shows a close view of the 55A83 DISA wedge-probe.

ii) The 55A0891 DISA V-probe:

The substrate of this probe is shaped like a wedge, the sharp edge of which has the shape of a V. The legs of the V-probe are perpendicular to each other and each of them consists of a nickel film protected by a quartz layer. Photo. 6 shows a close view of the 55A0891 DISA V-probe.

5.3.2 DISA Equipment

Units of DISA equipment were used in different arrangements to accomplish the experimental measurements of the flow characteristics in question. The basic three circuits used during the experimental work are listed below.

i) The circuit used to measure the velocity U and the turbulence intensity u' is shown diagramatically in Fig. 14. Photo. 7 shows a view of this set-up.

ii) The circuit used to measure the Reynolds stresses $-\rho\overline{uv}$ and the turbulence intensities u' and v' is shown diagramatically in Fig. 15. Photo. 8 shows a view of this set-up.

iii) The circuit used to measure the autocorrelation function $\rho(t)$ is shown diagramatically in Fig. 16. Photo. 9 is a view of this set-up.

5.4 Flow Visualization Equipment

i) Synchro-Lectric Viscometer:

This viscometer was used to measure the viscosity of the milling-yellow solution. Photo. 11 shows a view of the viscometer.

ii) Polariscope:

The polariscope used to view the shear patterns of the milling-yellow solution flow is shown in Photo. 12. Photo. 13 illustrates the polariscope mounted on top of the flume as used during the flow visualization experimental study.

iii) A 35 mm Nikon camera and 16 mm Bolex movie camera were used in photographing the shear patterns of the milling-yellow solution flow as viewed through the polariscope.

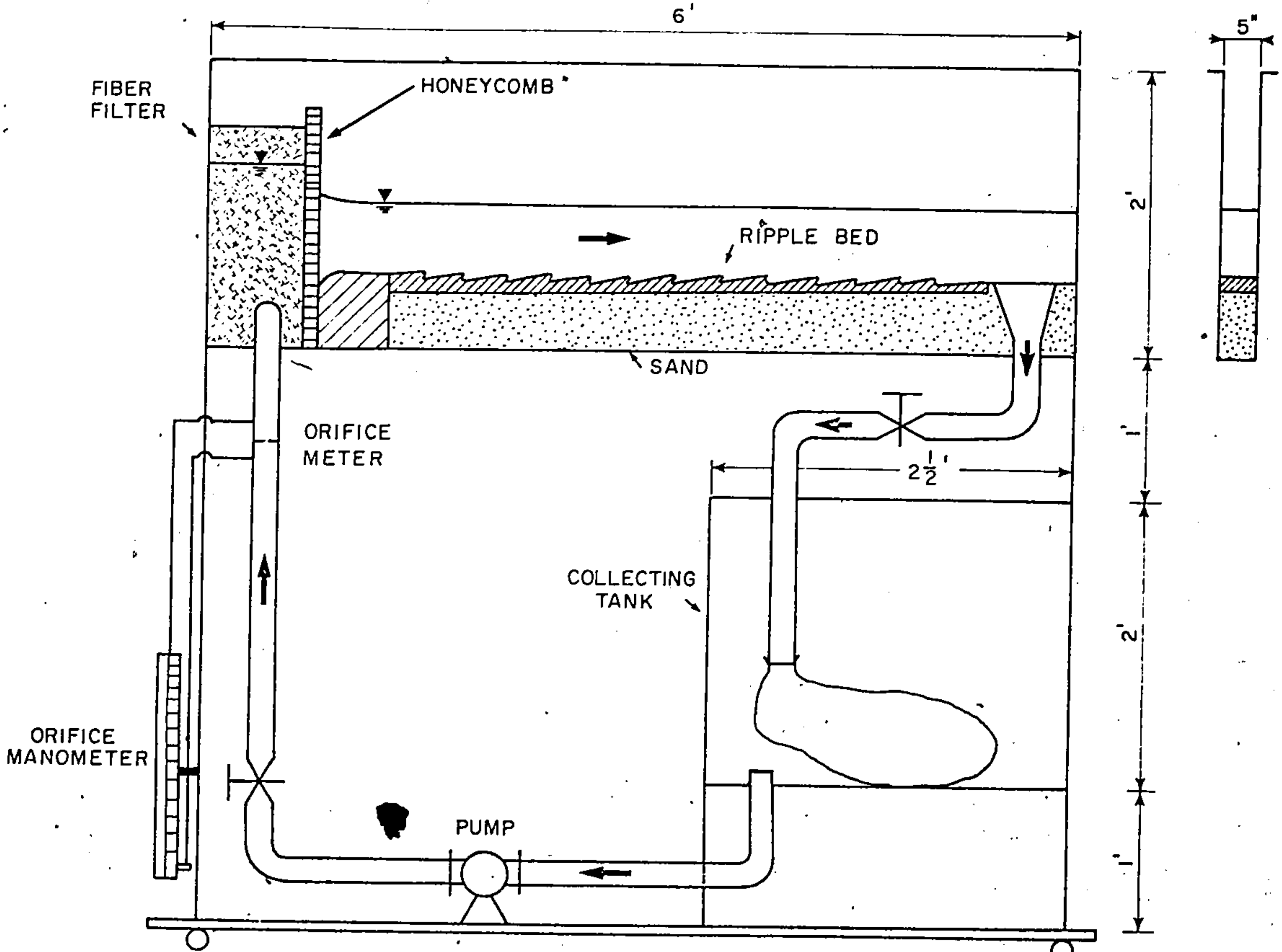

Fig.13 — Schematic layout and dimensions of the apparatus

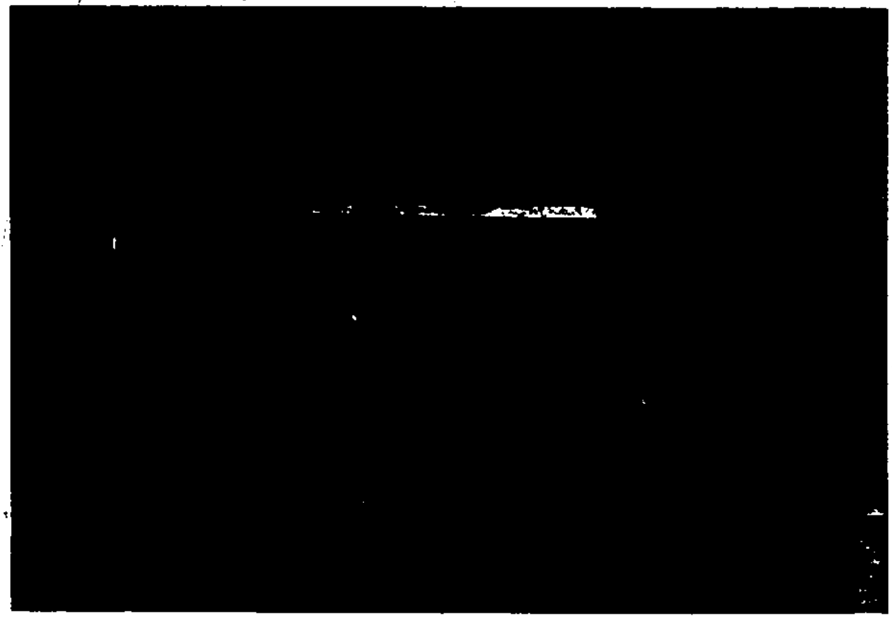

Photo. 1. A View of the Apparatus

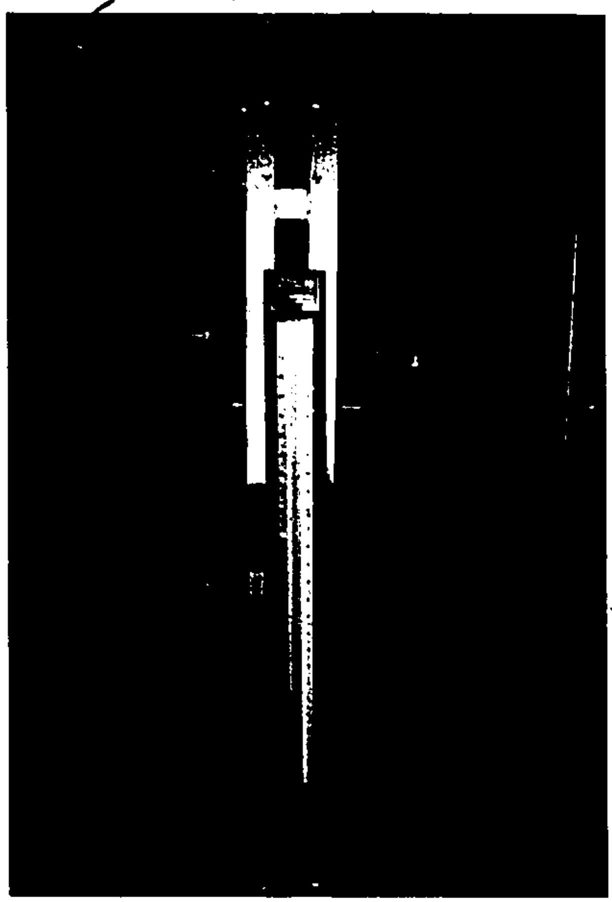

Photo. 2. End View of the Apparatus Showing Metering Equipment

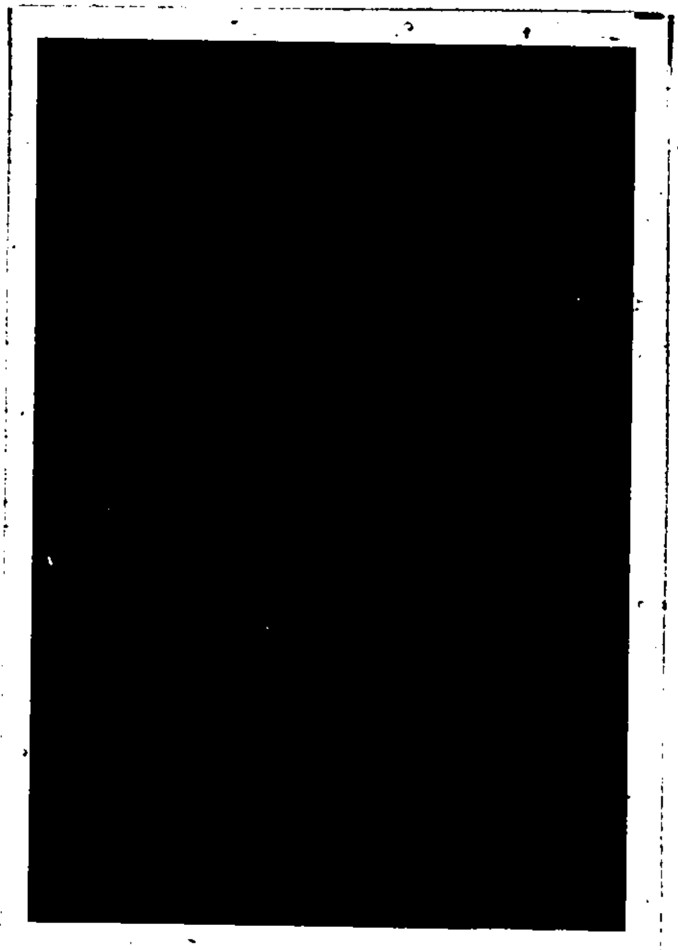

Photo. 3. A View of the Cast Ripple Bed (looking downstream)

(Flume Width = 5")

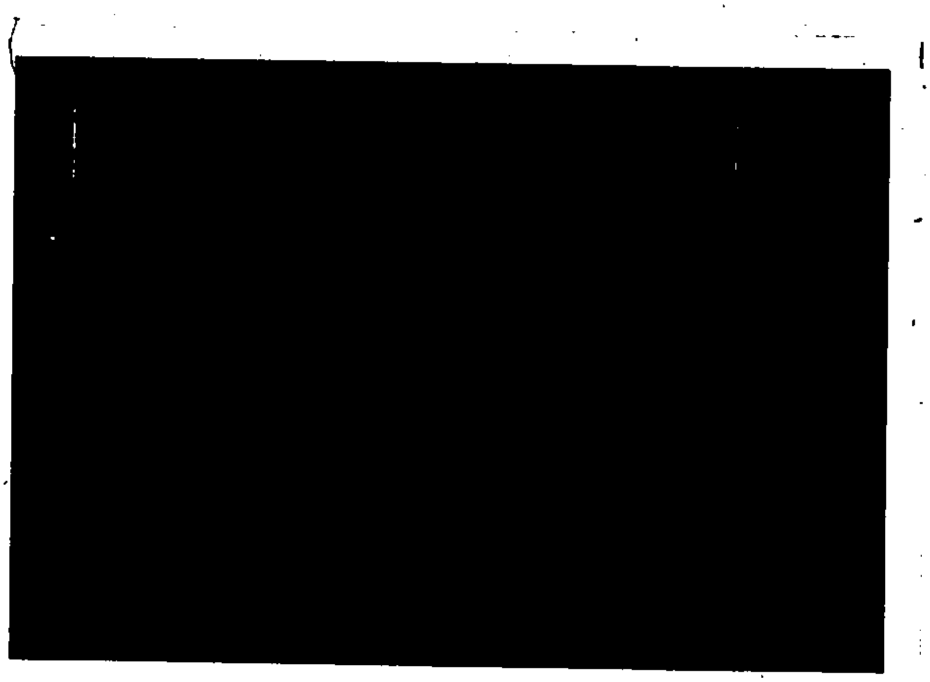

Photo. 4. A View of the Sand-Roughened Artificial Ripple Bed.

(5" Wide)

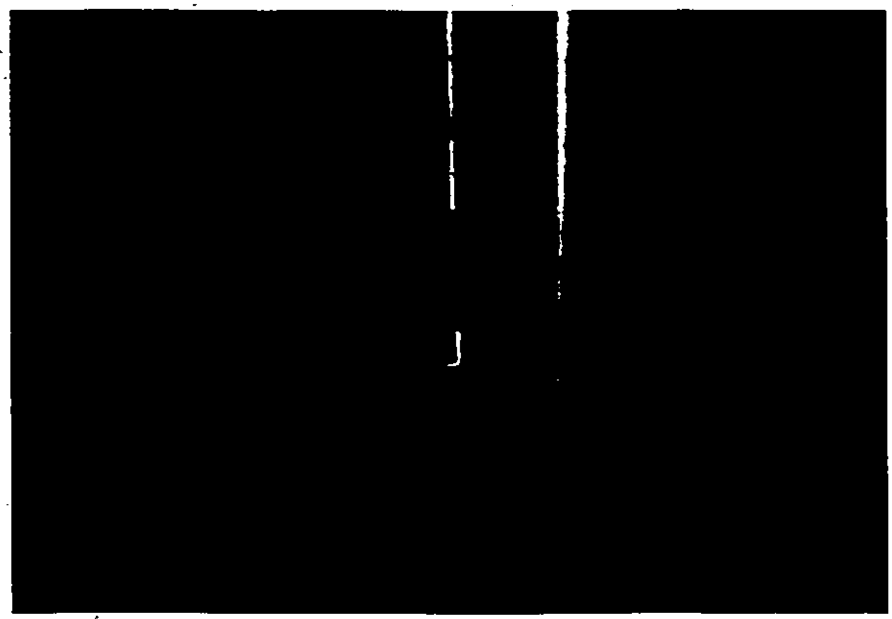

Photo. 5. A Close View of the 55A83 Wedge-Probe (Probe Support Diameter = 0.5")

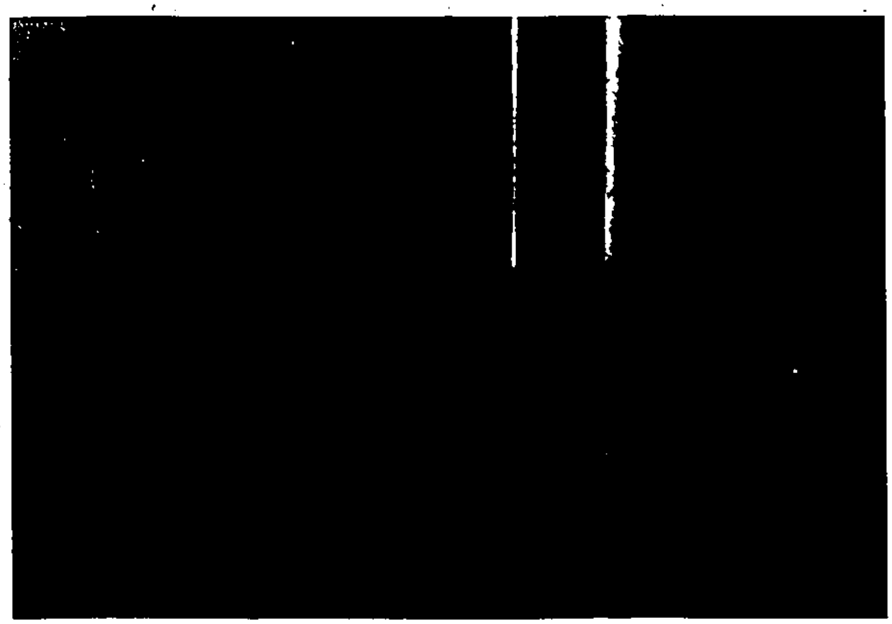

Photo. 6. A Close View of the 55A0891 V-Probe. "In the horizontal rather than the actual operating vertical position" (Probe Support Diameter = 0.5")

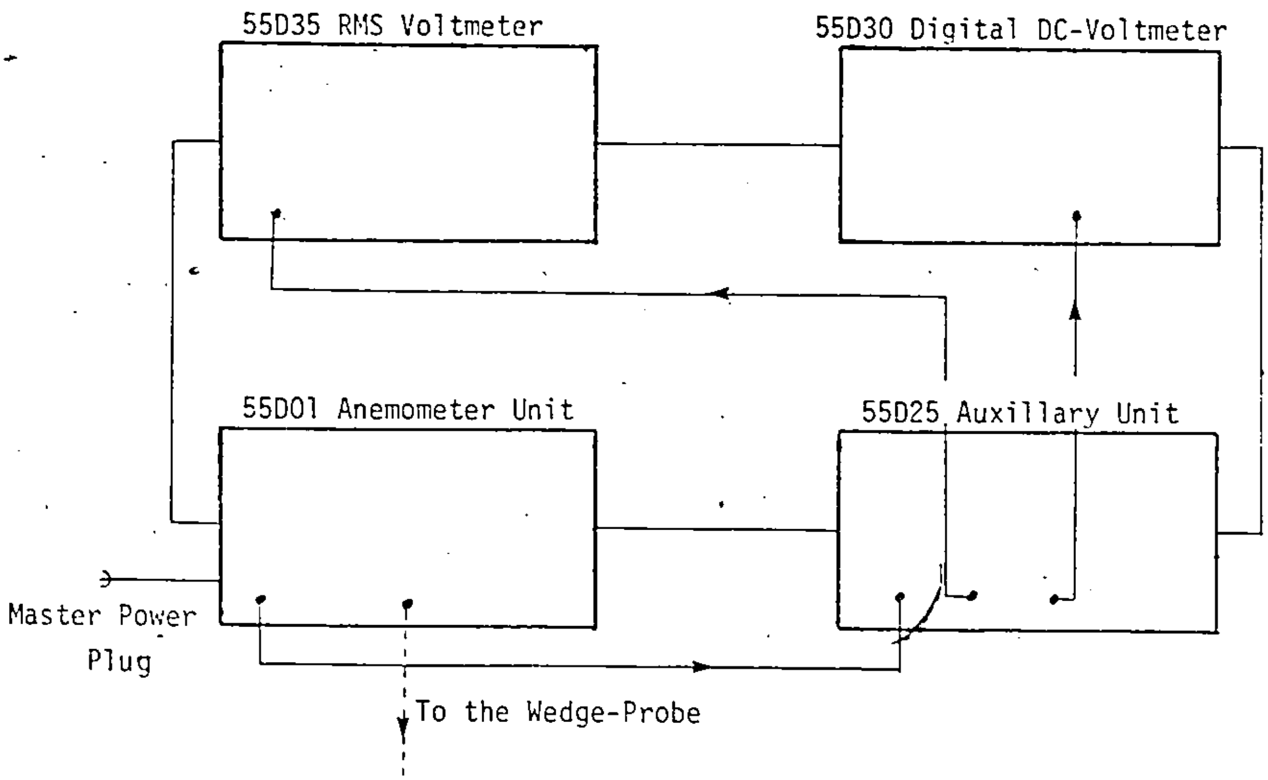

Fig. 14. The Circuit Used to Measure the Velocity U and the Turbulence Intensity u'

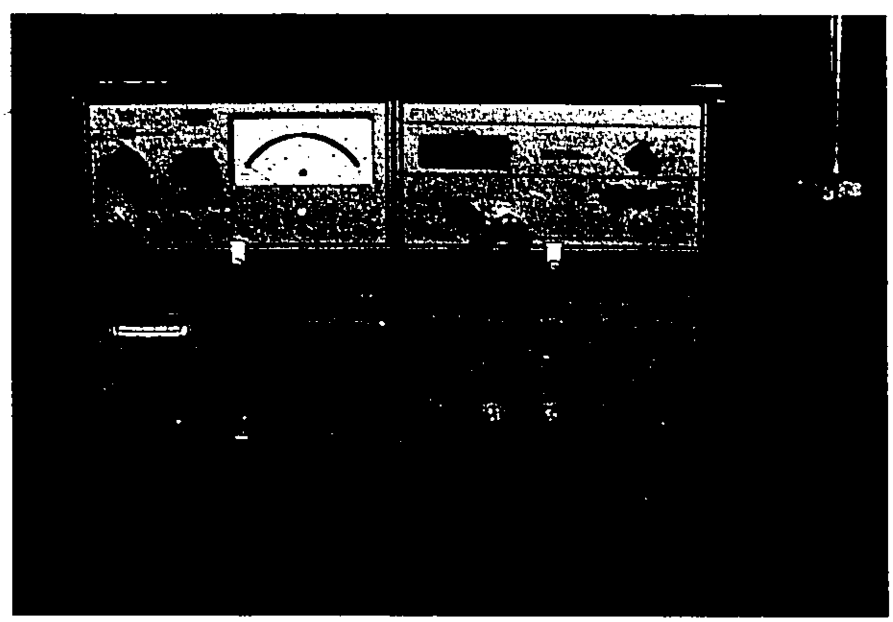

Photo. 7. A View of the Set-up Used to Measure the Longitudinal Velocity U and the Turbulence Intensity u'

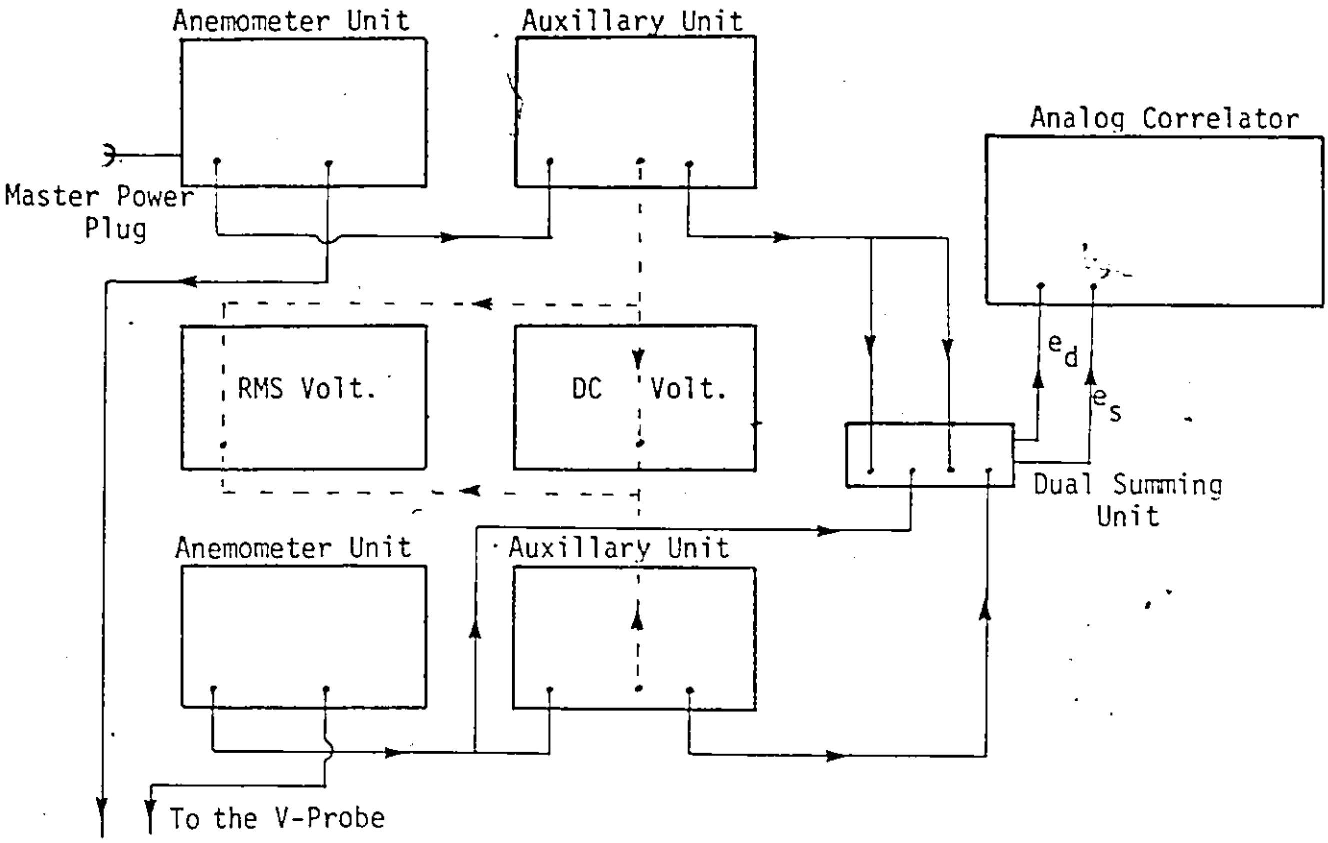

Fig. 15. The Circuit Used to Measure u', v', and $\overline{uv}$

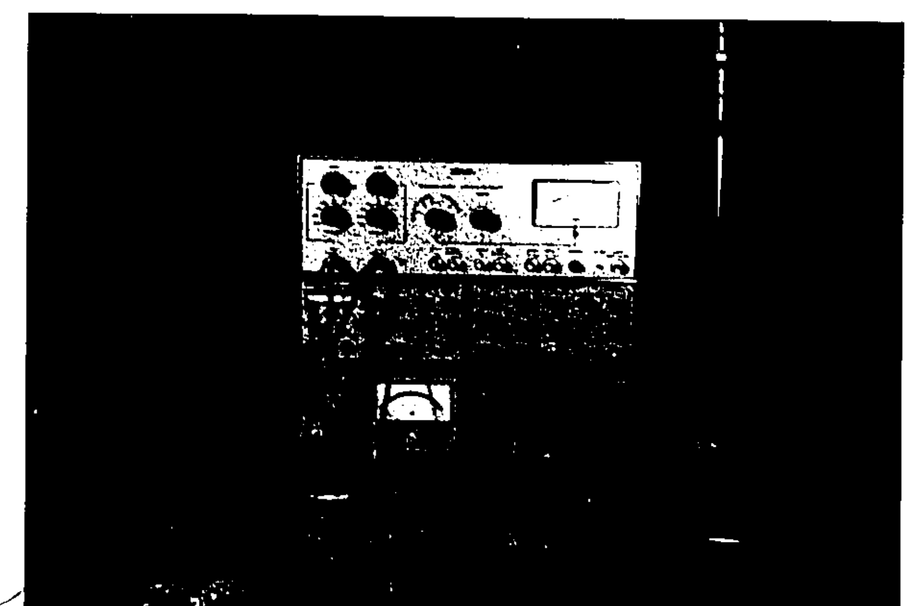

Photo. 8. A View of the Set-up Used to Measure u', v' and $\overline{uv}$

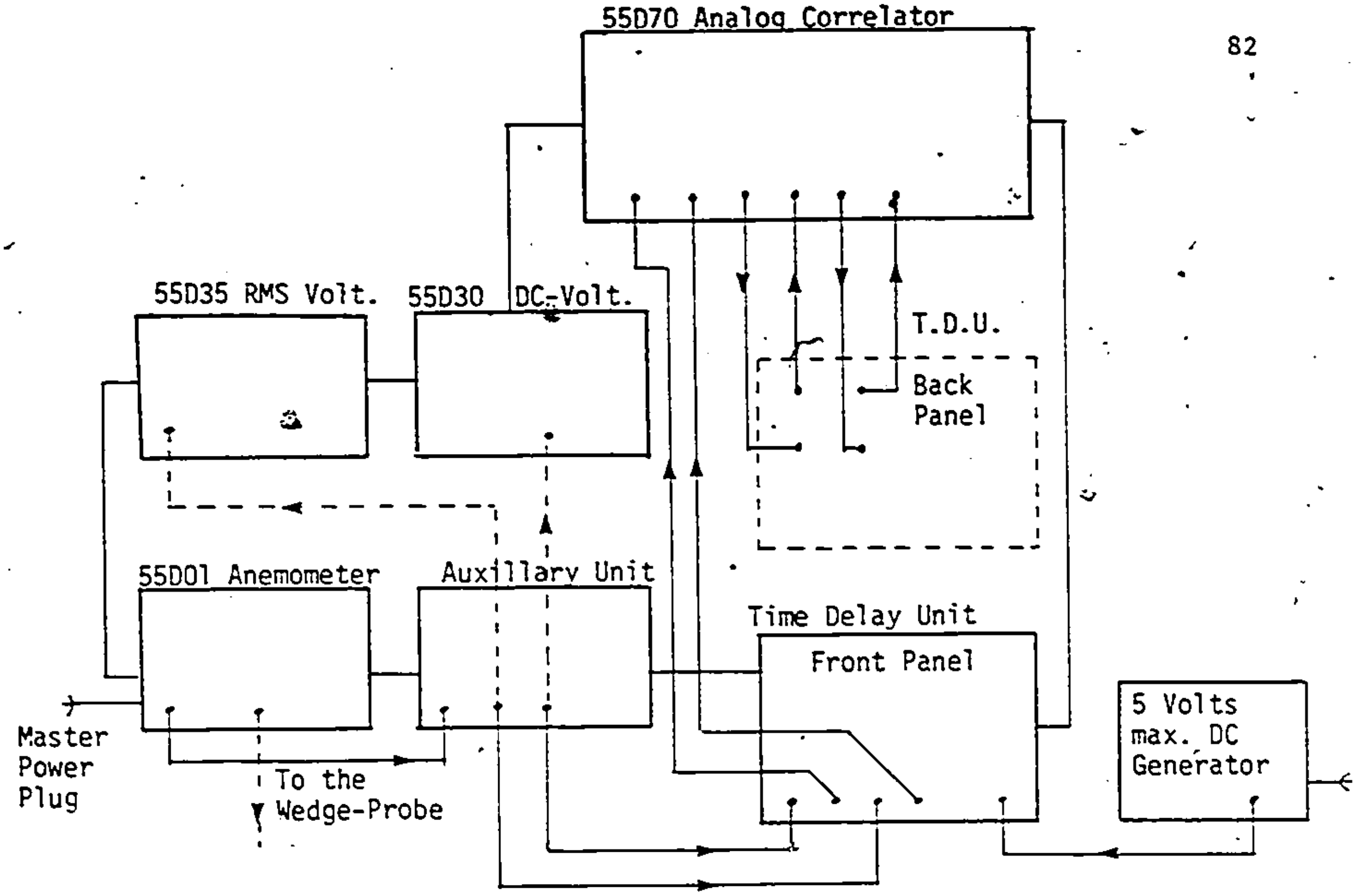

Fig. 16. The Circuit Used to Measure the Autocorrelation Function

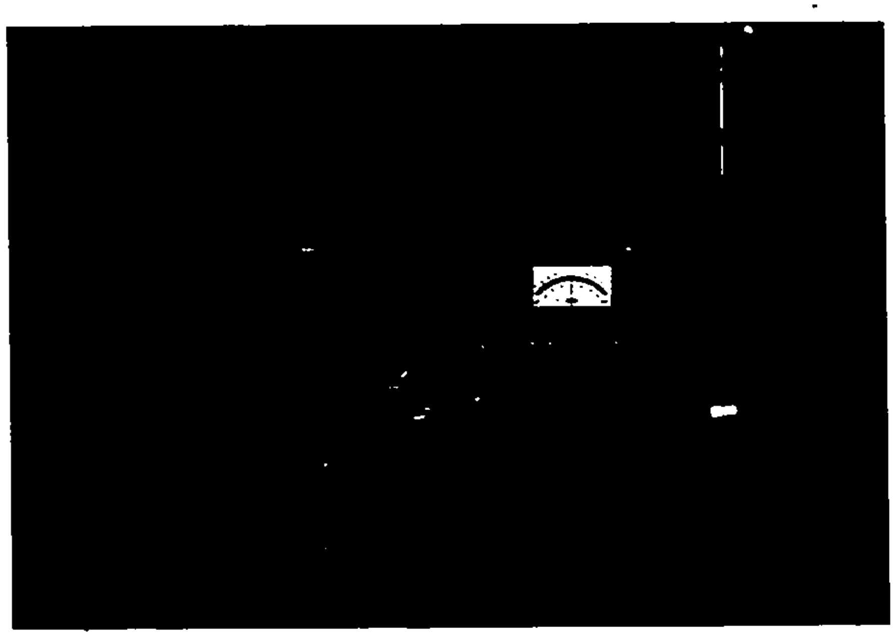

Photo. 9. A View of the Set-up Used to Measure the Autocorrelation Function

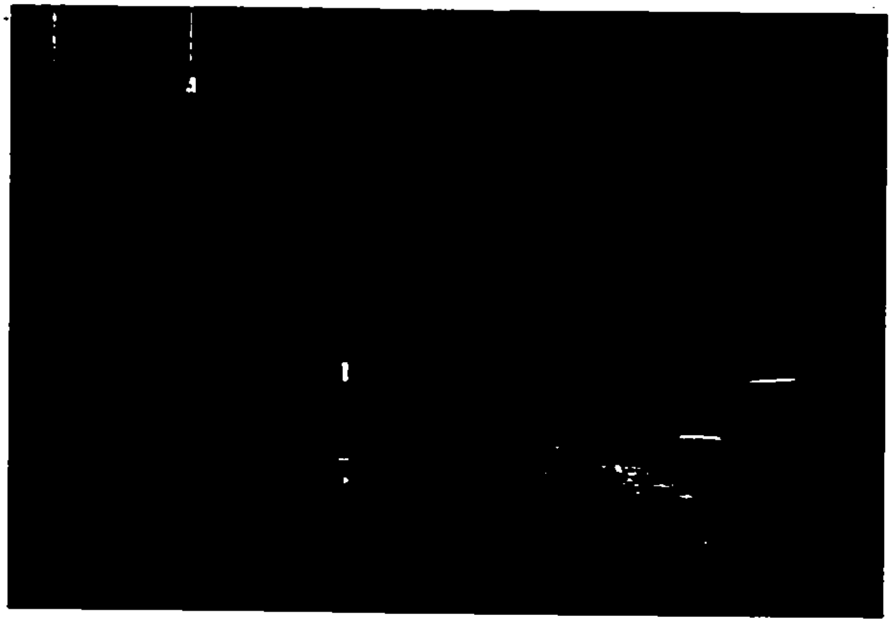

Photo. 10. A View of the Pitot-Tube and the Sloping Manometer (External Diameter of the Pitot-Tube = 0.125")

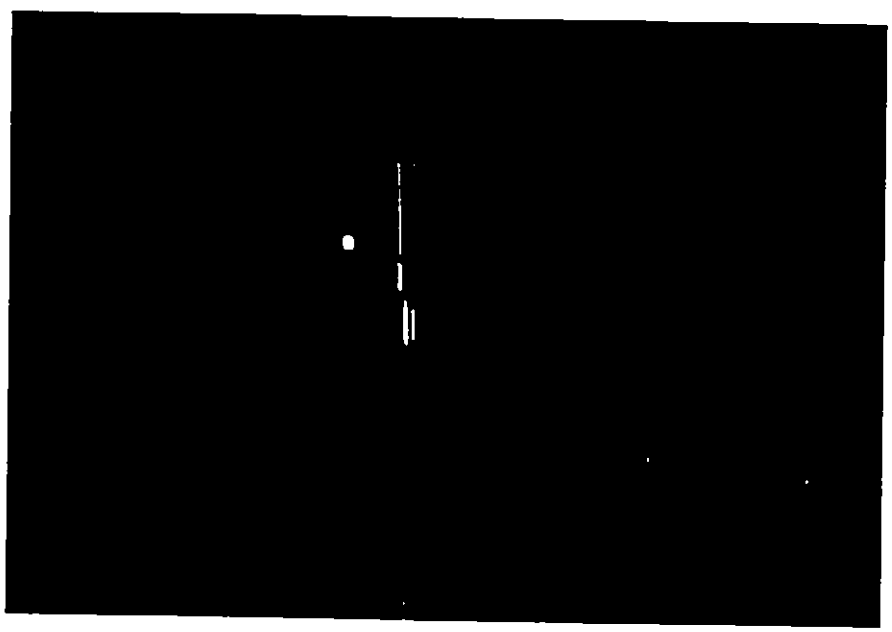

Photo. 11. A View of the Syndro-Lectric Viscometer.

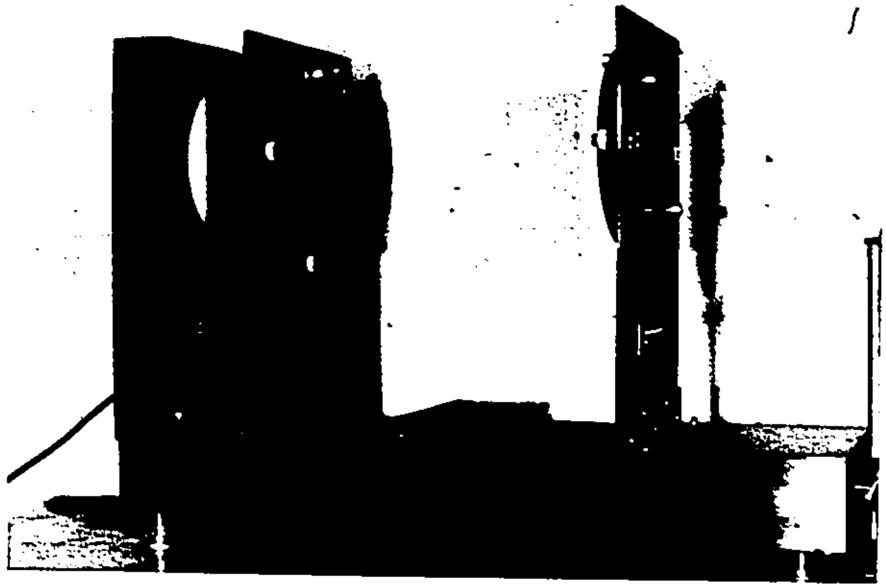

Photo. 12. A View of the Polariscope

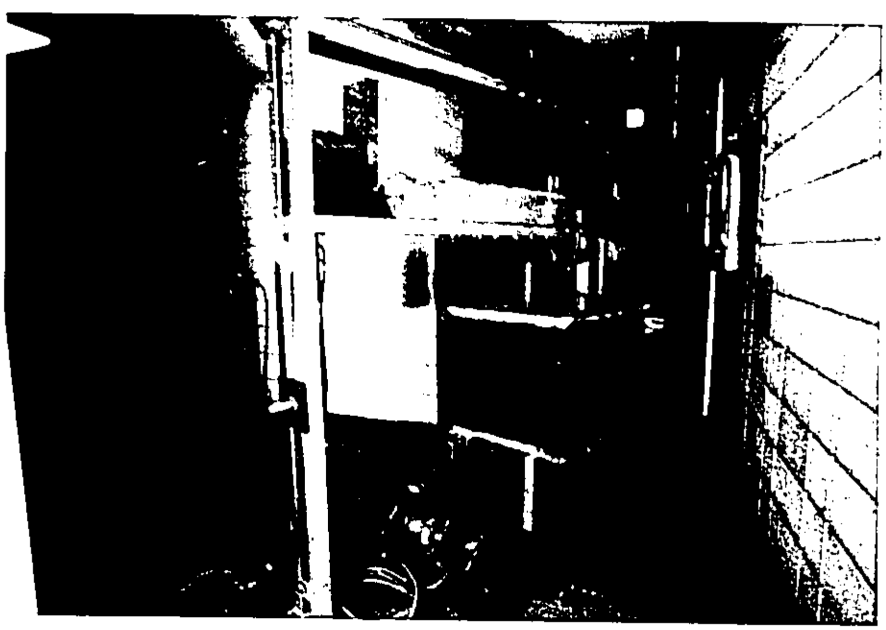

Photo. 13. A View of the Polariscope Mounted on the Top of the Flume.

CHAPTER SIX

EXPERIMENTAL PROCEDURES

The experimental study of this research can be divided into three sections:

1) Initiation and development of ripple formation whereas a series of tests was carried out in a natural mobile bed to establish the flow conditions at which the incipient and the developed ripples would form.

2) The hot-film anemometry in which the art of using hot-film anemometer techniques to measure the turbulent characteristics of water flow over rigid bed forms was applied.

3) The flow visualization in which the phenomena of double refraction of milling-yellow solution flowing over rigid beds was explored.

6.1 Initiation and Development of Ripple Formation in a Natural Mobile Bed

The first objective in the experimental study was to establish the flow conditions at which incipient ripples in a mobile sand bed would form. The flume was filled with a 0.2 mm graded sand to a depth of 6 inches. The sand was leveled throughout the length of the flume. A vertical plexiglass lever that ends with a 5 inch wide sharp edge scraper at the bottom and a horizontal arm at the top was used in leveling the sand. The dimensions of the lever were designed in such a way that with the arm sliding on top of the flume, the scraper is at 6 inches above the plexiglass bottom of the flume. The flume was slowly filled with water to a depth of 5 inches (12.7 cm) above the leveled sand bed. The depth of flow was held constant while the velocity was gradually increased by increasing the discharge. Constant flows were maintained for approximately half an hour to ascertain whether a ripple formation was developing. At a certain flow, the first appearance of sand particles sliding and/or rolling on the bed was observed.

The bed movement occured first in the upstream portion of the flume and gradually advanced downstream. The average velocity of this flow condition was recorded and defined as the incipient velocity. No definable bed pattern developed under the incipient velocity flow condition.

In order to establish a developed measurable ripple bed, the next series of tests were carried out at velocities slightly higher than the incipient velocity. The sand size and the flow depth were maintained as 0.2 mm and 5.0 inches respectively. Each flow was continued for three hours from the first appearance of the bed pattern. A flow with an average velocity 1.25 times the incipient velocity was selected as the best condition to represent the ripple bed.

The next step in the experimental measurements was to select a representative section where a symmetrical uniform transverse profile of the longitudinal velocity prevailed. For this purpose velocity distributions were constructed at 14 inches, 31 inches, and 44 inches downstream from the screen with the Pitot tube held at

2.5 inches above the bed. It was found that the transverse profile of the longitudinal velocity at 44 inches downstream from the screen is fairly uniform and, accordingly, this section was chosen as a representative one for further study.

Pitot tube measurements were taken at 44 inches (112 cm) downstream from the screen to:

1) establish the centreline velocity distribution throughout the depth of flow, and,

2) estimate the bed shear stress distribution along one ripple.

For the purpose of estimating the bed shear, the centre of the Pitot-tube was held (0.125 ± .005) inch, (3.0 ± 0.1) mm, normal to the ripple surface.

In the course of this experiment, the sand transport rate was estimated by observing the time elapsed for a ripple crest to travel a certain distance.

At the end of the experiment, the two valves were closed and the water was allowed to drain slowly so as not to disturb the bed pattern. Measurements of ripple lengths and heights were then taken along the flume by means of a point gauge.

6.2 Rigid Beds

6.2.1 Cast of the Natural Ripple Bed

While the sand bed was still wet, a one inch (2.5 cm) thick layer of watery Plaster of Paris was carefully poured over the bed forms. Spacers were located at one foot (30 cm) longitudinal intervals to prevent shrinkage cracks. The plaster impression was then used to make a mould which in turn was rubbed with a light grease and filled with a low slump sand mortar to produce a rigid casting of the original ripple bed. The 0.2 mm sand from the original bed was used to make the mortar. Photo. 3 shows a view of the cast of the natural ripple bed.

6.2.2. Artificial Ripple and Flat Beds.

An artificial ripple pattern was also made of plexiglass to form the smooth artificial ripple bed. The ripple lengths and heights, representing the average natural conditions, were 2.5 inches (6.4 cm) and 0.2 inch (0.5 cm) respectively. A coat of varnish was applied to the surface of the plexiglass and then, a layer of 0.2 mm sand was sprinkled to form the rough artificial ripple bed. Photo. 4 shows a view of the rough artificial ripple bed. Smooth and sand-roughened flat beds were constructed in a similar manner.

6.3 Hot-Film Anemometry

6.3.1. Measurements of Flow Characteristics over Rigid Beds

6.3.1.1 The Longitudinal Velocity "U"

Velocity measurements were performed by measuring the voltage "E" which must be supplied to a wedge-probe from the 55D01 Anemometer in order to keep the probe at a certain temperature higher than the temperature of the medium under measurement. The overheating ratio "a" was chosen as 1.05. The instantaneous value of the electic power supplied is assumed to be equal to the instantaneous thermal loss to the surroundings. The thermal loss depends on the nature, temperature, pressure and velocity of the medium under measurement, and on the probe used. If only the velocity is varied, the voltage "E" will be a direct measure of the velocity "U". A calibration analysis was performed to obtain the relation E = f(U). The hot-films were calibrated and repeatedly checked by a 1/8 inch (0.3 cm) diameter Pitot static tube connected to an inclined manometer. The method of calibration is described in Appendix I.

6.3.1.2 Turbulence Intensity "u'"

The root-mean-square of the voltage fluctuations were measured by the DISA 55D35 RMS Voltmeter. Subsequently these measurements were reduced to turbulence intensities by the simple relation given in Eq. 4.16, in which the sensitivity of the probe "S" is obtained from the calibration curve of the wedge-probe.

Photo. 7 shows a view of the set-up used in measuring the velocity U and the turbulence intensity u'. The wiring connections of the circuit is shown in Fig. 14. A close view of the 55A83 wedge-probe is shown in Photo. 5. The operating procedure of the 55D01 Anemometer using the wedge-probe to measure the velocity "U" and the turbulence intensity "u'" is given in Appendix I.

6.3.1.3 Reynolds Stresses "$-\rho\overline{uv}$"

The correlation between the longitudinal component "u" and the vertical component "v" of flow velocity fluctuations at a single point in the form $\overline{uv}$ and the turbulence intensities u' and v' were calculated from measurements taken with a V-probe connected to two DISA type 55D01 constant temperature anemometers, a 55D70 Analog Correlator and a Dual Summing Unit as shown in Fig. 15. The voltage fluctuations e_1 and e_2 sensed by the two films of the V-probe were fed to the Dual Summing Unit. The output from the Dual Summing Unit is simply the algebric addition and substraction of the input signals and identified as e_s and e_d respectively. The signals e_s and e_d were then fed to the 55D70 Analog Correlator where the correlation $\overline{e_s e_d}$ was recorded. The RMS of e_s and e_d were measured consecutively by means of the 55D35 RMS Voltmeter. A solution of three simultaneous equations given as 4.17, 4.18 and 4.19 will result in determining the correlation $\overline{uv}$ and the turbulence intensities u' and v', noting that:

S_1 and S_2 are the sensitivity factors of the two films of the V-probe.

Photo. 8 shows a view of the set-up used in determining the Reynolds stresses. A close view of the 55A0891 V-probe is shown in Photo. 6. The operating procedure of the 55D70 Analog Correlator with the V-probe to measure $\overline{uv}$, u' and v' is given in Appendix I.

6.3.1.4 Eulerian Macro and Micro Scales of Turbulence

The variation of the autocorrelation function $\rho(t)$ with the time "t" as defined in Eq. 4.20 at any fixed point in the flow field was achieved by inserting a Time Delay Unit 55D75 and a variable 5 Volts maximum DC generator in the circuit as shown in Fig. 16. The signal from the wedge-probe was delayed by different time intervals ranging from 0.1 millsec to 100 millsec. The original and delayed signals were fed to the 55D70 Analog correlator where the autocorrelation function was measured. The macro "Λ" and micro "λ" scales of turbulence were then calculated from Eqs. 4.21 and 4.22 respectively.

Photo. 9 shows a view of the set-up used in measuring the autocorrelation function $\rho(t)$. The operating procedure of the 55D75 Time Delay Unit and the 55D70 Analog Correlator to measure $\rho(t)$ is given in Appendix I.

6.3.2 Experimental Measurements on Rigid Beds

The average velocity and depth were set at the same conditions obtained for the mobile bed. Measurements over the rigid cast of the natural ripple bed included:

1) Centreline distribution throughout the depth of flow of velocity, turbulence intensities, turbulence scales and Reynolds stress at sections 14 inches, 21 inches, 31 inches, 37 inches, and 44 inches, (36 cm, 53 cm, 79 cm, 94 cm and 112 cm), downstream from the screen. The measurements were taken at ripple crests.
2) Longitudinal distributions along the flume centreline of velocity, turbulence intensities and Reynolds stress at 0.125 inch and 2.5 inches, (0.3 cm and 6.4 cm), above the ripple. The measurements were taken at ripple crests.
3) Velocity, turbulence intensities and Reynolds stress taken every half inch, (1.3 cm), along one ripple in the zone of low turbulence at 0.125 inch (0.3 cm) normal to the ripple and 2.5 inches

(6.4 cm) above the ripple.

The measurements were repeated for the sand-roughened artificial ripple bed. For the smooth artificial ripple bed, and the smooth and sand-roughened flat beds, only the measurements described in (1) and (2) were undertaken.

6.3.3 Precautions Observed in the Application of Hot Films in Water

1) The joint of the probe to the probe holder had to be completely watertight. This was achieved by applying a silicon rubber paste on the joint. The silicon paste solidified in a few hours.

2) Any voltage difference between the water and the hot film can cause a breakdown in the insulating quartz coating and thus, ruin the probe. To avoid such a voltage difference the water near the probe had to be grounded. This was achieved merely by using a wire with bare ends; one end was tied around the probe holder, and the other immersed in the water near the probe.

3) Drifting of the output voltage caused by the entrained gases, lint and dust particles in the water, was eliminated by frequently brushing the probe. Also, to keep the water as clean as possible:

   i) the collecting tank was permanently covered by a plexiglass sheet;

   ii) the flume was covered by a plastic sheet, when not in operation;

   iii) the water was drained and replaced by a clean fresh water occasionally.

6.4 Flow Visualization for Rigid Beds

6.4.1 General

When a flowing liquid with the property of double refraction is viewed in polarized light, visible interference patterns appear. These patterns can be quantitively related to the stresses in the moving liquid. Studies of this type have been made by past investigators, but they were hampered by liquids which were either extremely viscous or unstable in contact with common materials of construction.

It has been discovered recently that aqueous solutions of an organic dye, milling-yellow, exhibit strong double refraction characteristics and at the same time possess reasonably low viscosity and good stability.

6.4.2 Preparation of the Milling-Yellow Solution

Milling-yellow is almost insoluble in water at room temperature. However, it readily dissolves in boiling water and does not precipitate out when cooled.

Solutions containing different percentages ranging from 0.2 to 2.0 per cent of the dye by weight were tested against their stability, viscosity and birefringent quality. It was found that 1% by weight of milling-yellow gave a relatively clear and sensitive solution.

The water was gradually brought to boiling, then the dye, in a powdered form, was added and the mixture was continuously stirred to complete the dissolving of the dye. The solution was then allowed to cool in a room temperature environment. It was found that keeping the soution in opaque container would prolong and maintain its sensitivity.

6.4.3 Experimental Measurements

The absolute viscosity of the solution was measured by a Synchro-Lectric Viscometer. The principle of operation of the viscometer is simply rotating a cylinder in a fluid and measuring the torque necessary to overcome the viscous resistance to the induced movement. Photo. 11 shows a view of the viscometer.

Shear patterns for different flow conditions over the rigid natural ripple bed, a smooth and sand-roughened artificial ripple bed and a smooth and sand-roughened flat bed were viewed by a dark field circular polariscope. Slides and movie films were taken for those patterns.

Photo. 12 shows a view of the polariscope. Photo. 13 shows the equipment with the polariscope mounted on top of the flume.

6.5 Calibration Tests

The following calibration tests were performed as a part of the experimental work:

i) Calibration of the 1.5 inch orifice meter that was installed in the 2.5 inch pipe entering the flume to determine the constant C in the relation $Q = C\sqrt{H}$, where,

   Q - the flow rate in cubic feet per second, and

   H - the manometer reading in inches.

For this purpose four different flow rates were obtained by adjusting the two controlling valves on the apparatus and the reading on the manometer was recorded. In successive runs the manometer reading H was increased from 3 inches to 18 inches in 5 inch increments. For each flow rate a transverse velocity distribution was constructed from Pitot-tube measurements taken at 0.2 and 0.8 the flow depth. The discharge, $Q = \Sigma vdA$, and the constant C were calculated for each run. An average value of C was finally established.

ii) Calibration curves of the hot-film probes in the form, $E = f(U)$ were constructed where,

E - the DC-voltage read on the 55D30 Voltmeter, and

U - the mean velocity obtained from Pitot-tube measurements.

For this purpose the Pitot-tube was aligned side by side to the hot-film probe (wedge-probe or V-probe) at 1/8 of an inch apart in the horizontal plane. Numerous readings of the DC-Voltage and the corresponding velocity were taken in the velocity range of , (U = 0.25 to 1.10 ft./sec., that is, 0.08 to 0.34 m/s). The water temperature was recorded and the overheating ratio was kept at 1.05. A family of calibration curves for the wedge-probe and the V-probe were constructed for different operating temperatures.

CHAPTER SEVEN

EXPERIMENTAL RESULTS, DATA REDUCTION AND ERROR ANALYSIS

This chapter presents the results of the calibration tests. The experimental measurements of this study are then followed. They are further reduced to more significant parameters that are presented in sets of curves to facilitate the analysis which is discussed in Chapter nine. An error analysis of the experimental measurements is also included.

7.1 Results of the Calibration Tests

Calibration tests of the orifice meter and the hot-film probes were performed as described in the previous chapter. The results are given below.

i) A constant C = 0.041 was established in the discharge equation of the orifice meter $Q = C\sqrt{H}$ where

   Q - the rate of flow in cubic feet per second, and

   H - the manometer reading in inches.

ii) The calibration curves of the wedge-probe at temperatures 70° F, (21°C), and 80°F (27°C), are shown in Fig. 17. In the experimental range of velocity, (U = 0.50 to 1.10 ft./sec.), the calibration curves have nearly constant slope $(\frac{dE}{dU})$. This means that the wedge-probe has a constant sensitivity, if the water temperature and the overheating ratio are kept constant.

The sensitivities of the wedge-probe at 70°F, (21°C), and 80°F, (27°C), operating with overheating ratio a = 1.05, were estimated respectively as

$$S_{70} = \left(\frac{dE}{dU}\right)_{70} = 2.750 \text{ volts/ft./sec.}$$

and

$$S_{80} = \left(\frac{dE}{dU}\right)_{80} = 2.875 \text{ volts/ft./sec.}$$

The calibration curves of the V-probe at 70°F, (21°C), operating with overheating ratio a = 1.05 are shown in Fig. 18, which indicate that the sensitivity varies inversely with the velocity. The variation of the sensitivities of the two films of the V-probe with the velocity is shown in Fig. 19.

7.2 Initiation and Development of the Ripple Formation

The incipient ripple formation was observed at a mean velocity of (0.60 ± 0.05) ft./sec., (0.18 ± 0.02) m/s and a flow depth of 5.0 inches (12.7 cm). The flow condition to establish a developed ripple bed was achieved at a mean velocity 25 percent higher than the incipient velocity, that is 0.75 ft./sec. (0.23 m/s) under the flow depth of 5.0 inches. The Reynolds and Froude numbers of the average flow were 30,000 and 0.2 respectively.

In the natural mobile bed only the Pitot-tube was used during the experimental measurements. The use of hot-film probes was not practical since the delicate films could have been easily destroyed by the mobile sand particles.

Pitot-tube measurements were reduced, using Eq. 7.1 to calculate velocities at different points in the flow field.

$$\frac{p_t - p_s}{\gamma_w} = \frac{U^2}{2g} = \Delta h \cdot \sin\alpha\,(S.G. \; -1) \times \frac{1}{305} \qquad 7.1$$

where

p_t - the total pressure in $lbs./ft^2$.

p_s - the static pressure in $lbs./ft^2$.

U - the velocity at the tip of the Pitot-tube in ft./sec.

g - the gravitational acceleration = 32.2 $ft./sec^2$.

sin α - the slope of the manometer = $\frac{1}{10}$

Δh - the reading of the sloping manometer in mm.

γ_w - the specific weight of water = 62.4 $lbs./ft^3$.

S·G - the specific gravity of the liquid used in the manometer = 1.75.

From Eq. 7.1 the velocity U in feet per second is related to the manometer reading Δh in mm. as

$$U = 0.1258 \sqrt{\Delta h} \qquad 7.2$$

Table 1 gives the measured sloping manometer readings along with the calculated longitudinal velocities across the width of flume, taken at 2.5 inches (6.4 cm), above the bed for sections 14 inches (36 cm), 31 inches (79 cm), and 44 inches (112 cm) downstream from the screen. Fig. 20 shows the velocity distributions of the above mentioned three cross sections. By comparison, the velocity distribution at 44 inches downstream from the screen is fairly uniform and symmetrical. Also, the ripple pattern in this vicinity is more uniform than at the two upstream sections. For these reasons the section at 44 inches downstream from the screen is adopted as an appropriate location for quantitative and/or qualitative comparison among the different experimental techniques of measurements over the different beds.

Pitot tube measurements throughout the depth of flow, at a section 44 inches (112 cm) downstream from the screen above a ripple crest were also reduced, using Eq. 7.2, to give the centreline velocity distribution. Table 2 gives the measured sloping manometer readings at different points throughout the depth of flow, along with the calculated velocities. Fig. 21 shows the velocity distribution in a dimensionless form where

$\overline{U}$ - mean flow velocity = 0.75 ft./sec., (0.23 m/s), and

D - depth of flow = 5.0 inches, (12.7 cm).

The velocity and the shear stress distributions along a ripple 44 inches downstream from the screen were estimated from Pitot-tube measurements which were taken every 0.5 inch (1.3 cm) at a normal distance of 0.125 inch (0.3 cm), above the ripple bed.

The shear stress was calculated from the analytical relation between the dynamic pressure ($p_t - p_s$) and the bed shear (τ_o) as suggested by Hwang et al in 1963, (reference 31, page 111), and given by

$$\frac{p_t - p_s}{\tau_o} = 16.53 \left\{ \left(\log \frac{30y}{Ks}\right)^2 - \log \frac{30y}{Ks} \left[0.25 \left(\frac{dp'}{2y}\right)^2 + .0833 \left(\frac{dp'}{2y}\right)^4 + .00704 \left(\frac{dp'}{2y}\right)^6\right] + \left[0.25 \left(\frac{dp'}{2y}\right)^2 + .1146 \left(\frac{dp'}{2y}\right)^4 + .0586 \left(\frac{dp'}{2y}\right)^6 + \ldots\ldots\right] \right\} \qquad 7.3$$

where

d_p' – inside diameter of the Pitot tube = .046 inch (1.2 mm);

Ks – size of roughness = 0.2 mm;

y – the normal distance measured from the ripple bed = 0.125 inch

Using Eq. 7.1 and substituting the values of y, Ks and d_p' in the appropriate dimensions, Eq. 7.3 reduces to

$$\tau_o = 1.3 \times 10^{-4} \, \Delta h \qquad 7.4$$

where

τ_o – the bed shear stress in lbs./ft^2., and,

Δh – the reading of the sloping manometer in mms.

Eqs. 7.4 and 7.2 were used to calculate the shear stress and the velocity along the ripple respectively. Table 3 gives the measured sloping manometer readings along the ripple, along with the calculated shear stresses and velocities. Fig. 22 shows the dimensionless shear stress distribution along a ripple and the velocity at a normal distance of 0.125 inch (0.3 cm) above the ripple bed where

L – length of the ripple = 2.25 inches, (5.7 cm), and

$\overline{U}$ and D as given before

An empirical formula, to estimate the sand transport rate "q_B" from the mean ripple velocity u_r, height of ripple h_r, specific gravity of sand S_s and the porosity of sand m, was suggested[(16)] as

$$q_B = \frac{h_r}{2g} \cdot u_r \cdot \gamma_w \cdot S_s \cdot (1 - m) \qquad 7.5$$

The terms on the right hand side of eq. 7.5 were evaluated from the experimental observations as

h_r = 0.2 inch = .0167 ft., (0.5 cm)

u_r = 2.8×10^{-4} ft./sec., (8.5×10^{-3} cm/s)

S_s = 2.65

m = 0.4 (assumed)

γ_w = specific weight of water = 62.4 lbs./ft^3., (9800 N/m^3)

g = gravitational acceleration = 32.2 ft./sec^2., (9.81 m/s^2)

Using the above values, the sand transport rate was estimated as 7.1×10^{-6}lbm./sec./ft., (3.5×10^{-4} Kg/s/m), at an average bed shear, from Fig. 22, $\tau_o = 2.73 \times 10^{-3}$lbs./ft^2., (0.13 Pa).

The ripple lengths and heights as obtained from the point guage measurements are given in Table 4 and shown in Fig. 23.

7.3 Hot-Film Anemometry

7.3.1 Data Reduction of the Experimental Results

The correlation $\overline{uv}$ and the turbulence intensities u' and v' were calculated from the data measured by the V-probe. A computer programme was compiled to solve the three simultaneous Eqs. 4.17, 4.18 and 4.19 in the three unknowns u', v' and $\overline{uv}$. Appendix V contains the input and output printout of this computer programme with an illustrative flow chart.

Tables 5 and 6 give the measurements taken by the V-probe at different vertical and longitudinal sections, respectively, for different beds. Tables 7 and 8 give the measurements taken by the

V-probe every 0.5 inch (1.3 cm) along a ripple, at 44 inches downstream from the screen, at 0.125 inch (0.3 cm) normal to the ripple and 2.5 inches (6.4 cm) above the bed, respectively, for both the cast and sand-roughened artificial ripple beds.

The velocity at any point, U, was calculated as the average of three values. Using the calibration curve Fig. 18, two estimates of the velocity were attained from the measured DC voltages, E_1 and E_2, sensed by the two films denoted by subscripts (1) and (2) of the V-probe respectively. The third estimate of the velocity was obtained from the Pitot-tube measurement and using Eq. 7.2. The computer results of the correlation $\overline{uv}$ and the turbulence intensities u' and v' are also shown in Tables 5, 6, 7 and 8.

The Macro and Micro scales of turbulence were calculated from the measurements taken by the wedge-probe of the normalized auto-correlation function. The normalized autocorrelation function was measured for different time delays, ranging from 0.1 to 100 mill-seconds, at different points throughout the depth of flow.

Recalling the definition of the Macro scale of turbulence Λ as given in Eq. 4.21 by

$$\Lambda = \int_0^\infty \rho(t)\, dt$$

where $\rho(t)$ is the measured normalized autocorrelation function. The area under the time correlation curve, for any point in the flow field, gives an estimate of the Macro scale of turbulence in seconds at that point.

The Micro scale of turbulence, λ, was calculated using Eq. 4.22 given as

$$\rho(t) = 1 - \frac{t^2}{\lambda^2}$$

where $\rho(t)$ is the measured normalized autocorrelation function at time delay t = 1 millsecond.

The time correlation curves at different points in the flow field for different beds are shown on Plates 1 to 10 in Appendix II.

Table 9 gives the measurements taken by the wedge-probe of the normalized autocorrelation function. The velocity at any point, U, was calculated as the average of two values. One was obtained from the measured DC voltage and the appropriate calibration curve of Fig. 17. The second was obtained from the Pitot-tube measurement and using Eq. 7.2.

Also, the longitudinal turbulence intensity, u', was calculated from Eq. 4.16 given as

$$u' = \frac{e'}{S}$$

where $e' = \sqrt{\overline{e^2}}$ is the measured RMS of the AC voltage, and,

S = the sensitivity of the wedge-probe at the operating temperature.

The Macro and Micro scales of turbulence as deduced from the graphs in Appendix II are also given in Table 9.

7.3.2 Experimental Curves

Figs. 24 to 28 show in dimensionless form, the vertical distribution of velocity $\frac{U}{\overline{U}}$, turbulence intensities $\frac{u'}{\overline{U}}$ and $\frac{v'}{\overline{U}}$, turbulence scales $\frac{\Lambda\overline{U}}{D}$ and $\frac{\lambda\overline{U}}{D}$, and Reynolds stress $\frac{-\overline{uv}}{\overline{U}^2}$, at 44 inches (112 cm) downstream from the screen, for the five different beds tested in this study, namely

1) smooth flat bed,

2) sand-roughened flat bed,

3) smooth artificial ripple bed,

4) sand-roughened artificial ripple bed, and

5) cast of the natural ripple bed.

For the smooth and sand-roughened artificial ripple beds and the cast of the natural ripple bed, the measurements were taken vertically above a ripple crest.

Figs. 29 to 33 show in dimensionless form, the vertical distribution of velocity $\frac{U}{\overline{U}}$, turbulence intensities $\frac{u'}{\overline{U}}$ and $\frac{v'}{\overline{U}}$, turbulence scales $\frac{\Lambda\overline{U}}{D}$ and $\frac{\lambda\overline{U}}{D}$ and Reynolds stress $\frac{-\overline{uv}}{\overline{U}^2}$ at 14 inches (36 cm) downstream from the screen for the five different beds. Again, for the smooth and sand-roughheded artificial ripple beds, and the cast of the natural ripple bed, the measurements were taken vartically above a ripple crest.

Figs. 34 to 36 show in dimensionless form, the vertical distribution of velocity $\frac{U}{\overline{U}}$, turbulence intensities $\frac{u'}{\overline{U}}$ and $\frac{v'}{\overline{U}}$ and Reynolds stress $\frac{-\overline{uv}}{\overline{U}^2}$ for the cast of the natural ripple bed at 21 inches, 31 inches and 37 inches, (53 cm, 79 cm and 94 cm), downstream from the screen respectively. These three sections are located at ripple crests.

Figs. 37 to 41 show in dimensionless form, the longitudinal distribution of velocity $\frac{U}{\bar{U}}$, turbulence intensities $\frac{u'}{\bar{U}}$ and $\frac{v'}{\bar{U}}$ and Reynolds stress $\frac{-\overline{uv}}{\bar{U}^2}$ at 0.125 inch (0.3 cm) above the bed for the five different beds. To exclude the variation along ripples, the measurements for the cast of the natural bed and the rough and smooth artificial ripple beds were always taken above the ripple crests.

Figs. 42 to 46 show in dimensionless form, the longitudinal distribution of velocity $\frac{U}{\bar{U}}$, turbulence intensities $\frac{u'}{\bar{U}}$ and $\frac{v'}{\bar{U}}$ and Reynolds stress $\frac{-\overline{uv}}{\bar{U}^2}$ at 2.5 inches (6.4 cm) above the bed for the five different beds.

Figs. 47 and 48 show in dimensionless form, the distribution of velocity $\frac{U}{\bar{U}}$, turbulence intensities $\frac{u'}{\bar{U}}$ and $\frac{v'}{\bar{U}}$, and Reynolds stress $\frac{-\overline{uv}}{\bar{U}^2}$ along one ripple at 44 inches downstream from the screen, at 0.125 inch (0.3 cm) normal to the ripple and 2.5 inches (6.4 cm) above the bed, for the sand-roughened artificial ripple bed and the cast of the natural ripple bed respectively.

7.4 Flow Visualization

The viscosity of a solution containing one percent by weight of milling-yellow was measured by the Synchro-Lectric viscometer. Fig. 45 shows the shear stress - shear rate relation of the solution at temperature 71°F (22°C). The dynamic viscosity of the solution that is given by the slope of the shear stress - shear rate curve is 1.75×10^{-4} lb. sec./ft^2., (8.4×10^{-3} N.s./m^2), at 71°F, (22°C).

The vertical distribution of velocity and shear stress were calculated for the milling-yellow solution flowing over

1) Cast of a developed natural ripple bed,
2) sand-roughened flat bed,
3) smooth flat bed,
4) sand-roughened artificial ripple bed,
5) smooth artificial ripple bed.

In all cases the mean velocity was maintained at 0.75 ft/sec., (o.23 m/s), and the flow depth equal to 5.0 inches (12.7 cm). The Reynolds and Froude numbers of the average flow were 3,500 and 0.2 respectively. The following calculation procedure was applied in analyzing the photographed fringe patterns, viewed through the polariscope, to estimate the velocity and sheer stress distributions, for the five different beds:

a) The fringe number and the spacing between successive fringes were estimated from the photograph;

b) from the fact that the shear stress is zero at or near the free surface, the fringes were numbered in increasing order of one towards the bed, starting with zero for the first fringe appearing near the surface;

c) the vertical distribution of the shear stress τ was calculated as a function of f, from the relationship given in Eq. 4.28 as

$$\tau = N \cdot f$$

where

N – the fringe number

f – a sensitivity constant

d) for the milling-yellow solution flow, the shear stress and the velocity were assumed to obey Newton's law of viscous flow, that is,

$$\tau = \mu \cdot \frac{dU}{dy} \qquad 7.6$$

where

μ - the dynamic viscosity of the milling-yellow solution

$\frac{dU}{dy}$ - the velocity gradient

e) from Eqs. 4.28 and 7.6 the vertical velocity distribution was also calculated as a function of the sensitivity constant f;

f) from the velocity distribution obtained in part (e), and the known average flow velocity $\overline{U}$ = 0.75 ft./sec., (0.23 m/s), the sensitivity factor f was estimated;

g) the value of the sensitivity factor "f" was used in the distributions obtained in parts (c) and (e) above, to calculate the shear stress and the velocity distributions respectively.

Table 10 gives the observed fringe number and spacing along with the calculated velocity and shear stress distributions for the five different beds at 44 inches (112 cm) downstream from the screen.

Figs. 50 to 54 show in dimensionless form, the vertical distribution of the velocity $\frac{U}{\overline{U}}$ and the shear stress $\frac{\tau}{\rho \overline{U}^2}$ as calculated in Table 10. The isoshear pattern as viewed by the polariscope and also the isovelocity distribution of the flow conditions, $\overline{U}$ = 0.75 ft./sec. and D = 5.0 inches, over the different beds, at 44 inches (112 cm) downstream from the screen, are shown in Figs. 55 to 59. Fig. 60 shows in a dimensionless form, the shear stress distributions over the five beds.

Appendix III contains some selected photographs for various flow conditions over different beds.

7.5 Experimental Errors

The experimental data was subjected to certain errors and uncertainties as described below:

A) Errors associated with the Pitot-tube measurements:

i) Instrument precision: An instrument precision of ±1%, as suggested by the manufacturer, was assumed;

ii) Reading error: This error results from the accuracy of reading the sloping manometer. An accuracy of ±0.25 mm causes possible percentage errors in the observed velocity and the average bed shear in the order of ±0.5% and ±1.0% respectively;

iii) Positioning error: An error in positioning the probe, at a specified point in the flow field, was inevitable as a result of the probe size, the refraction through the plexiglass flume and the accuracy of the measuring device. A special attention was given in positioning the probe at the 0.125 inch normal to the ripple surface. The proper inclination was achieved by placing two wedges of upper slope equal to the ripple slope under the horizontal plate holding the probe. The 0.125 inch was carefully measured and checked from the midpoint of the probe perpendicularly to the ripple surface. However, the above mentioned precautions in positioning the probe will not completely eliminate a possible error in positioning the probe. An error of ±1/32 inch still would be expected. This causes an estimate possible error in the velocity and bed shear of ±3% and ±6% respectively.

The possible net error in the velocity and shear stress resulting from the Pitot-tube measurements would be in the order of ±3.2% and ±6.4% respectively.

B) Errors associated with the hot-film anemometry measurements:

i) Instrument precision: The ±1% instrument precision, as suggested by the manufacturer, was also assumed in the anemometry instrumentation;

ii) Reading error: A fluctuation in the DC Voltage of the 55D30 Voltmeter of ±.05 volts was observed. This results in a possible error of ±1.5% in the average velocity.

The fluctuation in the RMS Voltmeter was observed as ±.01 volts. This results in a possible error in estimating the bed turbulence intensity of ±5%.

A fluctuation of $\pm .01 \times 10^{-2}(\text{Volts})^2$ was experienced in the measurements, taken by the 55D70 Analog Correlator, for the purpose of calculating the Reynolds stresses. The resulting possible error in the shear stress was estimated as ±2%.

The possible errors in the Macro and Micro scales of turbulence were estimated as ±3% and ±6% respectively. This was based on an observed fluctuation of $\pm .01\ (\text{Volts})^2$ in the normalized autocorrelation function measured by the 55D70 Analog Correlator with the Wedge-probe as the sensing element;

iii) Calibrating error: A calibration error of the hot-film probes caused by the uncertainty in plotting the calibration curve will affect the Voltage/Velocity relationship and the sensitivities of the hot-films. Accordingly, a possible error in the velocity, the shear stress, and turbulence intensity were estimated as ±6%, ±12% and ±14% respectively. This estimation was based on a possible error in establishing the calibration curves;

iv) Positioning error: Following the same argument of the positioning error of the Pitot-tube probe, the possible error in the velocity, shear stress and turbulence intensity as a result of ±1/32 of an inch positioning error of the hot-film probes were estimated as ±3%, ±4% and ±6% respectively.

The possible net error in the velocity, shear stress and turbulence intensity resulting from the hot-film anemometry measurements would be in the order of ±7%, ±13% and ±16% respectively.

C) Errors associated with the flow visualization measurements:

i) A Viscosity Error: The viscosity of the milling-yellow solution is very temperature dependent. To keep the temperature effect to a minimum, the flow visualization part of the experimental work of this study was carried out in a temperature controlled laboratory of (71 ± 2)^{o}F.

The viscosity was also affected by the duration of mixing by the pump with a tendency of decreasing viscosity with increasing time of the run, to reach an asymptotic position. To overcome this uncontrollable error, the pictures and the viscosity measurements were taken after an approximate waiting period of 15 to 30 minutes.

The combined effect on the viscosity was estimated not to be more than ±20%.

ii) An error results from the interpretation of the photographs: The number and the spacing between successive fringes were subjected to human estimation. In order to keep this error to a minimum, the slides were projected to about 1.25 the prototype size and the measurements were taken from the enlarged projection.

The possible net error in the velocity and the shear stress as obtained from the flow visualization technique is estimated as ±10% and ±30% respectively.

D) A common error in the experimental study:

A common error in setting the ripple flow condition caused by:

i) a possible error of ±0.1 inch or ±2% in the desired flow depth of 5.0 inches.

ii) a possible error of ±0.25 inch or ±2.5% in the desired orifice meter manometer reading of 10.0 inches.

The combined effect results in a possible error of ±4% in the average velocity.

A summary of all possible errors in the velocity and shear stress measurements obtained from the Pitot-tube, the hot-film anemometry and the flow visualization techniques is given in the table on the following page.

TABLE "A" - POSSIBLE ERRORS IN EXPERIMENTAL MEASUREMENTS

(% of Average Observed Values of Velocity,

Shear Stress and Turbulence Intensity)

TECHNIQUE	TYPE OF ERROR	% ERROR IN VELOCITY	% ERROR IN SHEAR STRESS	% ERROR IN TURBULENCE INTENSITY
Pitot-Tube	Instrument precision	1.0	2.0	—
	Reading	0.5	1.0	—
	Positioning	3.0	6.0	—
	Net Error	3.2	6.4	—
Hot-Film	Instrument precision	1.0	1.0	1.0
	Reading	1.5	2.0	5.0
	Calibrating	6.0	12.0	14.0
	Positioning	3.0	4.0	6.0
	Net Error	7.0	13.0	16.0
Flow Visualization	Net Error	10.0	30.0	—

CHAPTER EIGHT

RESULTS OF THE COMPUTER SIMULATION

A computer programme to alternately solve the Poisson equation and Helmholtz vorticity equation, relating the stream function ψ and the vorticity ω of the flow pattern over a ripple bed, using the finite element technique, was developed and executed on the IBM 360/50 computer at the Computer Centre of the University of Windsor.

A region length of three ripples was considered to be appropriate for the mathematical representation of the problem. The ripple length and height were chosen as 2.5 inches, (6.4 cm), and 0.2 inch, (0.5 cm), respectively. These values were the average dimensions of the ripples observed in the experimental study.

The depth of flow and the average mean velocity were also set from the experimental data as 5.0 inches, (12.7 cm), and 0.75 ft./sec., (0.23 m/s), respectively.

Solutions of two different flow conditions were obtained:

1) the turbulent model to simulate the water flow over the ripple bed;

2) the laminar model to simulate the milling-yellow solution flow over the ripple bed.

The classical constant and logarithmic vertical velocity distributions were imposed as boundary condition at the entrance section for the turbulent and laminar models respectively.

Therefore, in the turbulent model, the velocity U, was given by

$$U = \overline{U} = 0.75 \text{ ft./sec.} \tag{8.1}$$

and the stream function ψ varied linearly with the depth y as

$$\psi = \overline{U}y \tag{8.2}$$

In the laminar model, the velocity U, was given by

$$U = C \ln \frac{y}{y'} \tag{8.3}$$

where

U - the flow velocity of a point at a distance y above the datum

y' - the height above datum where the velocity vanishes, and is equal to 0.2 inch at the entrance section

C - constant

The constant C was evaluated from equating the average velocity computed from Eq. 8.3 to the known mean flow velocity $\overline{U}$ = 0.75 ft./sec., and found equal to 0.313. Therefore, Eq. 8.3 can be written as

$$U = 0.313 \ln \frac{y}{y'} \tag{8.4}$$

The corresponding stream function reads

$$\psi = 0.313\ y \left[\ln \frac{y}{y'} - 1\right] + \text{constant} \tag{8.5}$$

The constant was obtained from the boundary condition that $\psi = 0$ at $y = y'$. Therefore, Eq. 8.5 can be written as

$$\psi = .313\, y \left[\ln \frac{y}{y'} - 1\right] + .0052 \qquad 8.6$$

Five streamlines, with decreasing spacing towards the bed, were arbitrary drawn in the region. The stream functions were calculated either from Eq. 8.2 for the turbulent model or Eq. 8.6 for the laminar model. The region was divided with vertical lines spaced half an inch, then the triangular elements were formed by connecting the adjacent nodal points.

Fig. 61 shows the typical arrangement of the 6-nodes triangular elements adopted to solve Poisson equation. The number of elements is 180. The total number of nodal points is 403, with 330 interior (unknown) nodes.

Fig. 62 shows the typical arrangement of the 3-nodes triangular elements employed in solving the Helmholtz equation. It has the same number of elements (180). The total number of nodes is 112, with 75 interior (unknown) nodes.

The ψ values for both the turbulent and laminar models are shown in Figs. 61 and 62.

Flow Chart 1 shows the main steps of the whole programme. The programme is divided into three main parts:

A) Solution of Laplace Equation:

1. In the first stage of the programme, the vorticity was assumed zero in the whole region. The following steps

were performed on every element:

i) the co-ordinates of the centroid were calculated, from the assigned global co-ordinates of the nodes;

ii) the local co-ordinates of the 6-nodes were calculated with respect to local axes located at the centroid of the element;

iii) the components of the matrix [C], as defined in Eq. 3.6, were calculated;

iv) the components of the inversion of the matrix [C], that is, $[C]^{-1}$, were evaluated, using subroutine MINV;

v) the values of α, that is, $(\alpha_1, \alpha_2, \ldots \alpha_6)$, were calculated using Eq. 3.9;

vi) the velocity components, at the centroid, were calculated, using Eqs. 3.53a and 3.53b;

vii) the components of the stiffness matrix [h], as defined in Eq. 3.29, were formed.

The following integration formulae over the triangle area were used in calculating the terms of the matrix [h]:

$$\int x \, dxdy = \int y \, dxdy = 0 \qquad 8.7$$

$$\int dxdy = \frac{1}{2} \begin{vmatrix} 1 & x_i & y_i \\ 1 & x_k & y_k \\ 1 & x_m & y_m \end{vmatrix} = \text{area of the triangle} = \Delta \qquad 8.8$$

$$\int x^2 \, dxdy = \frac{\Delta}{12} (x_i^2 + x_k^2 + x_m^2) \qquad 8.9$$

$$\int y^2 \, dxdy = \frac{\Delta}{12} (y_i^2 + y_k^2 + y_m^2) \qquad 8.10$$

$$\int xy \, dxdy = \frac{\Delta}{12} (x_i y_i + x_k y_k + x_m y_m) \qquad 8.11$$

where (x_i, y_i), (x_k, y_k) and (x_m, y_m) are the local co-ordinates of the three vertices of the triangular element, satisfying the condition

$$\frac{x_i + x_k + x_m}{3} = \frac{y_i + y_k + y_m}{3} = 0$$

The steps of calculation to form the Stiffness Matrix are shown in Flow Chart 2.

2. The Assembled Equations of the system were obtained as given by Eq. 3.32, with the term $\{F\} = 0$. The calculation steps of the assembled equations are shown in Flow Chart 3.

3. A solution of the 330 linearlzed simultaneous equations was achieved using an overrelaxation iteration method. Recalling that only the elements adjacent to the node i will contribute to $\frac{\partial \chi}{\partial \psi_i}$, in forming the assembled Eq. 3.32, a band width technique was introduced to simplify the solution. Examining Fig. 61, a band width of 45, which is the largest difference between any node i and all the nodes forming the adjacent elements, was selected. Different values of the relaxation parameter (OMEGA), the tolerance factor (EPS), and the time step Δt, were tested for optimum convergence. Acceptable

values of 1.0, .001, and .02 seconds for OMEGA, EPS and Δt respectively, were chosen. The steps of the iteration method are shown in the Flow Chart 4.

At this point in the programme, the first solution of the stream function ψ, was obtained.

B). Solution of Helmholtz Equation:

The procedure used is summarized in the following steps:

1. For the first time step, the vorticities of the interior nodes, and, also, the rate of change of vorticity, that is, $\frac{\partial \omega}{\partial t}$, of all the nodes, were assumed zero.

2. i) the vorticities of the surface nodes are zero,

   ii) the vorticities of the 16-nodes along the bed, were calculated, using the method of images.

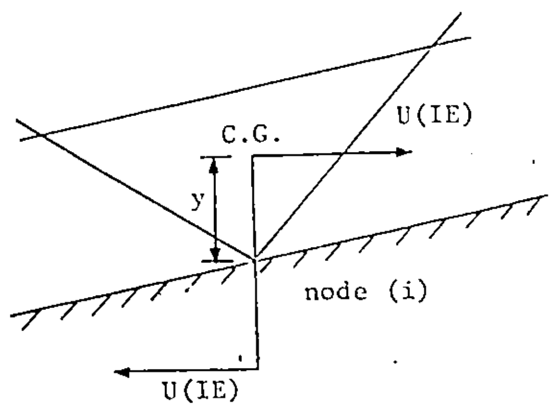

The above sketch shows the principle, where the velocity U is negatively reflected in the bed.

The vorticity can be written as

$$\omega(i) = \frac{U(IE)}{2y} \qquad 8.12$$

where

y - is the vertical distance of the centroid of the element (IE) above the bed.

iii) the vorticities of the 5-nodes at the entrance section were calculated either from Eq. 8.1 for the turbulent model, or Eq. 8.4 for the laminar model.

For the turbulent model, using Eq. 8.1, one obtains

$$\omega(i) = \frac{dU}{dy} = 0$$

and, for the laminar model, and using Eq. 8.4, gives

$$\omega(i) = \frac{dU}{dy} = \frac{.313}{y(i)}$$

where y(i) is the vertical distance of the node i above the bed, at the entrance section.

3. The following steps were performed on every element:

i) the vorticity was calculated as the arithmatic mean of the three nodal vorticities;

ii) the local co-ordinates of the 3-nodes, were calculated;

iii) the components of the matrix [CM], as defined in Eq. 3.41, were calculated;

iv) the components of the inversion of the matrix [CM], that is, $[CM]^{-1}$, were evaluated using subroutine MINV;

v) the terms β and γ were calculated using Eq. 3.54;

vi) the terms a, b and c at every node of the element, were calculated, using Eqs. 3.44a, 3.44b and 3.44c;

vii) the term $\overline{(\nu + \varepsilon)}^{e}$ was estimated according to the flow condition:

a) In the laminar model, ε was assumed equal to zero. A value, obtained from the experimental analysis of the viscosity of the milling-yellow solution, was used as:

$$\mu = 1.75 \times 10^{-4} \text{ lb.sec./ft}^2.$$

$$\rho = 1.94 \text{ slugs/ft}^3.$$

and

$$\nu = \frac{\mu}{\rho} = 9.02 \times 10^{-5} \text{ ft}^2\text{./sec.}$$

b) In the turbulent model, ε is affected by the boundary roughness. Von Kármán* suggested an expression of ε, assumed a constant within an element, in terms of the bed shear velocity and the relative elevation as:

$$\varepsilon = 0.4\sqrt{\frac{\tau_o}{\rho}}\, Z(1 - \frac{Z}{D}) \qquad 8.13*$$

where

* Reference (84), page 800

Z is the vertical distance of the centroid above the bed;

D is the depth of flow = 5.0 inches;

$\sqrt{\frac{\tau_o}{\rho}}$ is the bed shear velocity, an average value of 3.15×10^{-2} ft./sec. was selected based on the experimental results;*

and ν for water at 71°F = 1.06×10^{-5} ft^2./sec.;

viii) the term Q, in Eq. 3.51 was calculated with $\overline{C}^{e}$ defined by Eq. 3.52;

ix) the components of the stiffness matrix [h] in Eq. 3.50 were calculated;

x) the components of the matrix [p], in Eq. 3.62 were calculated where the formulae 8.7 to 8.11 were used.

The steps of the calculation are shown in Flow Chart 5.

4. The Assembled Equations of the system were obtained as given by Eq. 3.63. The assembly was constructed in two forms. The first set was built as suggested by Eq. 3.69, where the solution of the simultaneous linear equations results in the values of $\left\{\frac{\partial\omega}{\partial t}\right\}_{t=0}$, and obtained only once, that is, for the first time step. The second form of the assembly was built as given by Eq. 3.67 where the solution of the simultaneous linear equations results in the values of $\{\omega\}_t$. The steps of the calculation are shown in Flow Chart 6.

---

* The shear velocity can also be estimated as $\sqrt{gDS}$

5. The solution of the 75 linear simultaneous equations, in the unknown $\frac{\partial \omega}{\partial t}$ for the first time step and ω everytime step, was achieved by the same iteration method, used to solve for ψ. In here, the band width was 11.

6. The term $\frac{\partial \omega}{\partial t}$ in Eq. 3.67 was obtained as the solution of Eq. 3.69 for the first time step, and was calculated from Eq. 3.66, thereafter. The steps of the calculation are shown in Flow Chart 7.

C) Solution of Poisson Equation:

The values of ω, as the solution of Helmholtz equation, obtained from part (B), were inserted in the Poisson equation. The solution was achieved by following the same procedure described in part (A), with the addition of using Eq. 3.30 to calculate the term F for all the elements.

This results in a second improved solution of the stream function ψ.

D) Repeating parts (B) and (C), alternatively, a better solutions for ψ and ω, respectively, were obtained:

The final solution was achieved when the variation in the values of ω and ψ for any two successive solutions was negligible.

Once the final solution was obtained, the velocity components at the centroid of all the elements were calculated.

Also, the horizontal components of velocity, for five vertical sections 0.5 inch apart, along the length of the middle ripple were calculated.

The Finite Element Computer programme for both the laminar and turbulent models is given in Appendix V.

Figs. 63 and 64 show the finite element solution of the stream function for the laminar and turbulent flow models respectively.

Figs. 65 and 66 show in dimensionless form, the calculated vertical velocity distributions along the middle ripple for the laminar and turbulent models respectively.

Fig. 67 shows in dimentionless form, the variation of velocity $\frac{U}{\bar{U}}$ and shear stress $\frac{\tau_o}{\rho \bar{U}^2}$ distributions along the middle ripple at 0.125 inch above the bed for the laminar and turbulent models.

Tables 11 and 12 give the calculated shear stress, based on the computer velocity results. The following equations were used in the shear stress computations:

$$\tau_o = \mu_m \frac{dU}{dy} \qquad \text{for the laminar model}$$

$$\tau_o = (\mu_w + \lambda) \frac{dU}{dy} \qquad \text{for the turbulent model}$$

where

τ_o - the bed shear stress

μ_m - the dynamic viscosity of the milling-yellow solution

μ_w - the dynamic viscosity of water

λ - the eddy viscosity = $\frac{\varepsilon}{\rho}$

$\frac{dU}{dy}$ - the velocity gradient

FLOW CHART I General Layout of the Computer Programme of the finite element solution

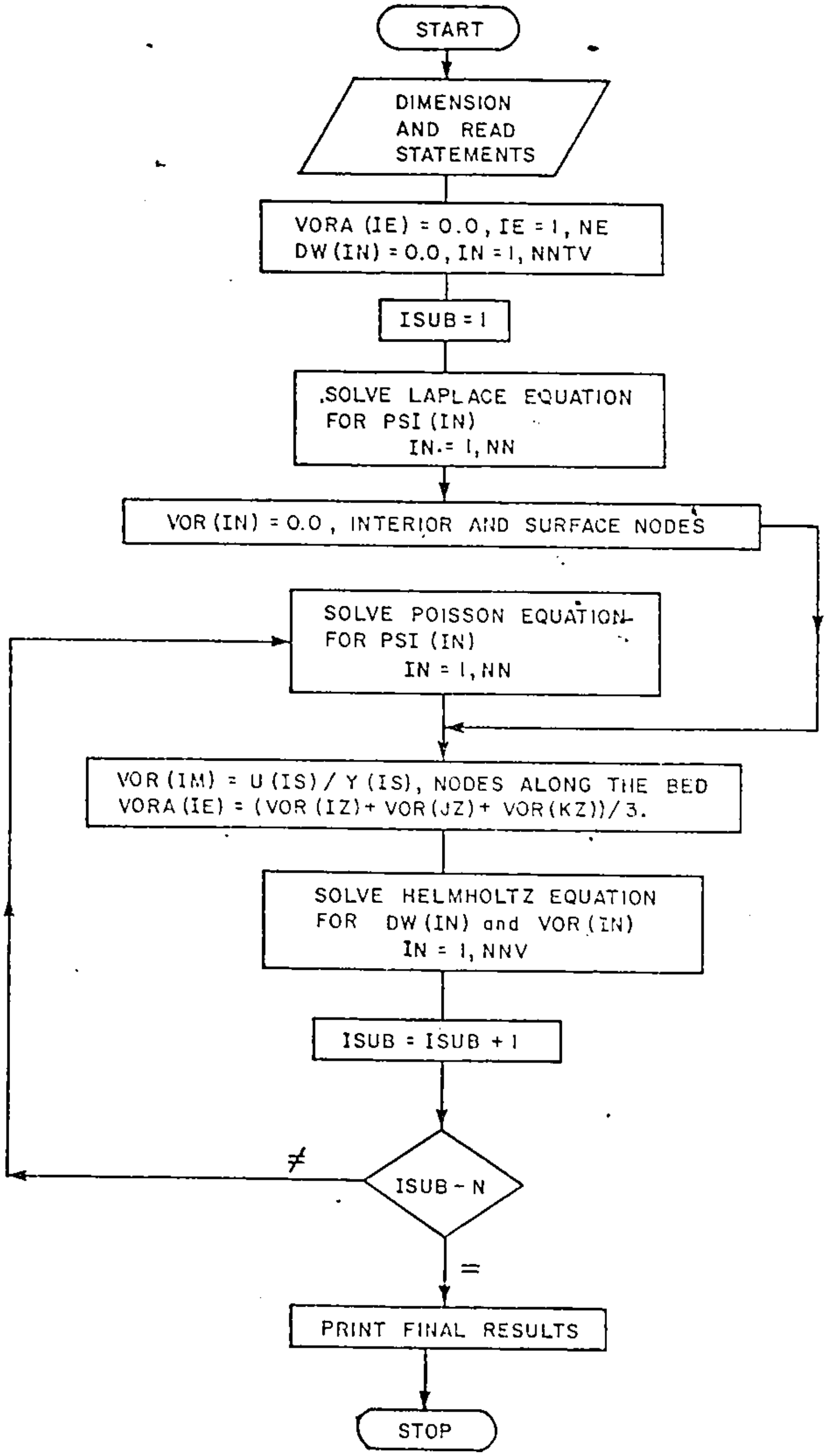

$DW = \frac{\partial \omega}{\partial t}$

VORA = VORTICITY OF AN ELEMENT

VOR = VORTICITY OF A NODE

FLOW CHART 2 STIFFNESS MATRIX [H] - Poisson Equation

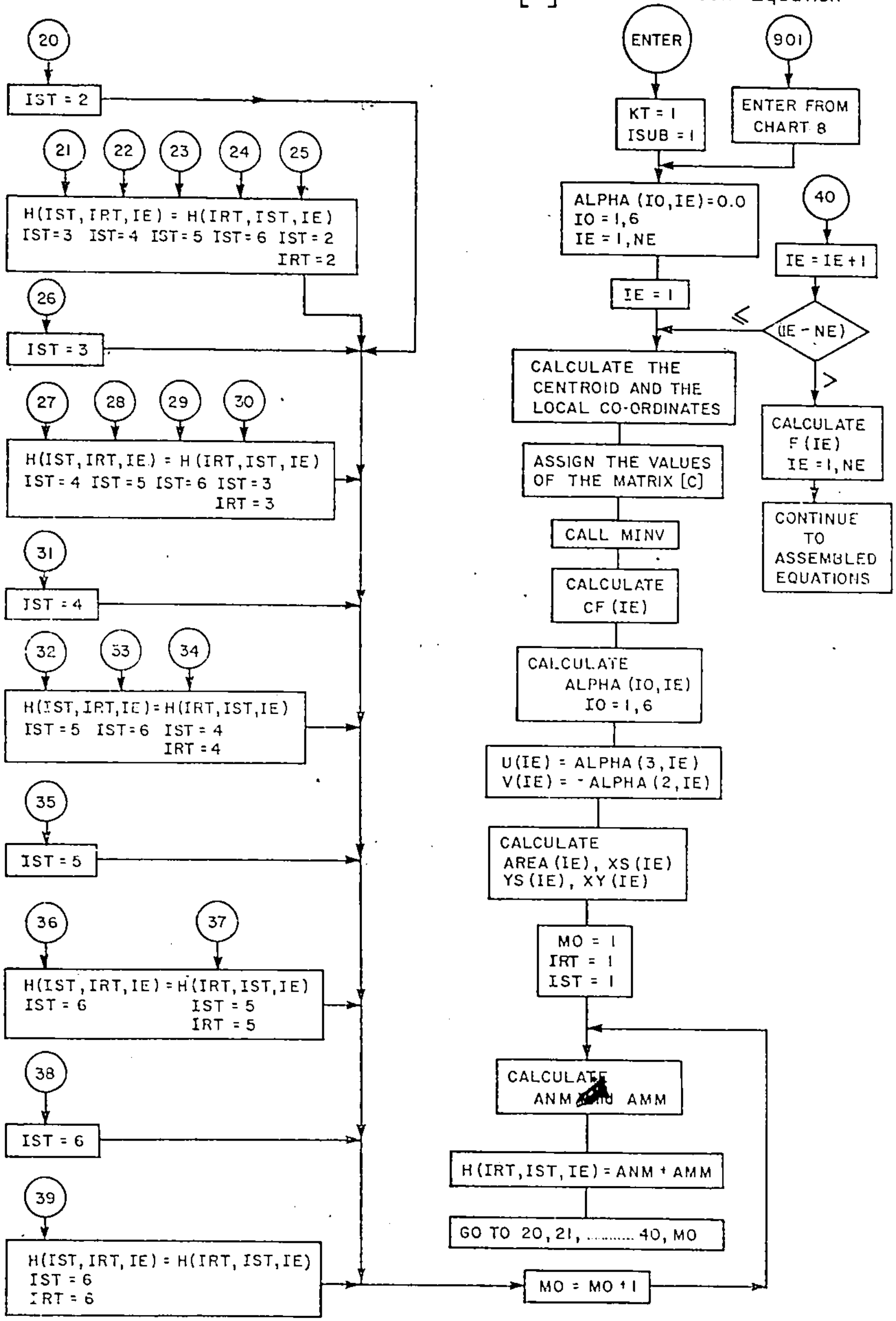

FLOW CHART 3 Assembled Equations - Poisson Equation

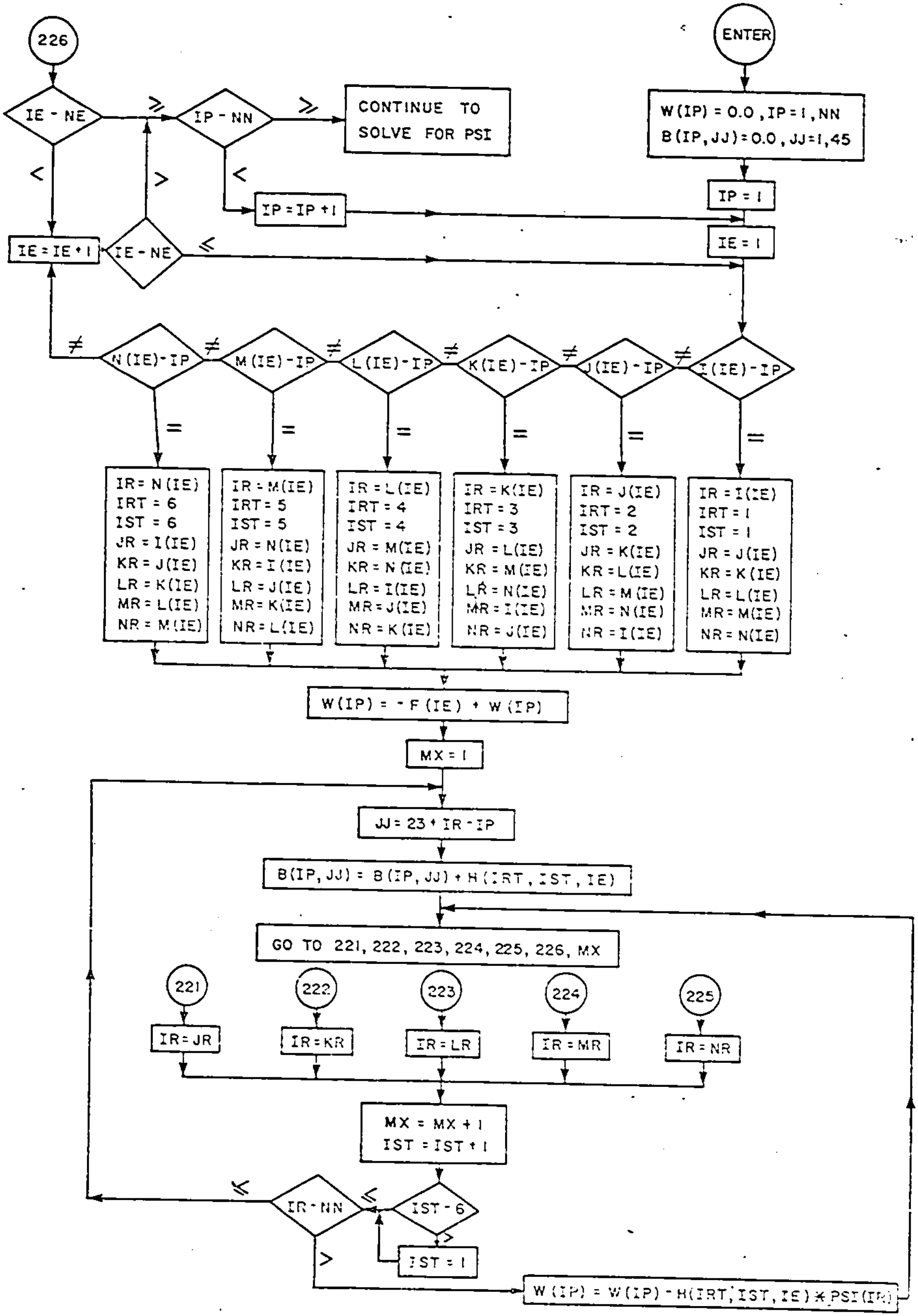

FLOW CHART 4 Solve for PSI - Poisson Equation

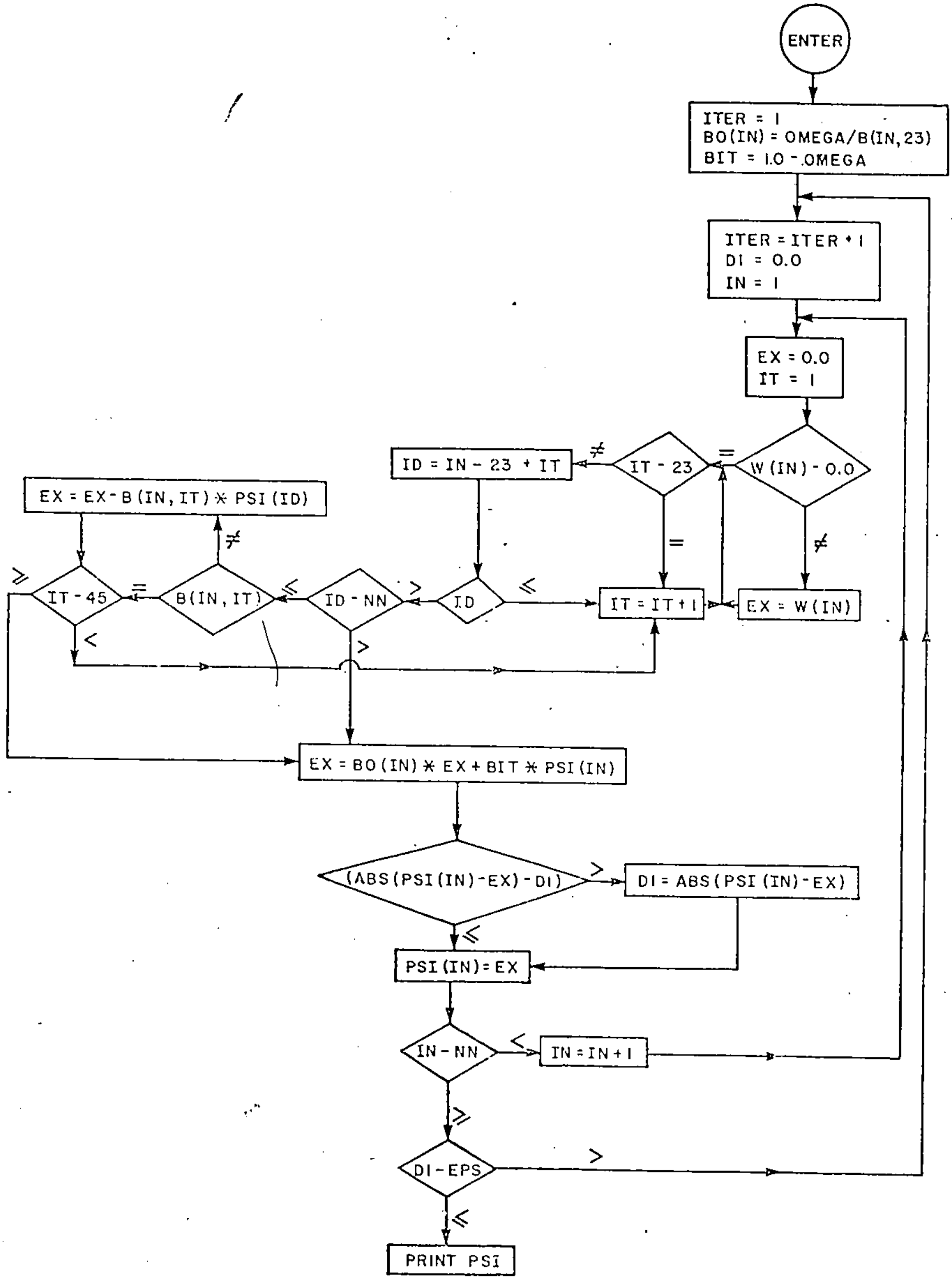

FLOW CHART 5 STIFFNESS MATRICES BPC and P = Helmholtz Equation

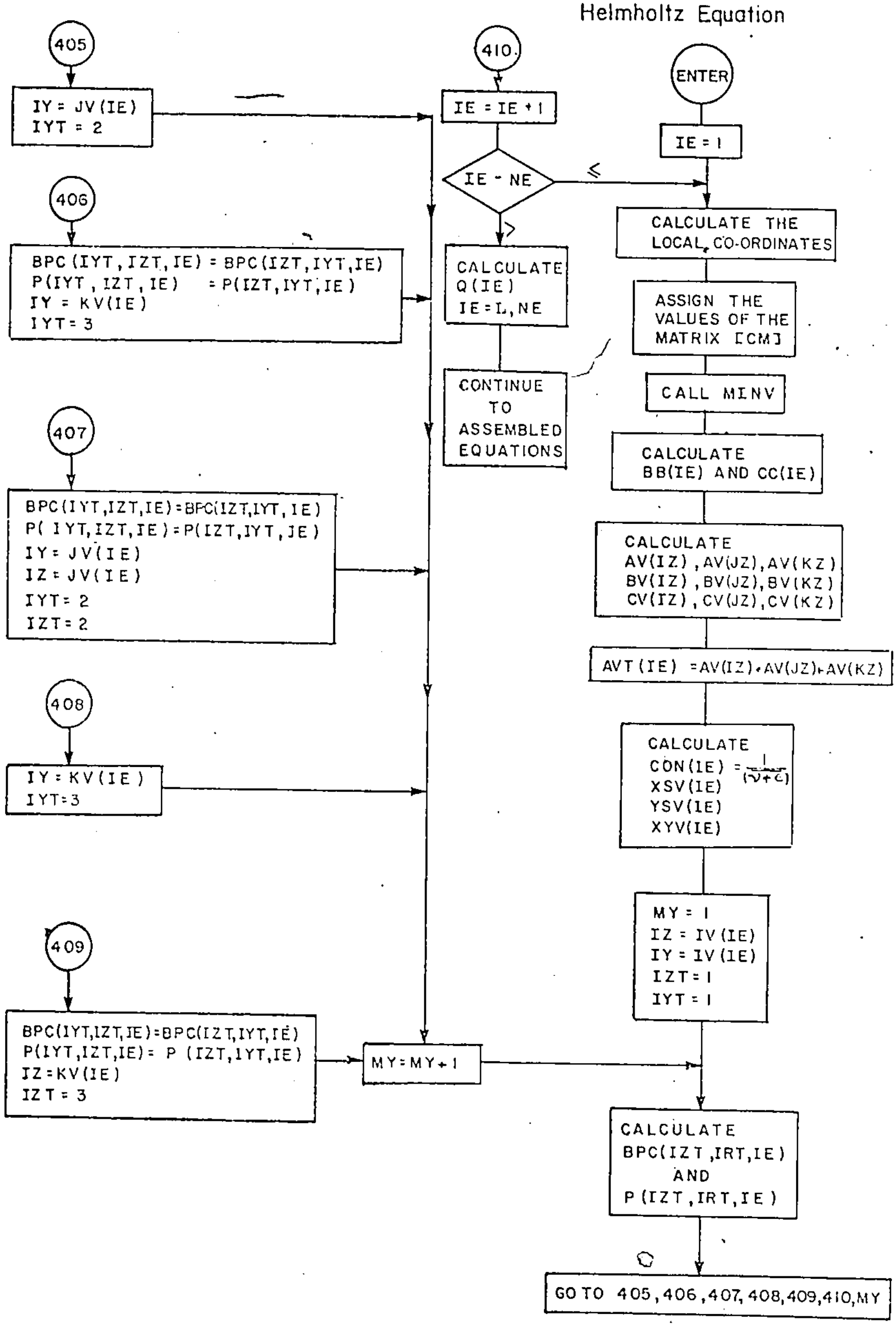

FLOW CHART 6 Assembled Equations - Helmholtz Equation

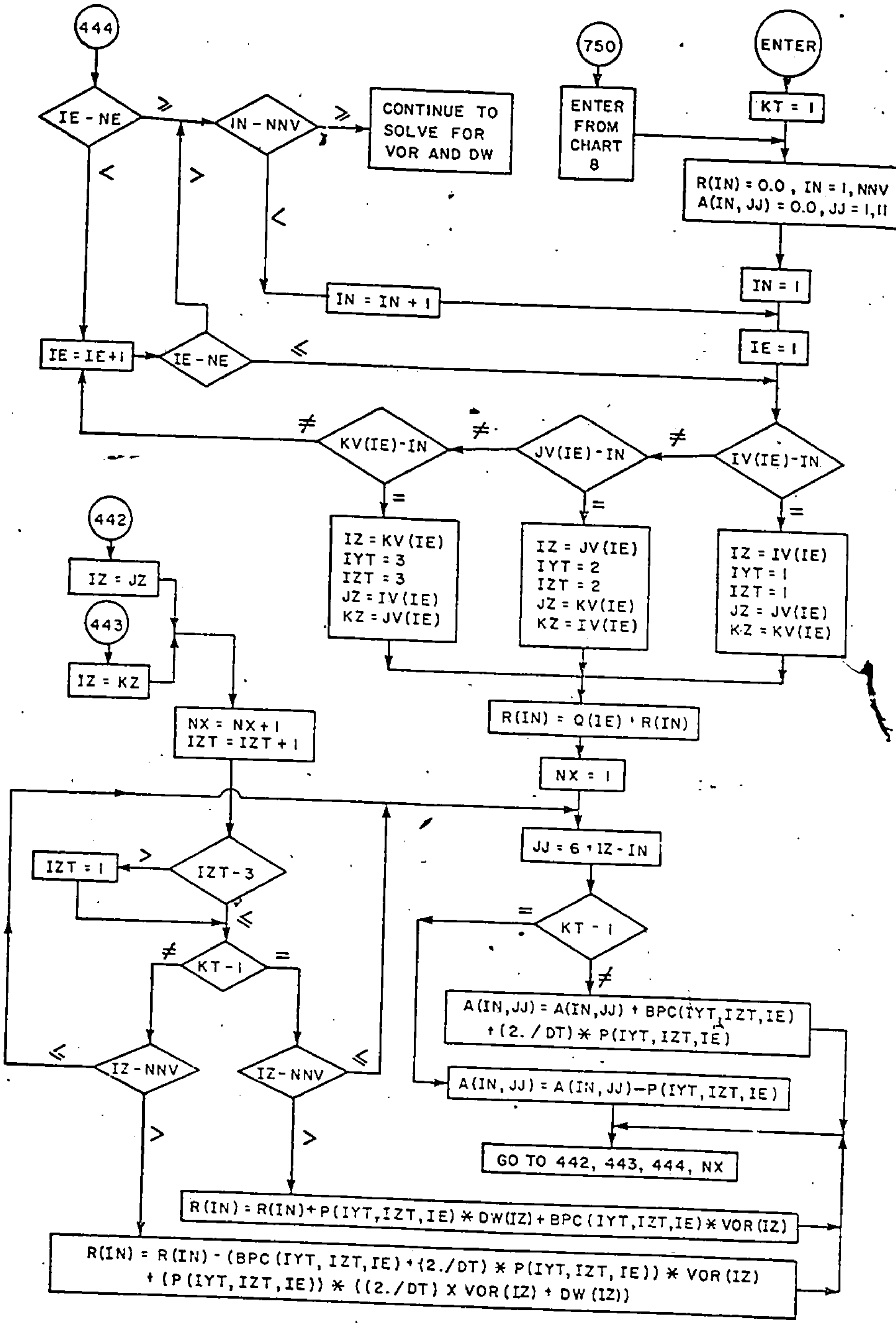

FLOW CHART 7 Solve for VOR and DW.- Helmholtz Equation

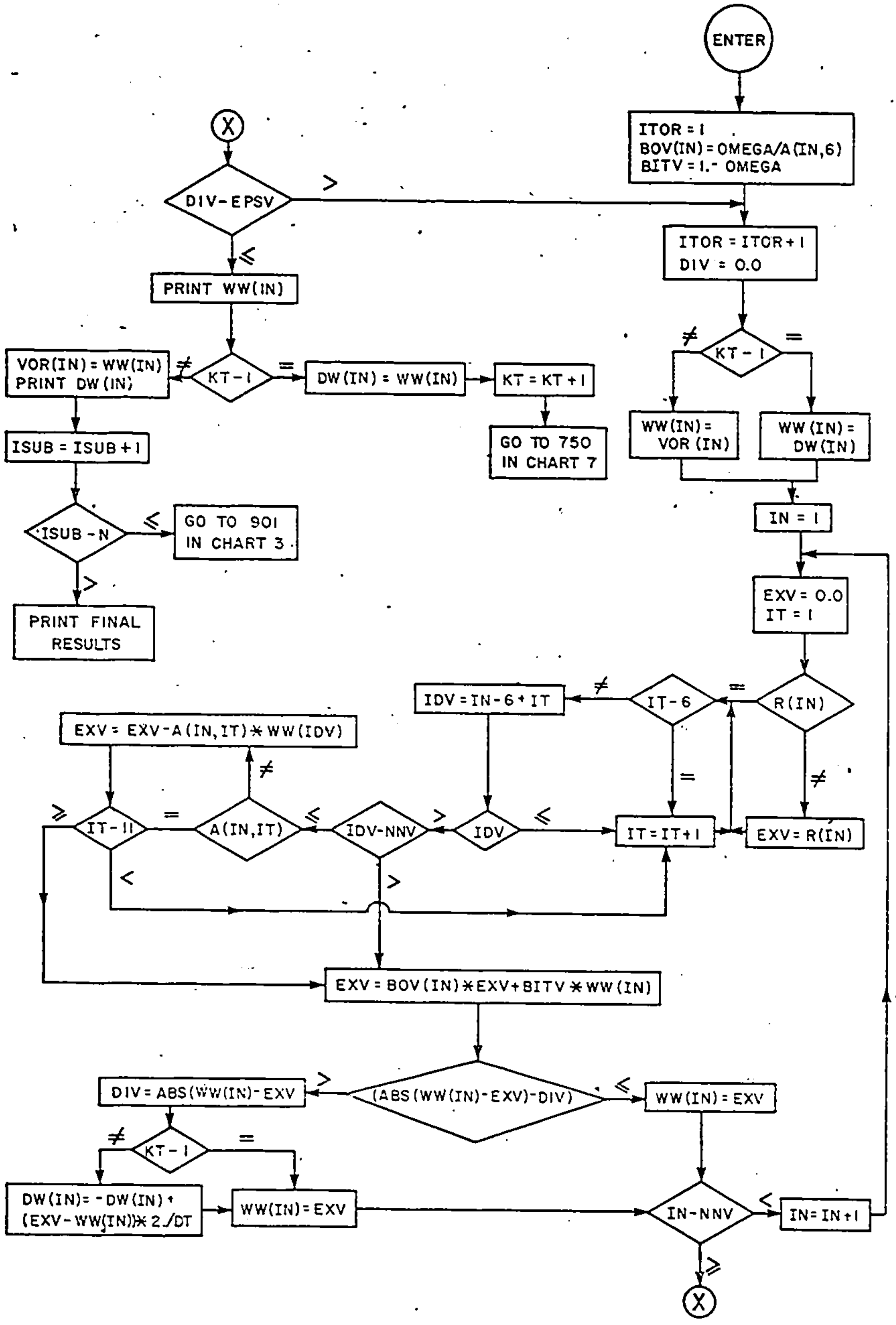

CHAPTER NINE

ANALYSIS AND DISCUSSION

An analysis and discussion of the experimental and mathematical results of this research is presented. This is followed by a comparison of the results of this study and those obtained from other researchers.

9.1 Discussion of the Experimental Data

9.1.1 Ripple Dimensions

Fig. 23 shows the variation of ripple lengths and heights along the centreline of the flume. Larger ripples labelled 1 through 7, (Zone I), of average length $\overline{L}_1$ = 3.55 inches (9.0 cm), and average height $\overline{h}_1$ = 0.43 inch (1.1 cm) occured at the entrance of the flume and extended to 35 inches downstream from the screen. Further downstream smaller size ripples labelled 8 through 14, (Zone II), with an average length of 2.25 inches (5.7 cm), and average height of 0.20 inch (0.5 cm) were observed. Statistical analysis on the ripple sizes (length and height) in the two zones was carried out to examine whether the ripple sizes in Zone I differ significantly from those of Zone II. First, F-tests were performed to investigate the validity of applying t-tests on the data. At the 5% level of significance the difference between the variances is not significant for both the length and height of ripples in the two zones. This verifies the applicability of the t-test, which in turn showed that the probability of the ripples in the two zones to be similar is less than 0.1%. In conclusion, the ripples in Zone I are significantly different than those in Zone II. Table 13 summarizes the statistical steps of performing the F and t-tests.

9.1.2 General Comments and Trends on the Hot-Film Anemometry Experimental Curves

Figs. 24 to 28 of the dimensionless vertical distribution of longitudinal velocity $\frac{U}{\overline{U}}$, turbulence intensities $\frac{u'}{\overline{U}}$ and $\frac{v'}{\overline{U}}$, turbulence scales $\frac{\Lambda\overline{U}}{D}$ and $\frac{\lambda\overline{U}}{D}$, and Reynolds stress $\frac{-\overline{uv}}{\overline{U}^2}$ in Zone II at 44 inches (112 cm) downstream from the screen for the five different beds indicate:

1) The turbulence intensities and the shear stress increase from the free surface towards the bed.

2) The mean average longitudinal turbulence intensity measured at half depth of flow $\frac{d}{D} = 0.5$ for the five different beds is $\frac{u'}{\overline{U}} = 0.052$ with standard deviation S = 0.0[illegible]51. Zone II with a turbulence level less than 0.06 is arbitrarily defined as the zone of low turbulence.

3) At 0.125 inch above the bed, the shear stress and the turbulence intensities of the rigid cast of the natural ripple bed are 4 to 10 percent less than those measured above the rough artificial ripple bed, and 15 to 30 percent higher than those obtained from measurements above the rough flat bed.

4) At 0.125 inch above the bed, the shear stress and the turbulence intensities of the smooth artificial ripple bed are 10 to 15 percent less than those measured above the rough artificial ripple bed.

5) At 0.125 inch above the bed, the shear stress and the turbulence intensities of the rough and smooth flat bed vary by not more than 5 percent.

6) The turbulence scales approach a maximum at $\frac{d}{D}$ = 0.3 to 0.5, where $\frac{d}{D}$ is the ratio of the height above the bed, at the point of measurement to the depth of flow.

7) The macro to micro scales of turbulence bears a mean ratio of $\frac{\Lambda}{\lambda} = 8.5$ with standard deviation S = 1.39.

8) The macro scale of turbulence near the ripple surface expressed in the units of length ($\Lambda\bar{U}$) for the smooth artificial ripple, rough artificial ripple, and the cast of the natural ripple beds are 0.22 inch (0.56 cm), 0.28 inch (0.71 cm), and 0.29 inch (0.74 cm), respectively are in the same order as the ripple height of 0.2 inch (0.51 cm) and 0.22 inch (0.56 cm) for the artificial ripple and the rigid natural beds, respectively. It should be noted that the Taylor hypothesis of the relationship between the turbulence scales expressed in the units of time or length given by $\frac{\partial}{\partial t} = -\bar{U}\frac{\partial}{\partial x}$ is an approximate one and only applicable if the turbulent field is homogeneous in its average statistical structure.

9) The turbulence intensities indicate isotropic turbulence in the upper 1/2 to 2/3 of the flow depth. The non-isotropic turbulence is more pronounced near the bed.

Figs. 29 to 33 of the dimensionless vertical distribution of longitudinal velocity $\frac{U}{\bar{U}}$, turbulence intensities $\frac{u'}{\bar{U}}$ and $\frac{v'}{\bar{U}}$, turbulence scales $\frac{\Lambda\bar{U}}{D}$ and $\frac{\lambda\bar{U}}{D}$ and the Reynolds stress $\frac{-\overline{uv}}{\bar{U}^2}$, in Zone I, at 14 inches (36 cm) downstream from the screen for the five different beds indicate:

1) The maximum values of the shear stress and the turbulence intensities occur at $\frac{d}{D}$ = 0.3 to 0.5, decreasing, rather irregularly, towards the water surface and the bed.

2) The turbulence intensities at the free surface are higher than their values at the bed (except for the cast rigid ripple bed).

3) The mean average longitudinal turbulence intensity measured at half depth of flow $\frac{d}{D}$ = 0.5, for the five different beds is $\frac{u'}{\bar{U}}$ = 0.113 with standard deviation $\hat{S}$ = .0106. Zone I with turbulence level higher than 0.10 is arbitrarily defined as the zone of high turbulence.

4) The turbulence scales in the high turbulence zone are about twice as high as the corresponding values measured in the low turbulence zone.

5) The turbulence intensities indicate non-isotropic turbulence throughout the depth of flow.

Figs. 34 to 36 show the dimensionless vertical distribution of longitudinal velocity $\frac{U}{\bar{U}}$, turbulence intensities $\frac{u'}{\bar{U}}$ and $\frac{v'}{\bar{U}}$ and Reynolds stress $\frac{-\overline{uv}}{\bar{U}^2}$ for the cast rigid natural ripple bed at three intermediate sections, 21 inches, 31 inches and 37 inches, (53 cm, 79 cm, and 94 cm), downstream from the screen. They demonstrate the gradual change in the shear stress and turbulence intensities (shapes and values) from those shown in Figs. 33 and 28 taken at 14 inches (36 cm) and 44 inches (112 cm) downstream from the screen, respectively.

Figs. 37 to 41 of the dimensionless distribution of longitudinal velocity $\frac{U}{\bar{U}}$, turbulence intensities $\frac{u'}{\bar{U}}$ and $\frac{v'}{\bar{U}}$ and Reynolds stress $\frac{-\overline{uv}}{\bar{U}^2}$

at 0.125 inch (0.3 cm) above the bed for the five different beds along the centreline of flume indicate that the measured quantities vary along the length of flume with the general tendency of decreasing in the downstream direction. It should be noted that the distribution of the measured quantities does not reflect the variation along ripples since the measurements were always taken above crest points for the cast of the natural ripple bed and the sand-roughened and smooth artificial ripple beds. These measurements indicate that a turbulent boundary layer exists at y/D = 0.025, through the measured portion of the bed.

Figs. 42 to 46 of the dimensionless distribution of longitudinal velocity $\frac{U}{\overline{U}}$, turbulence intensities $\frac{u'}{\overline{U}}$ and $\frac{v'}{\overline{U}}$ and Reynolds stress $\frac{-\overline{uv}}{\overline{U}^2}$ at 2.5 inches (6.4 cm) above the bed for the five different beds along the centreline of flume indicate that the turbulence intensities and the shear stress decrease rapidly along the first 10 inches (25 cm) of flume and continue to decrease in the downstream direction, yet reach more stabilized values at about 35 inches (89 cm) downstream from the screen (the zone of low turbulence). This is an indication of continual dissipation of the grid turbulence and the establishment of the fully developed flow in the downstream direction.

Figs. 47 and 48 of the dimensionless distribution of velocity $\frac{U}{\overline{U}}$, turbulence intensities $\frac{u'}{\overline{U}}$ and $\frac{v'}{\overline{U}}$ and Reynolds stress $\frac{-\overline{uv}}{\overline{U}^2}$ along one ripple at 44 inches downstream from the screen, at 0.125 inch (0.3 cm) normal to the bed, i.e., y/D = .025, or, $y/\delta_1 = 5.7$, and 2.5 inches (6.4 cm) above the bed, i.e., y/D = .50, for the rough artificial ripple bed and the cast of the natural ripple bed, respectively indicate:

1) At y/D = .025, i.e., 0.125 inch (0.3 cm) normal to the bed, the shear stress increases gradually, moving downstream along the ripple, approaching a maximum value at $\frac{l}{L} \approx 0.4$, then decreases slightly up to the ripple crest, where $\frac{l}{L}$, at the point of measurement, is the ratio of the distance measured downstream from the crest of the previous ripple to the ripple length.

2) A wake in the lee of the previous ripple, due to separation, causes the measured quantities at y/D = .025, i.e., 0.125 inch (0.3 cm) normal to the bed to reach zero and reverse in the range $\frac{l}{L} = 0.0$ to 0.15.

3) At y/D = .025, i.e., 0.125 inch (0.3 cm) normal to the bed, the measured turbulence intensities and the Reynolds stress for the cast of the natural ripple bed vary by not more than 4 percent from those obtained for the rough artificial ripple bed.

4) At y/D = 0.5, i.e., 2.5 inches (6.4 cm) above the bed, the turbulence intensities and the shear stress decrease slightly moving in the downstream direction.

9.1.3 General Comments on the Flow Visualization Experimental Curves

Figs. 50 to 54 of the dimensionless vertical distribution of longitudinal velocity $\frac{U}{\bar{U}}$ and shear stress $\frac{\tau}{\rho \bar{U}^2}$ above the ripple crest at 44 inches (112 cm) downstream the screen for the five different beds indicate:

1) The bed shear stress over the cast natural ripple bed is slightly higher (10%) than the bed shear over the rough artificial ripple bed. This is within the possible 30% experimental error in the shear stress measurements by the flow visualization technique.
2) Under the same flow conditions and bed geometry, the bed shear for the sand-roughened bed is about 50% higher than that for the smooth plexiglass bed. The higher shear stress over the sand-roughened bed is partly due to the effect of grain roughness and also due to the non-Newtonian behaviour of the milling-yellow solution. The milling-yellow solution has long chain molecules that may accumulate on the sand grains and exaggerate the friction to an extent of possible earlier transition from laminar to turbulent boundary layer.
3) There is no appreciable difference in the shear stress calculated for the flat and artificial ripple beds of the same texture (smooth or rough).
4) The vertical distribution of longitudinal velocity follows the parabolic distribution of laminar flow.

Figs. 55 to 59 of the isoshear and isovelocity distributions for the five different beds indicate:

1) For a rough boundary, the fringe pattern, near the bed, shows

greater density than that viewed for a smooth boundary.

2) Separation of flow just downstream from the ripple crest, extending to $\frac{l}{L} \approx 0.15$, is clearly visible.

Fig. 60 shows the shear stress distribution in a dimensionless form, $\frac{\tau}{\rho U^2}$, along a ripple for the smooth and sand-roughened artificial ripple beds and the cast of the natural ripple bed estimated from the isoshear patterns at 0.125 inch normal to the ripple surface. The estimated shear stresses at 0.125 inch above the sand-roughened and smooth flat beds are also indicated on Fig. 60.

The flow visualization qualitative results of this study have proven their merit as a visual tool in examining the shear pattern in the flow field and the separation and reattachment in the lee of the ripple. However, the quantitative results of the velocity and shear stress adopting the Newtonian approach of the relation between the shear stress and the velocity gradient obviously has its limitations when applied on a non-Newtonian fluid. Also the high estimated error (±20%) in determining the viscosity of the milling-yellow solution would directly affect the accuracy in the shear stress calculations.

9.2 Discussion of the Mathematical Model

9.2.1 General Comments

Figs. 63 and 64 show the finite element solution of the stream function for the laminar and turbulent flow models, respectively. The solution gives the reattachment in the lee of the ripples as a result of flow separation. The separation in both models occured at $\frac{l}{L} = 0$ and the reattachment at $\frac{l}{L} \approx 0.15$. This agrees with the experimental observations in the milling-yellow and water flows, as illustrated in Figs. 57 and 47 respectively.

Figs. 65 and 66 show the calculated vertical velocity distributions along the middle ripple for the laminar and turbulent models, respectively. In the laminar flow model, the velocity profiles follow the parabolic distribution. They compare quite well with the velocity distribution, (Fig. 52), obtained from the flow visualization study. In the turbulent flow model, the velocity is almost constant throughout the depth of flow, except close to the bed, where it decreases in the zone $\frac{d}{D} \leq 0.1$, to reach zero at the bed.

Fig. 67, of the variation of velocity $\frac{U}{\bar{U}}$, and shear stress $\frac{\tau}{\rho \bar{U}^2}$ along the middle ripple at 0.125 inch above the bed for the laminar and turbulent models indicates:

> Moving downstream along the ripple, the shear stress is zero or negative in the range of $0 \leq \frac{l}{L} \leq 0.15$, then increases to reach a stabilized value at $\frac{l}{L} \approx 0.3$. This shear stays almost constant in the range $0.3 \leq \frac{l}{L} \leq 0.8$. Moving further downstream, the shear stress increases slightly to reach its maximum value at the crest. The same trend applied to the velocity.

9.2.2 Limitations of the Mathematical Model

The finite element model was subjected to the following errors or limitations:

1) Errors of idealization: In developing the finite element model, it was assumed that the physical system was two dimensional. The side wall effect certainly has an appreciable role in discrediting

this assumption. This would be a contributing factor to the difference between the experimental and numerical results.

2) Discretization and grid size errors: In theory, the true minimizing distribution is only achieved as the element size approaches zero. However, a reasonable grid distribution was chosen, in which the element size was inversely proportional to its importance. The elements near the bed had the smallest areas, while the free surface elements had the largest areas. It is believed that the grid used in computation is an acceptable compromise between the element density and the computation time.

3) Limitation of the governing equations and the assumed boundary conditions: The following assumptions used in the numerical solution of the finite element technique are open to questions:

   i) using Eq. 8.13, to estimate the eddy viscosity ε in the term $\overline{(\nu + \varepsilon)}$ for the turbulent model;

   ii) the assumption that the convective term in Helmholtz equation is a constant within an element;

   iii) the imposed boundary condition, based on the method of images, to calculate the vorticities along the bed;

   iv) The effect of neglecting the change in momentum transfer caused by wake turbulence;

   v) the imposed rectangular and logarithmic vertical velocity distributions at the entrance section for the turbulent and laminar models respectively. These velocity distributions, assumed as the upstream boundary condition, would probably lead to a slightly higher bed shear, since the development length of three ripples is rather short. This could be improved by re-cycling the computed downstream velocity profile;

vi) the selected parameters Δt, OMEGA and EPS as .02 seconds, 1.0 and .001, respectively, as well as the number of time steps could have a minor influence on the final results.

In general, all the above mentioned assumptions are acceptable in that a stable solution was achieved. For future research, modifications and refinements on these assumptions should help to improve the accuracy of the simulation.

9.3 Correlation of the Experimental and Mathematical Results

9.3.1 Experimental Results

The experimental measurements taken along the rough artificial ripple bed and the cast of the natural ripple bed are further investigated to examine the significance of the observed differences. The procedure to achieve a meaningful evaluation is to plot the results obtained over the rough artificial ripple bed with their ranges of experimental error. The results obtained from measurements over the cast of the natural ripple bed are also indicated on the same curves. The magnitude of the experimental errors is given in Table A.

Fig. 68 shows in dimensionless form the correlation obtained from the hot-film anemometry measurements over the cast natural and rough artificial ripple beds of the velocity, turbulence intensities and the shear stress. Fig. 69 shows in dimensionless form the correlation obtained from the Pitot-tube measurements over the cast natural and rough artificial ripple beds of the velocity and the shear stress.

The variation of the measured values over the cast of the natural ripple bed, as shown, lies within the experimental error of the corresponding values measured over the rough artificial ripple bed. This leads to the conclusion that a two-dimensional ripple bed can reproduce the main turbulence features of the flow over the three-dimensional cast of a natural ripple bed.

A comparison between the hot-film anemometry and the Pitot-tube experimental techniques was accomplished. A calibration factor (cor) was first determined by plotting the shear stress measurements, $\frac{\tau_o}{\rho\bar{U}^2}$, taken by the Pitot-tube versus the Reynolds stresses $\frac{-\overline{uv}}{\bar{U}^2}$ calculated from the hot-film measurements. Fig. 70 shows all the measurements taken at 0.125 inch normal to the bed for the sand-roughened flat, sand-roughened artificial ripple and the cast of the natural ripple beds. The measurements at mid-flow depth in the zone of low turbulence are also indicated in Fig. 70, where the shear stress τ was calculated from, $\tau = \tau_o\ (1 - y/D)$. The fitting of the best line in the form $\frac{\tau_o}{\rho\bar{U}^2} = \text{cor.} \left(\frac{-\overline{uv}}{\bar{U}^2}\right)$, that is based on the method of least squares, yielded an overall calibration factor cor = 1.35.

This means that on a statistical basis, the shear stress measured by the Pitot-tube is 35% higher than that measured by the hot-film technique. However, the high calibration factor of 1.35 can be explained partly by position difference. This is due to the fact that the shear stress measured by the Pitot-tube is the bed shear at the ripple surface, while the hot-film anemometry estimates the shear stress at the point of measurement, i.e., 0.125 inch above the ripple surface. Examining Figs. 27 and 28 of the vertical shear stress distribution, a factor of 1.15 representing the ratio of bed shear and the shear stress at 0.125 inch above the bed was estimated.

Figs. 71 and 72 illustrate the comparison between the hot-film anemometry and the Pitot-tube techniques in measuring the velocity at 0.125 inch normal to the ripple and the bed shear stress over the sand-roughened artificial ripple and the cast of the natural ripple beds respectively. The shear stresses measured by the hot-film were multiplied by 1.15, and the increased values were assumed to represent the bed shear. Figs. 71 and 72 indicate that:

1) The shear stress variation along the ripple measured by the hot-film anemometry and the Pitot-tube techniques has the same trend.

2) The shear stresses measured by the two techniques are almost within the range of experimental error. However, the shear stresses measured by the Pitot-tube are consistently (10 to 20)% higher than that measured by the hot-film anemometry.

3) The velocities measured by the two techniques are within the range of experimental error in the zone $0.3 < \frac{l}{L} < 0.8$. However, the hot-film technique showed higher velocities than those measured by the Pitot-tube for $\frac{l}{L} > 0.8$ and $\frac{l}{L} < 0.3$.

9.3.2 Experimental and Mathematical Results

Fig. 73 shows the shear stress variation along a ripple obtained from:

i) the mathematical model of the turbulent flow condition;

ii) the Pitot-tube measurements over the natural mobile ripple bed;

iii) the Pitot-tube and the hot-film anemometry measurements over the rough artificial ripple bed.

The factor of 1.15 is again applied to the hot-film measurements. The increased shear stress is assumed to indicate the bed shear. From these curves, it is noted:

1) The variation in the shear stress measured by the Pitot-tube over the mobile and the sand-roughened artificial ripple beds lies within the range of experimental error for $\frac{l}{L} \geq 0.4$. However, the shear stress over the mobile bed is about (5 to 10)% higher than that measured over the sand-roughened artificial ripple bed for $\frac{l}{L} \leq 0.8$.

2) The shear stress obtained from the turbulent mathematical model correlates reasonably well with the shear stress measured experimentally by the Pitot-tube for $\frac{l}{L} \leq 0.8$.

3) The shear stress obtained from the mathematical model has its highest value at the ripple crest. This was not observed experimentally by either the hot-film anemometry or the Pitot-tube techniques. The probable explanation is that the momentum transfer and thus the shear stress near the crest in the physical model has been affected by the upstream wake; this was not incorporated in the mathematical model.

Fig. 74 shows the shear stress variation along a ripple obtained from:

i) the mathematical model of the laminar flow condition;

ii) the flow visualization technique over cast of the natural ripple and smooth and sand-roughened artificial ripple beds.

From these curves, it is noted:

1) The shear stress estimated from the flow visualization technique over the cast of the natural ripple and the sand-roughened artificial

ripple beds is (30 to 40)% higher than that obtained from the mathematical laminar flow model.

2) The results of the mathematical laminar model is only 10% higher than that obtained by the flow visualization technique over the smooth artificial ripple bed.

In conclusion, the mathematical laminar model is more represented by the milling-yellow solution flow over smooth ripple bed. As pointed earlier, sand bed friction is possibly exaggerated by the accumulation of long chain molecules on the sand grains that may cause earlier transition from laminar to turbulent boundary layer.

9.3.3 Boundary Layer Theory

The following section is an attempt to apply the boundary layer theory as a qualitative explanation for the experimental and mathematical results obtained in this study.

A boundary layer will develop along the ripple starting downstream from the wake. Applying the momentum principle, an equation in the form

$$\tau_o \simeq \frac{C\rho U^2}{(R_x)^n} = \frac{C\rho U^2}{\left(\frac{Ul_x}{\nu}\right)^n} \qquad 9.1^*$$

can be deduced where

τ_o is the boundary shear stress;

C is a constant;

n is an exponent.

C and n vary according to whether the boundary layer is laminar or turbulent.

---

* Reference (100) pp. 262 to 264

For laminar boundary layer*

$C = 0.322$ and $n = 0.5$

For turbulent boundary layer*

$C = .029$ and $n = 0.2$

R_x is the Reynolds number based on a representative length l_x;

ν and ρ are the kinematic viscosity and the density of the flowing fluid, respectively;

$l_x = l_o + x_*$

where

x_* = the distance measured from the reattachment to the point of measurement;

and $l_o \propto$ the ripple length "L".

For the purpose of this analysis, one may assume

l_o = one ripple length = L

U is the velocity of the undistrubed flow outside the laminar sublayer in the turbulent flow case

Substituting the above constants in Eq. 9.1 one obtains:

In the case of laminar boundary layer:

$$\tau_o = \frac{0.322\ \rho\ \nu^{0.5}\ U^{1.5}}{l_x^{0.5}} \qquad 9.2$$

and, in the case of turbulent boundary layer

$$\tau_o = \frac{.029\ \rho\ \nu^{0.2}\ U^{1.8}}{l_x^{0.2}} \qquad 9.3$$

The effect of the grain roughness on the boundary layer was evaluated

---

* Reference (100) pp. 262 to 264

from the average Reynolds number at the bed $R_e{*} = \frac{U_*K}{\nu}$. A value of 55 < $R_e{*}$ < 5 classifies the boundary as hydraulically smooth or rough. In this study an average value of $R_e{*} = 2.3$ was estimated. This is based on:

U_* = shear velocity = $\sqrt{\frac{\tau_o}{\rho}}$ = 3.75×10^{-2} ft./sec.

K = grain roughness = 0.2 mm = 6.56×10^{-4} ft.

ν = kinematic viscosity of water at $70^oF = 1.06 \times 10^{-5}$ ft^2./sec.

The thickness of the laminar sublayer can also be estimated from Nikuradse's* experiments on the effect of wall roughness on the boundary sublayer thickness. Nikuradse proposed that at $R_e{*} = 2.3$, $\frac{U_*\delta_1}{\nu} \simeq 6.5$ or, the boundary sublayer thickness $\delta_1 = 18.4 \times 10^{-4}$ ft. = 0.56 mm. Therefore, the boundary layer in this study is classified as hydraulically smooth.

From the above a velocity measured at 0.125 inch (3.0 mm) normal to the ripple surface lied outside the laminar sublayer thickness. Accordingly, this velocity is accepted to represent the velocity of the undisturbed flow as defined in Eq. 9.1.

Further refinement in Eq. 9.3 of the shear stress equation in the turbulent boundary layer was suggested by Zaghloul[119] in the form:

$$\tau_o = \frac{.029\ \rho\ \nu^{0.2}\ U^{1.8}}{l_x^{\ 0.2}} \cdot \left(\frac{\varepsilon_{ripple}}{\varepsilon_{flat\ bed}}\right)^{0.2} \qquad 9.4$$

---

* Reference (39) p. 485

where

ε_{ripple} = the eddy viscosity at 0.125 inch normal to the ripple;

$\varepsilon_{flat\ bed}$ = the eddy viscosity at 0.125 inch above the flat bed

Moreover, the eddy viscosity can be expressed in terms of the turbulence intensity u' and the macro scale of turbulence Λ as given by:

$$\varepsilon_{ripple}/\varepsilon_{flat\ bed} = (\Lambda \cdot u')_{ripple}/(\Lambda \cdot u')_{flat\ bed} \qquad 9.5$$

Assuming average values of x_* and U along the ripple the Reynolds number R_x for the water and milling-yellow solutions can be estimated as

$$R_x \text{ (water flow)} = 0.2 \times 10^5;$$

$$R_x \text{ (milling-yellow solution flow)} = 0.2 \times 10^4.$$

Experimental investigations indicate that the transition between laminar to turbulent boundary layers occur at values of R_x ranging between 10^5 and 10^6 for the case of undisturbed approaching flow over smooth plate with well sharpened edge. These conditions do not exist in the flow over the ripple beds of this study. The grain roughness and the high free stream turbulence of flow entering the flume would initiate a turbulent boundary layer at much lower R_x. From the above, it is assumed that a turbulent boundary layer will prevail under water flow over ripples, and only a laminar boundary layer may develop with milling-yellow solution flow.

Therefore, the boundary shear stress associated with the milling-yellow solution flow over ripples can be estimated from Eq. 9.2, that reduces to

$$\frac{\tau_o}{\rho \overline{U}^2} = \frac{0.322\ \nu_m^{0.5}\ U^{1.5}}{\overline{U}^2 \cdot 1_x^{0.5}} \qquad 9.6$$

And, the boundary shear stress associated with water flow over ripple can be estimated from Eq. 9.4, that reduces to

$$\frac{\tau_o}{\rho \overline{U}^2} = \frac{0.029\ \nu_w^{0.2}\ U^{1.8}}{\overline{U}^2 \cdot 1_x^{0.2}} \cdot ({}^{\varepsilon}\text{ripple}/{}^{\varepsilon}\text{flat bed})^{0.2} \qquad 9.7$$

where

ν_m = Kinematic viscosity of milling-yellow at 70°F = 9.02×10^{-5} ft^2./sec.

ν_w = Kinematic viscosity of water at 70°F = 1.06×10^{-5} ft^2./sec.

$\overline{U}$ = Average flow velocity = 0.75 ft./sec.

U = Flow velocity at 0.125 inch normal to the ripple surface

Fig. 75 shows the results of applying Eq. 9.7 on the hot-film anemometry experimental data of water flow over sand-roughened artificial ripple bed. On the same graph, the shear stress calculations obtained from the Pitot-tube and the hot-film anemometry before and after calibration are also shown.

Fig. 76 shows the results of applying Eq. 9.7 on the hot-film anemometry experimental data of water flow over cast of the natural ripple bed. On the same graph, the shear stress calculations obtained from the Pitot-tube and the hot-film anemometry before and after calibration are also shown.

Fig. 77 shows the results of applying Eq. 9.7 on the mathematical turbulent model data along with the shear stress obtained from the mathematical model.

The results of applying Eq. 9.6 on the mathematical laminar model data is shown in Fig. 74 along with the shear stress obtained from the mathematical model and the flow visualization study. The milling-yellow solution will behave as a non-Newtonian fluid, which may account for the poor agreement between Eq. 9.6 and the measured data.

Table 14 contains the calculations of the shear stress along the ripple based on the boundary layer theory.

The general observation on this analysis is that the trend of the shear stress along the ripple based on the boundary layer theory agrees with the mathematical model. The highest shear stress occured always near the ripple crest. The same argument concerning the effect of the upstream wake on the momentum transfer and consequently the shear stress in the physical model is not incorporated in the boundary layer theory.

A more general resistance equation can be written as:

$$\tau_T = \bar{\tau}_{og} + \tau_D \qquad 9.8$$

where

τ_T is the total shear

$\bar{\tau}_{og}$ is the bed shear due to skin friction

τ_D is the form drag

The skin friction is defined as:

$$\bar{\tau}_{og} = \frac{\int_o^L \tau_o \, dL}{L}$$ and estimated from Eq. 9.7

The form drag can be estimated from:

$$\tau_D = \frac{F_D}{L} = \frac{1}{2} C_d \rho \frac{h}{L} \bar{U}^2 \qquad 9.9$$

where

C_d is a drag coefficient depending on the ripple steepness $(\frac{h}{L})$, and sharpness of the ripple crest. Based on analysis of the work of Khanna[(50)], Raudkivi[(77)] and Sheen[(90)], a relation in the form $C_d \approx (2 \text{ to } 3) \frac{h}{L}$ is suggested. The higher factor is used for a sharp crest and the lower factor for rounded crest. In this study,

h is the ripple height = 0.2 inch

L is the ripple length = 2.5 inches

$\bar{U}$ is the average mean velocity = 0.75 ft./sec.

C_d is the drag coefficient = 0.2 (assumed)

Applying Eq. 9.9 to the ripple formation of this study, an average form drag τ_D = 0.0087 lb./ft^2. is obtained.

Using Eq. 9.7, an average bed shear $\bar{\tau}_{og}$ = .0031 lb./ft^2. is estimated. This suggests a ratio of $\frac{\tau_D}{\bar{\tau}_{og}} \approx 2.8$ which agrees with Khanna[(50)] and Raudkivi[(77)] findings of a ratio of form drag to friction drag $\frac{\tau_D}{\bar{\tau}_{og}} \approx 2$.

Richardson and Simons[(82)] has suggested a flow resistance equation for the ripple regime in the form:

$$\frac{C}{\sqrt{g}} = (7.66 - \frac{0.30}{U_*}) \log D + \frac{0.13}{U_*} + 11 \qquad 9.10$$

where

$\frac{C}{\sqrt{g}}$ is the dimensionless Chezy discharge coefficient;

D is the average depth of flow = 5.0 inches;

U_* is the shear velocity $= \sqrt{\frac{\tau_T}{\rho}} = 0.078$ ft./sec.

(estimated from Eq. 9.8)

Applying Eq. 9.10, a Chezy coefficient, $\frac{C}{\sqrt{g}} = 11.2$, is obtained. This is within the range proposed for ripple formation given by Richardson and Simons as $7.8 \leq \frac{C}{\sqrt{g}} \leq 12.4$.

In conclusion, under known flow conditions that initiate a ripple regime in a sand bed, Eqs. 9.7, 9.9 and 9.10 can be used to estimate the bed shear, form drag and Chezy coefficient, respectively.

9.4 Comparison With Other Investigators

9.4.1 Shear Stress Along a Ripple

The experimental results of the shear stress along the ripple bed obtained in this study and those reported by other researchers are shown in Fig. 78. A brief description of each is given as follows:

Curves (1) and (2) are the shear stress as obtained in this study over the sand-roughened artificial ripple bed measured by the Pitot-tube and the hot-film anemometry techniques, respectively. It should be noted that Curve (2) represents the calibrated hot-film anemometry measurements.

Curve (3) is Raudkivi's[77] experimental results of the bed shear measured by a Pitot-tube of a water flow over a reproduced ripple form of smooth galvanized metal sheet. The ripple length and height were 15.0 inches and 0.9 inch, respectively, with the ripple height to length ratio of 0.06. The average flow depth and mean velocity were reported as 4.96 inches and 0.98 ft./sec., respectively. The bed shear variation is steadily increasing in the downstream direction, beyond the wake zone, from $\frac{\tau_o}{\rho U^2} = 10.7 \times 10^{-4}$ to reach its maximum of $\frac{\tau_o}{\rho U^2} = 35 \times 10^{-4}$ at the crest.

Sheen[90] carried out his experiments on the same flume and the ripple model form of Raudkivi except that the smooth steel surface was roughened with the same sand used in forming the ripples. Pitot-tube measurements were taken at four locations along the ripple (Curve 4). Sheen claimed that the trend of the rough boundary shear is similar to that of the smooth boundary measurements by Raudkivi, although the scatter was considerable.

Sheen has also measured the Reynolds shear $-\rho\overline{uv}$ at 0.25 inch above the ripple surface using the hot-film technique (Curve 5). He pointed out the disagreement between the Reynolds shear and the bed shear measured by the Pitot-tube (Curve 4). He explained the discrepancy by either the large convergence of flow or the effect of viscosity if the hot-film measurements were taken inside the turbulent boundary layer. Also, the Pitot-tube measurements may have been affected by wake turbulence and periodic pressure gradient. The roughness Reynolds number, $\frac{U_* K}{\nu}$, varied from 2.9 at the trough to 6.0 at the ripple crest and the thickness of the laminar sublayer was always greater than the grain size. Thus, a hydraulically smooth turbulent boundary layer prevailed in Sheen's experiment.

The results reported by Khanna[50] based on experiments in a 1 ft. by 1 ft. wind tunnel using the techniques of hot-wire anemometry in the medium of air over smooth waves to represent sand waves are indicated by Curve (6). The ripple length and height were 12.0 inches and 0.8 inch, respectively, with a height to length ratio of 0.07. The average mean velocity was 54 ft./sec. His results showed the same trend reported by Raudkivi of increasing bed shear stress along the ripple to reach its highest value at the crest with an average value of $\frac{\tau_o}{\rho \bar{U}^2} = 15.0 \times 10^{-4}$. Khanna derived a relation for the inner region, to calculate the bed shear stress that is based on Prandtl's mixing theory in the form:

$$\frac{U}{U_*} = 5.6 \log \frac{U_* y}{\nu} + 4.9 \qquad 9.11$$

The results reported by Jonys[43] based on experiments in a water flume over a mobile bed of light weight material of specific gravity of 1.041 and D_{50} = 1.4 mm are indicated by Curve (7). Jonys's experiments showed a range of ripple lengths of 10 to 20 inches, ripple heights of 0.32 to 1.4 inches, with ripple height to length ratio ranging from .03 to 0.11. The flow depths investigated were in the range of 1.8 to 3.7 inches. An estimated mean average velocity of 2.5 inch/sec. was used in plotting Curve (7). The bed shear increases downstream from the wake to reach its maximum at $\frac{l}{L}$ = 0.75, then decreases to zero shear at the crest. Jonys gave an explanation of the difference in his results from those reported by Raudkivi and Khanna, based on the permable effect of the mobile bed. He stated that the decreasing boundary shear approaching the crest may be due to the seepage flow effect that will be induced from both sides toward the low pressure zone immediately upstream of the crest. Jonys used a similar equation to Khanna in determining the shear stress in the form:

$$U_* = \sqrt{\frac{\tau}{\rho}} = \frac{1}{5.75} \frac{dU}{d(\log y)} \qquad 9.12$$

where the velocity was measured by the hydrogen bubble technique.

The average bed shear on the ripple surface in the range of $0.55 \leq \frac{l}{L} \leq 0.85$ is $\frac{\tau_o}{\rho U^2} = 125 \times 10^{-4}$, and the roughness Reynolds number $\frac{U_* K}{\nu} \simeq 10$. The fall velocity was estimated as $v_s = .06$ ft./sec. from the following equation:

$$1.33 \frac{gd}{v_s} \left(\frac{S_s - S_f}{S_f} \right) = C_d = \phi(R) \qquad 9.13*$$

where

S_s = specific gravity of bed material

S_f = specific gravity of fluid

d = diameter of bed material

v_s = the settling velocity

R = Reynolds number = $\frac{v_s d}{\nu}$

C_d = coefficient of drag

Eq. 9.13 applies beyond Stokes law at Reynolds number $R > 0.1$.

Applying Eq. 9.13 on the experimental data of this study, a fall velocity $v_s = .08$ ft./sec. is obtained. An equivalent fall diameter of Jonys's bed material was estimated from

$$(d_{50})^2_{\text{equivalent}} = \frac{(v_s) \text{ Jonys}}{(v_s) \text{ this study}} \cdot (d_{50})^2_{\text{this study}}$$

or $(d_{50})_{\text{equivalent}} \simeq 0.17$ mm which satisfies the requirement for ripple formation ($d_{50} < 0.6$ mm). However, the following observations can be made on Jonys work:

1) The depth of flow in relation with the ripple dimensions would lead to a significant surface wave effect on his ripples. This,

---

* Reference (85) p. 779

in part, explains the high dimensionless bed shear $\frac{\tau_o}{\rho U^2}$ of 125×10^{-4} in comparison with the values of bed shear obtained by other researchers.

2) Seepage conductivity K is proportional to the diameter square of the bed material, i.e., $K \propto d_{50}^2$. Accordingly, the seepage conductivity of Jonys's work is about 50 times that of the mobile bed in this study.

3) The bed surface in Jonys's experiment is not hydraulically smooth. A smooth turbulent boundary layer existed in Sheen's experiment and in this study.

A comparison of the results of the shear stress distribution along a ripple surface as shown in Fig. 78 leads to the following comments:

1) Some of the differences could be explained by the variation of the technique used (Pitot-tube, hot-film or wire or hydrogen bubble), the flowing fluid (air or water), surface condition (smooth or rough) and the bed regime (rigid or mobile). The accuracy of different techniques is demonstrated by Curves (4) and (5) of the shear stress on the same bed under the same flow conditions, as reported by Sheen, using the Pitot-tube and the hot-film anemometry techniques. Raudkivi and Khanna reported similar results for smooth ripple surfaces. The high shear stress reported by Jonys was explained earlier by the effect of the surface wave. The zero shear stress at the crest is also explained by the high seepage conductivity encountered in his experiments.

2) Comparing the shear distribution, along the ripple, of this study with that of other researchers shows an agreement in trend

with the distributions reported by Sheen and Jonys and an agreement in the order of magnitude, but not shape, with the distributions reported by Raudkivi, Khanna and Sheen's Pitot-tube measurements. The average of Sheen's hot-film and Pitot-tube results is in good agreement with this study.

3) While the ripples reported by different investigators have similar dimensions, the ripples observed in this study were much smaller. However, the height of ripple to length ratio is similar. The ripples in this study represent the early stage of the ripple regime for fine sands.

9.4.2 Turbulence Intensities

Fig. 79 shows a comparison of the turbulence intensity $\frac{u'}{\bar{U}}$, and the velocity $\frac{U}{\bar{U}}$, along a ripple as obtained in this study with that reported by Sheen(90). The hot-film technique was used in both investigations. The measurements were taken at 0.25 inch and 0.125 inch above the ripple surface in Sheen's experiments and this study, respectively. The following observations can be made:

1) At the ripple surface, the two studies showed an increase in the turbulence intensity from the reattachment reaching a maximum at $\frac{l}{L} \approx 0.4$, then the intensity decreases in the downstream direction up to the ripple crest. However, Sheen's experiments showed higher turbulence than that measured in this study. The turbulence intensity $\frac{u'}{\bar{U}}$ of this study varied between .07 to .09 while in Sheen's experiments it varied between .09 to 0.15. This is probably a result of the significantly larger ripple heights used

by Sheen, i.e. 0.9 inch compared to 0.2 inch of this study.

2) The velocity measured by Sheen at y = 0.25 inch above a ripple of height h_r = 0.9 inch has been affected by the wake much more than the velocity measured in this study at y = 0.125 inch above a ripple of height h_r = 0.2 inch. This could be explained by the difference in the ratio of ripple height to depth of measurement above bed (h_r/y) used in the two studies. These ratios are 3.6 and 1.6 in Sheen's experiments and in this study, respectively. A higher (h_r/y) of Sheen's experiments resulted in relatively lower velocity and higher turbulence intensity along the ripple from downstream the reattachment to at least $\frac{l}{L}$ = 0.6.

3) At half flow depth the velocity and the turbulence intensity of the two investigations are quite similar. Average turbulence intensities $\frac{u'}{\bar{U}}$ of 0.050 and 0.055 are reported in this study and Sheen's experiments, respectively.

9.4.3 Regimes of Ripples

Several sets of dimensionless numbers have been introduced to define the regimes in which the different types of bed forms develop.

Shields(93) in 1936, in his early evaluation of particle motion, considered the parameters important to the initiation of particle motion to be the particle diameter, the specific weight of the submerged particle, the density and viscosity of the flowing fluid and the shear stress at the bed.

Liu(60) in 1957 introduced the fall velocity for a single particle as an important variable in the initial growth of bed forms and concluded that many of the variables involved in the interaction between water and individual sediment particles such as size, shape and submerged weight could be lumped in the fall velocity. He also showed that his parameters are equivalent to Shield's for the special case of spheres. Simons and Richardson[96] developed a set of dimensionless curves where the Froude number is introduced to define the bed regimes.

Along these lines other researchers, e.g. Garde and Raju[27], and Hill[38], have developed different criteria for bed regimes.

An attempt was made to correlate the ripples observed in this study with the previously published work. The following parameters are selected:

Size of bed material, d	=	0.2 mm
Specific gravity of sand	=	2.65
Kinematic viscosity of water, ν at 70°F	=	1.06×10^{-5} ft^2./sec.
Density of water, ρ	=	1.94 slug/ft^3.
Fall velocity, "v_s" = 25 mm/sec.	=	0.08 ft./sec.
Average bed shear velocity, $U_* = \sqrt{\frac{\tau_o}{\rho}}$	=	3.75×10^{-2} ft./sec.
Average mean velocity, $\overline{U}$	=	0.75 ft./sec.
Flow depth, D	=	5 inches

Figs. 80 to 87 show the experimental correlation of the results of this study on the regime maps of several investigators. The correlations fall inside the ripple zone of Figs. 81, 83 and 87 suggested by Hill[38] and Simmons and Richardson [95,96], and near ripples in Figs. 80, 82, 84, 85 and 86 proposed by Liu[60], Shields[93], Simons[31], and , Garde and Raju[27]. The experimental correlations developed from Jonys's data are also shown on Figs. 80, 84 and 86. The bed forms reported by Jonys appear to be ripples.

The tendency of the bed regime to fall slightly below ripples could be explained by the smaller ripple dimension incurred in this study in comparison with ripple dimensions reported by others. This argument is supported by the fact that the ripple size is not introduced in the dimensionless parameters of Figs. 80 to 87.

Flow characteristics near the bed such as turbulence level, shear stress and velocity are important facotrs in bed regime. If any of these factors was higher than normal, ripples could form when other researchers found no bed material movement. In conclusion the bed forms observed in this study are classified as ripples, possibly in the early stage of the ripple regime for fine sands.

Thomas(102) has introduced a correlation of periodic phenomena of sediment transport in horizontal pipes and open channels where the periodic height and length are introduced in an equation in the form:

$$\frac{\bar{U}^2}{g_L \cdot L_r} \Big/ \left(\frac{\rho_s - \rho}{\rho}\right) = \frac{1}{2\pi}\left[\tfrac{1}{4}\left(\frac{u_r^2}{g_L \quad h_r}\right)\left(\frac{D}{h_r}\right)^{5/3}\left(\frac{D}{d_r}\right)^{2/3}\right]^{0.258} \qquad 9.14$$

where

$\bar{U}$ - mean velocity of flow

L_r - periodic wave length = ripple length

h_r - height of the periodic phenomenon = ripple height

u_r - ripple velocity

d_r - particle diameter

D - depth of flow

ρ_s - particle density

ρ - density of water

g_L - gravitational acceleration

This correlation is shown in Fig. 88. A good agreement of the experimental data of this study with Thomas's correlation within the ±25% scatter was achieved. However, it should be noted that introducing the depth of flow as a parameter in Thomas's correlation does not agree with the generally accepted theory that ripples are independent of flow depth.

9.4.4 Theories of Ripple Formation

In this section three theories that explain the origin of ripples and the reason for their occurence are discussed.

The first approach was adopted by Yalin[116], in which he arrived by the process of elimination at the conclusion that the occurence of ripples is caused by the instability of the surface of the granular medium itself. In his physical model he assumed that the particle Reynolds number R_e* is small, i.e. that the influence of viscosity is large. In this case, the mechanical individuality of grains becomes restricted and the granular medium turns into what he described by the term "plastic medium". Under a continuous action of the shear stress τ_o, the plane surface of the plastic medium would soon lose its stability and would deform into a wavelike shape. Also, the slightest incidental ridge that might be present on the bed surface can result in the deviation of τ_o from its standard value and consequently induce the instability. Once these infinitesimal amplitude waves are established, the waves will soon grow in time to the ripple wave length. He stated that the wave length "L" is essentially a property of the plastic medium and may or may not depend on the shear stress. If the wave length is only a function of the plastic medium then:

$$L = f(\rho, u, d) \qquad 9.15$$

i.e., $L = \text{const.}\, d$

where d is the particle diameter.

If the wave length does depend on τ_o, then

$$L = f(\rho, u, d, \tau_o) \qquad 9.16$$

i.e., $L = \phi(R_e^*) \cdot d$

Yalin did not believe that turbulence is a factor in ripple occurence; on the contrary, he stated that the turbulence in the vicinity of the bed inhibits ripples.

Liu[60] has also attempted to explain the occurence of ripples by using the concept of instability of the laminar sublayer on the interface of two different fluids moving relative to each other. The lower fluid represents the granular medium and the upper fluid being the tractive fluid. Liu's approach differs from Yalin in that the waves on the interface are caused by the deviation in velocities rather than the shear stress.

Raudkivi[79], on the other hand, suggested that the mobility of grains and the occurence of bed forms is a function of the turbulent agitation and temporal mean shear, the turbulence makes the particles mobile and the shear stress transports them. Raudkivi described the mechanism of ripple formation starting from the threshold of grain movement passing a disturbance in the plane grain boundary that is created by a chance piling-up. This surface disturbance establishes an interface or surface of discontinuity in the flow. In the shear flow of the interface zone the turbulence intensity is high and the grains are stirred-up by the turbulent agitation where the interface reattaches itself to the grain boundary. From the reattachment point downstream the turbulent agitation decreases and also a boundary layer develops. Because of the reduced agitation some of the material made mobile at the reattachment point cannot be supported and settles out as it passes downstream. This leads to the formation of a second disturbance and so on. The bed-form development propagates gradually downstream from the point of the initial disturbance until the steady state condition is established. Along the established ripple form the turbulent agitation is maximum at the reattachment region and decreases from there downstream, partly because of diffusion and decay and partly because of the convergence of flow. The ripple form travels by erosion of sand on the upstream face and by deposition in the lee of the ripple.

Based on the experimental observations and results of this study, it is believed that Raudkivi's explanation of ripple formation is more realistic. The turbulence does play an important role in ripple formation. Larger ripples have been observed in the high turbulence zone while smaller size ripples occured in the low turbulence zone (Fig. 23). The description of the turbulence intensity along a ripple as given by Raudkivi was obtained experimentally by Sheen and in this study (Fig. 79). The highest turbulence intensity occured just downstream from the reattachment and decreased further downstream as far as the to the ripple crest. An explanation of the smaller size ripples reported in this study in comparison with Sheen's experiments can now be given as the dependency of ripple size on the turbulence intensity. Higher turbulence intensities may lead to longer ripples at the transitional stage from flat bed to developed ripples.

The presence of free stream turbulence in this study may have caused initial motion to occur at velocities lower than the critical values suggested by Shields. Once a ripple occurs in a relatively high turbulence or high shear zone, a ripple pattern tends to propagate downstream apparently because of the disturbance of the initial form.

Yalin(117) has indicated that the development of ripples can increase by a factor of about 2 in a duration as long as 400 hours. In a period of three hours of the present study, the ripple dimensions in the high turbulence zone were about twice the size of those observed in the low turbulence zone. This may lead to the conclusion that the high free turbulence encountered in this study has accelerated the development of ripples.

CHAPTER TEN

CONCLUSIONS AND RECOMMENDATIONS

On the basis of the experimental and mathematical analyses of this thesis, the following conclusions were drawn:

1) A comparison of the turbulence characteristics over the cast of the natural ripple and the artificial triangular ripple beds indicates that the essential velocity and turbulence features of flow over the three-dimensional cast of a natural ripple bed have been reproduced, within the range of experimental error, by the flow over two-dimensional sand-roughened artificial ripple bed.
2) The shear distribution over the mobile ripple bed was found to be very similar to the shear distribution over the cast of the natural ripple bed and the roughened artificial ripple bed.
3) Although the experimental results of the boundary shear stress along a ripple, obtained by the Pitot-tube technique, were 10 to 20 percent higher than those obtained by the hot-film anemometry technique, both methods showed the same trend in the shear stress variation along the ripple surface. After adjustment for depth and calibration of the V-probe, the results were in good agreement.
4) The macro scale of turbulence near the ripple surface is of the same order as the ripple height.
5) In this study, solutions of milling-yellow were found to be

satisfactory for qualitative visual studies of the velocity and shear patterns produced by viscous fluids.

6) A stable numerical solution of stream function, vorticity, velocity, shear stress distributions and the flow pattern separation was achieved using the finite element technique to solve the Poisson and Helmholtz form of the Navier-Stokes and Reynolds Equations for laminar and turbulent flow models. The mathematical and experimental results show fairly good agreement for both the viscous and turbulent flow conditions.

7) An analysis based on the boundary layer theory indicated that the shear stress variation along the ripple surface could be accounted for by:

   i) a rapid increase in shear immediately downstream of the point of reattachment;

   ii) a tendency for shear to decrease as the boundary layer develops;

   iii) a compensating increase in shear due to the increase in velocity near the bed as a result of the flow contraction due to the ripple form;

   iv) the increase in the eddy viscosity because of the separation from the preceding ripple tending to increase the shear near the reattachment point.

On the basis of the investigations of this thesis the following topics are suggested for future study:

1) The finite element models described herein could be extended to include different bed forms, such as dunes;

2) The milling-yellow solution has proved its usefulness as a qualitative flow visualization technique, which could be extended to cover different areas in fluid mechanics, such as flow under sluice gates and around spur-dikes;

3) The turbulence characteristics should be checked by laser anemometry to assess the accuracy of the hot-film technique;

4) Additional studies should be made in a large flume to permit a greater flow establishment distance;

5) The effect of free stream turbulence on ripple formation should be investigated.

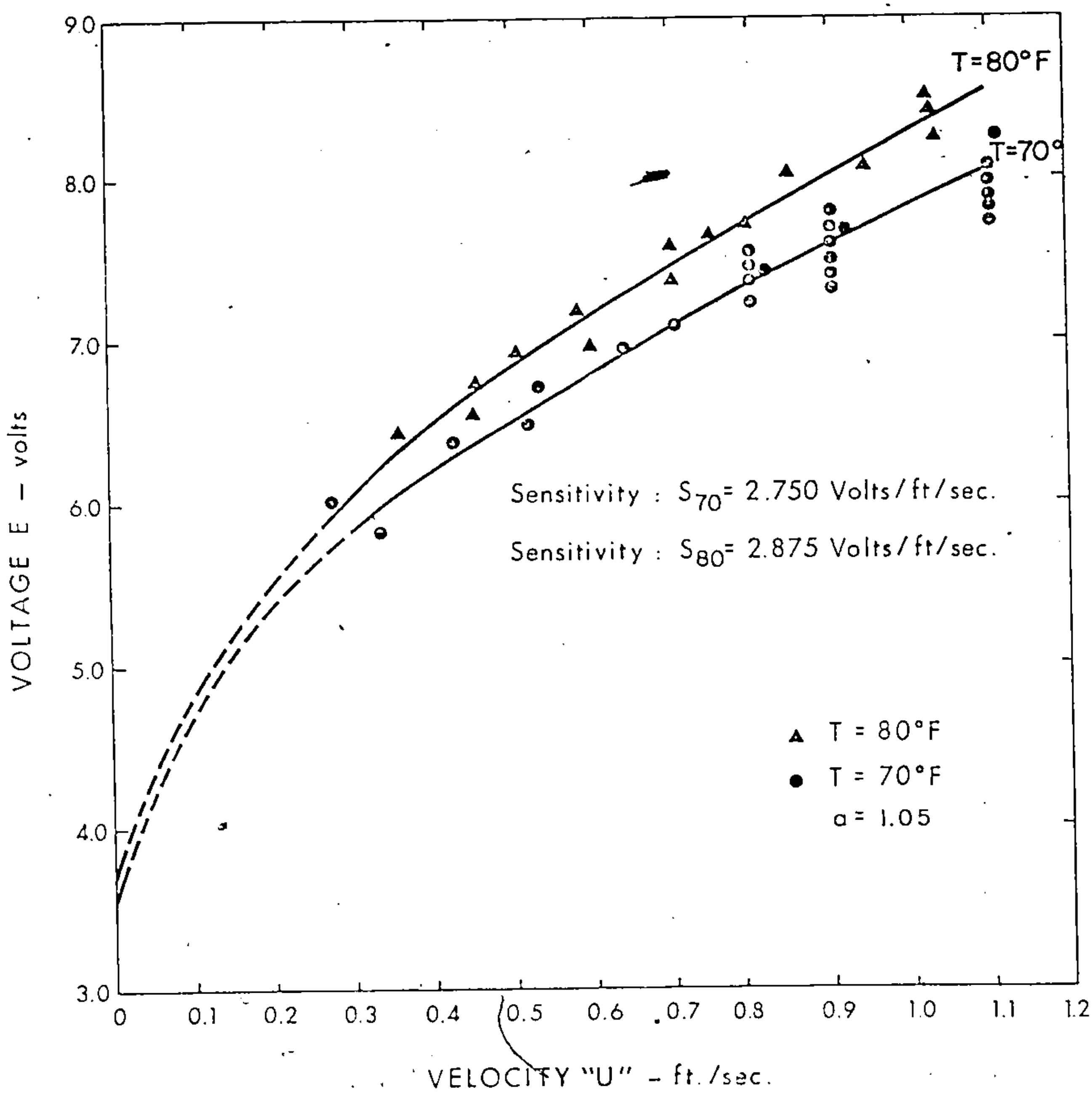

Fig. 17 — Calibration curves of the wedge probe 55 A 83.

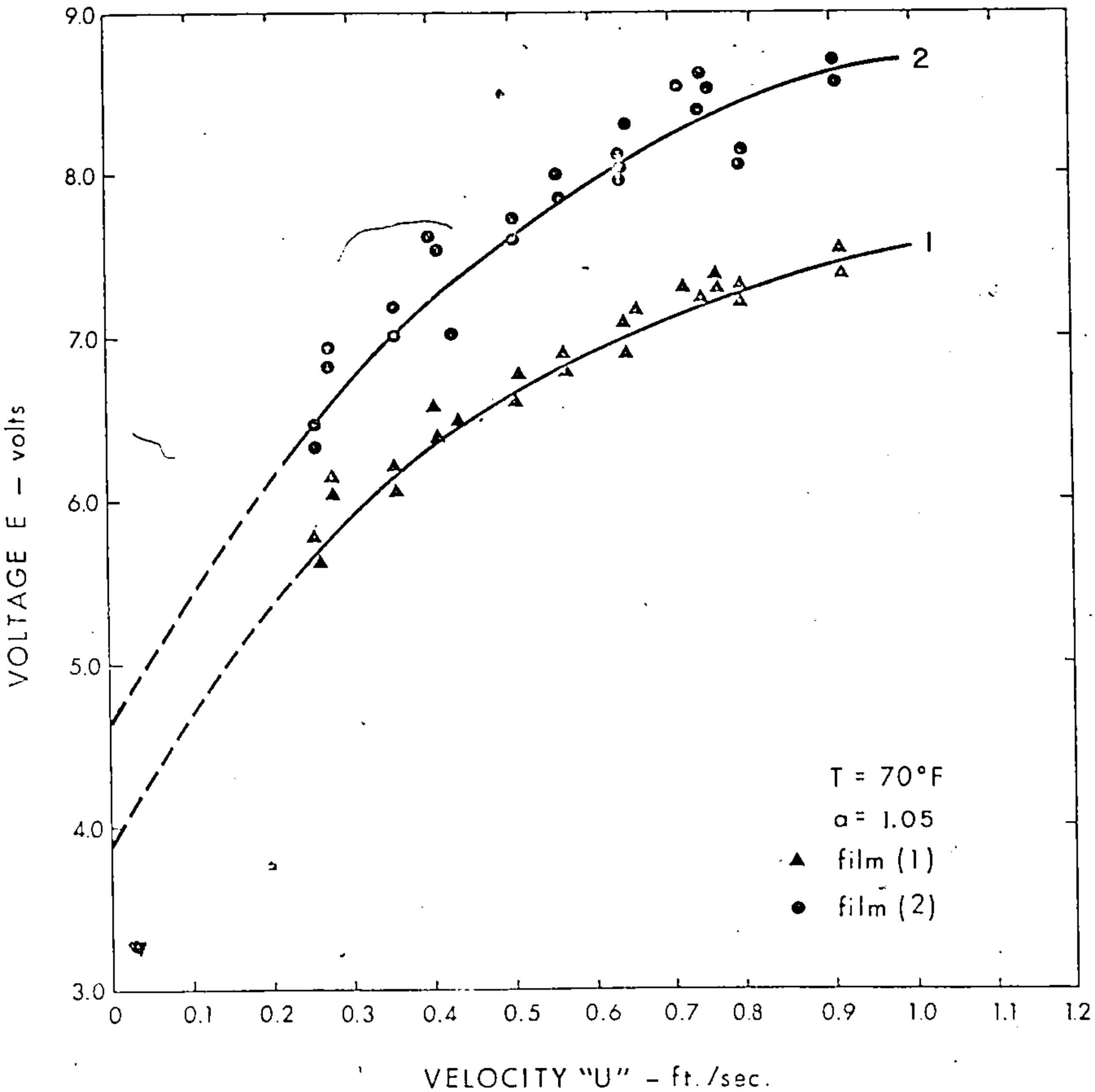

Fig. 18 — Calibration curves of the V-probe 55 A.0891

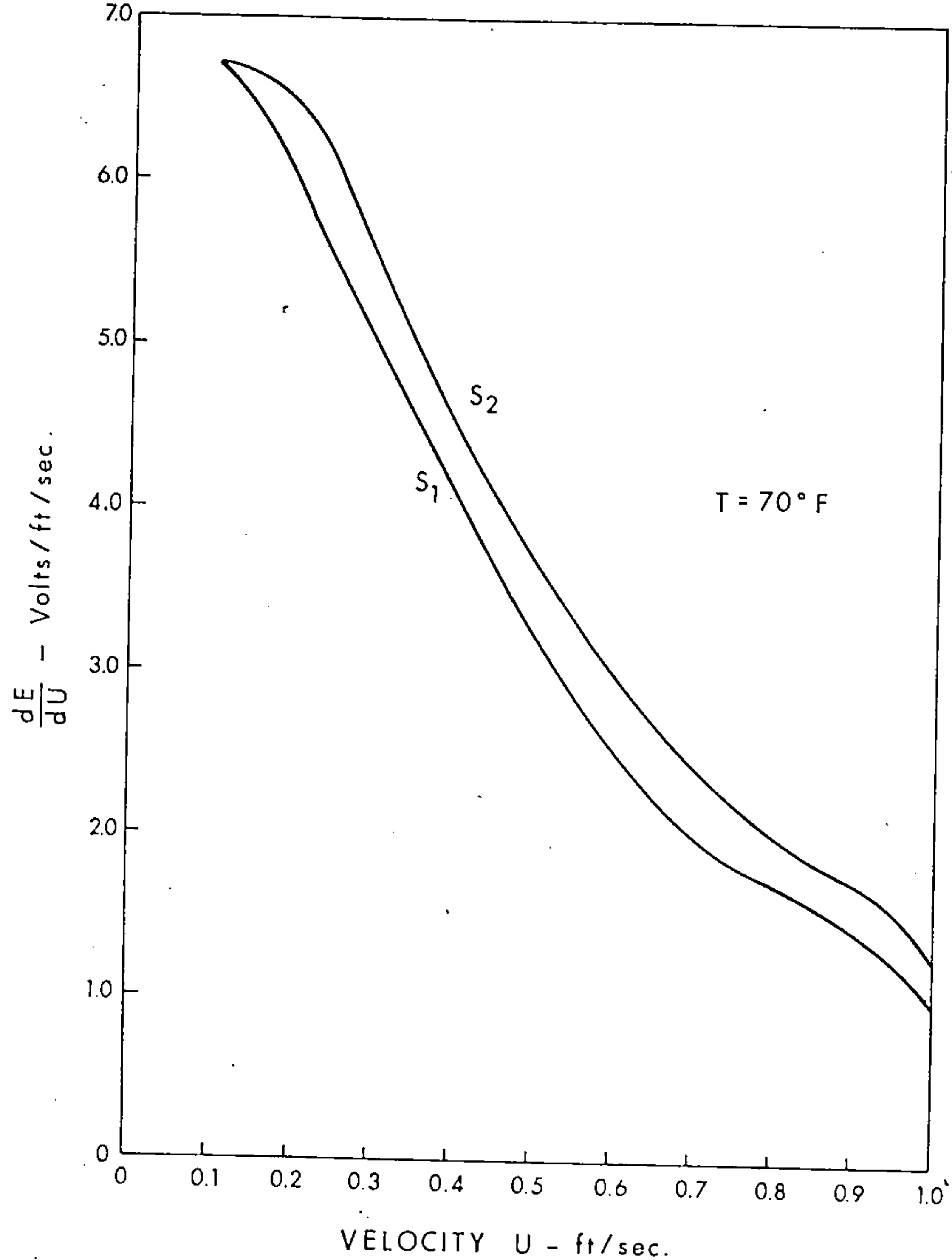

Fig. 19— Sensitivity curves of the V-probe 55A0891

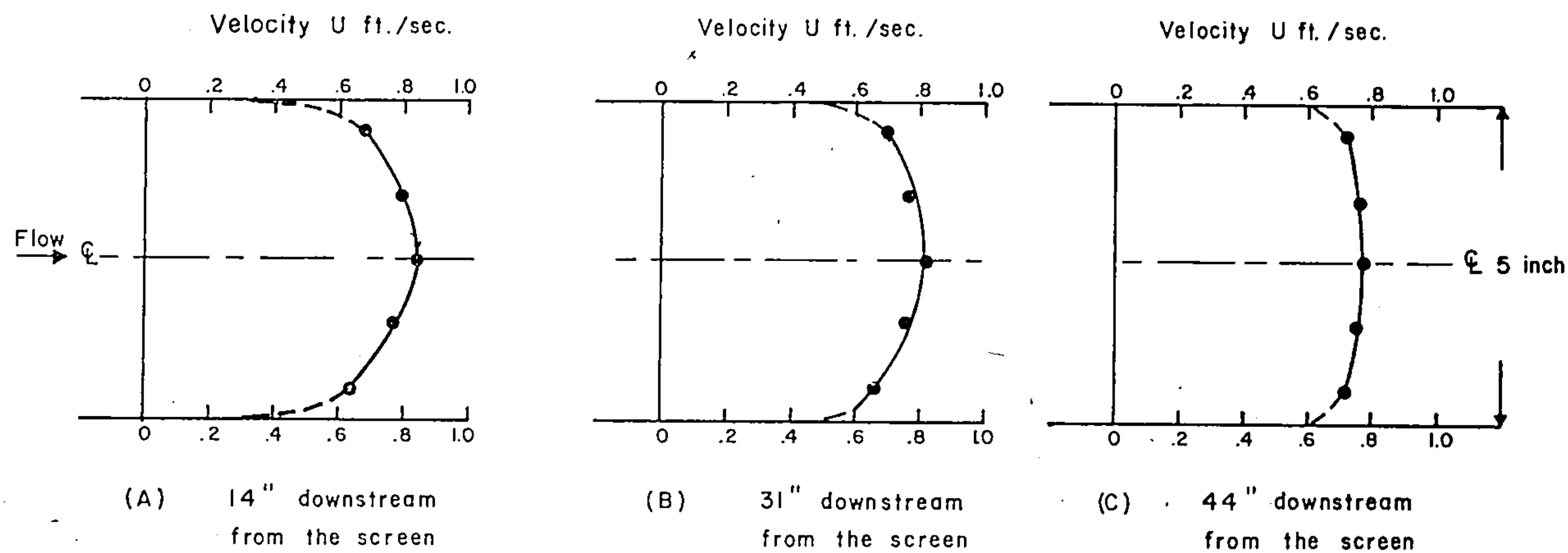

Fig. 20 — Transverse profiles of the longitudinal velocity along the flume at 2.5" above the bed.

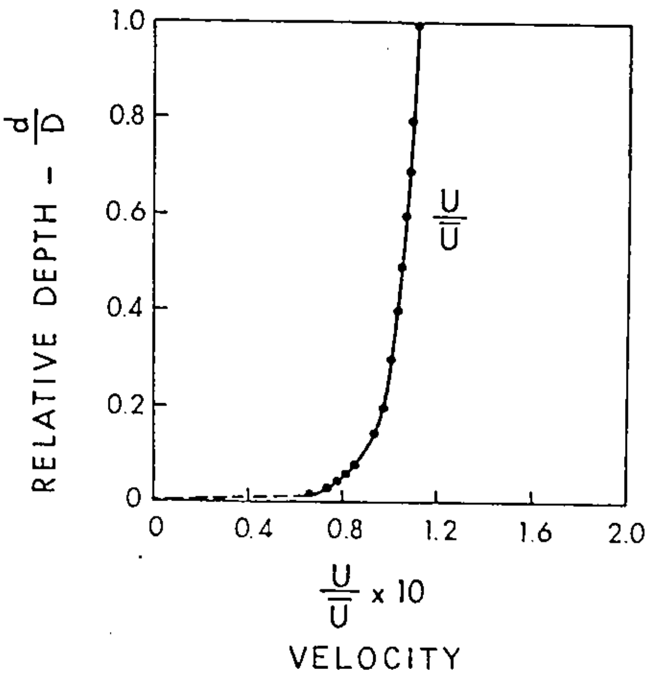

Fig. 21 — Distribution of the velocity taken 44" D/S from the screen above ripple crest for the natural mobile bed - obtained from the pitot - tube measurements.

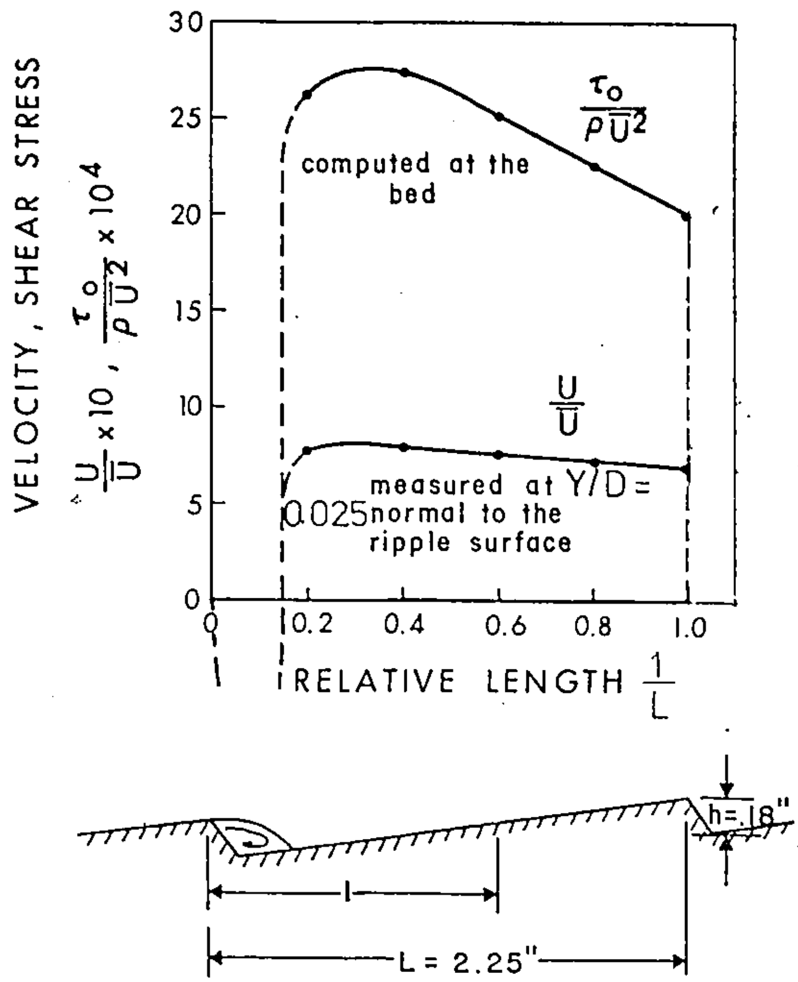

Fig.22 — Variation of velocity and shear stress along one ripple 44" D/S from the screen for the natural mobile bed - obtained from the pitot - tube measurements.

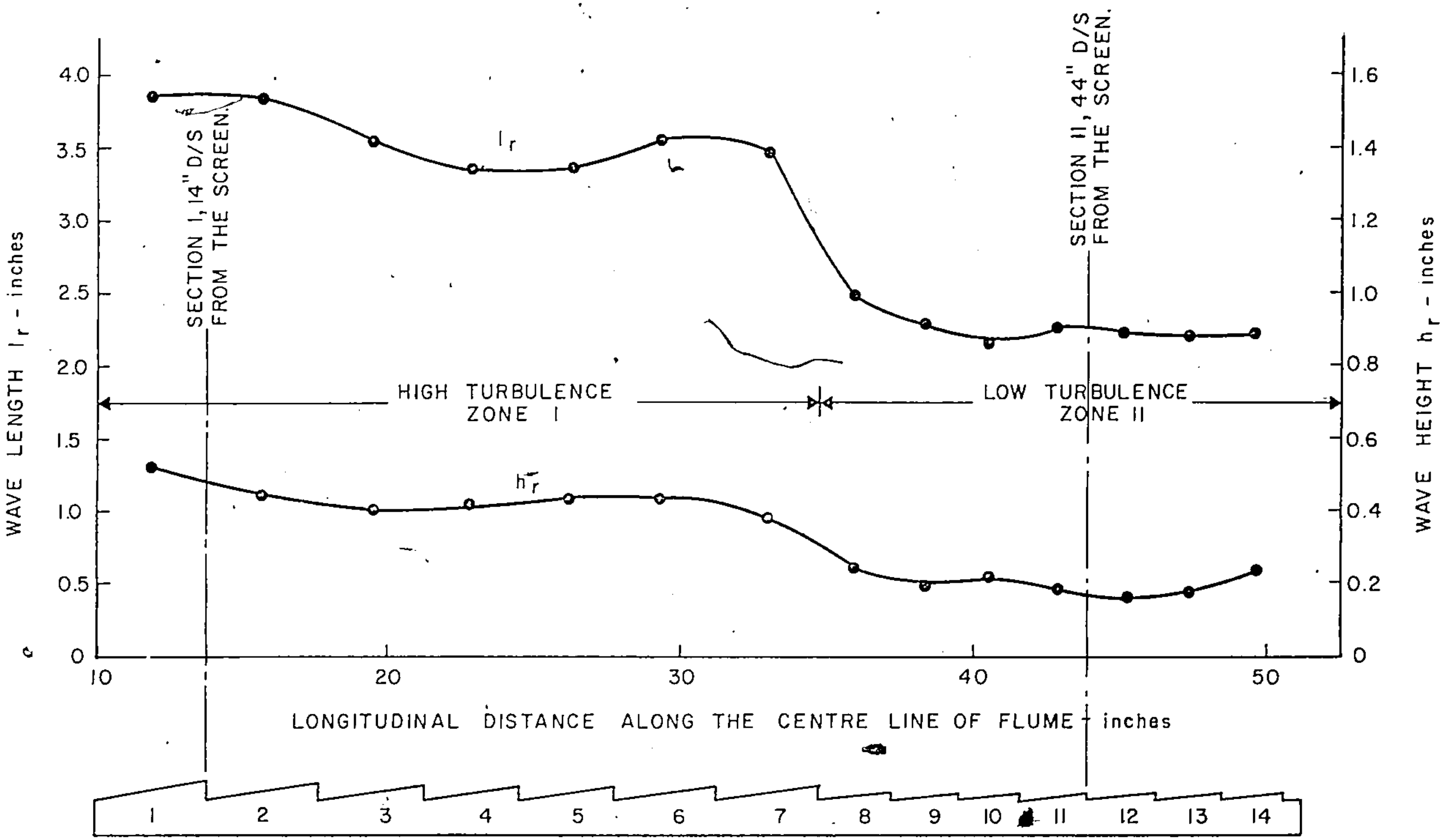

Fig. 23 — Variation of the ripple lengths and heights along the flume.

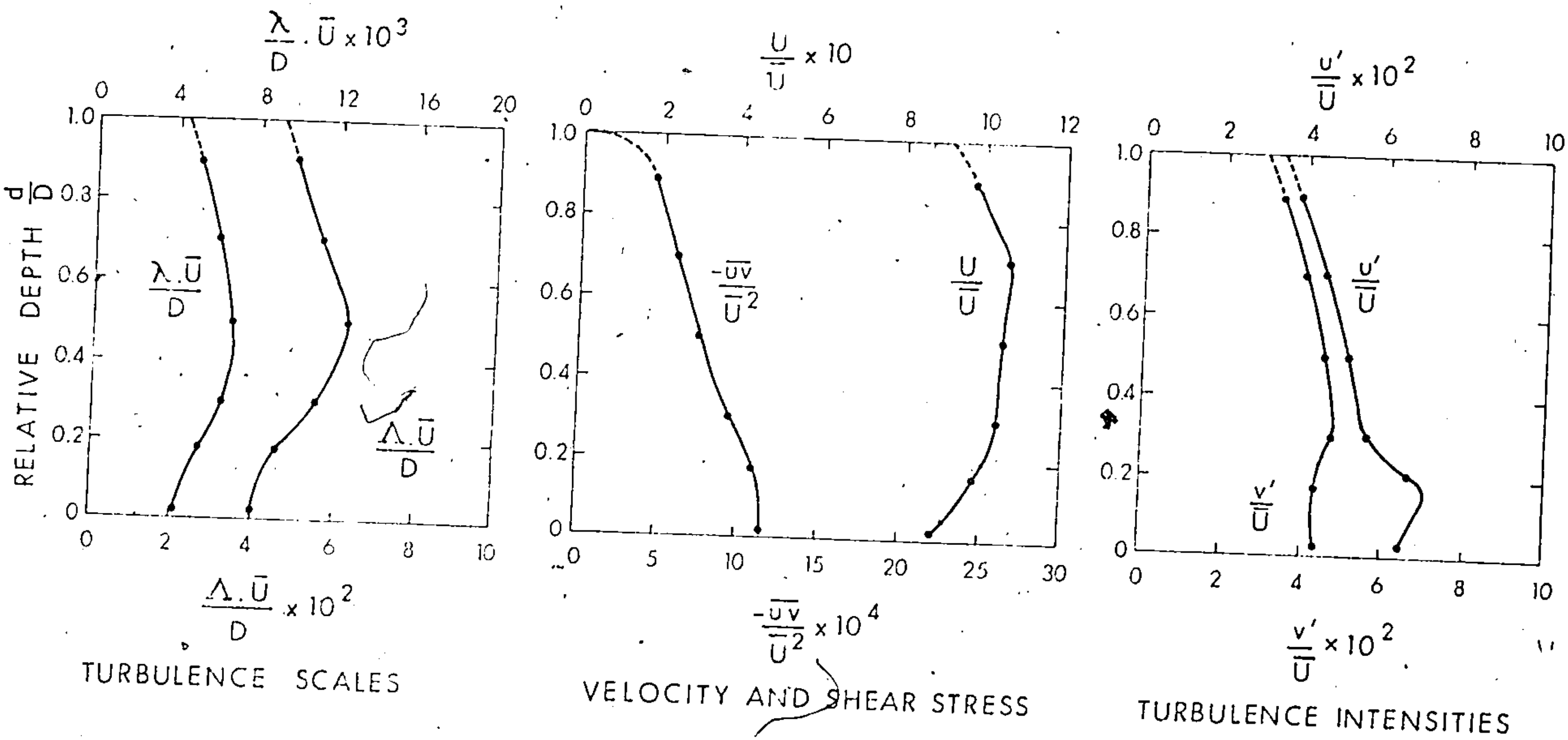

Fig. 24 — Vertical distribution of velocity and turbulence data for a smooth flat bed 44" D/S from the screen - obtained from hot-film anemometer measurements.

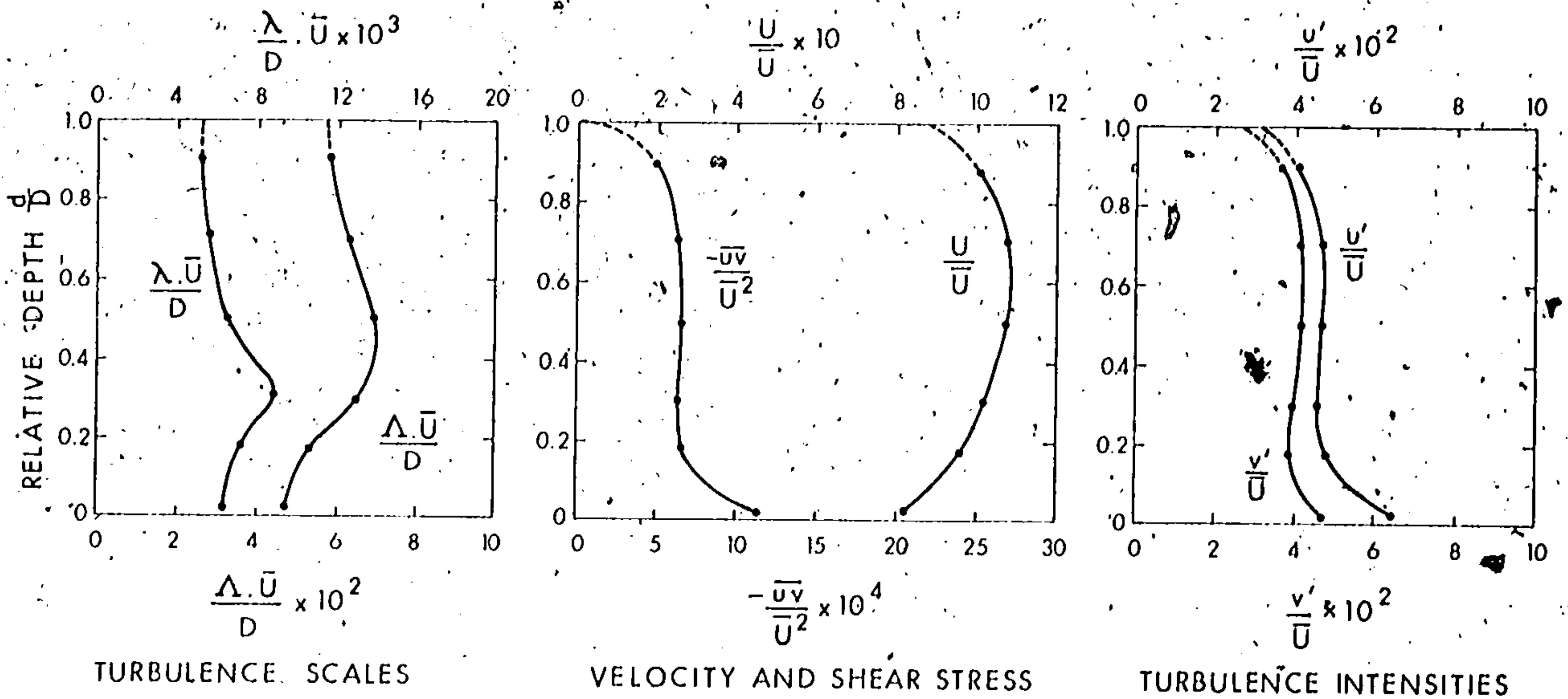

Fig. 25 — Vertical distribution of velocity and turbulence data for a rough flat bed 44" D/S from the screen - obtained from hot-film anemometer measurements.

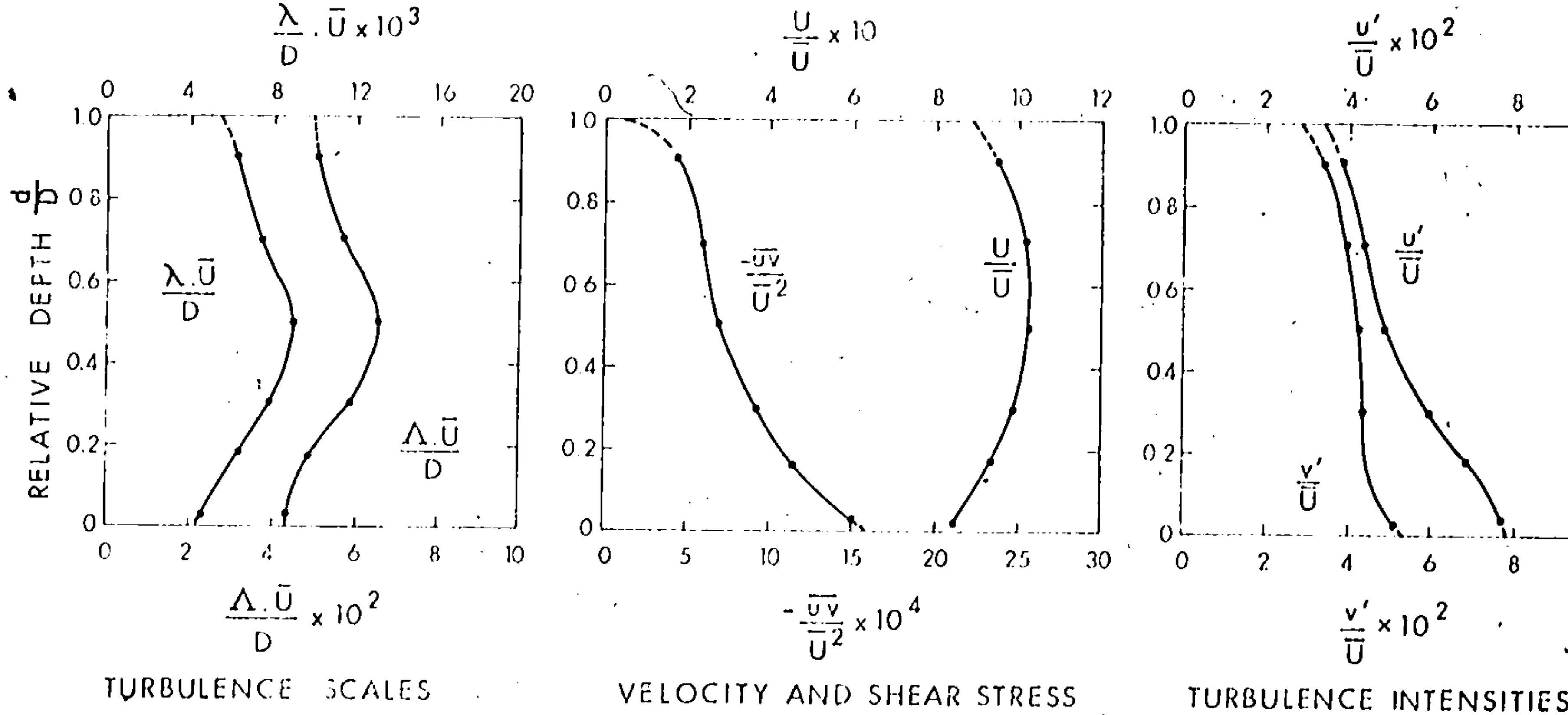

Fig. 26 — Vertical distribution of velocity and turbulence data for a smooth artificial ripple bed 44" D/S from the screen at ripple crest - obtained from hot-film anemometer measurements.

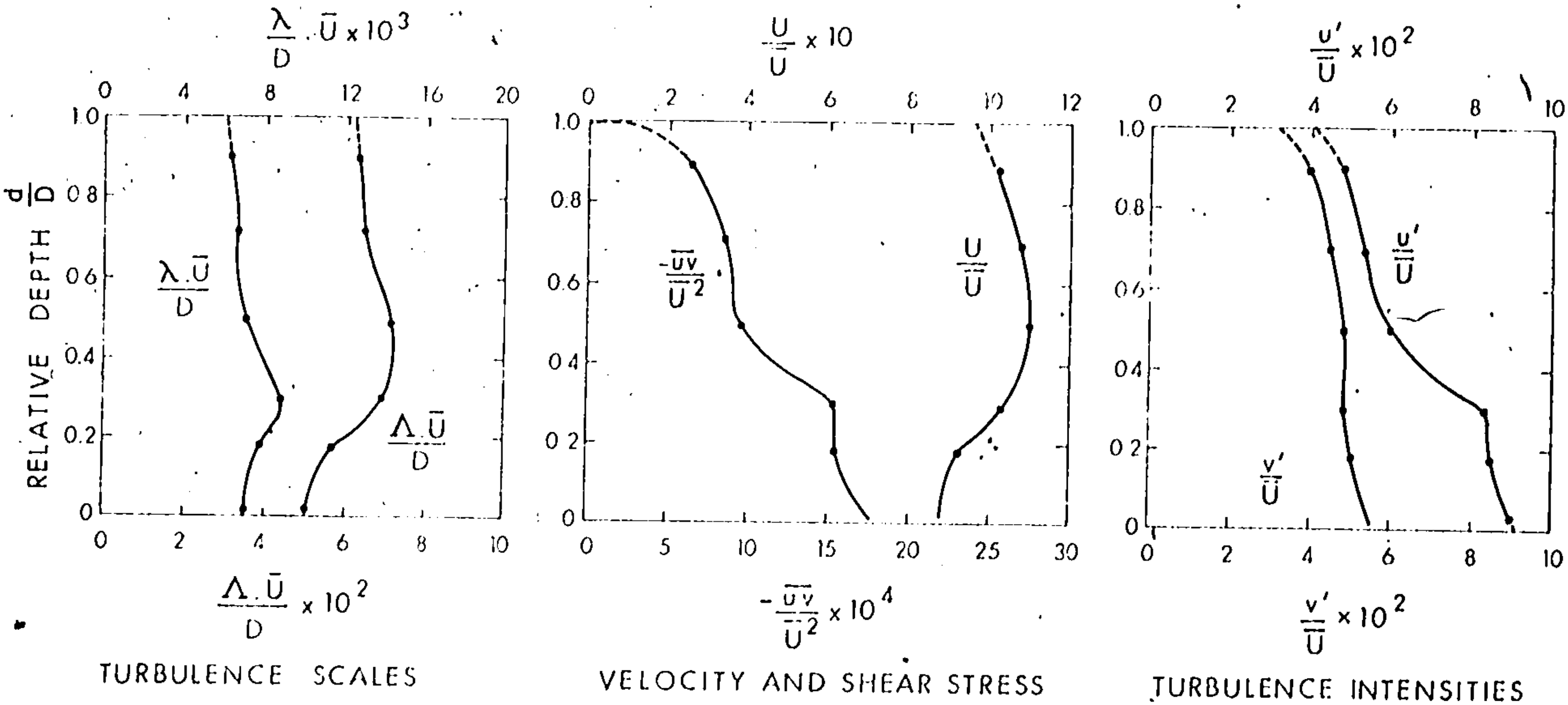

Fig. 27 — Vertical distribution of velocity and turbulence data for a rough artificial ripple bed 44" D/S from the screen at ripple crest - obtained from hot-film anemometer measurements.

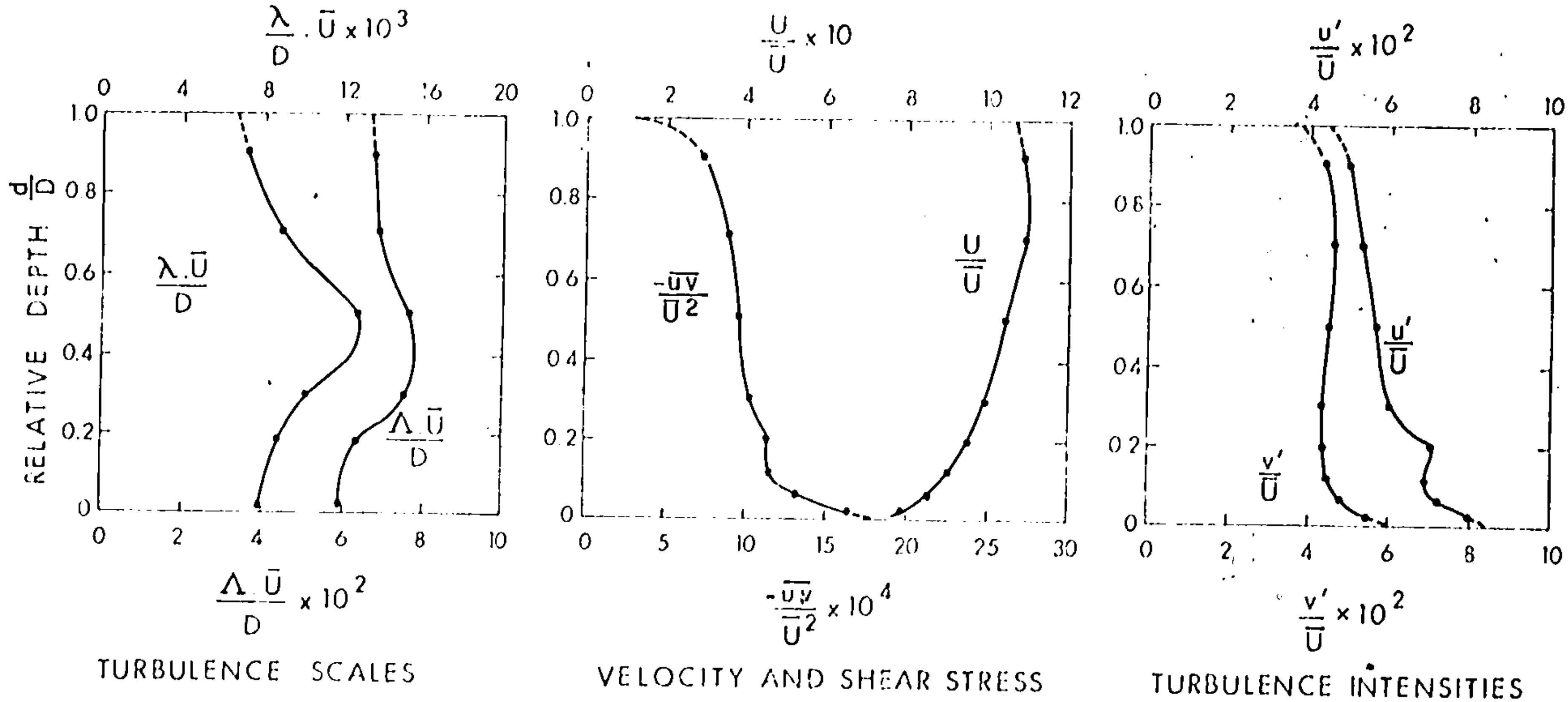

Fig. 28 — Vertical distribution of velocity and turbulence data for a cast of a natural ripple bed 44" D/S from the screen at ripple crest - obtained from hot-film anemometer measurements.

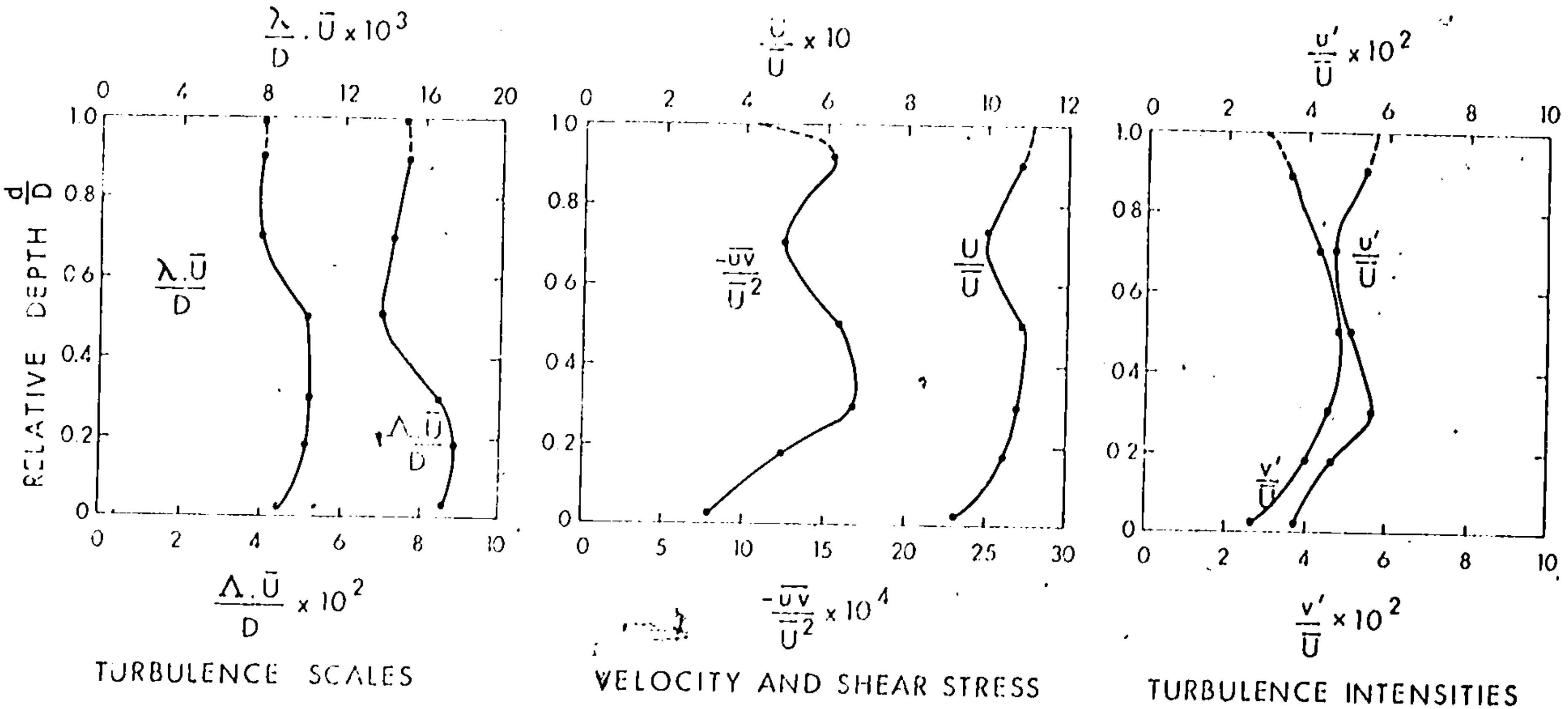

Fig. 29 — Vertical distribution of velocity and turbulence data for a smooth flat bed 14" D/S from the screen - obtained from hot - film anemometer measurements.

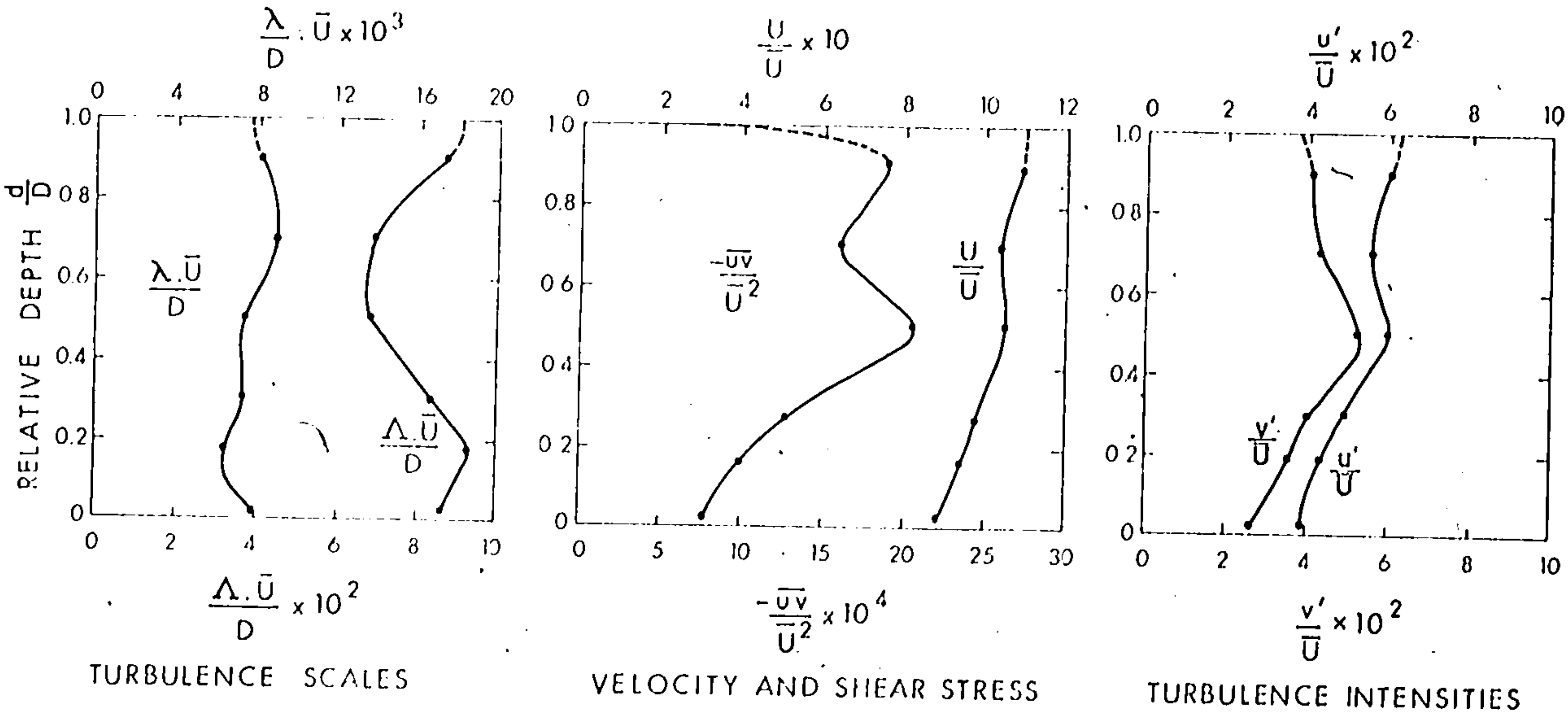

Fig. 30 — Vertical distribution of velocity and turbulence data for a rough flat bed 14" D/S from the screen - obtained from hot - film anemometer measurements;

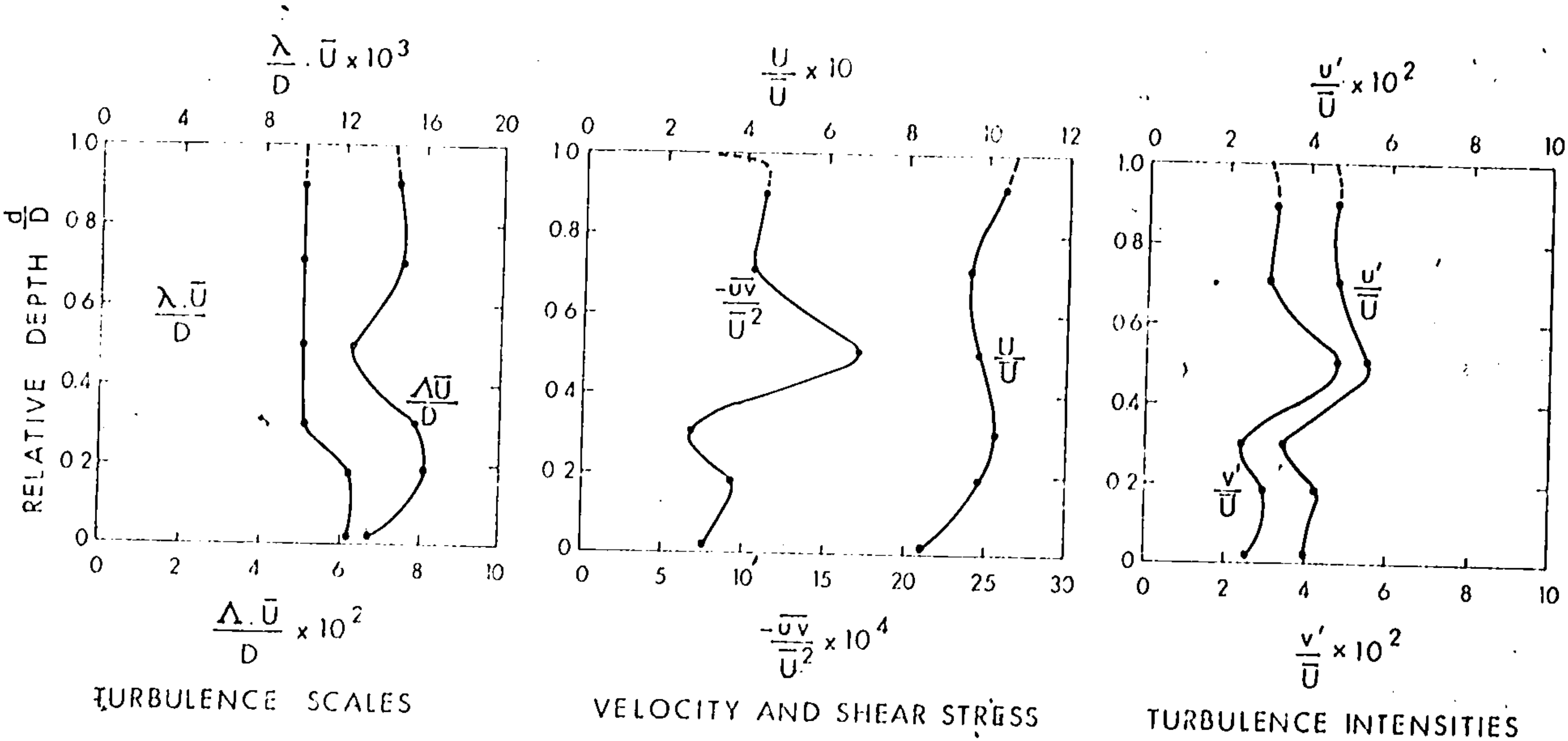

Fig. 31 — Vertical distribution of velocity and turbulence data for a smooth artificial ripple bed 14" D/S from the screen at ripple crest - obtained from hot - film anemometer measurements.

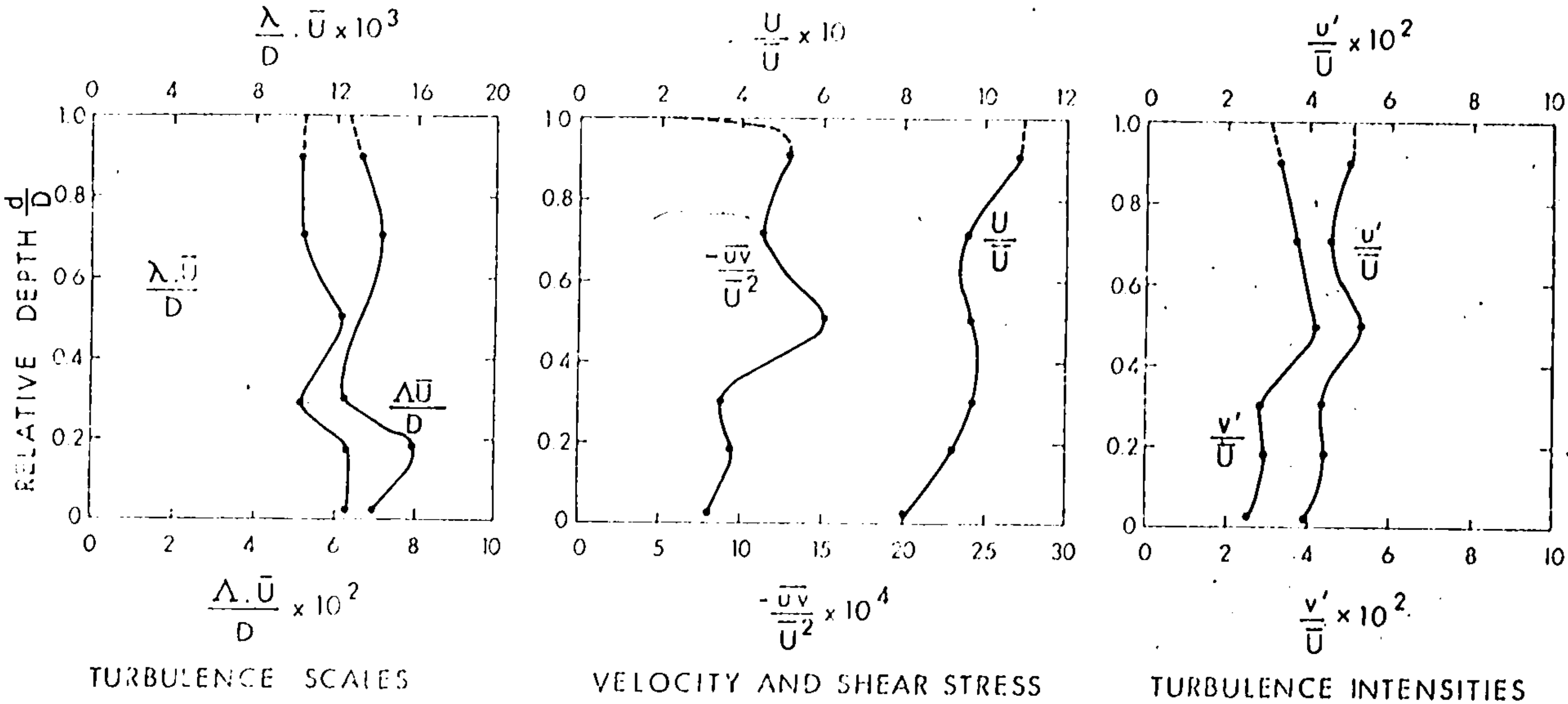

Fig. 32 Vertical distribution of velocity and turbulence data for a rough artificial ripple bed 14" D/S from the screen at ripple crest - obtained from hot-film anemometer measurements.

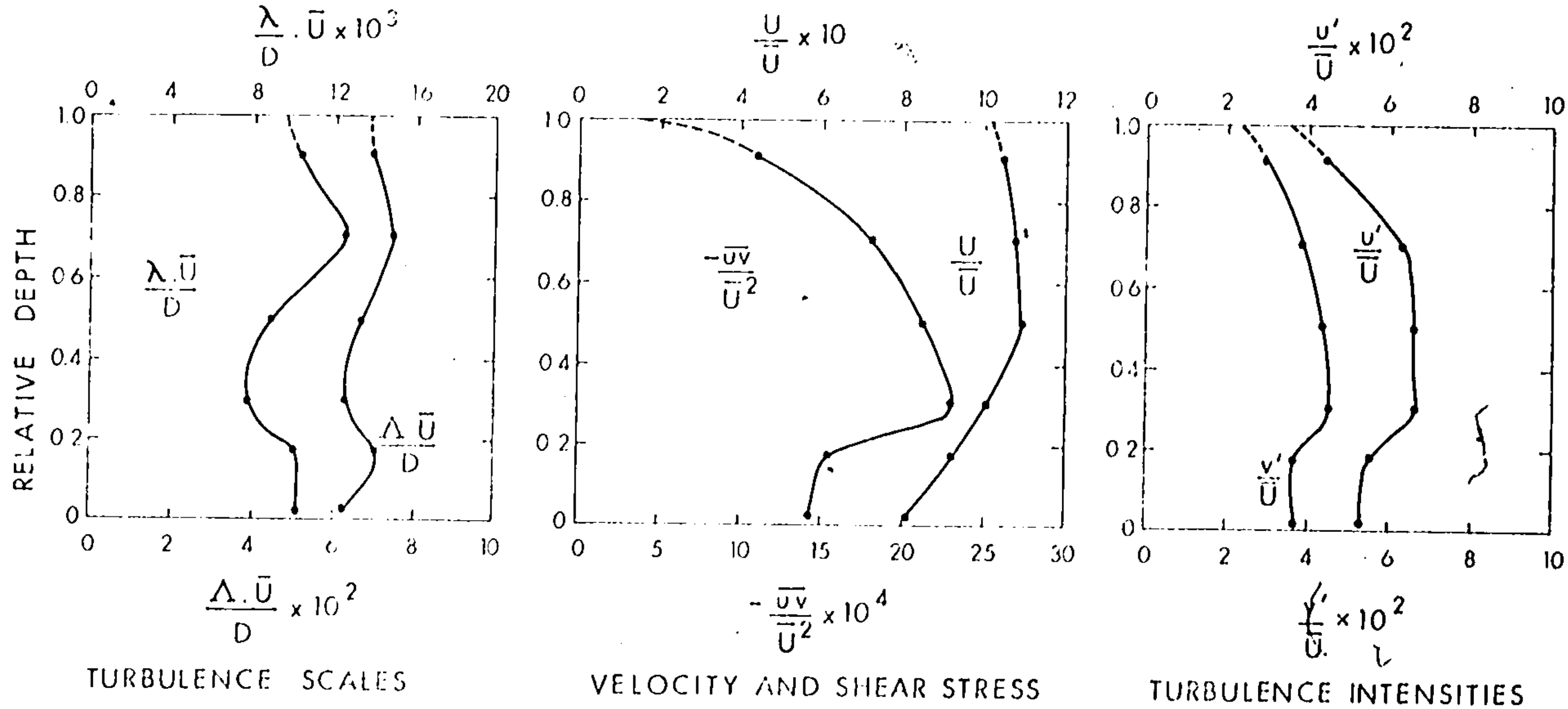

Fig. 33 — Vertical distribution of velocity and turbulence data for a cast of a natural ripple bed 14" D/S from the screen at ripple crest - obtained from hot-film anemometer measurements.

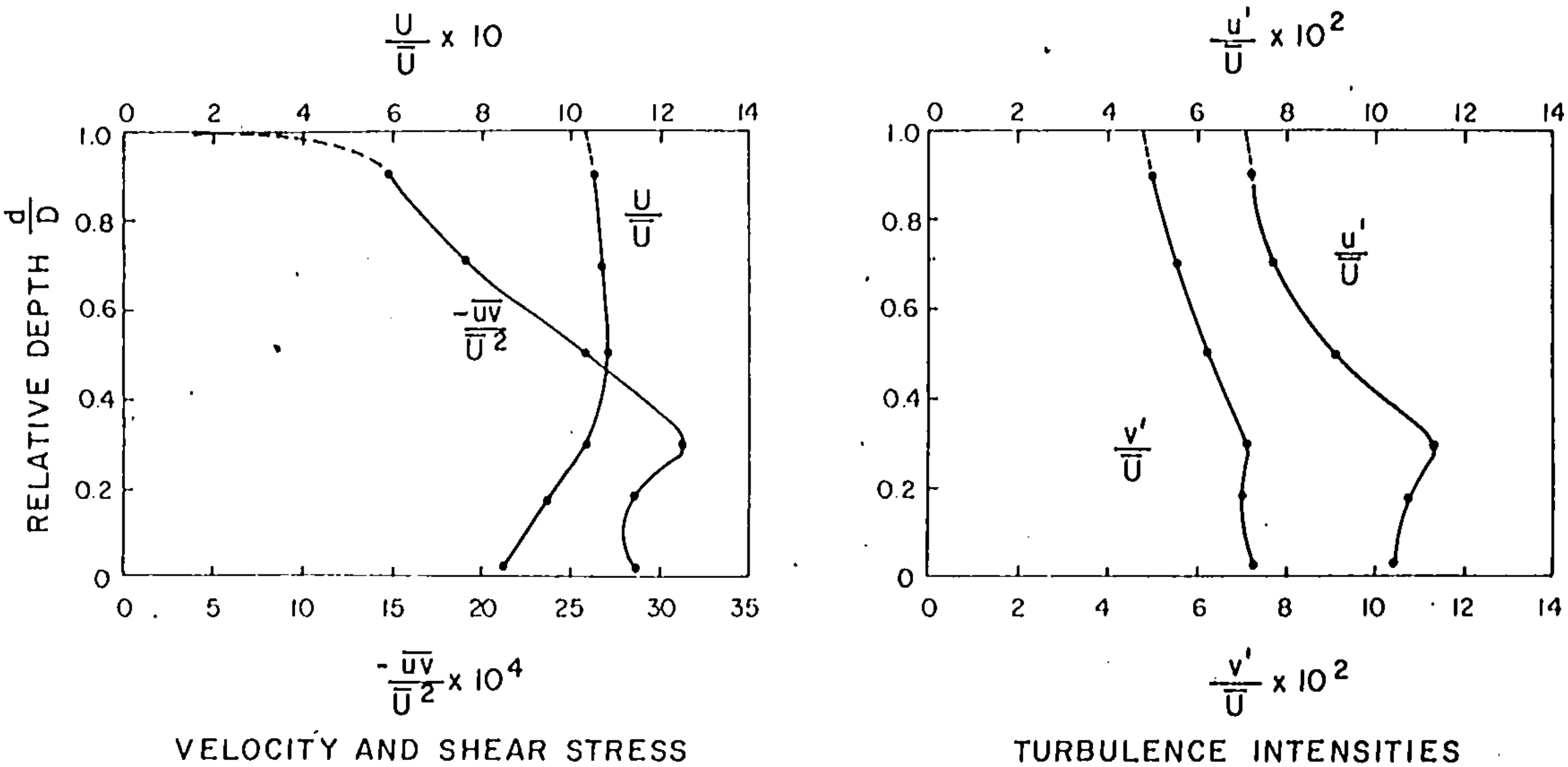

Fig. 34 — Vertical distribution of velocity and turbulence data for a cast of a natural ripple bed 21" D/S from the screen at ripple crest - obtained from hot-film anemometer measurements.

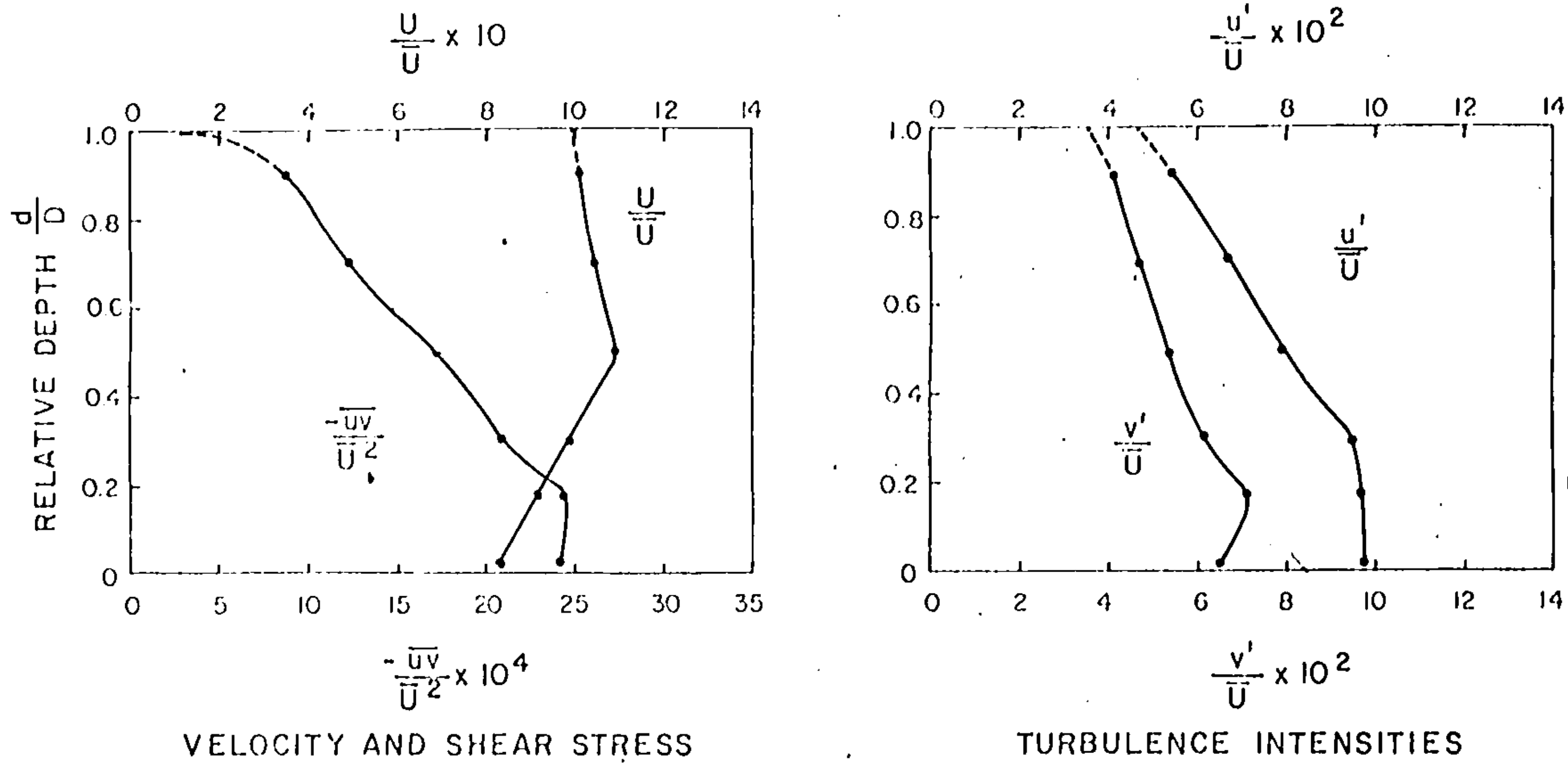

Fig. 35 — Vertical distribution of velocity and turbulence data for a cast of a natural ripple bed 31" D/S from the screen at ripple crest - obtained from hot film anemometer measurements.

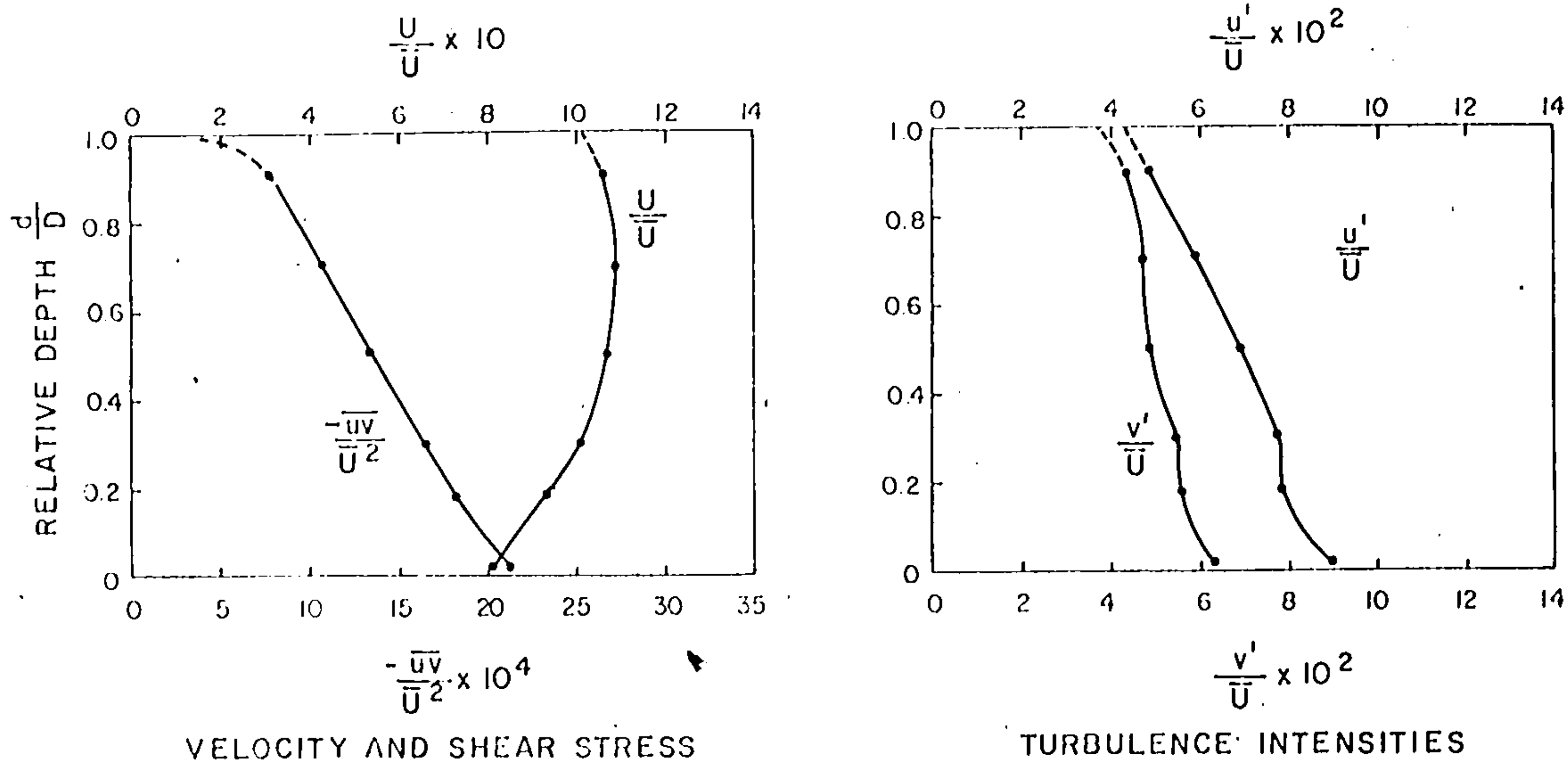

Fig. 36 — Vertical distribution of velocity and turbulence data for a cast of a natural ripple bed 37" D/S from the screen at ripple crest - obtained from hot film anemometer measurements.

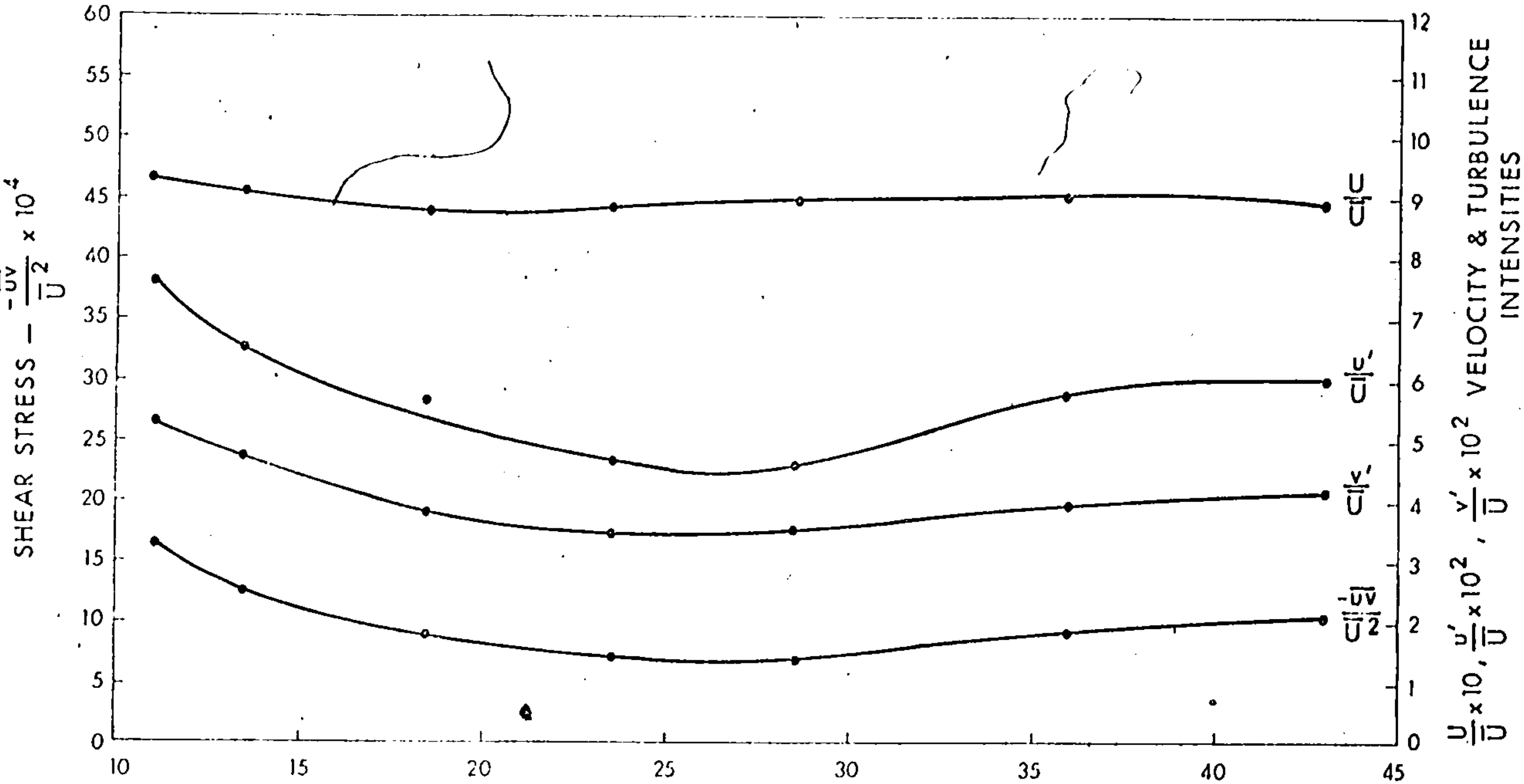

Fig. 37 — Velocity and turbulence data along a smooth flat bed 0.125" above the floor obtained from the hot-film anemometer measurements.

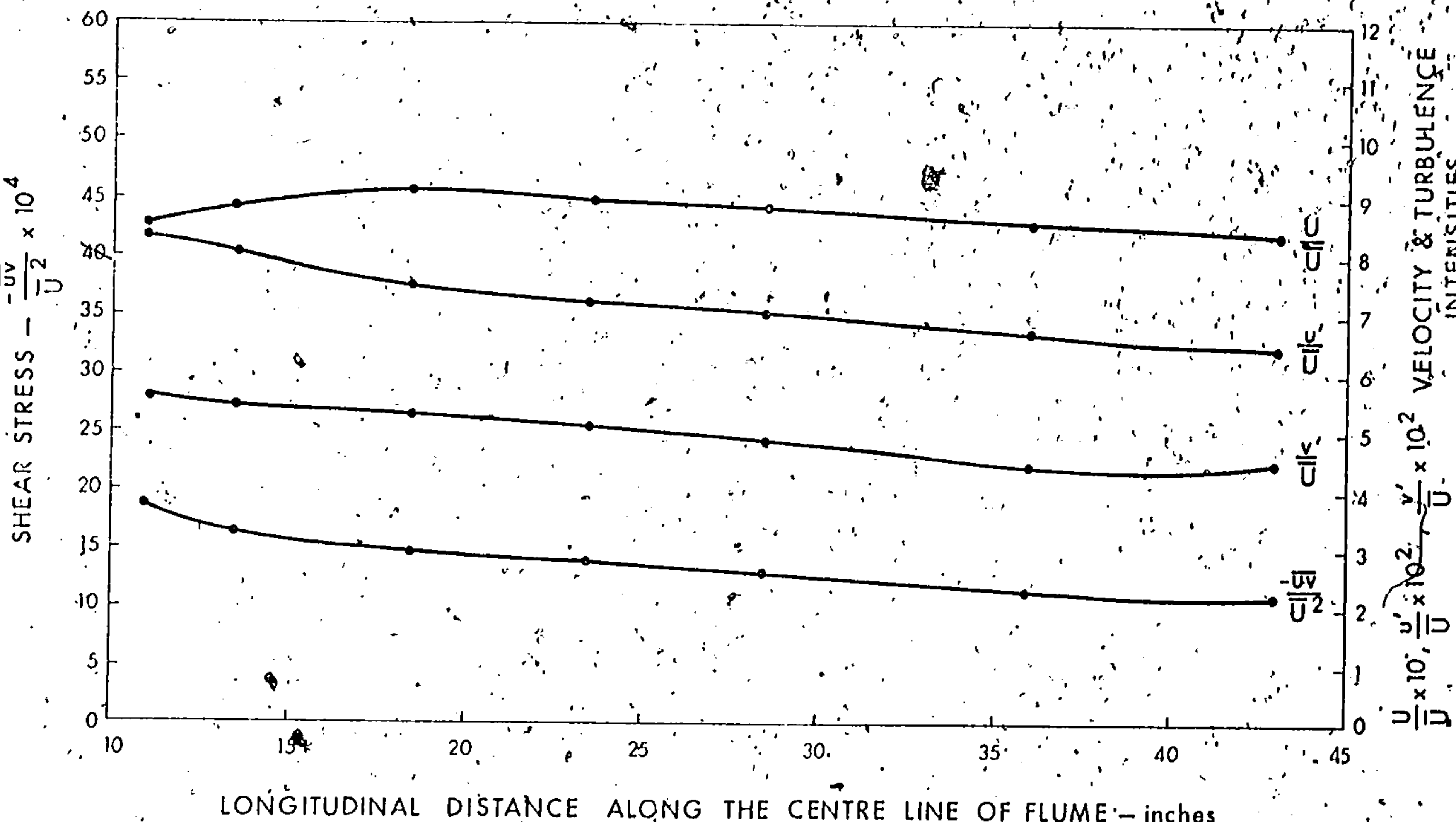

Fig. 38 – Velocity and turbulence data alone a rough flat bed 0.125" above the floor obtained from the hot-film anemometer measurements.

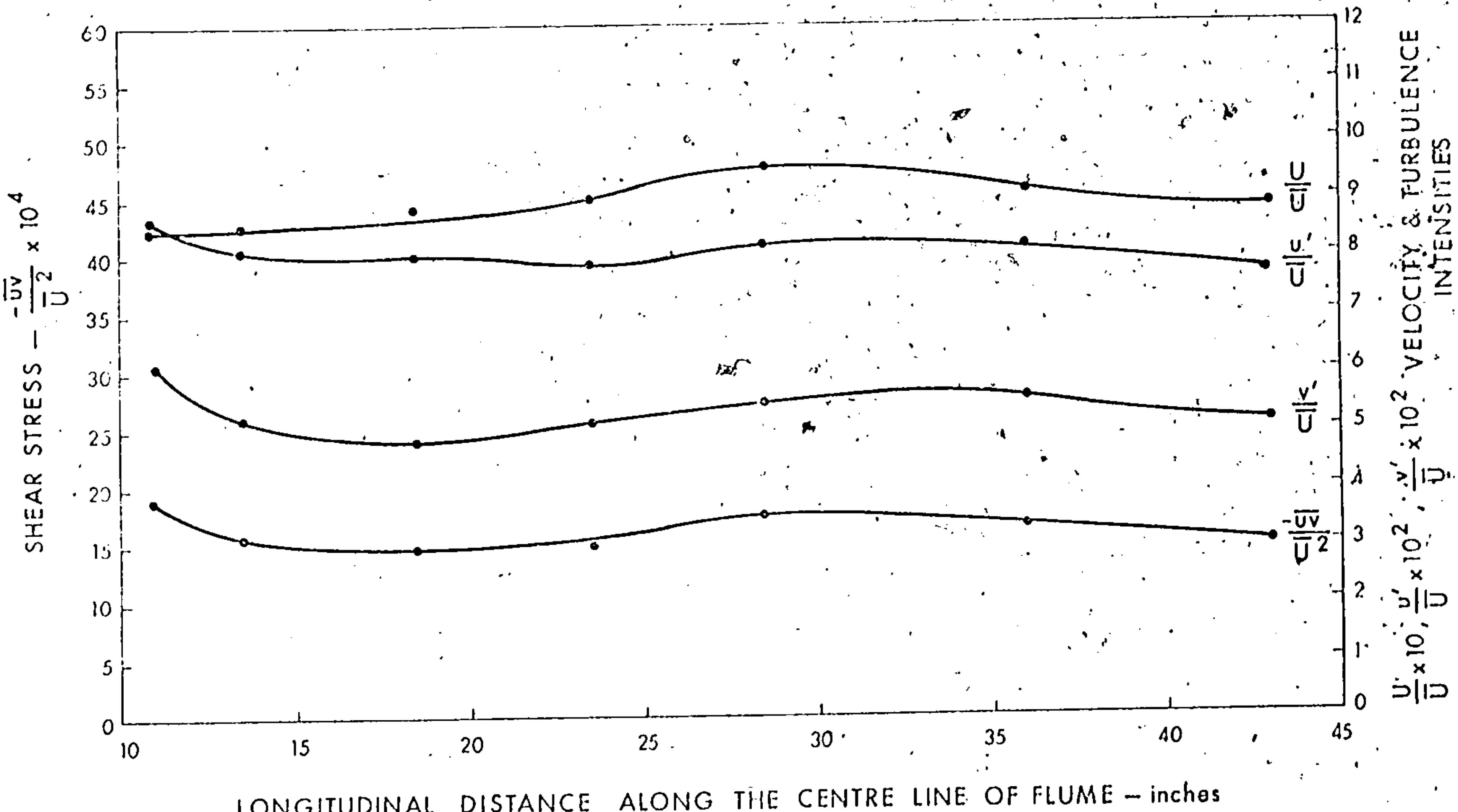

Fig. 39 – Velocity and turbulence data along a smooth artificial ripple bed 0.125" above ripple crests obtained from the hot-film anemometer measurements.

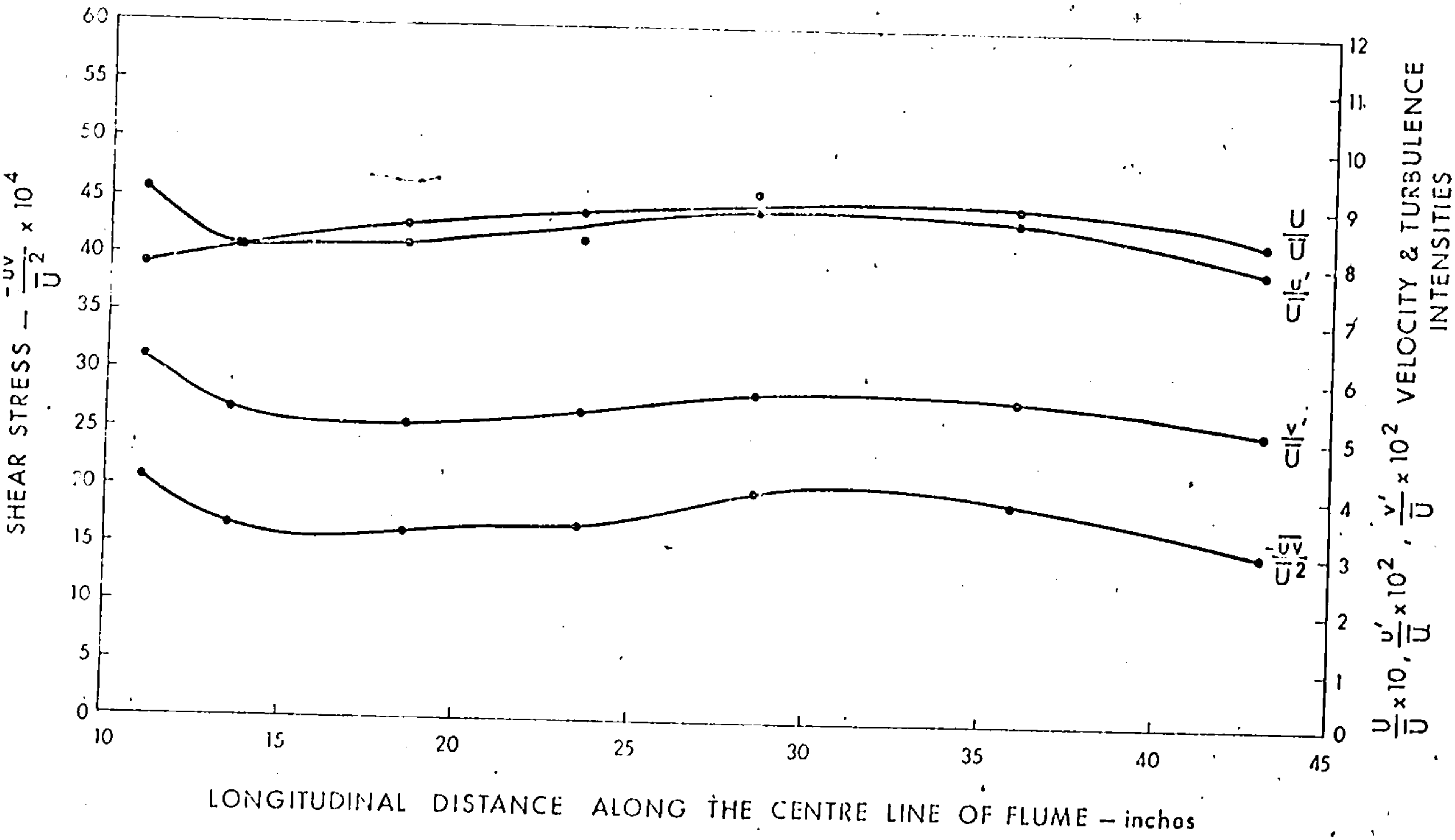

Fig. 40 – Velocity and turbulence data along a rough artificial ripple bed 0.125" above ripple crests obtained from the hot-film anemometer measurements.

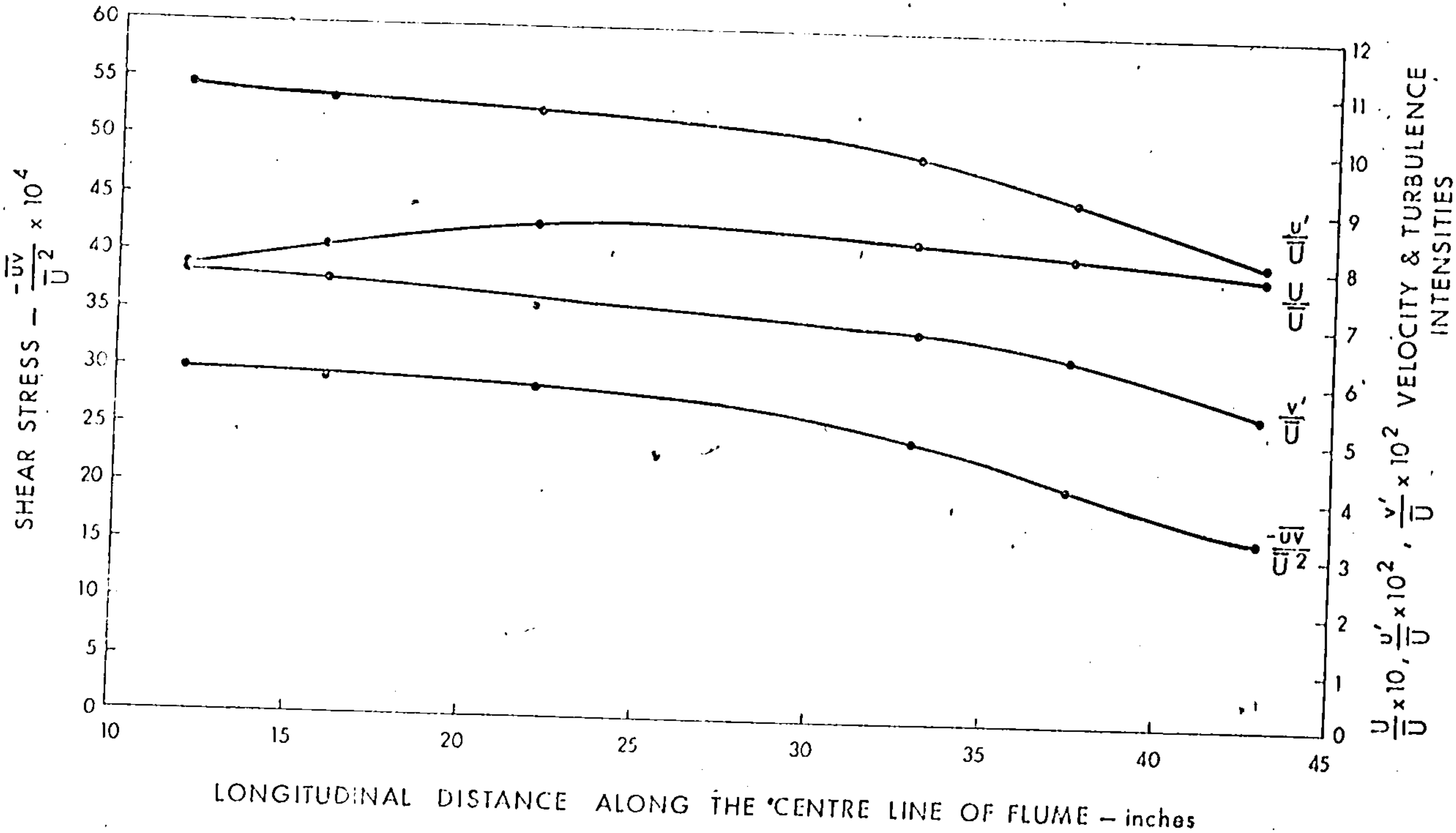

Fig. 41 – Velocity and turbulence data along a cast of a natural ripple bed 0.125" above ripple crests obtained from the hot-film anemometer measurements.

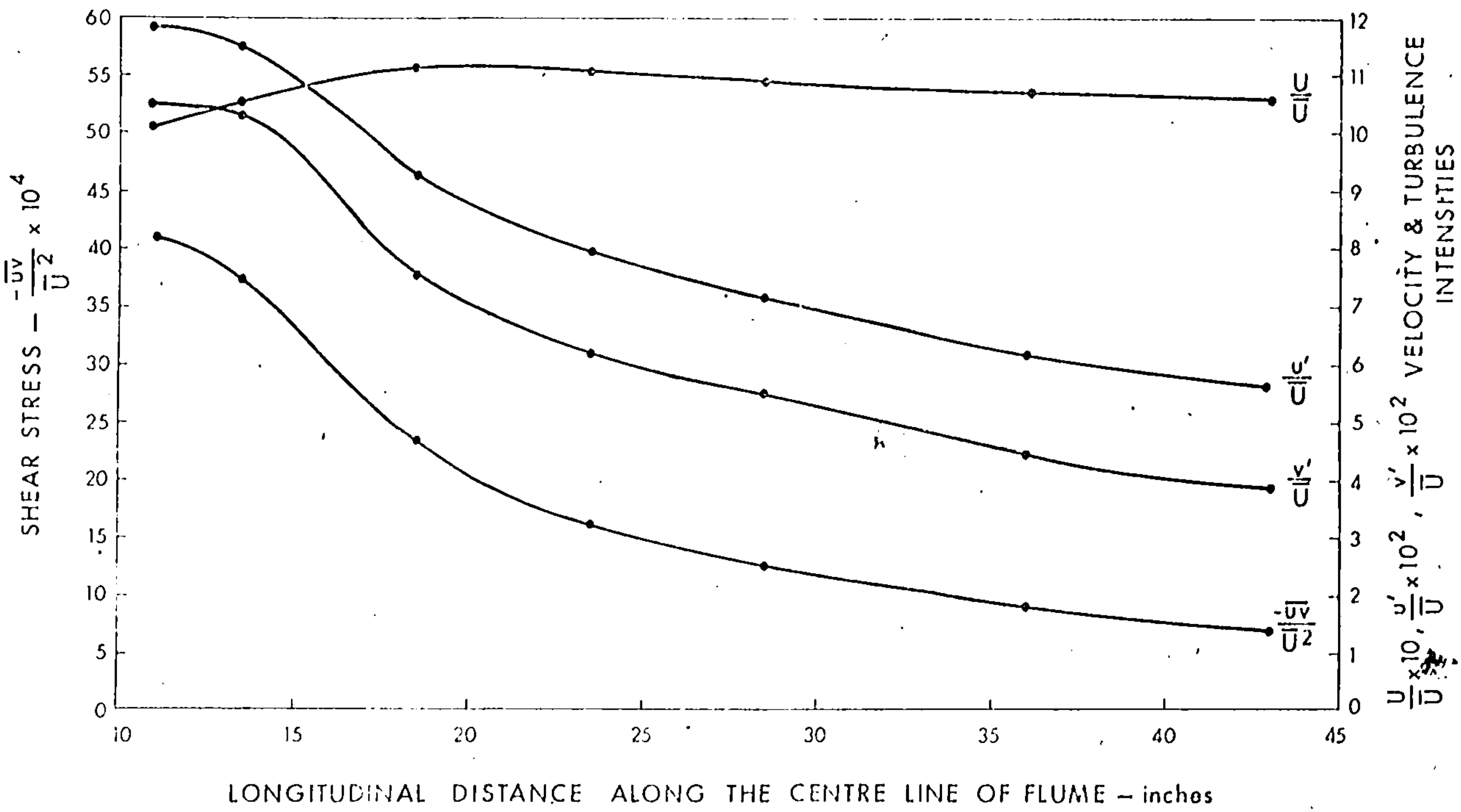

Fig. 42 – Velocity and turbulence data along a smooth flat bed 2.5" above the floor obtained from the hot-film anemometer measurements.

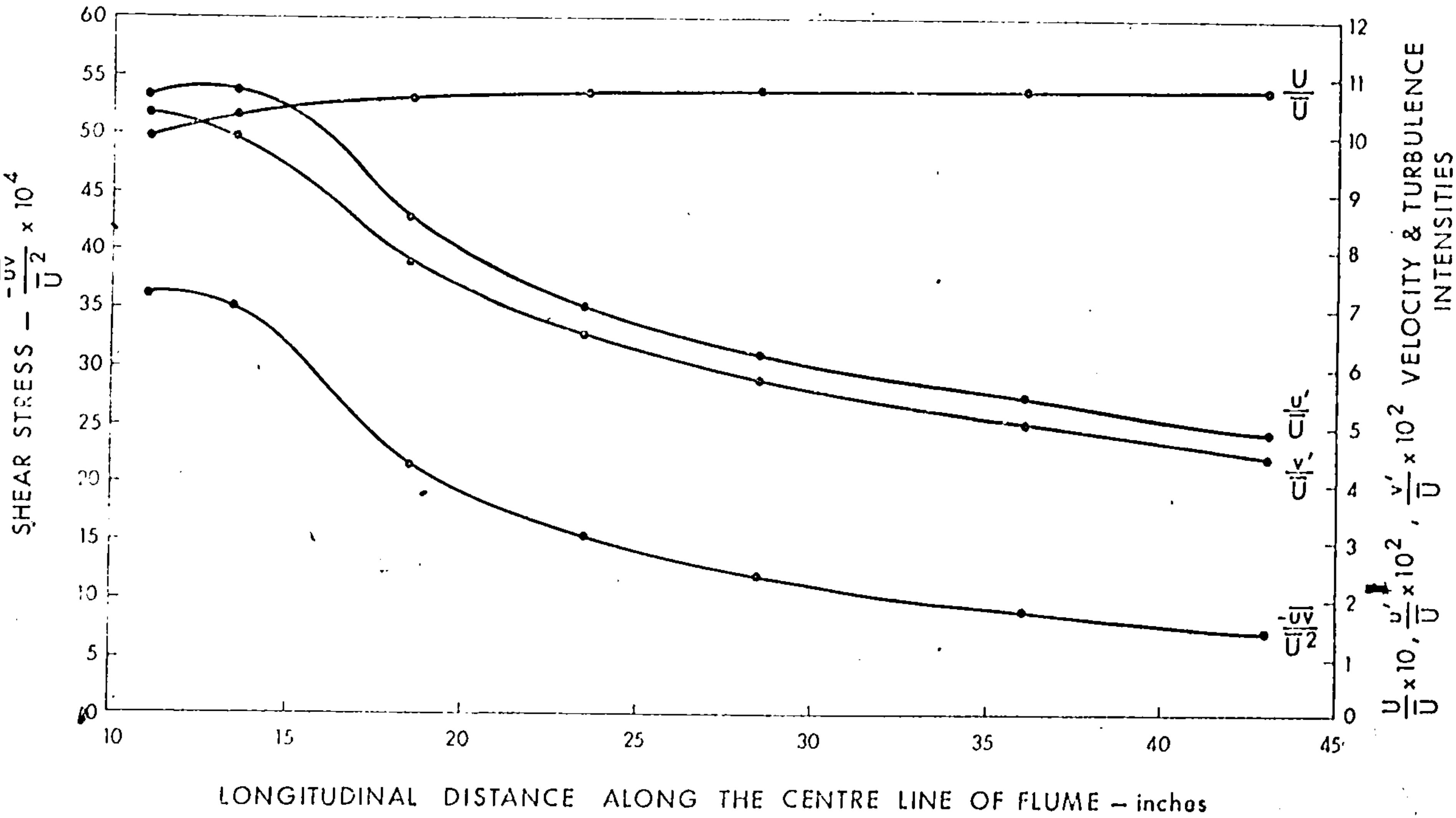

Fig. 43 – Velocity and turbulence data along a rough flat bed 2.5" above the floor obtained from the hot-film anemometer measurements.

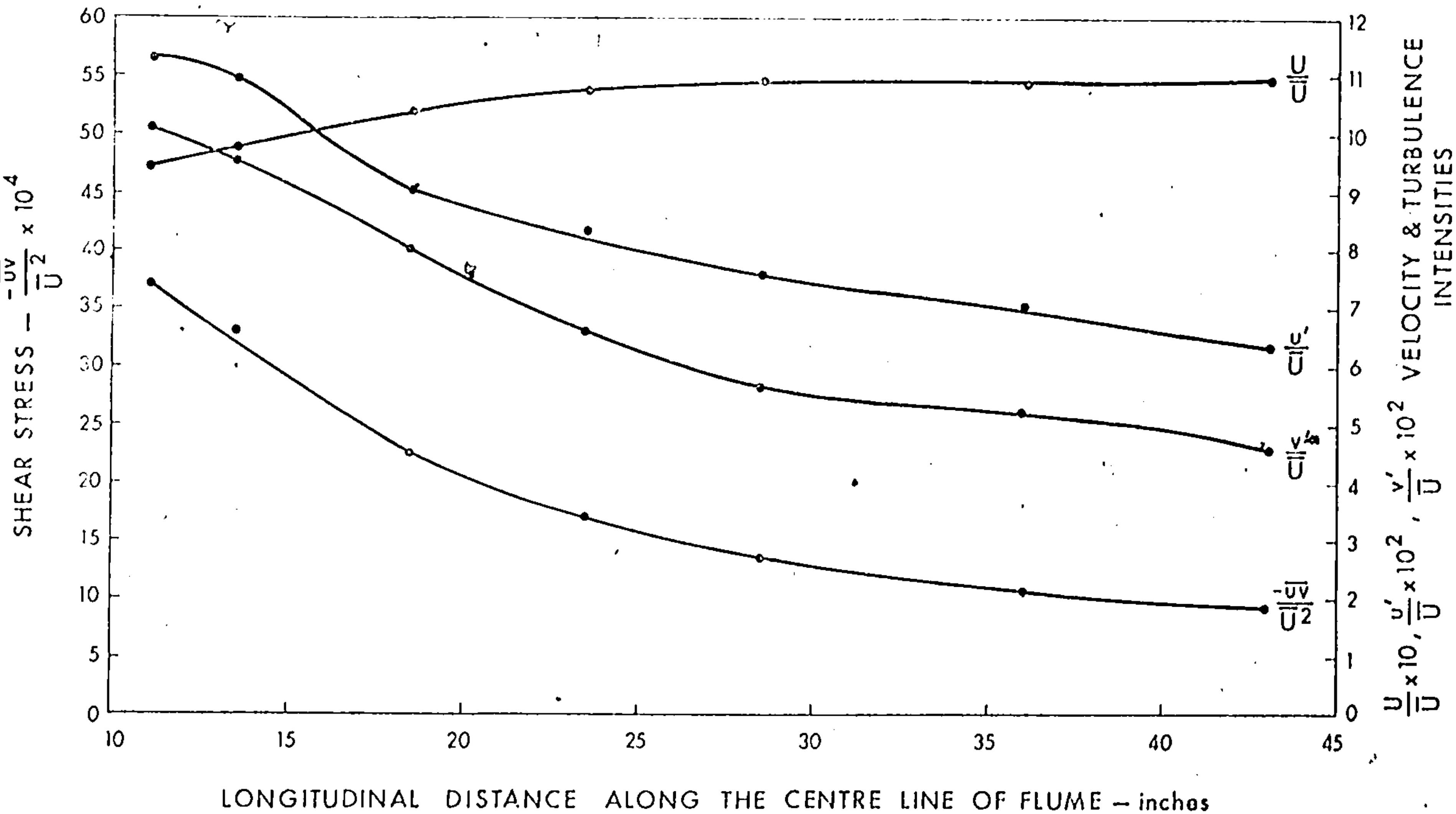

Fig. 44 — Velocity and turbulence data along a smooth artifical ripple bed 2.5" above the floor obtained from the hot-film anemometer measurements.

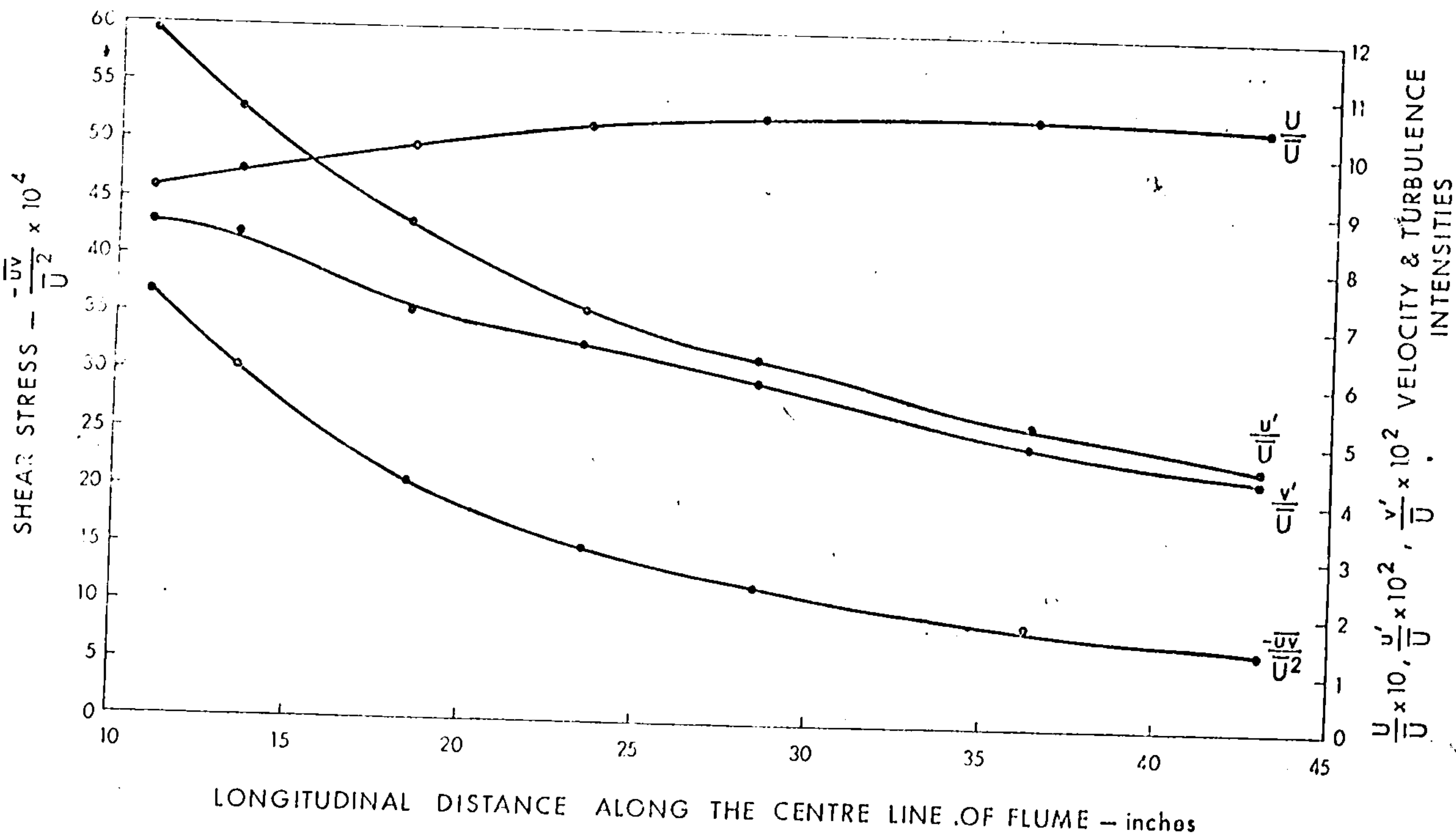

Fig. 45 – Velocity and turbulence data along a rough artificial ripple bed 2.5" above the floor obtained from the hot-film anemometer measurements.

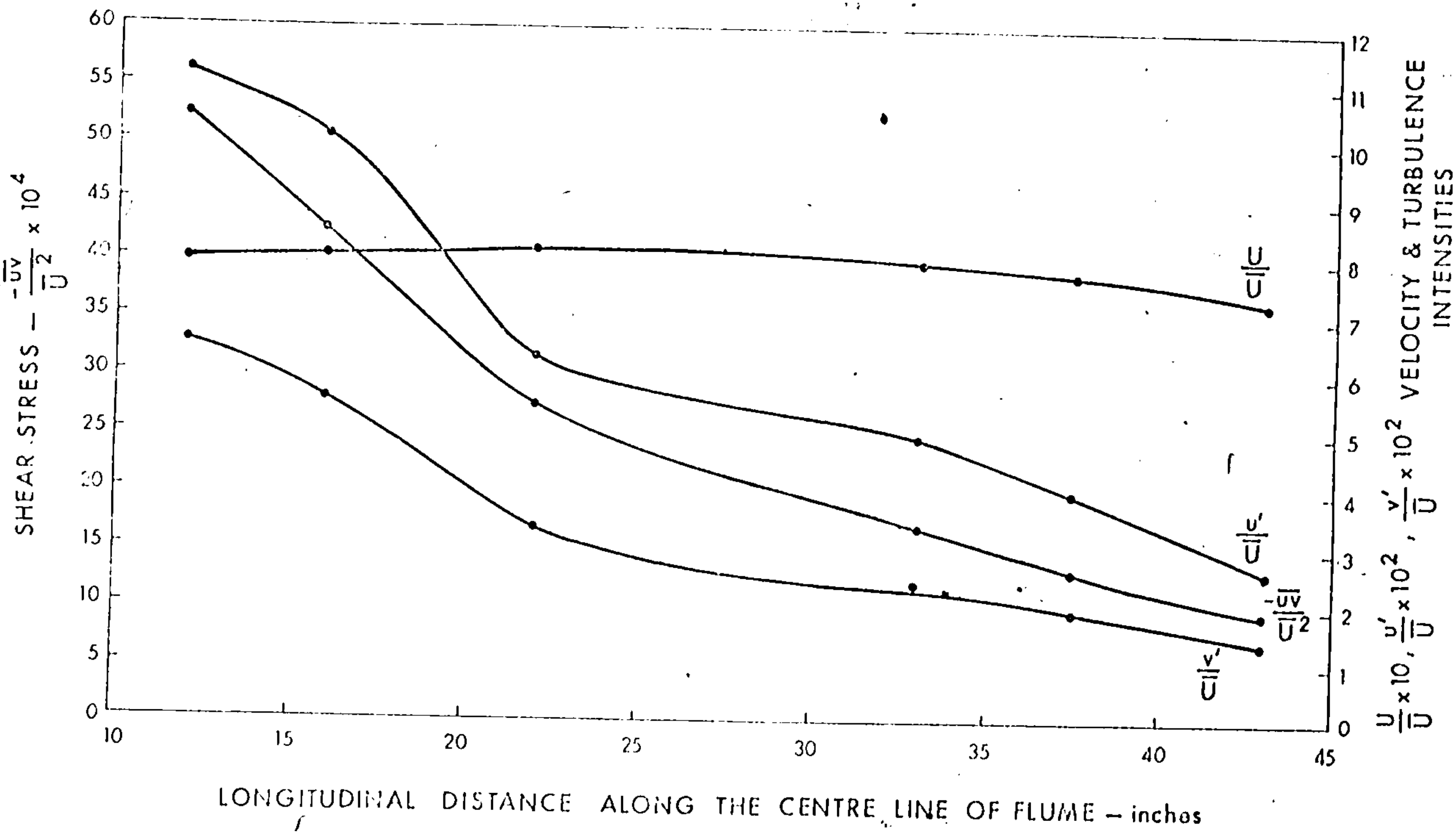

Fig. 46 – Velocity and turbulence data along a cast of a natural ripple bed 2.5" above the floor obtained from the hot-film anemometer measurements.

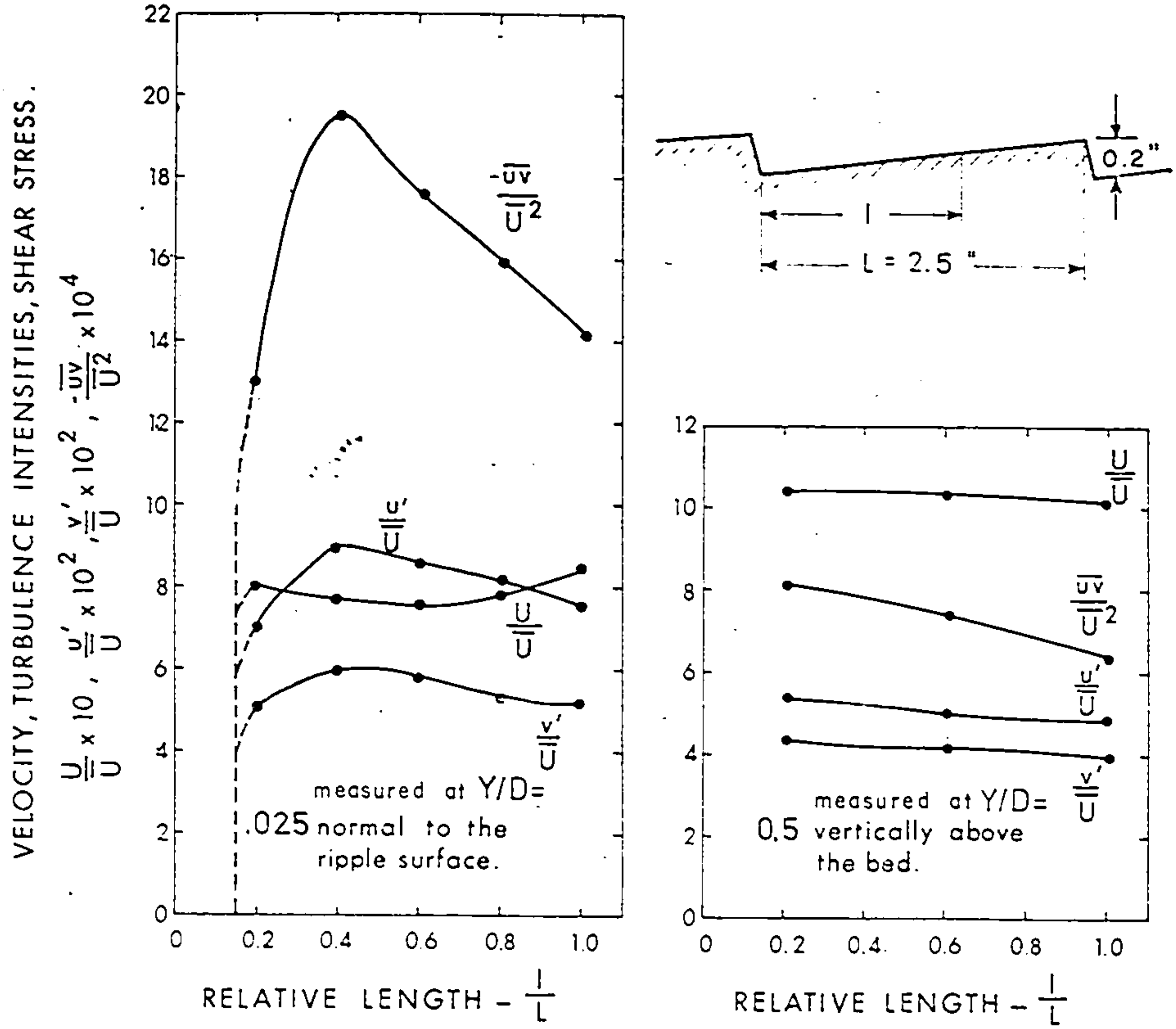

Fig. 47 — Velocity, turbulence intensities and shear stress variations along one ripple 44" D/S from the screen in a rough artifical ripple bed - obtained from the hot-film anemometer measurements.

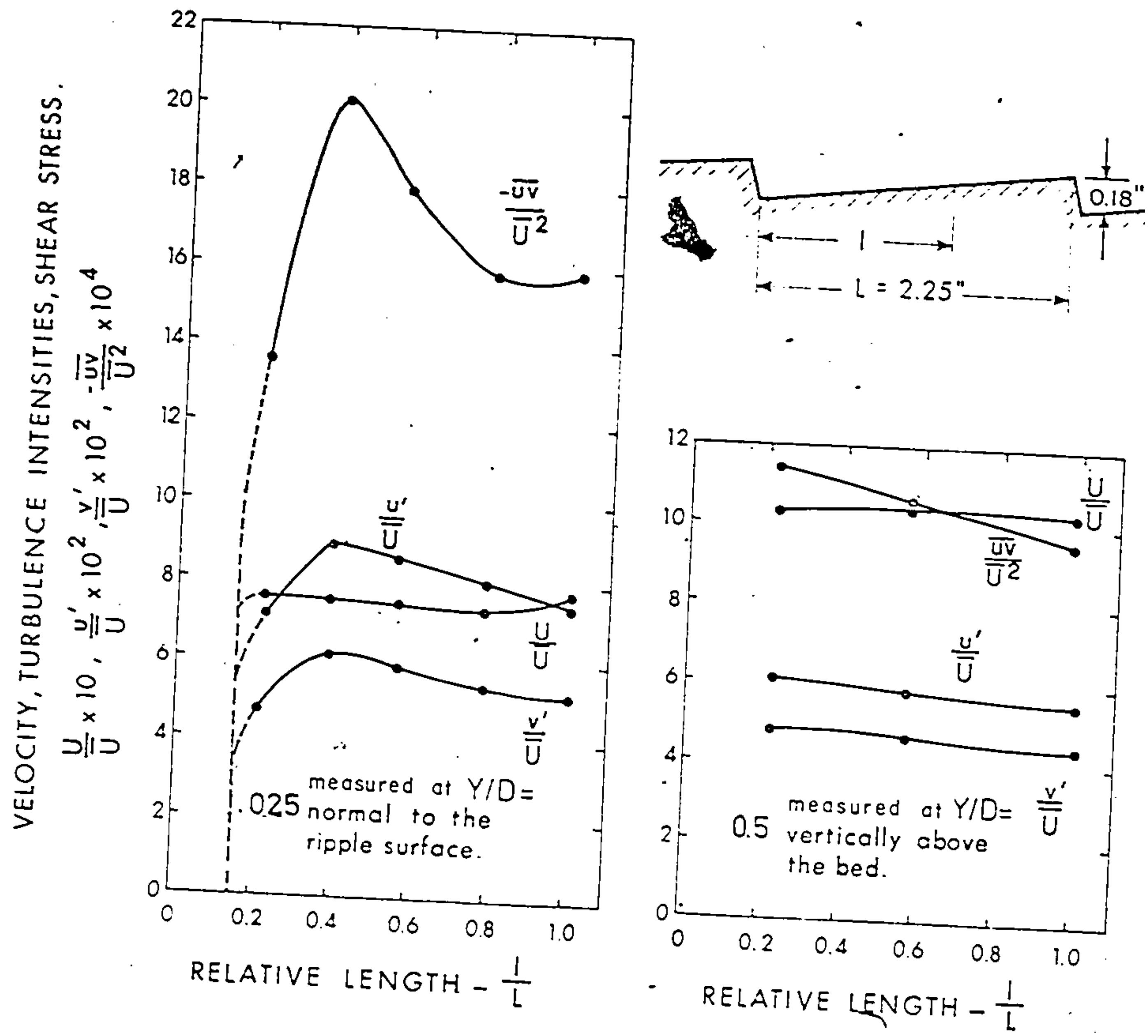

Fig. 48 – Velocity, turbulence intensities and shear stress variations along one ripple 44" D/S from the screen in a cast of a natural ripple bed - obtained from the hot-film anemometer measurements.

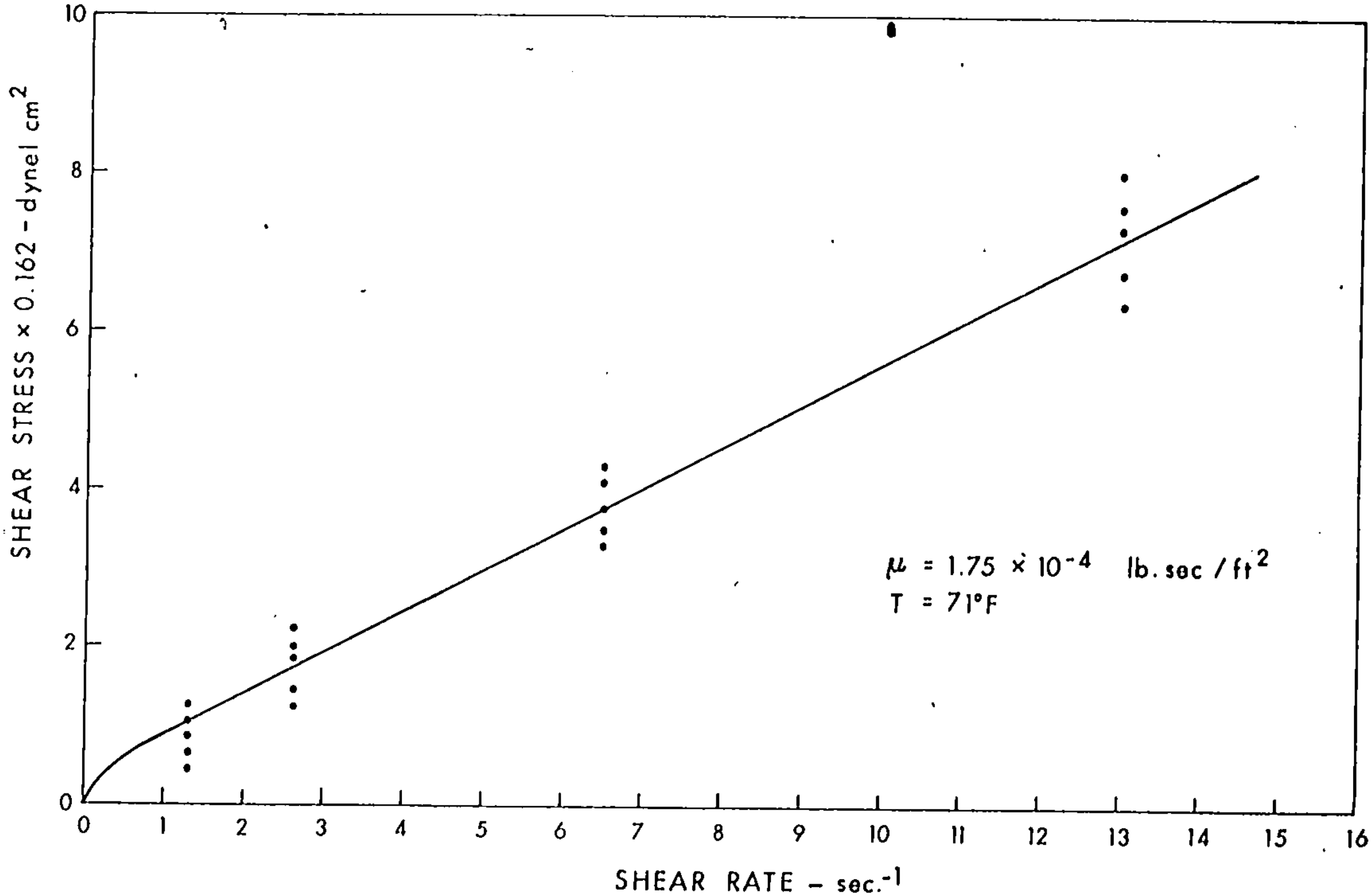

Fig. 49 – Viscosity of milling - yellow solution

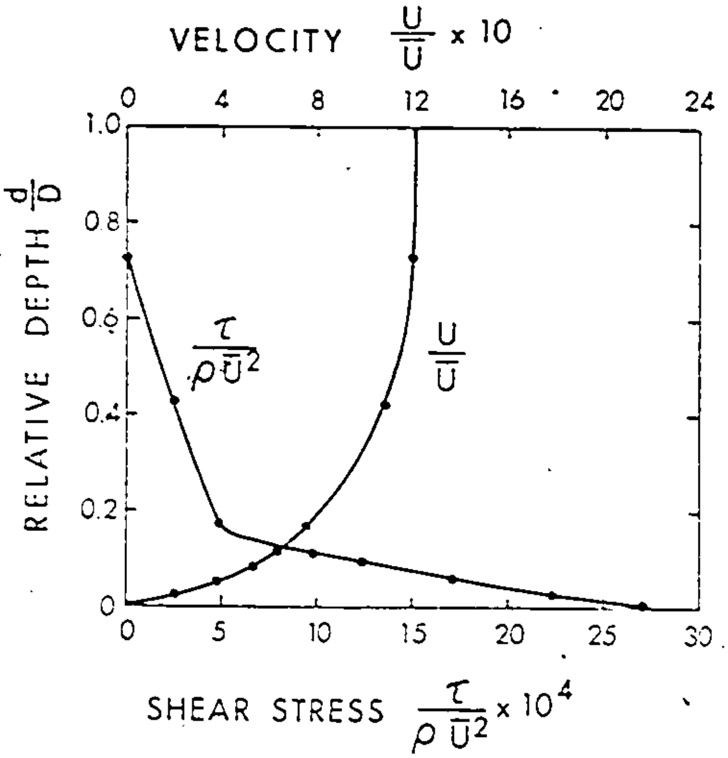

Fig. 50 — Velocity and shear stress distributions over a cast of a natural ripple bed, above ripple crest 44" D/S from the screen - obtained from flow visualization analysis.

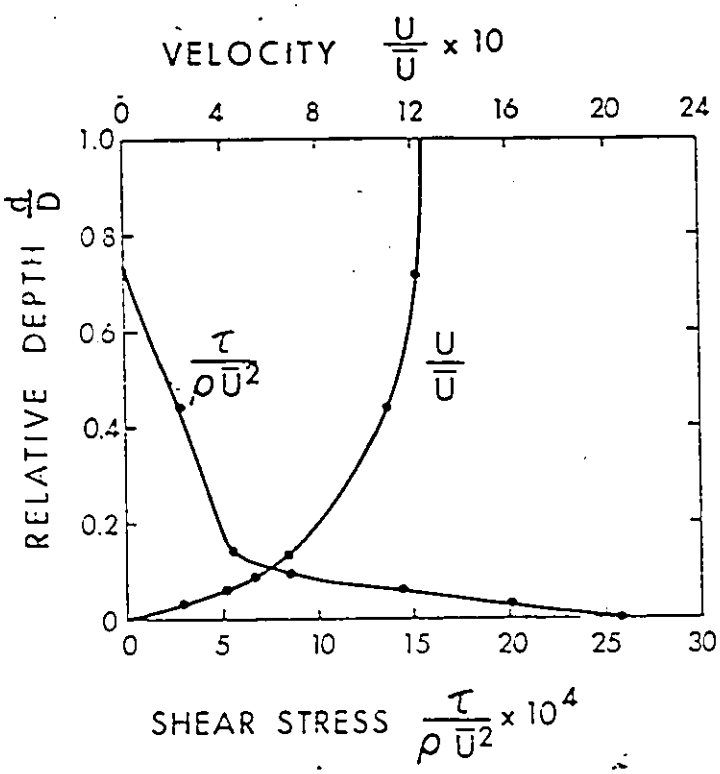

Fig. 51 — Velocity and shear stress distributions over a rough artifical ripple bed, above ripple crest 44" D/S from the screen - obtained from flow visualization analysis.

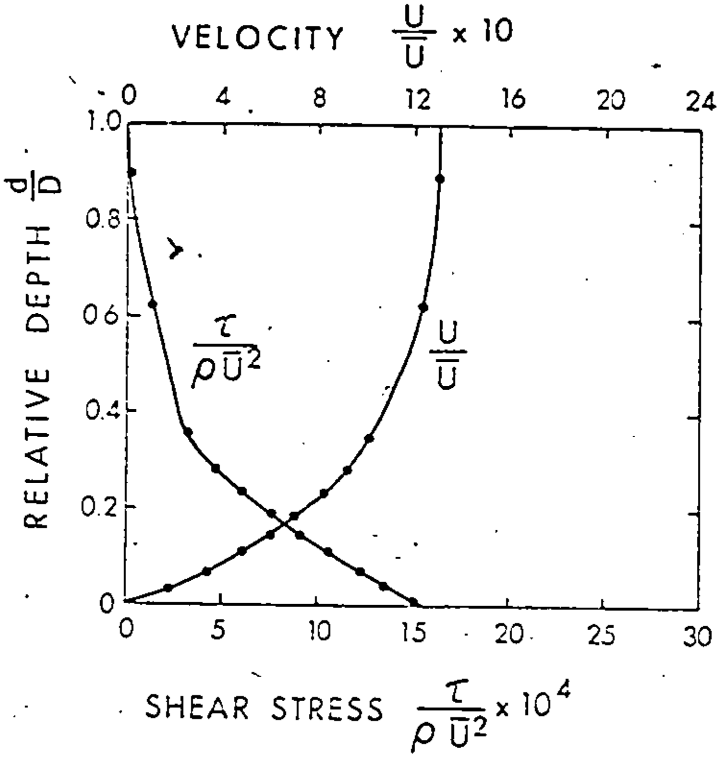

Fig. 52 — Velocity and shear stress distributions over a smooth artifical ripple bed, above ripple crest 44" D/S from the screen - obtained from flow visualization analysis.

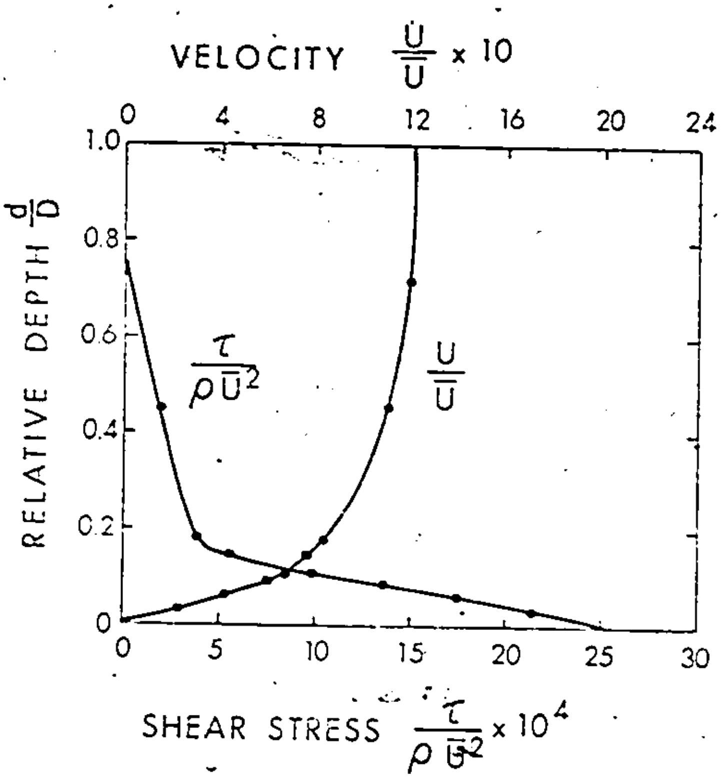

Fig. 53 — Velocity and shear stress distributions over a rough flat bed 44" D/S from the screen - obtained from flow visualization analysis

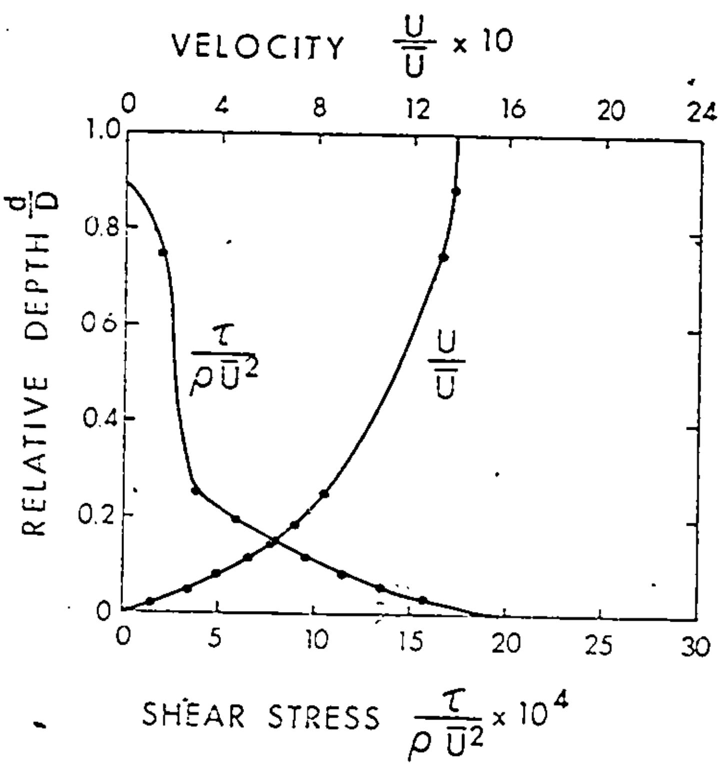

Fig. 54 — Velocity and shear stress distributions over a smooth flat bed 44" D/S from the screen - obtained from flow visualization analysis.

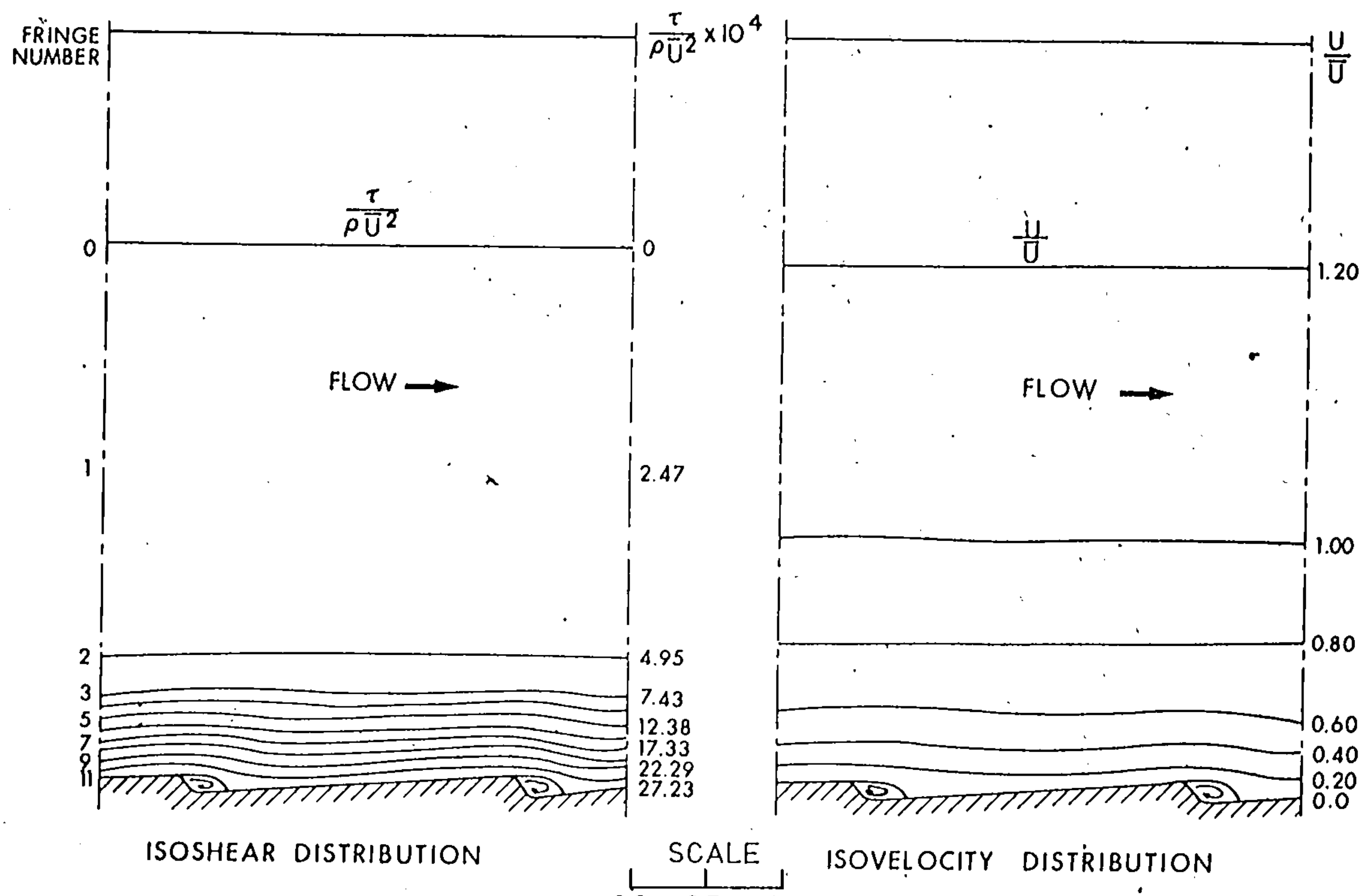

Fig. 55 — Isoshear and Isovelocity patterns over a cast of a natural ripple bed 44" D/S from the screen - obtained from flow visualization analysis.

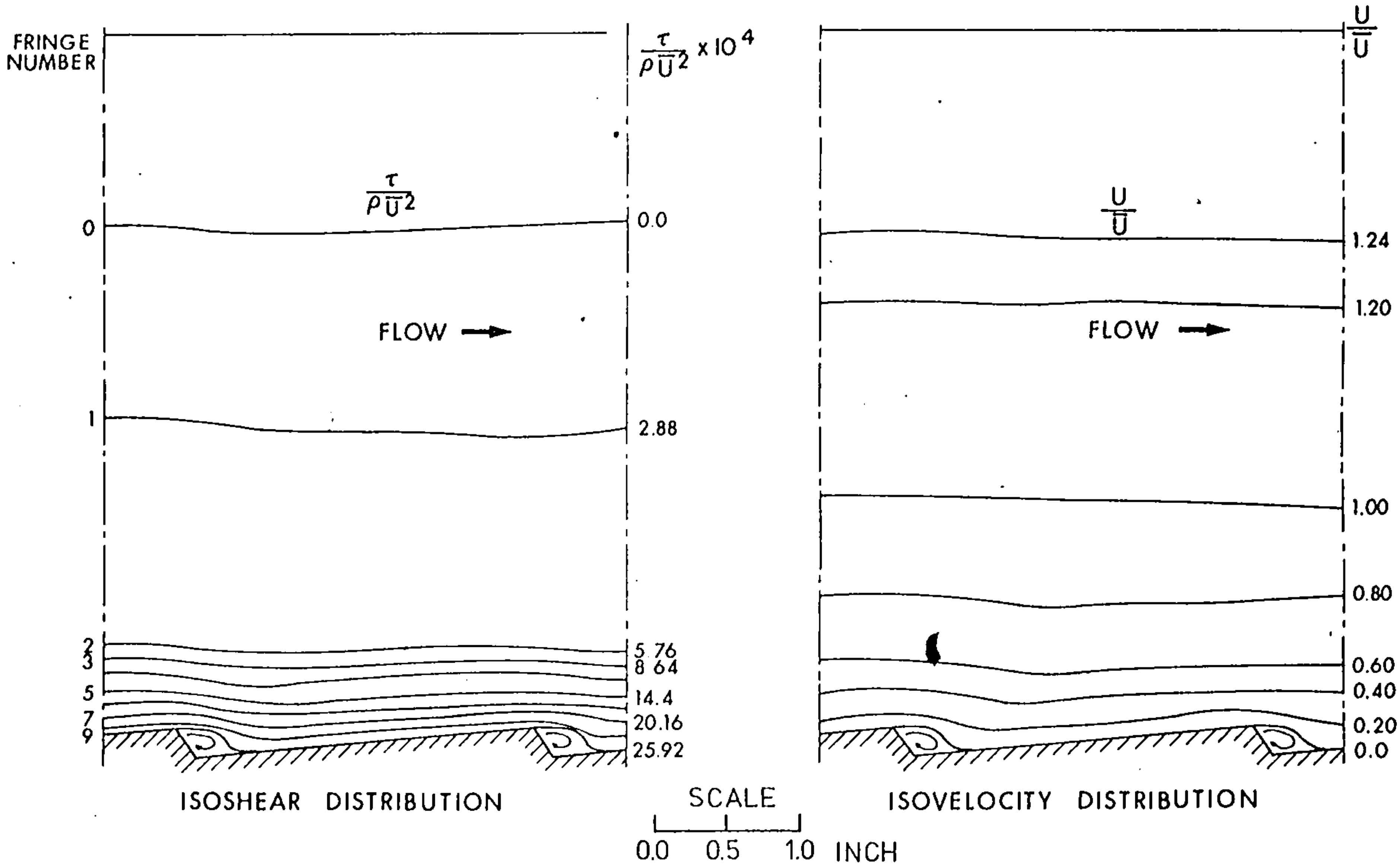

Fig. 56 — Isoshear and Isovelocity patterns over a rough artificial ripple bed 44" D/S from the screen - obtained from flow visualization analysis.

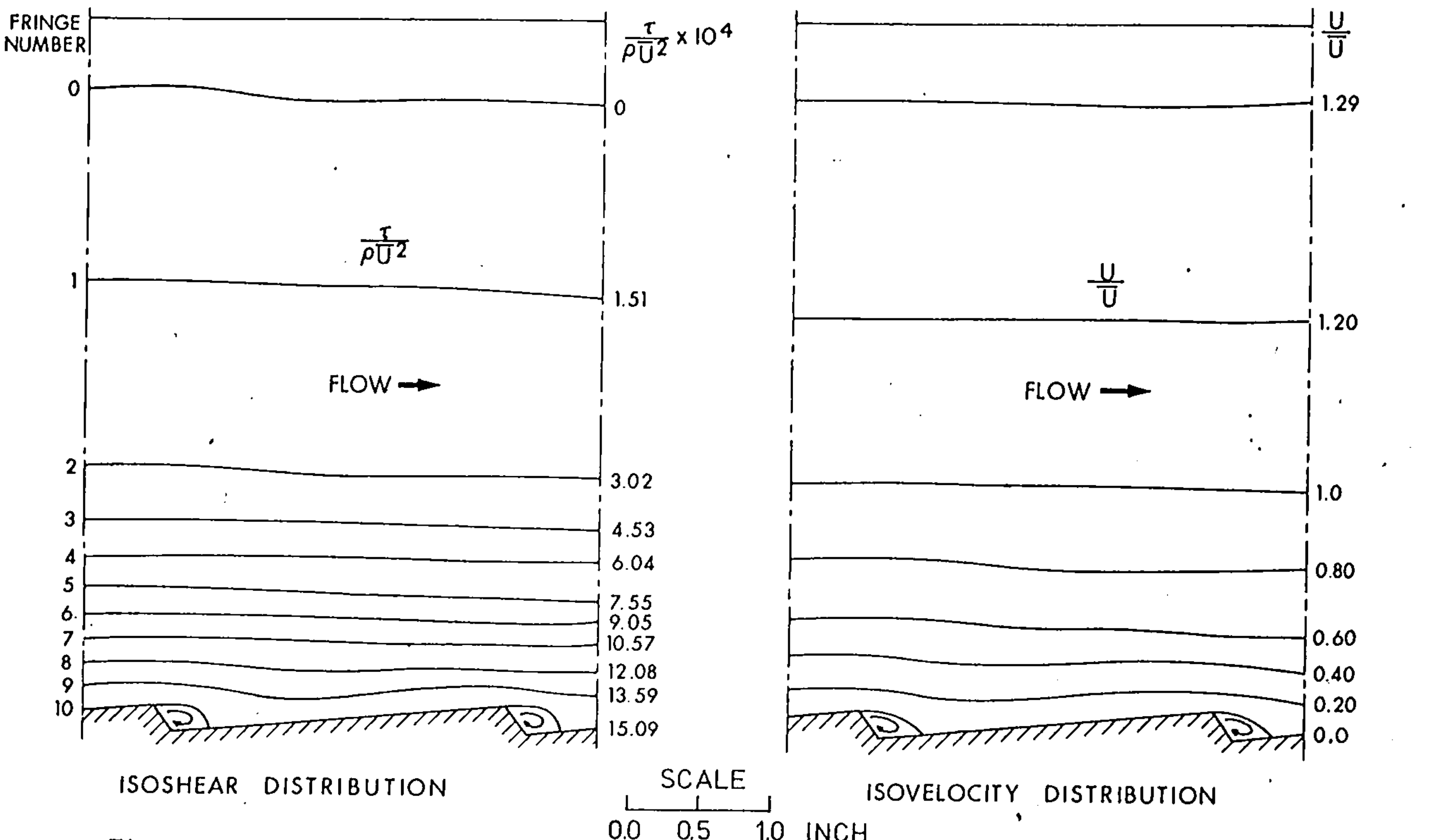

Fig. 57 — Isoshear and Isovelocity patterns over a smooth artificial ripple bed 44" D/S from the screen - obtained from flow visualization analysis.

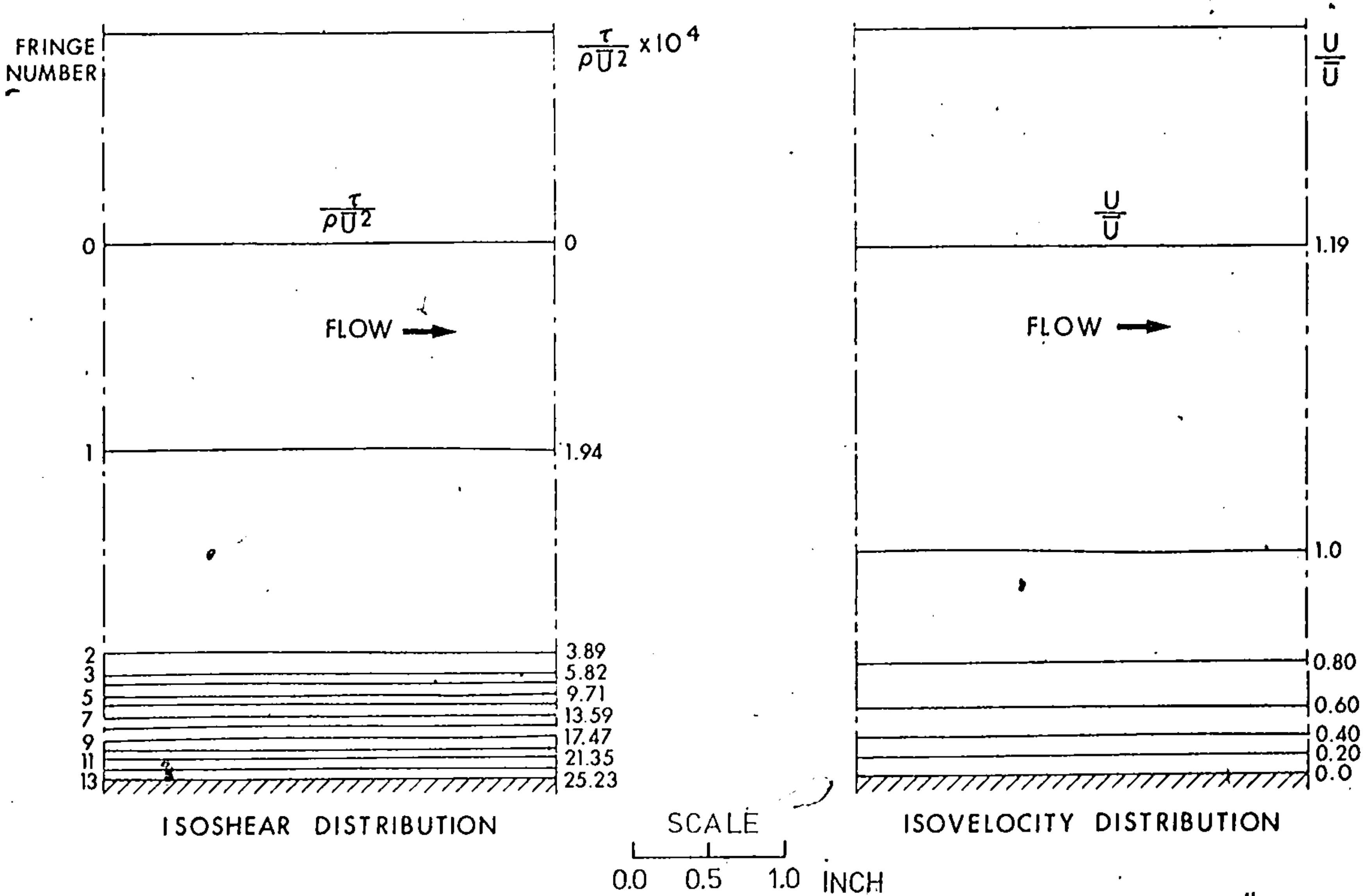

Fig. 58 — Isoshear and Isovelocity patterns over a rough flat bed 44" D/S from the screen obtained from flow visualization analysis.

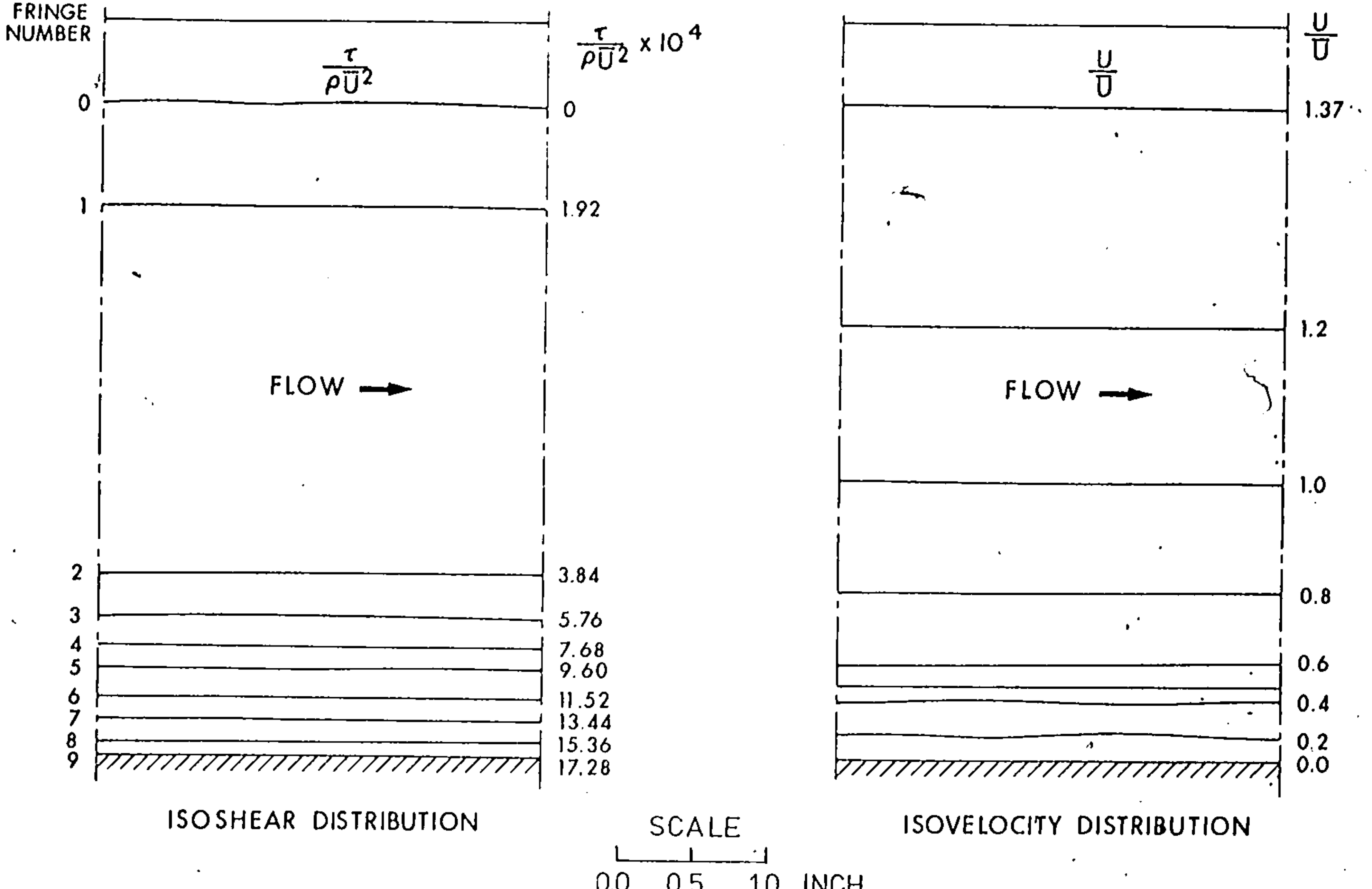

Fig. 59 — Isoshear and Isovelocity patterns over a smooth flat bed 44" D/S from the screen obtained from flow visualization analysis.

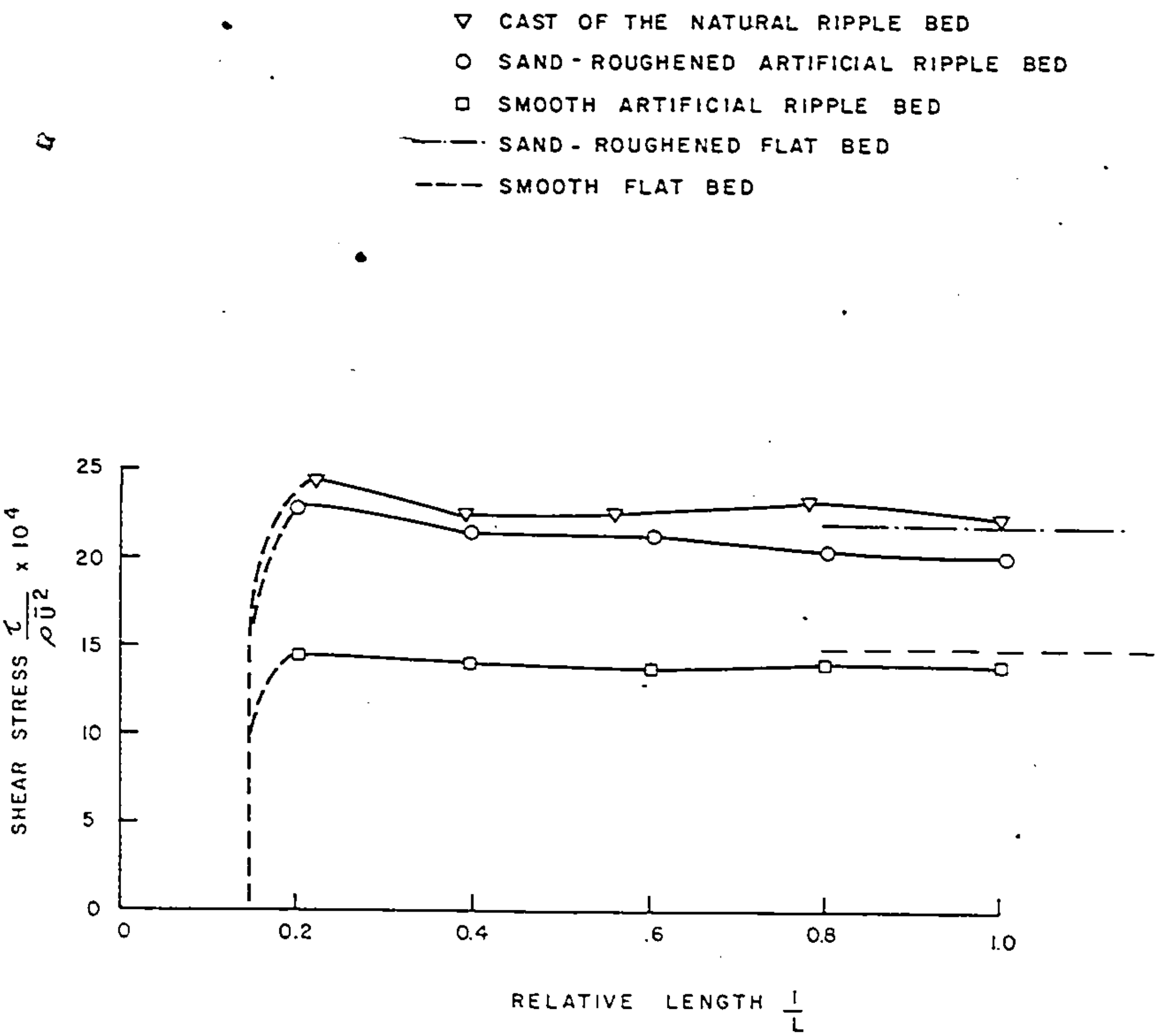

Fig. 60 — Shear stress variation at 0.125" above the bed, obtained from flow visualization technique.

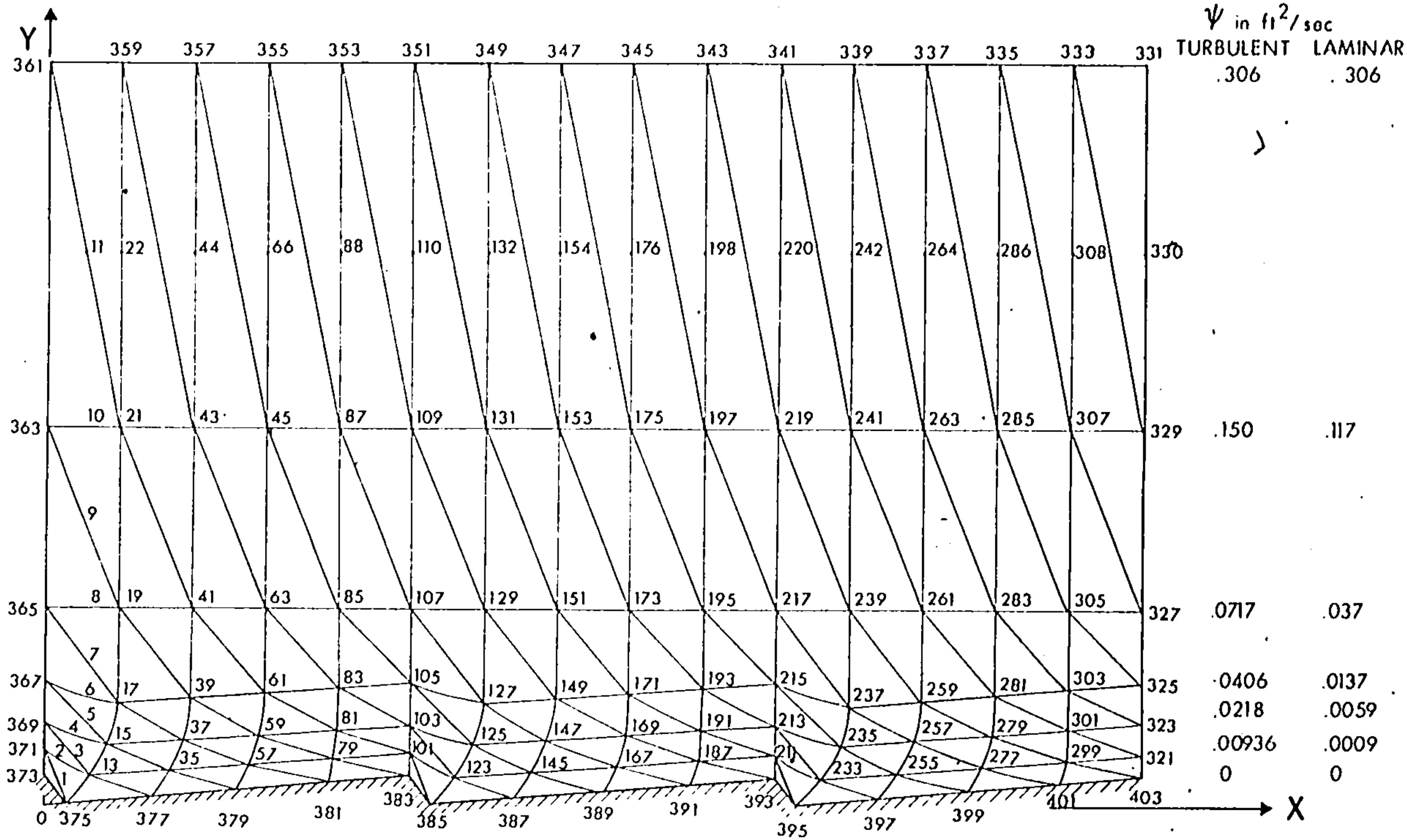

Fig. 61 — The typical arrangement of the six nodes triangular elements of the finite element method.

NUMBER OF ELEMENTS = 180
NUMBER OF UNKNOWN NODES = 330
TOTAL NUMBER OF NODES = 403

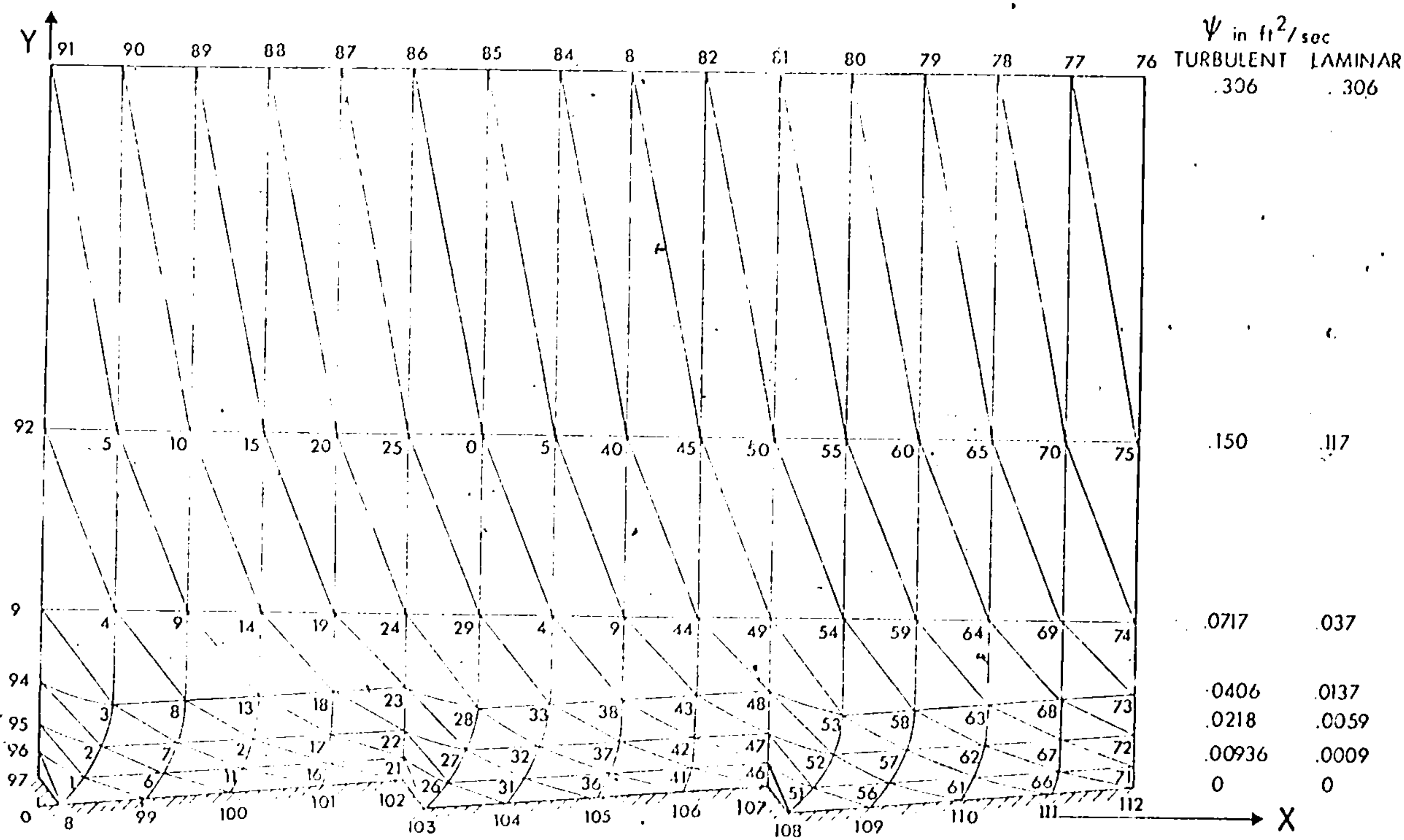

Fig. 62 — The typical arrangement of the three nodes triangular elements of the finite element method.

NUMBER OF ELEMENTS = 180
NUMBER OF UNKNOWN NODES = 75
TOTAL NUMBER OF NODES = 112

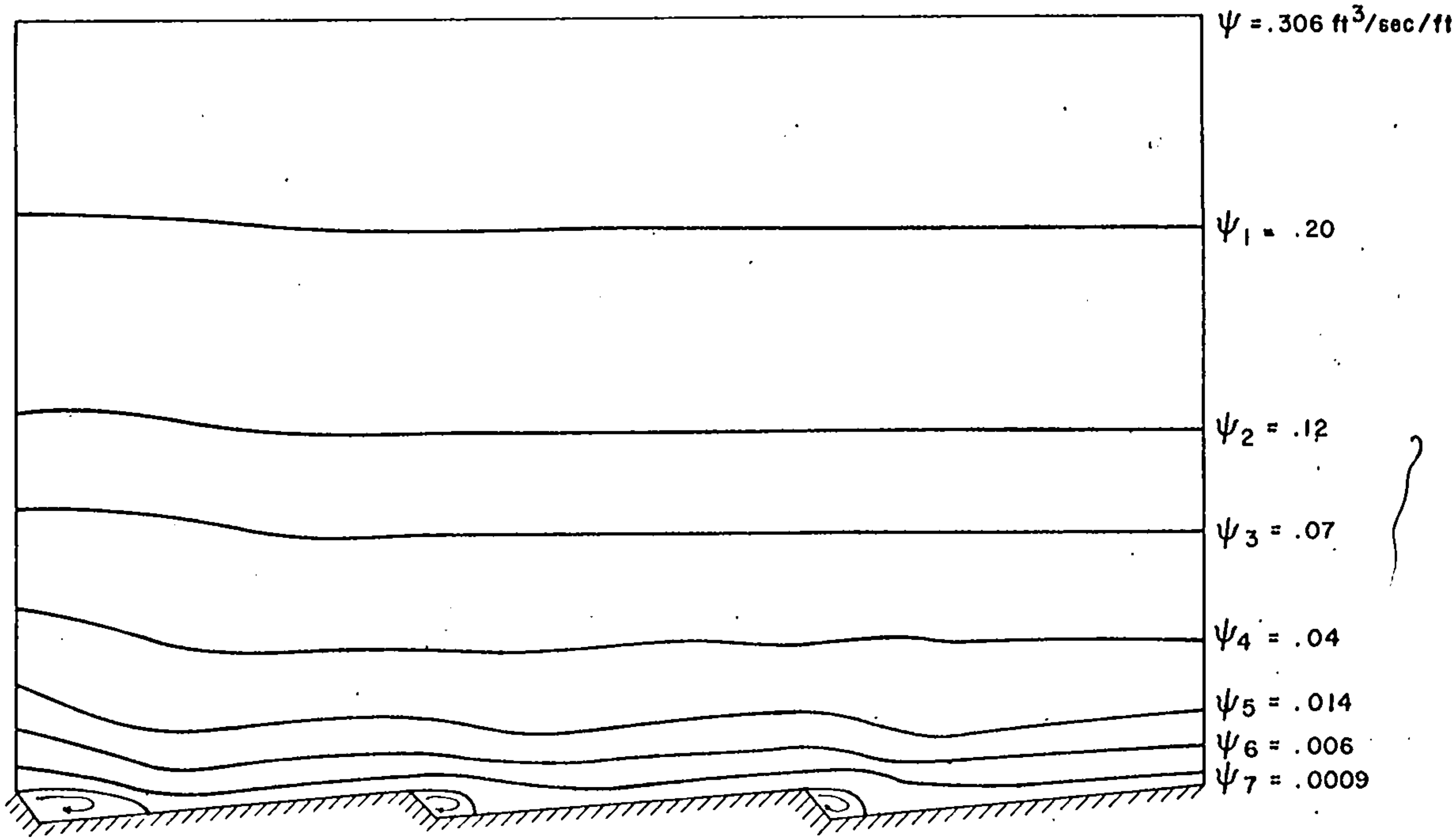

Fig. 63 - Finite element solution of the stream function for laminar flow, ψ = .306 ft ^{3}/sec. / ft.

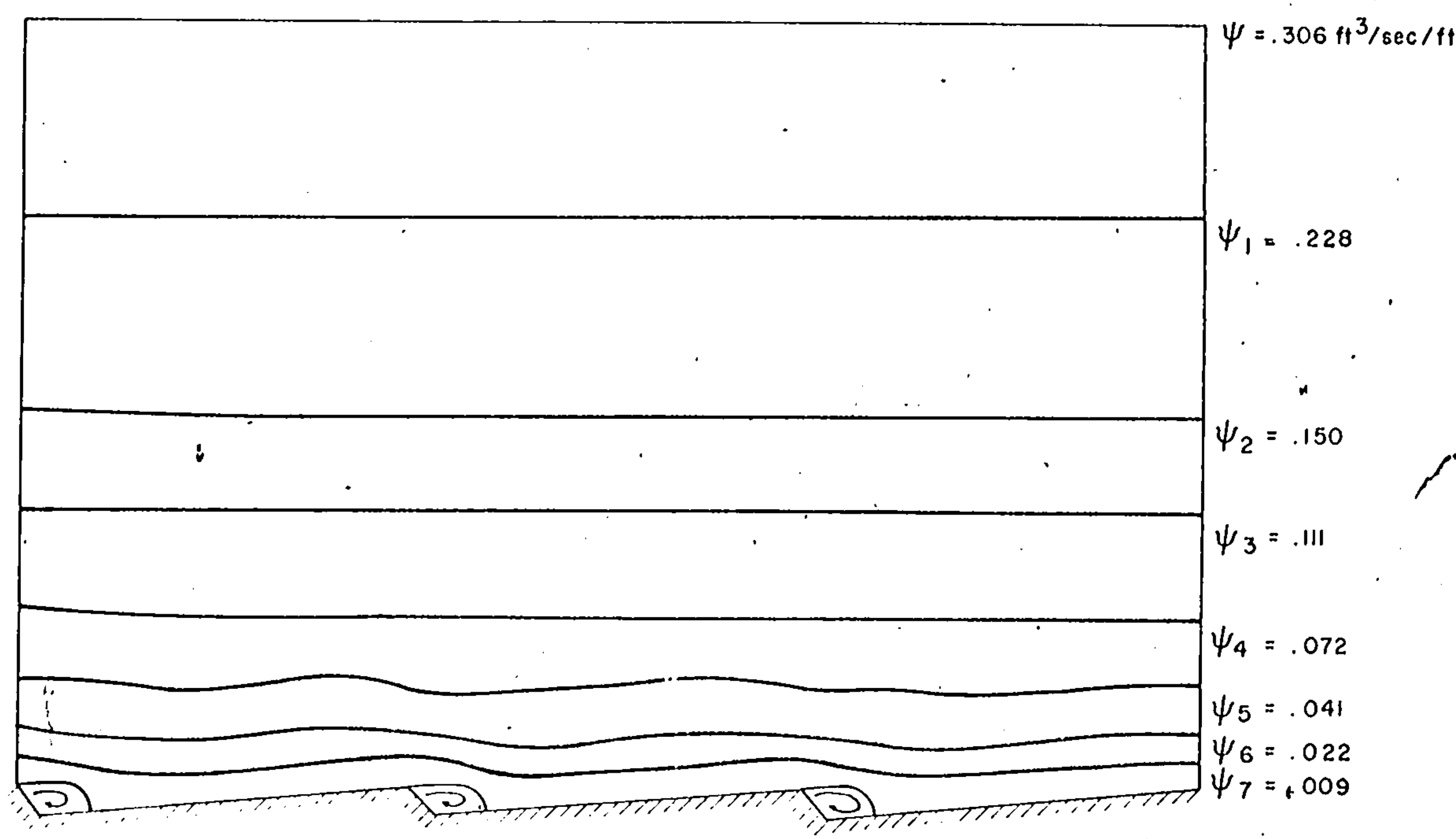

Fig. 64 — Finite element solution of the stream function for turbulent flow, $\psi = .306\ ft^3/sec./ft.$

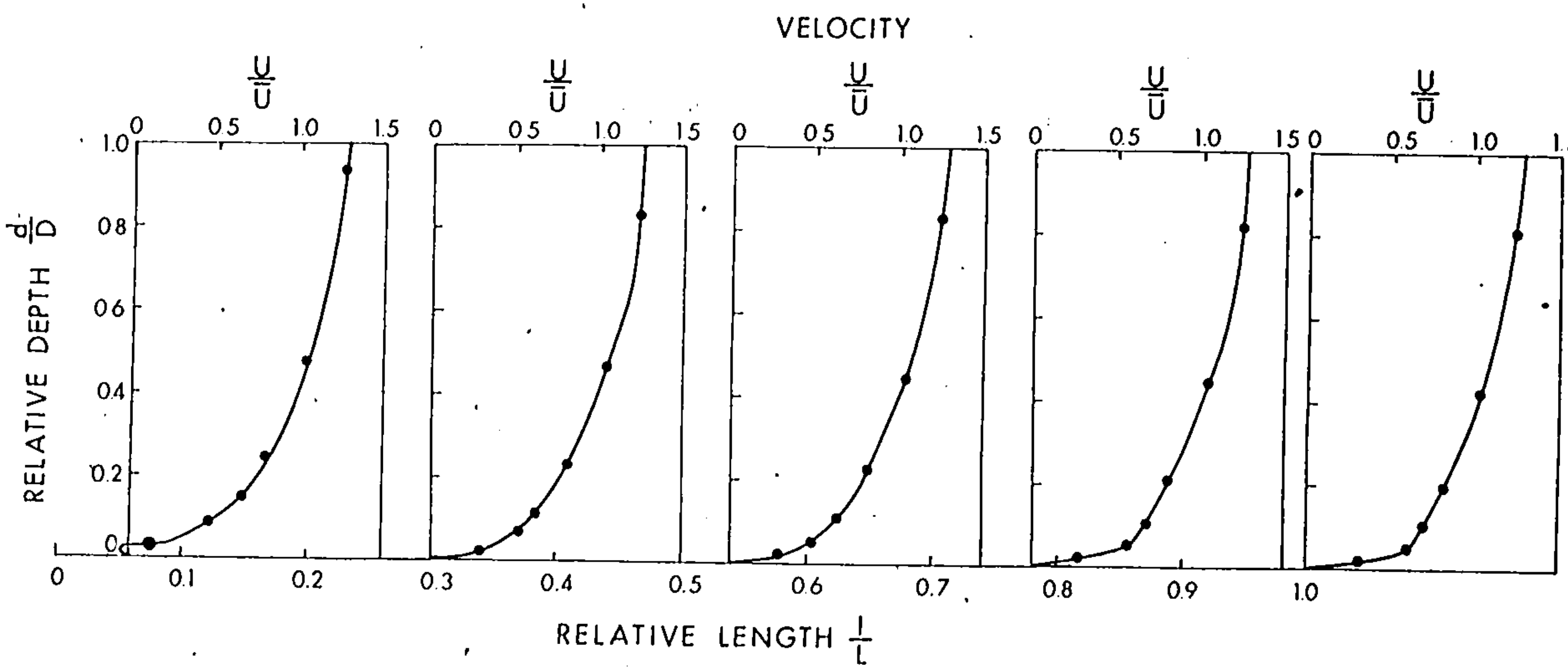

Fig. 65 — Theoretical velocity distribution along the middle ripple for laminar flow.

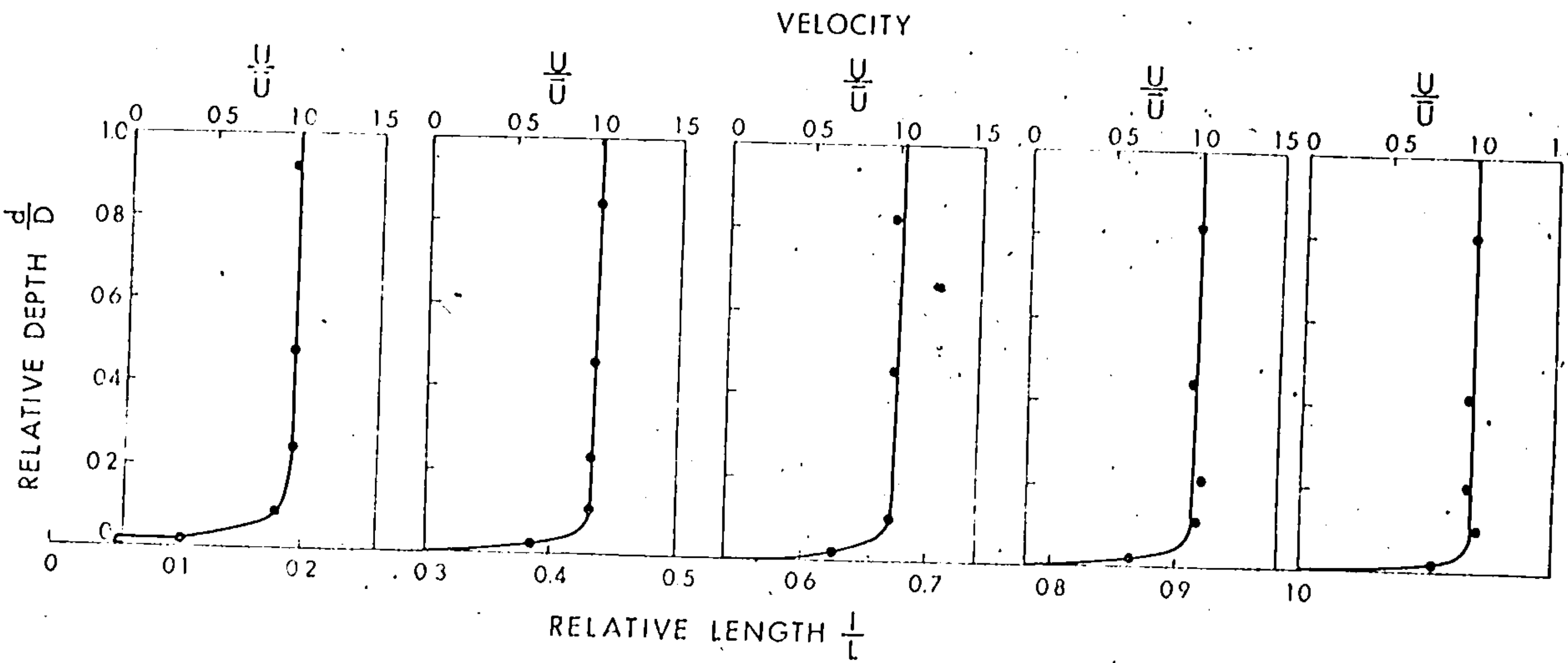

Fig. 66 - Theoretical velocity distribution along the middle ripple—for turbulent flow.

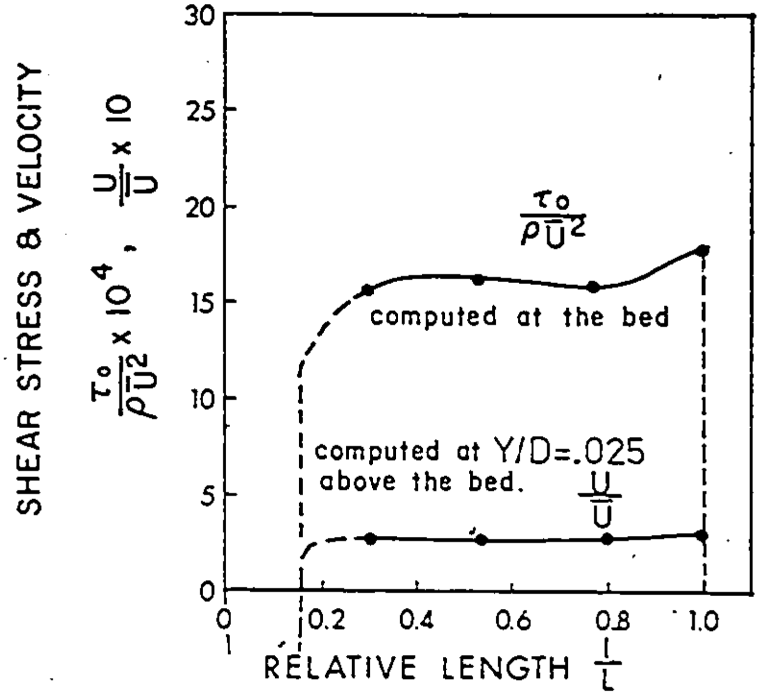

a) Laminar flow model.

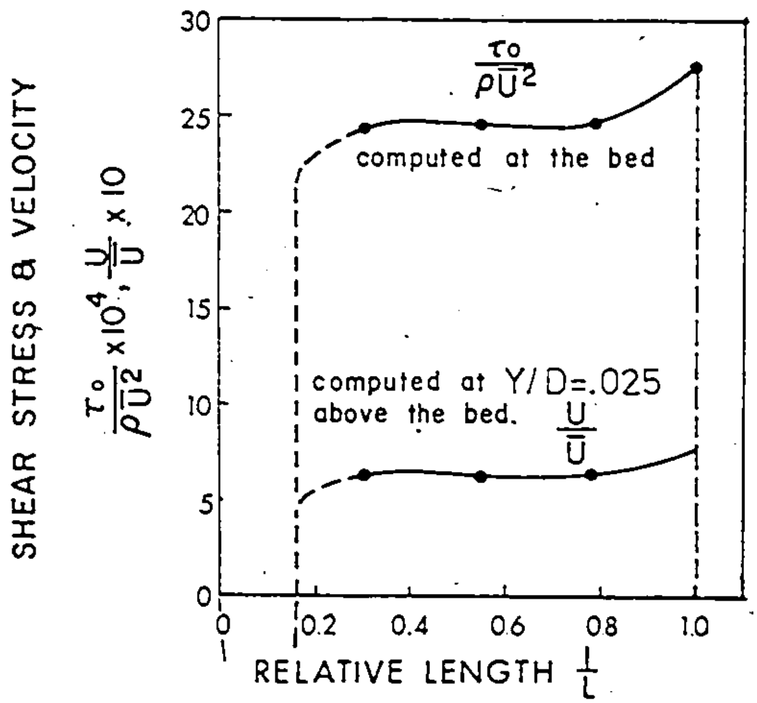

b) Turbulent flow model.

Fig. 67 - Velocity and shear stress distributions along the ripple obtained from the mathematical model.

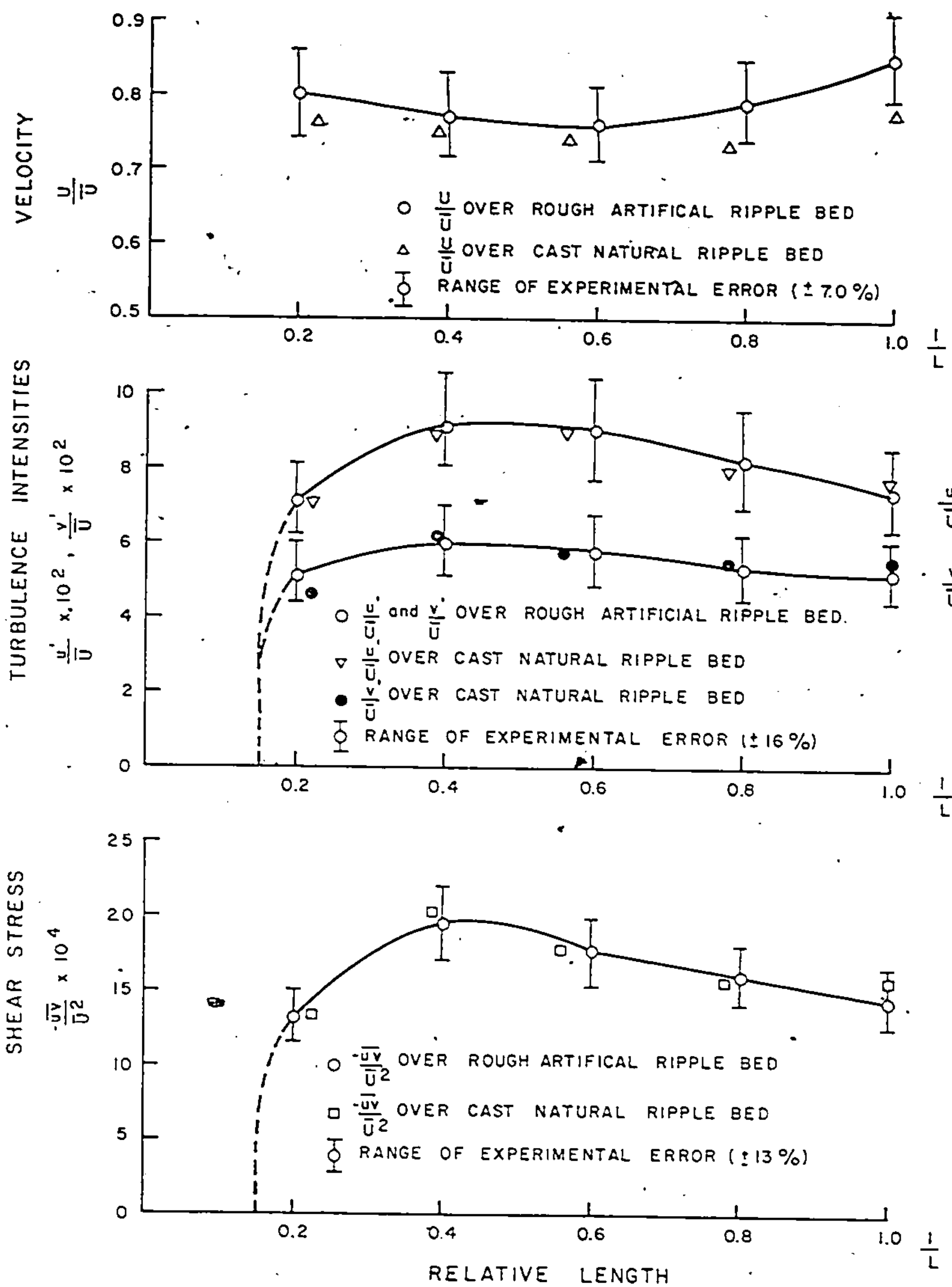
VELOCITY
OVER ROUGH ARTIFICAL RIPPLE BED
OVER CAST NATURAL RIPPLE BED
RANGE OF EXPERIMENTAL ERROR (± 7.0 %)
TURBULENCE INTENSITIES
and OVER ROUGH ARTIFICIAL RIPPLE BED.
OVER CAST NATURAL RIPPLE BED
OVER CAST NATURAL RIPPLE BED
RANGE OF EXPERIMENTAL ERROR (± 16 %)
SHEAR STRESS
OVER ROUGH ARTIFICAL RIPPLE BED
OVER CAST NATURAL RIPPLE BED
RANGE OF EXPERIMENTAL ERROR (± 13 %)
RELATIVE LENGTH

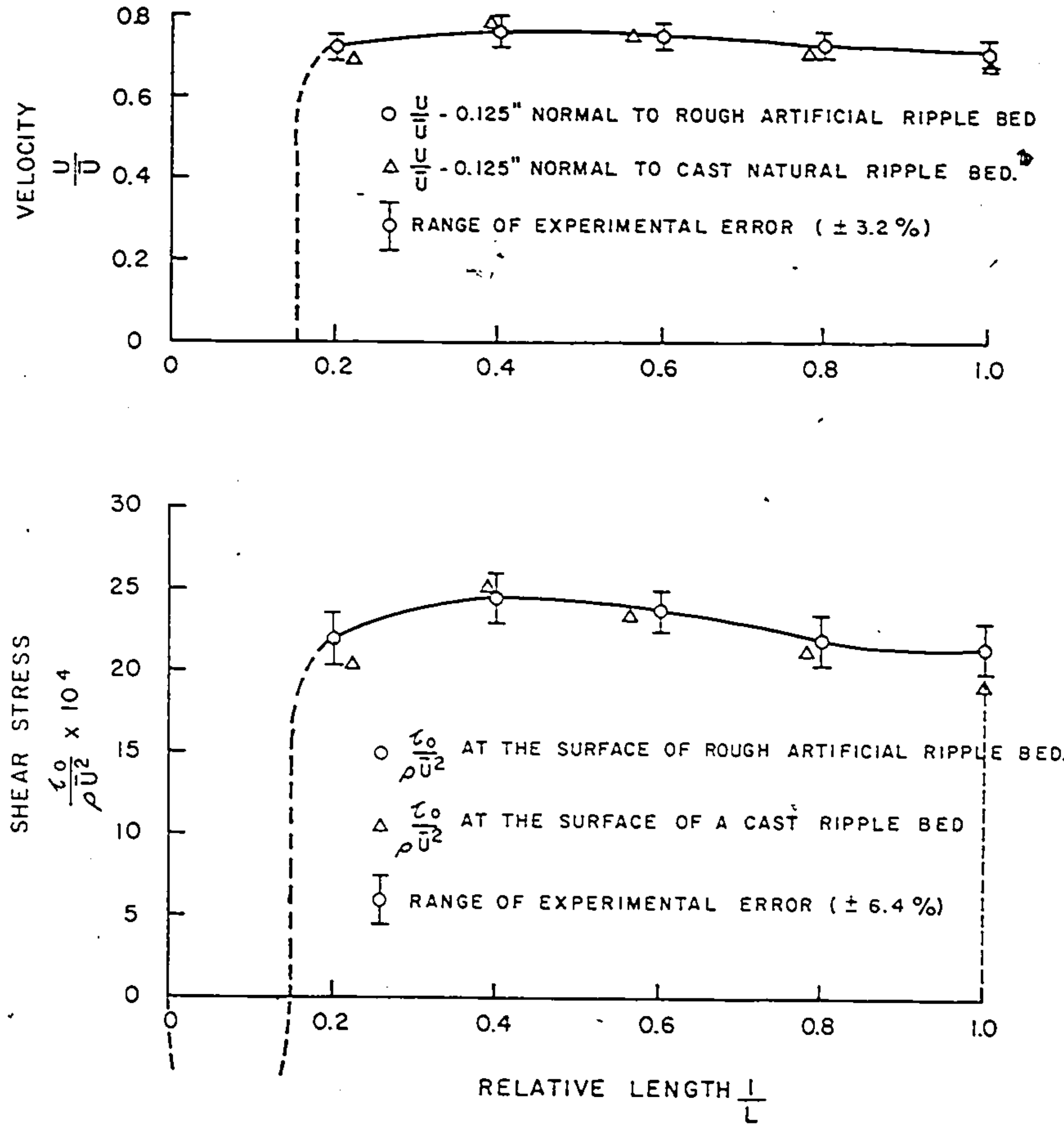

Fig. 69 — Correlation of pitot-tube measurements over the cast natural and rough artifical ripple beds.

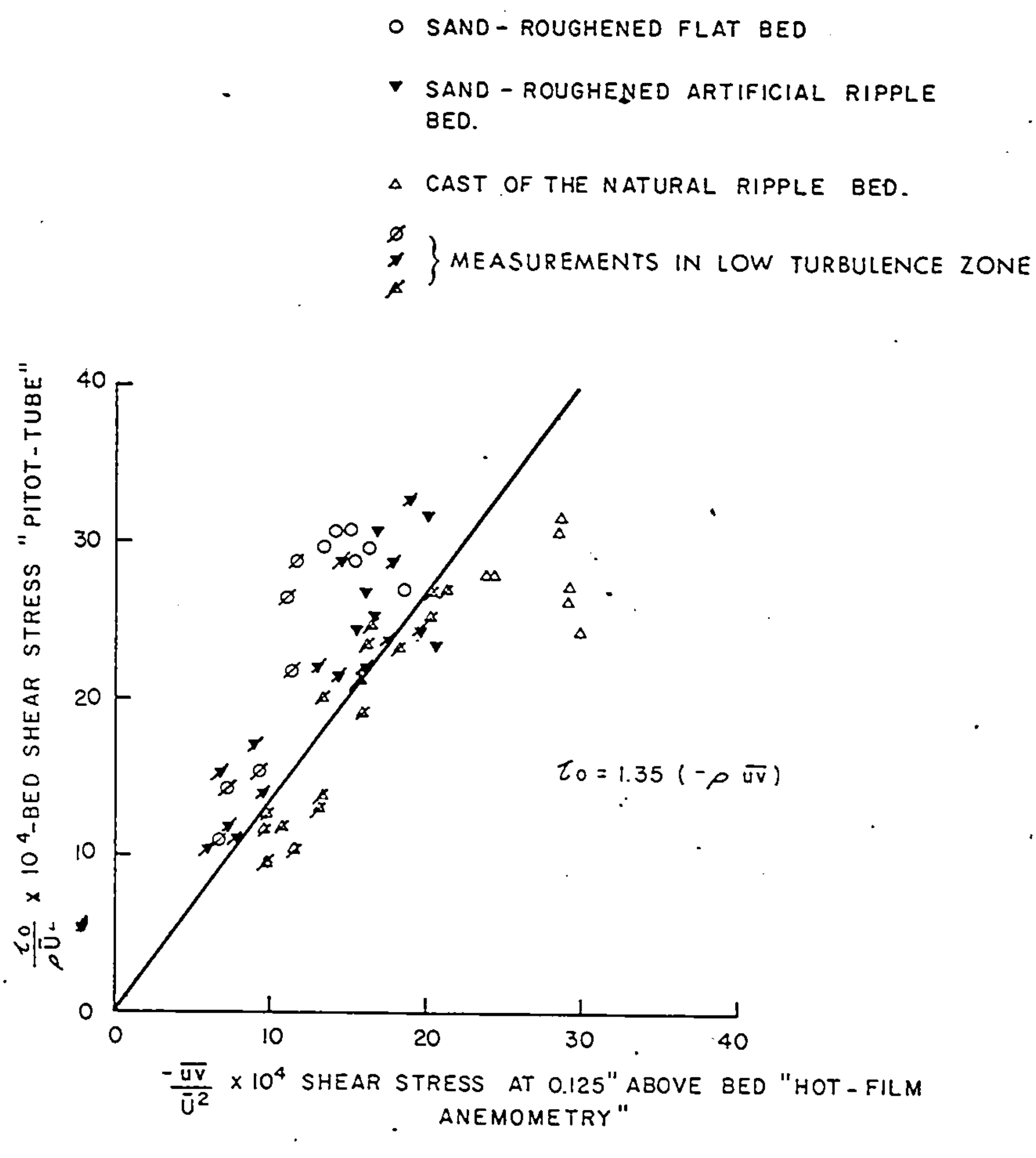

Fig. 70 — Reynolds shear stress-obtained from hot-film anemometry measurements versus bed shear stress measured by the pitot-tube.

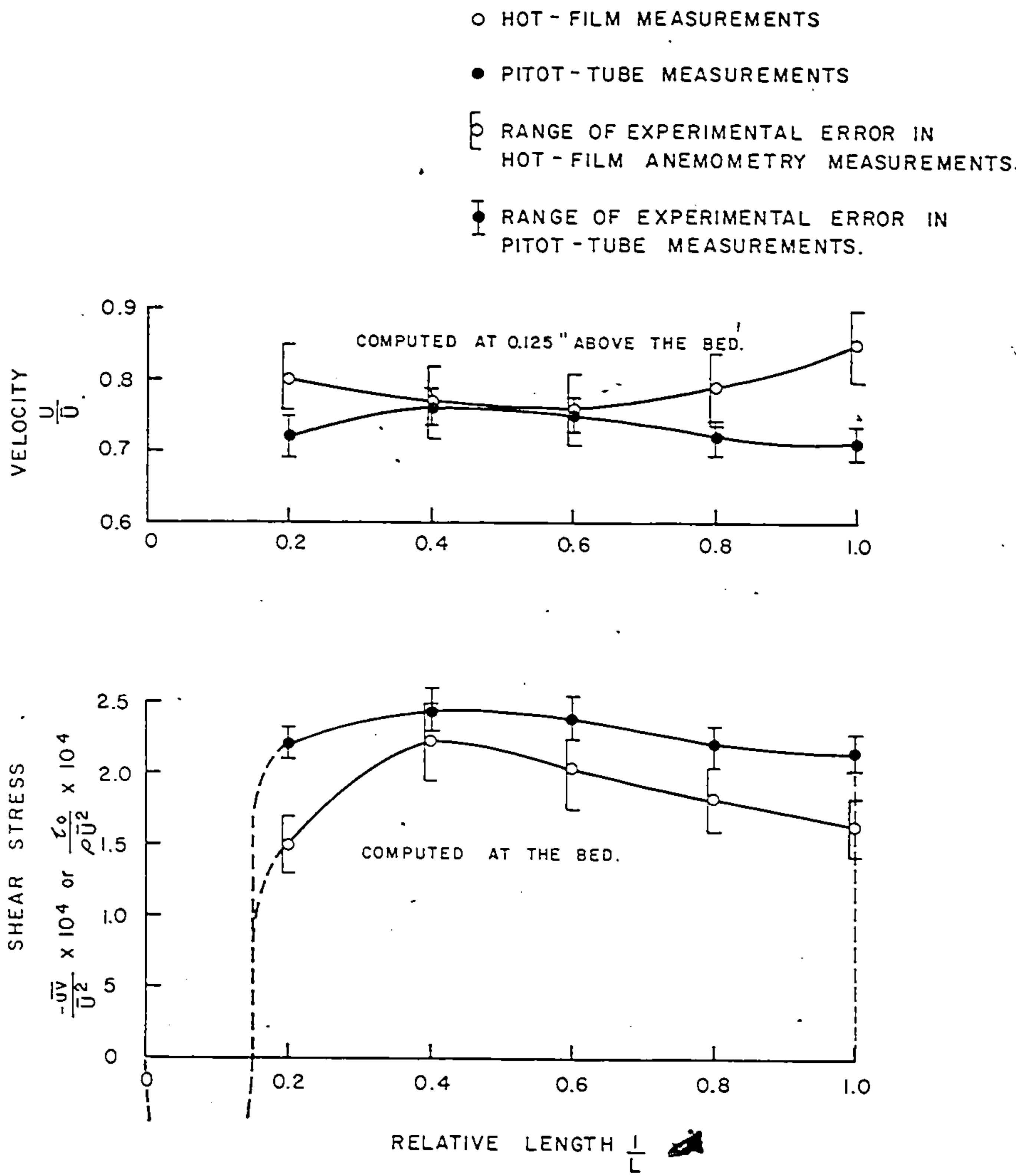

Fig. 71 — Comparison between the hot-film anemometry and pitot-tube measurements over rough artificial ripple bed.

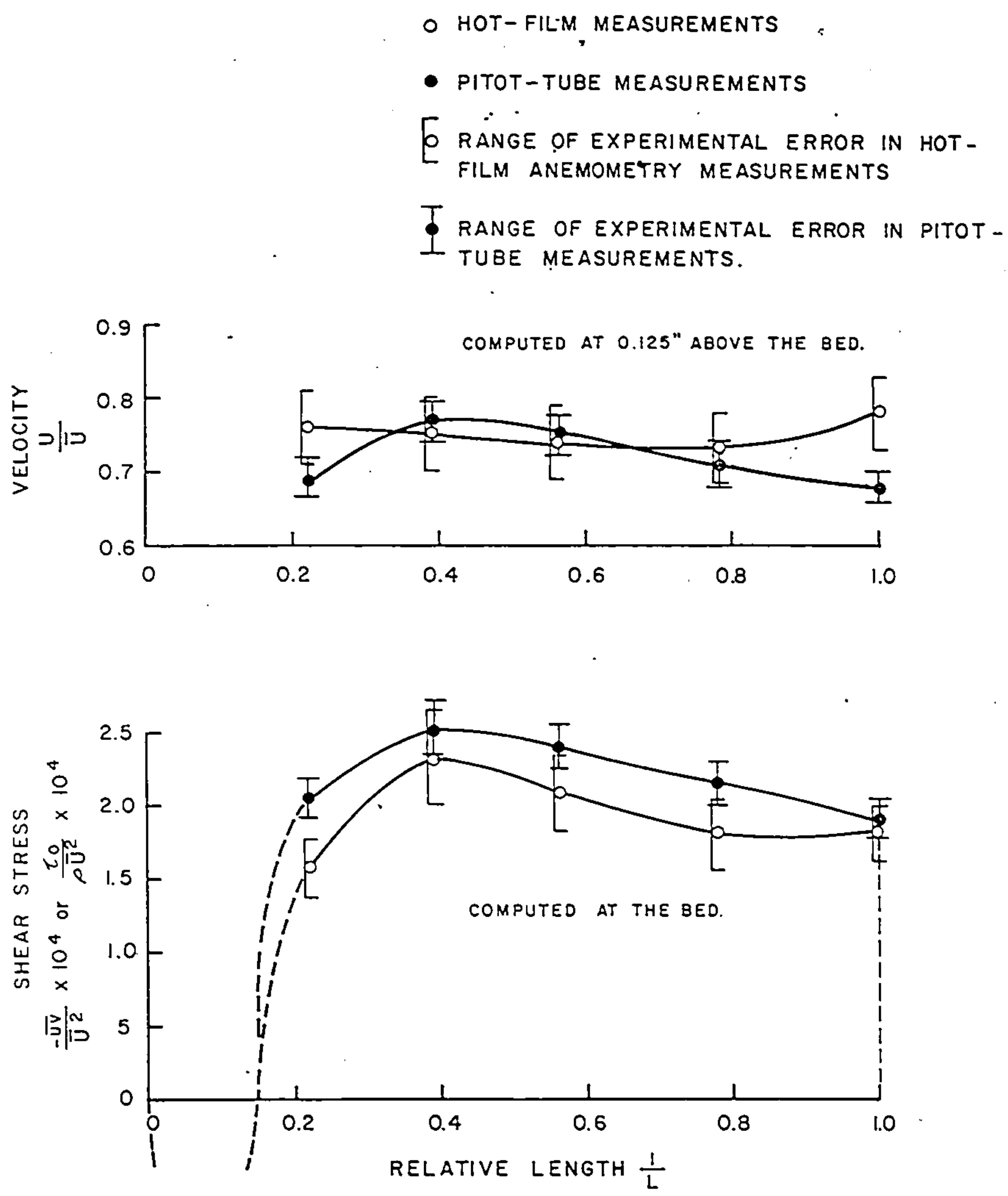

Fig. 72 — Comparison between the hot-film anemometry and pitot tube measurements over cast of a natural ripple bed.

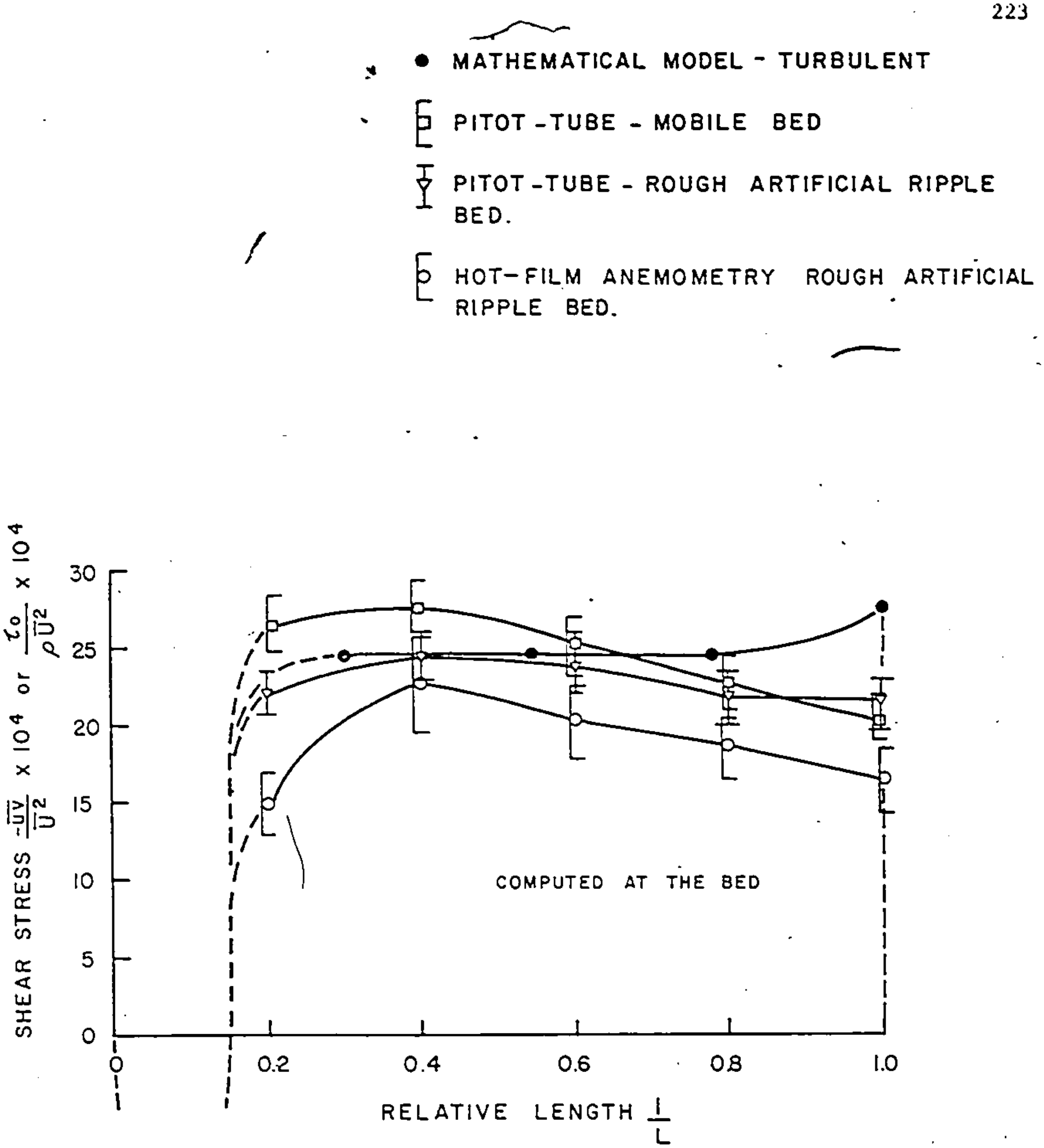

Fig. 73 — Mathematical and experimental results of the shear stress.

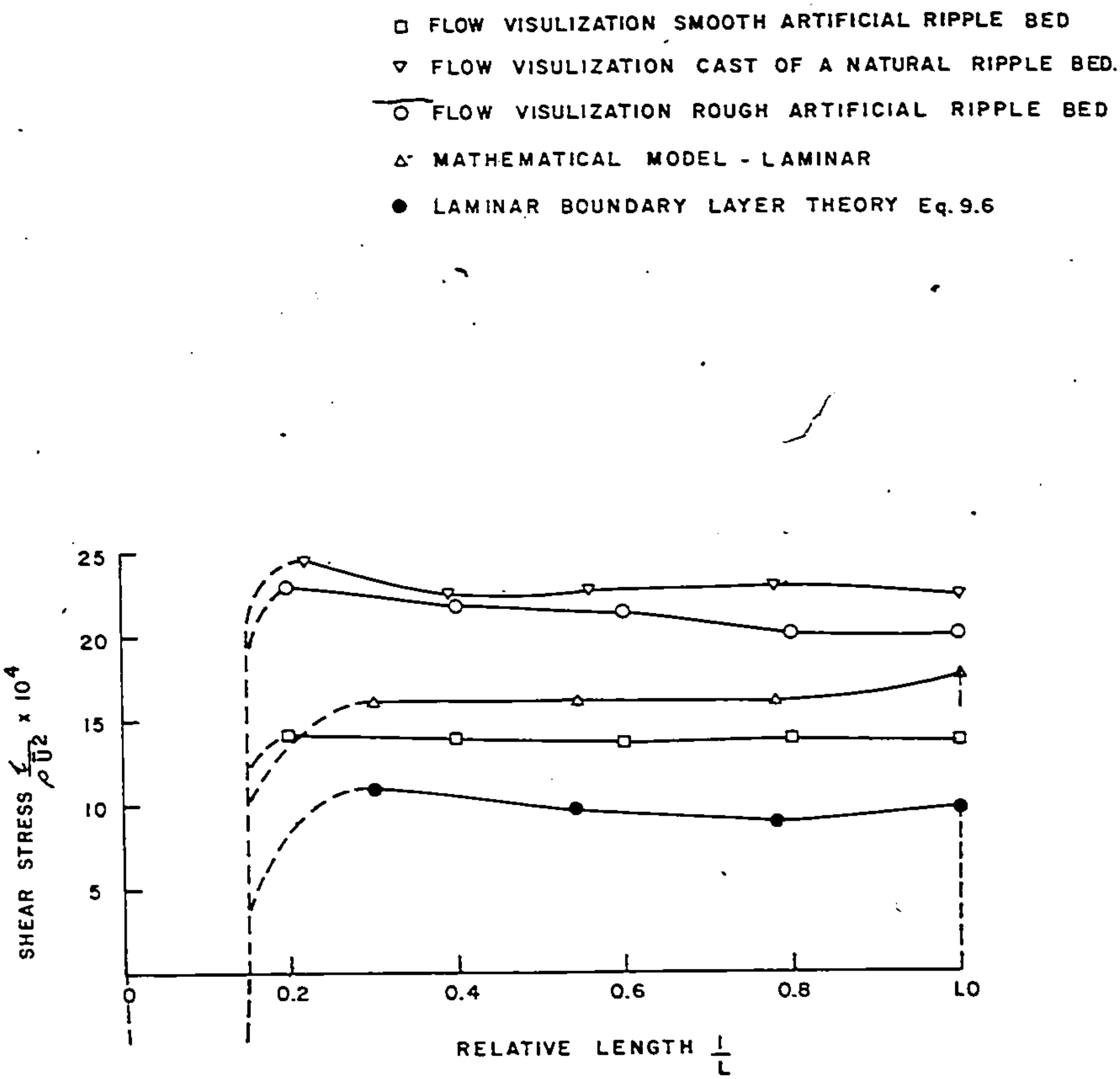

Fig. 74 – Comparison of the shear stress obtained from the flow visualization, the mathematical laminar model and the boundary layer theory.

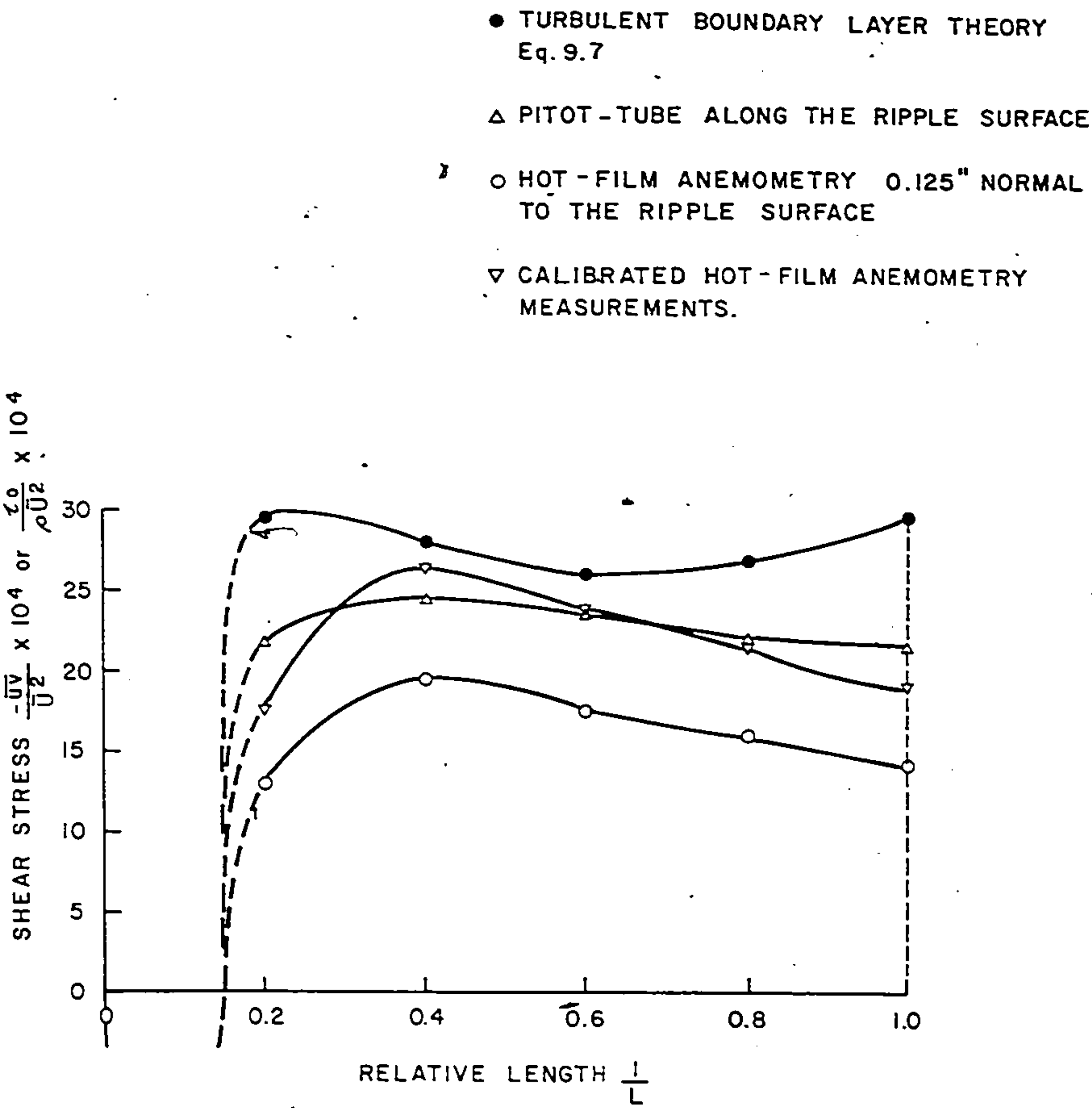

Fig. 75 — Comparison of the shear stress obtained from the boundary layer theory with those obtained experimentally for the sand-roughened artificial ripple bed.

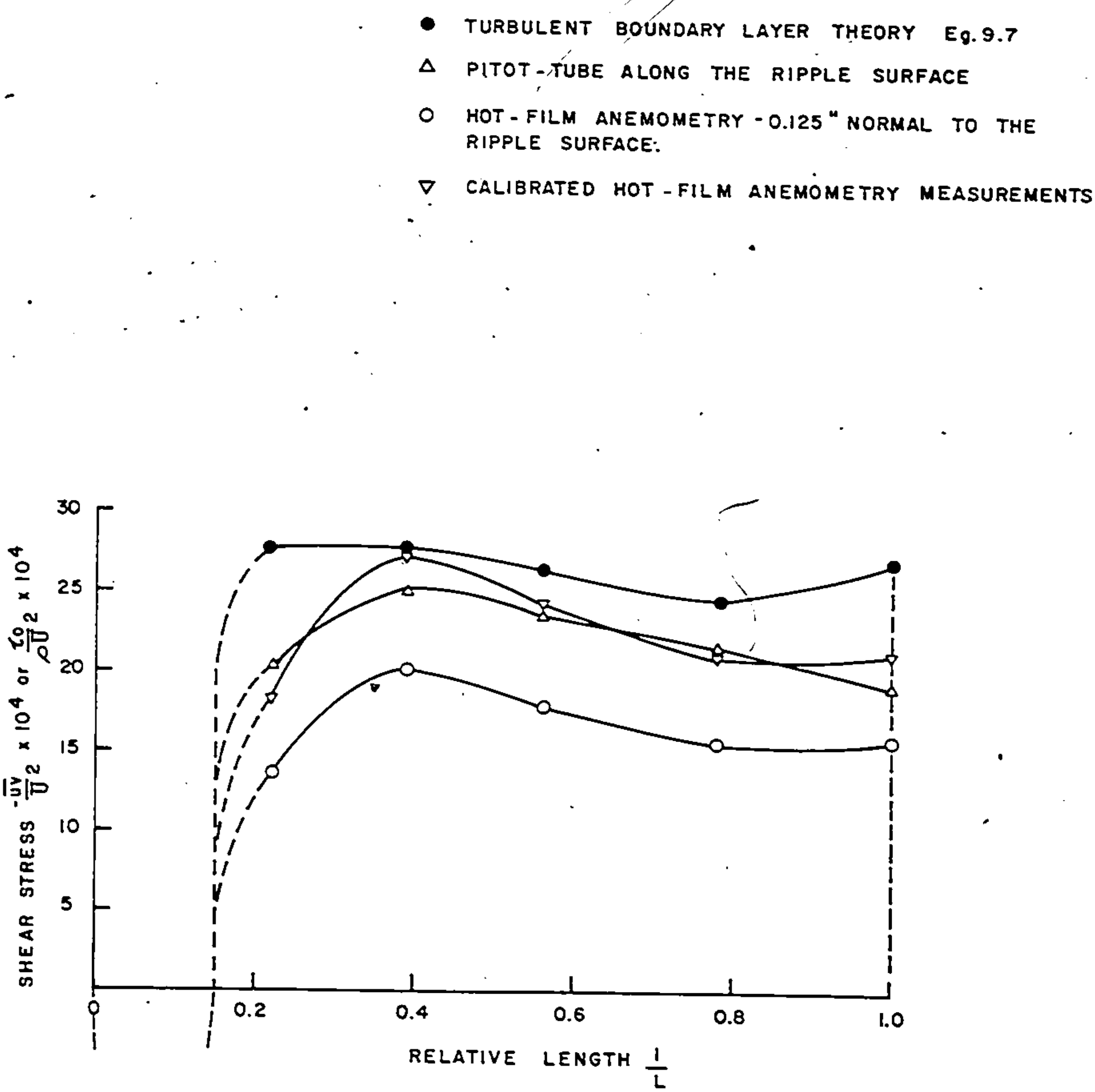

Fig. 76 — Comparison of the shear stress, obtained from the boundary layer theory with those obtained experimentally for the cast of the natural ripple bed.

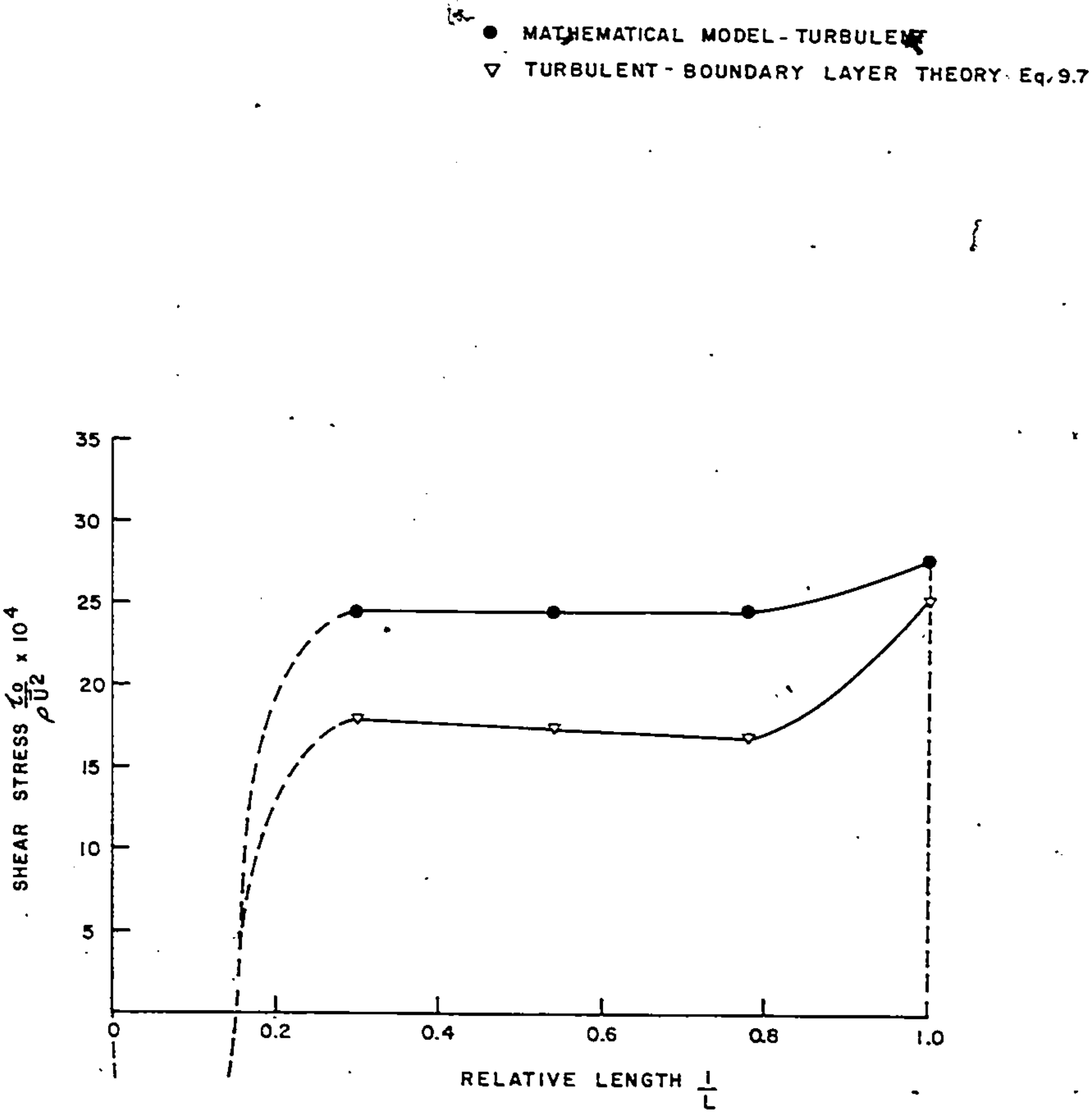

Fig. 77 — Comparison of the shear stress, obtained from the boundary layer theory with the mathematical turbulent model.

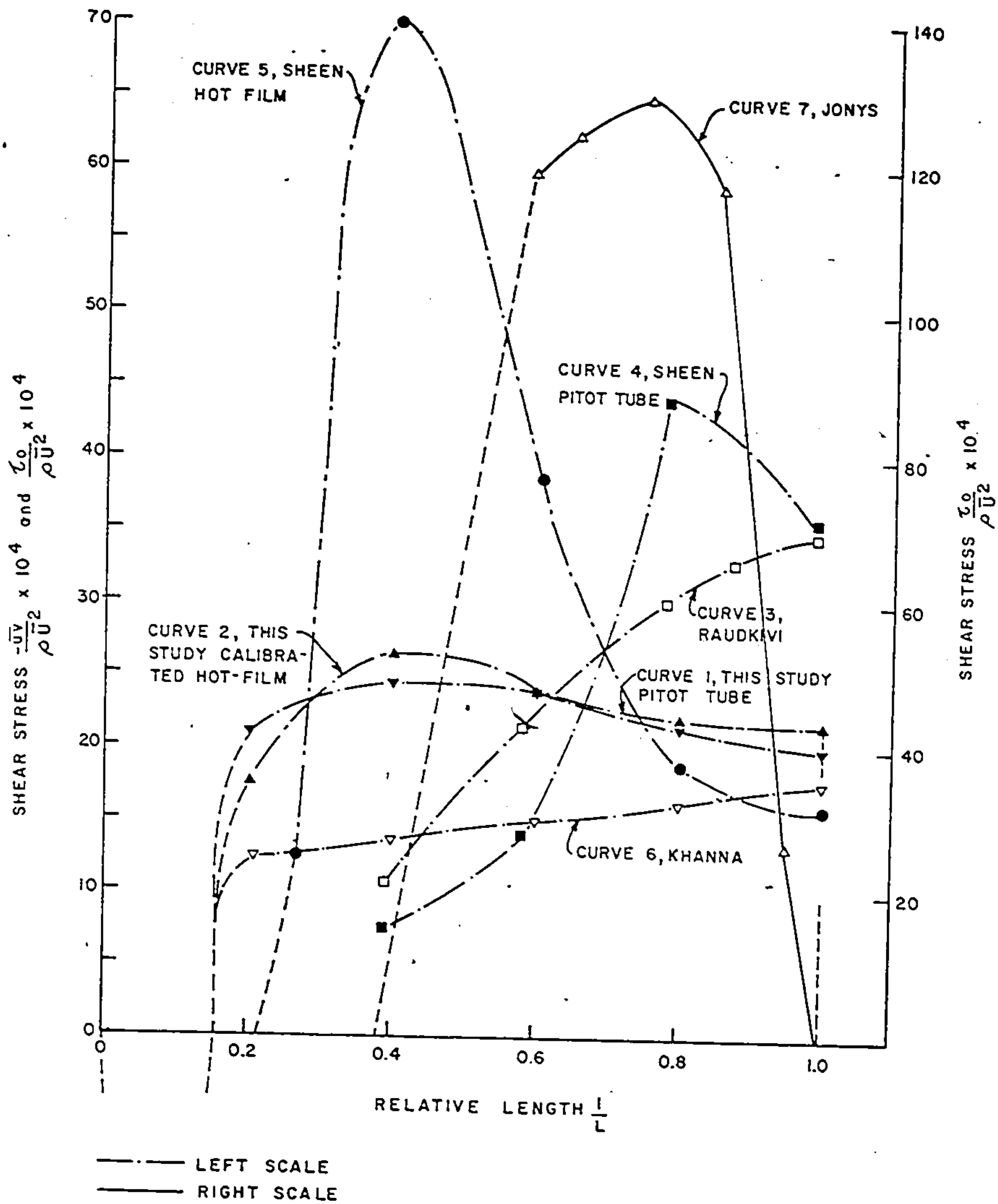

Fig. 78 – Comparison of shear stress distributions along a ripple reported by different researchers.

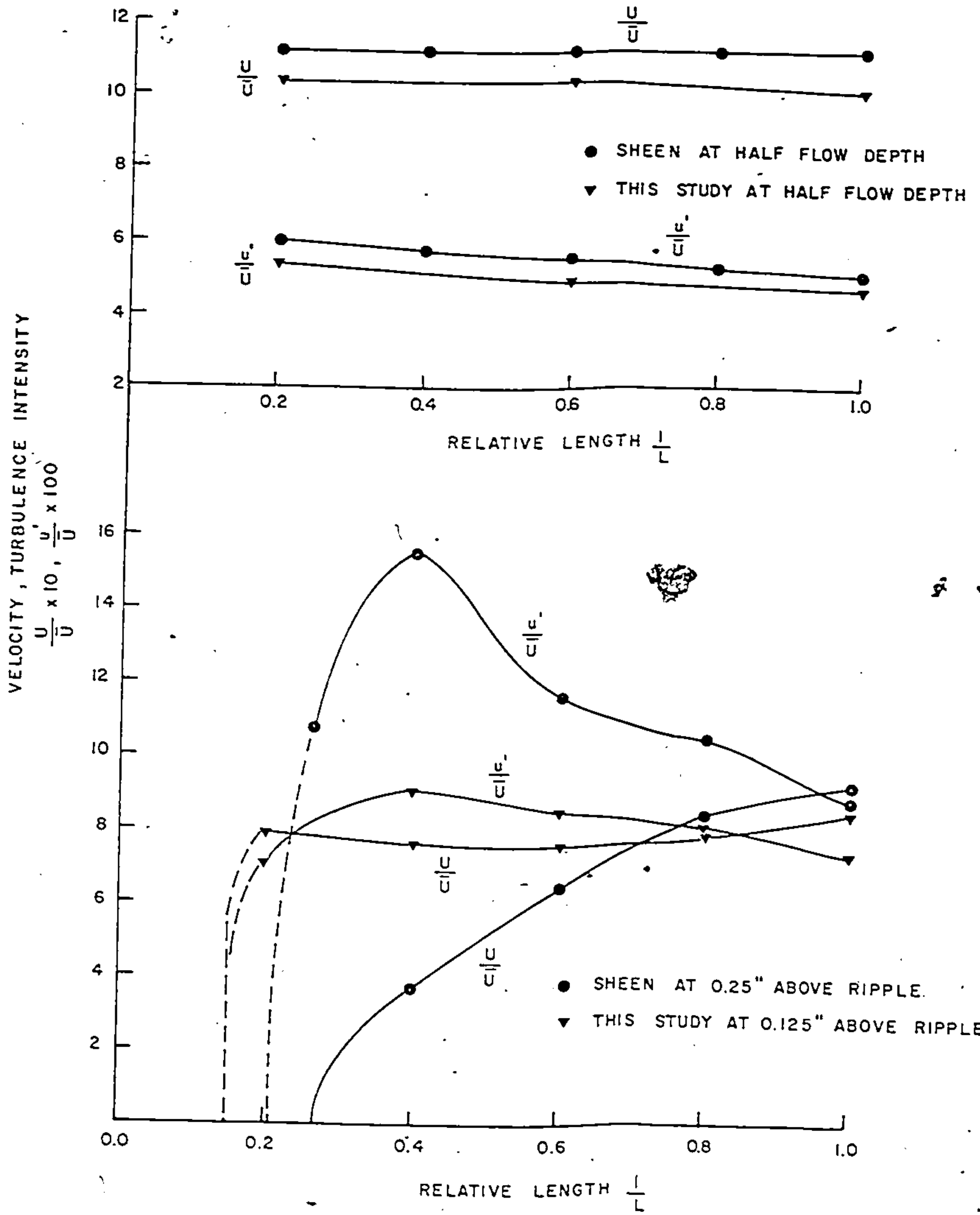

Fig. — 79 Comparison of turbulence intensities and velocities near ripple surface and at mid flow depth.

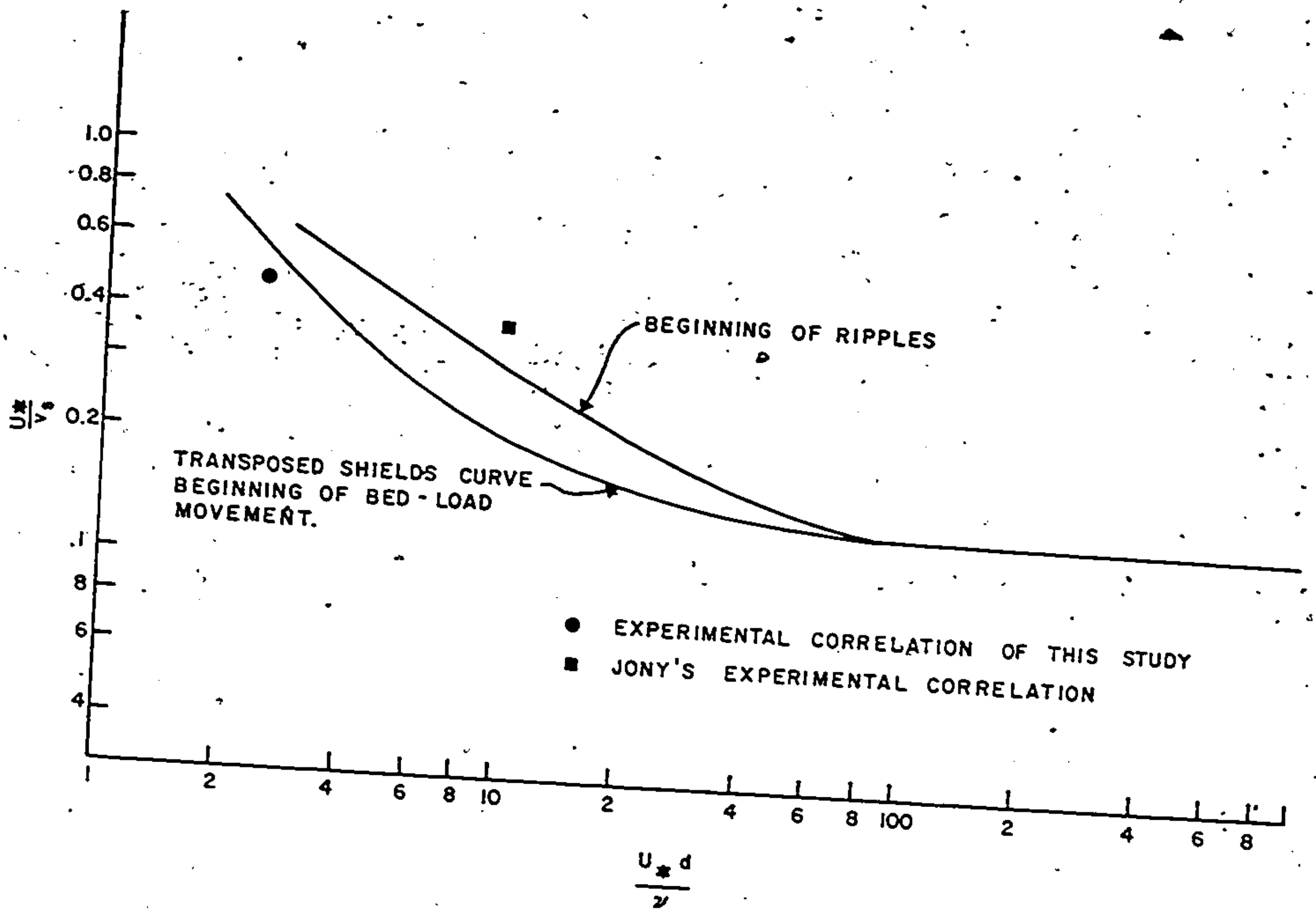

Fig. 80 — Relationship between beginning of bed-load movement and formation of ripples suggested by Liu ref. 60 pg. 1197-20

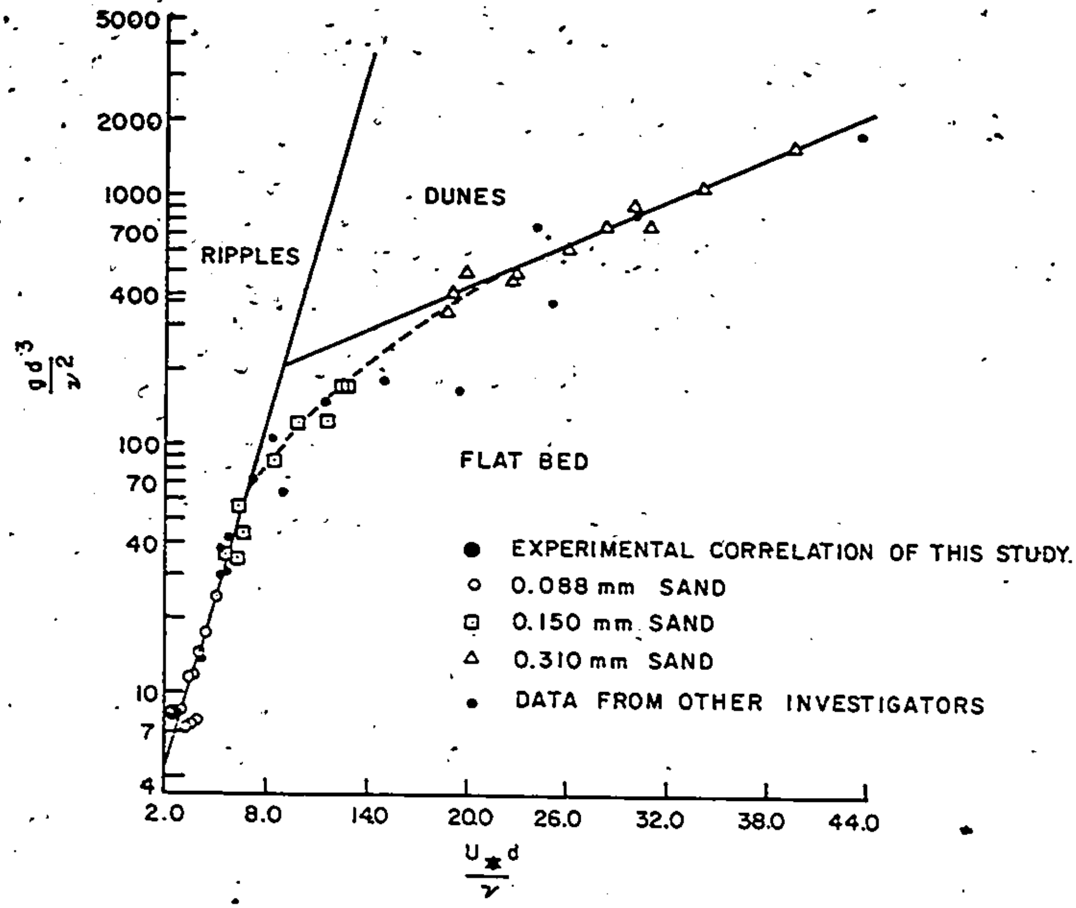

Fig. 81 — Criteria for bed forms as proposed by HILL ref. 38 pg. 1553

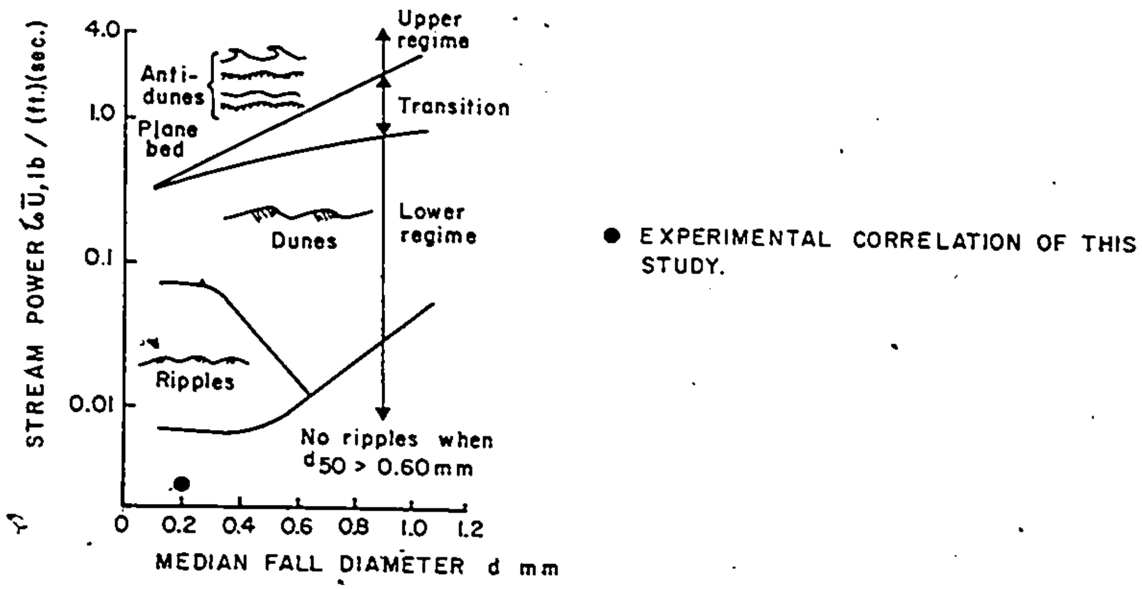

Fig. 82 — Relation of bedforms to stream power and grain diameter after Simons 1963 ref. 31 pg. 282

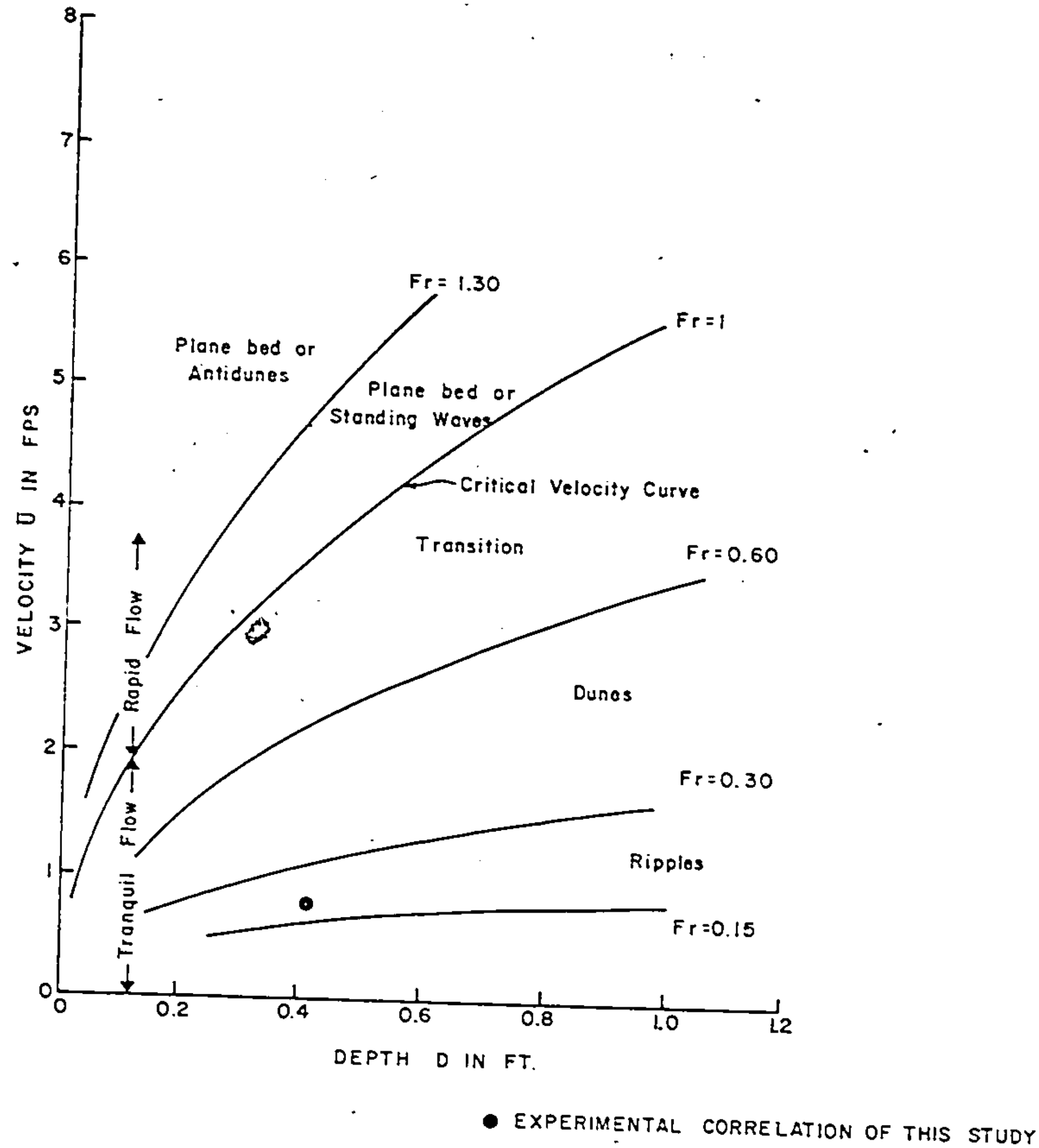

Fig. 83 — Variation of velocity $\bar{U}$ with depth D as proposed by Simons and Richardson — ref. 95 pg. 92

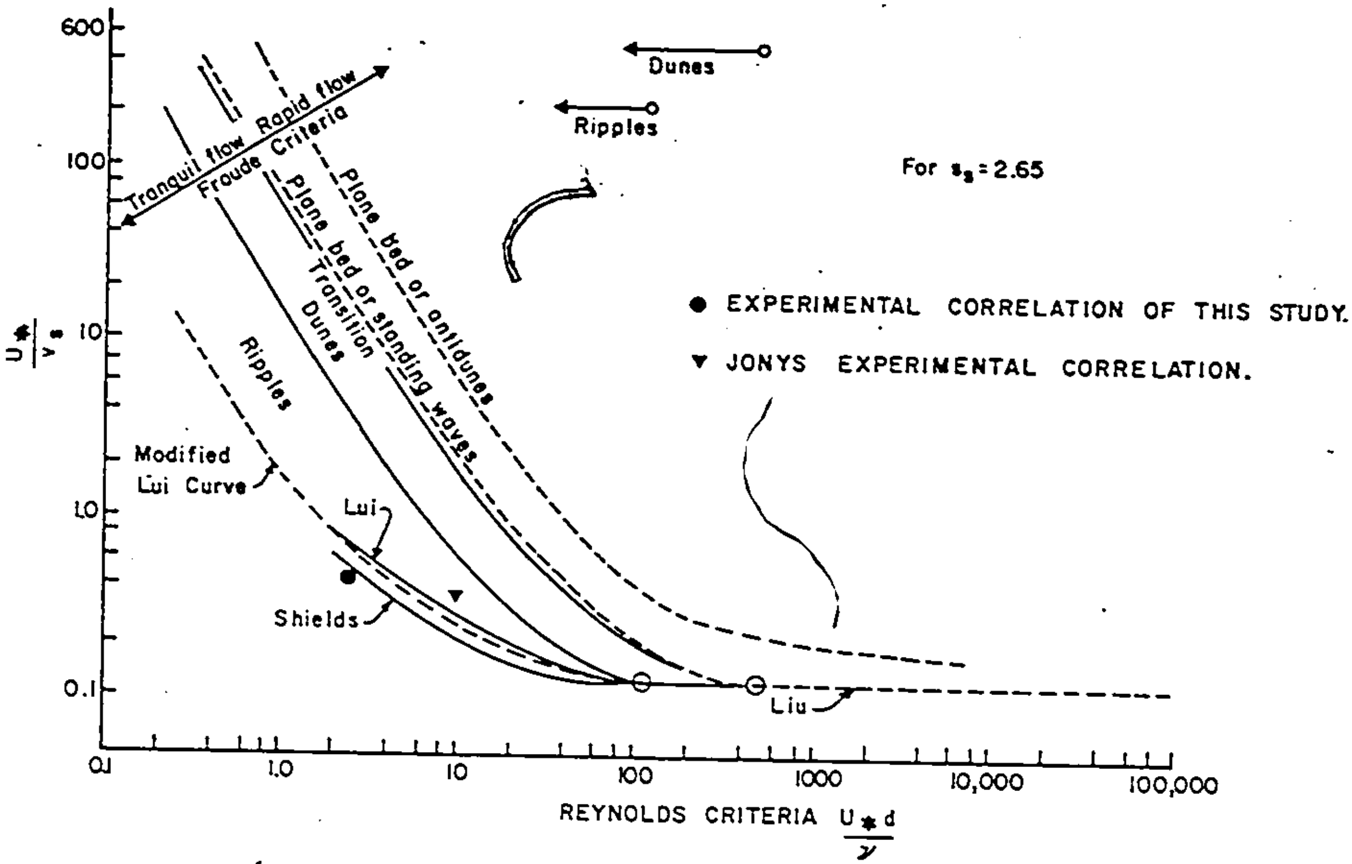

Fig. 84 — Criteria for bedforms, after Simons 1961 ref. 31 pg. 280

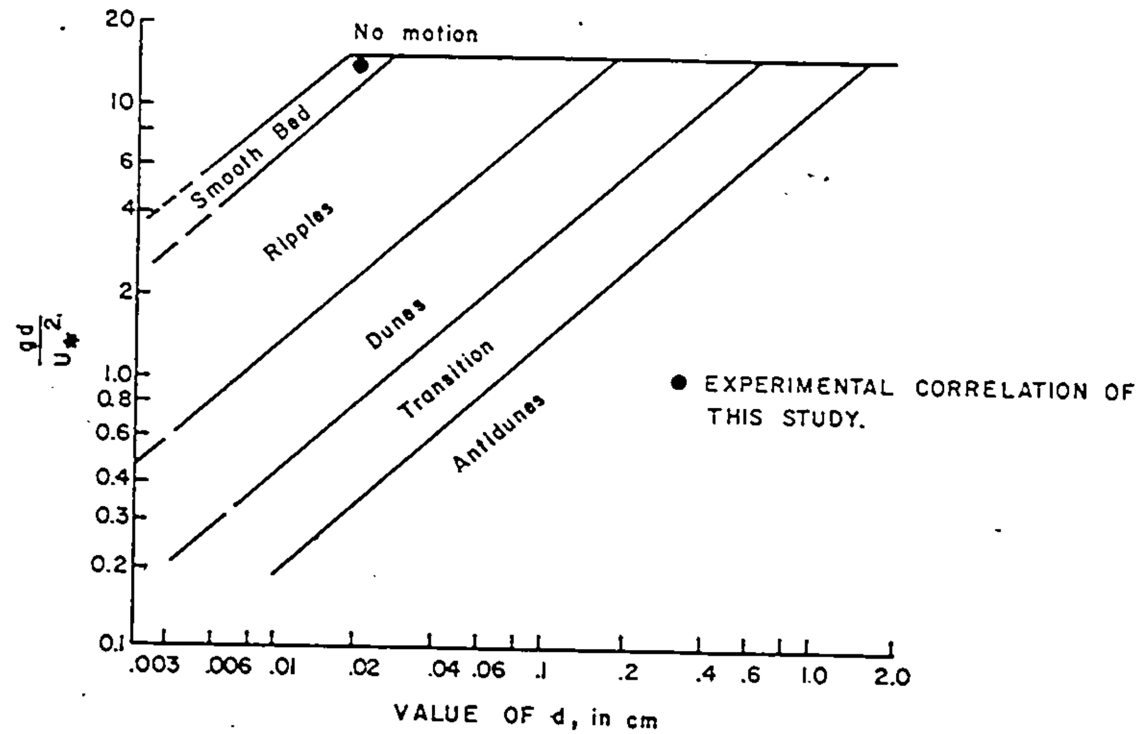

Fig. 85 — Regime criterion as proposed by Garde and Raju ref. 27 pg. 159.

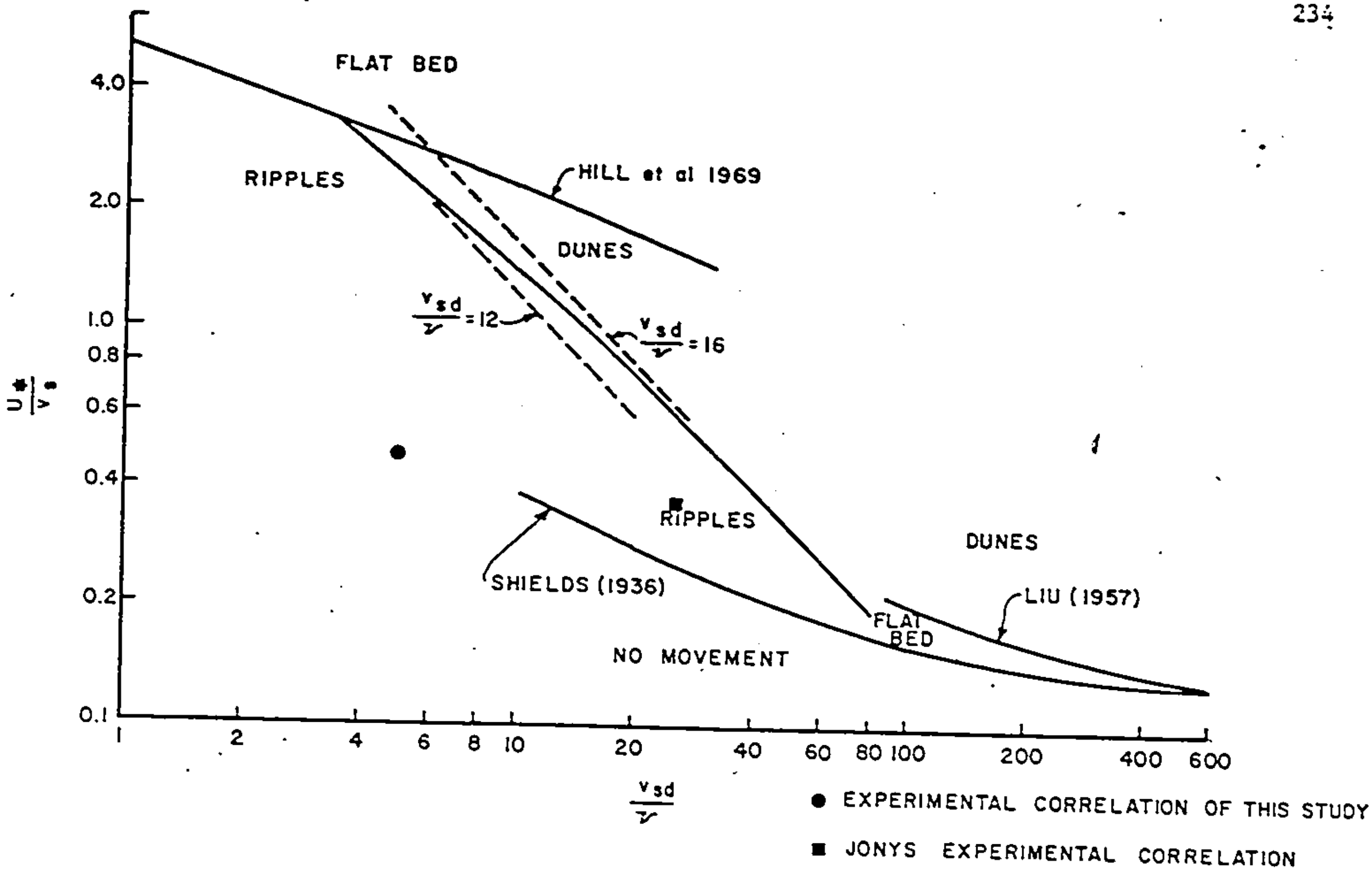

Fig. 86 – Regimes of ripples and dunes $\frac{U_*}{V_s}$ vs $\frac{V_s d}{\nu}$ ref. 92 pg. 10-6

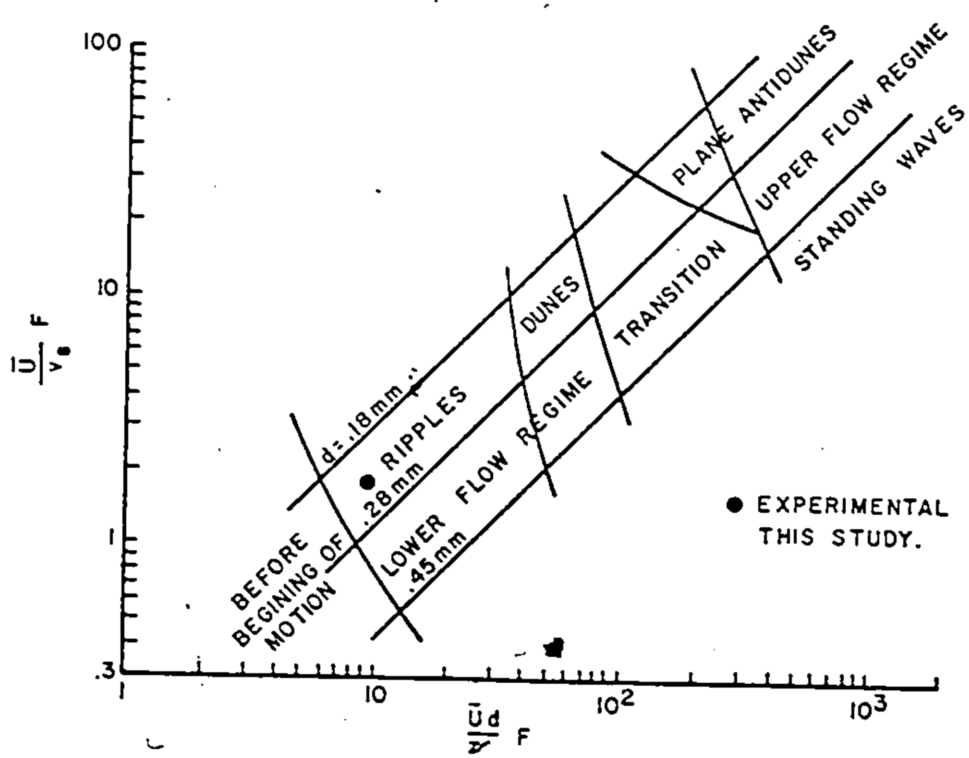

Fig. 87 – Forms of bed roughness in alluvial channels as proposed by Simons and Richardson ref. 96 pg. 102

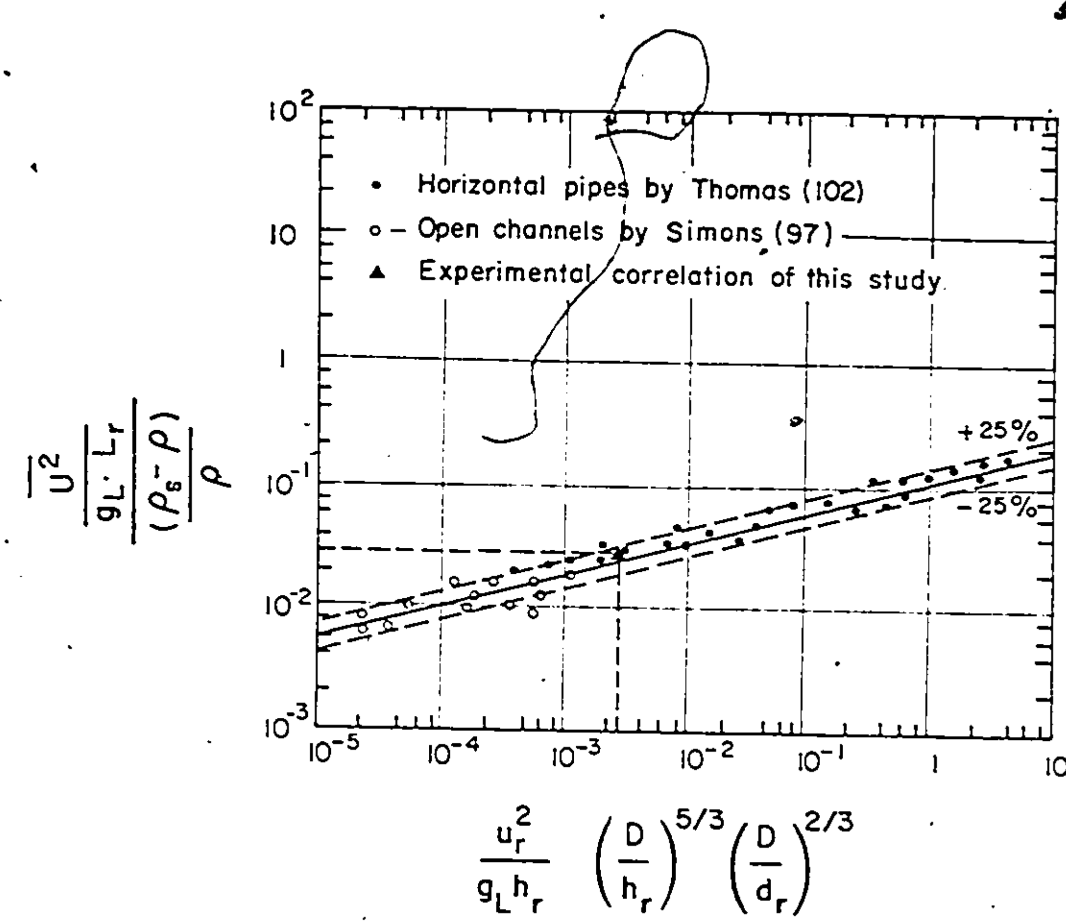

Fig. 88 - Correlation of periodic phenomenon observed in suspension transport in horizontal pipes and open channels. (After Thomas. ref. (102) pg. 534)

Appendix I

CALIBRATION AND OPERATING PROCEDURES IN HOT-FILM ANEMOMETRY

I.1 Procedure used in calibrating the hot-film probes:

Series of tests were carried out to establish a sound and reliable method of calibration of the hot-film probes. They were calibrated by a Pitot-static tube of 0.125 inch (0.32 cm), external diameter and 0.046 inch (0.12 cm), internal diameter. The method of calibration is summarized as follows:

i) The pump was started. The two controlling valves were adjusted to obtain a reasonable flow. Enough time was allowed to reach a steady condition.

ii) The Pitot-tube and the hot-film were held side by side, with 1/8 of an inch (0.32 cm), apart, at the same point in the flow. The tip of the Pitot-tube was adjusted to coincide with the hot-film in the same vertical plane perpendicular to the direction of flow.

iii) Enough time was allowed for the reading of the sloping manometer to reach a stable position.

iv) The water temperature was recorded. The DISA 55D01 Anemometer unit was put in operation as explained in the next section (I.2).

v) The DC voltage on the 55D30 Voltemeter and the sloping manometer reading were recorded simultaneously at the operating temperature.

APPENDIX I

CALIBRATION AND OPERATING PROCEDURES IN HOT-FILM ANEMOMETRY

vi) In case of unstable or drifting DC voltage was observed, step (v) was repeated after cleaning the hot-film of any dirt or air bubbles with a fine brush. While brushing the hot-film, the loop control of the anemometer unit has to be in the STD BY position.

vii) In case of calibrating the V-probe, the DC oltage of the two films were recorded along with the sloping manometer reading.

viii) The measurements were repeated at different points in the flow field, with the alignment described in step (ii) intact.

ix) The whole procedure was repeated for different flow conditions to cover a wide range of velocity.

x) The temperature at every point was measured and an adjustment in the cold resistance and the operating resistance was made for any change in temperature to maintain the same value of the over heating ratio "a" = 1.05.

xi) The calibration procedure covered a range of velocity and temperature variations which were expected in the actual experimental study.

xii) The sloping manometer readings were transferred to velocities using Eq. 7.2.

xiii) A set of calibration curves were constructed for both the Wedge and V-probes for different temperatures ($70^{o}F$ to $80^{o}F$) - Figs. 17 and 18.

I.2 Operating the 55D01 Anemometer

The procedure used in operating the 55D01 Anemometer (Fig. 89) with the Wedge-probe in water to measure the velocity U and the turbulence intensity u' is summarized as follows:

i) Turn the instrument ON and allow a sufficient warm up time - about 15 minutes.

ii) Check the line voltage, by turning the METER SWITCH all the way to the left, the meter deflects all the way to the right.

iii) With the METER SWITCH in its second position, set the CURRENT ADJ. control, using a fine screwdriver, for a meter reading of 3.5 mA on the upper scale.

iv) Set the control OUTPUT BIAS for half scale meter deflection, with the other controls set as follows:

Meter Switch at 1, 3, 10 or 30

Loop Control at STD BY

Decade Resistance at 00.00

Bridge Ratio at 1:20

HF Filter at 1

Gain Adj Fully left at 1

Input bias at approximately mid-scale

LF response at High

Temperature - Resistance Switch at Neutral.

v) Connect the 5 meters probe cable to the probe support which ends with a shorting probe. Adjust the ZERO OHMS with a screwdriver, so that there is no meter deflection when Temperature-Resistance switch is depressed.

vi) Replace the shorting probe with the wedge probe. Place the probe in water and record its temperature. Set decade resistance to a value that gives no meter deflection when

Temperature-Resistance switch is depressed. The reading of the decade resistance gives the cold resistance R_o in ohms of the probe at the recorded temperature.

vii) The operating resistance $R = a \cdot R_o$ where a = overheating ratio, chosen as 1.05.

viii) To measure the velocity U at any point in the flow field, set the decade box to read R, then turn the loop control to INT. A reading of a DC voltage on the meter can be transferred to velocity by using the appropriate calibration curve. For more precise results, the DC voltage can also be read on the 55D30 Digital DC Voltemeter.

ix) To calculate the turbulence intensity, u', the root-mean-square of the voltage $\sqrt{\overline{e^2}}$ is measured by the 55D35 RMS voltmeter. u' and $\sqrt{\overline{e^2}}$ are related as given by Eq. 4.16.

I.3 Operating the 55D70 Analog Correlator

The procedure used in operating the 55D70 Analog Correlator (Fig. 90) with the V-probe to measure the cross correlation factor $R = \overline{e_s \cdot e_d}$, $\sqrt{\overline{e_s^2}}$ and $\sqrt{\overline{e_d^2}}$ is summarized as follows:

i) Set RANGE VOLTS switches (2) and (4) to 10V and turn variable GAIN controls (1) and (3) fully clockwise to the CAL position.

ii) Apply signals to be correlated e_s and e_d, from Dual Summing Unit, through INPUT A and INPUT B of the correlator.

iii) To bring the signals on channel A within the dynamic range for the measurement channel, set MEASUREMENT FUNCTION switch to $\overline{e_A^2}$ and INTEGRATION TIME CONSTANT switch to 0.1 sec. Turn RANGE VOLTS (2) counterclockwise until meter reads between red mark and + 0.1 on upper right scale. Select time constant so that meter deflection does not fluctuate.

iv) To bring signals on channel B within the dynamic range for the measurement channel, repeat the procedure explained in step (iii).

v) To measure the cross-correlation factor R, turn MEASUREMENT FUNCTION switch to CORR. FACTOR R and set TIME CONSTANT switch so that meter deflection does not fluctuate. The upper scale meter reading R' in volts square, is proportional to R, where $R = G_A \cdot G_B \cdot R'$.
G_A and G_B are settings of the RANGE VOLTS switches for channels A and B respectively.

vi) The RMS of e_s and e_d were measured consecutively by means of the 55D35 RMS Voltmeter.

I.4 Operating the 55D75 Time Delay

The Procedure used in operating the 55D75 Time Delay Unit (Fig. 91) with the 55D70 Analog Correlator (Fig. 90) to measure the cross correlation coefficient ρ(t) is summarized as follows:

i) Set RANGE VOLTS switches (2) and (4) of the correlator to 10 Volts and turn variable GAIN CONTROLS (1) and (3) fully counterclockwise.

ii) The signal from the Wedge-probe is fed to the Time Delay Unit, where a specified time delay can be applied according to the DELAY RANGE switch of the Time Delay Unit, and, the DC Voltage supplied by the DC generator to the Time Delay Unit in such a way:

a) If the DC voltage is 5 volts, the time delay is the value specified on the Delay-Range switch.

b) If the DC voltage is any other value "V" less than 5 volts, the time delay is the value specified on the Delay-Range switch multiplied by the ratio $\frac{V}{5} < 1$.

iii) Apply signals to be correlated, from the Time Delay Unit, through INPUT A and INPUT B of the correlator.

iv) To normalize the signal on channel A, set MEASUREMENT FUNCTION to the $\overline{e_A^2}$ position and INTEGRATING TIME CONSTANT to 0.1 sec. Turn RANGE VOLTS switch (2) counterclockwise until meter reads between red mark and 0.1 on upper right scale. Select time constant so that meter deflection does not fluctuate. Turn GAIN control (1) clockwise until meter needle deflects to red mark.

v) To normalize the signal on channel B, repeat the procedure explained in step (iv).

vi) To measure the cross-correlation function ρ, set MEASUREMENT FUNCTION switch to the CORR. COEFFICIENT range providing greatest possible meter sensitivity. Select time constant so that meter deflection does not fluctuate.

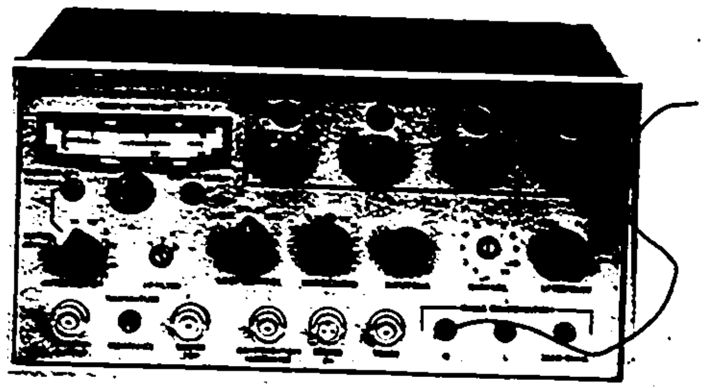

Fig. 89 - DISA Type 55D01 Anemometer Unit.

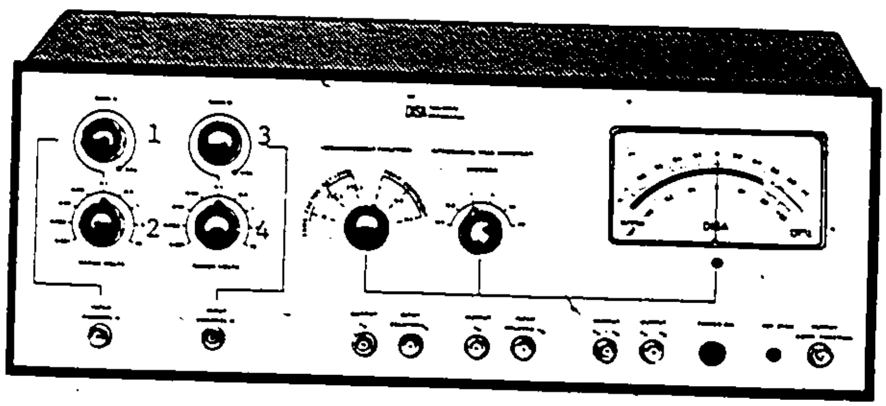

Fig. 90 - DISA Type 55D70 Analog Correlator

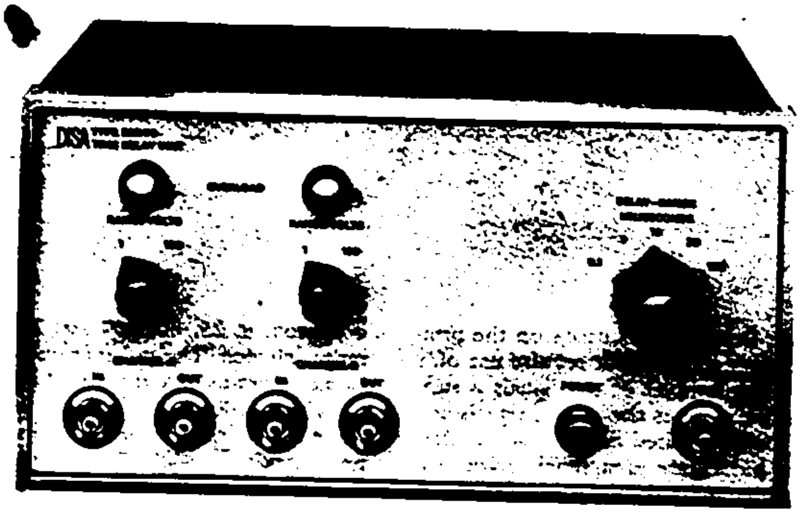

Fig. 91 - DISA Type 55D75 Time Delay Unit.

APPENDIX II

AUTOCORRELATION PLATES

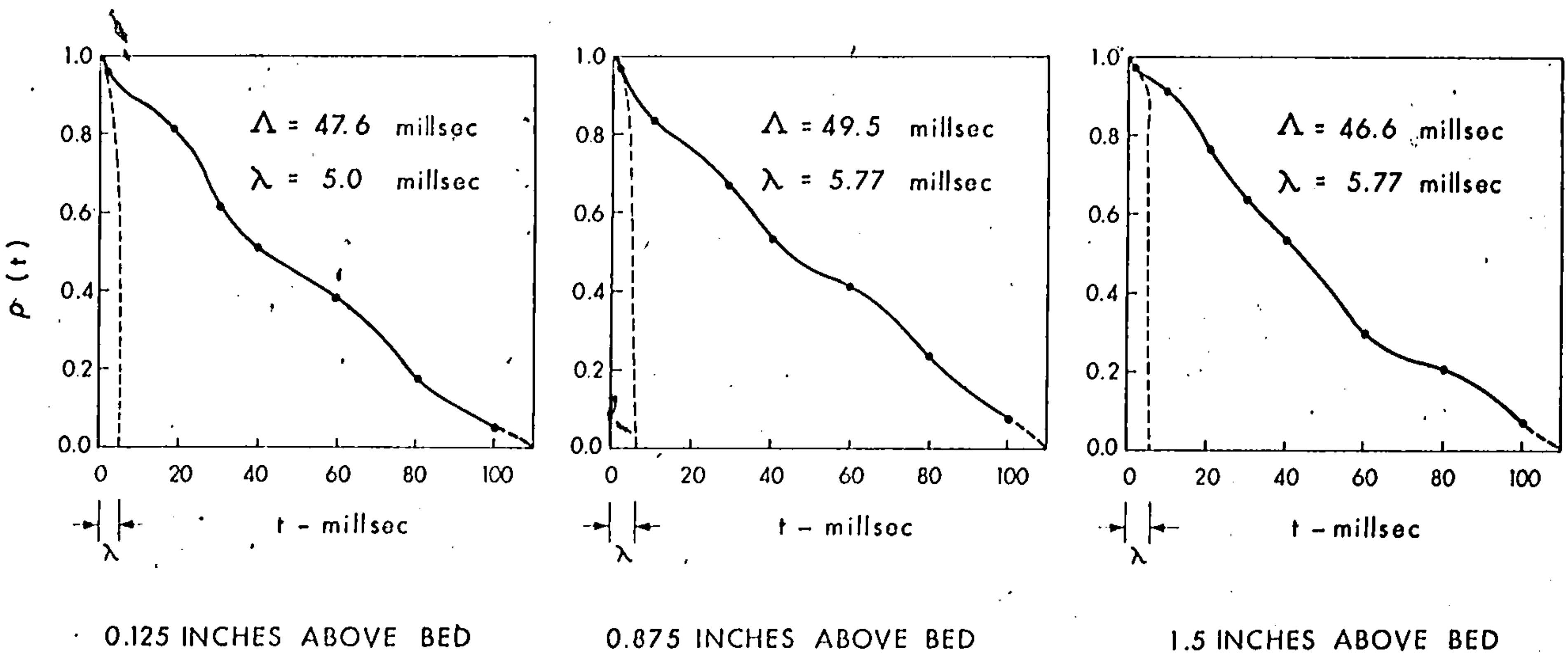

PLATE 1a — Time correlations for a smooth flat bed section 14.0 inches D/S from the screen.

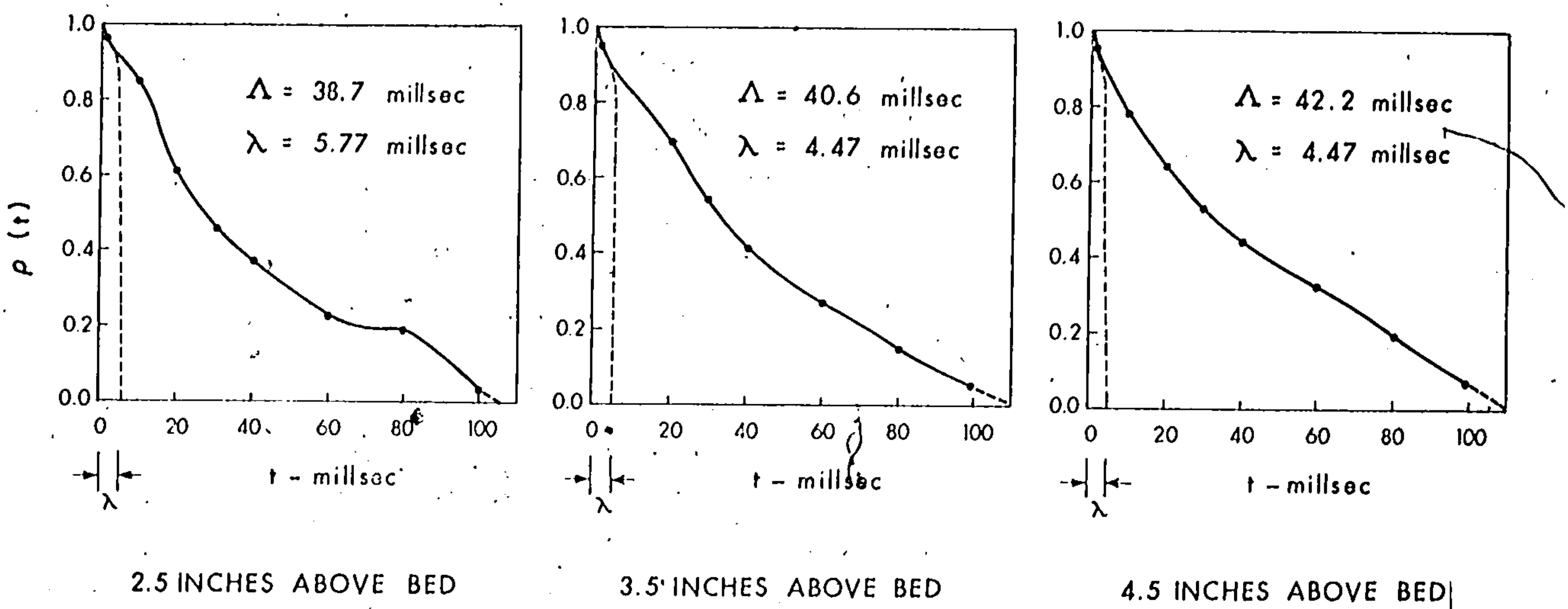

PLATE 1b — Time correlations for a smooth flat bed section 14.0 inches D/S from the screen.

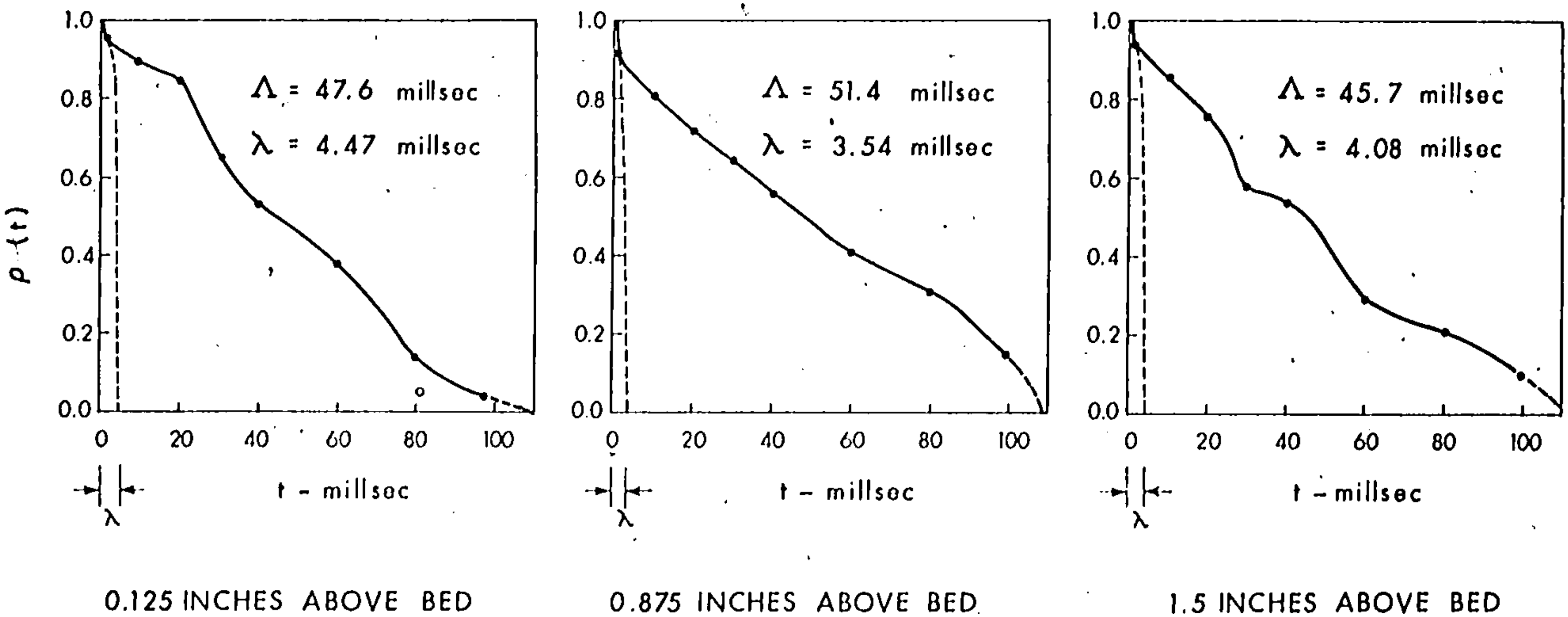

PLATE 2a — Time correlations for a rough flat bed section 14.0 inches D/S from the screen.

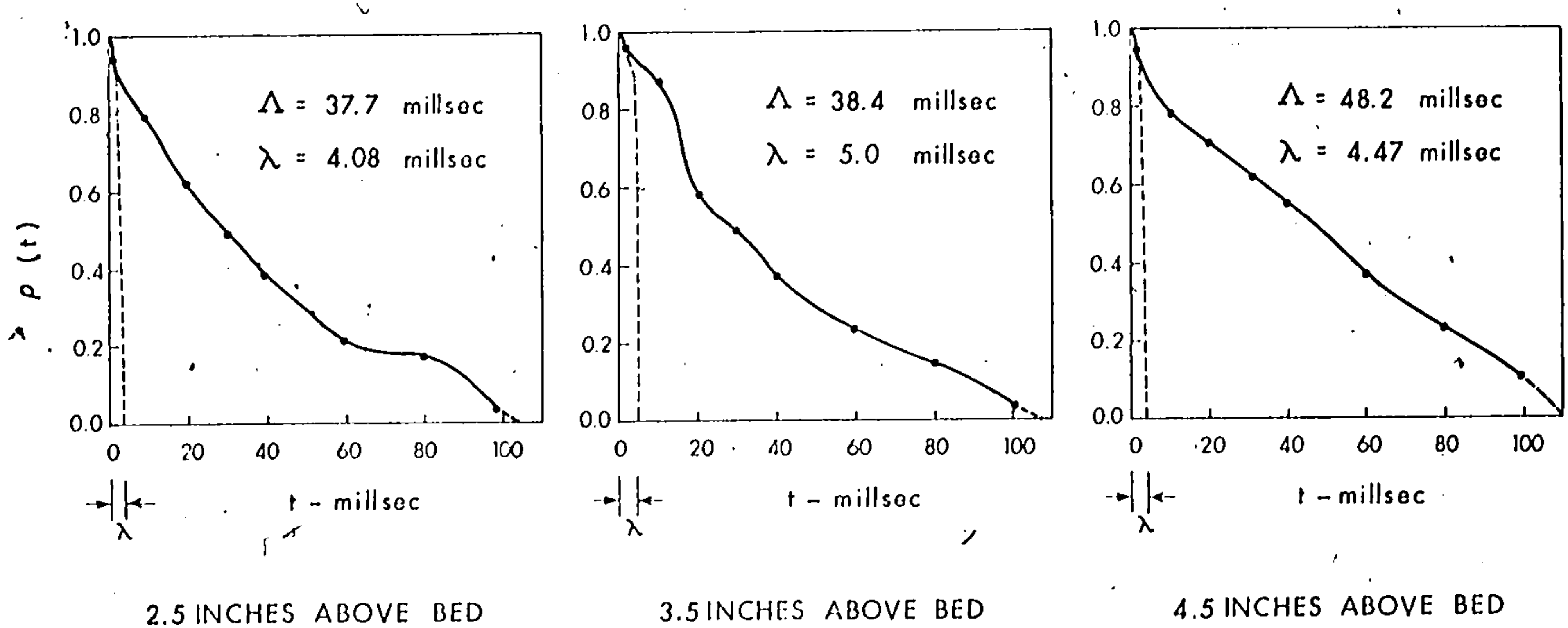

PLATE 2b— Time correlations for a rough flat bed section 14.0 inches D/S from the screen.

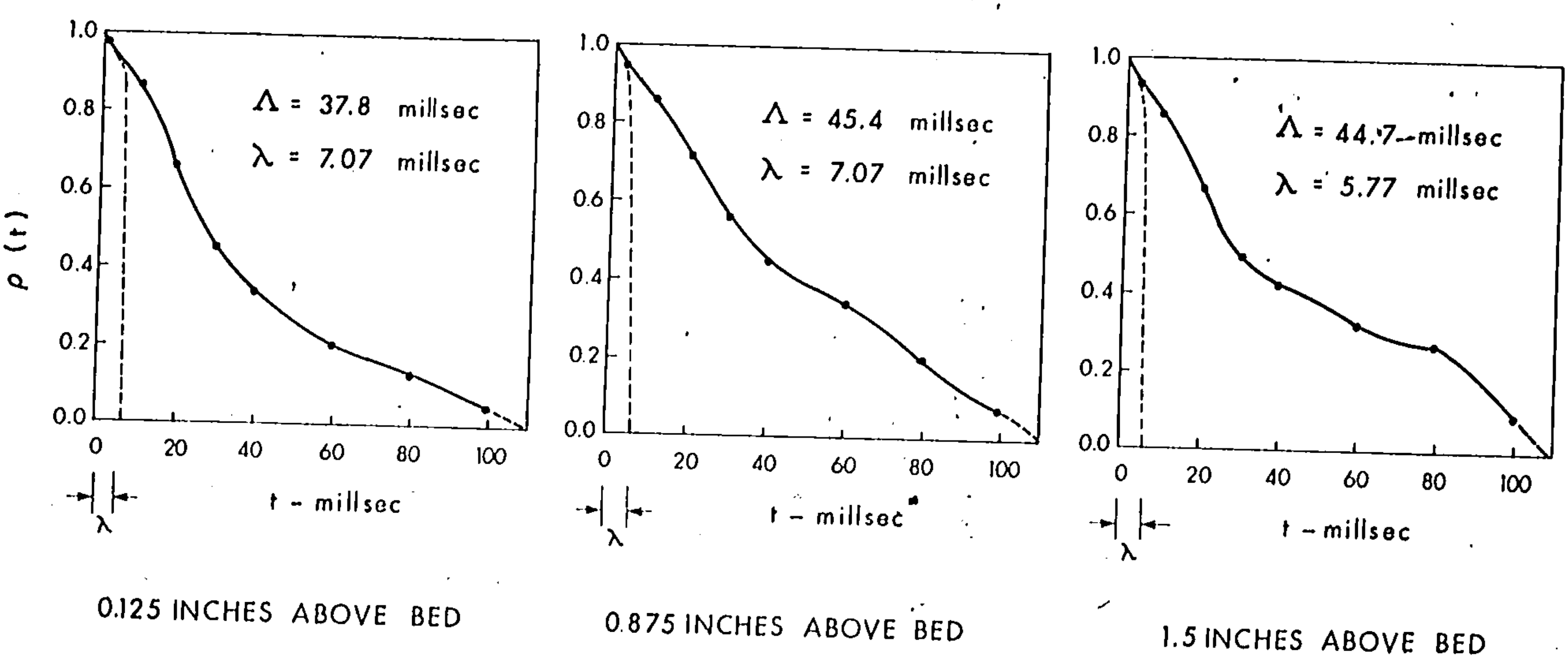

PLATE 3a — Time correlations for a smooth artificial ripple bed section 14.0 inches D/S from the screen.

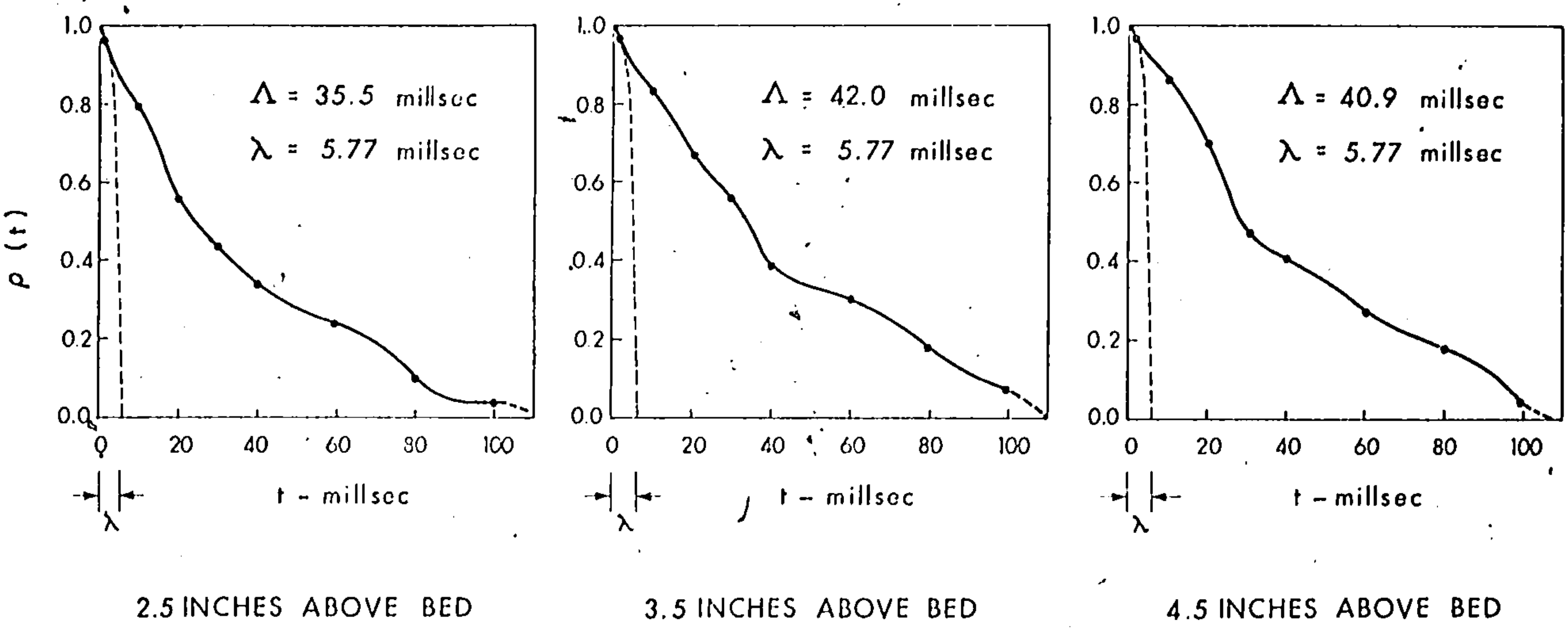

PLATE 3b— Time correlations for a smooth artificial ripple bed section 14.0 inches D/S from the screen.

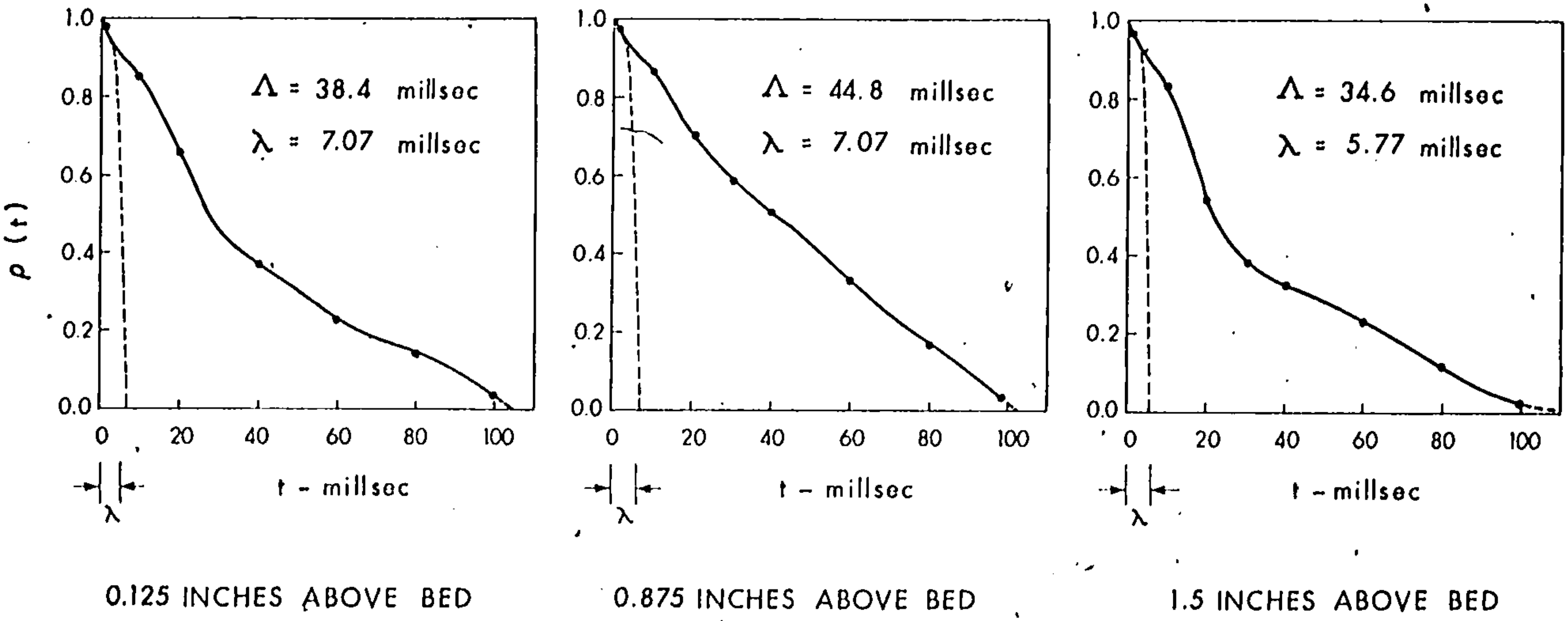

PLATE 4a — Time correlations for a rough artificial ripple bed section 14.0 inches D/S from the screen.

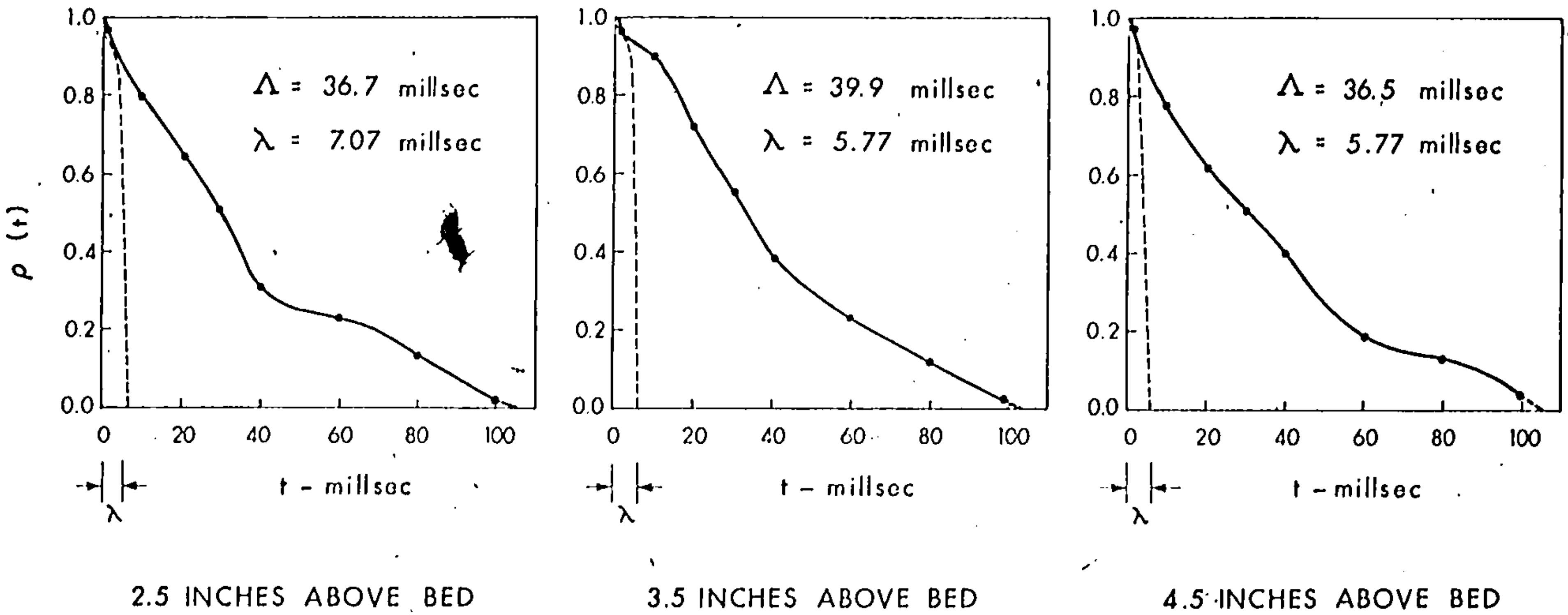

PLATE 4b— Time correlations for a rough artificial ripple bed section 14.0 inches D/S from the screen.

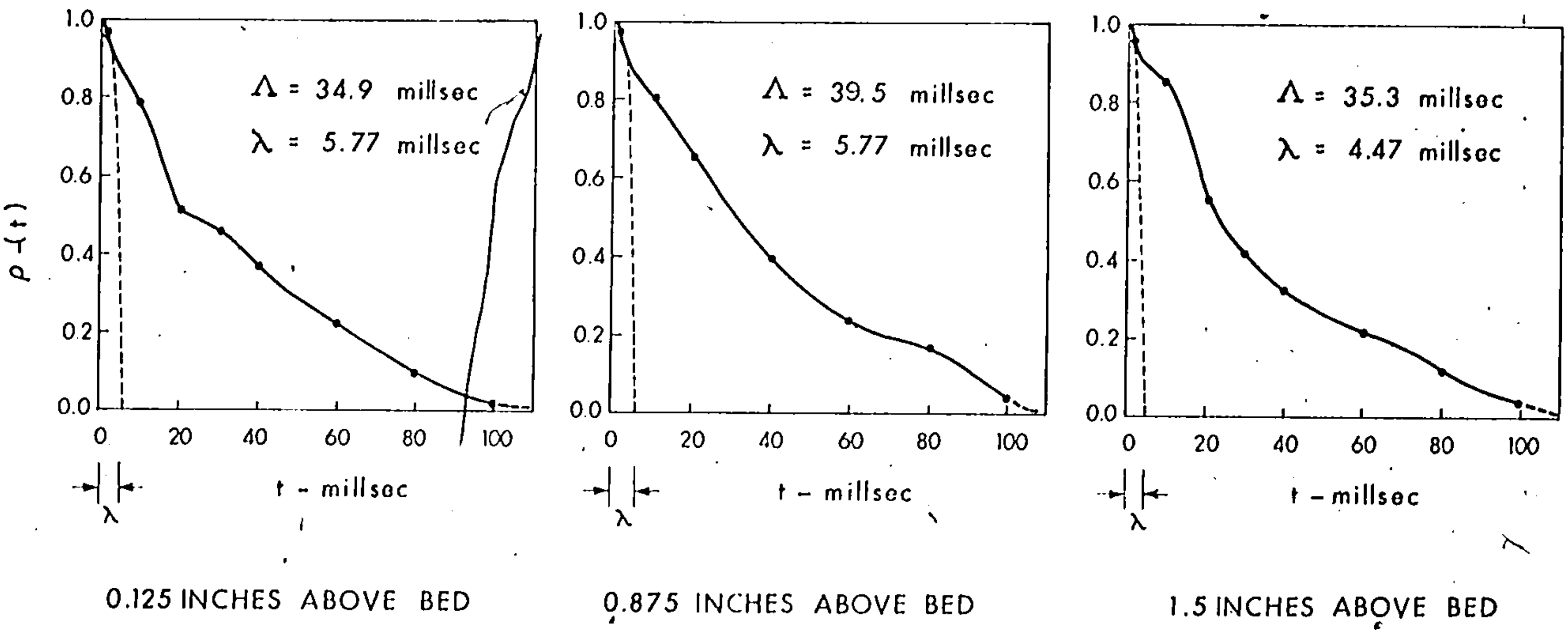

PLATE 5a — Time correlations for a cast of a natural ripple bed section 14.0 inches D/S from the screen.

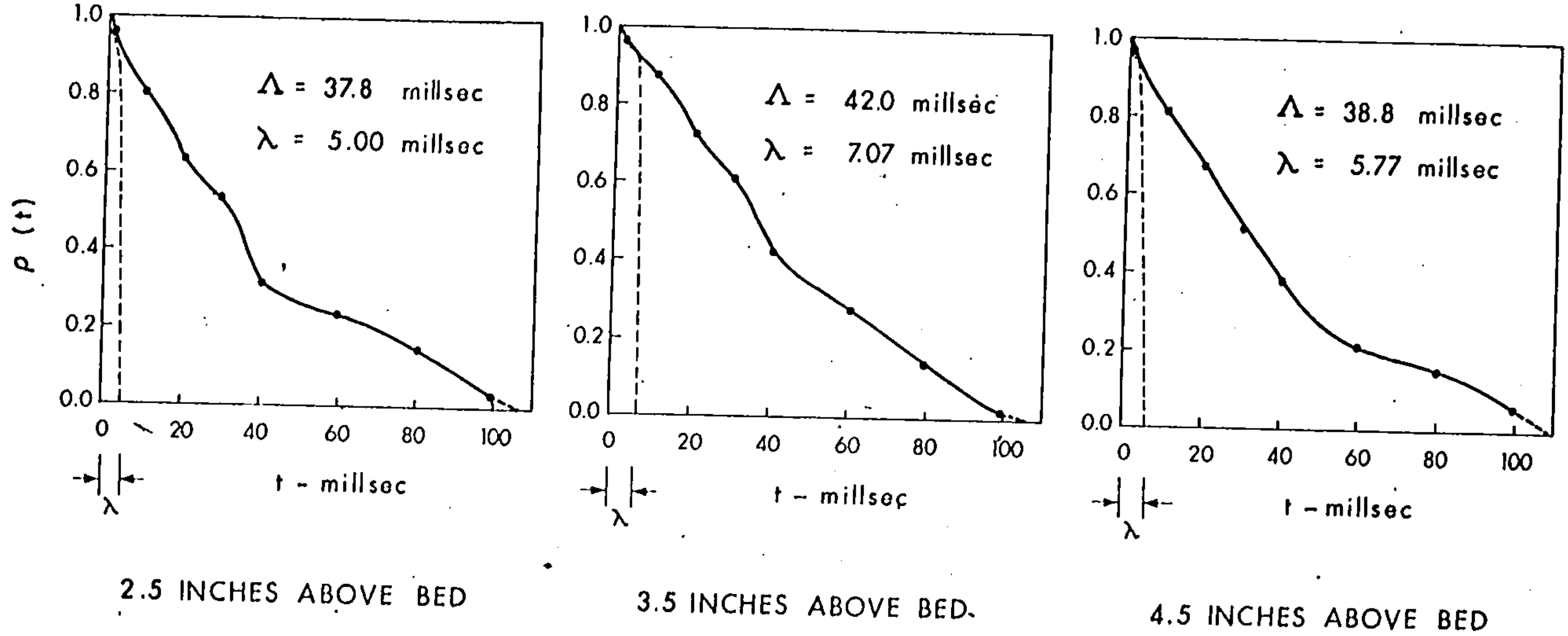

PLATE 5b— Time correlations for a cast of a natural ripple bed section 14.0 inches D/S from the screen.

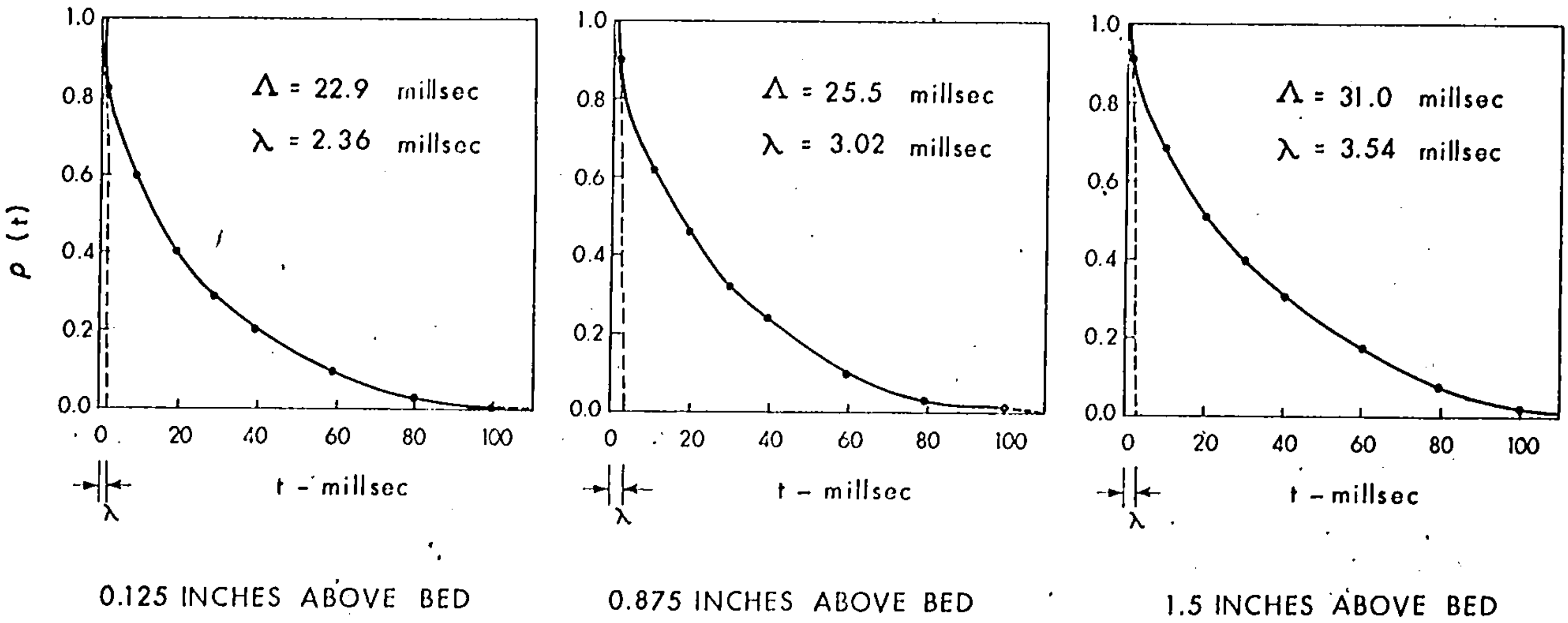

PLATE 6a– Time correlations for a smooth flat bed section 44.0 inches D/S from the screen.

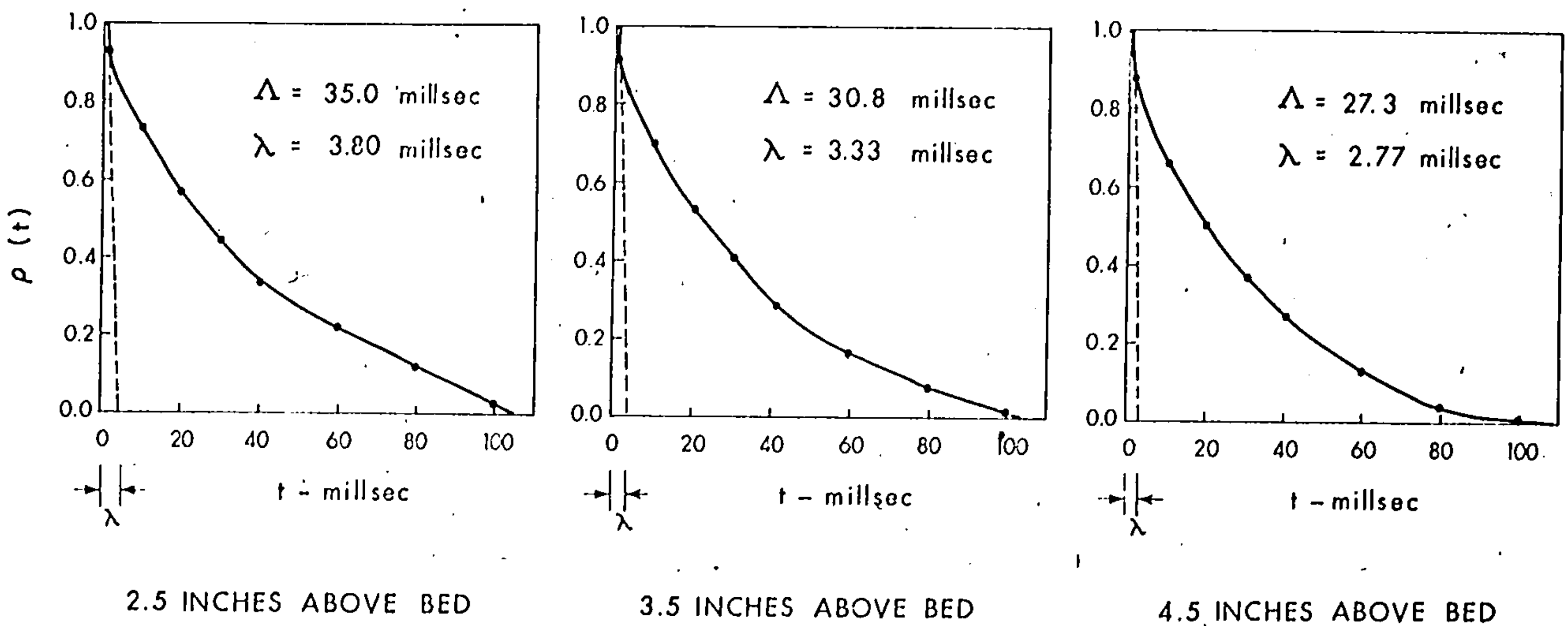

PLATE 6b— Time correlations for a smooth flat bed section 44.0 inches D/S from the screen.

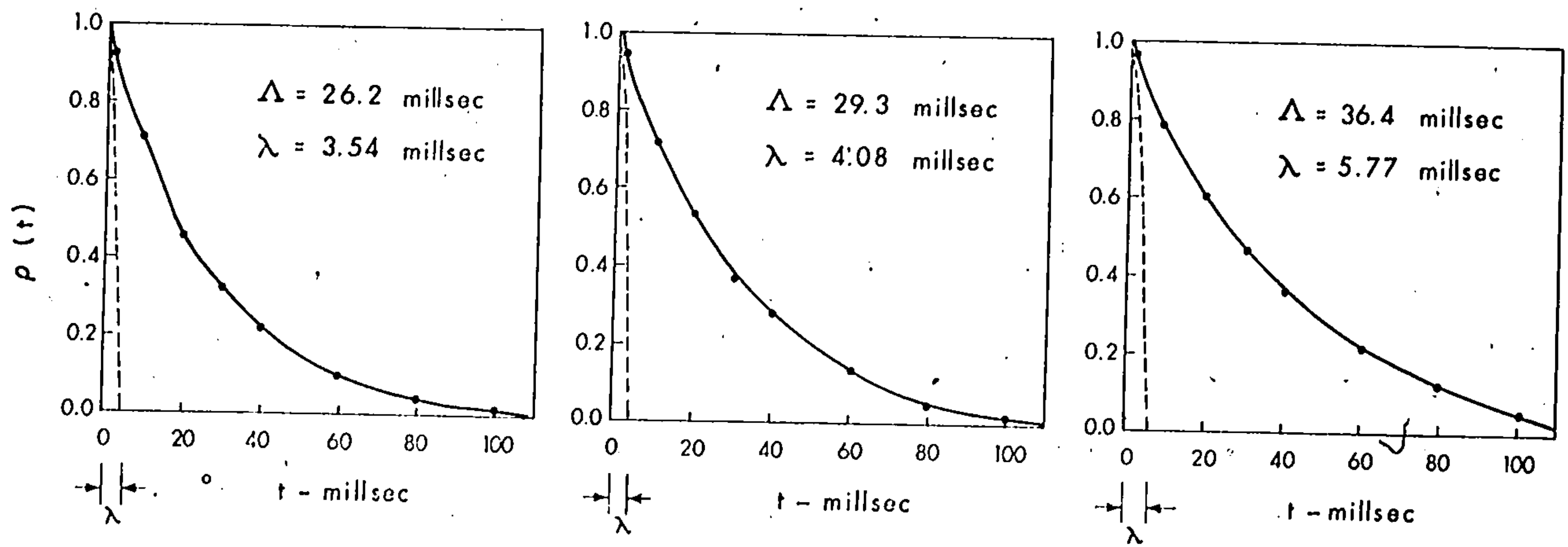

0.125 INCHES ABOVE BED   0.875 INCHES ABOVE BED   1.5 INCHES ABOVE BED

PLATE 7a — Time correlations for a rough flat bed section 44.0 inches D/S from the screen.

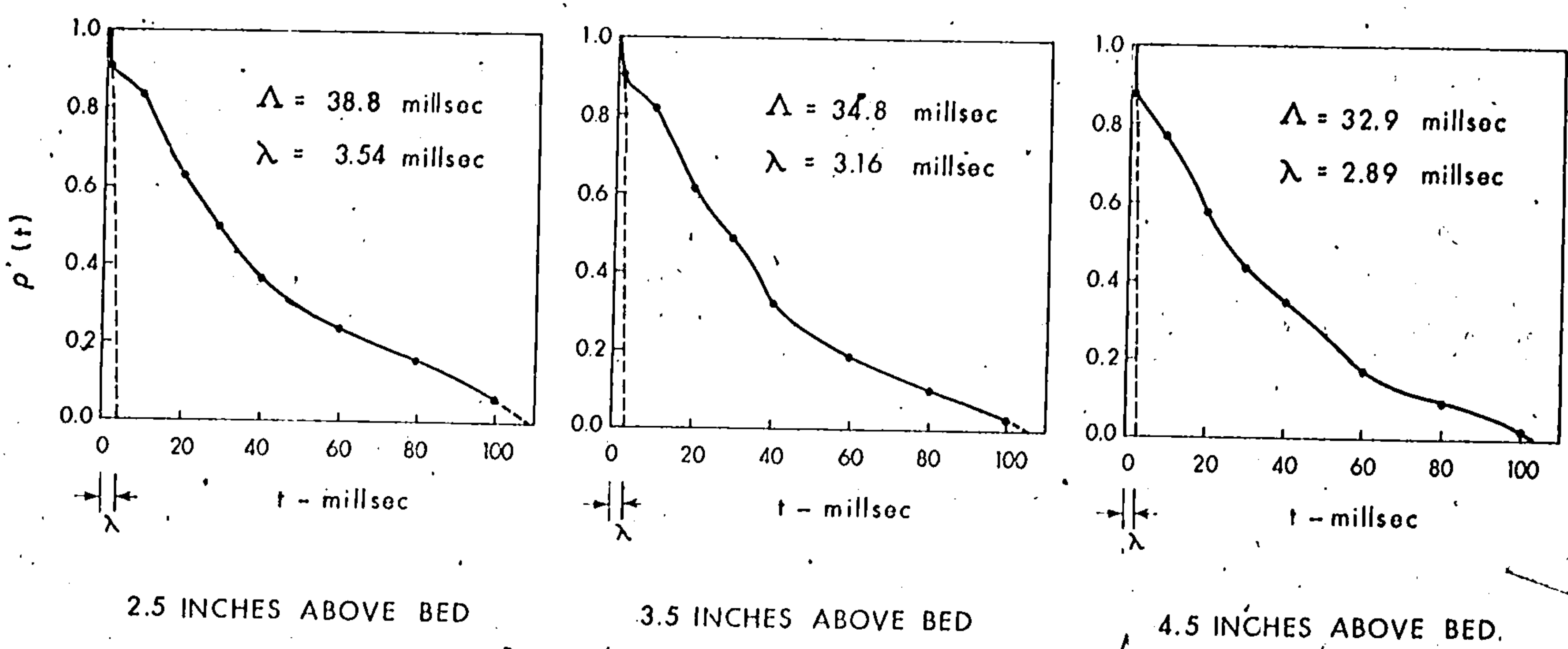

PLATE 7b— Time correlations for a rough flat bed section 44.0 inches D/S from the screen.

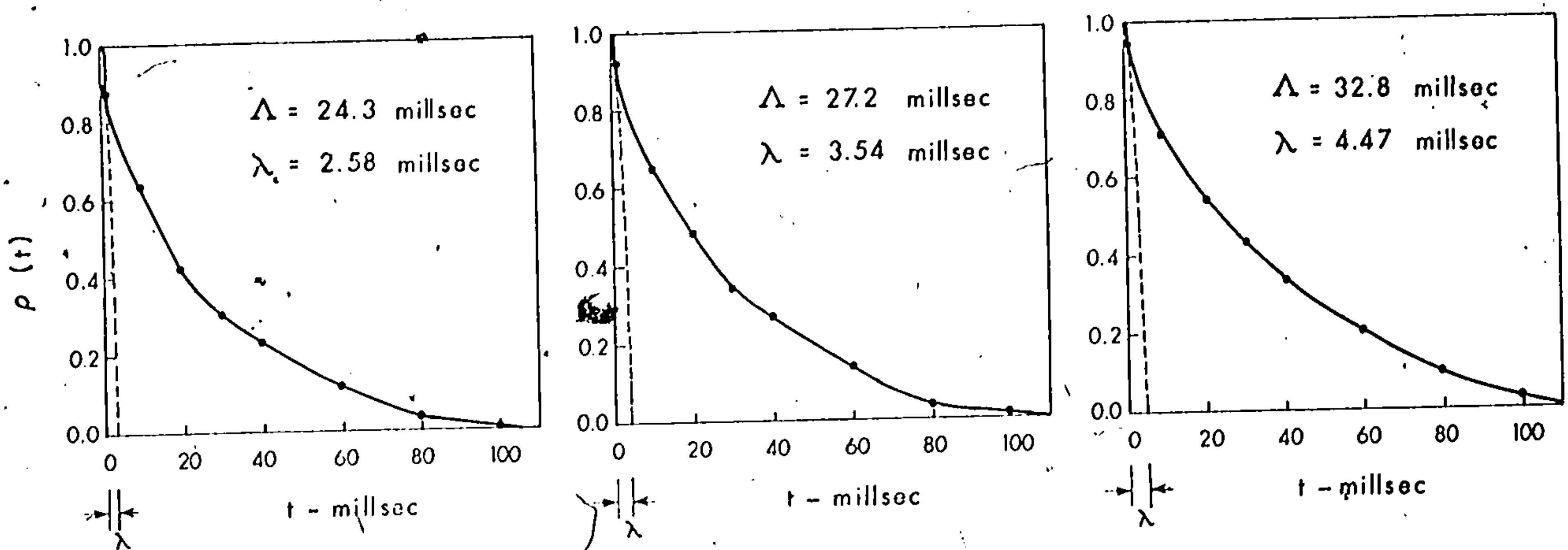

0.125 INCHES ABOVE BED | 0.875 INCHES ABOVE BED | 1.5 INCHES ABOVE BED

PLATE 8a — Time correlations for a smooth artificial bed section 44.0 inches D/S from the screen.

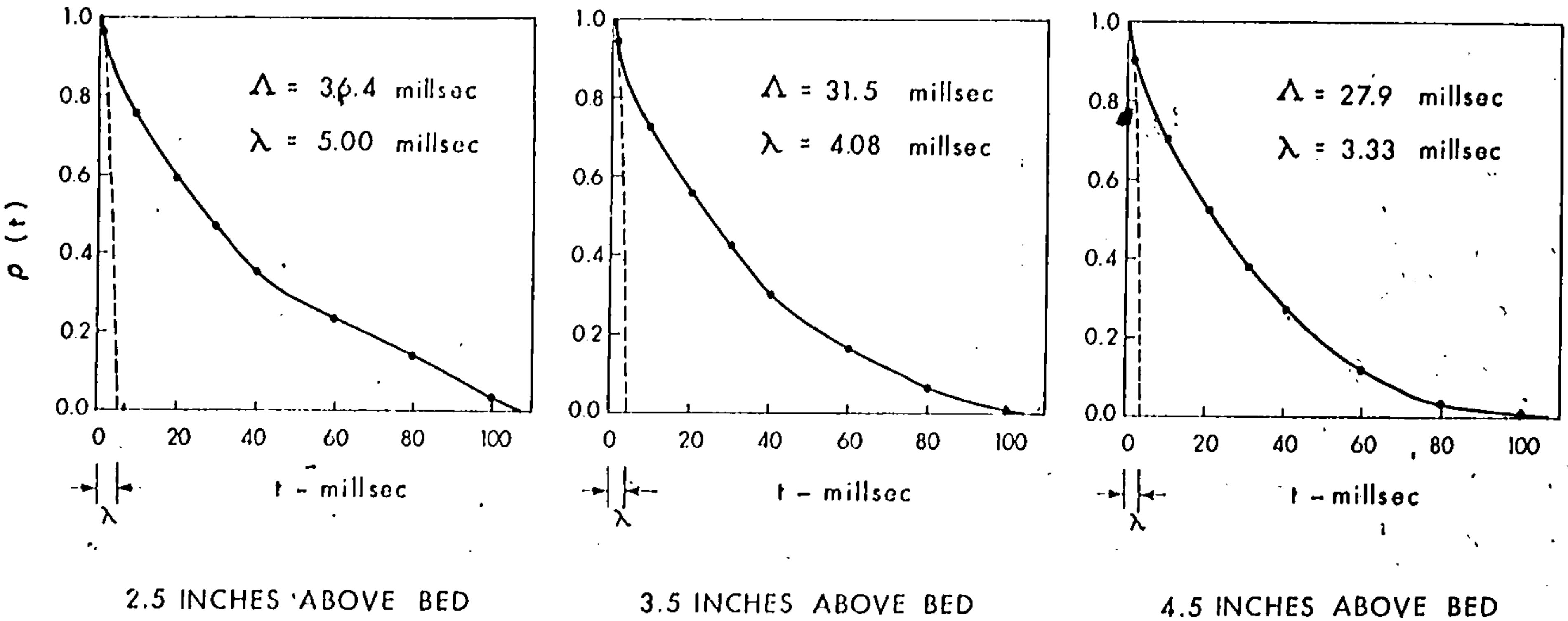

PLATE 8b— Time correlations for a smooth artificial bed section 44.0 inches D/S from the screen.

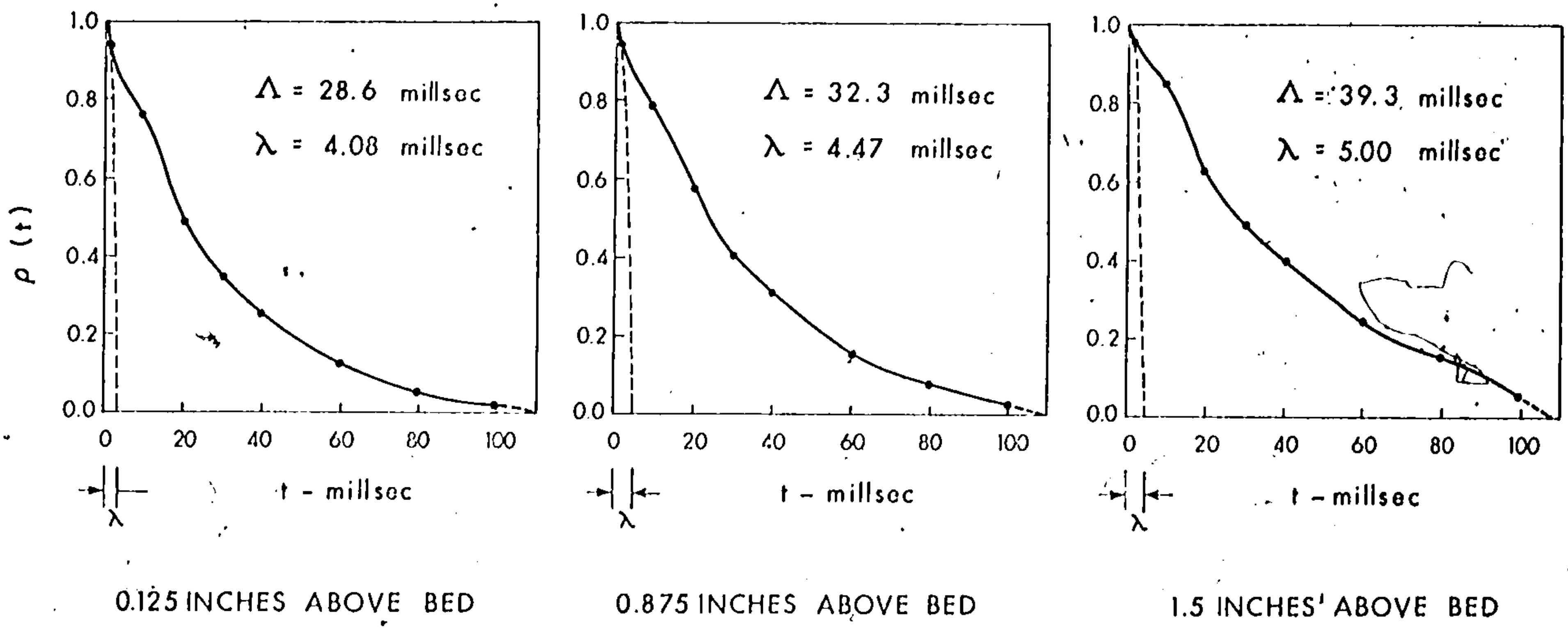

PLATE 9a— Time correlations for a rough artificial bed section 44.0 inches D/S from the screen.

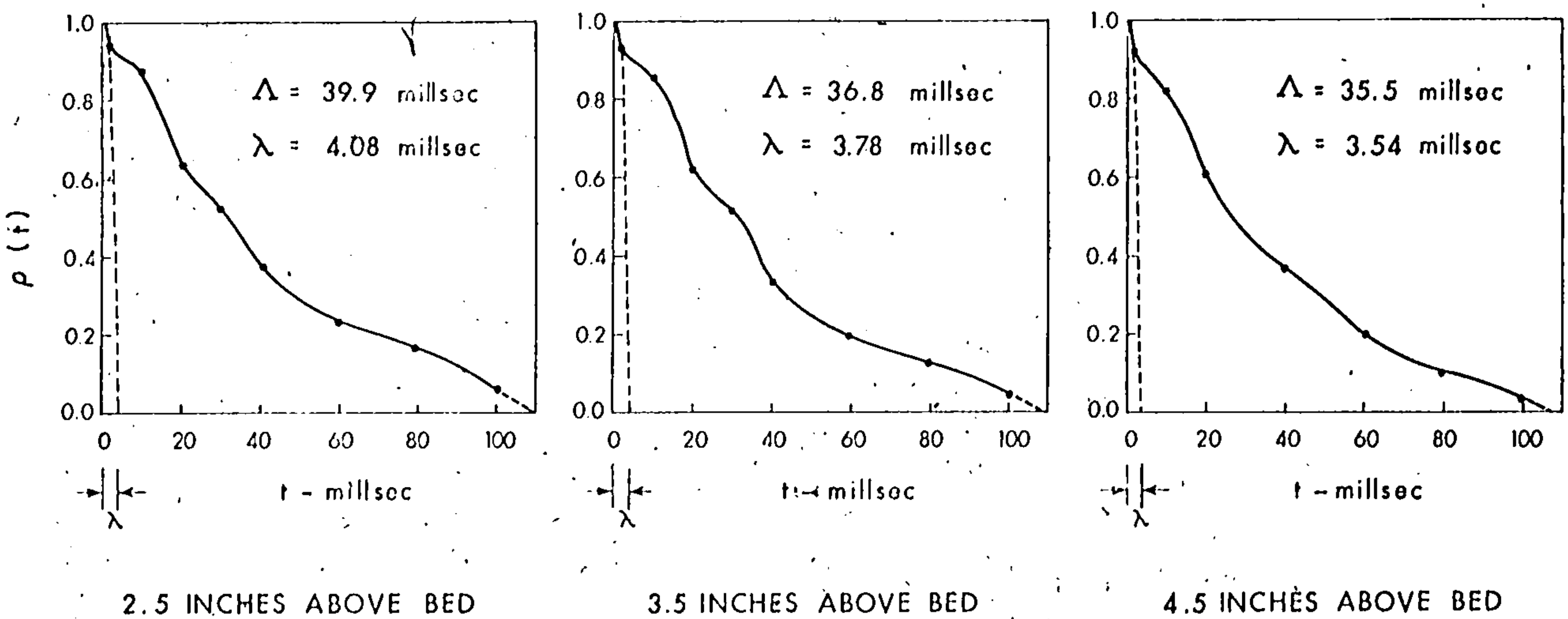

PLATE 9b — Time correlations for a rough artificial bed section 44.0 inches D/S from the screen.

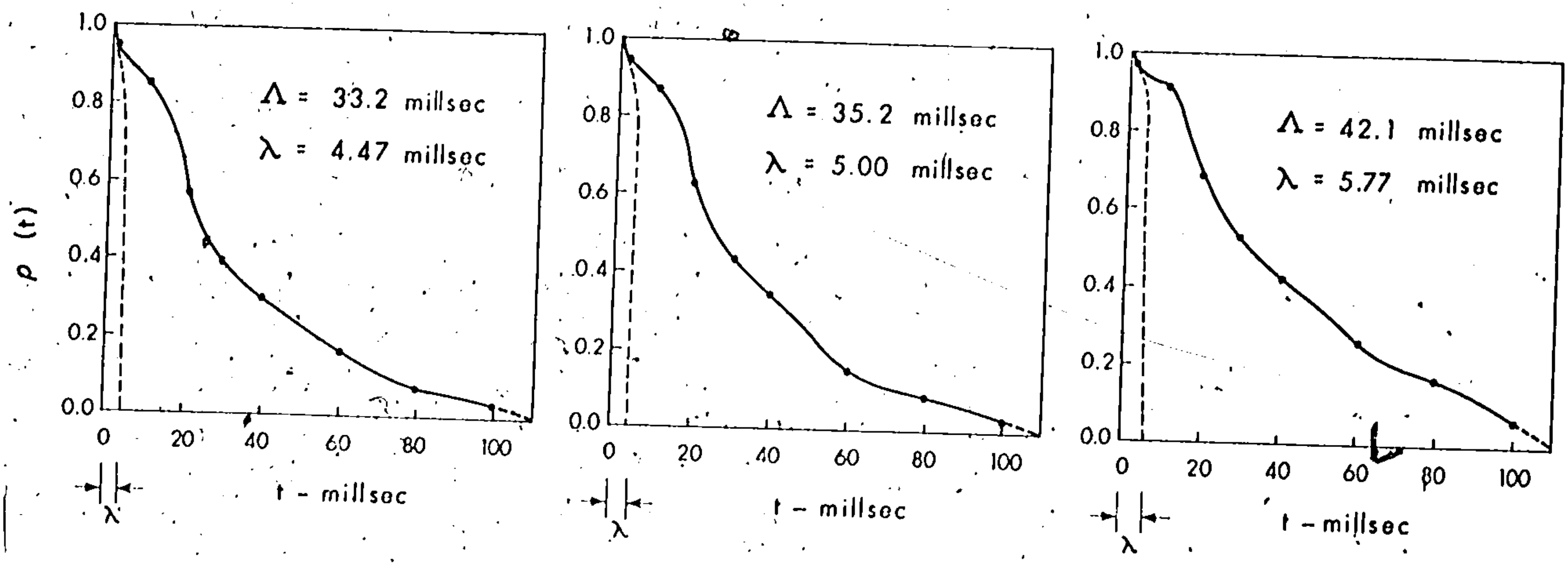

0.125 INCHES ABOVE BED

0.875 INCHES ABOVE BED

1.5 INCHES ABOVE BED

PLATE 10a– Time correlations for a cast of a natural ripple bed section 44.0 inches D/S from the screen.

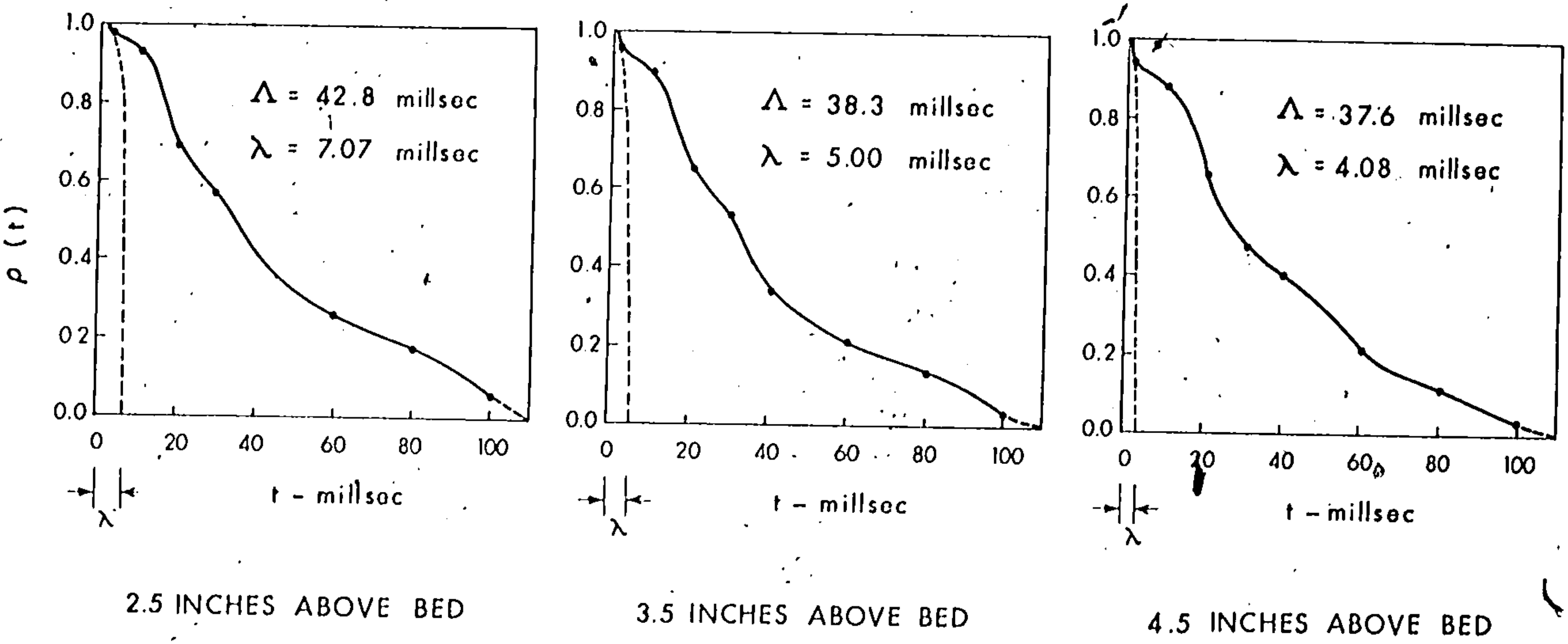

PLATE 10b– Time correlations for a cast of a natural ripple bed section 44.0 inches D/S from the screen.

APPENDIX III

PHOTOGRAPHS FROM THE FLOW VISUALIZATION STUDY

Photograph 14. Smooth Flat Bed.
Ripple Flow Condition.
D = 5.00 in., Q = 0.13 ft.^{3}/sec., $\bar{U}$ = 0.75 ft./sec.

Photograph 15. Smooth Artificial Ripple Bed.
Ripple Flow Condition.
D = 5.00 in., Q = 0.13 ft.^{3}/sec., $\bar{U}$ = 0.75 ft./sec.

Photograph 16. Rough Flat Bed.
Ripple Flow Condition.
$D = 5.00$ in., $Q = 0.13$ ft.^{3}/sec., $\bar{U} = 0.75$ ft./sec.

Photograph 17. Rough Artificial Ripple Bed.
Ripple Flow Condition.
$D = 5.00$ in., $Q = 0.13$ ft.^{3}/sec., $\bar{U} = 0.75$ ft./sec.

Photograph 18. Cast of a Natural Ripple Bed.
Flow Conditions Less Than That For Ripples.
D = 4.25 in., Q = 0.07 ft.^{3}/sec., $\bar{U}$ = 0.45 ft./sec.

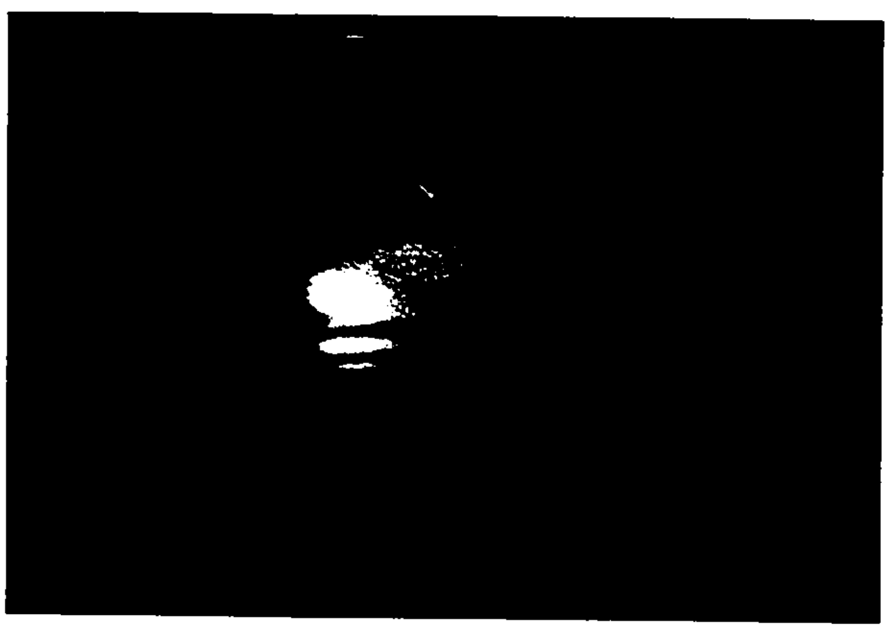

Photograph 19. Cast of a Natural Ripple Bed.
Flow Conditions Less Than That For Ripples.
D = 5.50 in., Q = 0.09 ft.^{3}/sec., $\bar{U}$ = 0.48 ft./sec.

Photograph 20. Smooth Flat Bed.

Flow Conditions Exceed Ripple Condition.

D = 4.75 in., Q = 0.14 ft.^{3}/sec., $\bar{U}$ = 0.85 ft./sec.

Photograph 21. Rough Flat Bed.

Flow Conditions Less Than That For Ripples.

D = 4.75 in., Q = 0.10 ft.^{3}/sec., $\bar{U}$ = 0.61 ft./sec.

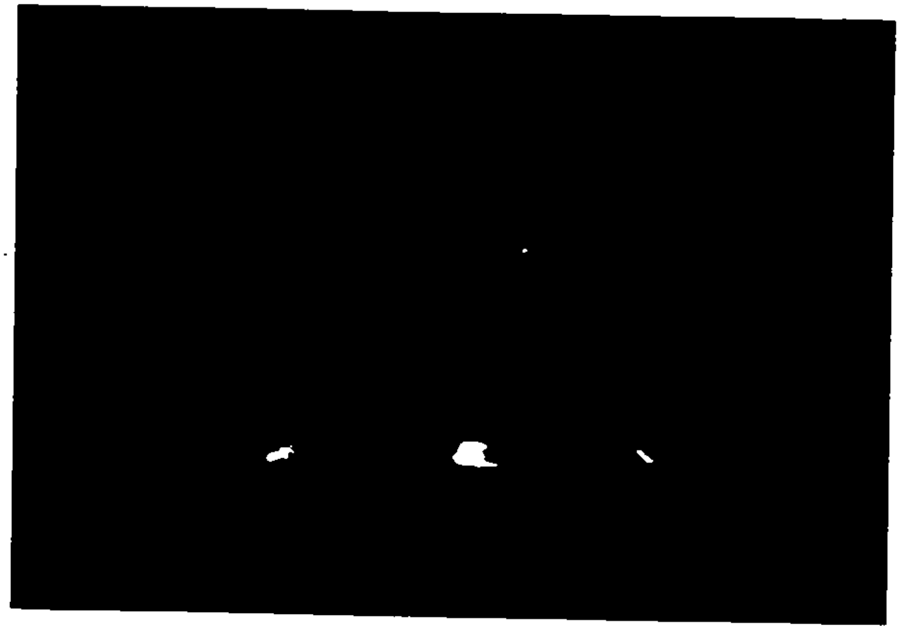

Photograph 22. Smooth Flat Bed - Filter OFF.
Ripple Flow Condition.
D = 5.00 in., Q = 0.13 ft.^{3}/sec., $\bar{U}$ =0.75 ft./sec.

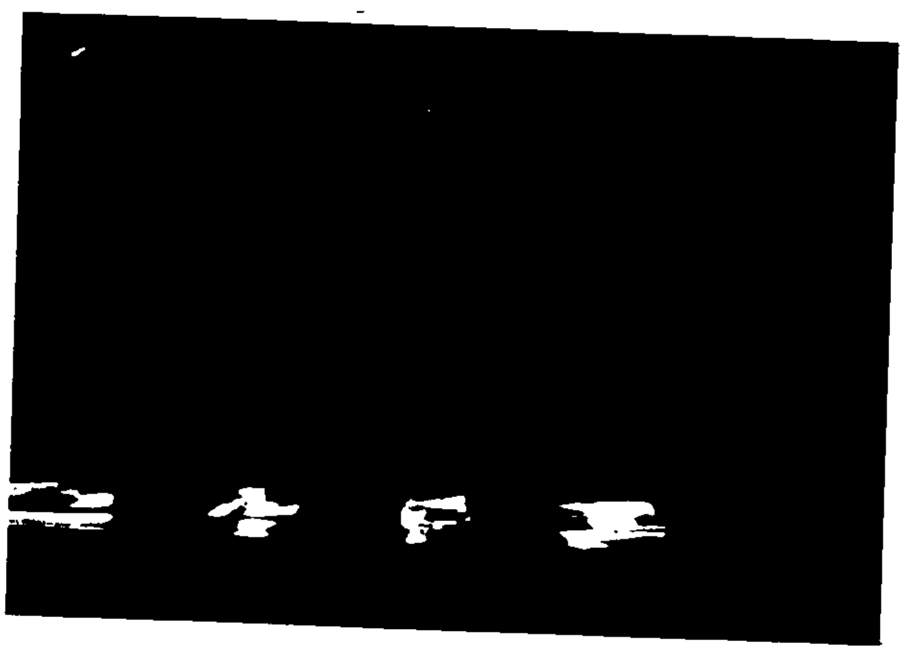

Photograph 23. Smooth Artificial Ripple Bed - Filter OFF.
Ripple Flow Condition.
D = 5.00 in., Q = 0.13 ft.^{3}/sec., $\bar{U}$ = 0.75 ft./sec.

APPENDIX IV

TABLES

TABLE 1. Transverse Measurements of Longitudinal Velocity At Different Sections Downstream The Screen At 2.5 Inches Above the Bed.

Distance D/S the Screen inches	Location of Pitot-tube across the width of flume inches	Sloping Manometer Reading Δh mms	Velocity U ft./sec.
14	0.5	29.0	0.68
	1.5	39.5	0.79
	2.5	45.0	0.84
	3.5	37.5	0.77
	4.5	26.0	0.64
31	0.5	31.0	0.70
	1.5	37.5	0.77
	2.5	42.5	0.82
	3.5	35.5	0.75
	4.5	28.0	0.67
44	0.5	33.0	0.72
	1.5	36.5	0.76
	2.5	38.5	0.78
	3.5	35.5	0.75
	4.5	33.0	0.72

$U = 0.1258 \sqrt{\Delta h}$

TABLE 2. Velocity Measurements Throughout The Depth Of Flow In The Mobile Bed Using The Pitot-Tube

Location of the Pitot-tube above the bed "d" inches	Relative depth $\frac{d}{D}$	Sloping manometer reading Δh mms.	Velocity U ft./sec.	$\frac{U}{\bar{U}}$
0	0	0	0	0
0.0625	0.0125	15.0	0.49	0.65
0.1	0.02	17.0	0.52	0.69
0.2	0.04	22.0	0.59	0.79
0.3	0.06	23.5	0.61	0.81
0.4	0.08	26.0	0.64	0.86
0.5	0.10	28.0	0.67	0.89
0.7	0.14	31.0	0.70	0.93
1.0	0.20	34.0	0.73	0.98
1.5	0.30	36.0	0.76	1.01
2.0	0.40	37.5	0.77	1.03
2.5	0.50	38.0	0.78	1.04
3.0	0.60	39.0	0.79	1.05
3.5	0.70	41.0	0.81	1.08
4.0	0.80	43.0	0.83	1.10

D = depth of flow = 5.00 inches

$\bar{U}$ = mean flow velocity = 0.75 ft./sec.

$U = 0.1258\sqrt{\Delta h}$.

TABLE 3. Velocity And Shear Stress Measurements Along A Ripple In A Mobile Bed Using The Pitot-Tube

Distance D/S the ripple "1" inches	Relative length $\frac{1}{L}$	Sloping manometer reading Δh mms.	Velocity U ft./sec.	$\frac{U}{\bar{U}}$	Shear Stress $\tau \times 10^4$ lb./ft.^{2}	$\frac{\tau}{\rho\bar{U}^2} \times 10^4$
2.25	1.00	17.0	0.52	0.69	22.1	20.3
1.80	0.80	19.0	0.55	0.73	24.7	22.6
1.35	0.60	21.0	0.58	0.77	27.3	25.0
0.90	0.40	23.0	0.60	0.80	29.9	27.4
0.45	0.20	22.0	0.59	0.79	28.6	26.2
0.10	0.05	0	0	0	0	0

L = length of the ripple = 2.25 inches

$\bar{U}$ = mean flow velocity = 0.75 ft./sec.

ρ = flow density = 1.94 slugs/ft.^{3}

$U = 0.1258 \cdot \sqrt{\Delta h}$

$\tau = 1.3 \times 10^{-4} \cdot \Delta h$.

TABLE 4. Ripple Lengths and Heights Along The Flume

Ripple No.	Ripple Height Inch	Ripple Length Inch
1	0.52	3.86
2	0.45	3.83
3	0.40	3.52
4	0.42	3.32
5	0.44	3.35
6	0.43	3.55
7	0.38	3.45
8	0.24	2.48
9	0.20	2.28
10	0.22	2.16
11*	0.18	2.25
12	0.16	2.22
13	0.18	2.20
14	0.22	2.18

* The tested ripple in the cast of the natural ripple bed.

TABLE 5-a. Results Of Vertical Velocity And Turbulence Characteristics At 44 Inches Downstream From The Screen For A Smooth Flat Bed Obtained From the V-Probe Measurements

Relative depth d/D	Temperature °F	Voltage E_1 Volts	Voltage E_2 Volts	Sloping manometer reading "Δh" mms.	Velocity ft./sec. obtained from E_1	Velocity ft./sec. obtained from E_2	Velocity ft./sec. "pitot-tube"	Average Velocity U ft./sec.	$\overline{e_s \cdot e_d} \times 10^2$ (Volts)^2	$\sqrt{\overline{e_s^2}}$ Volts	$\sqrt{\overline{e_d^2}}$ Volts	"S_1" Volts/ft./sec.	"S_2" Volts/ft./sec.	$\frac{U}{\bar{U}}$	$\frac{u'}{\bar{U}} \times 10^2$	$\frac{v'}{\bar{U}} \times 10^2$	$-\frac{\overline{uv}}{\bar{U}^2} \times 10^4$
.025	71	7.14	8.25	27.0	.68	.68	.65	.67	0.71	.23	.15	2.64	2.16	0.89	6.56	4.39	11.59
.175	72	7.26	8.45	33.5	.75	.77	.73	.75	0.44	.21	.125	2.25	1.85	1.00	6.97	4.27	11.08
.3	73	7.37	8.54	37.5	.78	.79	.77	.78	0.35	.16	.135	2.14	1.76	1.04	5.61	4.77	9.30
.5	73	7.37	8.61	39.5	.78	.80	.79	.79	0.23	.145	.125	2.09	1.71	1.05	5.21	4.52	7.52
.7	74	7.44	8.63	40.5	.79	.81	.80	.80	0.20	.125	.11	2.07	1.70	1.06	4.53	4.01	6.04
.9	75	7.33	8.43	34.5	.73	.72	.74	.73	0.186	.12	.105	2.33	1.91	0,97	3.88	3.41	4.43

D = depth of flow = 5.00 inches

$\bar{U}$ = mean flow velocity = 0.75 ft./sec.

TABLE 5-b. Results Of Vertical Velocity And Turbulence Characteristics At 44 Inches Downstream From The Screen For A Sand-Roughened Flat Bed Obtained From The V-Probe Measurements

Relative depth d/D	Temperature °F	Voltage E_1 Volts	Voltage E_2 Volts	Sloping manometer reading "Δh" mms.	Velocity ft./sec. obtained from E_1	Velocity ft./sec. obtained from E_2	Velocity ft./sec. "Pitot-tube"	Average Velocity U ft./sec.	$\overline{e_s \cdot e_d} \times 10^2$ (Volts)^2	$\sqrt{\overline{e_s^2}}$ Volts	$\sqrt{\overline{e_d^2}}$ Volts	"S_1" Volts/ft./sec.	"S_2" Volts/ft./sec.	$\frac{U}{\bar{U}}$	$\frac{u'}{\bar{U}} \times 10^2$	$\frac{v'}{\bar{U}} \times 10^2$	$-\frac{\overline{uv}}{\bar{U}^2} \times 10^4$
.025	70	7.05	8.08	20.0	.66	.64	.56	.62	0.80	.250	.175	2.91	2.38	0.83	6.47	4.61	11.29
.175	71	7.25	8.40	31.0	.74	.75	.70	.73	0.29	.145	.120	2.33	1.91	0.97	4.68	3.92	6.49
.3	71	7.30	8.50	35.5	.77	.79	.75	.77	0.25	.130	.120	2.20	1.80	1.02	4.47	4.13	6.42
.5	72	7.35	8.55	38.5	.80	.82	.78	.80	0.23	.125	.115	2.06	1.69	1.07	4.57	4.23	6.67
.7	73	7.42	8.60	40.5	.81	.82	.80	.81	0.21	.125	.110	2.03	1.67	1.08	4.63	4.09	6.38
.9	74	7.30	8.55	36.5	.72	.77	.76	.75	0.20	.120	.110	2.27	1.86	0.99	3.99	3.67	4.94

D = depth of flow = 5.00 inches

$\bar{U}$ = mean flow velocity = 0.75 ft./sec.

TABLE 5-c. Results Of Velocity And Turbulence Characteristics At 44 Inches Downstream From The Screen For A Smooth Artificial Ripple Bed Obtained From The V-Probe Measurements

Relative depth d/D	Temperature °F	Voltage E_I Volts	Voltage E_2 Volts	Sloping manometer reading "Δh" mms.	Velocity ft./sec. obtained from E_1	Velocity ft./sec. obtained from E_2	Velocity ft./sec. "Pitot-tube"	Average Velocity U ft./sec.	$\overline{e_s \cdot e_d} \times 10^2$ (Volts)^2	$\sqrt{\overline{e_s^2}}$ Volts	$\sqrt{\overline{e_d^2}}$ Volts	"S_1" Volts/ft./sec.	"S_2" Volts/ft./sec.	$\frac{U}{\bar{U}}$	$\frac{u'}{\bar{U}} \times 10^2$	$\frac{v'}{\bar{U}} \times 10^2$	$-\frac{\overline{uv}}{\bar{U}^2} \times 10^4$
.025	74	7.17	8.28	23.5	.65	.66	.61	.64	0.95	.29	.183	2.78	2.28	0.85	7.81	5.07	15.02
.175	75	7.29	8.37	31.0	.71	.69	.70	.70	0.52	.23	.140	2.49	2.03	0.93	6.93	4.35	11.22
.3	76	7.45	8.57	33.0	.77	.76	.72	.75	0.43	.175	.130	2.27	1.86	0.99	5.80	4.39	9.64
.5	76	7.43	8.64	36.5	.76	.79	.76	.77	0.26	.140	.120	2.20	1.80	1.02	4.80	4.15	6.83
.7	77	7.48	8.67	34.5	.76	.78	.74	.76	0.23	.13	.115	2.24	1.83	1.01	4.37	3.89	5.87
.9	78	7.37	8.56	31.0	.70	.73	.70	.71	0.21	.125	.110	2.46	2.02	0.94	3.83	3.39	4.37

D = depth of flow = 5.00 inches

$\bar{U}$ = mean flow velocity = 0.75 ft./sec.

TABLE 5-d. Results Of Vertical Velocity And Turbulence Characteristics At 44 Inches Downstream From The Screen For A Sand-Roughened Artificial Ripple Bed Obtained From The V-Probe Measurements

Relative depth d/D	Temperature °F	Voltage E_1 Volts	Voltage E_2 Volts	Sloping manometer reading "Δh" mms.	Velocity ft./sec. obtained from E_1	Velocity ft./sec. obtained from E_2	Velocity ft./sec. "Pitot-tube"	Average Velocity U ft./sec.	$\overline{e_s \cdot e_d} \times 10^2$ (Volts)^2	$\sqrt{\overline{e_s^2}}$ Volts	$\sqrt{\overline{e_d^2}}$ Volts	"S_1" Volts/ft./sec.	"S_2" Volts/ft./sec.	$\frac{U}{\bar{U}}$	$\frac{u'}{\bar{U}} \times 10^2$	$\frac{v'}{\bar{U}} \times 10^2$	$-\frac{\overline{uv}}{\bar{U}^2} \times 10^4$
.025	75	7.22	8.32	26.0	.67	.67	.64	.66	0.90	.32	.195	2.70	2.20	0.88	8.89	5.56	17.71
.175	76	7.30	8.45	29.0	.69	.70	.68	.69	0.75	.285	.165	2.54	2.08	0.92	8.40	5.01	15.61
.3	77	7.46	8.71	36.5	.75	.80	.76	.77	0.57	.24	.135	2.18	1.78	1.03	8.25	4.81	15.52
.5	77	7.63	8.75	43.5	.84	.82	.83	.83	0.28	.155	.125	1.98	1.62	1.10	5.88	4.80	9.51
.7	78	7.61	8.67	39.5	.83	.78	.79	.80	0.30	.145	.12	2.06	1.69	1.07	5.29	4.43	8.41
.9	79	7.57	8.70	33.5	.78	.77	.73	.76	0.25	.14	.115	2.22	1.82	1.01	4.75	3.93	6.42

D = depth of flow = 5.00 inches

$\bar{U}$ = mean flow velocity = 0.75 ft./sec.

TABLE 5-e. Results Of Vertical Velocity And Turbulence Characteristics At 44 Inches Downstream From The Screen For A Cast Of A Natural Ripple Bed Obtained From The V-Probe Measurements

Relative depth d/D	Temperature °F	Voltage E_1 Volts	Voltage E_2 Volts	Sloping manometer reading "Δh" mms.	Velocity ft./sec. obtained from E_1	Velocity ft./sec. obtained from E_2	Velocity ft./sec. "Pitot-tube"	Average Velocity U ft./sec.	$\overline{e_s \cdot e_d} \times 10^2$ (Volts)^2	$\sqrt{\overline{e_s^2}}$ Volts	$\sqrt{\overline{e_d^2}}$ Volts	"S_1" Volts/ft./sec.	"S_2" Volts/ft./sec.	$\frac{U}{\bar{U}}$	$\frac{u'}{\bar{U}} \times 10^2$	$\frac{v'}{\bar{U}} \times 10^2$	$-\frac{\overline{uv}}{\bar{U}^2} \times 10^4$
.025	72	6.93	8.00	21.0	.59	.60	.58	.59	1.35	.335	.22	3.16	2.58	0.78	7.97	5.36	16.44
.0625	73	7.12	8.20	24.0	.65	.65	.62	.64	0.89	.26	.17	2.78	2.28	0.85	7.03	4.71	13.12
.125	74	7.17	8.40	27.5	.65	.70	.66	.67	0.68	.24	.15	2.66	2.18	0.89	6.77	4.35	11.47
.2	75	7.27	8.46	31.0	.70	.73	.70	.71	0.55	.23	.14	2.46	2.02	0.94	7.00	4.37	11.45
.3	75	7.33	8.52	33.5	.73	.76	.73	.74	0.48	.18	.13	2.29	1.87	0.99	5.93	4.37	10.31
.5	76	7.47	8.66	36.5	.78	.80	.76	.78	0.40	.16	.125	2.17	1.77	1.03	5.57	4.41	9.62
.7	77	7.61	8.77	40.5	.83	.83	.80	.82	0.32	.14	.12	2.00	1.64	1.09	5.28	4.56	9.03
.9	78	7.59	8.73	40.5	.82	.81	.80	.81	0.25	.13	.115	2.03	1.67	1.08	4.81	4.28	7.22

D = depth of flow = 5.00 inches

$\bar{U}$ = mean flow velocity = 0.75 ft./sec.

TABLE 5-f. Results Of Vertical Velocity And Turbulence Characteristics At 14 Inches Downstream From The Screen For A Smooth Flat Bed Obtained From The V-Probe Measurements

Relative depth d/D	Temperature °F	Voltage E_1 Volts	Voltage E_2 Volts	Sloping manometer reading "Δh" mms.	Velocity ft./sec. obtained from E_1	Velocity ft./sec. obtained from E_2	Velocity ft./sec. "Pitot-tube"	Average Velocity U ft./sec.	$\overline{e_s \cdot e_d} \times 10^2$ (Volts)^2	$\sqrt{\overline{e_s^2}}$ Volts	$\sqrt{\overline{e_d^2}}$ Volts	"S_1" Volts/ft./sec.	"S_2" Volts/ft./sec.	$\frac{U}{\bar{U}}$	$\frac{u'}{\bar{U}} \times 10^2$	$\frac{v'}{\bar{U}} \times 10^2$	$-\frac{\overline{uv}}{\bar{U}^2} \times 10^4$
.025	73	7.24	8.38	28.0	.71	.72	.67	.70	0.79	.25	.17	2.49	2.03	0.93	7.56	5.27	15.36
.175	74	7.45	8.59	38.5	.80	.79	.78	.79	0.82	.26	.218	2.09	1.71	1.05	9.36	7.91	24.87
.3	75	7.53	8.59	40.5	.84	.79	.80	.81	1.05	.31	.245	2.03	1.67	1.08	11.43	9.13	34.13
.5	75	7.49	8.67	41.5	.82	.83	.81	.82	1.00	.27	.26	2.00	1.64	1.09	10.17	9.81	32.84
.7	76	7.38	8.62	34.5	.73	.78	.74	.75	0.93	.28	.255	2.25	1.85	1.00	9.33	8.53	25.21
.9	77	7.63	8.79	38.5	.84	.84	.78	.82	1.05	.295	.185	2.00	1.64	1.09	11.07	7.13	30.92

D = depth of flow = 5.00 inches

$\bar{U}$ = mean flow velocity = 0.75 ft./sec.

TABLE 5-g. Results Of Vertical Velocity And Turbulence Characteristics At 14 Inches Downstream From The Screen For A Sand-Roughened Flat Bed Obtained From The V-Probe Measurements

Relative depth d/D	Temperature °F	Voltage E_1 Volts	Voltage E_2 Volts	Sloping manometer reading "Δh" mms.	Velocity ft./sec. obtained from E_1	Velocity ft./sec. obtained from E_2	Velocity ft./sec. "Pitot-tube"	Average Velocity U ft./sec.	$\overline{e_s \cdot e_d} \times 10^2$ (Volts)^2	$\sqrt{\overline{e_s^2}}$ Volts	$\sqrt{\overline{e_d^2}}$ Volts	"S_1" Volts/ft./sec.	"S_2" Volts/ft./sec.	$\frac{U}{\bar{U}}$	$\frac{u'}{\bar{U}} \times 10^2$	$\frac{v'}{\bar{U}} \times 10^2$	$-\frac{\overline{uv}}{\bar{U}^2} \times 10^4$
.025	72	7.14	8.27	26.0	.68	.69	.64	.67	0.89	.27	.18	2.64	2.16	0.89	7.68	5.24	15.36
.175	73	7.26	8.38	30.0	.72	.72	.69	.71	0.92	.28	.225	2.44	2.00	0.95	8.61	7.00	20.30
.3	73	7.31	8.50	33.5	.75	.77	.73	.75	1.08	.305	.24	2.27	1.86	0.99	10.09	8.03	27.48
.5	74	7.44	8.61	38.5	.79	.80	.78	.79	1.35	.33	.29	2.09	1.71	1.05	11.88	10.51	41.37
.7	75	7.34	8.63	39.5	.74	.81	.79	.78	1.16	.31	.24	2.14	1.76	1.04	10.85	8.51	31.79
.9	75	7.51	8.65	41.5	.83	.82	.81	.82	1.28	.32	.21	2.00	1.64	1.09	12.01	8.08	37.51

D = depth of flow = 5.00 inches

$\bar{U}$ = mean flow velocity = 0.75 ft./sec.

TABLE 5-h. Results Of Vertical Velocity And Turbulence Characteristics At 14 Inches Downstream From The Screen For A Smooth Artificial Ripple Bed Obtained From The V-Probe Measurements

Relative depth d/D	Temperature °F	Voltage E_1 Volts	Voltage E_2 Volts	Sloping manometer reading "Δh" mms.	Velocity ft./sec. obtained from E_1	Velocity ft./sec. obtained from E_2	Velocity ft./sec. "Pitot-tube"	Average Velocity U ft./sec.	$\overline{e_s \cdot e_d} \times 10^2$ (Volts)^2	$\sqrt{\overline{e_s^2}}$ Volts	$\sqrt{\overline{e_d^2}}$ Volts	"S_1" Volts/ft./sec.	"S_2" Volts/ft./sec.	$\frac{U}{\bar{U}}$	$\frac{u'}{\bar{U}} \times 10^2$	$\frac{v'}{\bar{U}} \times 10^2$	$-\frac{\overline{uv}}{\bar{U}^2} \times 10^4$
.025	74	7.15	8.28	24.0	.64	.66	.62	.64	0.96	.295	.185	2.78	2.28	0.85	7.95	5.12	15.34
.175	75	7.33	8.52	33.5	.73	.76	.73	.74	0.82	.26	.175	2.29	1.87	0.99	8.55	5.88	19.09
.3	75	7.36	8.61	36.5	.75	.80	.76	.77	0.60	.20	.135	2.18	1.78	1.03	6.92	4.79	13.81
.5	76	7.36	8.55	35.5	.72	.75	.75	.74	1.25	.34	.295	2.29	1.87	0.99	11.17	9.76	34.68
.7	77	7.41	8.58	31.0	.72	.74	.70	.72	0.95	.30	.19	2.39	1.95	0.96	9.43	6.13	21.56
.9	78	7.57	8.65	36.5	.81	.77	.76	.78	0.86	.27	.18	2.14	1.76	1.04	9.44	6.44	22.56

D = depth of flow = 5.00 inches

$\bar{U}$ = mean flow velocity = 0.75 ft./sec.

TABLE 5-1. Results Of Vertical Velocity And Turbulence Characteristics At 14 Inches Downstream From The Screen For A Sand-Roughened Artificial Ripple Bed Obtained From The V-Probe Measurements

Relative depth d/D	Temperature °F	Voltage E_1 Volts	Voltage E_2 Volts	Sloping manometer reading "Δh" mms.	Velocity ft./sec. obtained from E_1	Velocity ft./sec. obtained from E_2	Velocity ft./sec. "Pitot-tube"	Average Velocity U ft./sec.	$\overline{e_s \cdot e_d} \times 10^2$ (Volts)^2	$\sqrt{\overline{e_s^2}}$ Volts	$\sqrt{\overline{e_d^2}}$ Volts	"S_1" Volts/ft./sec.	"S_2" Volts/ft./sec.	$\frac{U}{\bar{U}}$	$\frac{u'}{\bar{U}} \times 10^2$	$\frac{v'}{\bar{U}} \times 10^2$	$-\frac{\overline{uv}}{\bar{U}^2} \times 10^4$
.025	74	7.05	8.13	22.0	.60	.61	.59	.60	1.15	.32	.20	3.04	2.48	0.80	7.92	5.08	15.52
.175	75	7.27	8.40	28.0	.70	.70	.67	.69	0.96	.30	.195	2.54	2.08	0.92	8.85	5.89	19.08
.3	76	7.36	8.55	33.0	.72	.75	.72	.73	0.725	.265	.175	2.33	1.91	0.97	8.52	5.75	17.46
.5	76	7.36	8.53	33.5	.72	.74	.73	.73	1.23	.33	.255	2.30	1.91	0.97	10.63	8.32	29.90
.7	77	7.43	8.53	32.0	.73	.72	.71	.72	1.02	.29	.23	2.41	1.97	0.95	9.05	7.27	22.76
.9	77	7.59	8.75	39.5	.82	.82	.79	.81	0.93	.27	.17	2.03	1.67	1.08	9.96	6.45	25.53

D = depth of flow 5.00 inches

$\bar{U}$ = mean flow velocity = 0.75 ft./sec.

TABLE 5-j. Results Of Vertical Velocity And Turbulence Characteristics At 14 Inches Downstream From The Screen For A Cast Of A Natural Ripple Bed Obtained From The V-Probe Measurements

Relative depth d/D	Temperature °F	Voltage E_1 Volts	Voltage E_2 Volts	Sloping manometer reading "Δh" mms.	Velocity ft./sec. obtained from E_1	Velocity ft./sec. obtained from E_2	Velocity ft./sec. "Pitot-tube"	Average Velocity U ft./sec.	$\overline{e_s \cdot e_d} \times 10^2$ (Volts)^2	$\sqrt{\overline{e_s^2}}$ Volts	$\sqrt{\overline{e_d^2}}$ Volts	"S_1" Volts/ft./sec.	"S_2" Volts/ft./sec.	$\frac{U}{\bar{U}}$	$\frac{u'}{\bar{U}} \times 10^2$	$\frac{v'}{\bar{U}} \times 10^2$	$-\frac{\overline{uv}}{\bar{U}^2} \times 10^4$
.025	75	7.10	8.16	22.0	.62	.62	.59	.61	2.05	.42	.29	2.97	2.43	0.81	10.63	7.48	29.08
.175	76	7.34	8.42	28.0	.71	.69	.67	.69	1.74	.37	.24	2.54	2.08	0.92	10.95	7.28	31.38
.3	76	7.43	8.62	34.5	.76	.78	.74	.76	1.95	.395	.26	2.22	1.82	1.01	13.36	9.00	46.47
.5	77	7.63	8.75	40.5	.84	.82	.80	.82	1.4	.35	.22	2.00	1.64	1.09	13.12	8.47	42.47
.7	78	7.59	8.71	38.5	.82	.80	.78	.80	1.29	.34	.20	2.06	1.69	1.07	12.36	7.51	36.59
.9	79	7.53	8.78	37.5	.76	.81	.77	.78	1.05	.24	.16	2.14	1.76	1.04	8.45	5.80	22.29

D = depth of flow = 5.00 inches

$\bar{U}$ = mean flow velocity = 0.75 ft./sec.

TABLE 5-k. Results Of Vertical Velocity And Turbulence Characteristics At 21 Inches Downstream From The Screen For A Cast Of A Natural Ripple Bed Obtained From The V-Probe Measurements

Relative depth d/D	Temperature °F	Voltage E_1 Volts	Voltage E_2 Volts	Sloping manometer reading "Δh" mms.	Velocity ft./sec. obtained from E_1	Velocity ft./sec. obtained from E_2	Velocity ft./sec. "Pitot-tube"	Average Velocity U ft./sec.	$\overline{e_s \cdot e_d} \times 10^2$ (Volts)^2	$\sqrt{\overline{e_s^2}}$ Volts	$\sqrt{\overline{e_d^2}}$ Volts	"S_1" Volts/ft./sec.	"S_2" Volts/ft./sec.	$\frac{U}{\bar{U}}$	$\frac{u'}{\bar{U}} \times 10^2$	$\frac{v'}{\bar{U}} \times 10^2$	$-\frac{\overline{uv}}{\bar{U}^2} \times 10^4$
.025	76	7.13	8.33	27.0	.61	.66	.65	.64	1.86	.39	.26	2.78	2.28	0.85	10.52	7.17	28.68
.175	76	7.32	8,51	31.0	.70	.73	.70	.71	1.4	.35	.22	2.44	2.00	0.95	10.76	6.95	28.59
.3	77	7.50	8.74	35.5	.77	.79	.75	.77	1.2	.33	.20	2.18	1.78	1.03	11.37	7.09	31.43
.5	77	7.59	8.77	41.5	.82	.83	.81	.82	1.05	.24	.16	2.00	1.64	1.09	9.05	6.21	25.78
.7	78	7.52	8.75	40.5	.78	.82	.80	.80	0.80	.21	.15	2.06	1.69	1.07	7.69	5.63	18.88
.9	79	7.57	8.78	38.5	.78	.81	.78	.79	0.60	.20	.135	2.09	1.71	1.05	7.21	4.99	14.93

D = depth of flow ≐ 5.00 inches

$\bar{U}$ = mean flow velocity = 0.75 ft./sec.

TABLE 5-1. Results Of Vertical Velocity And Turbulence Characteristics At 31 Inches Downstream From The Screen For A Cast Of A Natural Ripple Bed Obtained From the V-Probe Measurements

Relative depth d/D	Temperature °F	Voltage E_1 Volts	Voltage E_2 Volts	Sloping manometer reading "Δh" mms.	Velocity ft./sec. obtained from E_1	Velocity ft./sec. obtained from E_2	Velocity ft./sec. "Pitot-tube"	Average Velocity U ft./sec.	$\overline{e_s \cdot e_d} \times 10^2$ (Volts)^2	$\sqrt{\overline{e_s^2}}$ Volts	$\sqrt{\overline{e_d^2}}$ Volts	"S_1" Volts/ft./sec.	"S_2" Volts/ft./sec.	$\frac{U}{\bar{U}}$	$\frac{u'}{\bar{U}} \times 10^2$	$\frac{v'}{\bar{U}} \times 10^2$	$-\frac{\overline{uv}}{\bar{U}^2} \times 10^4$
.025	75	7.10	8.20	23.5	.62	.63	.61	.62	1.65	.38	.25	2.91	2.38	0.83	9.80	6.60	24.25
.175	76	7.27	8.48	29.0	.67	.72	.68	.69	1.20	.33	.24	2.54	2.08	0.92	9.75	7.20	24.39
.3	76	7.39	8.55	33.5	.74	.75	.73	.74	0.80	.29	.18	2.29	1.87	0.99	9.49	6.05	20.80
.5	77	7.61	8.79	39.5	.83	.84	.79	.82	0.62	.21	.14	2.00	1.64	1.09	7.89	5.40	17.19
.7	78	7.48	8.71	38.5	.76	.80	.78	.78	0.50	.19	.13	2.14	1.76	1.04	6.67	4.65	12.16
.9	79	7.53	8.65	37.5	.76	.75	.77	.76	0.40	.16	.12	2.22	1.82	1.01	5.43	4.15	8.89

D = depth of flow = 5.00 inches

$\bar{U}$ = mean flow velocity = 0.75 ft./sec.

TABLE 5-m. Results Of Vertical Velocity And Turbulence Characteristics At 37 Inches Downstream From The Screen For A Cast Of A Natural Ripple Bed Obtained From The V-Probe Measurements

Relative Depth d/D	Temperature °F	Voltage E_1 Volts	Voltage E_2 Volts	Sloping manometer reading "Δh" mms.	Velocity ft./sec. obtained from E_1	Velocity ft./sec obtained from E_2	Velocity Ft./sec. "Pitot-tube"	Average Velocity U ft. sec.	$\overline{e_s \cdot e_d} \times 10^2$ (Volts)^2	$\sqrt{\overline{e_s^2}}$ Volts	$\sqrt{\overline{e_d^2}}$ Volts	"S_1" Volts/ft./sec.	"S_2" Volts/ft./sec.	$\frac{U}{\bar{U}}$	$\frac{u'}{\bar{U}} \times 10^2$	$\frac{v'}{\bar{U}} \times 10^2$	$-\frac{\overline{uv}}{\bar{U}^2} \times 10^4$
.025	73	7.00	8.15	23.0	.60	.63	.60	.61	1.5	.36	.245	2.97	2.43	0.81	9.11	6.32	21.23
.175	74	7.25	8.46	29.0	.69	.73	.68	.70	1.0	.26	.18	2.49	2.03	0.93	7.88	5.59	18.03
.3	75	7.38	8.57	34.5	.76	.78	.74	.76	0.7	.23	.16	2.22	1.82	1.01	7.79	5.53	16.48
.5	75	7.45	8.63	39.5	.80	.81	.79	.80	0.5	.19	.13	2.06	1.69	1.07	6.93	4.85	13.24
.7	76	7.52	8.66	42.5	.81	.80	.82	.81	0.4	.16	.125	2.03	1.67	1.08	5.92	4.69	10.65
.9	77	7.50	8.71	40.5	.77	.80	.80	.79	0.3	.135	.120	2.09	1.71	1.05	4.88	4.37	7.91

D = depth of flow = 5.00 inches

$\bar{U}$ = mean flow velocity = 0.75 ft./sec.

TABLE 6-a. Results Of Longitudinal Velocity And Turbulence Characteristics Along The Flume At 0.125 Inches Above The Floor For Smooth Flat Bed Obtained From The V-Probe Measurements

Distance downstream the screen inches	Temperature °F	Voltage E_1 Volts	Voltage E_2 Volts	Sloping manometer reading "Δh" mms.	Velocity ft./sec. obtained from E_1	Velocity ft./sec. obtained from E_2	Velocity Ft./sec. "Pitot-tube"	Average Velocity U ft./sec.	$\overline{e_s \cdot e_d} \times 10^2 (\text{Volts})^2$	$\sqrt{\overline{e_s^2}}$ Volts	$\sqrt{\overline{e_d^2}}$ Volts	"S_1" Volts/ft./sec.	"S_2" Volts/ft./sec.	$\frac{U}{\bar{U}}$	$\frac{u'}{\bar{U}} \times 10^2$	$\frac{v'}{\bar{U}} \times 10^2$	$-\frac{\overline{uv}}{\bar{U}^2} \times 10^4$
11.0	74	7.29	8.40	30.0	.71	.70	.69	.70	0.90	.25	.172	2.49	2.03	0.93	7.57	5.33	16.41
13.5	75	7.20	8.41	28.0	.66	.71	.67	.68	0.75	.225	.160	2.58	2.12	0.91	6.55	4.76	12.34
18.5	76	7.15	8.37	27.5	.62	.67	.66	.65	0.62	.205	.135	2.72	2.23	0.87	5.67	3.84	9.05
23.5	77	7.30	8.45	26.0	.66	.68	.64	.66	0.51	.165	.12	2.70	2.20	0.88	4.64	3.45	7.11
28.5	77	7.32	8.47	27.0	.67	.69	.65	.67	0.49	.160	.12	2.66	2.18	0.89	4.55	3.48	6.90
36.0	78	7.37	8.42	28.0	.70	.67	.67	.68	0.58	.20	.13	2.61	2.13	0.90	5.77	3.87	9.39
43.0	78	7.30	8.47	27.5	.66	.69	.66	.67	0.69	.21	.14	2.66	2.18	0.89	5.95	4.07	10.29

D = depth of flow = 5.00 inches

$\bar{U}$ = mean flow velocity = 0.75 ft./sec.

TABLE 6-b. Results Of Longitudinal Velocity And Turbulence Characteristics Along The Flume At 0.125 Inches Above The Floor For A Sand-Roughened Flat Bed Obtained From The V-Probe Measurements

Distance downstream the screen inches	Temperature °F	Voltage E_1 Volts	Voltage E_2 Volts	Sloping manometer reading "Δh" mms.	Velocity ft./sec. obtained from E_1	Velocity ft./sec. obtained from E_2	Velocity Ft./sec. "Pitot-tube"	Average Velocity U ft./sec.	$\overline{e_s \cdot e_d} \times 10^2 (\text{Volts})^2$	$\sqrt{\overline{e_s^2}}$ Volts	$\sqrt{\overline{e_d^2}}$ Volts	"S_1" Volts/ft./sec.	"S_2" Volts/ft./sec.	$\frac{U}{\bar{U}}$	$\frac{u'}{\bar{U}} \times 10^2$	$\frac{v'}{\bar{U}} \times 10^2$	$-\frac{\overline{uv}}{\bar{U}^2} \times 10^4$
11.0	75	7.15	8.28	24.0	.64	.66	.62	.64	1.24	.315	.205	2.83	2.31	0.85	8.37	5.60	18.42
13.5	76	7.25	8.37	27.0	.66	.67	.65	.66	0.92	.290	.190	2.70	2.2	0.88	8.08	5.43	16.30
18.5	77	7.34	8.50	27.5	.68	.70	.66	.68	0.85	.260	.180	2.58	2.12	0.91	7.56	5.33	15.08
23.5	78	7.30	8.47	27.5	.66	.69	.66	.67	0.80	.255	.175	2.64	2.16	0.89	7.25	5.09	13.88
28.5	79	7.32	8.50	27.0	.65	.68	.65	.66	0.78	.255	.170	2.70	2.2	0.88	7.12	4.85	13.21
36.0	79	7.23	8.47	26.0	.61	.67	.64	.64	0.76	.250	.160	2.78	2.28	0.85	6.75	4.43	11.59
43.0	80	7.30	8.45	24.0	.62	.65	.62	.63	0.75	.245	.165	2.86	2.34	0.84	6.44	4.44	10.93

D = depth of flow = 5.00 inches

$\bar{U}$ = mean flow velocity = 0.75 ft./sec.

TABLE 6-c. Results Of Longitudinal Velocity And Turbulence Characteristics Along The Flume At 0.125 Inches Above The Floor For A Smooth Artificial Ripple Bed Obtained From The V-Probe Measurements

Distance downstream the screen inches	Temperature °F	Voltage E_1 Volts	Voltage E_2 Volts	Sloping manometer reading "Δh" mms.	Velocity ft./sec. obtained from E_1	Velocity ft./sec. obtained from E_2	Velocity Ft./sec. "Pitot-tube"	Average Velocity U ft./sec.	$\overline{e_s \cdot e_d} \times 10^2 (\text{Volts})^2$	$\sqrt{\overline{e_s^2}}$ Volts	$\sqrt{\overline{e_d^2}}$ Volts	"S_1" Volts/ft./sec.	"S_2" Volts/ft./sec.	$\frac{U}{\bar{U}}$	$\frac{u'}{\bar{U}} \times 10^2$	$\frac{v'}{\bar{U}} \times 10^2$	$-\frac{\overline{uv}}{\bar{U}^2} \times 10^4$
11.0	76	7.15	8.33	23.5	.62	.66	.61	.63	1.23	.322	.227	2.86	2.34	0.84	8.45	6.08	18.74
13.5	76	7.17	8.33	25.0	.63	.66	.63	.64	0.96	.295	.185	2.78	2.28	0.85	7.95	5.12	15.34
18.5	77	7.30	8.45	26.0	.66	.68	.64	.66	0.87	.285	.165	2.70	2.20	0.88	7.93	4.75	15.02
23.5	77	7.32	8.47	27.0	.67	.69	.65	.67	0.84	.270	.175	2.64	2.16	0.89	7.68	5.11	14.83
28.5	78	7.44	8.53	28.0	.74	.72	.67	.71	0.93	.265	.170	2.44	2.00	0.95	8.16	5.37	17.67
36.0	79	7.40	8.55	27.0	.69	.70	.65	.68	0.90	.28	.185	2.58	2.12	0.91	8.13	5.49	16.50
43.0	80	7.40	8.55	26.0	.66	.68	.64	.66	0.86	.275	.180	2.70	2.20	0.88	7.67	5.15	14.90

D = depth of flow = 5.00 inches

$\bar{U}$ = mean flow velocity = 0.75 ft./sec.

TABLE 6-d. Results Of Longitudinal Velocity And Turbulence Characteristics Along The Flume At 0.125 Inches Above The Floor For A Sand-Roughened Artificial Ripple Bed Obtained From The V-Probe Measurements

Distance downstream the screen inches	Temperature °F	Voltage E_1 Volts	Voltage E_2 Volts	Sloping manometer reading "Δh" mms.	Velocity ft./sec. obtained from E_1	Velocity ft./sec. obtained from E_2	Velocity Ft./sec. "Pitot-tube"	Average Velocity U ft./sec.	$\overline{e_s \cdot e_d} \times 10^2 (\text{Volts})^2$	$\sqrt{\overline{e_s^2}}$ Volts	$\sqrt{\overline{e_d^2}}$ Volts	"S_1" Volts/ft./sec.	"S_2" Volts/ft./sec.	$\frac{U}{\bar{U}}$	$\frac{u'}{\bar{U}} \times 10^2$	$\frac{v'}{\bar{U}} \times 10^2$	$-\frac{\overline{uv}}{\bar{U}^2} \times 10^4$
11.0	72	6.93	8.00	21.0	.59	.60	.58	.59	1.59	.38	.255	3.16	2.58	0.78	9.04	6.20	20.50
13.5	73	7.03	8.11	23.0	.61	.62	.60	.61	1.20	.32	.205	2.97	2.43	0.81	8.09	5.32	16.52
18.5	74	7.17	8.25	24.0	.65	.65	.62	.64	1.00	.305	.185	2.78	2.28	0.85	8.21	5.13	16.05
23.5	75	7.17	8.32	27.5	.65	.67	.66	.66	1.00	.30	.185	2.71	2.22	0.87	8.31	5.27	16.75
28.5	75	7.20	8.35	28.0	.66	.68	.67	.67	1.14	.32	.19	2.64	2.16	0.89	9.09	5.57	19.96
36.0	76	7.25	8.37	29.0	.66	.67	.68	.67	1.10	.31	.195	2.66	2.18	0.89	8.73	5.64	18.90
43.0	77	7.15	8.35	26.0	.60	.65	.64	.63	0.95	.30	.19	2.86	2.34	0.84	7.87	5.11	14.90

D = depth of flow = 5.00 inches

$\bar{U}$ = mean flow velocity = 0.75 ft./sec.

TABLE 6-e. Results Of Longitudinal Velocity And Turbulence Characteristics Along The Flume At 0.125 Inches Above The Floor For A Cast Of A Natural Ripple Bed Obtained From The V-Probe Measurements

Distance downstream the screen inches	Temperature °F	Voltage E_1 Volts	Voltage E_2 Volts	Sloping manometer reading "Δh" mms.	Velocity ft./sec. obtained from E_1	Velocity ft./sec. obtained from E_2	Velocity Ft./sec. "Pitot-tube"	Average Velocity U ft./sec.	$\overline{e_s \cdot e_d} \times 10^2 (\text{Volts})^2$	$\sqrt{\overline{e_s^2}}$ Volts	$\sqrt{\overline{e_d^2}}$ Volts	"S_1" Volts/ft./sec.	"S_2" Volts/ft./sec.	$\frac{U}{\bar{U}}$	$\frac{u'}{\bar{U}} \times 10^2$	$\frac{v'}{\bar{U}} \times 10^2$	$-\frac{\overline{uv}}{\bar{U}^2} \times 10^4$
12.0	74	7.00	8.10	20.5	.57	.60	.57	.58	2.35	.46	.32	3.19	2.61	0.7[illegible]	10.83	7.68	29.72
16.0	75	7.05	8.20	23.0	.60	.63	.60	.61	2.05	.42	.29	2.97	2.43	0.81	10.63	7.48	29.08
22.0	75	7.12	8.25	26.0	.63	.65	.64	.64	1.86	.395	.26	2.83	2.31	0.85	10.49	7.08	28.44
33.0	76	7.08	8.33	23.5	.59	.66	.61	.62	1.65	.38	.255	2.91	2.38	0.83	9.81	6.72	24.41
37.5	77	7.15	8.30	23.0	.60	.63	.60	.61	1.5	.36	.245	3.00	2.46	0.81	9.00	6.25	20.62
43.0	77	7.13	8.20	21.0	.59	.60	.58	.59	1.35	.335	.22	3.16	2.58	0.78	7.97	5.36	16.44

D = depth of flow = 5.00 inches

$\bar{U}$ = mean flow velocity = 0.75 ft./sec.

TABLE 6-f. Results Of Longitudinal Velocity And Turbulence Characteristics Along The Flume at 2.5 Inches Above The Floor For A Smooth Flat Bed Obtained From The V-Probe Measurements

Distance downstream the screen inches	Temperature °F	Voltage E_1 Volts	Voltage E_2 Volts	Sloping manometer reading "Δh" mms.	Velocity ft./sec. obtained from E_1	Velocity ft./sec. obtained from E_2	Velocity Ft./sec. "Pitot-tube"	Average Velocity U ft./sec.	$\overline{e_s \cdot e_d} \times 10^2 (\text{Volts})^2$	$\sqrt{\overline{e_s^2}}$ Volts	$\sqrt{\overline{e_d^2}}$ Volts	"S_1" Volts/ft./sec.	"S_2" Volts/ft./sec.	$\frac{U}{\bar{U}}$	$\frac{u'}{\bar{U}} \times 10^2$	$\frac{v'}{\bar{U}} \times 10^2$	$-\frac{\overline{uv}}{\bar{U}^2} \times 10^4$
11.0	73	7.33	8.50	35.5	.76	.77	.75	.76	1.50	.35	.31	2.24	1.83	1.01	11.77	10.48	40.71
13.5	74	7.44	8.61	38.5	.79	.80	.78	.79	1.10	.32	.285	2.09	1.71	1.05	11.51	10.31	37.03
18.5	75	7.55	8.67	41.5	.85	.83	.81	.83	0.65	.24	.195	1.97	1.61	1.11	9.16	7.52	22.92
23.5	76	7.56	8.74	42.5	.83	.84	.82	.83	0.48	.21	.16	1.98	1.62	1.10	7.96	6.15	16.53
28.5	76	7.56	8.68	42.5	.83	.81	.82	.82	0.35	.19	.145	2.00	1.64	1.09	7.12	5.49	12.57
36.0	77	7.50	8.75	41.5	.77	.82	.81	.80	0.28	.17	.12	2.06	1.69	1.07	6.17	4.43	9.16
43.0	78	7.57	8.71	39.5	.81	.80	.79	.80	0.21	.155	.105	2.07	1.70	1.06	5.60	3.85	7.09

D = depth of flow = 5.00 inches

$\bar{U}$ = mean flow velocity = 0.75 ft./sec.

TABLE 6-8. Results of Longitudinal Velocity And Turbulence Characteristics Along The Flume At 2.5 Inches Above The Floor For A Sand-Roughened Flat Bed Obtained From The V-Probe Measurements

Distance downstream the screen inches	Temperature °F	Voltage E_1 Volts	Voltage E_2 Volts	Sloping manometer reading "Δh" mms.	Velocity ft./sec. obtained from E_1	Velocity ft./sec. obtained from E_2	Velocity Ft./sec. "Pitot-tube"	Average Velocity U ft./sec.	$\overline{e_s \cdot e_d} \times 10^2$ (Volts)^2	$\sqrt{\overline{e_s^2}}$ Volts	$\sqrt{\overline{e_d^2}}$ Volts	"S_1" Volts/ft./sec.	"S_2" Volts/ft./sec.	$\frac{U}{\bar{U}}$	$\frac{u'}{\bar{U}} \times 10^2$	$\frac{v'}{\bar{U}} \times 10^2$	$-\frac{\overline{uv}}{\bar{U}^2} \times 10^4$
11.0	74	7.36	8.52	34.5	.75	.76	.74	.75	1.41	.32	.31	2.27	1.86	1.0	10.63	10.31	36.09
13.5	75	7.36	8.59	37.5	.75	.79	.77	.77	1.23	.31	.287	2.18	1.78	1.03	10.73	9.97	35.24
18.5	76	7.47	8.64	40.5	.78	.79	.80	.79	0.70	.235	.210	2.09	1.71	1.05	8.47	7.60	21.35
23.5	77	7.54	8.73	40.5	.79	.81	.80	.80	0.50	.19	.185	2.06	1.69	1.07	6.95	6.77	15.45
28.5	77	7.55	8.75	41.5	.80	.82	.81	.81	0.38	.17	.165	2.04	1.68	1.08	6.25	6.08	12.12
36.0	78	7.57	8.71	39.5	.81	.80	.79	.80	0.30	.152	.137	2.06	1.69	1.07	5.55	5.03	9.23
43.0	79	7.64	8.82	38.5	.82	.83	.78	.81	0.24	.132	.120	2.03	1.67	1.08	4.88	4.47	7.31

D = depth of flow = 5.00 inches

$\bar{U}$ = mean flow velocity = 0.75 ft./sec.

TABLE 6-h. Results Of Longitudinal Velocity And Turbulence Characteristics Along The Flume At 2.5 Inches Above The Floor For A Smooth Artificial Ripple Bed Obtained From The V-Probe Measurements

Distance downstream the screen inches	Temperature °F	Voltage E_1 Volts	Voltage E_2 Volts	Sloping manometer reading "Δh" mms.	Velocity ft./sec. obtained from E_1	Velocity ft./sec. obtained from E_2	Velocity Ft./sec. "Pitot-tube"	Average Velocity U ft./sec.	$\overline{e_s \cdot e_d} \times 10^2 (Volts)^2$	$\sqrt{\overline{e_s^2}}$ Volts	$\sqrt{\overline{e_d^2}}$ Volts	"S_1" Volts/ft./sec.	"S_2" Volts/ft./sec.	$\frac{U}{\bar{U}}$	$\frac{u'}{\bar{U}} \times 10^2$	$\frac{v'}{\bar{U}} \times 10^2$	$-\frac{\overline{uv}}{\bar{U}^2} \times 10^4$
11.0	74	7.29	8.43	31.0	.71	.72	.70	.71	1.65	.37	.33	2.46	2.02	0.94	11.29	10.12	36.85
13.5	74	7.34	8.48	32.0	.74	.74	.71	.73	1.25	.34	.295	2.33	1.91	0.97	10.95	9.56	32.98
18.5	75	7.44	8.55	35.5	.79	.77	.75	.77	0.72	.26	.23	2.18	1.78	1.03	8.97	7.99	22.51
23.5	76	7.50	8.63	39.5	.80	.81	.79	.80	0.49	.23	.18	2.06	1.69	1.07	8.36	6.61	17.23
28.5	77	7.59	8.71	41.5	.82	.80	.81	.81	0.37	.205	.15	2.03	1.67	1.08	7.55	5.59	13.26
36.0	77	7.57	8.75	40.5	.81	.82	.80	.81	0.29	.19	.14	2.03	1.67	1.08	6.99	5.21	11.04
43.0	78	7.63	8.79	40.5	.84	.82	.80	.82	0.22	.17	.12	2.00	1.64	1.09	6.35	4.55	8.91

D = depth of flow = 5.00 inches

$\bar{U}$ = mean flow velocity = 0.75 ft./sec.

TABLE 6-1. Results Of Longitudinal Velocity And Turbulence Characteristics Along The Flume At 2.5 Inches Above The Floor For A Sand-Roughened Artificial Ripple Bed Obtained From The V-Probe Measurements

Distance downstream the screen inches	Temperature °F	Voltage E_1 Volts	Voltage E_2 Volts	Sloping manometer reading "Δh" mms.	Velocity ft./sec. obtained from E_1	Velocity ft./sec. obtained from E_2	Velocity Ft./sec. "Pitot-tube"	Average Velocity U ft./sec.	$\overline{e_s \cdot e_d} \times 10^2$ (Volts)^2	$\sqrt{\overline{e_s^2}}$ Volts	$\sqrt{\overline{e_d^2}}$ Volts	"S_1" Volts/ft./sec.	"S_2" Volts/ft./sec.	$\frac{U}{\bar{U}}$	$\frac{u'}{\bar{U}} \times 10^2$	$\frac{v'}{\bar{U}} \times 10^2$	$-\frac{\overline{uv}}{\bar{U}^2} \times 10^4$
11.0	75	7.25	8.40	29.0	.69	.70	.68	.69	1.95	.40	.285	2.55	2.09	0.91	11.77	8.55	36.73
13.5	76	7.34	8.48	31.0	.71	.72	.70	.71	1.41	.34	.27	2.44	2.00	0.95	10.47	8.41	30.28
18.5	77	7.43	8.65	35.5	.73	.77	.75	.75	0.82	.26	.21	2.27	1.86	0.99	8.60	7.03	20.59
23.5	78	7.50	8.67	36.5	.77	.78	.76	.77	0.50	.205	.19	2.18	1.78	1.03	7.09	6.59	14.97
28.5	78	7.50	8.71	37.5	.77	.80	.77	.78	0.40	.18	.17	2.14	1.76	1.04	6.32	5.97	11.93
36.0	79	7.51	8.80	40.5	.75	.82	.80	.79	0.32	.145	.135	2.09	1.71	1.05	5.24	4.89	9.00
43.0	80	7.56	8.81	39.5	.75	.80	.79	.78	0.24	.13	.125	2.14	1.76	1.04	4.57	4.40	6.67

D = depth of flow = 5.00 inches

$\bar{U}$ = mean flow velocity = 0.75 ft./sec.

TABLE 6-j. Results Of Longitudinal Velocity And Turbulence Characteristics Along The Flume At 2.5 Inches Above The Floor For A Cast Of A Natural Ripple Bed Obtained From The V-Probe Measurements

Distance downstream the screen inches	Temperature °F	Voltage E_1 Volts	Voltage E_2 Volts	Sloping manometer reading "Δh" mms.	Velocity ft./sec. obtained from E_1	Velocity ft./sec. obtained from E_2	Velocity Ft./sec. "Pitot-tube"	Average Velocity U ft./sec.	$\overline{e_s \cdot e_d} \times 10^2 (\text{Volts})^2$	$\sqrt{\overline{e_s^2}}$ Volts	$\sqrt{\overline{e_d^2}}$ Volts	"S_1" Volts/ft./sec.	"S_2" Volts/ft./sec.	$\frac{U}{\bar{U}}$	$\frac{u'}{\bar{U}} \times 10^2$	$\frac{v'}{\bar{U}} \times 10^2$	$-\frac{\overline{uv}}{\bar{U}^2} \times 10^4$
12.0	73	7.44	8.62	41.5	.82	.83	.81	.82	1.8	.38	.25	2.01	1.65	1.09	14.17	9.56	52.12
16.0	74	7.47	8.67	42.5	.81	.83	.82	.82	1.4	.35	.22	2.00	1.64	1.09	13.12	8.47	42.47
22.0	75	7.51	8.69	42.5	.83	.84	.82	.83	1.05	.24	.16	1.97	1.61	1.11	9.21	6.33	26.86
33.0	75	7.54	8.67	41.5	.82	.83	.81	.82	0.62	.21	.14	2.00	1.64	1.09	7.89	5.40	17.19
37.5	76	7.50	8.68	39.5	.80	.81	.79	.80	0.50	.19	.13	2.06	1.69	1.07	6.93	4.85	13.24
43.0	77	7.50	8.71	37.5	.77	.80	.77	.78	0.40	.16	.125	2.17	1.77	1.03	5.57	4.41	9.62

D = depth of flow = 5.00 inches

$\bar{U}$ = mean flow velocity = 0.75 ft./sec.

TABLE 7-a. Results Of Velocity And Turbulence Characteristics Along A Ripple 44 Inches Downstream From The Screen At .125 Inches Normal To The Floor For A Sand-Roughened Artificial Ripple Bed Obtained From The V-Probe Measurements

Relative length 1/L	Temperature °F	Voltage E_1 Volts	Voltage E_2 Volts	Sloping manometer reading "Δh", mms.	Velocity ft./sec. obtained from E_1	Velocity ft./sec. obtained from E_2	Velocity Ft./sec. "Pitot-tube"	Average Velocity U ft./sec.	$\overline{e_s \cdot c_d} \times 10^2$ (Volts)^2	$\sqrt{\overline{e_s^2}}$ Volts	$\sqrt{\overline{c_d^2}}$ Volts	"S_1" Volts/ft./sec.	"S_2" Volts/ft./sec.	$\frac{U}{\bar{U}}$	$\frac{u'}{\bar{U}} \times 10^2$	$\frac{v'}{\bar{U}} \times 10^2$	$-\frac{\overline{uv}}{\bar{U}^2} \times 10^4$	$\frac{\tau}{\rho \bar{U}^2} \times 10^4$ "Pitot-tube"
1.0	73	7.22	8.32	18.0	.70	.69	.53	.64	0.90	.28	.19	2.83	2.31	.85	7.4	5.2	14.2	21.5
0.8	74	7.03	8.23	18.5	.59	.64	.54	.59	1.20	.34	.215	3.12	2.55	.79	8.2	5.3	16.0	22.0
0.6	75	7.00	8.05	20.0	.57	.58	.56	.57	1.40	.37	.245	3.25	2.66	.76	8.5	5.8	17.6	23.8
0.4	75	7.00	8.10	20.5	.57	.60	.57	.58	1.50	.385	.250	3.19	2.61	.77	9.1	6.0	19.5	24.4
0.2	76	7.20	8.21	18.5	.64	.62	.54	.60	0.95	.285	.200	3.04	2.48	.80	7.1	5.1	13.0	22.0

D = depth of flow = 5.00 inches

L = ripple length = 2.50 inches

$\bar{U}$ = mean flow velocity = 0.75 ft./sec.

TABLE 7-b. Results Of Velocity And Turbulence Characteristics Along A Ripple 44 Inches Downstream From The Screen At 0.125 Inches Normal To The Floor For A Cast Of A Natural Ripple Bed Obtained From The V-Probe Measurements

Relative lenght 1/L	Temperature °F	Voltage E_1 Volts	Voltage E_2 Volts	Sloping manometer reading "Δh" mms.	Velocity ft./sec. obtained from E_1	Velocity ft./sec. obtained from E_2	Velocity ft./sec. "Pitot-tube"	Average Velocity U ft./sec.	$\overline{e_s \cdot e_d} \times 10^2$ (Volts)^2	$\sqrt{\overline{e_s^2}}$ Volts	$\sqrt{\overline{e_d^2}}$ Volts	"S_1" Volts/ft./sec.	"S_2" Volts/ft./sec.	$\frac{U}{\bar{U}}$	$\frac{u'}{\bar{U}} \times 10^2$	$\frac{v'}{\bar{U}} \times 10^2$	$-\frac{\overline{uv}}{\bar{U}^2} \times 10^4$	$\frac{\tau}{\rho \bar{U}^2} \times 10^4$ "Pitot-tube"
1.0	75	7.10	8.23	16.0	.62	.64	.51	.59	1.35	.32	.215	3.16	2.58	.78	7.6	5.3	15.8	19.1
0.78	76	7.00	8.05	18.0	.55	.57	.53	.55	1.45	.365	.24	3.44	2.81	.73	8.0	5.4	15.7	21.5
0.56	76	6.97	8.10	20.0	.54	.58	.56	.56	1.60	.38	.255	3.38	2.76	.74	8.5	5.8	18.0	23.8
0.39	77	7.00	8.10	21.0	.53	.57	.58	.56	1.80	.395	.265	3.32	2.72	.75	8.9	6.1	20.2	25.0
0.22	78	7.12	8.23	17.0	.58	.61	.52	.57	1.30	.305	.195	3.25	2.66	.76	7.1	4.6	13.6	20.3

D = depth of flow = 5.00 inches

L = ripple length = 2.25 inches

$\bar{U}$ = mean flow velocity = 0.75 ft./sec.

TABLE 8-a. Results Of Velocity And Turbulence Characteristics Along A Ripple 44 Inches Downstream From The Screen At 2.5 Inches Above The Floor For A Sand-Roughened Artificial Ripple Bed Obtained From The V-Prove Measurements

Relative length 1/L	Temperature °F	Voltage E_1 Volts	Voltage E_2 Volts	Sloping manometer reading "Δh" mms.	Velocity ft./sec. obtained from E_1	Velocity ft./sec. obtained from E_2	Velocity Ft./sec. "Pitot-tube"	Average Velocity U ft./sec.	$\overline{e_s \cdot e_d} \times 10^2$ (Volts)^2	$\sqrt{\overline{e_s^2}}$ Volts	$\sqrt{\overline{e_d^2}}$ Volts	"S_1" Volts/ft./sec.	"S_2" Volts/ft./sec.	$\frac{U}{\bar{U}}$	$\frac{u'}{\bar{U}} \times 10^2$	$\frac{v'}{\bar{U}} \times 10^2$	$-\frac{\overline{uv}}{\bar{U}^2} \times 10^4$
1.0	76	7.41	8.62	35.5	.75	.78	.75	.76	.25	.14	.115	2.22	1.82	1.01	4.75	3.93	6.42
0.6	77	7.48	8.65	38.5	.76	.77	.78	.77	.28	.145	.12	2.18	1.78	1.03	5.01	4.19	7.41
0.2	77	7.52	8.65	39.5	.78	.77	.79	.78	.30	.15	.125	2.14	1.76	1.04	5.27	4.43	8.04

D = depth of flow = 5.00 inches

L = ripple length = 2.50 inches

$\bar{U}$ = mean flow velocity = 0.75 ft./sec.

TABLE 8-b. Results Of Velocity And Turbulence Characteristics Along A Ripple 44 Inches Downstream From The Screen At 2.5 Inches Above The Floor For A Cast Of A Natural Ripple Bed Obtained From The V-Probe Measurements

Relative length l/L	Temperature °F	Voltage E_1 Volts	Voltage E_2 Volts	Sloping manometer reading "Δh" mms.	Velocity ft./sec. obtained from E_1	Velocity ft./sec. obtained from E_2	Velocity Ft./sec. "Pitot-tube"	Average Velocity U ft./sec.	$\overline{e_s \cdot e_d} \times 10^2 (\text{Volts})^2$	$\sqrt{\overline{e_s^2}}$ Volts	$\sqrt{\overline{e_d^2}}$ Volts	"S_1" Volts/ft./sec.	"S_2" Volts/ft./sec.	$\frac{U}{\bar{U}}$	$\frac{u'}{\bar{U}} \times 10^2$	$\frac{v'}{\bar{U}} \times 10^2$	$-\frac{\overline{uv}}{\bar{U}^2} \times 10^4$
1.0	74	7.45	8.57	36.5	.80	.78	.76	.78	.40	.16	.125	2.17	1.77	1.03	5.57	4.41	9.62
0.56	75	7.38	8.61	38.5	.76	.80	.78	.78	.45	.165	.13	2.14	1.76	1.04	5.8	4.64	10.54
0.22	76	7.45	8.57	38.5	.77	.76	.78	.77	.49	.175	.135	2.18	1.78	1.03	5.07	4.76	11.43

D = depth of flow = 5.00 inches

L = ripple length = 2.25 inches

$\bar{U}$ = mean flow velocity = 0.75 ft./sec.

Table 9-a. Results Of Vertical Velocity And Turbulence Characteristics At 44 Inches Downstream From The Screen For A Smooth Flat Bed Obtained From The Wedge Probe Measurements

Relative depth d/D	Temperature ^oF	Voltage E Volts	Sloping manometer reading "Δh" mms	Velocity ft./sec. obtained from E	Velocity ft./sec. "Pitot-tube"	Average Velocity U ft./sec.	$\sqrt{\overline{e_s^2}}$ Volts	Sensitivity "S" Volts/ft./sec.	$\frac{u'}{\bar{U}} \times 10^2$	Macro Scale Λ millsec.	Micro Scale λ millsec.	$\frac{\Lambda.\bar{U}}{D} \times 10^2$	$\frac{\lambda.\bar{U}}{D} \times 10^3$
0.025	72	7.15	27.5	.70	.66	.68	.14	2.775	6.73	22.9	2.36	4.12	4.25
0.175	73	7.31	33.0	.74	.72	.73	.15	2.788	7.17	25.5	3.02	4.59	5.44
0.3	74	7.56	37.5	.81	.77	.79	.12	2.800	5.71	31.0	3.54	5.58	6.37
0.5	75	7.55	40.5	.80	.80	.80	.11	2.813	5.21	35.0	3.78	6.30	6.84
0.7	75	7.52	43.5	.79	.83	.81	.10	2.813	4.74	30.8	3.33	5.54	5.99
0.9	76	7.43	36.5	.74	.76	.75	.085	2.825	4.01	27.3	2.77	4.91	4.99

D = depth of flow = 5.00 inches

$\bar{U}$ = mean flow velocity = 0.75 ft./sec.

Table 9-b. Results Of Vertical Velocity And Turbulence Characteristics At 44 Inches Downstream From The Screen For A Sand-Roughened Flat Bed Obtained From The Wedge Probe measurements

Relative depth d/D	Temperature ^{o}F	Voltage E Volts	Sloping manometer reading "Δh" mms	Velocity ft./sec. obtained from E	Velocity ft./sec. "Pitot-tube"	Average Velocity U ft./sec.	$\sqrt{\overline{e_s^2}}$ Volts	Sensitivity "S" Volts/ft./sec.	$\frac{u'}{\bar{U}} \times 10^2$	Macro Scale Λ millsec.	Micro Scale λ millsec.	$\frac{\Lambda.\bar{U}}{D} \times 10^2$	$\frac{\lambda.\bar{U}}{D} \times 10^3$
0.025	75	7.13	24.0	.66	.62	.64	.14	2.813	6.64	26.2	3.54	4.72	6.37
0.175	75	7.33	31.0	.72	.70	.71	.11	2.813	5.21	29.3	4.08	5.27	7.34
0.3	76	7.53	33.5	.77	.73	.75	.10	2.825	4.72	36.4	5.00	6.55	9.00
0.5	77	7.63	38.5	.80	.78	.79	.09	2.838	4.23	38.8	3.54	6.98	6.37
0.7	78	7.75	42.5	.82	.82	.82	.09	2.850	4.21	34.8	3.16	6.26	5.69
0.9	79	7.60	38.5	.76	.78	.77	.085	2.863	3.96	32.9	2.89	5.92	5.20

D = depth of flow = 5.00 inches

$\bar{U}$ = mean flow velocity = 0.75 ft./sec.

Table 9-c. Results Of Vertical Velocity And Turbulence Characteristics At 44 Inches Downstream From The Screen For A Smooth Artificial Ripple Bed Obtained From The Wedge Probe measurements

Relative depth d/D	Temperature ^oF	Voltage E Volts	Sloping manometer reading "Δh" mms	Velocity ft./sec. obtained from E	Velocity ft./sec. "Pitot-tube"	Average Velocity U ft./sec.	$\sqrt{\overline{e_s^2}}$ Volts	Sensitivity "S" Volts/ft./sec.	$\frac{u'}{\bar{U}} \times 10^2$	Macro Scale Λ millsec.	Micro Scale λ millsec.	$\frac{\Lambda.\bar{U}}{D} \times 10^2$	$\frac{\lambda.\bar{U}}{D} \times 10^3$
0.025	73	7.16	27.0	.69	.65	.67	.155	2.788	7.41	24.3	2.58	4.37	4.64
0.175	74	7.35	29.0	.74	.68	.71	.15	2.800	7.14	27.2	3.54	4.90	6.37
0.3	75	7.49	34.5	.78	.74	.76	.125	2.813	5.93	32.8	4.47	5.90	8.05
0.5	76	7.59	38.5	.80	.78	.79	.10	2.825	4.72	36.4	5.00	6.55	9.00
0.7	76	7.45	37.5	.75	.77	.76	.09	2.825	4.25	31.5	4.08	5:67	7.34
0.9	77	7.40	33.0	.72	.72	.72	.08	2.838	3.76	27.9	3.33	5.02	5.99

D = depth of flow = 5.00 inches

$\bar{U}$ = mean flow velocity = 0.75 ft./sec.

Table 9-d. Results Of Vertical Velocity And Turbulence Characteristics At 44 Inches Downstream From The Screen For A Sand-Roughened Artificial Ripple Bed Obtained From The Wedge Probe Measurements

Relative depth d/D	Temperature ^{o}F	Voltage E Volts	Sloping manometer reading "Δh" mms	Velocity ft./sec. obtained from E	Velocity ft./sec. "Pitot-tube"	Average Velocity U ft./sec.	$\sqrt{\overline{e_s^2}}$ Volts	Sensitivity "S" Volts/ft./sec.	$\frac{u'}{\bar{U}} \times 10^2$	Macro Scale Λ millsec.	Micro Scale λ millsec.	$\frac{\Lambda.\bar{U}}{D} \times 10^2$	$\frac{\lambda.\bar{U}}{D} \times 10^3$
0.025	75	7.13	23.0	.66	.60	.63	.195	2.813	9.24	28.6	4.08	5.15	7.34
0.175	76	7.27	27.0	.69	.65	.67	.18	2.825	8.5	32.3	4.47	5.81	8.05
0.3	77	7.63	38.5	.80	.78	.79	.17	2.838	7.99	39.3	5.00	7.07	9.00
0.5	78	7.67	42.5	.80	.82	.81	.13	2.850	6.08	39.9	4.08	7.18	7.34
0.7	79	7.79	40.5	.82	.80	.81	.115	2.863	5.36	36.8	3.78	6.62	6.80
0.9	80	7.75	34.5	.80	.74	.77	.10	2.875	4.64	35.5	3.54	6.39	6.37

D = depth of flow = 5.00 inches

$\bar{U}$ = mean flow velocity = 0.75 ft./sec.

Table 9-e. Results Of Vertical Velocity And Turbulence Characteristics At 44 Inches Downstream From The Screen For A Cast Of A Natural Ripple Bed Obtained From The Wedge Probe Measurements

Relative depth d/D	Temperature ^oF	Voltage E Volts	Sloping manometer reading "Δh" mms	Velocity ft./sec. obtained from E	Velocity ft./sec. "Pitot-tube"	Average Velocity U ft./sec.	$\sqrt{\overline{e_s^2}}$ Volts	Sensitivity "S" Volts/ft./sec.	$\frac{u}{\bar{U}} \times 10^2$	Macro Scale Λ millsec.	Micro Scale λ millsec.	$\frac{\Lambda.\bar{U}}{D} \times 10^2$	$\frac{\lambda.\bar{U}}{D} \times 10^3$
0.025	74	6.98	23.0	.62	.60	.61	.17	2.800	8.10	33.2	4.47	5.98	8.05
0.175	75	7.20	31.0	.68	.70	.69	.145	2.813	6.87	35.2	5.00	6.34	9.00
0.3	76	7.40	32.0	.73	.71	.72	.13	2.825	6.14	42.1	5.77	7.58	10.39
0.5	76	7.64	37.5	.81	.77	.79	.12	2.825	5.66	42.8	7.07	7.70	12.73
0.7	77	7.71	40.5	.82	.80	.81	.115	2.838	5.40	38.3	5.00	6.89	9.00
0.9	78	7.71	41.5	.81	.81	.81	.10	2.850	4.68	37.6	4.08	6.77	7.34

D = depth of flow = 5.00 inches

$\bar{U}$ = mean flow velocity = 0.75 ft./sec.

Table 9-f. Results Of Vertical Velocity And Turbulence Characteristics At 14 Inches Downstream From The Screen For A Smooth Flat Bed Obtained From The Wedge Probe Measurements

Relative depth d/D	Temperature ^oF	Voltage E Volts	Sloping manometer reading "Δh" mms	Velocity ft./sec. obtained from E	Velocity ft./sec. "Pitot-tube"	Average Velocity U ft./sec.	$\sqrt{\overline{e_s^2}}$ Volts	Sensitivity "S" Volts/ft./sec.	$\frac{u'}{\bar{U}} \times 10^2$	Macro Scale Λ millsec.	Micro Scale λ millsec.	$\frac{\Lambda.\bar{U}}{D} \times 10^2$	$\frac{\lambda.\bar{U}}{D} \times 10^3$
0.025	76	7.33	27.0	.71	.65	.68	.16	2.825	7.55	47.6	5.00	8.57	9.00
0.175	77	7.57	36.5	.78	.76	.77	.195	2.838	9.16	49.5	5.77	8.91	10.39
0.3	77	7.60	41.5	.79	.81	.80	.25	2.838	11.75	46.6	5.77	8.38	10.39
0.5	78	7.75	40.5	.82	.80	.81	.22	2.850	10.29	38.7	5.77	6.97	10.39
0.7	79	7.63	39.5	.77	.79	.78	.20	2.863	9.31	40.6	4.47	7.31	8.05
0.9	80	7.72	41.5	.79	.81	.80	.24	2.875	11.13	42.2	4.47	7.60	8.05

D = depth of flow = 5.00 inches

$\bar{U}$ = mean flow velocity = 0.75 ft./sec.

Table 9-g. Results Of Vertical Velocity And Turbulence Characteristics At 14 Inches Downstream From The Screen For A Sand-Roughened Flat Bed Obtained From The Wedge Probe Measurements

Relative depth d/D	Temperature °F	Voltage E Volts	Sloping manometer reading "Δh" mms	Velocity ft./sec. obtained from E	Velocity ft./sec. "Pitot-tube"	Average Velocity U ft./sec.	$\sqrt{\overline{e_s^2}}$ Volts	Sensitivity "S" Volts/ft./sec.	$\frac{u'}{\bar{U}} \times 10^2$	Macro Scale Λ millsec.	Micro Scale λ millsec.	$\frac{\Lambda . \bar{U}}{D} \times 10^2$	$\frac{\lambda . \bar{U}}{D} \times 10^3$
0.025	72	7.02	26.0	.66	.64	.65	.16	2.775	7.69	47.6	4.47	8.57	8.05
0.175	73	7.22	28.0	.71	.67	.69	.185	2.788	8.85	51.4	3.54	9.25	6.37
0.3	74	7.38	32.0	.75	.71	.73	.21	2.800	10.00	45.7	4.08	8.23	7.34
0.5	74	7.51	38.5	.80	.78	.79	.25	2.800	11.91	37.7	4.08	6.79	7.34
0.7	75	7.45	38.5	.76	.78	.77	.24	2.813	11.38	38.4	5.00	6.91	9.00
0.9	76	7.53	38.5	.78	.78	.78	.25	2.825	11.80	48.2	4.47	8.68	8.05

D = depth of flow

$\bar{U}$ = mean flow velocity = 0.75 ft./sec.

Table 9-h. Results Of Vertical Velocity And Turbulence Characteristics At 14 Inches Downstream From The Screen For A Smooth Artificial Ripple Bed Obtained From The Wedge Probe Measurements

Relative depth d/D	Temperature ^{o}F	Voltage E Volts	Sloping manometer reading "Δh" mms	Velocity ft./sec. obtained from E	Velocity ft./sec. "Pitot-tube"	Average Velocity U ft./sec.	$\sqrt{\overline{e_s^2}}$ Volts	Sensitivity "S" Volts/ft./sec.	$\frac{u'}{\bar{U}} \times 10^2$	Macro Scale Λ millsec.	Micro Scale λ millsec.	$\frac{\Lambda.\bar{U}}{D} \times 10^2$	$\frac{\lambda.\bar{U}}{D} \times 10^3$
0.025	74	7.09	26.0	.66	.64	.65	.17	2.800	8.10	37.8	7.07	6.80	12.73
0.175	75	7.30	33.5	.71	.73	.72	.18	2.813	8.53	45.4	7.07	8.17	12.73
0.3	76	7.45	35.5	.75	.75	.75	.145	2.825	6.84	44.7	5.77	8.05	10.39
0.5	77	7.46	33.0	.74	.72	.73	.23	2.838	10.81	35.5	5.77	6.39	10.39
0.7	77	7.46	31.0	.74	.70	.72	.195	2.838	9.16	42.0	5.77	7.56	10.39
0.9	78	7.61	33.0	.78	.72	.75	.20	2.850	9.36	40.9	5.77	7.36	10.39

D = depth of flow = 5.00 inches

$\bar{U}$ = mean flow velocity = 0.75 ft./sec.

Table 9-1. Results Of Vertical Velocity And Turbulence Characteristics At 14 Inches Downstream From The Screen For A Sand-Roughened Artificial Ripple Bed Obtained From The Wedge Probe Measurements

Relative depth d/D	Temperature ^oF	Voltage E Volts	Sloping manometer reading "Δh" mms	Velocity ft./sec. obtained from E	Velocity ft./sec. "Pitot-tube"	Average Velocity U ft./sec.	$\sqrt{\overline{e_s^2}}$ Volts	Sensitivity "S" Volts/ft./sec.	$\frac{u'}{\bar{U}} \times 10^2$	Macro Scale Λ millsec.	Micro Scale λ millsec.	$\frac{\Lambda.\bar{U}}{D} \times 10^2$	$\frac{\lambda.\bar{U}}{D} \times 10^3$
0.025	75	7.11	23.5	.65	.61	.63	.17	2.813	8.06	38.4	7.07	6.91	12.73
0.175	76	7.40	28.0	.73	.67	.70	.18	2.825	8.50	44.8	7.07	8.06	12.73
0.3	76	7.56	32.0	.79	.71	.75	.175	2.825	8.26	34.6	5.77	6.23	10.39
0.5	77	7.53	33.0	.76	.72	.74	.22	2.838	10.34	36.7	7.07	6.61	12.73
0.7	78	7.46	28.0	.73	.67	.70	.20	2.850	9.36	39.9	5.77	7.18	10.39
0.9	79	7.68	37.5	.79	.77	.78	.215	2.863	10.01	36.5	5.77	6.57	10.39

D = depth of flow = 5.00 inches

$\bar{U}$ = mean flow velocity = 0.75 ft./sec.

Table 9-j. Results Of Vertical Velocity And Turbulence Characteristics At 14 Inches Downstream From The Screen For A Cast Of A Natural Ripple Bed Obtained From The Wedge Probe Measurements

Relative depth d/D	Temperature ^{o}F	Voltage E Volts	Sloping manometer reading "Δh" mms	Velocity ft./sec. obtained from E	Velocity ft./sec. "Pitot-tube"	Average Velocity U ft./sec.	$\sqrt{\overline{e_s^2}}$ Volts	Sensitivity "S" Volts/ft./sec.	$\frac{u'}{\bar{U}} \times 10^2$	Macro Scale Λ millsec.	Micro Scale λ millsec.	$\frac{\Lambda.\bar{U}}{D} \times 10^2$	$\frac{\lambda.\bar{U}}{D} \times 10^3$
0.025	73	7.04	23.5	.65	.61	.63	.23	2.788	11.00	34.9	5.77	6.28	10.39
0.175	74	7.29	31.0	.72	.70	.71	.235	2.800	11.19	39.5	5.77	7.11	10.39
0.3	75	7.49	33.5	.77	.73	.75	.27	2.813	12.80	35.3	4.47	6.35	8.25
0.5	76	7.64	39.5	.81	.79	.80	.27	2.825	12.74	37.8	5.00	6.80	9.00
0.7	76	7.56	42.5	.79	.82	.81	.255	2.825	12.04	42.0	7.07	7.56	12.73
0.9	77	7.57	40.5	.78	.80	.79	.185	2.838	8.69	38.8	5.77	6.98	10.39

D = depth of flow = 5.00 inches

$\bar{U}$ = mean flow velocity = 0.75 ft./sec.

TABLE 10-a. Results of Velocity and Shear Stress Throughout the Depth of Flow at 44 inches D/S From the Screen for a smooth flat bed. Obtained from the Flow Visualization Analysis.

Distance Between Successive fringes Inches	Relative depth $\frac{d}{D}$	Fringe Number N	$\frac{\tau}{\rho \bar{U}^2} \times 10^4$	$\frac{U}{\bar{U}}$
0	0	9	17.28	0
0.10	.02	8	15.63	0.11
0.15	.05	7	13.44	0.26
0.15	.08	6	11.52	0.39
0.20	0.12	5	9.60	0.54
0.15	0.15	4	7.68	0.63
0.20	0.19	3	5.76	0.72
0.30	0.25	2	3.84	0.82
2.50	0.75	1	1.92	1.32
0.70	0.89	0	0.00	1.37
0.55	1.00	0	0.00	1.37

D = depth of Flow = 5.00 Inches.

$\bar{U}$ = Mean Flow velocity = 0.75 ft./sec.

τ = Shear stress = $\mu \frac{dU}{dy}$ = N.f.

μ = dynamic viscosity of milling - yellow solution = 1.75×10^{-4} lb. sec./ft.^{2} at 71°F.

$\frac{dU}{dy}$ = Velocity gradient .

N = fringe number.

f = Sensitivity factor = 2.10×10^{-4} lb/ft^2.

ρ = density of milling-yellow solution = 1.94 slugs/ft^3.

TABLE 10-b. Results of Velocity and Shear Stress Throughout the Depth of Flow at 44 inches D/S From the Screen for a sand-roughened flat bed. Obtained from the flow Visualization Analysis.

Distance Between Successive fringes Inches	Relative depth $\frac{d}{D}$	Fringe Number N	$\frac{\tau}{\rho \bar{U}^2} \times 10^4$	$\frac{U}{\bar{U}}$
0	0	13	25.23	0
.144	.03	11	21.35	0.23
.144	.06	9	17.47	0.43
.144	.09	7	13.59	0.59
.144	.12	5	9.71	0.69
.144	.14	3	5.82	0.77
.14	.17	2	3.89	0.83
1.38	.45	1	1.94	1.11
1.38	.72	0	0.00	1.19
1.38	1.00	0	0.00	1.19

D = depth of flow = 5.00 inches

$\bar{U}$ = mean flow velocity = 0.75 ft./sec.

τ = shear stress = $\mu \frac{dU}{dy}$ = N.f.

μ = dynamic viscosity of milling-yellow solution

= 1.75×10^{-4} lb.sec./ft^2. at 71°F

$\frac{dU}{dy}$ = velocity gradient

N = fringe number

f = sensitivity factor = 2.12×10^{-4} lb./ft^2.

ρ = density of milling-yellow solution = 1.94 slugs/ft^3.

TABLE 10-c. Results of Velocity and Shear Stress Throughout the Depth of Flow at 44 inches D/S From the Screen for a smooth artificial ripple bed. Obtained from the Flow Visualization Analysis.

Distance Between Successive fringes Inches	Relative depth $\frac{d}{D}$	Fringe Number N	$\frac{\tau}{\rho \bar{U}^2} \times 10^4$	$\frac{U}{\bar{U}}$
0	0	10	15.09	0
0.18	.040	9	13.59	0.18
0.18	.070	8	12.08	0.34
0.18	.110	7	10.57	0.48
0.18	.140	6	9.05	0.60
0.18	.180	5	7.55	0.71
0.25	.230	4	6.04	0.82
0.25	.280	3	4.53	0.92
0.35	.35	2	3.02	1.01
1.35	.62	1	1.51	1.22
1.35	.89	0	0.00	1.29
.55	1.0	0	0.00	1.29

D = depth of flow = 5.00 inches

$\bar{U}$ = mean flow velocity = 0.75 ft./sec.

τ = shear stress = $\mu \frac{dU}{dy}$ = N.f.

μ = dynamic viscosity = 1.75 x 10^{-4} lb.sec./ft^2. at 71°F

$\frac{dU}{dy}$ = velocity gradient

N = fringe number

f = sensitivity factor = 1.65 x 10^{-4} lb./ft^2.

ρ = density of milling-yellow solution = 1.94 slugs/ft^3.

TABLE 10-d. Results of Velocity and Shear Stress Throughout the Depth of Flow at 44 inches D/S From the Screen for a Sand - roughened artificial ripple bed. Obtained from the flow visualization Analysis.

Distance Between Successive fringes Inches	Relative depth $\frac{d}{D}$	Fringe Number N	$\frac{\tau}{\rho \bar{U}^2} \times 10^4$	$\frac{U}{\bar{U}}$
0	0	9	25.92	0
.15	.03	7	20.16	0.24
.15	.06	5	14.40	0.41
.15	.09	3	8.64	0.55
.21	.13	2	5.76	0.64
1.54	.44	1	2.88	1.11
1.40	.72	0	0.00	1.24
1.40	1.00	0	0.00	1.24

D = depth of flow = 5.00 inches

$\bar{U}$ = mean flow velocity = 0.75 ft./sec.

τ = shear stress = $\mu \frac{dU}{dy}$ = N.f.

μ = dynamic viscosity of milling-yellow solution

= 1.75×10^{-4} lb.sec./ft^2. at 71°F

$\frac{dU}{dy}$ = velocity gradient

N = fringe number

f = sensitivity factor = 3.14×10^{-4} lb./ft^2.

ρ = density of milling-yellow solution = 1.94 slugs/ft^3.

TABLE 10-e. Results of Velocity and Shear Stress Throughout the Depth of Flow at 44 inches D/S From the Screen for a cast of a natural ripple bed. Obtained from the Flow Visualization Analysis.

Distance Between Successive fringes Inches	Relative depth $\frac{d}{D}$	Fringe Number N	$\frac{\tau}{\rho \bar{U}^2} \times 10^4$	$\frac{U}{\bar{U}}$
0	.0	11	27.23	0
.125	.025	9	22.29	0.21
.125	.05	7	17.33	0.39
.150	.08	5	12.38	0.54
.150	.11	3	7.43	0.65
.250	.16	2	4.95	0.75
1.300	.42	1	2.47	1.09
1.500	.72	0	0.00	1.21
1.400	1.00	0	0.00	1.21

D = depth of flow = 5.00 inches

$\bar{U}$ = mean flow velocity = 0.75 ft./sec.

τ = shear stress = $\mu \frac{dU}{dy}$ = N.f.

μ = dynamic viscosity of milling-yellow solution = 1.75×10^{-4} lb.sec./ft^2. at 71°F.

$\frac{dU}{dy}$ = velocity gradient

N = fringe number

f = sensitivity factor = 2.70×10^{-4} lb./ft^2.

ρ = density of milling-yellow solution = 1.94 slugs/ft^3.

Table 11. The Calculated Shear Stress Based On The Computed Velocities At 0.125 Inches Above The Bed Of The Mathematical Model In The Laminar Flow Condition

Relative length $\frac{l}{L}$	Velocity U ft./sec.	$\frac{U}{\bar{U}}$	$\frac{\tau}{\rho \bar{U}^2} \times 10^4$
1.00	0.23	0.31	17.68
0.78	0.21	0.28	16.18
0.54	0.21	0.28	16.13
0.30	0.21	0.28	16.17
0.06	0	0	0

D = depth of flow = 5.00 inches

L = ripple length = 2.50 inches

$\bar{U}$ = mean flow velocity = 0.75 ft./sec.

$\tau = \mu \frac{dU}{dy}$

μ = dynamic viscosity of the milling yellow
= 1.75×10^{-4} lb.sec./ft.^{2} at 71°F

ρ = density of the milling yellow
= 1.94 slugs/ft.^{3}

$\frac{dU}{dy}$ = velocity gradient

Table 12. The Calculated Shear Stress Based On The Computed Velocities At 0.125 Inches Above The Bed Of The Mathematical Model In The Turbulent Flow Condition

Relative length $\frac{l}{L}$	Velocity U ft./sec.	$\frac{U}{\bar{U}}$	$\frac{\tau}{\rho\ \bar{U}^2} \times 10^4$
1.0	0.60	0.80	27.63
0.78	0.47	0.63	24.42
0.54	0.47	0.63	24.40
0.30	0.47	0.63	24.41
0.06	0	0	0

D = depth of flow = 5.00 inches

L = ripple length = 2.50 inches

$\bar{U}$ = mean flow velocity = 0.75 ft./sec.

$\tau = (\nu + \varepsilon)\rho \cdot \frac{dU}{dy}$

ε = eddy viscosity

ρ = density of water = 1.94 slugs/ft.^{3}

ν = kinematic viscosity of water

= 1.06×10^{-5} ft.^{2}/sec. at 70°F

$\frac{dU}{dy}$ = velocity gradient

TABLE 13-b. Statistical Evaluation of Ripple Length In Zones I and II

Zone	Ripple No.	Length L Inches	$(L - \overline{L})$	$(L - \overline{L})^2$
	1	3.86	+0.31	.0961
	2	3.83	+0.28	.0784
	3	3.52	-0.03	.0009
1	4	3.32	-0.23	.0529
	5	3.35	-0.20	.0400
	6	3.55	0	0
	7	3.45	-0.10	.0100
	$n_1 = 7$	$\overline{L}_1 = 3.55$	$\Sigma(L - \overline{L}_1) = 0$	$\Sigma(L - \overline{L}_1)^2 = 0.2783$
	8	2.48	+0.23	.0529
	9	2.28	+0.03	.0009
	10	2.16	-0.09	.0081
2	11	2.25	0	0
	12	2.22	-0.03	.0009
	13	2.20	-0.05	.0025
	14	2.18	-0.07	.0049
	$n_2 = 7$	$\overline{L}_2 = 2.25$	$\Sigma(L - \overline{L}_2) = 0$	$\Sigma(L - \overline{L}_2)^2 = .0702$

Statistical Procedure*

$$S_1^2 = \frac{\Sigma(L - \overline{L}_1)^2}{n_1 - 1} = .046$$

$$S_2^2 = \frac{\Sigma(L - \overline{L}_2)^2}{n_2 - 1} = .0117$$

$$F = \frac{S_1^2}{S_2^2} = 3.93$$

Table A-10 gives F = 4.28 at the 5.1 level of significance.

Therefore, the difference between the variance is not significant.

$$S_c^2 = \frac{S_1^2 (n_1 - 1) + S_2^2 (n_2 - 1)}{(n_1 - 1) + (n_2 - 1)} = .029$$

$$S_c = 0.17$$

$$S_d = S_c \sqrt{\frac{n_1 + n_2}{n_1 n_2}} = .091$$

$$t = \frac{\overline{L}_1 - \overline{L}_2}{S_d} = 14.3$$

Table A-8 gives t = 4.318 at 0.1 percent level of significance.

Therefore, the ripple lengths in Zones I and II are significantly different.

* Tables A-8 and A-10 refer to Reference 45.

TABLE 13-a. Statistical Evaluation of Ripple Height In Zones I and II

Zone	Ripple No.	Height h Inches	$h - \overline{h}$	$(h - \overline{h})^2$
	1	0.52	+.086	.007396
	2	0.45	+.016	.000256
	3	0.40	-.034	.001156
1	4	0.42	-.015	.000225
	5	0.44	+.006	.000036
	6	0.43	-.005	.000025
	7	0.38	-.054	.002916
	$n_1 = 7$	$\overline{h}_1 = 0.434$	$\Sigma(h - \overline{h}_1) = 0$	$\Sigma(h - \overline{h}_1)^2 = 0.01201$
	8	0.24	+.04	.0016
	9	0.20	0	0
	10	0.22	+.02	.0004
2	11	0.18	+.02	.0004
	12	0.16	-.04	.0016
	13	0.18	-.02	.0004
	14	0.22	+.02	.0004
	$n_2 = 7$	$\overline{h}_2 = 0.20$	$\Sigma(h - \overline{h}_2) = 0$	$\Sigma(h - \overline{h}_2)^2 = .0048$

Statistical Procedure*

$$S_1^2 = \frac{\Sigma(h - \overline{h}_1)^2}{n_1 - 1} = .002$$

$$S_2^2 = \frac{\Sigma(h - \overline{h}_2)^2}{n_2 - 1} = .0008$$

$$F = \frac{S_1^2}{S_2^2} = 2.5$$

Table A-10 gives F = 4.28 at the 5% level of significance.

Therefore, the difference between the variance is not significant.

$$S_c^2 = \frac{S_1^2\,(n_1 - 1) + S_2^2\,(n_2 - 1)}{(n_1 - 1) + (n_2 - 1)} = .0014$$

$$S_c = .0374$$

$$S_d = S_c \cdot \sqrt{\frac{n_1 + n_2}{n_1 n_2}} = .02$$

$$t_1 = \frac{\overline{h}_1 - \overline{h}_2}{S_d} = 11.7$$

Table A-8 gives t = 4.318 at 0.1 percent level of significance.

Therefore, the ripple heights in Zones I and II are significantly different.

* Tables A-8 and A-10 refer to Reference 45.

TABLE 14-a. Application of Boundary Layer Theory In Determining Shear Stress Distribution Along The Rough-Artificial Ripple Bed

$\frac{l}{L}$	1	0.8	0.6	0.4	0.2
U ft./sec. From Table 7a	0.64	0.59	0.57	0.58	0.60
$U^{1.8}$	0.4478	0.3868	0.3636	0.3751	0.3987
$\frac{u'}{U} \times 10^2$ From Table 7a	7.4	8.2	8.5	9.1	7.1
$\left(\frac{\varepsilon_{ripple}}{\varepsilon_{flat}}\right)^{0.2}$	1.040	1.061	1.069	1.084	1.031
$l_x = L + x$ ft.	0.385	0.343	0.302	0.260	0.218
$l_x^{0.2}$	0.826	0.808	0.787	0.764	0.738
$\frac{\tau_o}{\rho \bar{U}^2} \times 10^4$	29.4	26.6	25.8	27.8	29.2

$$\frac{\varepsilon_{ripple}}{\varepsilon_{flat}} = \frac{u'_{ripple}}{u'_{flat}} \cdot \frac{\Lambda_{ripple}}{\Lambda_{flat}}$$

$\left(\frac{u'}{\bar{U}}\right)_{flat} = 6.64 \times 10^{-2}$ (Table 9b)

$\left(\frac{\Lambda \bar{U}}{D}\right)_{flat} = 4.72 \times 10^{-2}$ (Table 9b)

$\left(\frac{\Lambda \bar{U}}{D}\right)_{ripple} = 5.15 \times 10^{-2}$ (Table 9d)

TABLE 14-b. Application of Boundary Layer Theory In Determining Shear Stress Distribution Along The Cast Of The Natural Ripple Bed

$\frac{l}{L}$	1.0	0.78	0.56	0.39	0.22
U ft./sec. From Table 7b	0.59	0.55	0.56	0.56	0.57
$U^{1.8}$	0.3868	0.3409	0.3522	0.3522	0.3636
$\frac{u'}{U} \times 10^2$ From Table 7b	7.6	8.0	8.5	8.9	7.1
$\left(\frac{\varepsilon_{ripple}}{\varepsilon_{flat}}\right)^{0.2}$	1.077	1.088	1.102	1.112	1.063
$l_x = L + x$ ft.	0.3465	0.3055	0.2645	0.2325	0.201
$l_x^{0.2}$	0.809	0.789	0.766	0.747	0.725
$\frac{\tau_o}{\rho \overline{U}^2} = 10^4$	26.9	24.6	26.4	27.3	27.8

$$\frac{\varepsilon_{ripple}}{\varepsilon_{flat}} = \frac{u'_{ripple}}{u'_{flat}} \cdot \frac{\Lambda_{ripple}}{\Lambda_{flat}}$$

$\left(\frac{u'}{\overline{U}}\right)_{flat} = 6.64 \times 10^{-2}$ (Table 9b)

$\left(\frac{\Lambda \overline{U}}{D}\right)_{flat} = 4.72 \times 10^{-2}$ (Table 9b)

$\left(\frac{\Lambda \overline{U}}{D}\right)_{ripple} = 5.98 \times 10^{-2}$ (Table 9c)

TABLE 14-c. Application of Boundary Layer Theory In Determining Shear Stress Distribution Using The Mathematical Turbulent Flow Data

$\frac{l}{L}$	1.0	0.78	0.54	0.30	0.06
U ft./sec. From Table 12	0.60	0.47	0.47	0.47	0
$U^{1.8}$	0.3987	0.2569	0.2569	0.2569	0
$\left(\frac{\varepsilon_{ripple}}{\varepsilon_{flat}}\right)^{0.2}$ Assumed	1	1	1	1	—
$l_x = l + x$ ft.	0.385	0.340	0.290	0.240	—
$l_x^{0.2}$	0.826	0.806	0.781	0.751	—
$\frac{\tau_o}{\rho U^2} \times 10^4$	25.2	16.6	17.2	17.9	0

TABLE 14-d. Application of Boundary Layer Theory In Determining Shear Stress Distribution Using The Mathematical Laminar Flow Data

$\frac{l}{L}$	1.0	0.78	0.54	0.30	0.06
U ft./sec. From Table 11	0.23	0.21	0.21	0.21	0
$U^{1.5}$	0.110	0.096	0.096	0.096	—
$l_x = L + x$ ft.	0.385	0.340	0.290	0.240	—
$l_x^{0.5}$	0.6248	0.5827	0.5381	0.4895	—
$\frac{\tau_o}{\rho U^2} \times 10^4$	9.6	9.0	9.7	10.7	0

APPENDIX V

COMPUTER PROGRAMMES

FLOW CHART Analysis of Hot Anemometry measurements

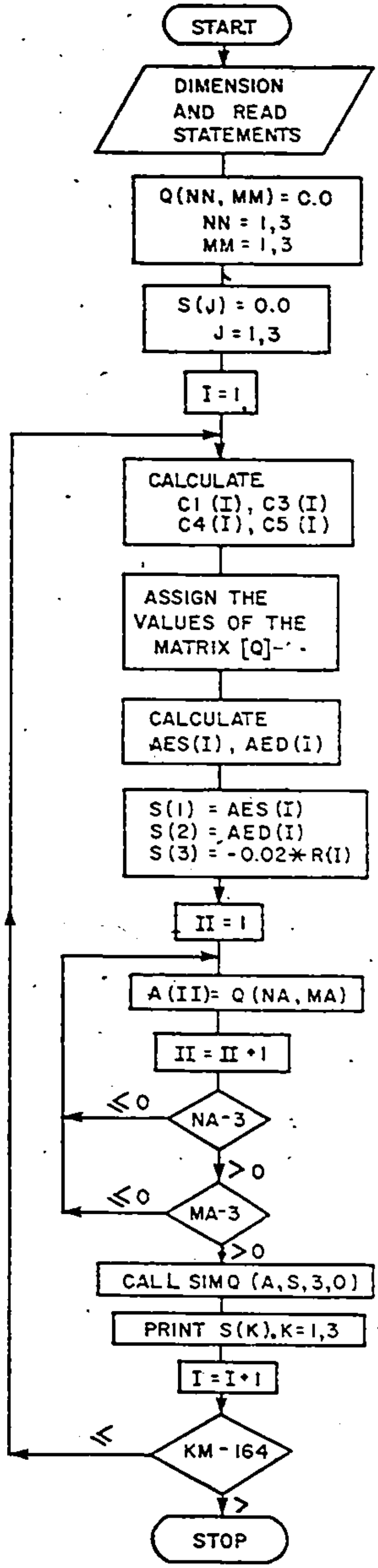

Analysis of the Hot-Film Anemometry Measurements:

```
      DIMENSION ES(200),ED(200),P(200)
      DIMENSION Q(3,3),S(3),A1(200),A2(200),A(9)
      DIMENSION AES(200),AED(200)
      DIMENSION C1(200),C2(200),C3(200),C4(200),C5(200)
      DIMENSION SS(3)
      KM=164
      READ(5,1)(P(I),ES(I),ED(I),A1(I),A2(I),I=1,KM)
    1 FORMAT (5F10.5)
      PRINT11,(P(I),ES(I),ED(I),A1(I),A2(I),I=1,KM)
   11 FORMAT (7X,5F10.5)
      DO 2 NN=1,3
      DO 2 MM=1,3
      Q(NN,MM)=0.0
    2 CONTINUE
      DO 3 J=1,3
      S(J)=0.0
    3 CONTINUE
      DO 4 I=1,KM
      C1(I)=(A1(I)+A2(I))**2
      C3(I)=(A1(I)-A2(I))**2
      C4(I)=2.0*((A1(I))**2-(A2(I))**2)
      C5(I)=2.0*(C1(I)+C3(I))
      Q(1,1)=C1(I)
      Q(2,1)=C3(I)
      Q(3,1)=C4(I)
      Q(1,2)=C4(I)
      Q(2,2)=C4(I)
      Q(3,2)=C5(I)
      Q(1,3)=C3(I)
      Q(2,3)=C1(I)
      Q(3,3)=C4(I)
      AES(I)=ES(I)**2
      AED(I)=ED(I)**2
      S(1)=AES(I)
      S(2)=AED(I)
      S(3)=-.02*P(I)
      II=1
      DO 7 MA=1,3
      DO 7 NA=1,3
      A(II)=Q(NA,MA)
      II=II+1
    7 CONTINUE
      CALL SIMQ (A,S[illegible]0)
      PRINT 5,(S(K),[illegible],3)
    5 FORMAT (7X,3F1[illegible])
      SS(1)=ABS(S(1))
      SS(3)=ABS(S(3))
      RMSU=SQRT(SS(1))
      RMSV=SQRT(SS(3))
    6 FORMAT (7X,5HRMSU=F15.7,10X,5HRMSV=F15.7)
      PRINT 6,RMSU,RMSV
    4 CONTINUE
      STOP
      END
```

```
C                                                                       SIMQ
C        ...............................................................SIMQ
C                                                                       SIMQ
C        SUBROUTINE SIMQ                                                SIMQ
C                                                                       SIMQ
C        PURPOSE                                                        SIMQ
C           OBTAIN SOLUTION OF A SET OF SIMULTANEOUS LINEAR EQUATIONS,  SIMQ
C           AX=B                                                        SIMQ
C                                                                       SIMQ
C        USAGE                                                          SIMQ
C           CALL SIMQ(A,B,N,KS)                                         SIMQ
C                                                                       SIMQ
C        DESCRIPTION OF PARAMETERS                                      SIMQ
C           A - MATRIX OF COEFFICIENTS STORED COLUMNWISE.  THESE ARE    SIMQ
C               DESTROYED IN THE COMPUTATION.  THE SIZE OF MATRIX A IS  SIMQ
C               N BY N.                                                 SIMQ
C           B - VECTOR OF ORIGINAL CONSTANTS (LENGTH N). THESE ARE      SIMQ
C               REPLACED BY FINAL SOLUTION VALUES, VECTOR X.            SIMQ
C           N - NUMBER OF EQUATIONS AND VARIABLES. N MUST BE .GT. ONE.  SIMQ
C           KS - OUTPUT DIGIT                                           SIMQ
C                0 FOR A NORMAL SOLUTION                                SIMQ
C                1 FOR A SINGULAR SET OF EQUATIONS                      SIMQ
C                                                                       SIMQ
C        REMARKS                                                        SIMQ
C           MATRIX A MUST BE GENERAL.                                   SIMQ
C           IF MATRIX IS SINGULAR , SOLUTION VALUES ARE MEANINGLESS.    SIMQ
C           AN ALTERNATIVE SOLUTION MAY BE OBTAINED BY USING MATRIX     SIMQ
C           INVERSION (MINV) AND MATRIX PRODUCT (GMPRD).                SIMQ
C                                                                       SIMQ
C        SUBROUTINES AND FUNCTION SUBPROGRAMS REQUIRED                  SIMQ
C           NONE                                                        SIMQ
C                                                                       SIMQ
C        METHOD                                                         SIMQ
C           METHOD OF SOLUTION IS BY ELIMINATION USING LARGEST PIVOTAL  SIMQ
C           DIVISOR. EACH STAGE OF ELIMINATION CONSISTS OF INTERCHANGINGSIMQ
C           ROWS WHEN NECESSARY TO AVOID DIVISION BY ZERO OR SMALL      SIMQ
C           ELEMENTS.                                                   SIMQ
C           THE FORWARD SOLUTION TO OBTAIN VARIABLE N IS DONE IN        SIMQ
C           N STAGES. THE BACK SOLUTION FOR THE OTHER VARIABLES IS      SIMQ
C           CALCULATED BY SUCCESSIVE SUBSTITUTIONS. FINAL SOLUTION      SIMQ
C           VALUES ARE DEVELOPED IN VECTOR B, WITH VARIABLE 1 IN B(1),  SIMQ
C           VARIABLE 2 IN B(2),........, VARIABLE N IN B(N).            SIMQ
C           IF NO PIVOT CAN BE FOUND EXCEEDING A TOLERANCE OF 0.0,      SIMQ
C           THE MATRIX IS CONSIDERED SINGULAR AND KS IS SET TO 1. THIS  SIMQ
C           TOLERANCE CAN BE MODIFIED BY REPLACING THE FIRST STATEMENT. SIMQ
C                                                                       SIMQ
C        ...............................................................SIMQ
C                                                                       SIMQ
      SUBROUTINE SIMQ(A,B,N,KS)                                         SIMQ
      DIMENSION A(9),B(3)                                               SIMQ
C                                                                       SIMQ
C        FORWARD SOLUTION                                               SIMQ
C                                                                       SIMQ
      TOL=0.0                                                           SIMQ
      KS=0                                                              SIMQ
      JJ=-N                                                             SIMQ
      DO 65 J=1,N                                                       SIMQ
      JY=J+1                                                            SIMQ
                                                                        SIMQ
```

```
      JJ=JJ+N+1                                                         SIMQ
      BIGA=0                                                            SIMQ
      IT=JJ-J                                                           SIMQ
      DO 30 I=J,N                                                       SIMQ
C                                                                       SIMQ
C        SEARCH FOR MAXIMUM COEFFICIENT IN COLUMN                       SIMQ
C                                                                       SIMQ
      IJ=IT+I                                                           SIMQ
      IF(ABS(BIGA)-ABS(A(IJ))) 20,30,30                                 SIMQ
   20 BIGA=A(IJ)                                                        SIMQ
      IMAX=I                                                            SIMQ
   30 CONTINUE                                                          SIMQ
C                                                                       SIMQ
C        TEST FOR PIVOT LESS THAN TOLERANCE (SINGULAR MATRIX)           SIMQ
C                                                                       SIMQ
      IF(ABS(BIGA)-TOL) 35,35,40                                        SIMQ
   35 KS=1                                                              SIMQ
      RETURN                                                            SIMQ
C                                                                       SIMQ
C        INTERCHANGE ROWS IF NECESSARY                                  SIMQ
C                                                                       SIMQ
   40 I1=J+N*(J-2)                                                      SIMQ
      IT=IMAX-J                                                         SIMQ
      DO 50 K=J,N                                                       SIMQ
      I1=I1+N                                                           SIMQ
      I2=I1+IT                                                          SIMQ
      SAVE=A(I1)                                                        SIMQ
      A(I1)=A(I2)                                                       SIMQ
      A(I2)=SAVE                                                        SIMQ
C                                                                       SIMQ
C        DIVIDE EQUATION BY LEADING COEFFICIENT                         SIMQ
C                                                                       SIMQ
   50 A(I1)=A(I1)/BIGA                                                  SIMQ
      SAVE=B(IMAX)                                                      SIMQ
      B(IMAX)=B(J)                                                      SIMQ
      B(J)=SAVE/BIGA                                                    SIMQ
C                                                                       SIMQ
C        ELIMINATE NEXT VARIABLE                                        SIMQ
C                                                                       SIMQ
      IF(J-N) 55,70,55                                                  SIMQ
   55 IQS=N*(J-1)                                                       SIMQ
      DO 65 IX=JY,N                                                     SIMQ
      IXJ=IQS+IX                                                        SIMQ
      IT=J-IX                                                           SIMQ
      DO 60 JX=JY,N                                                     SIMQ
      IXJX=N*(JX-1)+IX                                                  SIMQ
      JJX=IXJX+IT                                                       SIMQ
   60 A(IXJX)=A(IXJX)-(A(IXJ)*A(JJX))                                   SIMQ
   65 B(IX)=B(IX)-(B(J)*A(IXJ))                                         SIMQ
C                                                                       SIMQ
C        BACK SOLUTION                                                  SIMQ
C                                                                       SIMQ
   70 NY=N-1                                                            SIMQ
      IT=N*N                                                            SIMQ
      DO 80 J=1,NY                                                      SIMQ
      IA=IT-J                                                           SIMQ
      IB=N-J                                                            SIMQ
      IC=N                                                              SIMQ
```

```
      DO 80 K=1,J                                                      SIMQ
      B(IB)=B(IB)-A(IA)*B(IC)                                          SIMQ
      IA=IA-N                                                          SIMQ
   80 IC=IC-1                                                          SIMQ
      RETURN                                                           SIMQ
      END                                                              SIMQ
```

1.24000	0.21500	0.20500	2.83000	2.31000
0.92000	0.29000	0.19000	2.70000	2.20000
0.85000	0.26000	0.18000	2.58000	2.12000
0.80000	0.25500	0.17500	2.64000	2.16000
0.78[illegible]00	0.25500	0.17000	2.70000	2.20000
0.7[illegible]000	0.25000	0.16000	2.78000	2.28000
0.75000	0.24500	0.16500	2.86000	2.34000
1.41000	0.32000	0.31000	2.27000	1.86000
1.23000	0.31000	0.28700	2.18000	1.78000
0.70000	0.23500	0.21000	2.09000	1.71000
0.50000	0.19000	0.18500	2.06000	1.69000
0.38000	0.17000	0.16500	2.04000	1.68000
0.30000	0.15200	0.13700	2.06000	1.69000
0.24000	0.13200	0.12000	2.03000	1.67000
0.80000	0.25000	0.17500	2.91000	2.38000
0.29000	0.14500	0.12000	2.33000	1.91000
0.25000	0.13000	0.12000	2.20000	1.80000
0.23000	0.12500	0.11500	2.06000	1.69000
0.21000	0.12500	0.11000	2.03000	1.67000
0.20000	0.12000	0.11000	2.27000	1.86000
0.89000	0.27000	0.18000	2.64000	2.16000
0.92000	0.28000	0.22500	2.44000	2.00000
1.08000	0.30500	0.24000	2.27000	1.86000
1.35000	0.33000	0.29000	2.09000	1.71000
1.16000	0.31000	0.24000	2.14000	1.76000
1.28000	0.32000	0.21000	2.00000	1.64000
0.90000	0.25000	0.17200	2.49000	2.03000
0.75000	0.22500	0.16000	2.58000	2.12000
0.62000	0.20500	0.13500	2.72000	2.23000
0.51000	0.16500	0.12000	2.70000	2.20000
0.49000	0.16000	0.12000	2.66000	2.18000
0.58000	0.20000	0.13000	2.61000	2.13000
0.69000	0.21000	0.14000	2.66000	2.18000
1.50000	0.35000	0.31000	2.24000	1.83000
1.10000	0.32000	0.28500	2.09000	1.71000
0.65000	0.24000	0.19500	1.97000	1.61000
0.48000	0.21000	0.16000	1.98000	1.62000
0.35000	0.19000	0.14500	2.00000	1.64000
0.28000	0.17000	0.12000	2.06000	1.69000
0.21000	0.15500	0.10500	2.07000	1.70000
0.71000	0.23000	0.15000	2.64000	2.16000
0.44000	0.21000	0.12500	2.25000	1.85000
0.35000	0.16000	0.13500	2.14000	1.76000
0.23000	0.14500	0.12500	2.09000	1.71000
0.20000	0.12500	0.11000	2.07000	1.70000
0.18600	0.12000	0.10500	2.33000	1.91000
0.79000	0.25000	0.17000	2.49000	2.03000
0.82000	0.26000	0.21800	2.09000	1.71000
1.05000	0.31000	0.24500	2.03000	1.6[illegible]000
1.00000	0.27000	0.26000	2.00000	1.64000
0.93000	0.28000	0.25500	2.25000	1.85000
1.05000	0.29500	0.18500	2.00000	1.64000
1.59000	0.38000	0.25500	3.16000	2.58000
1.20000	0.32000	0.20500	2.97000	2.43000
1.00000	0.30500	0.18500	2.78000	2.28000
1.00000	0.30000	0.18500	2.71000	2.22000
1.14000	0.32000	0.19000	2.64000	2.16000
1.10000	0.31000	0.19500	2.66000	2.18000
0.95000	0.30000	0.19000	2.86000	2.34000

1.95000	0.40000	0.28500	2.55000	2.09000
1.41000	0.34000	0.27000	2.44000	2.00000
0.82000	0.26000	0.21000	2.27000	1.86000
0.50000	0.20500	0.19000	2.18000	1.78000
0.40000	0.13000	0.17000	2.14000	1.76000
0.32000	0.14500	0.13500	2.09000	1.71000
0.24000	0.13000	0.12500	2.14000	1.76000
0.95000	0.29000	0.18300	2.78000	2.28000
0.52000	0.23000	0.14000	2.49000	2.03000
0.43000	0.17500	0.13000	2.27000	1.86000
0.26000	0.14000	0.12000	2.20000	1.80000
0.23000	0.13000	0.11500	2.24000	1.83000
0.21000	0.12500	0.11000	2.46000	2.02000
1.15000	0.32000	0.20000	3.04000	2.48000
0.96000	0.30000	0.19500	2.54000	2.08000
0.72500	0.26500	0.17500	2.33000	1.91000
1.23000	0.33000	0.25500	2.33000	1.91000
1.02000	0.29000	0.23000	2.41000	1.97000
0.93000	0.27000	0.17000	2.03000	1.67000
1.23000	0.32200	0.22700	2.86000	2.34000
0.96000	0.29500	0.18500	2.78000	2.28000
0.87000	0.28500	0.16500	2.70000	2.20000
0.84000	0.27000	0.17500	2.64000	2.16000
0.93000	0.26500	0.17000	2.44000	2.00000
0.90000	0.28000	0.18500	2.58000	2.12000
0.86000	0.27500	0.18000	2.70000	2.20000
1.65000	0.37000	0.33000	2.46000	2.02000
1.25000	0.34000	0.29500	2.33000	1.91000
0.72000	0.26000	0.23000	2.18000	1.78000
0.49000	0.23000	0.19000	2.06000	1.69000
0.37000	0.20500	0.15000	2.03000	1.67000
0.29000	0.19000	0.14000	2.03000	1.67000
0.22000	0.17000	0.12000	2.00000	1.64000
0.90000	0.32000	0.19500	2.70000	2.20000
0.75000	0.28500	0.16500	2.54000	2.08000
0.57000	0.24000	0.13500	2.18000	1.78000
0.28000	0.15500	0.12500	1.98000	1.62000
0.30000	0.14500	0.12000	2.06000	1.69000
0.25000	0.14000	0.11500	2.22000	1.82000
0.96000	0.29500	0.18500	2.78000	2.28000
0.82000	0.26000	0.17500	2.29000	1.87000
0.60000	0.20000	0.13500	2.18000	1.78000
1.25000	0.34000	0.29500	2.29000	1.87000
0.95000	0.30000	0.19000	2.39000	1.95000
0.86000	0.27000	0.18000	2.14000	1.76000
2.35000	0.46000	0.32000	3.19000	2.61000
2.05000	0.42000	0.29000	2.97000	2.43000
1.86000	0.39500	0.26000	2.83000	2.31000
1.65000	0.38000	0.25500	2.91000	2.38000
1.50000	0.36000	0.24500	3.00000	2.46000
1.35000	0.33500	0.22000	3.16000	2.58000
1.80000	0.33000	0.25000	2.01000	1.65000
1.40000	0.35000	0.22000	2.00000	1.64000
1.05000	0.24000	0.16000	1.97000	1.61000
0.62000	0.21000	0.14000	2.00000	1.64000
0.50000	0.19000	0.13000	2.06000	1.69000
0.40000	0.16000	0.12500	2.17000	1.77000
1.35000	0.33500	0.22000	3.16000	2.58000
0.89000	0.26000	0.17000	2.78000	2.28000
0.68000	0.24000	0.15000	2.66000	2.18000

0.55000	0.23000	0.14000	2.46000	2.07000
1.48000	-0.18000	0.13000	2.29000	1.87000
0.40000	0.15000	0.12500	2.17000	1.77000
0.32000	0.14000	0.12000	2.00000	1.64000
0.75000	0.13000	0.11500	2.03000	1.67000
2.05000	0.42000	0.29000	2.97000	2.43000
1.74000	0.37000	0.24000	2.54000	2.08000
1.95000	0.39500	0.26000	2.22000	1.82000
1.40000	0.35000	0.22000	2.00000	1.64000
1.29000	0.34000	0.20000	2.06000	1.69000
1.05000	0.24000	0.16000	2.14000	1.76000
1.86000	0.39000	0.26000	2.78000	2.28000
1.40000	0.35000	0.22000	2.44000	2.00000
1.20000	0.33000	0.20000	2.18000	1.78000
1.05000	0.24000	0.16000	2.00000	1.64000
0.80000	0.21000	0.15000	2.06000	1.69000
0.60000	0.20000	0.13500	2.09000	1.71000
1.65000	0.38000	0.25000	2.91000	2.38000
1.20000	0.33000	0.24000	2.54000	2.08000
0.80000	0.29000	0.18000	2.29000	1.87000
0.62000	0.21000	0.14000	2.00000	1.64000
0.50000	0.19000	0.13000	2.14000	1.76000
0.40000	0.16000	0.12000	2.22000	1.82000
1.50000	0.36000	0.24500	2.97000	2.43000
1.00000	0.26000	0.18000	2.49000	2.03000
0.70000	0.23000	0.16000	2.22000	1.82000
0.50000	0.19000	0.13000	2.06000	1.69000
0.40000	0.16000	0.12500	2.03000	1.67000
0.30000	0.13500	0.12000	2.09000	1.71000
0.90000	0.29000	0.19000	2.83000	2.31000
1.20000	0.34000	0.21500	3.12000	2.55000
1.40000	0.37000	0.24500	3.25000	2.66000
1.50000	0.33500	0.25000	3.19000	2.61000
0.95000	0.28500	0.20000	3.04000	2.48000
1.35000	0.32000	0.21500	3.16000	2.58000
1.45000	0.36500	0.24000	3.44000	2.81000
1.60000	0.38000	0.25500	3.38000	2.76000
1.80000	0.39500	0.26500	3.32000	2.72000
1.30000	0.30500	0.19500	3.25000	2.66000
0.25000	0.14000	0.11500	2.22000	1.82000
0.28000	0.14500	0.12000	2.18000	1.78000
0.30000	0.15000	0.12500	2.14000	1.76000
0.40000	0.16000	0.12500	2.17000	1.77000
0.45000	0.16500	0.13000	2.14000	1.76000
0.49000	0.17500	0.13500	2.18000	1.78000

Output

```
 0.00394737 -0.00103614  0.00175992
RMSU=       0.0623281          RMSV=       0.0419514
 0.00367264 -0.00091700  0.00165244
RMSU=       0.0606023          RMSV=       0.0406503
 0.00321079 -0.00084770  0.00160190
RMSU=       0.0566639          RMSV=       0.0400238
 0.00296399 -0.00078139  0.00145585
RMSU=       0.0544425          RMSV=       0.0381556
 0.00284604 -0.00074281  0.00132562
RMSU=       0.0533483          RMSV=       0.0364091
 0.00255922 -0.00065242  0.00110381
RMSU=       0.0505888          RMSV=       0.0332236
 0.00233180 -0.00061505  0.00110653
RMSU=       0.0482888          RMSV=       0.0332646
 0.00634759 -0.00202990  0.00597455
```

```
RMSU=        0.0796717          RMSV=       0.0772952
  0.00647163 -0.00178218  0.0055[illegible]699
RMSU=        0.0804474          RMSV=       0.0747462
  0.00403218 -0.00120137  0.00325397
RMSU=        0.0634995          RMSV=       0.0570436
  0.00271354 -0.00086928  0.00257390
-----------------------------------------------------
RMSU=        0.0520917          RMSV=       0.0507829
  0.00220100 -0.00068238  0.00207381
RMSU=        0.0469148          RMSV=       0.0455940
  0.00173159 -0.00051926  0.00142029
RMSU=        0.0416124          RMSV=       0.0376368
  0.00134212 -0.00041089  0.00111911
-----------------------------------------------------
RMSU=        0.0366349          RMSV=       0.0334532
  0.00234859 -0.00063484  0.00119800
RMSU=        0.0484623          RMSV=       0.0346122
  0.00123342 -0.00036522  0.00086125
RMSU=        0.0351200          RMSV=       0.0293471
  0.00111876 -0.00036061  0.00096093
-----------------------------------------------------
RMSU=        0.0334479          RMSV=       0.0309989
  0.00117531 -0.00037483  0.00100297
RMSU=        0.0342828          RMSV=       0.0316697
  0.00120222 -0.00035865  0.00094227
RMSU=        0.0346730          RMSV=       0.0306964
  0.00089200 -0.00027910  0.00075582
-----------------------------------------------------
RMSU=        0.0298664          RMSV=       0.0274921
  0.00332148 -0.00086438  0.00154591
RMSU=        0.0576323          RMSV=       0.0393181
  0.00417629 -0.00114219  0.00275339
RMSU=        0.0646242          RMSV=       0.0524728
  0.00572508 -0.00154641  0.00362755
-----------------------------------------------------
RMSU=        0.0755643          RMSV=       0.0602291
  0.00794487 -0.00232713  0.00621007
RMSU=        0.0891340          RMSV=       0.0788040
  0.00662803 -0.00178830  0.00407255
RMSU=        0.0814127          RMSV=       0.0638165
  0.00811006 -0.00211014  0.00366647
-----------------------------------------------------
RMSU=        0.0900559          RMSV=       0.0605514
  0.00323040 -0.00092280  0.00160241
RMSU=        0.0568366          RMSV=       0.0400301
  0.00241537 -0.00069372  0.00127155
RMSU=        0.0491464          RMSV=       0.0356588
  0.00180777 -0.00050885  0.00082683
-----------------------------------------------------
RMSU=        0.0425179          RMSV=       0.0287546
  0.00120853 -0.00039981  0.00066376
RMSU=        0.0347639          RMSV=       0.0258604
  0.00116312 -0.00038817  0.00068026
RMSU=        0.0341046          RMSV=       0.0260819
  0.00187867 -0.00052903  0.00083987
-----------------------------------------------------
RMSU=        0.0433437          RMSV=       0.0289806
  0.00198812 -0.00057845  0.00093187
RMSU=        0.0445884          RMSV=       0.0305266
  0.00779384 -0.00229035  0.00618377
RMSU=        0.0882828          RMSV=       0.0786369
  0.00744824 -0.00208248  0.00596701
-----------------------------------------------------
RMSU=        0.0863032          RMSV=       0.0772464
  0.00472124 -0.00128850  0.00317830
RMSU=        0.0687113          RMSV=       0.0563764
  0.00356760 -0.00093040  0.00212571
RMSU=        0.0597294          RMSV=       0.0461054
  0.00284782 -0.00070691  0.00169881
```

```
RMSU=        0.0533650                 RMSV=       0.0412167
  0.00214595 -0.00051483   0.00110470
RMSU=        [illegible]               RMSV=       [illegible]
  0.00176059 -0.00039885   0.00083703
RMSU=        0.0419594                 RMSV=       0.0289315
  0.00241547 -0.00065146   0.00108270
--------------------------------------------------------------
RMSU=        0.0491475                 RMSV=       0.0329044
  0.00273518 -0.00062267   0.00102497
RMSU=        0.0522990                 RMSV=       0.0320151
  0.00177282 -0.00052292   0.00128330
RMSU=        0.0421049                 RMSV=       0.0358231
  0.00152913 -0.00042310   0.00115139
--------------------------------------------------------------
RMSU=        0.0391041                 RMSV=       0.0339322
  0.00115736 -0.00034004   0.00090694
RMSU=        0.0340200                 RMSV=       0.0301134
  0.00084399 -0.00024944   0.00065440
RMSU=        0.0290516                 RMSV=       0.0255812
  0.00321385 -0.00086377   0.00155703
--------------------------------------------------------------
RMSU=        0.0567349                 RMSV=       0.0394593
  0.00492594 -0.00139864   0.00352161
RMSU=        0.0701851                 RMSV=       0.0593431
  0.00734896 -0.00192004   0.00468864
RMSU=        0.0857261                 RMSV=       0.0684736
  0.00581443 -0.00184683   0.00541047
--------------------------------------------------------------
RMSU=        0.0762524                 RMSV=       0.0735559
  0.00490152 -0.00141777   0.00409822
RMSU=        0.0700108                 RMSV=       0.0640173
  0.00688415 -0.00173915   0.00285977
RMSU=        0.0829708                 RMSV=       0.0534768
  0.00459371 -0.00115322   0.00215974
--------------------------------------------------------------
RMSU=        0.0677769                 RMSV=       0.0464730
  0.00368164 -0.00092942   0.00159026
RMSU=        0.0606765                 RMSV=       0.0398780
  0.00379731 -0.00090304   0.00147811
RMSU=        0.0616223                 RMSV=       0.0384462
  0.00387483 -0.00094203   0.00155713
--------------------------------------------------------------
RMSU=        0.0622482                 RMSV=       0.0394605
  0.00465163 -0.00112322   0.00174497
RMSU=        0.0682029                 RMSV=       0.0417728
  0.00429553 -0.00106282   0.00179178
RMSU=        0.0655403                 RMSV=       0.0423295
  0.00348130 -0.00083787   0.00146782
--------------------------------------------------------------
RMSU=        0.0590025                 RMSV=       0.0383122
  0.00780088 -0.00206582   0.00410565
RMSU=        0.0883226                 RMSV=       0.0640754
  0.00616249 -0.00170313   0.00397499
RMSU=        0.0785015                 RMSV=       0.0630475
  0.00416584 -0.00115831   0.00277439
--------------------------------------------------------------
RMSU=        0.0645433                 RMSV=       0.0526725
  0.00282515 -0.00084243   0.00244342
RMSU=        0.0531521                 RMSV=       0.0494310
  0.00224183 -0.00067085   0.00200951
RMSU=        0.0473480                 RMSV=       0.0448276
  0.00154369 -0.00050570   0.00134782
--------------------------------------------------------------
RMSU=        0.0392898                 RMSV=       0.0367127
  0.00117379 -0.00037473   0.00108916
RMSU=        0.0342607                 RMSV=       0.0330025
  0.00343760 -0.00084490   0.00144139
RMSU=        0.0586310                 RMSV=       0.0379657
  0.00270680 -0.00063131   0.00105982
--------------------------------------------------------------
```

```
RMSU=        0.0520269           RMSV=      0.0325548
  0.00189240 -0.00054181  0.00107973
RMSU=        0.0435017           RMSV=      0.0328592
  0.00129221 -0.00039427  0.00096393
RMSU=        0.0359474           RMSV=      0.0310472
  0.00107807 -0.00033012  0.00085395
-----------------------------------------------------
RMSU=        0.0328340           RMSV=      0.0292224
  0.00082063 -0.00024604  0.00064329
RMSU=        0.0286467           RMSV=      0.0253632
  0.00352287 -0.00087330  0.00145368
RMSU=        0.0593538           RMSV=      0.0381272
  0.00441080 -0.00107260  0.00195136
-----------------------------------------------------
RMSU=        0.0654139           RMSV=      0.0441742
  0.00408258 -0.00098210  0.00185802
RMSU=        0.0638551           RMSV=      0.0431047
  0.00635263 -0.00168208  0.00388791
RMSU=        0.0797034           RMSV=      0.0623531
  0.00461101 -0.00128014  0.00296812
-----------------------------------------------------
RMSU=        0.0679044           RMSV=      0.0544804
  0.00558242 -0.00143634  0.00233769
RMSU=        0.0747156           RMSV=      0.0483496
  0.00402459 -0.00105443  0.00207630
RMSU=        0.0634397           RMSV=      0.0455664
  0.00355[illegible]17 -0.00086334  0.00147263
-----------------------------------------------------
RMSU=        0.0596253           RMSV=      0.0333749
  0.00354210 -0.00084452  0.00126937
RMSU=        0.0595155           RMSV=      0.0356283
  0.00331626 -0.00083416  0.00146288
RMSU=        0.0575870           RMSV=      0.0382476
  0.00374332 -0.00093411  0.00162626
-----------------------------------------------------
RMSU=        0.0611827           RMSV=      0.0403270
  0.00371453 -0.00092802  0.00169542
RMSU=        0.0609469           RMSV=      0.0411754
  0.00330535 -0.00083838  0.00148612
RMSU=        0.0574922           RMSV=      0.0385502
  0.00717252 -0.00207265  0.00576385
-----------------------------------------------------
RMSU=        0.0846907           RMSV=      0.0759200
  0.00674723 -0.00185482  0.00514200
RMSU=        0.0821415           RMSV=      0.0717078
  0.00452992 -0.00126569  0.00358286
RMSU=        0.0673047           RMSV=      0.0598570
  0.00392909 -0.00096910  0.00245699
-----------------------------------------------------
RMSU=        0.0626825           RMSV=      0.0495680
  0.00319818 -0.00074547  0.00175832
RMSU=        0.0565524           RMSV=      0.0419324
  0.00274343 -0.00062142  0.00152666
RMSU=        0.0523778           RMSV=      0.0390724
  0.00226884 -0.00050062  0.00116366
-----------------------------------------------------
RMSU=        0.0476323           RMSV=      0.0341124
  0.00445006 -0.00099618  0.00174068
RMSU=        0.0667087           RMSV=      0.0417215
  0.00396631 -0.00087808  0.00141105
RMSU=        0.0629787           RMSV=      0.0375639
  0.00383627 -0.00087333  0.00129948
-----------------------------------------------------
RMSU=        0.0619376           RMSV=      0.0360483
  0.00194781 -0.00053479  0.00129311
RMSU=        0.0441340           RMSV=      0.0359599
  0.00157775 -0.00047313  0.00110200
RMSU=        0.0397209           RMSV=      0.0331964
  0.00126379 -0.00036084  0.00086934
```

RMSU=	0.0355499	RMSV=	0.0294846
0.00355517	-0.00084334	0.00147263	
RMSU=	0.0596253	RMSV=	0.0383749
0.00410319	-0.00107349	0.00194460	
RMSU=	0.0640561	RMSV=	0.0440976
0.00269462	-0.00077734	0.00129174	
RMSU=	0.0519097	RMSV=	0.0359407
0.00701940	-0.00195138	0.00535119	
RMSU=	0.0837818	RMSV=	0.0731518
0.00500245	-0.00121309	0.00211114	
RMSU=	0.0707290	RMSV=	0.0459471
0.00501813	-0.00126933	0.00232989	
RMSU=	0.0708387	RMSV=	0.0482690
0.00659145	-0.00167225	0.00331253	
RMSU=	0.0811878	RMSV=	0.0575546
0.00634509	-0.00163595	0.00314783	
RMSU=	0.0796561	RMSV=	0.0561055
0.00620056	-0.00160013	0.00281[illegible]	
RMSU=	0.0787436	RMSV=	0.0530943
0.00540960	-0.00137275	0.00254441	
RMSU=	0.0735500	RMSV=	0.0504421
0.00455519	-0.00115975	0.00219832	
RMSU=	0.0674922	RMSV=	0.0468863
0.00357663	-0.00092534	0.00161948	
RMSU=	0.0598049	RMSV=	0.0402428
0.01130686	-0.00293241	0.00513319	
RMSU=	0.1063337	RMSV=	0.0716463
0.00967871	-0.00238916	0.00403085	
RMSU=	0.0983804	RMSV=	0.0634890
0.00477529	-0.00151074	0.00225299	
RMSU=	0.0691035	RMSV=	0.0474657
0.00350364	-0.00096682	0.00163626	
RMSU=	0.0591915	RMSV=	0.0404507
0.00270131	-0.00074532	0.00132256	
RMSU=	0.0519742	RMSV=	0.0363670
0.00174763	-0.00054103	0.00109837	
RMSU=	0.0418047	RMSV=	0.0331417
0.00357663	-0.00092534	0.00161948	
RMSU=	0.0598049	RMSV=	0.0402428
0.00277388	-0.00073777	0.00124747	
RMSU=	0.0526676	RMSV=	0.0353195
0.00257630	-0.00064487	0.00106306	
RMSU=	0.0507573	RMSV=	0.0326046
0.00275180	-0.00064382	0.00107648	
RMSU=	0.0524576	RMSV=	0.0328098
0.00197831	-0.00057957	0.00107343	
RMSU=	0.0444782	RMSV=	0.0327632
0.00174763	-0.00054103	0.00109837	
RMSU=	0.0418047	RMSV=	0.0331417
0.00156822	-0.00050755	0.00117188	
RMSU=	0.0396008	RMSV=	0.0342327
0.00130373	-0.00040610	0.00103272	
RMSU=	0.0361072	RMSV=	0.0321359
0.00634509	-0.00163595	0.00314783	
RMSU=	0.0796561	RMSV=	0.0561055
0.00673583	-0.00176542	0.00298338	
RMSU=	0.0820721	RMSV=	0.0546203
0.01003233	-0.00261400	0.00456103	
RMSU=	0.1001615	RMSV=	0.0675354
0.00967871	-0.00238916	0.00403085	

```
RMSU=        0.[illegible]                RMSV=        0.0634[illegible]
   0.00859470 -0.00205787   0.0031[illegible]685
RMSU=        0.0927130                   RMSV=        0.0562748
   0.00401333 -0.00125356   0.00188929
RMSU=        0.0633509                   RMSV=        0.0434659
   0.00623100 -0.00161280   0.00288315
------------------------------------------------------------------
RMSU=        0.0789367                   RMSV=        0.0538344
   0.00650600 -0.00160767   0.00270990
RMSU=        0.0806598                   RMSV=        0.0520567
   0.00727271 -0.00176804   0.00283374
RMSU=        0.0852902                   RMSV=        0.0532329
   0.00471274 -0.00144949   0.00217373
------------------------------------------------------------------
RMSU=        0.0679172                   RMSV=        0.0466232
   0.00332833 -0.00106230   0.00177722
RMSU=        0.0576916                   RMSV=        0.0421571
   0.00292400 -0.00083960   0.00140080
RMSU=        0.0540740                   RMSV=        0.0374273
   0.00540867 -0.00136352   0.00245234
------------------------------------------------------------------
RMSU=        0.0735437                   RMSV=        0.0495211
   0.00534622 -0.00137153   0.00291372
RMSU=        0.0731179                   RMSV=        0.0540252
   0.00507506 -0.00117040   0.00205683
RMSU=        0.0712395                   RMSV=        0.0453522
   0.00350364 -0.00096682   0.00163626
------------------------------------------------------------------
RMSU=        0.0591915                   RMSV=        0.0404507
   0.00249520 -0.00068430   0.00122077
RMSU=        0.0499520                   RMSV=        0.0349396
   0.00165800 -0.00049988   0.00096500
RMSU=        0.0407186                   RMSV=        0.0310644
   0.00466065 -0.00119359   0.00225058
------------------------------------------------------------------
RMSU=        0.0682690                   RMSV=        0.0474403
   0.00349691 -0.00101355   0.00175595
RMSU=        0.0591346                   RMSV=        0.0419041
   0.00340790 -0.00092737   0.00171871
RMSU=        0.0583772                   RMSV=        0.0414573
   0.00270131 -0.00074532   0.00132256
------------------------------------------------------------------
RMSU=        0.0519742                   RMSV=        0.0363670
   0.00197485 -0.00059924   0.00123926
RMSU=        0.0444393                   RMSV=        0.0352031
   0.00134032 -0.00044462   0.00107275
RMSU=        0.0366103                   RMSV=        0.0327529
   0.00311382 -0.00079386   0.00149618
------------------------------------------------------------------
RMSU=        0.0558816                   RMSV=        0.0386805
   0.00376098 -0.00090118   0.00158102
RMSU=        0.0613268                   RMSV=        0.0397621
   0.00409791 -0.00098725   0.00187481
RMSU=        0.0640149                   RMSV=        0.0432990
   0.00460562 -0.00109863   0.00203158
------------------------------------------------------------------
RMSU=        0.0678647                   RMSV=        0.0450730
   0.00279981 -0.00073362   0.00143279
RMSU=        0.0529132                   RMSV=        0.0378522
   0.00327156 -0.00088777   0.00154899
RMSU=        0.0571975                   RMSV=        0.0393573
   0.00357261 -0.00088529   0.00161673
------------------------------------------------------------------
RMSU=        0.0597713                   RMSV=        0.0402086
   0.00401504 -0.00101017   0.00188789
RMSU=        0.0633643                   RMSV=        0.0434498
   0.00448185 -0.00113686   0.00210654
RMSU=        0.0669466                   RMSV=        0.0458971
   0.00280410 -0.00076555   0.00121359
------------------------------------------------------------------
```

RMSU=	0.0527538	RMSV=	0.0348766
0.00126379	-0.00036084	[illegible]	
RMSU=	0.0355499	RMSV=	0.0294846
0.00141491	-0.00041702	0.00098808	
RMSU=	0.0376153	RMSV=	0.0314338
0.00155690	-0.00045188	0.00110056	
RMSU=	0.0394576	RMSV=	0.0331747
0.00174763	-0.00054103	0.00109837	
RMSU=	0.0418047	RMSV=	0.0331417
0.00189393	-0.00059253	0.00120860	
RMSU=	0.0435194	RMSV=	0.0347649
0.00206993	-0.00064338	0.00127105	
RMSU=	0.0454965	RMSV=	0.0356517

```
      DIMENSION I(200),J(200),K(200),L(200),M(200),N(200)
      DIMENSION PSI(450),X(450),Y(450),XL(450),YL(450),XO(30),YO(30)
      DIMENSION LL(6),MM(6),C(6,6),H(6,6,200),W(750),BO(350)
      DIMENSION B(330,45),XS(200),YS(200),XY(200),AREA(200)
      DIMENSION CM(3,3),LC(3),MC(3),BB(200),CC(200),BPC(3,3,200),Z(200)
      DIMENSION VOR(200),ALPHA(6,200),XG(200),YG(200),U(200),V(200)
      DIMENSION F(200),IV(200),JV(200),KV(200),XV(120),YV(120),R(80)
      DIMENSION XLV(120),YLV(120),XSV(200),YSV(200),XYV(200),AV(200)
      DIMENSION BV(200),CV(200),G(200),A(75,11),DW(120),LZ(80),MZ(80)
      DIMENSION P(3,3,200),VORA(200),BOV(80),WA(80),YB(200),COM(200)
      DIMENSION CF(200),AVT(200)
      READ 1,NE,NN,NNT,NNV,NNTV
    1 FORMAT (5X,5I5)
      READ 2,(I(IE),J(IE),K(IE),L(IE),M(IE),N(IE),IV(IE),JV(IE),KV(IE),
     2IE=1,NE)
    2 FORMAT (5X,9I5)
      READ 3,(PSI(IN),X(IN),Y(IN),IN=1,NNT)
    3 FORMAT (5X,3F10.5)
      READ 5,(XV(IN),YV(IN),IN=1,NNTV)
    5 FORMAT (2F10.5)
      READ 6,(YB(IE),IE=1,NE)
    6 FORMAT (12F6.3)
      READ 9,(XO(IN),YO(IN),IN=1,30)
    9 FORMAT (2F10.5)
      READ 8,OMEGA,EPS,DT,EPSV
    8 FORMAT (7X,4F13.8)
      PRINT 701,NE,NN,NNT,NNV,NNTV
  701 FORMAT (7X,5I5)
      PRINT 702,(I(IE),J(IE),K(IE),L(IE),M(IE),N(IE),IV(IE),JV(IE),
     5KV(IE),IE=1,NE)
  702 FORMAT (7X,9I5)
      PRINT 703,(PSI(IN),X(IN),Y(IN),IN=1,NNT)
  703 FORMAT (7X,3F10.5)
      PRINT 704,(XV(IN),YV(IN),IN=1,NNTV)
  704 FORMAT (7X,2F10.5)
      PRINT705,(YB(IE),IE=1,NE)
  705 FORMAT (7X,12F5.3)
      PRINT 706,(XO(IN),YO(IN),IN=1,30)
  706 FORMAT (7X,2F10.5)
      PRINT8,OMEGA,EPS,DT,EPSV
      DO 16 IE=1,NE
   16 VORA(IE)=0.0
      DO 17 IN=1,NNTV
   17 DW(IN)=0.0
      KT=1
      ISUB=1
  901 CONTINUE
      DO 41 IE=1,NE
      DO 41 IO=1,6
   41 ALPHA(IO,IE)=0.0
      IE=1
   13 IR=I(IE)
      JR=J(IE)
      KR=K(IE)
      LR=L(IE)
      MR=M(IE)
      NR=N(IE)
```

```
      XG(IE)=(X(IR)+X(MR)+X(KF))/?.
      YG(IE)=(Y(IR)+Y(MR)+Y(KR))/?.
      XL(IR)=(X(IR)-XG(IE))/12.
      XL(JR)=(X(JR)-XG(IE))/12.
      XL(KR)=(X(KR)-XG(IE))/12.
      XL(LR)=(X(LR)-XG(IE))/12.
      XL(MR)=(X(MR)-XG(IE))/12.
      XL(NR)=(X(NR)-XG(IE))/12.
      YL(IR)=(Y(IR)-YG(IE))/12.
      YL(JR)=(Y(JR)-YG(IE))/12.
      YL(KR)=(Y(KR)-YG(IE))/12.
      YL(LR)=(Y(LR)-YG(IE))/12.
      YL(MR)=(Y(MR)-YG(IE))/12.
      YL(NR)=(Y(NR)-YG(IE))/12.
      C(1,1)=1.
      C(1,2)=XL(IR)
      C(1,3)=YL(IR)
      C(1,4)=XL(IR)*XL(IR)
      C(1,5)=XL(IR)*YL(IR)
      C(1,6)=YL(IR)*YL(IR)
      C(2,1)=1.
      C(2,2)=XL(JR)
      C(2,3)=YL(JR)
      C(2,4)=XL(JR)*XL(JR)
      C(2,5)=XL(JR)*YL(JR)
      C(2,6)=YL(JR)*YL(JR)
      C(3,1)=1.
      C(3,2)=XL(KR)
      C(3,3)=YL(KR)
      C(3,4)=XL(KR)*XL(KR)
      C(3,5)=XL(KR)*YL(KR)
      C(3,6)=YL(KR)*YL(KR)
      C(4,1)=1.
      C(4,2)=XL(LR)
      C(4,3)=YL(LR)
      C(4,4)=XL(LR)*XL(LR)
      C(4,5)=XL(LR)*YL(LR)
      C(4,6)=YL(LR)*YL(LR)
      C(5,1)=1.
      C(5,2)=XL(MR)
      C(5,3)=YL(MR)
      C(5,4)=XL(MR)*XL(MR)
      C(5,5)=XL(MR)*YL(MR)
      C(5,6)=YL(MR)*YL(MR)
      C(6,1)=1.
      C(6,2)=XL(NR)
      C(6,3)=YL(NR)
      C(6,4)=XL(NR)*XL(NR)
      C(6,5)=XL(NR)*YL(NR)
      C(6,6)=YL(NR)*YL(NR)
      CALL MINV (C,6,D,LL,MM)
      CF(IE)=C(1,1)+C(1,2)+C(1,3)+C(1,4)+C(1,5)+C(1,6)
      DO 52 IO=1,6
      JO=1
   51 CONTINUE
      GO TO (43,44,45,46,47,48),JO
   43 IR=IR
      GO TO 42
   44 IR=JR
      GO TO 42
```

```
   45 IR=KR
      GO TO 42
   46 IR=LR
      GO TO 42
   47 IR=MR
      GO TO 42
   48 IR=NR
   42 ALPHA(IO,IE)=ALPHA(IO,IE)+C(IO,JO)*PSI(IR)
      JO=JO+1
      IF(JO-6) 51,51,52
   52 CONTINUE
      U(IE)=ALPHA(?,IE)
      V(IE)=-ALPHA(2,IE)
      IF(KT-1) 40,1000,41
 1000 AREA(IE)=(X(IR)*(Y(KR)-Y(MR))+X(KR)*(Y(MR)-Y(IR))+X(MR)*(Y(IR)-
     4Y(KR)))/144.
      XS(IE)=XL(IR)*XL(IR)+XL(KR)*XL(KR)+XL(MR)*XL(MR)
      YS(IE)=YL(IR)*YL(IR)+YL(KR)*YL(KR)+YL(MR)*YL(MR)
      XY(IE)=XL(IR)*YL(IR)+XL(KR)*YL(KR)+XL(MR)*YL(MR)
      MO=1
      IRT=1
      IST=1
    7 ANM=AREA(IE)*(C(2,IRT)*C(2,IST)+(1./3.)*XS(IE)
     5*C(4,IRT)*C(4,IST)+(1./12.)*YS(IE)*C(5,IRT)*C(5,IST)+(1./6.)
     5*XY(IE)*(C(3,IRT)*C(4,IST)+C(4,IRT)*C(5,IST)))
      AMM=AREA(IE)*(C(3,IRT)*C(3,IST)+(1./12.)*XS(IE)*
     8C(5,IRT)*C(5,IST)+(1./3.)*YS(IE)*C(6,IRT)*C(6,IST)
     8+(1./6.)*XY(IE)*(C(6,IRT)*C(5,IST)+C(5,IRT)*C(6,IST)))
      H(IRT,IST,IE)=ANM+AMM
      GO TO (20,21,22,23,24,25,26,27,28,29,30,31,32,33,34,35,36,37,38
     2,39,40),MO
   20 IST=2
      GO TO 15
   15 MO=MO+1
      GO TO 7
   21 H(IST,IRT,IE)=H(IRT,IST,IE)
      IST=3
      GO TO 15
   22 H(IST,IRT,IE)=H(IRT,IST,IE)
      IST=4
      GO TO 15
   23 H(IST,IRT,IE)=H(IRT,IST,IE)
      IST=5
      GO TO 15
   24 H(IST,IRT,IE)=H(IRT,IST,IE)
      IST=6
      GO TO 15
   25 H(IST,IRT,IE)=H(IRT,IST,IE)
      IST=2
      IRT=2
      GO TO 15
   26 IST=3
      GO TO 15
   27 H(IST,IRT,IE)=H(IRT,IST,IE)
      IST=4
      GO TO 15
   28 H(IST,IRT,IE)=H(IRT,IST,IE)
      IST=5
      GO TO 15
   29 H(IST,IRT,IE)=H(IRT,IST,IE)
```

```
      IST=6
      GO TO 15
   30 H(IST,IRT,IE)=H(IRT,IST,IE)
      IST=3
      IRT=3
      GO TO 15
   31 IST=4
      GO TO 15
   32 H(IST,IRT,IE)=H(IRT,IST,IE)
      IST=5
      GO TO 15
   33 H(IST,IRT,IE)=H(IRT,IST,IE)
      IST=6
      GO TO 15
   34 H(IST,IRT,IE)=H(IRT,IST,IE)
      IST=4
      IRT=4
      GO TO 15
   35 IST=5
      GO TO 15
   36 H(IST,IRT,IE)=H(IRT,IST,IE)
      IST=6
      GO TO 15
   37 H(IST,IRT,IE)=H(IRT,IST,IE)
      IST=5
      IRT=5
      GO TO 15
   38 IST=6
      GO TO 15
   39 H(IST,IRT,IE)=H(IRT,IST,IE)
      IST=6
      IRT=6
      GO TO 15
   40 CONTINUE
      IE=IE+1
      IF(IE-NE) 13,13,14
   14 CONTINUE
      DO 54 IE=1,NE
   54 F(IE)=VORA(IE)*AREA(IE)*CF(IE)
C     ASSEMBLE EQUATIONS
      DO 190 IP=1,NN
      W(IP)=0.0
      DO 190 JJ=1,45
  190 B(IP,JJ)=0.0
      IP=1
  195 IE=1
  200 IF(I(IE)-IP) 201,202,201
  201 IF(J(IE)-IP) 203,204,203
  203 IF(K(IE)-IP) 205,206,205
  205 IF(L(IE)-IP) 207,208,207
  207 IF(M(IE)-IP) 209,210,209
  209 IF(N(IE)-IP) 211,212,211
  211 IE=IE+1
      IF(IE-NE) 213,213,214
  213 GO TO 200
  202 IP=I(IE)
      IRT=1
      IST=1
      JP=J(IE)
      KP=K(IE)
```

```
      LR=L(IE)
      MR=M(IE)
      NR=N(IE)
      GO TO 215
  204 IR=J(IE)
      IRT=2
      IST=2
      JR=K(IE)
      KR=L(IE)
      LR=M(IE)
      MR=N(IE)
      NR=I(IE)
      GO TO 215
  206 IR=K(IE)
      IRT=3
      IST=3
      JR=L(IE)
      KR=M(IE)
      LR=N(IE)
      MR=I(IE)
      NR=J(IE)
      GO TO 215
  208 IR=L(IE)
      IRT=4
      IST=4
      JR=M(IE)
      KR=N(IE)
      LR=I(IE)
      MR=J(IE)
      NR=K(IE)
      GO TO 215
  210 IR=M(IE)
      IRT=5
      IST=5
      JR=N(IE)
      KR=I(IE)
      LR=J(IE)
      MR=K(IE)
      NR=L(IE)
      GO TO 215
  212 IR=N(IE)
      IRT=6
      IST=6
      JR=I(IE)
      KR=J(IE)
      LR=K(IE)
      MR=L(IE)
      NR=M(IE)
  215 W(IR)=-F(IE)+W(IR)
      MX=1
  220 JJ=23+IR-IR
      B(IR,JJ)=B(IR,JJ)+H(IRT,IST,IE)
      GO TO (221,222,223,224,225,226),MX
  221 IR=JR
  230 MX=MX+1
      IST=IST+1
      IF(IST-6) 231,231,232
  232 IST=1
  231 IF(IR-NN) 225,220,240
  240 W(IR)=W(IR)-H(IRT,IST,IE)*PSI(IR)
```

```
      GO TO (221,222,223,224,225,226),MX
  222 IR=KR
      GO TO 230
  223 IR=LR
      GO TO 230
  224 IR=MR
      GO TO 230
  225 IR=NR
      GO TO 230
  226 IF(IE-NE) 211,214,214
  214 IF(IR-NN) 241,242,242
  241 IR=IR+1
      GO TO 195
  242 CONTINUE
C     SOLVE FOR PSI(IN)
      ITER=1
 1001 DO 300 IN=1,NN
  300 BO(IN)=OMEGA/B(IN,23)
      BIT=(1.-OMEGA)
  301 ITER=ITER+1
      PRINT 90,ITER
   90 FORMAT (7X,I3)
   70 CONTINUE
      DI=0.0
      IN=1
  302 EX=0.0
      IT=1
      IF(W(IN)-0.0) 303,304,303
  303 EX=W(IN)
  304 CONTINUE
  260 IF(IT-23) 305,307,305
  305 ID=IN-23+IT
      IF(ID) 307,307,360
  360 IF(ID-NN) 361,361,308
  361 IF(B(IN,IT)-0.0) 362,363,362
  362 EX=EX-B(IN,IT)*PSI(ID)
  363 IF(IT-45) 307,308,308
  307 IT=IT+1
      GO TO 260
  308 EX=BO(IN)*EX+BIT*PSI(IN)
      IF(ABS(PSI(IN)-EX)-DI) 320,320,321
  321 DI=ABS(PSI(IN)-EX)
  320 PSI(IN)=EX
  370 IF(IN-NN) 330,331,331
  330 IN=IN+1
      GO TO 302
  331 IF(DI-EPS) 340,340,301
  340 PRINT 350,(PSI(IN),IN=1,NN)
  350 FORMAT (7X,6F10.6/7X,5F10.6)
      IF(KT-1) 830,830,831
  830 CONTINUE
      DO 57 IN=1,96
   57 VOR(IN)=0.0
  831 CONTINUE
      VOR(97)=12.*U(1)/(YG(1)-YB(1))
      DO 56 IN=1,15
      IM=IN+97
      IS=12*IN-10
      VOR(IM)=12.*U(IS)/(YG(IS)-YB(IS))
   56 CONTINUE
```

```
400 IE=1
401 IZ=IV(IE)
    JZ=JV(IE)
    KZ=KV(IE)
    VORA(IE)=(VOR(IZ)+VOR(JZ)+VOR(KZ))/3.
    XLV(IZ)=(XV(IZ)-XG(IE))/12.
    XLV(JZ)=(XV(JZ)-XG(IE))/12.
    XLV(KZ)=(XV(KZ)-XG(IE))/12.
    YLV(IZ)=(YV(IZ)-YG(IE))/12.
    YLV(JZ)=(YV(JZ)-YG(IE))/12.
    YLV(KZ)=(YV(KZ)-YG(IE))/12.
    CM(1,1)=1.
    CM(1,2)=XLV(IZ)
    CM(1,3)=YLV(IZ)
    CM(2,1)=1.
    CM(2,2)=XLV(JZ)
    CM(2,3)=YLV(JZ)
    CM(3,1)=1.
    CM(3,2)=XLV(KZ)
    CM(3,3)=YLV(KZ)
    CALL MINV (CM,3,D,LC,MC)
    BB(IE)=CM(2,1)*VOR(IZ)+CM(2,2)*VOR(JZ)+CM(2,3)*VOR(KZ)
    CC(IE)=CM(3,1)*VOR(IZ)+CM(3,2)*VOR(JZ)+CM(3,3)*VOR(KZ)
    AV(IZ)=XLV(JZ)*YLV(KZ)-XLV(KZ)*YLV(JZ)
    AV(JZ)=XLV(KZ)*YLV(IZ)-XLV(IZ)*YLV(KZ)
    AV(KZ)=XLV(IZ)*YLV(JZ)-XLV(JZ)*YLV(IZ)
    BV(IZ)=YLV(JZ)-YLV(KZ)
    BV(JZ)=YLV(KZ)-YLV(IZ)
    BV(KZ)=YLV(IZ)-YLV(JZ)
    CV(IZ)=XLV(KZ)-XLV(JZ)
    CV(JZ)=XLV(IZ)-XLV(KZ)
    CV(KZ)=XLV(JZ)-XLV(IZ)
    AVT(IE)=AV(IZ)+AV(JZ)+AV(KZ)
    IF (KT-1) 2250,2250,410
2250 CONTINUE
    Z(IE)=YG(IE)-YB(IE)
    CON(IE)=1./((.00105*Z(IE)*(1.-Z(IE)/9.))+.0000106)
    XSV(IE)=XLV(IZ)*XLV(IZ)+XLV(JZ)*XLV(JZ)+XLV(KZ)*XLV(KZ)
    YSV(IE)=YLV(IZ)*YLV(IZ)+YLV(JZ)*YLV(JZ)+YLV(KZ)*YLV(KZ)
    XYV(IE)=XLV(IZ)*YLV(IZ)+XLV(JZ)*YLV(JZ)+XLV(KZ)*YLV(KZ)
    MY=1
    IZ=IV(IE)
    IY=IV(IE)
    IZT=1
    IYT=1
402 BPC(IZT,IYT,IE)=(BV(IZ)*BV(IY)+CV(IZ)*CV(IY))/(4.*AREA(IE))
    P(IZT,IYT,IE)=CON(IE)*(AV(IZ)*AV(IY)+(1./12.)*XSV(IE)*BV(IZ)
   5*BV(IY)+(1./12.)*YSV(IE)*CV(IZ)*CV(IY)+(1./12.)*XYV(IE)*BV(IZ)
   5*CV(IY))/(4.*AREA(IE))
    GO TO (405,406,407,408,409,410),MY
405 IY=JV(IE)
    IYT=2
    GO TO 403
403 MY=MY+1
    GO TO 402
406 BPC(IYT,IZT,IE)=BPC(IZT,IYT,IE)
    P(IYT,IZT,IE)=P(IZT,IYT,IE)
    IY=KV(IE)
    IYT=3
    GO TO 403
```

```
  407 RPC(IYT,IZT,IF) [illegible](IZT,IYT,IF)
      P(IYT,I[illegible]T,I[illegible]) [illegible](I[illegible],IYT,I[illegible])
      IY=JV(I[illegible])
      IZ=JV(I[illegible])
      IYT=[illegible]
      IZT=[illegible]
      GO TO 4[illegible]
  40[illegible] IY=KV(I[illegible])
      IYT=[illegible]
      GO TO 4[illegible]
  4[illegible] RPC(IYT,IZT,I[illegible])[illegible](IZT,IYT,I[illegible])
      P(IYT,IZT,I[illegible])=P(IZT,IYT,I[illegible])
      IZ=KV(I[illegible])
      IZT=3
      GO TO 40[illegible]
  41[illegible] IF=IF+1
      IF(IF-[illegible]) 4[illegible],4[illegible],411
  411 CONTINUE
      DO 415 IF=1,[illegible]
  415 Q(IF)=C(N(I[illegible])[illegible](U(I[illegible])*BB(IF)+V(IF)*CC(IF)))*AVT(IF)/[illegible].
  750 DO 417 IN=1,NNV
      P(IN)=0.0
      DO 417 JJ=1,11
  417 A(IN,JJ)=0.0
      IN=1
  418 IF=1
  419 IF(IV(IF)-I[illegible]) 4[illegible],4[illegible],4[illegible]
  42[illegible] IF(JV(I[illegible])-I[illegible]) 4[illegible],4[illegible],4[illegible]
  422 IF(KV(I[illegible])-I[illegible]) 4[illegible],4[illegible],4[illegible]
  424 IF=I[illegible]+1
      IF(I[illegible]-[illegible]) 4[illegible],[illegible],[illegible]
  4[illegible] GO TO 4[illegible]
  4[illegible] IZ=IV(I[illegible])
      IYT=1
      IZT=1
      JZ=JV(I[illegible])
      KZ=KV(I[illegible])
      GO TO [illegible]
  4[illegible] IZ=JV(I[illegible])
      IYT=[illegible]
      IZT=2
      JZ=KV(I[illegible])
      KZ=IV(I[illegible])
      GO TO 44[illegible]
  42[illegible] IZ=KV(IF)
      IYT=3
      IZT=3
      JZ=IV(I[illegible])
      KZ=JV(I[illegible])
  44[illegible] P(IN)=P(IN)+[illegible](IN)
      NX=1
  5[illegible] JJ=[illegible]+IZ-IN
      IF(KT-1) 4[illegible],4[illegible],4[illegible]
  4[illegible]1 A(IN,JJ)=A(IN,JJ)-P(IYT,IZT,IF)
      GO TO 4[illegible]
  47[illegible] A(IN,JJ)=A(IN,JJ)+RPC(IYT,IZT,I[illegible])+(2./DT)*P(IYT,IZT,IF)
  4[illegible] GO TO (44[illegible],44[illegible],4[illegible]),NX
  442 IZ=JZ
  445 NX=NX+1
      IZT=IZT+1
```

```
      IF(IZT-[illegible]) [illegible]
 [illegible] IZT=1
 [illegible] IF([illegible]) [illegible]
 [illegible] IF (IZ-NNV) [illegible],448
 401 IF (IZ-NNV) [illegible],472
 448 R(IN)=R(IN)+P(IYT,IZT,IE)*[illegible](IZ)+[illegible](IYT,IZT,I[illegible])*VO[illegible](IZ)
      GO TO [illegible]
 472 R(IN)=R(IN)-([illegible](IYT,IZT,IE)+([illegible]/DT)*[illegible](IYT,I[illegible]T,I[illegible]))*V[illegible](IZ)
     3+(P(IYT,IZT,I[illegible]))*(([illegible]/DT)*V[illegible](IZ)+DA(IZ))
 4[illegible] GO TO (442,44[illegible],4[illegible]),NX
 443 IZ=KZ
      GO TO 44[illegible]
 44[illegible] IF(I[illegible]-[illegible]) [illegible]
 4[illegible] IF(IN-[illegible]V) [illegible]
 4[illegible] IN=IN+1
      GO TO 41[illegible]
 45[illegible] CONTINUE
 905 ITER=1
      DO 91[illegible] IN=1,NNV
 91[illegible] [illegible]V(IN)=[illegible](I[illegible])
      DITV=1.-[illegible]
 9[illegible]7 ITER=ITER+1
      PRINT 9[illegible],IT[illegible]
      IF(ITE[illegible]-1[illegible]) [illegible]1,[illegible]1,9[illegible]
 [illegible]11 CONTINUE
      DIV=[illegible]
      IF(K1-1) [illegible]
 4[illegible] DO [illegible] IN=1,NNV
 5[illegible] [illegible](IN)=[illegible](IN)
      GO TO [illegible]
 4[illegible] DO [illegible] IN=1,NNV
 [illegible] [illegible](IN)=V[illegible](I[illegible])
 [illegible] IN=1
 [illegible] EXV=[illegible]
      IT=1
      IF ([illegible](I[illegible])-[illegible]) [illegible]14
 914 EXV=[illegible](IN)
 915 CONTINUE
 91[illegible] IF (IT-[illegible]) [illegible]
 917 IDV=IN-[illegible]+IT
      IF(IDV) [illegible]
 92[illegible] IF (IDV-N[illegible]V) [illegible]
 921 IF (A(I[illegible],IT)-[illegible]) [illegible]
 9[illegible]1 EXV=EXV-A(I[illegible],IT)*[illegible](I[illegible]V)
 9[illegible]2 IF (IT-1[illegible]) [illegible]
 918 IT=IT+1
      GO TO [illegible]
 9[illegible] EXV=[illegible]V(IN)[illegible]
      IF (A[illegible]([illegible](IN)-[illegible])-[illegible]V) [illegible]
 [illegible]41 DIV=ABS([illegible](IN)-[illegible]XV)
      IF(KT-1) [illegible]
 1025 [illegible](IN)=[illegible](I[illegible])+([illegible]V-[illegible](IN))[illegible]/DT
 [illegible] [illegible](IN)=[illegible]XV
 [illegible] IF (IN-NNV) [illegible]
 [illegible] IN=IN+1
      GO TO [illegible]
 [illegible]3 IF(DIV-[illegible]V) [illegible]
 9[illegible] PRINT [illegible]1,([illegible](IN),IN=1,NNV)
 [illegible]1 FORMAT ([illegible]X,[illegible])
      IF(KT-1) [illegible]
```

```
  961 DO 962 IN=1,NNV
  962 DX(IN)=WW(IN)
      KT=KT+1
      GO TO 750
  960 DO 963 IN=1,NNV
  963 VDP(IN)=WW(IN)
      PRINT 951,(DX(IN),IN=1,NNV)
      ISUB=ISUB+1
      IF (ISUB-9) 901,901,902
  902 PRINT 810,(U(IE),IE=1,NE)
      PRINT 810,(V(IE),IE=1,NE)
      PRINT 810,(XG(IE),IE=1,NE)
      PRINT 810,(YG(IE),IE=1,NE)
  810 FORMAT (7X,6F11.6/7X,6F11.6)
      PRINT 820,(CON(IE),IE=1,NE)
  820 FORMAT (7X,6F11.4/7X,6F11.4)
      DO 850 IN=1,30
      IE=2*IN+60
      U(IE)=ALPHA(3,IE)+ALPHA(5,IE)*(XG(IN)-XG(IE))/12.
     5+2.*ALPHA(6,IE)*(YG(IN)-YG(IE))/12.
      PRINT 840,U(IE)
  840 FORMAT (7X,F12.8)
  850 CONTINUE
      STOP
      END
```

Input-Data of the Turbulent and Laminar Models:

180	332	403	75	112				
373	374	375	1	371	372	97	98	96
371	1	375	12	13	2	96	96	1
371	2	13	3	369	370	96	1	95
369	3	13	14	15	4	95	1	2
369	4	15	5	367	368	95	2	94
367	5	15	16	17	6	94	2	3
367	6	17	7	365	366	94	3	93
365	7	17	18	19	8	93	3	4
365	8	19	9	363	364	93	4	92
363	9	19	20	21	10	92	4	5
363	10	21	11	361	362	92	5	91
361	11	21	22	359	360	91	5	90
375	376	377	23	13	12	98	99	1
13	23	377	34	35	24	1	99	6
13	24	35	25	15	14	1	6	2
15	25	35	36	37	26	2	6	7
15	26	37	27	17	16	2	7	3
17	27	37	38	39	28	3	7	8
17	28	39	29	19	18	3	8	4
19	29	39	40	41	30	4	8	9
19	30	41	31	21	20	4	9	5
21	31	41	42	43	32	5	9	10
21	32	43	33	359	22	5	10	90
359	33	43	44	357	358	90	10	89
377	378	379	45	35	34	99	100	6
35	45	379	56	57	46	6	100	11
35	46	57	47	37	36	6	11	7
37	47	57	58	59	48	7	11	12
37	48	59	49	39	38	7	12	8
39	49	59	60	61	50	8	12	13
39	50	61	51	41	40	8	13	9
41	51	61	62	63	52	9	13	14
41	52	63	53	43	42	9	14	10
43	53	63	64	65	54	10	14	15
43	54	65	55	357	44	10	15	89
357	55	65	66	355	356	89	15	88
379	380	381	67	57	56	100	101	11
57	67	381	78	79	68	11	101	16
57	68	79	69	59	58	11	15	12
59	69	79	80	81	70	12	16	17
59	70	81	71	61	60	12	17	13
61	71	81	82	83	72	13	17	18
61	72	83	73	63	62	13	18	14
63	73	83	84	85	74	14	18	19
63	74	85	75	65	64	14	19	15
65	75	85	86	87	76	15	19	20
65	76	87	77	355	66	15	20	88
355	77	87	88	353	354	88	20	87
381	382	383	89	79	78	101	102	16
79	89	383	100	101	90	16	102	21
79	90	101	91	81	80	16	21	17
81	91	101	102	103	92	17	21	22
81	92	103	93	83	82	17	22	18
83	93	103	104	105	94	18	22	23
83	94	105	95	85	84	18	22	19
85	95	105	106	107	96	19	23	24

35	96	127	97	87	86	19	24	22
97	97	107	108	109	13	20	24	25
87	[illegible]	109	[illegible]	353	88	20	25	27
353	99	109	110	351	352	87	25	86
383	384	335	111	101	100	102	103	21
101	111	385	122	123	112	21	103	26
101	112	123	113	103	102	21	26	22
103	113	123	124	125	114	22	26	27
103	114	125	115	105	104	22	27	23
105	115	125	126	127	116	23	27	[illegible]
105	116	127	117	107	106	23	28	24
107	117	127	128	129	118	24	28	[illegible]
107	118	129	119	109	108	24	29	25
109	119	129	130	131	120	25	29	30
109	120	131	121	351	110	25	30	85
351	121	131	132	349	350	86	30	85
335	386	387	133	123	122	102	104	26
123	133	387	144	145	134	26	104	31
123	134	145	135	125	124	26	31	27
125	135	145	146	147	136	27	31	32
125	136	147	137	127	126	27	32	28
127	137	147	148	149	138	28	32	33
127	138	149	139	129	128	28	33	29
129	139	149	150	151	140	29	33	34
129	140	151	141	131	130	29	34	30
131	141	151	152	153	142	30	34	35
131	142	153	143	349	132	30	35	85
349	143	153	154	347	348	85	35	84
387	388	389	155	145	144	104	105	31
145	155	389	166	167	156	31	105	36
145	156	167	157	147	146	31	36	32
147	157	167	168	169	158	32	36	37
147	158	169	159	149	148	32	37	33
149	159	169	170	171	160	33	37	38
149	160	171	161	151	150	33	38	34
151	161	171	172	173	162	34	38	39
151	162	173	163	153	152	34	39	35
153	163	173	174	175	164	35	39	40
153	164	175	165	347	154	35	40	84
347	165	175	176	345	346	84	40	83
389	390	391	177	167	166	105	106	36
167	177	391	188	189	178	36	106	41
167	178	189	179	169	168	36	41	37
169	179	189	190	191	180	37	41	42
169	180	191	181	171	170	37	42	38
171	181	191	192	193	182	38	42	43
171	182	193	183	173	172	38	43	39
173	183	193	194	195	184	39	43	44
173	184	195	185	175	174	39	44	40
175	185	195	196	197	186	40	44	45
175	186	197	187	345	176	40	45	83
345	187	197	198	343	344	83	45	82
391	392	393	199	189	188	106	107	41
189	199	393	210	211	200	41	107	46
189	200	211	201	191	190	41	46	42
191	201	211	212	213	202	42	46	47
191	202	213	203	193	192	42	47	43
193	203	213	214	215	204	43	47	48
193	204	215	205	195	194	43	48	44
195	205	215	216	217	206	44	48	40

196	206	217	207	197	196	44	49	45
197	207	217	218	219	198	45	49	50
197	208	[illegible]	209	340	198	45	50	[illegible]
343	209	219	220	341	342	82	50	31
393	394	395	221	211	210	107	106	46
211	221	395	232	233	222	46	106	51
211	222	233	223	213	212	46	51	47
213	223	233	234	235	224	47	51	52
213	224	235	225	215	214	47	52	48
215	225	235	236	237	226	48	52	53
215	226	237	227	217	216	48	53	49
217	227	237	238	239	228	49	53	54
217	228	239	229	219	218	49	54	50
219	229	239	240	241	230	50	54	55
219	230	341	231	341	220	50	55	31
341	231	241	242	339	340	81	55	80
395	396	397	243	233	232	108	109	51
233	243	397	254	255	244	51	109	56
233	244	255	245	235	234	51	56	52
235	245	255	256	257	246	52	56	57
235	246	257	247	237	236	52	57	53
237	247	257	258	259	248	53	57	58
237	248	259	249	239	238	53	58	54
239	249	259	260	261	250	54	58	59
239	250	261	251	241	240	54	59	55
241	251	261	262	263	252	55	59	60
241	252	263	253	339	242	55	60	80
339	253	263	264	337	338	80	60	79
397	398	399	265	255	254	109	110	56
255	265	399	276	277	266	56	110	61
255	266	277	267	257	256	56	61	57
257	267	277	278	279	268	57	61	62
257	268	279	269	259	258	57	62	58
259	269	279	280	281	270	58	62	63
259	270	281	271	261	260	58	63	59
261	271	281	282	283	272	59	63	64
261	272	283	273	263	262	59	64	60
263	273	283	284	285	274	60	64	65
263	274	285	275	337	264	60	65	79
337	275	285	286	335	336	79	65	78
399	400	401	287	277	276	110	111	61
277	287	401	298	299	238	61	111	66
277	288	299	289	279	278	61	66	62
279	289	299	300	301	290	62	66	67
279	290	301	291	281	280	62	67	63
281	291	301	302	303	292	63	67	68
281	292	303	293	283	282	63	68	64
283	293	303	304	305	294	64	68	69
283	294	305	295	285	284	64	69	65
285	295	305	306	307	296	65	69	70
285	296	307	297	335	286	65	70	78
335	297	307	308	333	334	78	70	77
401	402	403	309	299	298	111	112	66
299	309	403	320	321	310	66	112	71
299	310	321	311	301	300	66	71	67
301	311	321	322	323	312	67	71	72
301	312	323	313	303	302	67	72	68
303	313	323	324	325	314	68	72	73
303	314	325	315	305	304	68	73	69
305	315	325	326	327	316	69	73	74

305	316	327	317	307	306	69	74	70
307	317	327	328	320	318	70	74	75
307	318	329	319	332	308	70	75	77
333	319	329	330	331	332	77	75	76

ψ_T	X	Y	ψ_L
.00468	.075	.175	.00003
.00936	.15	.2625	.0009
.0156	.15	.3625	.0027
.0218	.225	.475	.0059
.0312	.225	.625	.0096
.0406	.25	.775	.0137
.0563	.25	1.025	.025
.0717	.25	1.35	.037
.111	.25	1.975	.072
.15	.25	2.60	.117
.228	.25	3.85	.204
.00468	.225	.0675	.00003
.00936	.3	.175	.0009
.0156	.375	.2875	.0027
.0218	.45	.400	.0059
.0312	.475	.55	.0096
.0406	.50	.7	.0137
.0563	.50	1.025	.025
.0717	.5	1.35	.037
.111	.50	1.975	.072
.15	.5	2.60	.117
.229	.5	3.85	.204
.00468	.525	.12	.00003
.00936	.575	.20	.0009
.0156	.65	.3125	.0027
.0218	.70	.425	.0059
.0312	.725	.575	.0096
.0406	.75	.7125	.0137
.0563	.75	1.0375	.025
.0717	.75	1.35	.037
.111	.75	1.975	.072
.150	.75	2.60	.117
.229	.75	3.85	.204
.00468	.80	.145	.00003
.00936	.85	.225	.0009
.0156	.90	.3375	.0027
.0218	.95	.450	.0059
.0312	.975	.5875	.0096
.0406	1.0	.725	.0137
.0563	1.0	1.0375	.025
.0717	1.0	1.350	.037
.111	1.0	1.975	.072
.150	1.0	2.6	.117
.228	1.0	3.85	.204
.00468	1.1	.1625	.00003
.00936	1.1375	.2375	.0009
.0156	1.1875	.35	.0027
.0218	1.2125	.4625	.0059
.0312	1.2375	.60	.0096
.0406	1.25	.75	.0137
.0563	1.25	1.0625	.025
.0717	1.25	1.35	.037
.111	1.25	1.975	.072
.150	1.25	2.60	.117
.228	1.25	3.85	.204
.00468	1.3875	.175	.00003

.00936	1.425	[illegible]	.0009
.0156	1.45	[illegible]	.0027
.0218	1.475	.475	.0059
.0312	1.4275	.625	.0096
.0406	1.5	.775	.0137
.0563	1.5	1.0625	.025
.0717	1.5	1.35	.037
.111	1.5	1.975	.072
.150	1.5	2.6	.117
.228	1.5	3.85	.204
.00468	1.6875	.20	.00003
.00936	1.7	.275	.0009
.0156	1.725	.3875	.0027
.0218	1.7375	.500	.0059
.0312	1.75	.65	.0096
.0406	1.75	.7375	.0137
.0563	1.75	1.075	.025
.0717	1.75	1.35	.037
.111	1.75	1.975	.072
.150	1.75	2.60	.117
.228	1.75	3.85	.204
.00468	1.9625	.225	.00003
.00936	1.975	.3	.0009
.0156	1.9875	.4125	.0027
.0218	2.0	.525	.0059
.0312	2.0	.6625	.0096
.0406	2.0	.8	.0137
.0563	2.0	1.075	.025
.0717	2.0	1.35	.037
.111	2.0	1.975	.072
.150	2.0	2.6	.117
.228	2.0	3.85	.204
.00468	2.2375	.25	.00003
.00936	2.2375	.325	.0009
.0156	2.25	.4375	.0027
.0218	2.25	.5375	.0059
.0312	2.25	.675	.0096
.0406	2.25	.825	.0137
.0563	2.25	1.1	.025
.0717	2.25	1.35	.037
.111	2.25	1.975	.072
.150	2.25	2.60	.117
.228	2.25	3.85	.204
.00468	2.50	.275	.00003
.00936	2.5	.35	.0009
.0156	2.5	.45	.0027
.0218	2.5	.55	.0059
.0312	2.5	.70	[illegible]
.0406	2.5	.85	.0137
.0563	2.5	1.1	.025
.0717	2.5	1.35	.037
.111	2.5	1.975	.072
.150	2.5	2.6	.117
.228	2.5	3.85	.204
.00468	2.575	.175	.00003
.00936	2.65	.2625	.0009
.0156	2.65	.3625	.0027
.0218	2.725	.475	.0059
.0312	2.725	.625	.0096
.0406	2.75	.775	.0137

.0563	2.75	1.02	.025
.0717	2.75	1.35	.037
.111	2.75	1.97	.072
.150	2.75	2.60	.117
.228	2.75	3.85	.204
.00468	2.725	.0875	.00003
.00936	2.8	.175	.0009
.0156	2.875	.2875	.0027
.0219	2.95	.4	.0059
.0312	2.975	.55	.0096
.0406	3.0	.7	.0137
.0563	3.0	1.025	.025
.0717	3.0	1.35	.037
.111	3.0	1.975	.072
.150	3.0	2.6	.117
.228	3.0	3.85	.204
.00468	3.025	.12	.00003
.00936	3.075	.2	.0009
.0156	3.15	.3125	.0027
.0218	3.2	.425	.0059
.0312	3.225	.575	.0096
.0406	3.25	.7125	.0137
.0563	3.25	1.0375	.025
.0717	3.25	1.35	.037
.111	3.25	1.975	.072
.150	3.25	2.60	.117
.228	3.25	3.85	.204
.00468	3.30	.145	.00003
.00936	3.35	.225	.0009
.0156	3.40	.3375	.0027
.0218	3.45	.45	.0059
.0312	3.475	.5875	.0096
.0406	3.50	.725	.0137
.0563	3.5	1.0375	.025
.0717	3.50	1.35	.037
.111	3.5	1.975	.072
.150	3.5	2.6	.117
.228	3.5	3.85	.204
.00468	3.6	.1625	.00003
.00936	3.6375	.2375	.0009
.0156	3.6875	.35	.0027
.0219	3.7125	.4625	.0059
.0312	3.7375	.60	.0096
.0406	3.75	.75	.0137
.0563	3.75	1.0625	.025
.0717	3.75	1.35	.037
.111	3.75	1.975	.072
.150	3.75	2.60	.117
.228	3.75	3.85	.204
.00468	3.8875	.175	.00003
.00936	3.925	.25	.0009
.0156	3.95	.3625	.0027
.0218	3.975	.475	.0059
.0312	3.9875	.625	.0096
.0406	4.0	.775	.0137
.0563	4.0	1.0625	.025
.0717	4.0	1.35	.037
.111	4.0	1.975	.072
.150	4.0	2.6	.117
.228	4.0	3.85	.204

.00468	4.1875	.2	.00003
.00936	4.2	.275	.0009
.0156	4.2[illegible]	.3[illegible]75	.0027
.0219	4.2375	.50	.0059
.0312	4.25	.65	.0096
.0406	4.25	.7875	.0137
.0563	4.25	1.075	.025
.0717	4.25	1.35	.037
.111	4.25	1.975	.072
.150	4.25	2.60	.117
.228	4.25	3.85	.204
.00468	4.4625	.225	.00003
.00936	4.475	.3	.0009
.0156	4.4875	.4125	.0027
.0218	4.5	.525	.0059
.0312	4.5	.6625	.0096
.0406	4.5	.8	.0137
.0563	4.5	1.075	.025
.0717	4.5	1.35	.037
.111	4.5	1.975	.072
.150	4.5	2.6	.117
.228	4.5	3.85	.204
.00468	4.7375	.25	.00003
.00936	4.7375	.325	.0009
.0156	4.75	.4375	.0027
.0218	4.75	.5375	.0059
.0312	4.75	.675	.0096
.0406	4.75	.825	.0137
.0563	4.75	1.10	.025
.0717	4.75	1.35	.037
.111	4.75	1.975	.072
.150	4.75	2.60	.117
.228	4.75	3.85	.204
.00468	5.0	.275	.00003
.00936	5.0	.35	.0009
.0156	5.0	.45	.0027
.0218	5.0	.55	.0059
.0312	5.0	.70	.0096
.0406	5.0	.85	.0137
.0563	5.0	1.10	.025
.0717	5.0	1.35	.037
.111	5.0	1.975	.072
.150	5.0	2.6	.117
.228	5.0	3.85	.204
.00468	5.075	.175	.00003
.00936	5.15	.2625	.0009
.0156	5.15	.3625	.0027
.0218	5.225	.475	.0059
.0312	5.225	.625	.0096
.0406	5.25	.775	.0137
.0563	5.25	1.025	.025
.0717	5.25	1.35	.037
.111	5.25	1.975	.072
.150	5.25	2.60	.117
.228	5.25	3.85	.204
.00468	5.225	.0875	.00003
.00936	5.3	.175	.0009
.0156	5.375	.2875	.0027
.0218	5.45	.4	.0059
.0312	5.475	.55	.0096

.00406	5.5	.7	.0137
.0563	5.5	1.025	.025
.0717	5.5	1.35	.037
.111	5.5	1.975	.072
.150	5.5	2.6	.117
.228	5.5	3.85	.204
.00468	5.575	.12	.00003
.00936	5.575	.20	.0009
.0156	5.65	.3125	.0027
.0218	5.7	.425	.0059
.0312	5.725	.575	.0096
.0406	5.75	.7125	.0137
.0563	5.75	1.0375	.025
.0717	5.75	1.35	.037
.111	5.75	1.975	.072
.150	5.75	2.6	.117
.228	5.75	3.85	.204
.00468	5.8	.145	.00003
.00936	5.85	.225	.0009
.0156	5.9	.3375	.0027
.0218	5.95	.45	.0059
.0312	5.975	.5875	.0096
.0406	6.0	.725	.0137
.0563	6.0	1.0375	.025
.0717	6.0	1.35	.037
.111	6.0	1.975	.072
.150	6.0	2.6	.117
.228	6.0	3.85	.204
.00468	6.1	.1625	.00003
.00936	6.1375	.2375	.0009
.0156	6.1875	.35	.0027
.0218	6.2125	.4625	.0059
.0312	6.2375	.60	.0096
.0406	6.25	.75	.0137
.0563	6.25	1.0625	.025
.0717	6.25	1.35	.037
.111	6.25	1.975	.072
.150	6.25	2.60	.117
.228	6.25	3.85	.204
.00468	6.3875	.175	.00003
.00936	6.425	.25	.0009
.0156	6.45	.3625	.0027
.0218	6.475	.475	.0059
.0312	6.4875	.625	.0096
.0406	6.5	.775	.0137
.0563	6.5	1.0625	.025
.0717	6.5	1.35	.037
.111	6.5	1.975	.072
.150	6.5	2.6	.117
.228	6.5	3.85	.204
.00468	6.6875	.2	.00003
.00936	6.7	.275	.0009
.0156	6.725	.3875	.0027
.0218	6.7375	.50	.0059
.0312	6.75	.65	.0096
.0406	6.75	.7875	.0137
.0563	6.75	1.075	.025
.0717	6.75	1.35	.037
.111	6.75	1.975	.072
.150	6.75	2.6	.117

.228	6.75	3.85	.204
.00469	6.9625	[illegible]	.00003
.00936	6.975	[illegible]	.0009
.0156	6.9875	.4125	.0027
.0218	7.0	.525	.0059
.0312	7.0	.6625	.0096
.0406	7.0	.8	.0137
.0563	7.0	1.075	.025
.0717	7.0	1.35	.037
.111	7.0	1.975	.072
.150	7.0	2.6	.117
.226	7.0	3.85	.204
.00468	7.2375	.25	.00003
.00936	7.2375	.325	.0009
.0156	7.25	.4375	.0027
.0218	7.25	.5375	.0059
.0312	7.25	.675	.0096
.0406	7.25	.825	.0137
.0563	7.25	1.1	.025
.0717	7.25	1.35	.037
.111	7.25	1.975	.072
.150	7.25	2.60	.117
.228	7.25	3.85	.204
.00469	7.5	.275	.00003
.00936	7.5	.35	.0009
.0156	7.5	.45	.0027
.0218	7.5	.55	.0059
.0312	7.5	.70	.0096
.0406	7.5	.85	.0137
.0563	7.5	1.1	.025
.0717	7.5	1.35	.037
.111	7.5	1.975	.072
.150	7.5	2.6	.117
.228	7.5	3.85	.204
.306	7.5	5.1	.306
.306	7.25	5.1	.306
.306	7.0	5.1	.306
.306	6.75	5.1	.306
.306	6.5	5.1	.306
.306	6.25	5.1	.306
.306	6.0	5.1	.306
.306	5.75	5.1	.306
.306	5.5	5.1	.306
.306	5.25	5.1	.306
.306	5.0	5.1	.306
.305	4.75	5.1	.306
.306	4.5	5.1	.306
.306	4.25	5.1	.306
.306	4.0	5.1	.306
.306	3.75	5.1	.306
.306	3.5	5.1	.306
.306	3.25	5.1	.306
.306	3.0	5.1	.306
.306	2.75	5.1	.306
.306	2.5	5.1	.306
.306	2.25	5.1	.306
.306	2.0	5.1	.306
.306	1.75	5.1	.306
.306	1.5	5.1	.306
.306	1.25	5.1	.306

.306	1.0	5.1	
.306	.7[illegible]	5.1	.306
.306	[illegible]	5.1	.306
.306	.25	5.1	.306
.306	.00	5.1	.306
.228	.00	3.65	.306
.150	.00	2.6	.204
.111	.00	1.975	.117
.0717	.00	1.35	.072
.0562	.00	1.10	.037
[illegible]	.00	.85	.025
.0312	.00	.70	.0137
.0218	.00	.55	.0096
.0156	.00	.45	.0059
.00936	.00	.35	.0027
.00468	.00	.275	.0009
.00	.00	.2	.00003
.00	.075	.10	.00
.00	.15	.00	.00
.00	.45	.03	.00
.00	.75	.06	.00
.00	1.05	.08	.00
.00	1.35	.10	.00
.00	1.65	.125	.00
.00	1.96	.15	.00
.00	2.225	.175	.00
.00	2.5	.2	.00
.00	2.575	.10	.00
.00	2.65	.00	.00
.00	2.95	.03	.00
.00	3.25	.06	.00
.00	3.55	.08	.00
.00	3.85	.10	.00
.00	4.15	.125	.00
.00	4.45	.15	.00
.00	4.725	.175	.00
.00	5.00	.2	.00
.00	5.275	.10	.00
.00	5.15	.00	.00
.00	5.45	.03	.00
.00	5.75	.06	.00
.00	6.05	.05	.00
.00	6.35	.10	.00
.00	6.65	.125	.00
.00	6.95	.15	.00
.00	7.225	.175	.00
.00	7.5	.2	.00
			.00

.3	.175
.45	.400
.5	.7
.5	1.35
.5	2.6
.85	.225
.95	.45
1.	.725
1.	1.35
1.	2.6
1.425	.25
1.475	.475
1.5	.775

1.5	1.35
1.5	2.6
1.975	.3
2.	.525
2.	.8
2.	1.35
2.	2.6
2.5	.35
2.5	.55
2.5	.85
2.5	1.35
2.5	2.6
2.8	.175
2.95	.4
3.	.7
3.	1.35
3.	2.6
3.35	.225
3.45	.45
3.5	.725
3.5	1.35
3.5	2.6
3.925	.25
3.975	.475
4.	.775
4.	1.35
4.	2.6
4.475	.3
4.5	.525
4.5	.8
4.5	1.35
4.5	2.6
5.	.35
5.	.55
5.	.85
5.	1.35
5.	2.6
5.3	.175
5.45	.4
5.5	.7
5.5	1.35
5.5	2.6
5.85	.225
5.95	.45
6.	.725
6.	1.35
6.	2.6
6.425	.25
6.475	.475
6.5	.775
6.5	1.35
6.5	2.6
6.975	.3
7.	.525
7.	.8
7.	1.35
7.	2.6
7.5	.35
7.5	.55
7.5	.85

7.5	1.35
7.5	2.6
7.5	5.1
7.	5.1
6.5	5.1
6.	5.1
5.5	5.1
5.	5.1
4.5	5.1
4.	5.1
3.5	5.1
3.	5.1
2.5	5.1
2.	5.1
1.5	5.1
1.	5.1
.5	5.1
.00	5.1
.00	2.6
.00	1.35
.00	.85
.00	.55
.00	.35
.00	.2
.15	.00
.75	.05
1.35	.1
1.95	.15
2.5	.2
2.65	.00
3.25	.05
3.85	.1
4.45	.15
5.	.2
5.15	.00
5.75	.05
6.35	.1
6.95	.15
7.5	.2

.1	.1	.1	.1	.1	.1	.1	.1	.1	.1	.1	.1
.03	.03	.03	.03	.03	.03	.03	.03	.03	.03	.03	.03
.08	.08	.08	.08	.08	.08	.08	.08	.08	.08	.08	.08
.125	.125	.125	.125	.125	.125	.125	.125	.125	.125	.125	.125
.175	.175	.175	.175	.175	.175	.175	.175	.175	.175	.175	.175
.1	.1	.1	.1	.1	.1	.1	.1	.1	.1	.1	.1
.03	.03	.03	.03	.03	.03	.03	.03	.03	.03	.03	.03
.08	.08	.08	.08	.08	.08	.08	.08	.08	.03	.08	.08
.125	.125	.125	.125	.125	.125	.125	.125	.125	.125	.125	.125
.175	.175	.175	.175	.175	.175	.175	.175	.175	.175	.175	.175
.1	.1	.1	.1	.1	.1	.1	.1	.1	.1	.1	.1
.03	.03	.03	.03	.03	.03	.03	.03	.03	.03	.03	.03
.08	.08	.08	.08	.08	.08	.08	.08	.08	.08	.08	.08
.125	.125	.125	.125	.125	.125	.125	.125	.125	.125	.125	.125
.175	.175	.175	.175	.175	.175	.175	.175	.175	.175	.175	.175

2.65	.125
2.65	.45
2.65	.775
2.65	1.25
2.65	2.4
2.65	4.65

F 585

3.25	.135
3.25	.35
3.25	.65
3.25	1.25
3.25	2.4
3.25	4.25
3.85	.225
3.85	.4
3.85	.675
3.85	1.25
3.85	2.4
3.85	4.25
4.45	.275
4.45	.45
4.45	.75
4.45	1.25
4.45	2.4
4.45	4.25
5.	.325
5.	.45
5.	.75
5.	1.25
5.	2.4
5.	4.25

1. .001 .02 .01

2
3
4

ψ "first time step"

0.004409	0.008775	0.015391	0.022039	0.030839	0.039540	0.056109
0.073156	0.111169	0.149998	0.227997			
0.002598	0.007139	0.013350	0.020082	0.028404	0.036579	0.054324
0.072998	0.111111	0.149979	0.228000			
0.004736	0.009510	0.016007	0.022659	0.030496	0.038126	0.055366
0.073418	0.111131	0.149986	0.227998			
0.004474	0.008940	0.015751	0.022700	0.031078	0.039415	0.055938
0.072718	0.111097	0.150003	0.227997			
0.002545	0.009072	0.014220	0.022060	0.030395	0.039169	0.053295
0.072657	0.111010	0.149990	0.228000			
0.004812	0.008911	0.015338	0.021695	0.030132	0.037594	0.055432
0.073458	0.111146	0.150004	0.227997			
0.004343	0.008813	0.015571	0.022329	0.031290	0.039359	0.056364
0.072888	0.111146	0.150018	0.227996			
0.004824	0.009182	0.015841	0.022421	0.030295	0.038731	0.056547
0.073375	0.111196	0.150017	0.227995			
0.004594	0.009173	0.016325	0.022572	0.031254	0.040613	0.057511
0.072717	0.111105	0.150009	0.227997			
0.005916	0.011267	0.017787	0.024230	0.033901	0.043014	0.057980
0.072877	0.111126	0.149996	0.227998			
0.004409	0.008775	0.015392	0.022040	0.030841	0.039544	0.056124
0.073177	0.111181	0.150003	0.227996			
0.002662	0.007173	0.013504	0.020178	0.028634	0.036884	0.054781
0.073407	0.111195	0.149990	0.227998			
0.004741	0.009512	0.016016	0.022668	0.030520	0.038156	0.055456
0.073519	0.111217	0.149996	0.227997			
0.004474	0.008940	0.015751	0.022700	0.031078	0.039416	0.055941
0.072721	0.111100	0.150005	0.227997			
0.002752	0.009385	0.014915	0.022666	0.031319	0.040082	0.054241
0.073287	0.111149	0.150008	0.227997			
0.004812	0.008937	0.015356	0.021735	0.030205	0.037720	0.055631
0.073635	0.111213	0.150017	0.227996			
0.004343	0.008814	0.015571	0.022330	0.031291	0.039362	0.056370
0.072897	0.111153	0.150021	0.227995			
0.004823	0.009183	0.015842	0.022425	0.030302	0.038751	0.056582
0.073416	0.111219	0.150024	0.227995			
0.004594	0.009173	0.016325	0.022572	0.031254	0.040613	0.057512
0.072719	0.111107	0.150010	0.227997			
0.005916	0.011267	0.017786	0.024230	0.033901	0.043014	0.057980
0.072878	0.111127	0.149996	0.227998			
0.004409	0.008775	0.015392	0.022040	0.030841	0.039544	0.056124
0.073178	0.111182	0.150003	0.227996			
0.002662	0.007173	0.013504	0.020178	0.028634	0.036884	0.054781
0.073407	0.111196	0.149990	0.227998			
0.004741	0.009512	0.016016	0.022668	0.030520	0.038156	0.055456
0.073519	0.111217	0.149996	0.227997			
0.004477	0.008928	0.015751	0.022697	0.031075	0.039367	0.055847
0.072639	0.111100	0.150008	0.227996			
0.002752	0.009385	0.014915	0.022666	0.031319	0.040082	0.054241
0.073287	0.111149	0.150009	0.227997			
0.004812	0.008937	0.015356	0.021735	0.030205	0.037720	0.055631
0.073635	0.111213	0.150017	0.227996			
0.004343	0.008814	0.015571	0.022329	0.031293	0.039364	0.056376
0.072892	0.111157	0.150022	0.227995			
0.004824	0.009133	0.015842	0.022425	0.030302	0.038751	0.056582

0.073416	0.111219	0.150024	0.227995			
0.004913	0.009127	0.016140	0.022339	0.030874	0.040085	0.057029
0.072418	0.111099	0.150014	0.227996			
0.004942	0.009832	0.016191	0.022571	0.032058	0.041436	0.056927
0.072392	0.111113	0.150013	0.227996			

$\left\{\frac{\partial \omega}{\partial t}\right\}_{t=0}$

0.24920E 02	-0.26265E 01	-0.63006E-01	-0.32552E 00	-0.44563E 00
0.33465E 02	-0.56063E 01	0.59536E 00	-0.60794E-02	0.17487E 00
0.38653E 02	-0.51482E 01	0.65316E 00	0.21930E 00	-0.71726E 00
0.37760E 02	-0.69380E 01	0.30373E-01	0.94423E-01	0.38538E 00
0.36934E 02	0.40640E 01	0.53540E 00	0.86364E-01	0.15614E 00
0.21149E 02	-0.26370E 01	-0.85711E 00	-0.32642E 00	0.20145E 00
0.33771E 02	-0.50394E 01	0.97627E 00	0.33017E 00	0.52703E-01
0.38618E 02	-0.55930E 01	0.46940E 00	-0.10525E 01	-0.91631E-01
0.37535E 02	-0.56604E 01	0.64465E 00	0.37798E 00	0.28433E 00
0.36920E 02	0.37592E 01	0.27558E 00	-0.24992E-01	-0.81379E 00
0.20681E 02	-0.25648E 01	0.18807E-01	-0.62919E-03	0.24369E 00
0.33734E 02	-0.50626E 01	0.67911E 00	0.30376E 00	0.14167E 00
0.38649E 02	-0.63121E 01	0.53029E 00	-0.21681E 00	0.13752E 00
0.37790E 02	-0.50298E 01	0.57981E 00	0.24745E 00	-0.69469E 00
0.45321E 02	-0.58833E 01	-0.70547E-01	-0.37218E 00	0.61100E-01

ω and $\frac{\partial \omega}{\partial t}$ "first time step"

0.24870E 00	-0.24765E-01	0.20975E-02	0.31294E-02	0.44287E-02
0.33043E 00	-0.43885E-01	0.28027E-02	-0.53124E-03	-0.16953E-02
0.38072E 00	-0.60561E-01	0.48255E-02	-0.28495E-02	0.71343E-02
0.37288E 00	-0.41740E-01	0.81176E-02	-0.14440E-02	-0.37758E-02
0.36447E 00	0.32303E-01	-0.39458E-02	-0.85703E-03	-0.15690E-02
0.20568E 00	-0.22753E-01	0.98436E-02	0.31607E-02	-0.19988E-02
0.33722E 00	-0.51245E-01	-0.81512E-03	-0.38947E-02	-0.50906E-03
0.38019E 00	-0.55898E-01	-0.66096E-02	0.97537E-02	0.94130E-03
0.37519E 00	-0.54366E-01	0.20121E-02	-0.42311E-02	-0.28027E-02
0.36456E 00	0.35281E-01	-0.13900E-02	0.24945E-03	0.80619E-02
0.21034E 00	-0.23428E-01	0.11769E-02	-0.62875E-04	-0.23820E-02
0.33756E 00	-0.51037E-01	0.20903E-02	-0.36490E-02	-0.13954E-02
0.37989E 00	-0.48769E-01	0.60619E-02	0.14718E-02	-0.13423E-02
0.37267E 00	-0.60611E-01	0.25916E-02	-0.29692E-02	0.69060E-02
0.42323E 00	-0.39263E-01	0.10895E-01	-0.31205E-02	-0.52726E-03
-0.49790E 02	-0.26265E 01	-0.63006E-01	-0.32552E 00	-0.44563E 00
-0.66508E 02	-0.56063E 01	0.59536E 00	-0.60794E-02	0.17487E 00
-0.76725E 02	-0.51482E 01	0.65316E 00	0.21930E 00	-0.71726E 00
0.37760E 02	-0.69380E 01	0.30373E-01	0.94423E-01	0.38538E 00
0.36934E 02	0.40640E 01	0.53540E 00	0.86364E-01	0.15614E 00

0.21149E 02	-0.26370E 01	-0.85711E 00	-0.32642E 00	0.20145E (
0.33771E 02	-0.50394E 01	0.97627E 00	0.33017E 00	0.52703E-
0.38618E 02	-0.55930E 01	0.46940E 00	-0.10525E 01	-0.91631E-(
0.37535E 02	-0.56604E 01	0.64465E 00	0.37798E 00	0.28433E (
0.36920E 02	0.37592E 01	0.27558E 00	-0.24992E-01	-0.81379E (
0.20681E 02	-0.25648E 01	0.18807E-01	-0.62919E-03	0.24369E (
0.33734E 02	-0.50626E 01	0.67911E 00	0.30376E 00	0.14167E (
0.38649E 02	-0.63121E 01	0.53029E 00	-0.21681E 00	0.13752E (
0.37790E 02	-0.50298E 01	0.57981E 00	0.24745E 00	-0.69469E (
-0.87644E 02	-0.58833E 01	-0.70547E-01	-0.37218E 00	0.61100E-(

ϕ "last time step"

2

-0.000175	0.001020	0.010439	0.018656	0.028213	0.037698	0.055511
0.073279	0.111697	0.150309	0.228020			
-0.001368	-0.000266	0.008293	0.015906	0.024541	0.033432	0.053027
0.072807	0.111373	0.150119	0.228007			
0.000009	0.001403	0.010591	0.018600	0.026949	0.035319	0.054222
0.073277	0.111610	0.150234	0.228014			
0.000070	0.001828	0.011702	0.020374	0.029648	0.038665	0.056069
0.073220	0.111755	0.150364	0.228028			
0.001091	0.005804	0.011746	0.018914	0.027908	0.037200	0.052427
0.072436	0.111170	0.150065	0.228000			
0.001574	0.005297	0.010773	0.017104	0.026269	0.034533	0.054134
0.073165	0.111506	0.150199	0.228007			
0.001837	0.006051	0.012540	0.019440	0.029215	0.037971	0.056134
0.073193	0.111730	0.150346	0.228023			
0.001946	0.006009	0.012069	0.018659	0.027228	0.036442	0.055689
0.073303	0.111669	0.150291	0.228015			
0.002657	0.007149	0.014617	0.021285	0.030490	0.040247	0.057711
0.073265	0.111798	0.150390	0.228031			
0.003392	0.007164	0.015617	0.022775	0.032731	0.042311	0.057963
0.073396	0.111849	0.150405	0.228034			
-0.000164	0.001038	0.010476	0.018708	0.028293	0.037798	0.055659
0.073447	0.111852	0.150422	0.228037			
-0.001391	-0.000143	0.008495	0.016174	0.025029	0.034046	0.053851
0.073653	0.111926	0.150430	0.228038			
0.000059	0.001490	0.010727	0.018768	0.027174	0.035583	0.054591
0.073677	0.111919	0.150434	0.228038			
0.000073	0.001833	0.011713	0.020391	0.029675	0.038700	0.056124
0.073288	0.111826	0.150417	0.228035			
0.000930	0.005642	0.011638	0.019356	0.028728	0.038196	0.053596
0.073560	0.111888	0.150425	0.228036			
0.001655	0.005422	0.010958	0.017365	0.026614	0.034953	0.054684
0.073725	0.111931	0.150443	0.228039			
0.001841	0.006062	0.012560	0.019471	0.029260	0.038034	0.056223
0.073299	0.111836	0.150421	0.[illegible]037			
0.001969	0.006054	0.012138	0.[illegible]759	0.027360	0.036616	0.055924
0.073556	0.111892	0.150435	0.[illegible]8038			
0.002658	0.007152	0.014623	0.021295	0.030506	0.040269	0.057744
0.073307	0.111843	0.150416	0.228036			
0.003393	0.007165	0.015620	0.022780	0.032740	0.042324	0.057983
0.073420	0.111876	0.150418	0.228036			
-0.000166	0.001025	0.010447	0.018647	0.028196	0.037660	0.055491
0.073288	0.111764	0.150391	0.228036			
-0.001391	-0.000143	0.008495	0.016175	0.025032	0.034050	0.053855
0.073658	0.111932	0.150432	0.228039			

0.000059	0.001490	0.010726	0.018764	0.027165	0.035563	0.054559
0.073641	0.111898	0.150427	0.228039			
0.000012	0.001655	0.011425	0.019961	0.029165	0.038147	0.055586
0.072853	0.111620	0.150350	0.228036			
0.000931	0.005642	0.011639	0.019357	0.028732	0.038202	0.053606
0.073574	0.111902	0.150431	0.228037			
0.001655	0.005472	0.010959	0.017366	0.026614	0.034951	0.054676
0.073715	0.111927	0.150441	0.228039			
0.001816	0.006019	0.012450	0.019311	0.029018	0.037749	0.055906
0.073010	0.111696	0.150369	0.228037			
0.001967	0.006051	0.012128	0.018741	0.027323	0.036560	0.055841
0.073471	0.111845	0.150417	0.228038			
0.002398	0.006765	0.013900	0.020435	0.029564	0.039317	0.056940
0.072659	0.111584	0.150335	0.228042			
0.002519	0.005701	0.013583	0.021131	0.031092	0.040891	0.056860
0.072633	0.111566	0.150338	0.228047			

2

0.21415E 00	-0.60522E-01	0.20368E-01	-0.38702E-02	0.60324E-
0.31243E 00	-0.12853E 00	0.31914E-01	-0.90231E-02	-0.10589E-
0.36301E 00	-0.13217E 00	0.35533E-01	-0.75117E-02	0.79040E-
0.35739E 00	-0.12819E 00	0.14896E-01	-0.24305E-02	-0.26636E-
0.36147E 00	-0.41791E-02	0.83123E-02	-0.75256E-02	-0.11784E-
0.18016E 00	-0.60589E-01	0.31606E-01	-0.12941E-02	0.15382E-
0.31203E 00	-0.13566E 00	0.25895E-01	-0.14961E-01	-0.15585E-
0.36327E 00	-0.12561E 00	0.40575E-01	0.87101E-02	0.22695E-
0.35939E 00	-0.14148E 00	0.60145E-02	-0.65420E-02	-0.28659E-
0.35506E 00	-0.12954E-02	0.11908E-01	-0.41462E-02	0.91158E-
0.18316E 00	-0.58296E-01	0.22444E-01	-0.58541E-02	-0.33467E-
0.30880E 00	-0.13826E 00	0.25648E-01	-0.14062E-01	-0.73161E-
0.37152E 00	-0.11140E 00	0.46990E-01	-0.29824E-02	-0.73704E-
0.34262E 00	-0.17735E 00	0.15363E-01	-0.61777E-02	0.66019E-
0.48150E 00	-0.31094E-01	0.91394E-02	0.42628E-02	-0.35654E-
-0.53819E 02	-0.92060E 01	-0.21479E-01	-0.32552E 00	-0.44563E
0.66494E 02	-0.14224E 02	0.59536E 00	-0.60794E-02	0.17487E
-0.76725E 02	-0.51482E 01	-0.21936E 01	0.21930E 00	-0.71726E
0.37760E 02	-0.69380E 01	0.30373E-01	0.94423E-01	0.38538E
0.36934E 02	0.40640E 01	0.53540E 00	0.86364E-01	0.15614E
0.21149E 02	-0.26370E 01	0.77255E 00	-0.32642E 00	0.20145E
0.33771E 02	-0.13745E 02	0.97627E 00	0.33017E 00	0.52703E-
0.38618E 02	-0.55930E 01	-0.20668E 01	-0.10525E 01	-0.91631E-
0.37535E 02	-0.56604E 01	0.64465E 00	0.37798E 00	0.28433E
0.36920E 02	0.37592E 01	-0.25058E 00	-0.24992E-01	-0.81379E
0.20681E 02	0.24769E 01	-0.12382E 00	-0.62919E-03	0.24369E
0.33734E 02	-0.13587E 02	0.67911E 00	-0.27805E 00	0.14167E
-0.38662E 02	-0.63121E 01	0.20493E 01	-0.21681E 00	0.13752E
0.37790E 02	-0.12745E 02	0.57981E 00	0.24745E 00	-0.69469E
0.87628E 02	-0.58833E 01	-0.70547E-01	-0.37218E 00	0.61100E-

0.367885	0.399258	0.723952	0.756325	0.729751	0.714878
0.732763	0.732147	0.745006	0.744511	0.748418	0.748619
0.125377	0.442757	0.663318	0.816494	0.723959	0.724442
0.723965	0.728391	0.737889	0.740894	0.747618	0.748415
0.237490	0.465718	0.726634	0.833193	0.746211	0.749670
0.734752	0.737024	0.737388	0.740425	0.747090	0.748274
0.243550	0.464025	0.761775	0.863686	0.776290	0.778431
0.751169	0.746886	0.739617	0.740802	0.746806	0.748153
0.372832	0.697719	0.838617	0.856321	0.797563	0.777220
0.756174	0.743977	0.739571	0.739937	0.746580	0.748053
0.307459	0.397372	0.768226	0.780046	0.754326	0.730053
0.737853	0.732235	0.736433	0.738421	0.746378	0.747989
0.137944	0.450565	0.671295	0.824315	0.733180	0.730929

0.727287	0.729497	0.734439	0.738125	0.746263	0.747974
0.241994	0.468313	0.730493	0.835931	0.749899	0.752454
0.736644	0.737963	0.736249	0.739373	0.746317	0.747998
0.244365	0.464644	0.762934	0.864588	0.777660	0.779506
0.752136	0.747525	0.739352	0.740408	0.746409	0.748016
0.373051	0.657908	0.838992	0.856600	0.798059	0.777629
0.756620	0.744280	0.739486	0.739702	0.746439	0.748020
0.307501	0.397375	0.768337	0.780111	0.754530	0.730213
0.738031	0.732302	0.736357	0.738310	0.746351	0.747986
0.137937	0.450572	0.671341	0.824285	0.733225	0.730657
0.727176	0.729357	0.734467	0.738256	0.746268	0.747980
0.241929	0.467813	0.730159	0.834607	0.748901	0.750496
0.735962	0.737808	0.736776	0.740167	0.746403	0.748039
0.241925	0.456296	0.758353	0.856092	0.772845	0.775170
0.751328	0.749762	0.741559	0.742786	0.746694	0.748107
0.339981	0.591632	0.812368	0.852512	0.792038	0.783418
0.762641	0.756249	0.745420	0.744366	0.746926	0.748078
-0.014369	0.059241	-0.089351	-0.078861	-0.074665	-0.049750
-0.037372	-0.026545	-0.009898	-0.007420	-0.000393	-0.000162
-0.085587	0.140979	-0.003055	0.062862	-0.009718	0.001597
-0.015102	-0.004712	-0.006105	-0.003771	-0.000232	-0.000178
-0.049644	0.148625	0.015700	0.089845	0.025872	0.024275
0.005337	0.006655	-0.001946	-0.000938	-0.000103	-0.000136
-0.046112	0.154874	0.024765	0.093957	0.029859	0.014457
0.007768	0.001985	-0.001301	-0.000915	-0.000211	-0.000119
-0.059857	0.037480	-0.031705	-0.015403	-0.005985	-0.028015
-0.006588	-0.010508	-0.002741	-0.001824	-0.000209	-0.000081
-0.076066	0.046981	-0.105381	-0.092060	-0.046663	-0.035635
-0.014670	-0.010083	-0.002363	-0.001349	-0.000091	-0.000054
-0.087338	0.143352	-0.000587	0.067062	-0.001351	0.008662
-0.002041	0.003911	0.000192	0.000596	0.000085	0.000001
-0.048474	0.149401	0.018373	0.091616	0.029979	0.027362
0.011600	0.010771	0.002078	0.001596	0.000129	0.000040
-0.045835	0.155049	0.025511	0.094441	0.031320	0.015498
0.010280	0.003594	0.000816	0.000456	0.000046	0.000055
-0.059805	0.037533	-0.031496	-0.015236	-0.005534	-0.027633
-0.005644	-0.009836	-0.001624	-0.001129	-0.000019	0.000007
-0.076049	0.046990	-0.105323	-0.092053	-0.046564	-0.035629
-0.014411	-0.009823	-0.001891	-0.001078	-0.000056	-0.000050
-0.087341	0.143353	-0.000599	0.067139	-0.001243	0.009091
-0.001533	0.004895	0.000706	0.001090	0.000114	-0.000000
-0.048450	0.149504	0.018647	0.092575	0.031100	0.030120
0.013991	0.014484	0.003567	0.002979	0.000232	0.000068
-0.045386	0.157151	0.028759	0.103137	0.038336	0.028296
0.018355	0.013119	0.003993	0.002721	0.000125	0.000009
-0.055290	0.067953	-0.008279	0.041181	0.018737	0.004424
0.009919	0.003063	0.001589	0.000479	-0.000244	-0.000163
0.050000	0.150000	0.100000	0.250000	0.150000	0.316667
0.166667	0.333333	0.166667	0.333333	0.166667	0.333333
0.400000	0.633333	0.533333	0.750000	0.633333	0.816667
0.666667	0.833333	0.666667	0.833333	0.666667	0.833333
0.983333	1.208332	1.074999	1.283333	1.141666	1.325000
1.166666	1.333333	1.166666	1.333333	1.166666	1.333333
1.574999	1.783333	1.624999	1.816666	1.658333	1.833333
1.666666	1.833333	1.666666	1.833333	1.666666	1.833333
2.141666	2.325000	2.158333	2.333333	2.166666	1.833333
2.166666	2.333333	2.166666	2.333333	2.166666	2.333333
2.549999	2.650000	2.599999	2.749999	2.650000	2.816667
2.666666	2.833333	2.666666	2.833333	2.666666	2.833333
2.900000	3.133332	3.033333	3.249999	3.133333	3.316667

3.166666	3.333333	3.166666	3.333333	3.166666	3.333333
3.483333	3.708332	3.574999	3.783333	3.641666	3.825000
3.666666	3.833333	3.666666	3.833333	3.666666	3.833333
4.074999	4.283333	4.124999	4.316666	4.158333	4.333333
4.166666	4.333333	4.166666	4.333333	4.166666	4.333333
4.641666	4.825000	4.658333	4.833333	4.666666	4.833333
4.666666	4.833333	4.666666	4.833333	4.666666	4.833333
5.049999	5.150000	5.099999	5.249999	5.150000	5.316667
5.166666	5.333333	5.166666	5.333333	5.166666	5.333333
5.399999	5.633331	5.533330	5.749994	5.633331	5.816666
5.666666	5.833333	5.666666	5.833333	5.666666	5.833333
5.983332	6.208328	6.074997	6.283330	6.141663	6.324997
6.166666	6.333333	6.166666	6.333333	6.166666	6.333333
6.574997	6.783330	6.624994	6.816666	6.658330	6.833333
6.666666	6.833333	6.666666	6.833333	6.666666	6.833333
7.141663	7.324997	7.158330	7.333333	7.166666	7.333333
7.166666	7.333333	7.166666	7.333333	7.166666	7.333333
0.183333	0.175000	0.358333	0.375000	0.600000	0.650000
0.966666	1.133332	1.766665	2.183332	3.433332	4.266665
0.078333	0.153333	0.266667	0.358333	0.516666	0.625000
0.925000	1.141665	1.766665	2.183332	3.433332	4.266665
0.128333	0.191667	0.308333	0.391666	0.550000	0.658333
0.949999	1.158333	1.766665	2.183332	3.433332	4.266665
0.166667	0.233333	0.341667	0.433333	0.591666	0.700000
0.974999	1.166666	1.766665	2.183332	3.433332	4.266665
0.216667	0.283333	0.391666	0.475000	0.625000	0.733333
0.999999	1.183332	1.766665	2.183332	3.433332	4.266665
0.183333	0.175000	0.358333	0.375000	0.600000	0.650000
0.966666	1.133332	1.766665	2.183332	3.433332	4.266665
0.078333	0.153333	0.266667	0.358333	0.516666	0.625000
0.925000	1.141665	1.766665	2.183332	3.433332	4.266665
0.128333	0.191667	0.308333	0.391666	0.550000	0.658333
0.949999	1.158333	1.766665	2.183332	3.433332	4.266665
0.166667	0.233333	0.341667	0.433333	0.591666	0.700000
0.974999	1.166666	1.766665	2.183332	3.433332	4.266665
0.216667	0.283333	0.391666	0.475000	0.625000	0.733333
0.999999	1.183332	1.766665	2.183332	3.433332	4.266665
0.183333	0.175000	0.358333	0.375000	0.600000	0.650000
0.966666	1.133332	1.766665	2.183332	3.433332	4.266665
0.078333	0.153333	0.266667	0.358333	0.516666	0.625000
0.925000	1.141665	1.766665	2.183332	3.433332	4.266665
0.128333	0.191667	0.308333	0.391666	0.550000	0.658333
0.949999	1.158333	1.766665	2.183332	3.433332	4.266665
0.166667	0.233333	0.341667	0.433333	0.591666	0.700000
0.974999	1.166666	1.766665	2.183332	3.433332	4.266665
0.216667	0.283333	0.391666	0.475000	0.625000	0.733333
0.999999	1.183332	1.766665	2.183332	3.433332	4.266665
10347.5078	11341.8906	3733.6438	3527.7344	2069.9673	1906.3079
1310.8462	1147.6240	849.4260	777.2175	849.4250	1351.7769
16431.3359	7304.3047	4043.0640	3005.6111	2119.2634	1782.5183
1278.5532	1088.9331	832.8220	770.4978	868.2529	1449.8250
16431.3281	7985.2188	4177.0859	3150.0962	2184.7876	1826.1147
1306.9329	1112.7676	844.4651	775.1594	854.5671	1378.0110
18523.5430	8204.4297	4381.3242	3180.8162	2198.4502	1835.1377
1330.8945	1140.9214	855.8826	779.9490	843.2517	1320.7666
18523.5156	8204.4258	4381.3242	3260.5212	2269.7649	1881.8755
1362.5498	1168.4502	869.6904	785.9565	831.7146	1264.0852
10347.5078	11341.8906	3733.6438	3527.7344	2069.9673	1906.3079
1310.8462	1147.6240	849.4260	777.2175	849.4250	1351.7769
16431.3359	7304.3047	4043.0640	3005.6111	2119.2634	1782.5183

1278.5532	1088.9331	832.8220	770.4978	868.2529	1449.8250
16431.3281	7985.2188	4177.0859	3150.0962	2184.7876	1826.1147
1306.9329	1112.7676	844.4651	775.1594	854.5671	1378.0110
18523.5430	8204.4297	4381.3242	3180.8162	2198.4502	1835.1377
1330.8945	1140.9214	855.8826	779.9490	843.2517	1320.7666
18523.5156	8204.4258	4381.3242	3260.5212	2269.7649	1881.8755
1362.5498	1168.4502	869.6904	785.9565	831.7146	1264.0852
10347.5078	11341.8906	3733.6438	3527.7344	2069.9673	1906.3079
1310.8462	1147.6240	849.4260	777.2175	849.4250	1351.7769
16431.3359	7304.3047	4043.0640	3005.6111	2119.2634	1782.5183
1278.5532	1088.9331	832.8220	770.4978	868.2529	1449.8250
16431.3281	7985.2188	4177.0859	3150.0962	2184.7876	1826.1147
1306.9329	1112.7676	844.4651	775.1594	854.5671	1378.0110
18523.5430	8204.4297	4381.3242	3180.8162	2198.4502	1835.1377
1330.8945	1140.9214	855.8826	779.9490	843.2517	1320.7666
18523.5156	8204.4258	4381.3242	3260.5212	2269.7649	1881.8755
1362.5498	1168.4502	869.6904	785.9565	831.7146	1264.0852

0.24278492

0.69021392
0.73933011
0.73792273
0.74093950
0.74900311
0.47193128

0.81478220
0.73039865
0.72976327
0.74027973
0.74793136
0.47165656

0.84347069
0.75056666
0.73640621
0.74074847
0.74795425
0.47513598

0.92269093
0.77876461
0.74529278
0.74105709
0.74797755
0.60270405

0.93734235
0.76994771
0.73832422
0.74026352
0.74797732

```
      DIMENSION I(200),J(200),K(200),L(200),M(200),N(200)
      DIMENSION LL(6),MM(6),C(5,6),H(5,6,200),A(350),R0(350)
      DIMENSION S(350,45),XS(200),YS(200),XY(200),APLA(200)
      DIMENSION CM(3,3),LC(3),MC(3),BR(200),CC(200),BPC(3,3,200),Z(200)
      DIMENSION VOR(200),ALPHA(6,200),XG(200),YG(200),U(200),V(200)
      DIMENSION F(200),IV(200),JV(200),KV(200),XV(120),YV(120),P(40)
      DIMENSION XLV(120),YLV(120),XSV(200),YSV(200),XYV(200),AV(200)
      DIMENSION BV(200),CV(200),Q(200),A(75,11),DW(120),IZ(30),MZ(30)
      DIMENSION PSI(450),X(450),Y(450),XL(450),YL(450),XO(30),YO(30)
      DIMENSION D(3,3,200),VORA(200),B3V(40),WW(30),YB(200),CON(200)
      DIMENSION CH(200),AVT(200)
      READ 1,NE,NN,NNT,NNV,NNTV
    1 FORMAT (5X,5I5)
      READ 2,(I(IE),J(IE),K(IE),L(IE),M(IE),N(IE),IV(IE),JV(IE),KV(IE),
     2IE=1,NE)
    2 FORMAT (5X,9I5)
      READ 3,(PSI(IN),X(IN),Y(IN),IN=1,NNT)
    3 FORMAT (5X,3F10.5)
      READ 5,(XV(IN),YV(IN),IN=1,NNTV)
    5 FORMAT (2F10.5)
      READ 6,(YB(IE),IE=1,NE)
    6 FORMAT (12F5.3)
      READ 9,(XO(IN),YO(IN),IN=1,30)
    9 FORMAT (2F10.5)
      READ 8,OMEGA,EPS,DT,EPSV
    8 FORMAT (7X,4F10.5)
      PRINT 701,NE,NN,NNT,NNV,NNTV
  701 FORMAT (7X,5I5)
      PRINT 702,(I(IE),J(IE),K(IE),L(IE),M(IE),N(IE),IV(IE),JV(IE),
     5KV(IE),IE=1,NE)
  702 FORMAT (7X,9I5)
      PRINT 703,(PSI(IN),X(IN),Y(IN),IN=1,NNT)
  703 FORMAT (7X,3F10.5)
      PRINT 704,(XV(IN),YV(IN),IN=1,NNTV)
  704 FORMAT (7X,2F10.5)
      PRINT705,(YB(IE),IE=1,NE)
  705 FORMAT (7X,12F5.3)
      PRINT 706,(XO(IN),YO(IN),IN=1,30)
  706 FORMAT (7X,2F10.5)
      PRINT8,OMEGA,EPS,DT,EPSV
      DO 16 IE=1,NE
   16 VORA(IE)=0.0
      DO 17 IN=1,NNTV
   17 DW(IN)=0.0
      KA=1
      ISUB=1
  901 CONTINUE
      DO 41 IE=1,NE
      DO 41 IO=1,6
   41 ALPHA(IO,IE)=0.0
      IE=1
   13 IR=I(IE)
      JR=J(IE)
      KR=K(IE)
      LR=L(IE)
      MR=M(IE)
      NR=N(IE)
```

```
      XG(IE)=(X(IR)+X(MR)+X(KR))/3.
      YG(IE)=(Y(IR)+Y(MR)+Y(KR))/3.
      XL(IR)=(X(IR)-XG(IE))/12.
      XL(JR)=(X(JR)-XG(IE))/12.
      XL(KR)=(X(KR)-XG(IE))/12.
      XL(LR)=(X(LR)-XG(IE))/12.
      XL(MR)=(X(MR)-XG(IE))/12.
      XL(NR)=(X(NR)-XG(IE))/12.
      YL(IR)=(Y(IR)-YG(IE))/12.
      YL(JR)=(Y(JR)-YG(IE))/12.
      YL(KR)=(Y(KR)-YG(IE))/12.
      YL(LR)=(Y(LR)-YG(IE))/12.
      YL(MR)=(Y(MR)-YG(IE))/12.
      YL(NR)=(Y(NR)-YG(IE))/12.
      C(1,1)=1.
      C(1,2)=XL(IR)
      C(1,3)=YL(IR)
      C(1,4)=XL(IR)*XL(IR)
      C(1,5)=XL(IR)*YL(IR)
      C(1,6)=YL(IR)*YL(IR)
      C(2,1)=1.
      C(2,2)=XL(JR)
      C(2,3)=YL(JR)
      C(2,4)=XL(JR)*XL(JR)
      C(2,5)=XL(JR)*YL(JR)
      C(2,6)=YL(JR)*YL(JR)
      C(3,1)=1.
      C(3,2)=XL(KR)
      C(3,3)=YL(KR)
      C(3,4)=XL(KR)*XL(KR)
      C(3,5)=XL(KR)*YL(KR)
      C(3,6)=YL(KR)*YL(KR)
      C(4,1)=1.
      C(4,2)=XL(LR)
      C(4,3)=YL(LR)
      C(4,4)=XL(LR)*XL(LR)
      C(4,5)=XL(LR)*YL(LR)
      C(4,6)=YL(LR)*YL(LR)
      C(5,1)=1.
      C(5,2)=XL(MR)
      C(5,3)=YL(MR)
      C(5,4)=XL(MR)*XL(MR)
      C(5,5)=XL(MR)*YL(MR)
      C(5,6)=YL(MR)*YL(MR)
      C(6,1)=1.
      C(6,2)=XL(NR)
      C(6,3)=YL(NR)
      C(6,4)=XL(NR)*XL(NR)
      C(6,5)=XL(NR)*YL(NR)
      C(6,6)=YL(NR)*YL(NR)
      CALL MINV (C,6,D,LL,MM)
      CF(IE)=C(1,1)+C(1,2)+C(1,3)+C(1,4)+C(1,5)+C(1,6)
      DO 52 IO=1,6
      JO=1
   51 CONTINUE
      GO TO (43,44,45,46,47,48),JO
   43 IR=IR
      GO TO 42
   44 IR=JR
      GO TO 42
```

```
45 IR=KR
   GO TO 42
46 IR=LR
   GO TO 42
47 IR=MR
   GO TO 42
48 IR=NR
42 ALPHA(IO,IE)=ALPHA(IO,IE)+C(IO,JO)*PSI(IR)
   JO=JO+1
   IF(JO-6) 51,51,52
52 CONTINUE
   U(IE)=ALPHA(3,IE)
   V(IE)=-ALPHA(2,IE)
   IF(KT-1) 43,1000,43
1000 APEA(IE)=(X(IR)*(Y(KR)-Y(MR))+X(KR)*(Y(MR)-Y(IR))+X(MR)*(Y(IR)-
  4Y(KR)))/144.
   XS(IE)=XL(IR)*XL(IR)+XL(KR)*XL(KR)+XL(MR)*XL(MR)
   YS(IE)=YL(IR)*YL(IR)+YL(KR)*YL(KR)+YL(MR)*YL(MR)
   XY(IE)=XL(IR)*YL(IR)+XL(KR)*YL(KR)+XL(MR)*YL(MR)
   MO=1
   IRT=1
   IST=1
 7 ANM=APEA(IE)*(C(2,IRT)*C(2,IST)+(1./3.)*XS(IE)
  5*C(4,IRT)*C(4,IST)+(1./12.)*YS(IE)*C(5,IRT)*C(5,IST)+(1./6.)
  5*XY(IE)*(C(5,IRT)*C(4,IST)+C(4,IRT)*C(5,IST)))
   AMM=APEA(IE)*(C(3,IRT)*C(3,IST)+(1./12.)*XS(IE)*
  3C(5,IRT)*C(5,IST)+(1./3.)*YS(IE)*C(6,IRT)*C(6,IST)
  3+(1./6.)*XY(IE)*(C(6,IRT)*C(5,IST)+C(5,IRT)*C(6,IST)))
   H(IRT,IST,IE)=ANM+AMM
   GO TO (20,21,22,23,24,25,26,27,28,29,30,31,32,33,34,35,36,37,38
  2,39,40),MO
20 IST=2
   GO TO 15
15 MO=MO+1
   GO TO 7
21 H(IST,IRT,IE)=H(IRT,IST,IE)
   IST=3
   GO TO 15
22 H(IST,IRT,IE)=H(IRT,IST,IE)
   IST=4
   GO TO 15
23 H(IST,IRT,IE)=H(IRT,IST,IE)
   IST=5
   GO TO 15
24 H(IST,IRT,IE)=H(IRT,IST,IE)
   IST=6
   GO TO 15
25 H(IST,IRT,IE)=H(IRT,IST,IE)
   IST=2
   IRT=2
   GO TO 15
26 IST=3
   GO TO 15
27 H(IST,IRT,IE)=H(IRT,IST,IE)
   IST=4
   GO TO 15
28 H(IST,IRT,IE)=H(IRT,IST,IE)
   IST=5
   GO TO 15
29 H(IST,IRT,IE)=H(IRT,IST,IE)
```

```
      IST=6
      GO TO 15
   30 H(IST,IRT,IE)=H(IRT,IST,IE)
      IST=3
      IRT=?
      GO TO 15
   31 IST=4
      GO TO 15
   32 H(IST,IRT,IE)=H(IRT,IST,IE)
      IST=5
      GO TO 15
   33 H(IST,IRT,IE)=H(IRT,IST,IE)
      IST=6
      GO TO 15
   34 H(IST,IRT,IE)=H(IRT,IST,IE)
      IST=4
      IRT=4
      GO TO 15
   35 IST=5
      GO TO 15
   36 H(IST,IRT,IE)=H(IRT,IST,IE)
      IST=6
      GO TO 15
   37 H(IST,IRT,IE)=H(IRT,IST,IE)
      IST=5
      IRT=5
      GO TO 15
   38 IST=6
      GO TO 15
   39 H(IST,IRT,IE)=H(IRT,IST,IE)
      IST=6
      IRT=6
      GO TO 15
   40 CONTINUE
      IE=IE+1
      IF(IE-NE) 13,13,14
   14 CONTINUE
      DO 54 IE=1,NE
   54 F(IE)=VOKA(IE)*AREA(IE)*CF(IE)
C     ASSEMBLE EQUATIONS
      DO 190 IP=1,NN
      W(IP)=0.0
      DO 190 JJ=1,45
  190 H(IP,JJ)=0.0
      IP=1
  195 IE=1
  200 IF(I(IE)-IP) 201,202,201
  201 IF(J(IE)-IP) 203,204,203
  203 IF(K(IE)-IP) 205,206,205
  205 IF(L(IE)-IP) 207,208,207
  207 IF(M(IE)-IP) 209,210,209
  209 IF(N(IE)-IP) 211,212,211
  211 IE=IE+1
      IF(IE-NE) 213,213,214
  213 GO TO 200
  202 IR=I(IE)
      IRT=1
      IST=1
      JR=J(IE)
      KR=K(IE)
```

```
      LR=L(IE)
      MR=M(IE)
      NR=N(IE)
      GO TO 215
  204 IR=J(IE)
      IRT=2
      IST=2
      JR=K(IE)
      KR=L(IE)
      LR=M(IE)
      MR=N(IE)
      NR=I(IE)
      GO TO 215
  206 IR=K(IE)
      IRT=3
      IST=3
      JR=L(IE)
      KR=M(IE)
      LR=N(IE)
      MR=I(IE)
      NR=J(IE)
      GO TO 215
  208 IR=L(IE)
      IRT=4
      IST=4
      JR=M(IE)
      KR=N(IE)
      LR=I(IE)
      MR=J(IE)
      NR=K(IE)
      GO TO 215
  210 IR=M(IE)
      IRT=5
      IST=5
      JR=N(IE)
      KR=I(IE)
      LR=J(IE)
      MR=K(IE)
      NR=L(IE)
      GO TO 215
  212 IR=N(IE)
      IRT=6
      IST=6
      JR=I(IE)
      KR=J(IE)
      LR=K(IE)
      MR=L(IE)
      NR=M(IE)
  215 W(IP)=-F(IE)+W(IP)
      MX=1
  220 JJ=25+IR-IP
      B(IP,JJ)=B(IP,JJ)+H(IRT,IST,IE)
      GO TO (221,222,223,224,225,226),MX
  221 IR=JR
  230 MX=MX+1
      IST=IST+1
      IF(IST-6) 231,231,232
  232 IST=1
  231 IF(IR-NN) 220,220,240
  240 W(IP)=W(IP)-H(IRT,IST,IE)*PSI(IR)
```

```
      GO TO (221,222,223,224,225,226),KX
  222 IP=KP
      GO TO 230
  223 IP=LR
      GO TO 230
  224 IP=MR
      GO TO 230
  225 IP=NR
      GO TO 230
  226 IF(IE-NF) 211,214,214
  214 IF(IP-NN) 241,242,242
  241 IP=IP+1
      GO TO 195
  242 CONTINUE
C     SOLVE FOR PSI(IN)
      ITER=1
 1001 DO 300 IN=1,NN
  300 BO(IN)=OMEGA/B(IN,23)
      BIT=(1.-OMEGA)
  301 ITER=ITER+1
      PRINT 90,ITER
   90 FORMAT (7X,I3)
   70 CONTINUE
      D1=0.0
      IN=1
  302 EX=0.0
      IT=1
      IF(W(IN)-0.0) 303,304,303
  303 EX=W(IN)
  304 CONTINUE
  260 IF(IT-23) 305,307,305
  305 ID=IN-23+IT
      IF(ID) 307,307,360
  360 IF(ID-NN) 361,361,308
  361 IF(B(IN,IT)-0.0) 362,363,362
  362 EX=EX-B(IN,IT)*PSI(ID)
  363 IF(IT-45) 307,308,308
  307 IT=IT+1
      GO TO 260
  308 EX=BO(IN)*EX+BIT*PSI(IN)
      IF(ABS(PSI(IN)-EX)-D1) 320,320,321
  321 D1=ABS(PSI(IN)-EX)
  320 PSI(IN)=EX
  370 IF(IN-NN) 330,331,331
  330 IN=IN+1
      GO TO 302
  331 IF(D1-EPS) 340,340,301
  340 PRINT 350,(PSI(IN),IN=1,NN)
  350 FORMAT (7X,5F10.6/7X,5F10.6)
      IF(KT-1) 830,830,831
  830 CONTINUE
      DO 57 IN=1,91
   57 VOR(IN)=0.0
  831 CONTINUE
      DO 55 IN=1,5
      IM=IN+91
      IB=361+2*IN
   55 VOR(IM)=3.75/Y(IB)
      VOR(97)=32.*U(1)/(YG(1)-YB(1))
      DO 56 IN=1,15
```

```
      IM=INI+2
      IS=12*IK-12
      VOR(IM)=2.*U(IM)/(YG(IS)-YG(IS))
   55 CONTINUE
  400 IE=1
  401 IZ=IV(IE)
      JZ=JV(IE)
      KZ=KV(IE)
      VORA(IE)=(VOR(IZ)+VOR(JZ)+VOR(KZ))/3.
      XLV(IZ)=(XV(IZ)-XG(IE))/12.
      XLV(JZ)=(XV(JZ)-XG(IE))/12.
      XLV(KZ)=(XV(KZ)-XG(IE))/12.
      YLV(IZ)=(YV(IZ)-YG(IE))/12.
      YLV(JZ)=(YV(JZ)-YG(IE))/12.
      YLV(KZ)=(YV(KZ)-YG(IE))/12.
      CM(1,1)=1.
      CM(1,2)=XLV(IZ)
      CM(1,3)=YLV(IZ)
      CM(2,1)=1.
      CM(2,2)=XLV(JZ)
      CM(2,3)=YLV(JZ)
      CM(3,1)=1.
      CM(3,2)=XLV(KZ)
      CM(3,3)=YLV(KZ)
      CALL MINV (CM,3,D,LC,MC)
      BB(IE)=CM(2,1)*VOR(IZ)+CM(2,2)*VOR(JZ)+CM(2,3)*VOR(KZ)
      CC(IE)=CM(3,1)*VOR(IZ)+CM(3,2)*VOR(JZ)+CM(3,3)*VOR(KZ)
      AV(IZ)=XLV(JZ)*YLV(KZ)-XLV(KZ)*YLV(JZ)
      AV(JZ)=XLV(KZ)*YLV(IZ)-XLV(IZ)*YLV(KZ)
      AV(KZ)=XLV(IZ)*YLV(JZ)-XLV(JZ)*YLV(IZ)
      BV(IZ)=YLV(JZ)-YLV(KZ)
      BV(JZ)=YLV(KZ)-YLV(IZ)
      BV(KZ)=YLV(IZ)-YLV(JZ)
      CV(IZ)=XLV(KZ)-XLV(JZ)
      CV(JZ)=XLV(IZ)-XLV(KZ)
      CV(KZ)=XLV(JZ)-XLV(IZ)
      AVT(IE)=AV(IZ)+AV(JZ)+AV(KZ)
      IF (KT-1) 2250,2250,410
 2250 CONTINUE
      CON(IE)=19400./1.75
      XSV(IE)=XLV(IZ)*XLV(IZ)+XLV(JZ)*XLV(JZ)+XLV(KZ)*XLV(KZ)
      YSV(IE)=YLV(IZ)*YLV(IZ)+YLV(JZ)*YLV(JZ)+YLV(KZ)*YLV(KZ)
      XYV(IE)=XLV(IZ)*YLV(IZ)+XLV(JZ)*YLV(JZ)+XLV(KZ)*YLV(KZ)
      MY=1
      IZ=IV(IE)
      IY=IV(IE)
      IZT=1
      IYT=1
  402 BPC(IZT,IYT,IE)=(BV(IZ)*BV(IY)+CV(IZ)*CV(IY))/(4.*AREA(IE))
      P(IZT,IYT,IE)=CON(IE)*(AV(IZ)*AV(IY)+(1./12.)*XSV(IE)*BV(IZ).
     5*BV(IY)+(1./12.)*YSV(IE)*CV(IZ)*CV(IY)+(1./12.)*XYV(IE)*BV(IZ)
     5*CV(IY))/(4.*AREA(IE))
      GO TO (405,406,407,408,409,410),MY
  405 IY=JV(IE)
      IYT=2
      GO TO 403
  403 MY=MY+1
      GO TO 402
  406 BPC(IYT,IZT,IE)=BPC(IZT,IYT,IE)
      P(IYT,IZT,IE)=P(IZT,IYT,IE)
```

```
      IY=KV(IF)
      IYT=3
      GO TO 4..
  407 BPC(IYT,IZT,IF)=BPC(IZT,IYT,IF)
      P(IYT,IZT,IF)=P(IZT,IYT,IF)
      IY=JV(IF)
      IZ=JV(IF)
      IYT=2
      IZT=2
      GO TO 4..
  408 IY=KV(IF)
      IYT=3
      GO TO 4..
  409 BPC(IYT,IZT,IF)=BPC(IZT,IYT,IF)
      P(IYT,IZT,IF)=P(IZT,IYT,IF)
      IZ=KV(IF)
      IZT=3
      GO TO 4..
  410 IF=IF+1
      IF(IF-NE) 4..,4..,411
  411 CONTINUE
      DO 415 IF=1,NE
  415 Q(IF)=[illegible]+V(IF)*CC(IF)))*AVT(IF)/2.
  755 DO 417 IN=1,N
      R(IN)=0.
      DO 417 JJ=1,..
  417 A(IN,JJ)=0.
      IN=1
  418 IF=1
  419 IF(IV(IF)-IN) 420,421,420
  420 IF(JV(IF)-IN) 422,423,422
  422 IF(KV(IF)-IN) 424,425,424
  424 IF=IF+1
      IF(IF-NE) 419,419,4..
  430 GO TO 4..
  421 IZ=IV(IF)
      IYT=1
      IZT=1
      JZ=JV(IF)
      KZ=KV(IF)
      GO TO 42.
  423 IZ=JV(IF)
      IYT=2
      IZT=2
      JZ=KV(IF)
      KZ=IV(IF)
      GO TO 4..
  425 IZ=KV(IF)
      IYT=3
      IZT=3
      JZ=IV(IF)
      KZ=JV(IF)
  4.. R(IN)=Q(IF)+R(IN)
      NX=1
  5.. JJ=.+IZ-IN
      IF(.T-1) 4..,4..,4..
  4.. A(IN,JJ)=A(IN,JJ)-.(IYT,IZT,IF)
      GO TO 4..
  47. A(IN,JJ)=A(IN,JJ)+BPC(IYT,IZT,IF)+(./.T)*P(IYT,IZT,IF)
  4.. GO TO (..,...,...),NX
```

```
44 IZ=IZ
44 NX=NX+1
   IZ1=IZ1+1
   IF(IZ1-?) 4..., ..., 4..
447 IZ1=1
4?? IF(KT-1) 4??, ..., ...
44? IF (IZ-NXV). ..., ..., 4...
44? IF (IZ-NXV)   ..., ..., ...
44? P(IN)=P(IN)+?(IY?,IZ?,I?)*( (IZ)+...(IY,IZ,I ) ... (IZ).
   GO TO 4..
47? P(IN)=P(IN)-( ?(IY?,IZ?,I?)*( ,Z?T) + (IY?,IZ?,I? ))*V? (IZ)
  *+(P(IY?,IZ?,I? ))*(( ,Z?T) ...(I?))(I?))
4?? GO TO (4..., ..., ...), ...
4?? IZ=?
   GO TO 4..
4?? IF(IT-? ) ..., ..., ...
45? IF(IN-N?V) ..., ..., ...
451 IN=IN+1
   GO TO 41
452 CONTINUE
9?? IT?=1
   DO 91? IN=1,??V
91? ?DV(IN)=...(IN,?)
   ?ITV=1.-...
9?7 IT?=IT?+1
   PRINT ...,IT?
   IF(IT?-1?) ..., ..., ...
911 CONTINUE
   DIV=?.?
   IF(KT-1) ..., ..., ...
4?? DO ?? IN=1,?V
55? ?X(IN)=?(IN)
   GO TO ?7?
4?1 DO ... IN=1,...
5?? ??(IN)=V?(IN)
57? IN=1
91? ?XV=?.
   IT=1
   IF (?(IN)-?.?) ..., ..., ...
914 ?XV=?(IN)
91? CONTINUE
91? IF (IT-?) ..., ..., ...
917 IDV=I?-...
   IF(IDV) ..., ..., ...
92? IF (IDV-?DV) ..., ..., ...
921 IF (A(IN,IT)-?.?) ..., ..., ...
9?1 ?XV=?XV-A(IN,IT)*?(IDV)
9?? IF (IT-??) ..., ..., ...
91? IT=IT+1
   GO TO 91?
9?? ?XV=?XV(IN)...?TV ...(IN)
   IF (ABS(??(IN)-?XV)-DIV) ..., ..., ...
941 DIV=A?S(??(IN)-?XV)
   IF(KT-1) ..., ..., ...
1?0? D?(IN)=...(IN)+(?XV-?(IN))*?.75?
94? ??(IN)=?XV
9?? IF (IN-N?V) ..., ..., 94?
942 IN=IN+1
   GO TO 91?
94? IF(DIV-??V) ..., ..., ...
```

```
950 PRINT 951,(DW(IN),IN=1,NNV)
951 FORMAT (7X,6E17.4)
    IF(KE-1) 960,961,960
961 DO 962 IN=1,NNV
962 DW(IN)=XW(IN)
    KT=KT+1
    GO TO 750
960 DO 963 IN=1,NNV
963 VOR(IN)=XW(IN)
    PRINT 951,(DW(IN),IN=1,NNV)
    ISUP=ISUP+1
    IF (ISUP-7) 901,901,902
902 PRINT 810,(U(IE),IE=1,NE)
    PRINT 810,(V(IE),IE=1,NE)
    PRINT 810,(XG(IE),IE=1,NE)
    PRINT 810,(YG(IE),IE=1,NE)
810 FORMAT (7X,6E11.6/7X,6E11.6)
    DO 850 IN=1,30
    IE=2*IN+60
    U(IE)=ALPHA(3,IE)+ALPHA(5,IE)*(XC(IN)-XG(IE))/12.
   5+2.*ALPHA(6,IE)*(YC(IN)-YG(IE))/12.
    PRINT 860,U(IE)
860 FORMAT (7X,E12.8)
850 CONTINUE
    STOP
    END
```

2
3
4
5
6

Output Laminar Model

ϕ "first time step"

0.000335	0.001844	0.003346	0.006598	0.010381	0.015266	0.024498
0.039551	0.074004	0.116702	0.204940			
0.000485	0.001712	0.003601	0.005975	0.009736	0.014240	0.026082
0.040736	0.075318	0.116884	0.205474			
0.001234	0.002631	0.004940	0.007526	0.011397	0.015834	0.027779
0.042134	0.076489	0.117347	0.206020			
0.001111	0.002352	0.004744	0.007434	0.011915	0.017019	0.028643
0.042262	0.076834	0.117628	0.206221			
0.001107	0.002408	0.004893	0.007715	0.012077	0.017108	0.028758
0.042073	0.076904	0.117745	0.206294			
0.001268	0.002476	0.004613	0.007153	0.011155	0.015506	0.027549
0.041990	0.076064	0.117307	0.205800			
0.001189	0.002618	0.005004	0.007882	0.012348	0.017299	0.02904[illegible]
0.042405	0.076918	0.117902	0.206256			
0.001359	0.002737	0.005030	0.007780	0.011691	0.016750	0.028930
0.042548	0.076755	0.117723	0.206131			
0.001257	0.002727	0.005239	0.008056	0.012566	0.018278	0.029929
0.042312	0.076965	0.117965	0.206301			
0.001408	0.002920	0.005496	0.008384	0.013508	0.019116	0.029964
0.042158	0.076980	0.117787	0.206320			
0.001111	0.002352	0.004748	0.007441	0.011932	0.017047	0.028736
0.042404	0.077025	0.117818	0.206332			
0.000572	0.001776	0.003858	0.006271	0.010223	0.014867	0.027493
0.042562	0.077062	0.117804	0.206329			
0.001244	0.002639	0.004974	0.007570	0.011488	0.015962	0.028145
0.042667	0.077083	0.117815	0.206332			
0.001107	0.002408	0.004894	0.007716	0.012080	0.017113	0.028777
0.042108	0.076963	0.117814	0.206333			
0.000609	0.002364	0.004326	0.007461	0.011800	0.017154	0.027158
0.042717	0.077037	0.117994	0.206317			
0.001281	0.002535	0.004688	0.007276	0.011370	0.015883	0.028257
0.042994	0.077103	0.118014	0.206321			
0.001189	0.002619	0.005005	0.007885	0.012354	0.017316	0.029090
0.042484	0.077023	0.118013	0.206324			
0.001359	0.002742	0.005038	0.007798	0.011726	0.016839	0.029109
0.042838	0.077094	0.118021	0.206323			
0.001257	0.002728	0.005289	0.008057	0.012567	0.018282	0.029938
0.042332	0.076996	0.118003	0.206325			
0.001408	0.002920	0.005496	0.008384	0.013509	0.019117	0.029968
0.042166	0.076997	0.117810	0.206333			
0.001111	0.002352	0.004748	0.007441	0.011932	0.017047	0.028734
0.042406	0.077047	0.117846	0.206343			
0.000572	0.001776	0.003858	0.006271	0.010223	0.014867	0.027494
0.042564	0.077066	0.117811	0.206334			
0.001107	0.002402	0.004889	0.007695	0.012034	0.017030	0.028709
0.042149	0.077202	0.117982	0.206498			
0.001244	0.002639	0.004974	0.007570	0.011488	0.015962	0.028146
0.042668	0.077085	0.117817	0.206332			
0.000609	0.002364	0.004326	0.007461	0.011800	0.017154	0.027159
0.042723	0.077046	0.118006	0.206325			
0.001281	0.002535	0.004688	0.007275	0.011370	0.015883	0.028257
0.042996	0.077106	0.118018	0.206324			
0.001189	0.002619	0.005005	0.007884	0.012350	0.017305	0.029067

0.042489	0.077121	0.118092	0.206386			
0.001359	0.002742	0.005039	0.007798	0.011728	0.016839	0.029110
0.042838	0.077074	0.118025	0.206321			
0.001226	0.002692	0.005170	0.007889	0.012326	0.018022	0.029822
0.042352	0.077476	0.118201	0.206670			
0.001173	0.002503	0.004941	0.007698	0.012903	0.018631	0.029875
0.042276	0.077825	0.118153	0.206911			

2
3
4
5

$\left\{\frac{\partial\omega}{\partial t}\right\}_{t=0}$

0.77232E 01	-0.34395E 00	0.93827E-01	-0.13131E 00	-0.44925E 00
0.78455E 01	-0.10678E 01	0.20804E-01	-0.84284E-01	0.14035E 00
0.10161E 02	-0.92306E 00	0.22984E 00	0.32346E 00	-0.50121E 00
0.97518E 01	-0.15419E 01	-0.18585E 00	-0.13069E-01	0.34648E 00
0.80050E 01	0.67663E 00	0.19664E 00	0.10110E 00	0.19042E 00
0.64838E 01	-0.49802E 00	-0.48470E 00	-0.25998E 00	0.13603E 00
0.81615E 01	-0.94850E 00	0.30195E 00	0.22846E 00	0.56978E-01
0.10187E 02	-0.93743E 00	0.91651E-01	-0.80322E 00	-0.14062E 00
0.96186E 01	-0.11579E 01	0.66052E-01	0.27038E 00	0.27454E 00
0.81666E 01	0.64903E 00	0.27259E 00	0.66571E-01	-0.94197E 00
0.62333E 01	-0.62279E 00	-0.14359E 00	-0.11675E 00	0.23137E 00
0.83572E 01	-0.81675E 00	0.32861E 00	0.51025E 00	0.23717E 00
0.98072E 01	-0.12647E 01	-0.18673E 00	-0.35164E 00	0.98236E-01
0.98492E 01	-0.83878E 00	0.32227E 00	0.35976E 00	-0.50290E 00
0.84270E 01	-0.97884E 00	-0.41321E 00	-0.28717E 00	0.62781E-01

2
3
4
5

ω and $\left\{\frac{\partial\omega}{\partial t}\right\}$ "first time step"

0.76071E-01	-0.35353E-02	0.17470E-02	0.28265E-02	0.52736E-02
0.81990E-01	-0.84755E-02	0.27483E-03	0.44397E-03	-0.14440E-02
0.99482E-01	-0.12092E-01	-0.47237E-03	-0.32772E-02	0.50136E-02
0.96634E-01	-0.59787E-02	0.30810E-02	0.68541E-04	-0.34582E-02
0.80820E-01	0.36704E-02	-0.18993E-02	-0.10081E-02	-0.19047E-02
0.61245E-01	-0.46984E-02	0.50328E-02	0.25881E-02	-0.13593E-02
0.83583E-01	-0.92629E-02	-0.17835E-02	-0.23514E-02	-0.56679E-03
0.98450E-01	-0.12088E-01	0.72865E-03	0.79479E-02	0.14092E-02
0.98104E-01	-0.97568E-02	0.59034E-03	-0.27592E-02	-0.27409E-02
0.79178E-01	0.39303E-02	-0.26627E-02	-0.66389E-03	0.94124E-02
0.63745E-01	-0.34486E-02	0.16272E-02	0.11585E-02	-0.23084E-02
0.81638E-01	-0.10582E-01	-0.20529E-02	-0.51691E-02	-0.23683E-02
0.10223E 00	-0.88171E-02	0.35104E-02	0.34352E-02	-0.97873E-03
0.95816E-01	-0.12942E-01	-0.19703E-02	-0.36546E-02	0.50278E-02
0.80032E-01	-0.36772E-02	0.51594E-02	0.28251E-02	-0.62149E-03
-0.15330E 02	-0.34395E 00	0.93827E-01	-0.13131E 00	-0.44925E 00
-0.16045E 02	-0.10678E 01	0.20804E-01	-0.84284E-01	0.14035E 00
-0.20109E 02	-0.92306E 00	0.22984E 00	0.32346E 00	-0.50121E 00
0.97518E 01	-0.15419E 01	-0.18585E 00	-0.13069E-01	0.34648E 00
0.80050E 01	0.67663E 00	0.19664E 00	0.10110E 00	0.19042E 00
0.64838E 01	-0.49802E 00	-0.48470E 00	-0.25998E 00	0.13603E 00
0.81615E 01	-0.94850E 00	0.30195E 00	0.22846E 00	0.56978E-01
0.10187E 02	-0.93743E 00	0.91651E-01	-0.80322E 00	-0.14062E 00
0.96186E 01	-0.11579E 01	0.66052E-01	0.27038E 00	0.27454E 00
0.81666E 01	0.64903E 00	0.27259E 00	0.66571E-01	-0.94197E 00
0.62333E 01	-0.62279E 00	-0.14359E 00	-0.11675E 00	0.23137E 00
0.83572E 01	-0.81675E 00	0.32861E 00	0.51025E 00	0.23717E 00
-0.20030E 02	-0.12647E 01	-0.18673E 00	-0.35164E 00	0.98236E-01
0.98492E 01	-0.83878E 00	0.32227E 00	0.35976E 00	-0.50290E 00
0.84270E 01	-0.97884E 00	-0.41321E 00	-0.28717E 00	0.62781E-01

2

-0.000219	0.000600	0.002485	0.005728	0.009883	0.014958	0.024654
0.039653	0.074583	0.116621	0.205396			
-0.001200	-0.001249	0.002044	0.005169	0.009503	0.014275	0.027089
0.041544	0.076788	0.117268	0.206370			
-0.000092	0.000547	0.004595	0.008453	0.013013	0.018076	0.030746
0.045402	0.079479	0.119089	0.207575			
-0.000033	0.000562	0.004881	0.008928	0.014379	0.020287	0.032760
0.046699	0.080795	0.120196	0.208199			
0.000042	0.000852	0.005411	0.009719	0.015116	0.020885	0.033386
0.047042	0.081385	0.120783	0.208514			
0.000379	0.001794	0.004197	0.007241	0.011969	0.016831	0.029651
0.044296	0.078333	0.118484	0.207040			
0.000829	0.002768	0.005906	0.009552	0.015104	0.020728	0.033470
0.047085	0.081182	0.120728	0.208370			
0.000861	0.002685	0.005585	0.008979	0.013745	0.019440	0.032582
0.046441	0.080293	0.119938	0.207916			
0.001105	0.003154	0.006708	0.010261	0.015665	0.022086	0.034665
0.047305	0.081589	0.121122	0.208596			
0.001244	0.002815	0.006854	0.010643	0.016713	0.023100	0.034731
0.047278	0.081697	0.121072	0.208666			
-0.000011	0.000595	0.004967	0.009059	0.014628	0.020639	0.033428
0.047590	0.081885	0.121272	0.208780			
-0.000627	-0.000075	0.003769	0.007414	0.012328	0.017869	0.031910
0.047653	0.081875	0.121204	0.208738			
0.000069	0.000782	0.005047	0.009017	0.013877	0.019167	0.032643
0.047779	0.081927	0.121259	0.208768			
0.000046	0.000858	0.005430	0.009750	0.015179	0.020986	0.033607
0.047361	0.081842	0.121273	0.208783			
0.000311	0.002240	0.005020	0.009016	0.014392	0.020580	0.031610
0.047717	0.081815	0.121313	0.208703			
0.000722	0.002413	0.005067	0.008382	0.013578	0.018893	0.032698
0.048001	0.081933	0.121402	0.208751			
0.000835	0.002787	0.005946	0.009627	0.015234	0.020948	0.033853
0.047640	0.081886	0.121429	0.208779			
0.000908	0.002796	0.005765	0.009277	0.014195	0.020143	0.033714
0.047910	0.081938	0.121429	0.208771			
0.001107	0.003158	0.006717	0.010278	0.015700	0.022156	0.034792
0.047507	0.081873	0.121424	0.208781			
0.001245	0.002816	0.006858	0.010650	0.016731	0.023133	0.034801
0.047387	0.081877	0.121274	0.208785			
-0.000011	0.000593	0.004962	0.009048	0.014614	0.020628	0.033444
0.047661	0.082043	0.121469	0.208943			
-0.000627	-0.000075	0.003769	0.007415	0.012332	0.017876	0.031933
0.047695	0.081951	0.121298	0.208797			
0.000032	0.000812	0.005356	0.009641	0.015070	0.020899	0.033611
0.047501	0.082213	0.121671	0.209161			
0.000069	0.000783	0.005048	0.009017	0.013879	0.019170	0.032657
0.047816	0.081998	0.121357	0.208836			
0.000312	0.002240	0.005021	0.009018	0.014399	0.020595	0.031644
0.047790	0.081925	0.121440	0.208785			
0.000722	0.002413	0.005068	0.008383	0.013581	0.018899	0.032715
0.048038	0.081996	0.1214[illegible]	0.208806			
0.000830	0.002778	0.005922	0.009595	0.015192	0.020913	0.033869
0.047728	0.082133	0.121709	0.209033			
0.000908	0.002796	0.005764	0.009275	0.014192	0.020142	0.033729
0.047955	0.082041	0.121565	0.208875			
0.001028	0.003044	0.006501	0.010038	0.015474	0.021977	0.034795

0.047639	0.082432	0.121917	0.209326			
0.000974	0.002328	0.006152	0.010093	0.016295	0.022833	0.034823
0.047573	0.082701	0.121924	0.209533			

2

0.64744E-01	-0.10026E-01	0.41247E-02	0.13246E-02	0.51491E-02
0.76434E-01	-0.24269E-01	0.48165E-02	-0.31297E-05	-0.10574E-02
0.95694E-01	-0.26678E-01	0.27140E-02	-0.45409E-02	0.51823E-02
0.93345E-01	-0.18122E-01	0.56852E-02	0.45599E-03	-0.27950E-02
0.81654E-01	-0.55248E-02	-0.10840E-02	-0.25349E-02	-0.21077E-02
0.53281E-01	-0.12439E-01	0.92834E-02	0.28292E-02	-0.58248E-03
0.76793E-01	-0.24414E-01	0.20765E-02	-0.40850E-02	-0.19187E-02
0.93853E-01	-0.26629E-01	0.41715E-02	0.81786E-02	0.20353E-02
0.95936E-01	-0.22393E-01	0.23767E-02	-0.23994E-02	-0.30687E-02
0.77632E-01	-0.58911E-02	-0.19051E-02	-0.21034E-02	0.90737E-02
0.55984E-01	-0.85249E-02	0.54246E-02	0.95464E-03	-0.98727E-03
0.73030E-01	-0.27934E-01	0.98015E-03	-0.63979E-02	-0.28639E-02
0.99731E-01	-0.21251E-01	0.86526E-02	0.37121E-02	-0.50821E-03
0.92395E-01	-0.28871E-01	-0.14240E-02	-0.50276E-02	0.45757E-02
0.87893E-01	-0.21225E-02	0.60026E-02	0.32379E-02	-0.39635E-03
-0.16791E 02	0.48624E-01	-0.10429E 00	-0.13131E 00	-0.44925E 00
-0.15732E 02	0.27502E 01	0.20804E-01	-0.84284E-01	0.14035E 00
-0.20109E 02	-0.92306E 00	0.22984E 00	0.32346E 00	-0.50121E 00
0.97518E 01	-0.15419E 01	-0.18585E 00	-0.13069E-01	0.34648E 00
0.80050E 01	0.67663E 00	0.19654E 00	0.10110E 00	0.19042E 00
0.64838E 01	-0.49802E 00	-0.49470E 00	-0.25998E 00	0.13603E 00
0.81615E 01	-0.94850E 00	0.30195E 00	0.22846E 00	0.56978E-01
0.10187E 02	-0.93743E 00	0.91651E-01	-0.80322E 00	-0.14062E 00
0.96186E 01	-0.11579E 01	0.66052E-01	0.27038E 00	0.27454E 00
0.81666E 01	0.64903E 00	0.27259E 00	0.66571E-01	-0.94197E 00
0.62333E 01	-0.62279E 00	-0.14359E 00	-0.11675E 00	0.23137E 00
0.83572E 01	0.26032E 01	0.32861E 00	0.51025E 00	0.23717E 00
-0.20030E 02	-0.12647E 01	-0.18673E 00	-0.35164E 00	0.98236E-01
0.98492E 01	-0.83876E 00	0.32227E 00	0.35976E 00	-0.50290E 00
0.84270E 01	-0.97884E 00	-0.41321E 00	-0.28717E 00	0.62781E-01

0.024841	0.077829	0.278089	0.293223	0.329312	0.370379
0.500949	0.532370	0.735089	0.776018	0.894640	0.944911
-0.011100	0.164255	0.249837	0.369710	0.363205	0.415505
0.490836	0.548081	0.695131	0.749255	0.886283	0.932964
0.097502	0.204023	0.335932	0.403796	0.417405	0.453356
0.520890	0.568056	0.687545	0.743537	0.879321	0.926591
0.104741	0.203850	0.361212	0.425324	0.447450	0.485274
0.545050	0.584530	0.689493	0.743545	0.875617	0.923382
0.148361	0.271555	0.395172	0.435278	0.474466	0.501294
0.560856	0.595049	0.691858	0.743517	0.873808	0.921841
0.112335	0.155165	0.364669	0.367802	0.448865	0.448370
0.549514	0.574429	0.689117	0.742184	0.872933	0.921137
0.052899	0.196308	0.306921	0.399262	0.414327	0.450494
0.528661	0.570535	0.686574	0.741649	0.872512	0.920839
0.105977	0.209779	0.346972	0.412080	0.433671	0.466994
0.536372	0.579207	0.687843	0.742713	0.872401	0.920736
0.105824	0.204833	0.363846	0.427442	0.452476	0.489787
0.551677	0.589797	0.691063	0.744123	0.872429	0.920704
0.148573	0.271735	0.395767	0.435812	0.476096	0.502783
0.563457	0.597302	0.692914	0.743985	0.872474	0.920699
0.112361	0.155159	0.364826	0.367865	0.449336	0.448711
0.550497	0.575232	0.689615	0.742486	0.872405	0.920644
0.052896	0.196319	0.306960	0.399304	0.414475	0.450640
0.529014	0.571113	0.686916	0.742041	0.872221	0.920437
0.105982	0.209706	0.346955	0.411864	0.433648	0.467023
0.536925	0.580594	0.688633	0.743437	0.872050	0.919819

0.105366	0.202787	0.362834	0.425422	0.451974	0.490497
0.553642	0.593922	0.693212	0.745163	0.871836	0.918425
0.138945	0.249948	0.387832	0.435468	0.477303	0.509962
0.570734	0.605634	0.698440	0.743956	0.871729	0.916011
-0.002173	0.055751	-0.125694	-0.072386	-0.117291	-0.086550
-0.127767	-0.104034	-0.113967	-0.076840	-0.058348	-0.029600
-0.053605	0.047058	-0.044722	0.007699	-0.068286	-0.023824
-0.083590	-0.048608	-0.066415	-0.042776	-0.029414	-0.015871
-0.024516	0.062855	-0.003284	0.042716	-0.004926	0.014381
-0.024466	-0.006844	-0.031357	-0.017588	-0.014075	-0.008152
-0.019076	0.068838	0.010738	0.054252	0.015709	0.023086
-0.000307	0.005058	-0.012999	-0.005799	-0.006194	-0.004038
-0.024054	0.026368	-0.008184	0.011035	-0.000799	0.001588
-0.001955	-0.000990	-0.006817	-0.001824	-0.002215	-0.001938
-0.029790	0.020219	-0.064204	-0.052109	-0.035390	-0.027825
-0.019920	-0.008559	-0.003662	0.000223	-0.000207	-0.000950
-0.038677	0.059919	-0.007043	0.031295	-0.012893	0.009231
-0.007068	0.005640	-0.000258	0.002752	0.000828	-0.000472
-0.020790	0.064505	0.005754	0.047491	0.010715	0.026168
0.007614	0.014732	0.002321	0.004389	0.001274	-0.000260
-0.018594	0.069123	0.012370	0.055423	0.020134	0.026606
0.010752	0.012744	0.002317	0.004027	0.001373	-0.000144
-0.023985	0.026426	-0.007824	0.011282	0.000201	0.002603
0.001[illegible]68	0.001760	-0.000245	0.002356	0.001379	-0.000140
-0.029782	0.020224	-0.064160	-0.052109	-0.035160	-0.027766
-0.019043	-0.007856	-0.001134	0.001571	0.001268	-0.000298
-0.038679	0.059917	-0.007050	0.031305	-0.012867	0.009317
-0.006842	0.005683	0.000158	0.002232	0.000864	-0.000840
-0.020787	0.064526	0.005802	0.047690	0.010916	0.026650
0.007713	0.014329	0.000883	0.001692	-0.000540	-0.002078
-0.018503	0.069630	0.013150	0.057882	0.021784	0.029713
0.011364	0.012308	-0.001658	-0.001871	-0.003174	-0.004071
-0.022431	0.036053	-0.000037	-0.032454	0.007802	0.012165
0.003323	0.000072	-0.008380	-0.008915	-0.006695	-0.006707
0.050000	0.150000	0.100000	0.250000	0.150000	0.316667
0.166667	0.333333	0.166667	0.333333	0.166667	0.333333
0.400000	0.633333	0.533333	0.750000	0.633333	0.816667
0.666667	0.833333	0.666667	0.833333	0.666667	0.833333
0.983333	1.208332	1.074999	1.283333	1.141666	1.325000
1.166666	1.333333	1.166666	1.333333	1.166666	1.333333
1.574999	1.783333	1.624999	1.816666	1.658333	1.833333
1.666666	1.833333	1.666666	1.833333	1.666666	1.833333
2.141666	2.325000	2.158333	[illegible]333333	2.166666	2.333333
2.166666	2.333333	2.166666	[illegible].333333	2.166666	2.333333
2.549999	2.650000	2.599999	2.749999	2.650000	2.816667
2.666666	2.833333	2.666666	2.833333	2.666666	2.833333
2.900000	3.133332	3.033333	3.249999	3.133333	3.316667
3.166666	3.333333	3.166666	3.333333	3.166666	3.333333
3.483333	3.708332	3.574999	3.783333	3.641666	3.825000
3.666666	3.833333	3.666666	3.833333	3.666666	3.833333
4.074999	4.283333	4.124999	4.316666	4.158333	4.333333
4.166666	4.333333	4.166666	4.333333	4.166666	4.333333
4.641666	4.825000	4.658333	4.833333	4.666666	4.833333
4.666666	4.833333	4.666666	4.833333	4.666666	4.833333
5.049999	5.150000	5.099999	5.249999	5.150000	5.316667
5.166666	5.333333	5.166666	5.333333	5.166666	5.333333
5.399999	5.633331	5.533330	5.749994	5.633331	5.816666
5.666666	5.833333	5.666666	5.833333	5.666666	5.833333
5.983332	6.208328	6.074997	6.283330	6.141663	6.324997
6.166666	6.333333	6.166666	6.333333	6.166666	6.333333

6.574997	6.783330	6.624994	6.816666	6.658330	6.833333
6.666666	6.833333	6.666666	6.833333	6.666666	6.833333
7.141663	7.324997	7.158330	7.333333	7.166666	7.333333
7.166666	7.333333	7.166666	7.333333	7.166666	7.333333
0.183333	0.175000	0.358333	0.375000	0.600000	0.650000
0.966666	1.133332	1.766665	2.183332	3.433332	4.266665
0.078333	0.153333	0.266667	0.358333	0.516666	0.625000
0.925000	1.141665	1.766665	2.183332	3.433332	4.266665
0.128333	0.191667	0.308333	0.391666	0.550000	0.658333
0.949999	1.158333	1.766665	2.183332	3.433332	4.266665
0.166667	0.233333	0.341667	0.433333	0.591666	0.700000
0.974999	1.166666	1.766665	2.183332	3.433332	4.266665
0.216667	0.283333	0.391666	0.475000	0.625000	0.733333
0.999999	1.183332	1.766665	2.183332	3.433332	4.266665
0.183333	0.175000	0.358333	0.375000	0.600000	0.650000
0.966666	1.133332	1.766665	2.183332	3.433332	4.266665
0.078333	0.153333	0.266667	0.358333	0.516666	0.625000
0.925000	1.141665	1.766665	2.183332	3.433332	4.266665
0.128333	0.191667	0.308333	0.391666	0.550000	0.658333
0.949999	1.158333	1.766665	2.183332	3.433332	4.266665
0.166667	0.233333	0.341667	0.433333	0.591666	0.700000
0.974999	1.166666	1.766665	2.183332	3.433332	4.266665
0.216667	0.283333	0.391666	0.475000	0.625000	0.733333
0.999999	1.183332	1.766665	2.183332	3.433332	4.266665
0.183333	0.175000	0.358333	0.375000	0.600000	0.650000
0.966666	1.133332	1.766665	2.183332	3.433332	4.266665
0.078333	0.153333	0.266667	0.358333	0.516666	0.625000
0.925000	1.141665	1.766665	2.183332	3.433332	4.266665
0.128333	0.191667	0.308333	0.391666	0.550000	0.658333
0.949999	1.158333	1.766665	2.183332	3.433332	4.266665
0.166667	0.233333	0.341667	0.433333	0.591666	0.700000
0.974999	1.166666	1.766665	2.183332	3.433332	4.266665
0.216667	0.283333	0.391666	0.475000	0.625000	0.733333
0.999999	1.183332	1.766665	2.183332	3.433332	4.266665

0.09075803
0.35369009
0.50025624
0.61064506
0.77988166
0.95040458
0.20704591
0.39406508
0.46079713
0.59690899
0.77825773
0.91965067
0.21057653
0.41567695
0.47027183
0.59847099
0.77755278
0.91948491
0.20616454
0.44905102
0.50218688
0.60504168
0.77712286
0.91943133
0.23362422
0.45859766

0.50040990
0.60646302
0.77583385
0.91941863

APPENDIX VI

BIBLIOGRAPHY

BIBLIOGRAPHY

1. Ahimaz, F.J., "Birefringent - Fluid Tests Using Scattered-light Technique", Experimental Mechanics, pp. 133-134, March, 1970.

2. Alcock, E.D., and Sadron, C.L., An Optical Method for Measuring the Distribution of Velocity Gradients in a Two Dimensional Flow, Physics, Vol. 6, pp. 92-95, 1935.

3. Anderson, A.G., The Characteristics of Sediment Waves Formed by Flow in Open Channels, Proceedings, The Third Midwestern Conference in Fluid Mechanics, Minneapolis, pp. 379-395, March, 1953.

4. Bagnold, R.A., The Movement of the Desert Sand, Proceedings, Royal Society, London, A. No. 892, Vol. 157, pp. 594-620, 1936.

5. Bagnold, R.A., The Flow of Cohesionless Grains in Fluids, Philosophical Transactions, Royal Soc. of London, Series A, Vol. 249, Dec. 1956, p. 235.

6. Bankoff, S.G., and Rosler, R.S., Constant Temperature Hot-Film Anemometer as a Tool in Liquid Turbulence Measurements, Rev. Sci. Inst., 33, n11, 1209, 1962.

7. Batchelor, Theory of Homogenous Turbulence, Cambridge, 1953.

8. Bogardi, J.J., The Total Sediment Load of Streams, Discussion, Proc. Paper No. 1856, ASCE, Vol. 84, No. HY 6, November 1958, p. 74.

9. Boussinesq, J., Essai sur la theorie des eaux courantes, Memoiries de L'Academie de Sciences de France, Vol. 23, 1877, pp. 218-228 (For recapitulation of Boussinesq's formulation, see Fourchheimer, P., Hydraulik, Teubner, Leipzig, 1930, pp. 237-242).

10. Breslin, J.P., and Macovsky, M.S., Effects of Turbulence Stimulation on the Boundary Layer and Resistance of a Ship Model as Detected by Hot-Wires, David Taylor, Model Basin Report 724, Aug. 1950.

11. Carruthers, P.A., Velocity Profiles for the Transition Region in an Open Rectangular Channel, M.S. Thesis Rice University, May 1963.

12. Chang, F.M., Ripple Concentration and Friction Factor, Journal of the Hydraulics Division, ASCE, Vol. 96, No. HY 2, Proc. Paper 7067, February 1970, pp. 417-430.

13. Chow, Ven Ti, Open Channel Hydraulics, McGraw-Hill, N.Y., 1959.

14. Clough, R.W., The Finite Element in Plane Stress Analysis, Proc. 2nd ASCE. Conf. on Electronic Computations, Pittsburgh, Pa., September, 1960.

15. Cooper, R.D., and Tulin, M.P., Turbulence Measurements with the Hot-Wire Anemometer, Agardograph, 12, Aug., 1955.

16. Crickmore, M.J., Effect of Flume Width on Bed-Form Characteristics, Journal of the Hydraulics Division, ASCE, Vol. 96, No. HY 2, Proc. Paper 7077, Feb., 1970, pp. 473-496.

17. Dally, J.W., and Riley, W.F., Experimental Stress Analysis, McGraw-Hill, N.Y., 1965.

18. Darby, R., Momentum Transfer in a Two Phase Liquid - Liquid System in Co-Current Stratified Flow, Ph.D. Thesis, Rice University, Oct., 1961.

19. Darwin, G.H., On the Formation of Ripple - Marks, Proceedings Royal Society, London, 1883.

20. Dell'osso, L., Turbulence Measurements in Water in an Open Channel With the Hot-Film Anemometer, Ph.D. Thesis, Rice University, 1966.

21. Einstein, H.A., and Barbarossa, N.L., River Channel Roughness, Transactions, ASCE, Vol. 117, 1952, p. 1121.

22. Engelund, F., Hydraulic Resistance of Alluvial Streams, Journal of the Hydraulics Division, ASCE, Vol. 92, No. HY 2, Proc. Paper 4739, March 1966, pp. 315-326.

23. Engelund, F., and Hansen, E., Investigations of Flow in Alluvial Streams, Bulletin No. 9, Hydraulics Laboratory Technical University of Denmark, 1966.

24. Exner, F.M., Uber die Wechselwirking Zwischen Wasser und Geschiebe in Flussen, Sitzungsber - ichte der Akademie der Wissenschaften, Wein, Heft 3-4, 1925.

25. Falkner, F.H., Studies of River Bed Material and Their Movements with Special Reference to Lower Mississippi River, Paper 17, U.S. Waterway Experimental Sta., Vicksburg, Miss., June, 1935.

26. Garde, R.J., and Albertson, M.L., Characteristics of Bed Forms and Regimes of Flow in Alluvial Channels, Colorado State University, Fort Collins, Colo., 1959.

27. Garde, R.J., and Raju, R.G., Regime Criteria for Alluvial Streams, J. of the Hydraulics Division, ASCE, Proc., Nov., 1963, pp. 153-164.

28. Garde, R.J., and Raju, R.G., Resistance Relationships for Alluvial Channel Flow, J. of the Hydraulics Division, ASCE, Vol. 92, No. HY 4, Proc. Paper 4869, July, 1966, pp. 77-100.

29. Gilbert, G.K., The Transportation of Debris by Running Water, Professional Paper 86, U.S.G.S., 1914.

30. Giratalla, M.K., and McCorquodale, J.A., Flow Over Natural and Artificial Ripples, International Association for Hydraulic Research, 1973.

31. Graf, W.H., Hydraulics of Sediment Transport, McGraw-Hill, N.Y., 1971.

32. Grant, H.L., Stewart, R.W., and Moilliet, A., Turbulence Spectra from a Tidal Channel, J. Fluid Mechanics, 12, 241, 1962.

33. Grant, H.L., Moilliet, A., and Stewart, R.W., A Spectrum of Turbulence at Very High Reynolds Number, Nature, 184, 808, 1959.

34. Grass, A.J., Initial Instability of Fine Bed Sand, J. of Hydraulics Division, ASCE, Vol. 96, No. HY 3, March, 1970, pp. 619-632.

35. Hauser, E.A., and Dewey, D.R., Visual Studies of Flow Patterns, The Journal of Physical Chemistry, Vol. 46, pp. 212-213, 1942.

36. Henderson, F.M., Open Channel Flow, The MacMillan Company, N.Y., 1966.

37. Hill, H.M., Bed Forms Due to a Fluid Stream, J. of the Hydraulics Division, ASCE, Vol. 92, March, 1966, pp. 127-143.

38. Hill, H.M., Srinivasan, V.S., and Unny, T.E., Instability of Flat Bed in Alluvial Channels, J. of the Hydraulics Division, ASCE, Vol. 95, Porc., Sept., 1969, pp. 1545-1558.

39. Hinze, J.O., Turbulence, McGraw Hill, N.Y., 1959.

40. Humphrey, R.H., Demonstration of Double Refraction Due to Motion of a Vanadium Pentoxide Sol. and Some Applications, Proceedings of the Physical Society of London, Vol. 35, pp. 217-218, 1923.

41. Inglis, C.C., Bed Ripples and Bed Dunes, Research Publication No. 13, Central Water Power Irrigation and Navigation Research Station, Poona, India, 1949, pp. 459-467.

42. Iwasa, Y., Computation Method of Surface Profiles of Water, Special Lecture 1963-1, Kwansai District Office, Japan Society of Civil Engineers, Jan., 1963, (in Japanese).

43. Jonys, C.K., An Experimental Study of Bed-Form Mechanics, Ph.D. Thesis, Civil Engineering Department, University of Alberta, 1973.

44. Jonys, C.K., Pressure and Shear Stress Distributions on Alluvial Bed-forms, 9th Proceeding of Hydrology Symposium, University of Alberta, 1973.

45. Kennedy, J.B., and Nevill, A.M., Basic Statistical Methods for Engineers and Scientists, International Textbook Company, Scranton, Pennsylvania, 1966.

46. Kennedy, J.F., The Mechanics of Dunes and Antidunes in Erodible-Bed Channels, J. of Fluid Mechanics, Vol. 16, 1963, pp. 521-544.

47. Kennedy, J.F., and Iwasa, Y., Free Surface Shear Flow Over a Wavy Bed, J. of the Hydraulics Division, ASCE, Vol. 94, Proc. March, 1968, pp. 431-454.

48. Kennedy, J.F., and Lovera, F., Friction Factors for Flat Bed Flows in Sand Channels, J. of the Hydraulics Division, ASCE, Vol. 95, Proc. July, 1969, pp. 1227-1234.

49. Kennedy, J.F., and Alam, A.M.Z., Friction Factors for Flow in Sand Bed Channels, J. of the Hydraulics Division, ASCE, Vol. 95, Nov., 1969, pp. 1973-1992.

50. Khanna, Sat Dev., Experimental Investigation of Form of Bed Roughness, J. of the Hydraulics Division, ASCE, Vol. 96, Proc. Oct.,1970, pp. 2029-2040.

51. King, L.V., On the Convection of Heat from Small Cylinders in a Stream of Fluid: Determination of the Convection Constants of Small Platinum Wires with Applications to Hot Wire Anemometry - Phil Trans. Roy. Soc., London, SA 214, 373, 1914.

52. Kramers, H., Physica 12, 61, 1946.

53. Lamb, H., Hydrodynamics, 6th Edition, Cambridge University Press, Cambridge, 1932.

54. Langbein, W.B., Hydraulic Criteria for Sand Waves, Transactions, Amer. Geophysical Union, Vol. 23, 1942.

55. Laufer, J., Investigation of Turbulent Flow in a Two Dimensional Channel, NACA Report 1053, 1951.

56. Laursen, E.M., et al, Pressure and Shear Distribution on Schematic Dunes, Technical Report 2, NSF G-7409, National Science Foundation, Washington, D.C., 1962.

57. Leliavsky, S., An Introduction to Fluvial Hydraulics, Dover Publications, Inc., N.Y., 1966.

58. Ling, S.C., Measurement of Flow Characteristics by the Hot-Film Technique, Ph.D. Thesis, State University of Iowa, 1955.

59. Ling, S.C., and Hubbard, P.G., The Hot-Film Anemometer: A New Device for Fluid Mechanics Research, J. Aero Sci., 23, 890, 1956.

60. Liu, H.K., Mechanics of Sediment - Ripple Formation, J. of the Hydraulics Division, ASCE, Vol. 83, April, 1957.

61. Massé, P., Ressaut et ligne d'eau dans les cours d'eau a pente variable, Revue Generale de L'Hydraulique, Vol. 4, No. 19, 1938, pp. 61-64.

62. Maxwell, J.C., On Double Refraction in a Viscous Fluid in Motion, The Scientific Papers of James Clerk Maxwell, edited by Niven, W.D., Vol. II, N.Y. Dover Publication, 1952, pp. 379-380.

63. McQuivey, R.S., Turbulence in a Hydrodynamically Rough and Smooth Open Channel Flow, Ph.D. Thesis, Colorado State University, 1967.

64. McQuivey, R.S., and Richardson, E.V., Measurement of Turbulence in Water, J. of the Hydraulics Division, ASCE, Vol. 94, Proc. March, 1968, pp. 411-430.

65. McQuivey, R.S., and Richardson, E.V., Some Turbulence Measurements in Open Channel Flow, J. of the Hydraulics Division, ASCE, Vol. 95, Proc. Jan., 1969, pp. 209-223.

66. Mercer, A.G., and Haque, M.I., Ripple Profiles Modeled Mathematically, J. of the Hydraulics Division, ASCE, Vol. 99, Proc. March 1973, pp. 441-459.

67. Milne- Thomson, L.M., Theoretical Hydrodynamics, 4th ed., The MacMillan Co., N.Y., 1960.

68. Ousterhout, D., Some Problems in Streaming Birefringence Flow Analysis, Ph.D. Thesis, Washington University, 1965.

69. Pai, Shih-I., Viscous Flow Theory, Vol. II, Turbulent Flow, D. Van Nostrand Co., Inc., Princeton, N.J., 1957.

70. Patterson, A.M., Development of a Hot-Wire Instrument for Ocean Turbulence Measurements, Pacific Naval Laboratory Technical Memorandum 57-2, 1957.

71. Patterson, A.M., Hot-Wire Turbulence Measurements in a Tidal Channel, Pacific Naval Laboratory Technical Memorandum, 1959.

72. Peebles, F.N., Prados, J.W., and Honeycutt, E.G., A Study of Laminar Flow Phenomena Utilizing a Double Refracting Liquid. Progress Report 1, The Engineering Experiment Station and The Department of Chemical Engineering, University of Tennessee, 1954.

73. Peebles, F.N., Garber, H.J., and Jury, S.H., Preliminary Studies of Flow Phenomena Utilizing a Double Refractive Liquid, Proceedings of the Third Mid-Western Conference on Fluid Mechanics, 1953.

74. Prados, J.W., and Peebles, F.N., Determination of the Flow Double Refraction Properties of Aqueous Milling-Yellow Dye Solutions, The Engineering Experiment Station and the Department of Chemical Engineering, University of Tennessee, Progress Report 2 in 1955, and Final Report, 1957.

75. Pratt, C.J., Bagnold Approach and Bed-Form Development, J. of the Hydraulics Division, ASCE, Vol. 99, Proc. Jan., 1973, pp. 121-137.

76. Raichlen, F., Some Turbulence Measurements in Water, J. of the Engineering Mechanics Division, ASCE, Vol. 93, Proc. April, 1967.

77. Raudkivi, A.J., Study of Sediment Ripple Formation, J. of the Hydraulics Division, ASCE, Vol. 89, Proc. Nov., 1963, pp. 15-33.

78. Raudkivi, A.J., Analysis of Resistance in Fluvial Channels, J. of the Hydraulics Division, ASCE, Vol. 93, Proc. Sept., 1967, pp. 73-84.

79. Raudkivi, A.J., Loose Boundary Hydraulics, Pergamon Press, 1967.

80. Resh, F.J., Hot-Film Turbulence Measurements in Water Flow, J. of the Hydraulics Division, ASCE, Vol. 96, Proc. March, 1970, pp. 787-800.

81. Reynolds, A.J., Waves on the Erodible Bed of an Open Channel, J. of Fluid Mechanics, Vol. 22, 1965, pp. [illegible]-133.

82. Richardson, E.V., and Simons, D.B., Resistance to Flow in Sand Channels, Proceedings, 12th Congress of the International Association for Hydraulic Research, Sept., 1967.

83. Rifai, M.F., and Smith, K., Flow Over Triangular Elements Simulating Dunes, J. of the Hydraulics Division, ASCE, Vol. 97, July, 1971, pp. 963-976.

84. Roberts, W.J., Experimental Dynamic Response of Fluid Lines, Dept. Mech. Eng., Purdue University, Internal Report, 1963.

85. Rouse, H., Engineering Hydraulics, John Wiley, Inc., 1950.

86. Sabin, C.M., An Analytical and Experimental Study of the Plane, Incompressible Turbulent Free Shear Layer with Arbitrary Velocity Ratio and Pressure Gradient, AFOSR TN 5443, Oc., 1963.

87. Sandborn, V.A., Metrology of Fluid Mechanics, Report No. CER 66VAS32, Dept. of Civil Engineering, Colorado State University, Fort Collins, Colo.,1966, p. 155.

88. Scheuner, J.R., A Birefracting Fluid Tunnel for Fundamental Fluid Flow Investigations, Doctor of Science Thesis, Washington University, 1964.

89. Schlichting, H., Boundary Layer Theory, McGraw-Hill, N.Y., 1968.

90. Sheen, S.J., Turbulence Over a Sand Ripple, Master of Engineering, University of Auckland, 1964.

91. Shen, H.W., Development of Bed Roughness in Alluvial Channels, J. of the Hydraulics Division, ASCE, Vol. 88, Proc., May, 1962, pp. 45-58.

92. Shen, H.W., River Mechanics, Vol. I, 1971.

93. Shields, A., Application of the Theory of Similarity and Turbulent Research to the Bed-Load Movement, Prussian Experimental Inst. for Hydraulic Engrg. and Ship Building, Berlin, Germany, 1936.

94. Shinohara, K., and Tsubaki, T., On the Characteristics of Sand-Waves Formed Upon the Beds of the Open-Channels and Rivers, Reports of Research Ins. for Applied Mechanics, Vol. VII, No. 25, 1959.

95. Simons, D.B., and Richardson, E.V., Resistance to Flow in Alluvial Channels, Proceedings, ASCE, Vol. 86, May, 1960.

96. Simons, D.B., and Richardson, E.V., Forms of Bed Roughness in Alluvial Channels, Proceedings, ASCE, Vol. 87, May, 1961.

97. Simons, D.B., Richardson, E.V., Hanshild, W.L., U.S. Geol. Survey, Colorado State University, Fort Collins, Colorado, Rept. No. CER 61DBS50, August, 1961.

98. Smith, K.H., Alluvial Channel Resistance to Bed Form, Proceedings ASCE, Vol. 94, January, 1968.

99. Squarer, D., Friction Factors and Bed Forms in Fluvial Channels, Proceedings, ASCE, Vol. 96, April, 1970.

100. Streeter, V.L., Fluid Mechanics, McGraw-Hill, Fifth Edition,

101. Tchen, Turbulent Flow, Princeton University Press.

102. Thomas, D.G., Periodic Phenomena Observed with Spherical Particles in Horizontal Pipes, Science, Vol. 144, May, 1964, pp. 534-536.

103. Thurston, G.B., and Schrag, J.L., Measurement of Dynamic Birefringence of a Thin Fluid Layer in Oscillatory Shear, Physics Department, Research Foundation, Oklahoma State University, Stillwater, 1961.

104. Tison, L.J., Origine des Ondes de Sable et des Bancs de Sable sans L'action des Courants, Association International de Recherches pour Travaux Hydrauliques, Third Meeting, Sept., 1949, Grenoble, France.

105. Townsend, Structure of Turbulent Shear Flow, Cambridge.

106. Vanoni, V.A., and Brooks, N.H., Laboratory Studies of the Roughness and Suspended Loads of Alluvial Streams, Report No. E-68, California Inst. of Tech., Pasadena, California, Dec., 1957.

107. Vanoni, V.A., and Hwang, L.S., Relation Between Bed Forms and Friction in Streams, Proceedings, ASCE, Vol. 93, May, 1967.

108. Velikanov, M.A., Formation of Sand Ripples on the Stream's Bottom, Rapport 13, International Association of Scientific Hydrology, 1936.

109. Von-Karmen, T., Sand Ripples in the Desert, Technian Year Book, 1947.

110. Wayland, H., and Sutera, S.P., Quantitative Analysis of Two-Dimensional Flow by Means of Streaming Birefringence, J. of Applied Physics, Vol. 32, 1961.

111. Wayland, H., Streaming Birefringence as a Hydrodynamic Research Tool - Applied to a Rotating Cylinder Apparatus Above the Transition Velocity, J. of Applied Physics, Vol. 26, 1955.

112. Wayland, H., Streaming Birefringence as a Qualitative and Quantitative Flow Visualization Tool, ASME, Annual Meeting Symposium on Flow Visualization, N.Y., 1960.

113. Wayland, H., Streaming Birefringence of Rigid Macro-Molecules in General Two-Dimensional Laminar Flow, J. of Chemical Physics, Vol. 33, 1960.

114. Williams, P.B., and Kemp, P.H., Initiation of Ripples on Flat Sediment Beds, J. of Hydraulics Division, ASCE, Proc., Vol. 97, April, 1971.

115. Williams, P.B., and Kemp, P.H., Initiation of Ripples by Artificial Disturbances, Proceedings, ASCE, Vol. 98, June, 1972

116 Yalin, M.S., Mechanics of Sediment Transport, Pergamon Press, 1972.

117 Yalin, M.S., On the Determination of Ripple Length, Technical Note, Proceedings, ASCE, Vol. 103, April, 1977.

118 Yang, C.T., Incipient Motion and Sediment Transport, Proceedings, ASCE, Vol. 99, Oct., 1973.

119 Zaghloul, N.A., Analytical and Experimental Investigations of Flow Around a Spur Dike, Ph.D. Thesis, Civil Engineering Department, University of Windsor, Windsor, Ontario, 1974.

120 Zienkiewicz, O.C., and Cheung, Y.K., The Finite Element Method in Structural and Continuum Mechanics, McGraw-Hill, N.Y., 1967.

APPENDIX VII

NOMENCLATURE

NOMENCLATURE

A	Component of the Light Vector
a	Overheating Ratio
a	Heat Transfer Coefficient
C	Chezy Coefficient
C	Constant
C_d	Drag Coefficient
cor	Calibration Coefficient of the V-probe
c_p	Specific Heat at Constant Pressure
D	Depth of Flow
d	Distance Above the Channel Bed
d	Equivalent Diameter of the Hot-Film Sensor
d'_p	Inside Diameter of the Pitot-tube
E	DC Voltage
e	Subscript Denotes an Element
e'	Root-Mean-Square of AC Voltage
f	Sensitivity Factor
F_D	Drag Force
g	Gravitational Acceleration
H	Reading of the Orifice Meter Manometer
h_r	Ripple Height
Δh	Reading of the Sloping Manometer
I	Electric Current
I	Intensity of Light
K_s	Size of Sand-Roughness

K	Heat Conductivity of Fluid
K	Bed Roughness
L	Ripple Length
l	Distance Along a Ripple Measured in the Downstream Direction
m	Porosity of Sand
N	Fringe Number
N_u	Nusselt Number
n	Index of Refraction
P	Pressure at a Point
P_r	Prandtl Number
Q	Rate of Flow
q_B	Rate of Sand Transport
R	Electric Resistance
R, R_e	Reynolds Number
$R_e{*}$	Roughness Reynolds Number
R_x	Reynolds Number Based on a Representation length l_x
S	Sensitivity Factor of Hot-Film Probe
S	Standard of Deviation
S.G	Specific Gravity
T	Temperature
t	Time
Δt	Time Step
U	Velocity Component in the X-Direction
$\overline{U}$	Mean Flow Velocity
$\vec{U}$	Velocity Vector

U_*	Shear Velocity
u	Velocity Fluctuation in the X-Direction
u'	Turbulence Intensity in the X-Direction
u_r	Ripple Velocity
$\overline{uv}$	Double Correlation of the Velocity Fluctuations
V	Velocity Component in the Y-Direction
v	Velocity Fluctuation in the Y-Direction
v'	Turbulence Intensity in the Y-Direction
v_s	Fall Velocity
X, Y, Z	Cartesian Co-ordinates
x_*	Distance Measured from the Reattachment Point
y	Distance above the bed
ψ	Stream Function
ε	Eddy Viscosity
Λ	Macro Scale of Turbulence
λ	Micro Scale of Turbulence
λ	Wave Length of Light
ω	Vorticity
ω	Circular Frequency of Light
μ	Dynamic Viscosity
ν	Kinematic Viscosity
ρ	Density
γ	Specific Weight
Σ	Summation
σ	Temperature Coefficient of the Electric Resistivity
τ	Shear Stress

τ_D	Form Drag
$\bar{\tau}_{og}$	Bed Shear Due to Skin Friction
τ_T	Total Shear
δ_1	Laminar Sublayer Thickness

VITA AUCTORIS

1941 Mahmoud Kamel Giratalla was born in Egypt, on December 12, 1941.

1964 In June, 1964, graduated from Ain Shams University, Cairo, Egypt, with the degree of Bachelor of Applied Science in Civil Engineering Department "Irrigation and Hydraulics Section".

1969 In October 1969, graduated from University of Windsor, Windsor, Ontario, Canada, with the degree of Master of Applied Science in Civil Engineering Department

1969 In October, 1969, enrolled at the University of Windsor, in a program leading to the degree of Doctor of Philosophy in Civil Engineering Department.

1973 In September, 1973, joined FENCO Consultants Ltd. in the capacity of Design Engineer in Edmonton, Alberta.

1976 In May, 1976, joined the Design and Construction Division, Department of Environment, Province of Alberta, as Design Project Engineer.